WORLD METEOROLOGICAL ORGANIZATION

NATIONAL AERONAUTICS AND SPACE ADMINISTRATION

FEDERAL AVIATION ADMINISTRATION

NATIONAL OCEANIC AND ATMOSPHERIC ADMINISTRATION

WMO GLOBAL OZONE RESEARCH AND MONITORING PROJECT

REPORT No. 11

THE STRATOSPHERE 1981
THEORY AND MEASUREMENTS

N82-18770 —
N82-18777

ERRATA

for

THE STRATOSPHERE 1981: THEORY AND MEASUREMENTS
WMO Global Ozone Research and
Monitoring Project Report No. 11

Note the following changes:

1. p.E-24. "Harwood....1976" should read:

   "Harwood R. S., Some recent investigations of the upper atmosphere by remote sounding satellites, Remote Sensing of the Terrestrial Environment, R. F. Peel, L. F. Curtis, and E. C. Barrett, editors, Colston Papers Vol. 28 (1976), Butterworth, London, pp. 111-125, 1977."

2. p.E-35. "Lee....1982" add: NASA Technical Memorandum 83259

3. p.E-50. "Pinto....1981" should read:

   "Pinto, J. P., Y. L. Young, D. Rind, G. L. Russell, J. A. Lerner, J. E. Hansen, and S. Hameed, A general circulation model study of atmospheric carbon monoxide, J. Geophys. Res., submitted, 1981.

4. p.I-2. "James K. Angel" should read "James K. Angell"

WORLD METEOROLOGICAL ORGANIZATION

NATIONAL AERONAUTICS AND SPACE ADMINISTRATION

FEDERAL AVIATION ADMINISTRATION

NATIONAL OCEANIC AND ATMOSPHERIC ADMINISTRATION

WMO GLOBAL OZONE RESEARCH AND MONITORING PROJECT

REPORT No. 11

May 1981

A meeting of experts on the state of the stratosphere held at Hampton, Virginia USA, 18-22 May 1981, organized in collaboration with the United Nations Environment Program.

THE STRATOSPHERE 1981
THEORY AND MEASUREMENTS

Printed January 1982

Copies of this report are available from:

World Meteorological Organization, Case Postale No. 5
Geneva 20, Switzerland

Stratosphere Physics and Chemistry Branch, Code 963
NASA/Goddard Space Flight Center
Greenbelt, Maryland 20771, USA

PREFACE

For a little over a decade, there has been considerable public and scientific interest in the question as to whether man can inadvertently modify the stratosphere and in particular the ozone layer allowing biologically harmful ultraviolet radiation to reach the ground. Specific reports on the impact of emission by the supersonic transport in the stratosphere and the release of chlorofluoromethanes in the troposphere have been published by individual nations, the Commission for the European Communities, the Organization for Economic Cooperation and Development, the United Nations Environment Program, and the World Meteorological Organization. In December 1980, officials from the World Meteorological Organization and three United States government agencies, the National Aeronautics and Space Administration, the Federal Aviation Administration, and the National Oceanic and Atmospheric Administration agreed to sponsor jointly a scientific workshop to summarize the present state-of-knowledge of the stratosphere and to assess the totality of man's impact.

The Goddard Space Flight Center of the National Aeronautics and Space Administration was asked to organize the workshop, which was held May 18-22, 1981. The workshop was centered around three working groups corresponding to the three chapters in the report. These three were a Trace Species Working Group chaired by Dr. Dieter Ehhalt of the Institut für Chemie der KFA, Jülich, Federal Republic of Germany, a Multidimensional Aspects Working Group chaired by Dr. James Holton, Washington University, Seattle, Washington, USA, and a Trends and Predictions Working Group chaired by Dr. Julius Chang, Lawrence Livermore National Laboratory, Livermore, California, USA. Five pre-workshop meetings were also held to address specific problems or to organize the written inputs to the workshop. These were a Modeling Working Group under the chairmanship of Dr. Chang, a Trace Species Working Group under the chairmanship of Dr. Ehhalt, a Solar Flux Working Group under the chairmanship of Dr. John Frederick, Goddard Space Flight Center, USA, a Trends Working Group under the chairmanship of Dr. Julius London, University of Colorado, Boulder, Colorado, USA, and a joint NASA/CODATA Working Group under the joint chairmanship of Dr. William DeMore of the Jet Propulsion Laboratory, California, USA, and Dr. J. Alistair Kerr, University of Birmingham, United Kingdom. The findings of the Solar Flux Working Group and the Reaction Rate Working Group have been placed in appendices to this report. The overall direction of the workshop was under the joint chairmanship of Dr. R. D. Hudson of the Goddard Space Flight Center and Dr. Rumen Bojkov of the World Meteorological Organization. Dr. Richard Stolarski, Dr. Marvin Geller, and Mrs. Edith Reed, all of the Goddard Space Flight Center, and Dr. Robert Watson, Upper Atmosphere Program Office, National Aeronautics and Space Administration were the co-chairman for the workshop and for the production of the report.

Each working group was further subdivided and prominent scientists active and expert in stratospheric and mesospheric studies were asked to prepare position papers to cover selected topics of research. In addition to the prepared position papers, pre-meetings, as discussed above, were held to assemble some of this material into a cohesive report. The position papers and these prepared reports were furnished to the participants before they came to the workshop. An important aspect of this work was that the modeling groups agreed on a common set of scenarios to study so that realistic model comparisons could be made at the workshop.

Over 100 scientists representing most of the institutions in the world engaged in upper atmospheric research attended the workshop. A complete list of the position paper authors and the participants in the workshop and in the pre-workshop meetings is given in an appendix. At the end of the workshop each working group prepared a summary document and these have been assembled into this report. Thus this report should represent current knowledge as of June 1981.

The basic theme for the workshop and the report was the comparison of theory and measurement. Thus in Chapter 1 measurements of trace species are compared with theoretical estimates; the similarities and the differences between these two sets of results are discussed in terms of the implications to the assessments found in Chapter 3. In Chapter 2 the available satellite data are compared with the prediction of two-dimensional and three-dimensional models. In Chapter 3 the theoretical predictions are compared with long term trends in both column content and altitude profile of ozone as observed from ground-based and satellite instruments. It should be stressed that this is not a consensus document. If more than one conclusion could be maintained by the scientific data, then both of these conclusions have been quoted. It is, after all, a significant test of the present state-of-knowledge if more than one scientific conclusion can be drawn from the same experimental data.

The World Meteorological Organization, the National Aeronautics and Space Administration, the Federal Aviation Administration, and the National Oceanic and Atmospheric Administration wish to express their thanks to the working group chairman, the position paper authors, and the participants at both the pre-workshop meetings and the workshop for the time and effort that they contributed to the preparation of this report.

CONTENTS

CHAPTER 1

TRACE SPECIES

CONTENTS (Continued)

CHAPTER 3

MODEL PREDICTIONS AND TREND ANALYSIS

CONTENTS (Continued)

CHAPTER 1

TRACE SPECIES

INTRODUCTION

The elements of a qualitative understanding of the stratosphere date back more than half a century to Chapman's pioneering work that explained the existence of the stratospheric ozone layer: Photolysis of oxygen in the Herzberg continuum, recombination of O with O_2 to form O_3, ozone photolysis from about 240 to 300 nm thereby heating the stratosphere and inverting its temperature profile, and the odd-oxygen destruction reaction, $O + O_3 \rightarrow O_2 + O_2$, four reactions in all, sufficed to provide a general picture. Extension and elaboration followed, first in 20-year intervals and then more closely spaced: HO_x chemistry by Bates and Nicolet in 1950, NO_x chemistry by Crutzen (1971) and by Johnston in 1971, ClO_x chemistry by Stolarski and Cicerone (1974) and Wofsy and McElroy (1974), until the present time when the number of chemical species has passed 35 and the number of reactions 130.

The story is both interesting and familiar, at least in historical outline. As a truly global problem of potential anthropogenic pollution of the atmosphere it has captured our imagination. A series of possible sources of pollutants has been considered: supersonic transport engine exhaust (NO_x), chlorofluoromethane photolysis and degradation (ClO_x), nuclear bomb tests (NO_x), rocket engine exhaust (ClO_x), fertilizer-induced N_2O (NO_x), and diverse halocarbons (ClO_x, BrO_x).

The perceived threat of an anthropogenic reduction of the Earth's ozone shield generated an active program of research in many countries, directed both towards a fuller understanding of the natural stratosphere and of its perturbation. This program faced the formidable task of bringing together and elucidating many different aspects of the problem: to help understand the transport and dynamics of the stratosphere, its complex chemistry and photochemistry, the intensity and variability of solar radiation, to describe the delicate interplay of these disciplines using mathematical models, and then to verify this understanding through elaborate field measurements of trace species concentrations. Even so, it is not enough to examine the stratosphere in isolation, since both its dynamics and its chemistry are linked with those of the troposphere. This requires the understanding, measurement, and modeling of tropospheric processes as well.

The outpouring of work on all aspects of this large problem during the past decade has been remarkable and its progress has been summarized and reviewed at regular intervals (CIAP 1975b, NAS, 1975, 1976 and 1979, NASA 1977 and 1979). It revolves principally, but not exclusively, around ozone, its formation and removal by catalytic sets of chain reactions whose net effects are equivalent to the odd-oxygen distribution steps:

$$O + O_3 \rightarrow 2O_2$$

$$O_3 + O_3 \rightarrow 3O_2$$

The families of trace species involved in these processes are best characterized in terms of three categories: source gases, active radicals, and sink gases. The active radicals take part directly in the odd oxygen removal processes, they are produced from relatively stable source species, and they are themselves removed via the formation of more or less stable sink gases that are ultimately removed from the atmosphere. For the NO_x trace species the active radicals are NO and NO_2 and the principal catalytic cycle is the well-known sequence:

$$NO + O_3 \rightarrow NO_2 + O_2$$

$$NO_2 + O \rightarrow NO + O_2$$

$$\text{Net } O + O_3 \rightarrow 2O_2$$

The source gas is N_2O and the main sink gases are HNO_3, HNO_4, and $ClNO_3$. For ClO_x trace species, the list of source gases is long, including $CFCl_3$, CF_2Cl_2, CCl_4, CH_3Cl, CH_3CCl_3, and other halocarbon compounds, the active radicals are Cl and ClO, and the sink gases are HCl, HOCl, and $ClNO_3$. The catalytic cycles are interlocked through fast exchange reactions, and the sink gases are capable of regenerating active radical species through chemical and photolytic steps.

Examples of radical interchange reactions are

$$ClO + NO \rightarrow Cl + NO_2$$

$$HO_2 + NO \rightarrow HO + NO_2$$

and of radical regeneration reactions

$$HO + HCl \rightarrow H_2O + Cl$$

$$HNO_3 + h\nu \rightarrow HO + NO_2$$

To set the stage for the critical discussion of the measurement of trace gas species and for the comparison with mathematical model calculations it is desirable to provide a framework that permits one to recognize which of the catalytic cycles and chemical steps are more or less important to our overall understanding of stratospheric processes. Figures 1-1, 1-2, and 1-3 show the source, radical, and sink species for the HO_x (Figure 1-1), NO_x (Figure 1-2), and ClO_x (Figure 1-3) cycles and their reactive interconnections. The numbers within the boxes are the molecular concentrations of the species in molecules/cm^3. The numbers within the arrows are the reaction fluxes in molecules/cm^3-sec. Both sets of numbers refer to an altitude of 30 km, noon local time, and mid-latitude. The relative magnitudes of the concentrations and of the fluxes permit us to appreciate at a glance the importance of species and of specific processes. The lifetime of any species for a given process is obtained by dividing the species concentration by the flux for that process. The chemical and photochemical rate parameters used in this calculation are those of the most recent recommendation by the NASA/CODATA Panel for Data Evaluation of Laboratory Measurements given in Appendix A of this report.

The relative contribution of the various catalytic cycles to the removal of odd oxygen as a function of altitude is shown in Table 1-1, based again on one-dimensional model calculations. Each column lists the local rate of a given removal process normalized to the local rate of odd oxygen production by oxygen photolysis. The column headings indicate the rate-limiting step in a given catalytic cycle. For example, in the NO_x cycle, the $NO + O_3$ rate is much larger than the $NO_2 + O$ rate, since NO_2 photolysis regenerates odd oxygen. The rate of odd oxygen destruction due to the NO_x catalytic cycle is therefore $2k_{NO_2}[NO_2][O]$ where the square brackets denote molecular concentrations and k_{NO_2} is the rate constant for the $O + NO_2$ reaction at the temperature corresponding to that altitude. The factor of two arises from the destruction of O_3 by $NO + O_3$ in the completion of one cycle in the homogeneous catalysis.

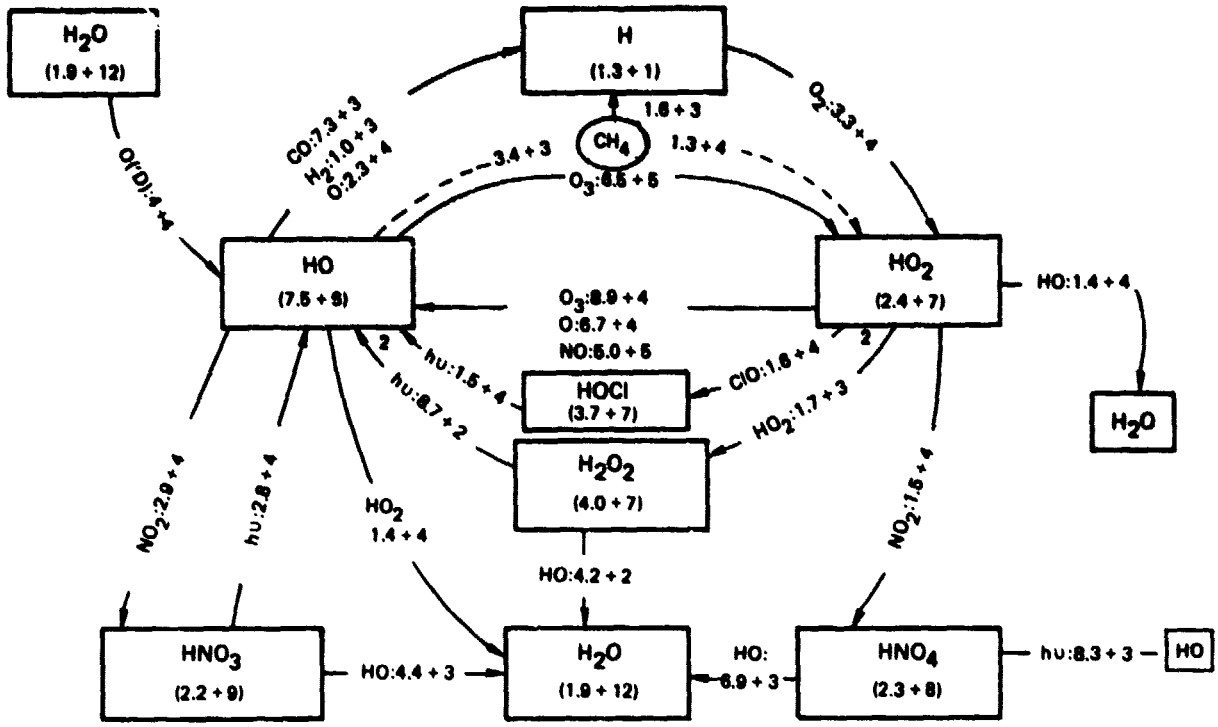

Figure 1-1. Chemical life cycles of HO_x trace species.

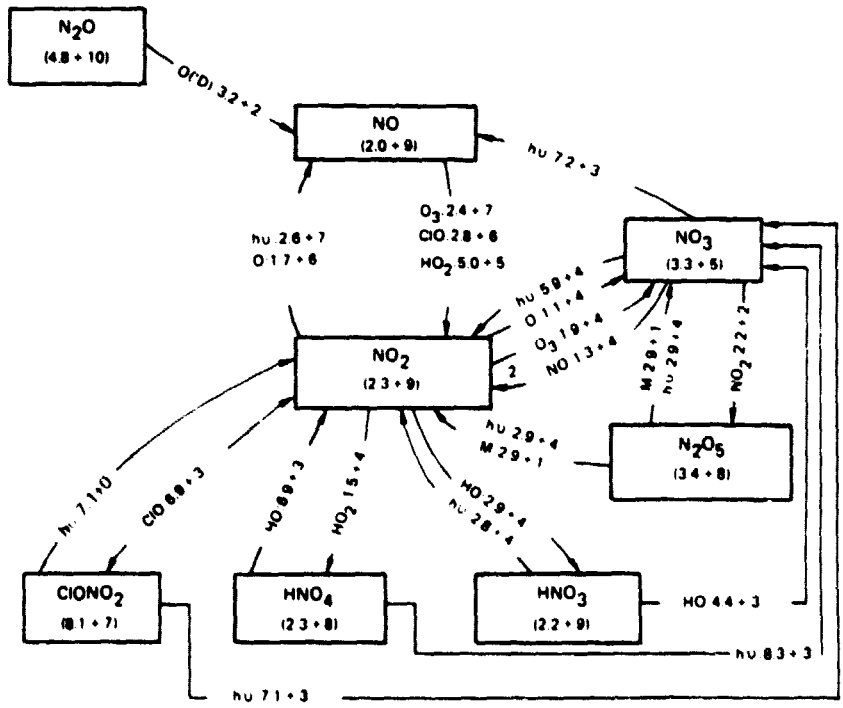

Figure 1-2. Chemical life cycles of NO_x trace species.

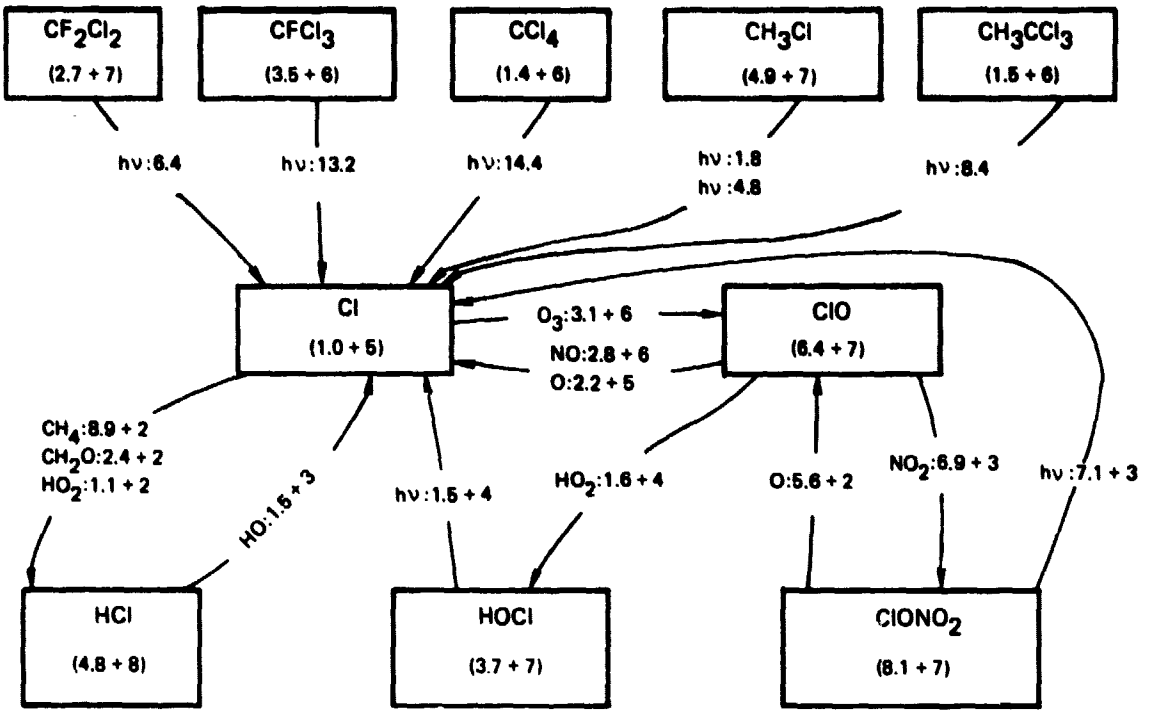

Figure 1-3. Chemical life cycles of ClO_x trace species.

Table 1-1
Relative Contributions of the Major Rate Limiting Chemical Reactions for the Catalytic Destruction of Ozone (24-Hour Average)

Altitude km	k (O) (O_3) (%)	k (NO_2) (O) (%)	k (ClO) (O) (%)	k (HO_2) (O) (%)	k (HO_2) (O_3) (%)
50	25	7	4	52	---
45	29	24	10	31	---
40	18	53	16	10	---
35	11	68	13	4	1
30	10	69	8	2	3
25	12	78	5	1	8
20	11	70	1	1	26

Note: All percentages are relative to the photolytic production rate of odd oxygen and do not include transport sources or sinks. At the upper altitude range, the contributions from a catalytic cycle involving (H, HO, HO_2) were not tabulated.

The fractional destruction rates add up approximately to unity at each altitude as they must in a steady-state model calculation. The apportioning among the different catalytic cycles cannot be used, however, to calculate the effect of increasing source gas concentrations, because the addition of one given trace species family affects the distribution of all other families among its radical and sink species.

The presentation of stratospheric measurement data is predicated on certain principles of critical evaluation and selection. To be included in the graphs to follow, data had to be obtained by well established and properly documented measurement techniques. Moreover, it was required that these techniques were continuously used and checked in series of experiments to show instrumental reproducibility under field conditions. For those trace species where many data sets meeting these criteria were available, a representative subset of all data may be shown in the interest of clarity of presentation. The important question of measurement uncertainties is treated individually in the various sections of this chapter. To provide a feel for measurement variance, the graphs show individual, original data points wherever possible.

Finally, while it is unfortunate that ozone concentration monitoring alone cannot be relied on, due to its extreme spatial and temporal variability, to permit the assessment of pollution effects, the rich harvest of our understanding of atmospheric processes justifies the large scientific effort. As this chapter shows, the present requirements are rigorous: to identify, understand, predict, and measure all the important trace species and thereby to attain a detailed insight into the chemical and dynamical properties of the stratosphere.

TROPOSPHERIC SOURCE GASES

The purpose of this section is to update the information previously published in NASA RP 1049. The information is summarized in Table 1-2, with short comments in the text where appropriate. The fourth and fifth columns contain the best estimates of representative values for the two hemispheres. In many cases, the value for the Southern Hemisphere is obtained by a combination of a relative latitude profile with one or a few absolute determinations at a northern site. For some of the more exotic gases, only one or a few measurements exist; these cases are called out in the remarks column. The references are not comprehensive, and are intended as an initial guide to the literature.

NITROGEN COMPOUNDS

Two major questions regarding N_2O were debated but could not be resolved in NASA RP 1049. These were (1) what is the absolute concentration of N_2O in the troposphere, and (2) is it changing steadily?

In the recent past the background tropospheric N_2O concentration has been measured to be between 290 and 350 ppb. While no firm agreement exists a majority of investigators currently report N_2O levels in the range of 295 to 315 ppb. The notable exception is the data of Rasmussen et al. (1981) who report N_2O levels of 330 to 335 ppb. A number of investigators are now updating their earlier data and report N_2O levels between 300 to 305 ppb. Given the direction of change it is reasonable to suggest that the best estimate of the background N_2O concentration is in the range of 300 to 310 ppb.

More important than the question of absolute concentration, is the nature of the temporal trends. Until early 1980 no conclusive evidence of either an increase or a decrease in N_2O concentration was available. It was, however, evident from available data that the change in N_2O

Table 1-2
Atmospheric Budgets

Chemical Group	Chemical	Dominant Source N. Natural A. Artificial	Tropospheric Mole Fraction (1981) Northern Hemisphere	Tropospheric Mole Fraction (1981) Southern Hemisphere	Average Growth Rate ppt/year	Technique*	Estimated Precision (%)	Estimated Accuracy (%)	Estimated Limit of Detection (pptv)	References	Remarks
			In pptv (10^{-12}) unless otherwise indicated								
Nitrogen Compounds	N_2O	N	302ppb	301ppb	600	GC-UPSD	0.5	3	<5ppb	Weiss et al. (1981)	Relative to CO_2. See Figures 1-4, 1-5, 1-13, 1-16, 1-17
	NH_3	N	295-315ppb	—	—	GC-ECD	1.0	3	<5ppb	(1)	Disagreement on absolute calibration.
	NO_x ($NO+NO_2$)	N,A	<1-10ppb	—	—	IRHS	—	—	<1ppb	Hoell et al. (1980)	Large seasonal changes.
			10-150	10-150	—	Chemi-luminescence	10	15	5	Kley et al. (1981)	Major stratospheric source.
Sulfur Compounds Compounds	COS	?	510±60	510±60		GC-FPD	10	15	20	Torres et al. (1980)	No known N-S differences. Source totally unknown.
	CS_2	A?	3-30	—		GC-FPD	10	15	10	Maroulis and Bandy (1980)	Data for surface near 40°N.
	SO_2	A?	122±85	90±20		GC-FPD	15	15	20	Maroulis et al. (1980)	~30% lower in marine boundary layer. See Figure 1-6.
	H_2S	N	0-100	—		GC-FPD	—	—	—	Sze and Ko 1980	Source no really known.
Fully fluorinated compounds	CF_4	A	65 ± 9	65 ± 9		GC-MS	10	15	<20	Penkett, et al. (1981)	Preliminary data from one place.
	C_2F_6	A	4 ± 1	4 ± 1		GC-MS	—	25	—	Penkett, et al. (1981)	
	SF_6	A	0.3-0.5	0.3-0.5		GC-ECD	—	25	0.05	Singh et al. 1979	
Chlorofluoro-carbons (others in text)	CCl_3F_2	A	300	270	30	ALL	2 to 5	10	1	See Figures	See Figures 1-9, 1-14, 1-20, and 1-21.
	CCl_3F	A	190	170	17		2 to 5	10	1	See Figures	See Figures 1-8, 1-15, 1-18, and 1-19.
	CCl_2FCClF_2	A	12-25	11-22			10	20	1	Singh et al. (1981)	
						GC-ECD	10	20	1	Rasmussen et al. (1981)	
	$CClF_2CClF_2$	A	15	13						Singh et al. (1981)	Data inconsistent with emissions.
						GC-MS	10	20	5	Rasmussen et al. (1980a)	
	$CHClF_2$	A	52	~2		GC-MS	—	—	—	Penkett et al. (1981)	
	CF_3Cl	A	3.4 + 0.6	3.4 ± 0.6							
Chlorocarbons	CH_3Cl	N	650	650	0		10	10	10	Singh et al. (1979), Rasmussen et al. (1980b)	Distribution uniform (Figure 1-22)
	CH_2Cl_2	A	35-50	20 (est)	—		10	20	10	Singh et al. (1981)	Data for surface near 40°N.
	$CHCl_3$	A	10-15	3 (est)	—	ALL	10	20	2	See Figures	
	CCl_4	A	135	130	0-7		5	15	1	Singh et al. (1981), NASA RP 1049	Serious difficulty with sample instability; results scattered.
	CH_2ClCH_2Cl	A	30-40	20 (est)	—	GC-ECD	10	20	10	Singh et al. (1981)	Data for surface near 40°N.
	CH_3CCl_3	A	165-180	120	13	GC-FID	10	20	10	Singh et al. (1981), Rasmussen et al. (1980b)	
	C_2HCl_3	A	10-15	<3	—	GC-MS	10	20	5	See Figures	
	C_2Cl_4	A	40-50	20	—		10	20	5	Singh et al. (1981)	

*GC–Gas chromatography, UPSD–Ultrasonic pulse shift detector, IRHS–Infra red heterodyne spectroscopy, FPD–Flame photometric detector, MS–Mass spectroscopy, NDIR–Nondispersive infrared, CC-AA–Chemical conversion atomic absorption, HeID–Helium ionization detector, ECD–Electron capture detector, FID–Far infrared detector.

Table 1-2
Atmospheric Budgets (continued)

Chemical Group	Chemical	Dominant Source N Natural A Artificial	Tropospheric Mole Fraction (1981) Northern Hemisphere	Tropospheric Mole Fraction (1981) Southern Hemisphere	Average Growth Rate ppt/year	Technique*	Estimated Precision (%)	Estimated Accuracy (%)	Estimated Limit of Detection (pptv)	References	Remarks
			In pptv (10^{-12}) unless otherwise indicated								
Bromine and Iodine Compounds	CH_3Br	A,N	5-15	–		ALL	10	20	1	Singh et al. (1981), Rasmussen & Khalil (1980)	
	$CBrF_3$	A	1	–			10	50	<1	Penkett et al. (1981)	Data Tentative
	CH_2BrCH_2Br	A	2-5	–			10	50	1	Singh et al. (1981)	
	CH_3I	A	2-5	3		GC-EDC	10	100	<1	Singh et al. (1981)	
Hydrocarbons CO_2, CO, H_2	CH_4	N,A	1690±50ppb	1620±30ppb	small or zero	GC-FID	1	5	5ppb	Hrisdt et al. (1980) JGR, (GAMETAG)	small increase suggested (Figure 1-26)
	C_2H_6	N,A	1000-1500	300-600		GC-FID	5	10	<5	Singh et al. (1979), Rudolph & Ehhalt (1981)	suggested (Figure 1-26) Hydrocarbons are often much larger over continents (Figure 1-27)
	C_2H_2	A	30-300			GC-FID	5	10	<5	Rudolph & Ehhalt (ibid)	<20 ppt seen at South Pole (Figures 1-28, 1-29)
	C_3H_8	*	100-300			GC-FID	5	10	<10	Cronn & Robinson (1979)	Figure 1-29.
	CO_2	N,A	336ppm	334ppm	1.5ppm/year	NDIR	0.1	0.1	–	Rudolph & Ehhalt (ibid)	Figure 1-23.
						GC-FID	0.2	1.0	5ppb		
	CO	N,A	70-200ppb	40-60ppb		CC-AA	2	5	1ppo		Figure 1-26. CO levels for marine free troposphere. Nonpolluted continental air has as high as 300 ppb.
	H_2	N,A	550ppb	520ppb	small or zero	GC-FID	2	5	5ppb		
						CC-AA	2	5	50ppb		Figure 1-25.
						GC-HeID	2	5	20ppb		

*GC–Gas chromatography, UPSD–Ultrasonic phase shift detector, IRHS–Infra red heterodyne spectroscopy, FPD–Flame photometric detector, MS–Mass spectroscopy, NDIR–Nondispersive infrared, CC-AA–Chemical conversion atomic absorption, HeID–Helium ionization detector, ECD–Electron capture detector, FID–Far infrared detector

levels over the last 3 or 4 years was less than ±0.5%/year. N_2O levels appeared to be uniform around the globe with a possibility of slightly higher N_2O values in the Southern Hemisphere.

The recent availability of N_2O data from Weiss (1981) has provided a more rigorous quantitative relationship on the growth and the hemispheric gradients of N_2O. Figure 1-4 shows the distribution of N_2O in the two hemispheres. All data are normalized to January 1, 1978. Figure 1-5 shows the N_2O trend over the last two decades. Weiss (1981) draws the following conclusions:

- N_2O levels in the Northern Hemisphere are on the average greater than the Southern Hemispheric levels. The difference is statistically significant and is estimated to be 0.8 ± 0.2 ppb.
- Atmospheric N_2O concentration is increasing slowly. During the period 1976 to 1980 a rate of increase of 0.5 ± 0.1 ppb/year (for January 1, 1978) or 0.2%/year was determined.
- With the help of a simplified model it is estimated that the N_2O concentration in the preindustrial unperturbed troposphere was between 281 and 291 ppb or about 3 to 5% below its current value. The concentration of N_2O by the year 2000 is projected to be 5 to 7% above the present value (i.e., 315 to 320 ppb).

Weiss presents limited evidence that N_2O is emitted by certain combustion sources. But there is little doubt that the dominant source is biological, and this source too has the potential of increasing with time.

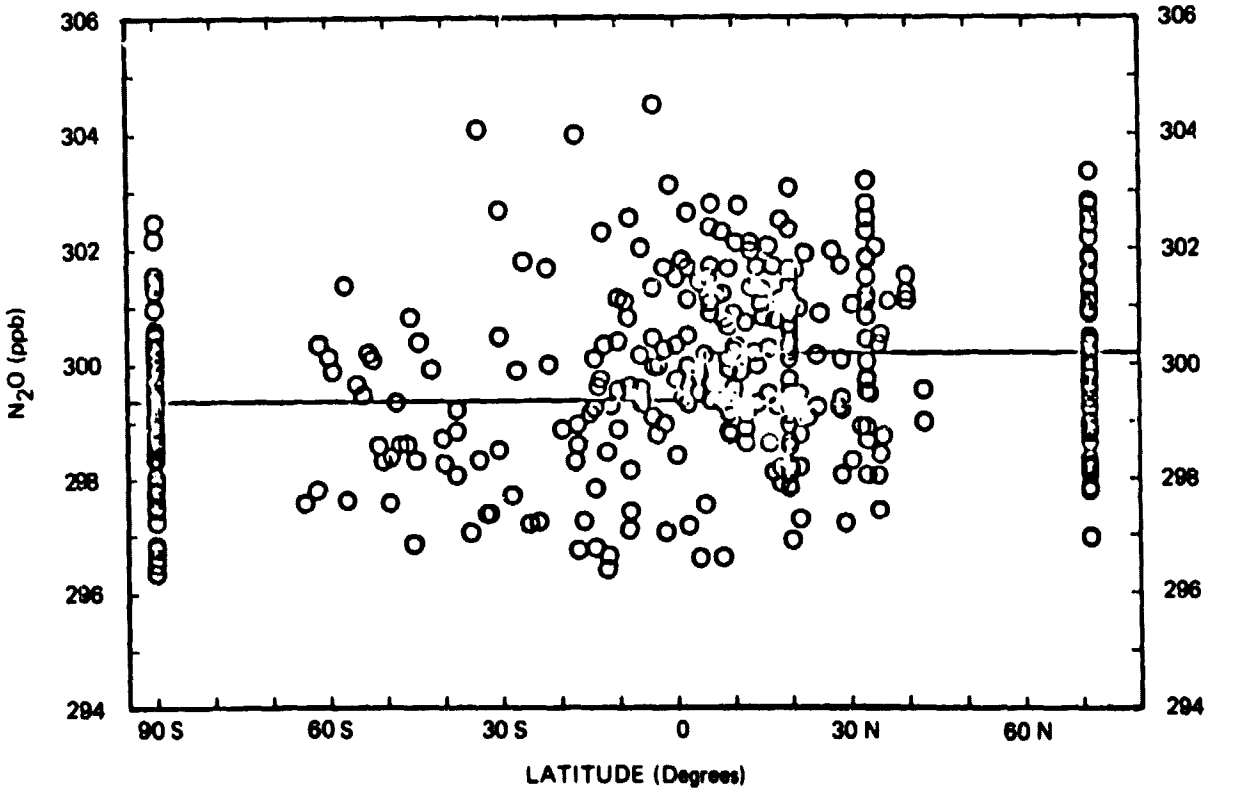

Figure 1-4. Latitudinal distribution of nitrous oxide.

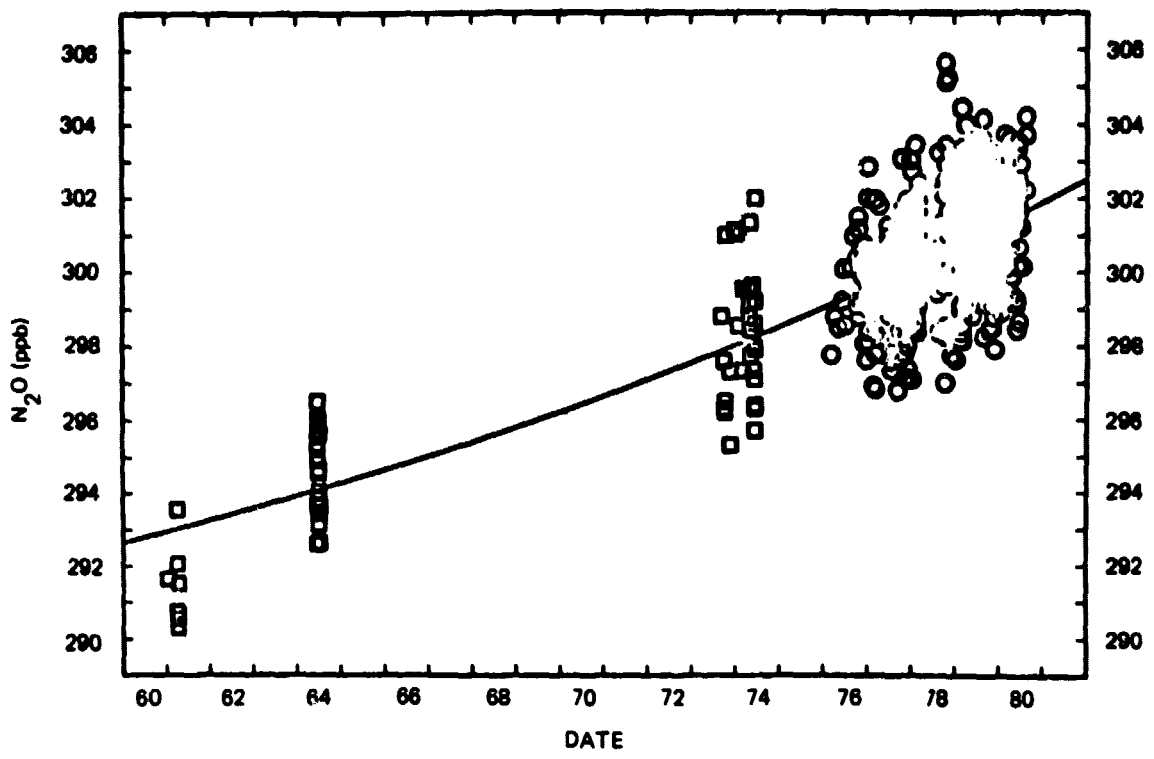

Figure 1-5. Growth of nitrous oxide over the last two decades.

Understanding of N_2O has improved considerably over the past 2 years. Indications are that the biological source is dominated by nitrification (oxidation of NH_4^+) rather than denitrification (reduction of NO_3). The yield of N_2O referenced with respect to oxidation of NH_4^+ is about 0.03% at high oxygen levels, but more than 10% at low oxygen levels, a nonlinearity which deserves continuing attention. The growth rate is thought to include contributions both from combustion and biological oxidation.

SULFUR COMPOUNDS

Concentrations of COS, CS_2, SO_2 and H_2S are given in Table 1-2. The tropospheric distributions of SO_2 (Maroulis et al., 1980) and COS (Torres et al., 1980) are shown in Figures 1-6 and 1-7. Reaction with HO is thought to provide the major sink for H_2S and for SO_2 in remote areas (e.g. Sze and Ko, 1980; Logan et al., 1979). Sources and sinks for COS and CS_2, and sources for background SO_2 are not well understood at present. Recent kinetic measurements suggest that the rates for reaction of HO with COS and CS_2 are rather slow (Ravishankara et al., Wine et al., 1980; Iyer and Rowland, 1980), in contrast to earlier studies (e.g., Kurylo, 1978). If the new measurements are correct, reaction with tropospheric HO provides a negligibly slow removal mechanism for CS_2 and COS. The uniform distribution of COS in the troposphere (see Figure 1-7) is consistent with a rather long lifetime for the gas. However concentrations of CS_2 are highly variable (Maroulis and Bandy, 1980) suggesting a short lifetime for this species. Reaction of CS_2 with atomic oxygen (Sze and Ko, 1981) and reactions of electronically excited CS_2 (Wine et al., 1981a) have been proposed as sinks for CS_2 and sources for COS. These proposals are speculative, and the budgets of the sulfur species remain poorly defined.

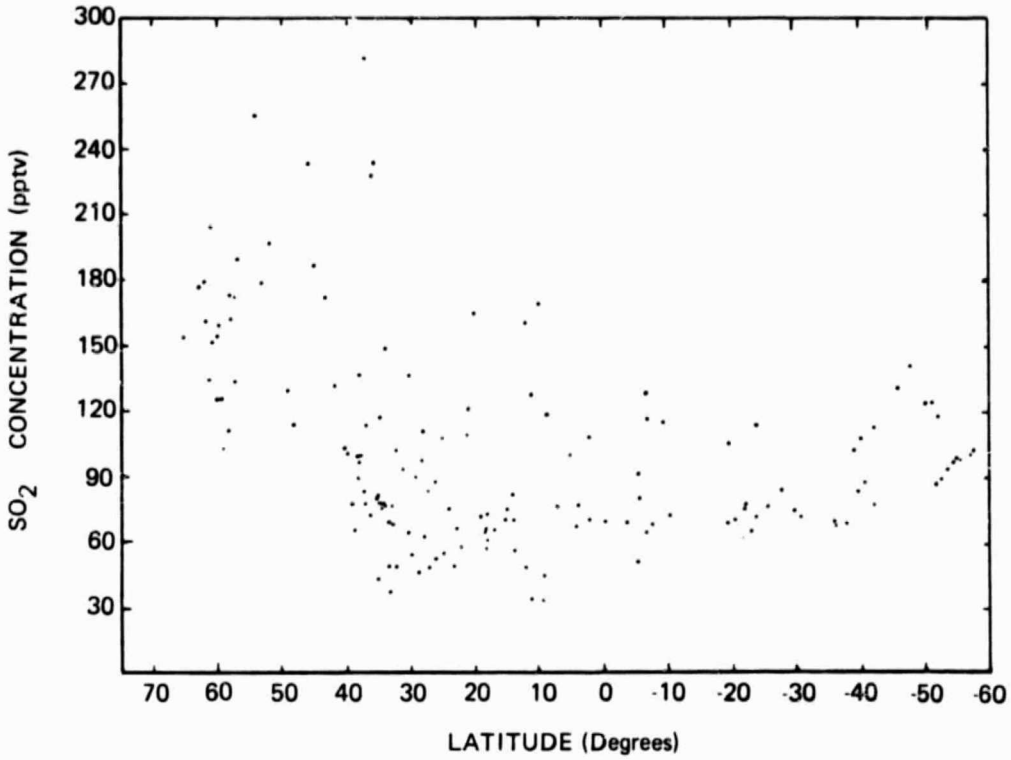

Figure 1-6. Plot of the individual free troposphere SO_2 data points as a function of latitude (Maroulis et al., 1980).

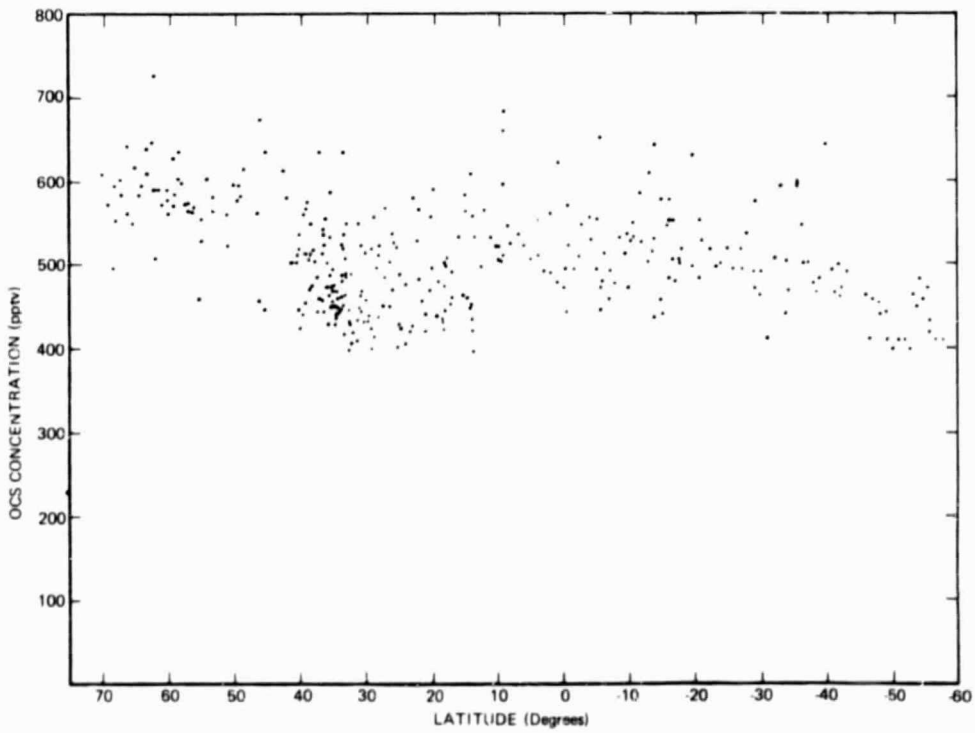

Figure 1-7. A plot of the GAMETAG COS data as a function of latitude (Torres et al., 1980).

HALOGENATED COMPOUNDS

Information about halogens in the atmosphere was reviewed recently by Cicerone (1981) and Jesson (1980). The concentrations of the halocarbons are given in Table 1-2. Recent measurements and budget analyses of different species are summarized below.

Methyl Chloride (CH_3Cl)

Singh et al. (1979) found concentrations of CH_3Cl nearly uniform with latitude during a Pacific cruise in November 1977. They reported concentrations of 615±100 pptv. Measurements by Rasmussen et al. (1980b) over the Pacific Ocean suggest that the concentration of CH_3Cl is higher in the boundary layer than in the free troposphere (~780 pptv vs. ~620 pptv) at equatorial latitudes. Concentrations measured over the North American continent, however, were independent of altitude. Observations of CH_3Cl at several remote locations (Alaska, Oregon, Hawaii, Samoa, the South Pole) are consistent with data from the latitudinal surveys (Rasmussen et al., 1980b). There is no evidence for a temporal trend in CH_3Cl (Rasmussen et al., 1980b); Singh et al., 1981).

The major sources for methyl chloride are thought to be the world's oceans and the burning of vegetation (Lovelock, 1975; Singh et al., 1979; Watson et al., 1980; Rasmussen et al., 1980b). Yields of CH_3Cl measured relative to CO_2 in a forest fire (Crutzen et al., 1979) and in laboratory combustion experiments (Rasmussen et al., 1980b) vary by two orders of magnitude. Elevated concentrations of CH_3Cl have been observed in volcanic emissions (Rasmussen et al., 1980b). Industrial manufacture of CH_3Cl provides a small fraction of the global source strength. Methyl chloride is removed from the atmosphere by reaction with HO, with a lifetime of ~1 year according to current models for tropospheric chemistry. The global removal rate for CH_3Cl by reaction with HO is 5×10^{12} gm yr^{-1} (Logan et al., 1981). This estimate is within the range of source strengths given by Watson et al. (1980), who favor the ocean as the dominant source for CH_3Cl. The observed yields of CH_3Cl in combustion may be combined with figures for global biomass burning (3×10^{15} gm C yr^{-1}; Crutzen et al., 1979; Logan et al., 1981) to estimate a range for the associated source of CH_3Cl, 2.5×10^{10} to 2.5×10^{12} gm yr^{-1}. Hence combustion could be a major source. More work is needed to resolve the question.

Chlorofluorocarbons (CCl_2F_2, CCl_3F)

Measurements of CCl_2F_2 and CCl_3F in the troposphere taken over the past decade are summarized in Figures 1-8 and 1-9. The concentrations of both compounds continue to increase at a rate of about 10% per year. Data from individual research groups are shown by different symbols in the figures. Discrepancies between different groups (e.g., Rasmussen et al., 1981a,b and Singh et al., 1979) were discussed in NASA RP 1049. The majority of the data for the Northern Hemisphere were taken at mid-latitudes. The locations of the southern measurements include Brazil, Australia and the South Pole. Two programs have been established to monitor concentrations of CCl_3F and CCl_2F_2 in remote locations; the Atmospheric Lifetime Experiment, sponsored by the Chemical Manufacturers Association, and the NOAA-GMCC program. These networks have been operating since 1978 and 1977, respectively. The data have not yet been published.

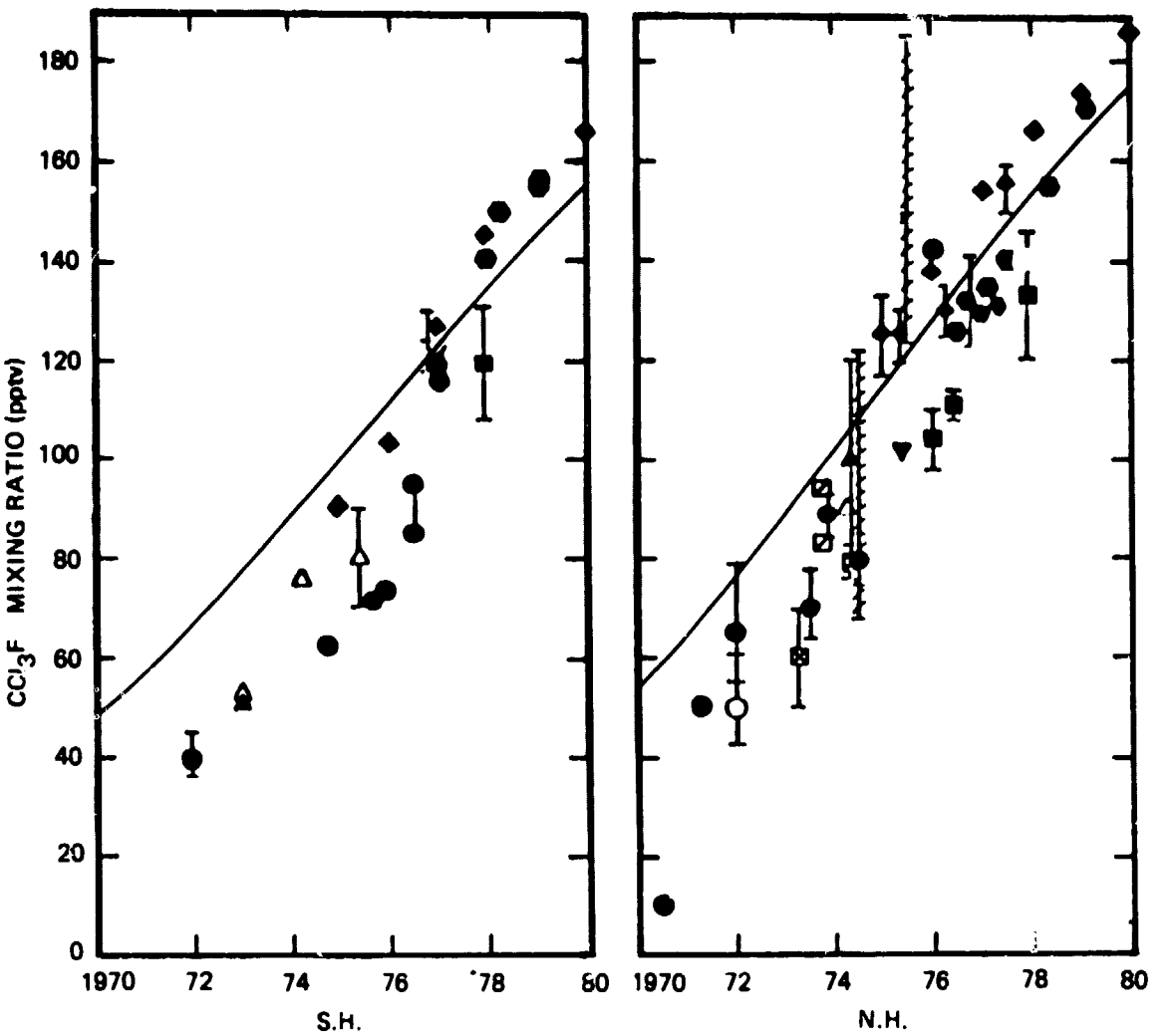

Figure 1-8. Measurements of CCl_3F in the Northern and Southern Hemispheres as a function of time. Each symbol represents data from a different group of investigators; ● (30°-90°), ○ (0-30°), ⋈, Lovelock (1971, 1972, 1974), Lovelock et al. (1973), Pack et al. (1977), NASA RP 1049 (1979); ▲ (30°-90°), △ (0-30°) Wilkness et al. (1973, 1975a, 1975b, 1978); ⊠ Zafonte et al. (1975), Hester et al. (1975), ⊡ Heidt et al. (1975; ■ Singh et al. (1971, 1977b, 1979); ◆ Grimsrud and Rasmussen (1975), Robinson et al. (1976), Cronn et al. (1977), Pierotti et al. (1978), Rasmussen et al. (1981a & b); × Fraser and Pearman (1978); + Tyson et al. (1978) ▼ Krey et al. (1977); ⋗ Goldan et al. (1980). The solid lines show results of the model calculations of Logan et al. (1981) which use release rates for CCl_3F and CCl_2F_2 given by Bauer (1979). The model assumes that 90% of the release takes place in Northern Hemisphere. Model results are mean hemispheric values.

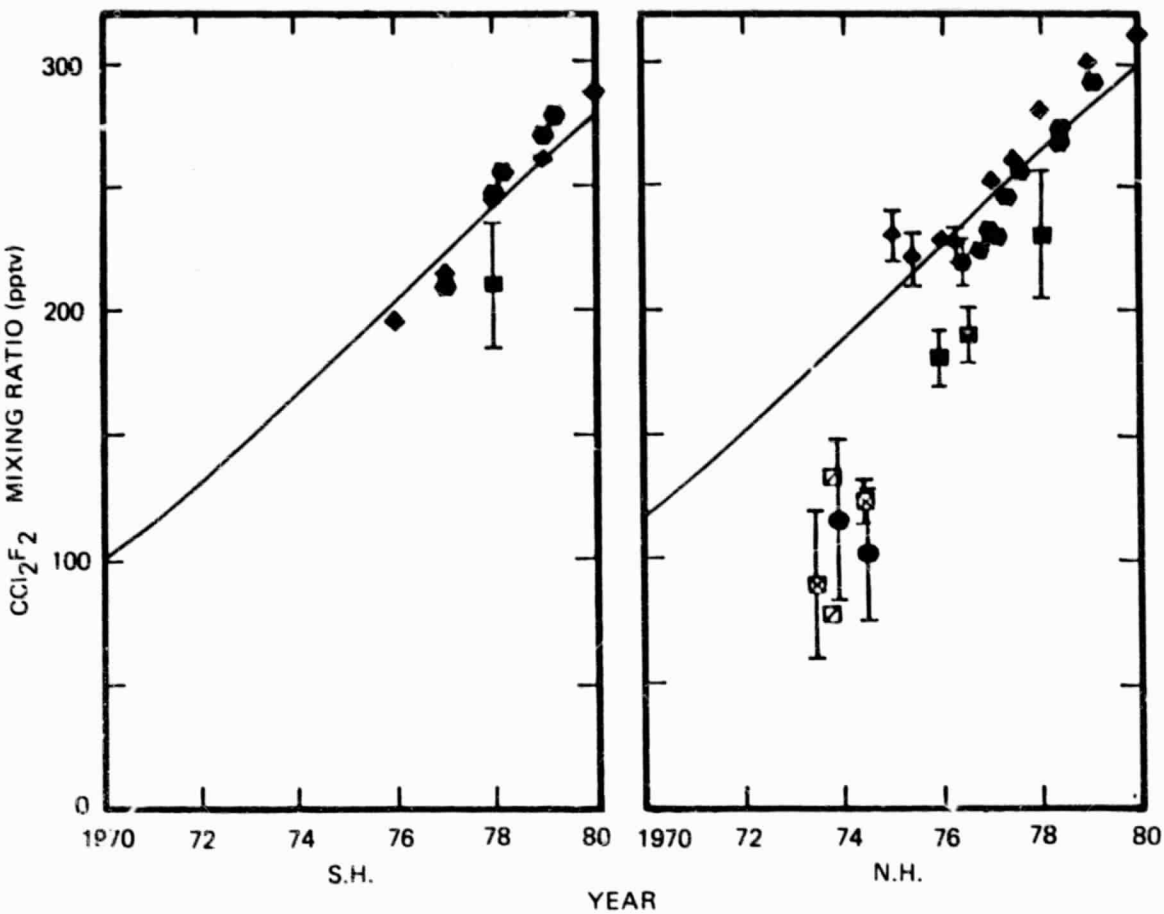

Figure 1-9 Measurements of CCl_2F_2 in the Northern and Southern Hemispheres as a function of time. Each symbol represents data from a different group of investigators; ● (30°-90°), ○ (0-30°), ⋇, Lovelock (1971, 1972, 1974), Lovelock et al. (1973), Pack et al. (1977), NASA RP 1049 (1979); ▲ (30°-90°), △ (0-30°) Wilkness et al. (1973, 1975a, 1975b, 1978); ⊠ Zafonte et al. (1975), Hester et al. (1975), ⧄ Heidt et al. (1975; ■ Singh et al. (1971, 1977b, 1979); ◆ Grimsrud and Rasmussen (1975), Robinson et al. (1976), Cronn et al. (1977), Pierotti et al. (1978), Rasmussen et al. (1981a & b); × Fraser and Pearman (1978); + Tyson et al. (1978) ▼ Krey et al. (1977); ● Goldan et al. (1980). The solid lines show results of the model calculations of Logan et al. (1981) which use release rates for CCl_3F and CCl_2F_2 given by Bauer (1979). The model assumes that 90% of the release takes place in Northern Hemisphere. Model results are mean hemispheric values.

Data for industrial production and for release to the atmosphere of CCl_2F_2 and CCl_3F are given by McCarthy et al. 1977 (see Bauer, 1979, for recent corrections). Recent figures for production and release are given below in Table 1-3 (CMA, 1981).

Table 1-3
Production and Release Rates of FC-11 and FC-12

Year	CCl_3F (FC-11)		CCl_2F_2 (FC-12)	
	Production	Release	Production	Release
1975	323.5	312.9	418.6	412.0
1976	349.9	304.1	449.8	395.7
1977	332.2	306.4	424.4	376.5
1978	321.2	291.0	414.1	347.6
1979	302.0	272.0	400.3	338.0
1980	302.2	257.4	393.4	333.7

Units: 10^9 gm yr^{-1}

Annual release of CCl_3F and CCl_2F_2 has been decreasing slowly since 1974. Production of these compounds in the U.S. decreased 45% between 1974 and 1979.

The major removal process for CCl_3F and CCl_2F_2 is photolysis in the stratosphere. Tropospheric removal processes of comparable efficiency have not been identified. A recent report concluded that destruction of these species by either photodecomposition or thermally induced decomposition on desert sands is unlikely to be important (NAS, 1979). Measurements of the increasing atmospheric burden of CCl_3F and CCl_2F_2 are generally consistent with this view, but some uncertainties remain. Data for CCl_3F from Mauna Loa and Tasmania were analyzed by Hyson et al. (1980) using a two-dimensional transport model. They concluded that the rate of increase of CCl_3F in the past 2 to 3 years exceeds that which should have occurred given the release data. Similarly, an analysis of budgets for CCl_3F, based on a four-box model indicates that the release data cannot quite account for concentrations measured in recent years by Rasmussen and coworkers (Logan et al., 1981; see Figure 1-8 and 1-9). Neither theoretical study allowed for tropospheric loss of chlorofluorocarbons. Discrepancies between these models and recent measurements are less than 10%.

Methyl Chloroform (CH_3CCl_3)

Measurements of CH_3CCl_3 are shown in Figure 1-10. Absolute calibration problems are more serious for methyl chloroform than for the chlorofluorocarbons. The measurements of Lovelock in 1975-1976 are clearly inconsistent with the work of Rasmussen and coworkers. Later measurements by Rasmussen and by Singh are significantly higher than the results of Rowland and coworkers.

The chemical industry provides the only known source for CH_3CCl_3 (Neely and Plonka, 1978). The gas is removed from the atmosphere primarily by reaction with tropospheric HO, and measurements of CH_3CCl_3 have been used to deduce mean concentrations for HO (Singh, 1977a, b; Lovelock, 1977). Preliminary analyses of data for CH_3CCl_3 suggests that the lifetime for the gas is 3 to 11 years (Lovelock, 1977; Singh, 1977a, b; Derwent and Eggleton, 1978; McConnell and Schiff, 1978; Neely and Plonka, 1978; Chang and Penner, 1978).

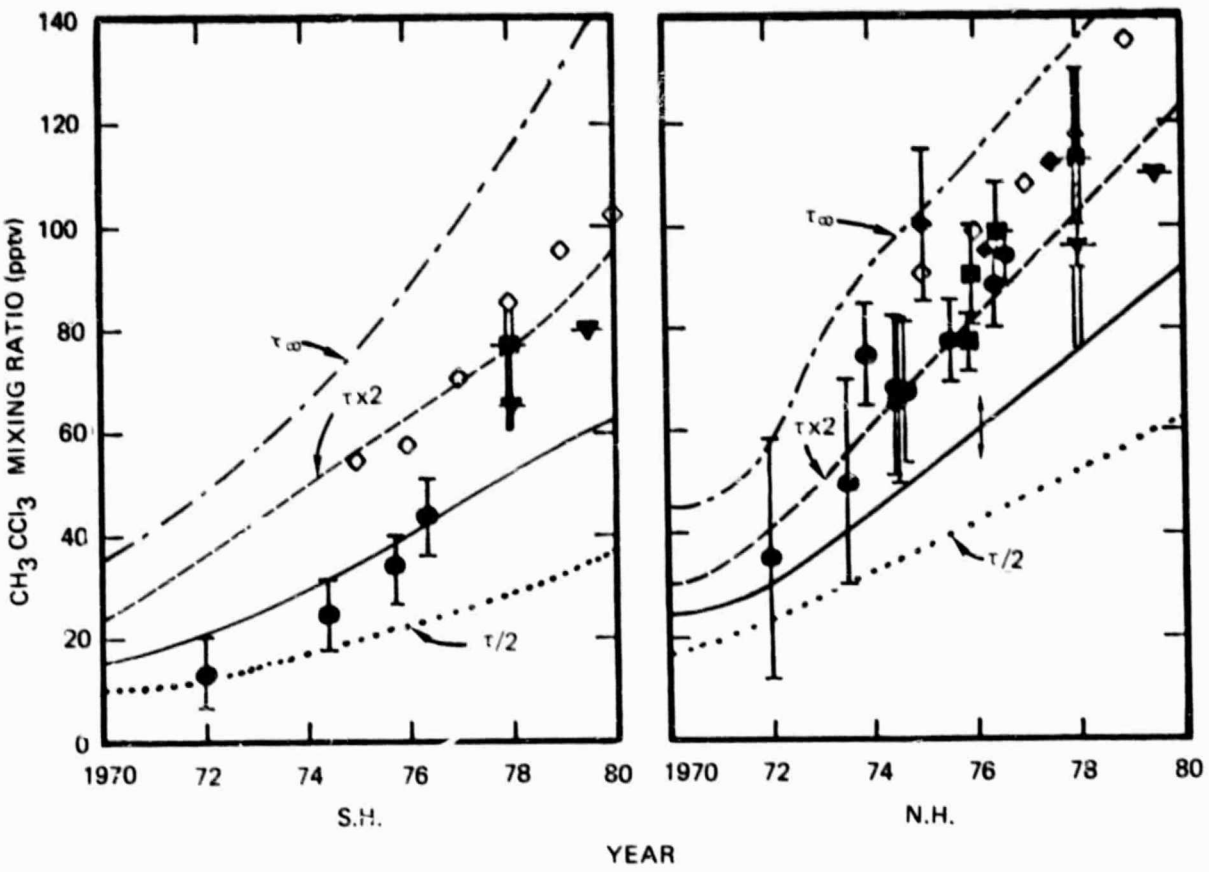

Figure 1-10. Measurements of CH_3CCl_3 in the Northern and Southern Hemispheres as a function of time. Each symbol represents data from a different group of investigators; ● Lovelock (1974, 1977); ◇ Rasmussen et al. (1981a & b); ◆ Grimsrud and Rasmussen (1975), Cronn et al. (1977), Pierotti et al. (1978); ⊟ (hemispheric mean), ▯ (range, 0-30°), ▮ (range, 30°-60°), Singh et al. (1979); ■ Singh et al. (1977a, 1977b); ▼ (1978, mid-latitude mean; 1979, hemispheric mean) Rowland et al. (1980). The lines show results of model calculations (Logan et al., 1981) which use release rates for CH_3CCl_3 given by Neely and Plonka (1978). It was assumed that 95% of the release takes place in the Northern Hemisphere. Model results are mean hemispheric values. The arrows (↕) show the range of concentrations from the model for mid-latitudes and the tropics. The solid lines give the results of the standard model. The troposphere is divided into four latitude zones of equal area with boundaries at 30°N, 0° and 30°S. In each latitude zone a mean HO profile is derived from marine and continental profiles, weighted by the appropriate area in each zone. The dashed curves show results in which HO concentrations from the standard model are multiplied by 0.5 while the dotted curves are for HO concentrations multiplied by two. The dot dash curves show results for an infinite tropospheric lifetime for CH_3CCl_3 (HO concentration = 0).

Recent laboratory studies have resolved earlier discrepancies in knowledge of the rate constant for the reaction of HO with CH_3CCl_3 (Kurylo et al., 1979; Jeong and Kaufman, 1979). The accuracy of the release rates provided by Neely and Plonka (1978) is difficult to determine as they do not account for release in Eastern Bloc countries (H. Farber, Dow Chemical, personal communication). Concentrations calculated for CH_3CCl_3 using these release data and model distributions for HO are somewhat smaller than observed concentrations of CH_3CCl_3 (Logan et al., 1981; Derwent and Eggleton, 1981). An underestimate in release rates of 25% would bring model results into agreement with some recent observations for CH_3CCl_3.

The release rate of CH_3CCl_3 increased exponentially between 1960 and 1975. The present day concentration of the gas is linearly proportional to the release rate, but depends less strongly on the removal rate. Hence it is difficult to place strict bounds on the globally averaged concentration for HO from an analysis of data for CH_3CCl_3, given the uncertainties in absolute concentrations and in the release rate (Logan et al., 1981). Measurements of CH_3CCl_3 appear to be consistant with a lifetime of 5 to 10 years, and with globally averaged HO concentrations of $\sim 7 \times 10^5$ molecules cm^{-3}.

Carbon Tetrachloride (CCl_4)

Measurements for CCl_4 are given in Figure 1-11. Again, there appear to be serious calibration inconsistencies between different research groups. The data in Figure 1-11, and measurements made in England (Penkett et al., 1979) and the western U.S. (Singh et al., 1979) suggest that the concentration of CCl_4 is increasing slowly.

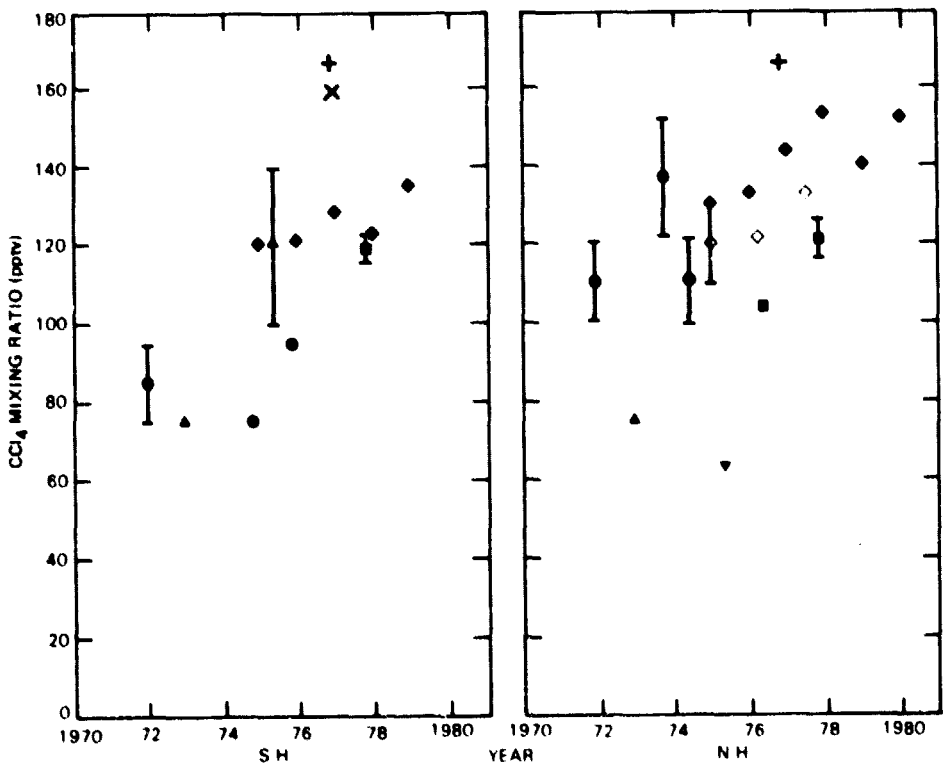

Figure 1-11. Measurements of CCl_4 in the Northern and Southern Hemispheres as a function of time. Each symbol represents data from a different group of investigators. The symbols are defined in Figure 1-8.

There are no known natural sources for CCl_4. Estimates for industrial production and release are subject to considerable uncertainty (Altshuller, 1976; Singh et al., 1976; Galbally, 1976). Only a small percentage of the total production is released to the atmosphere, and production figures are unavailable for many countries, including the U.S.S.R. and China. Production of CCl_4 in the U.S. has been decreasing since 1970 (U.S. International Trade Commission Reports).

Other Halocarbons

Observations of other halocarbons are summarized in Table 1-2. Two of these compounds, CF_4 and $CHClF_2$ (FC-22) have concentrations larger than 50 pptv. Industrial sources have been identified for all the halocarbons listed in Table 1-2 with the exceptions of $CHCl_2F$, CH_3Cl and CH_3I. Halocarbons which are unsaturated or contain hydrogen atoms are removed from the atmosphere by reaction with tropospheric HO. Kinetic data (Atkinson et al., 1979) may be used to estimate that the lifetimes of $CHCl_2F$, $CHCl_3$, CH_2Cl_2, CCl_2CCl_2, CH_3Br and CH_2BrCH_2Br are between 2 years and a few months. The lifetime of $CHClF_2$ is about 12 years while that of $CHClCCl_2$ is a few days. Methyl iodide is removed from the troposphere by photolysis within a few days (Chameides and Davis, 1980).

The aluminum industry is thought to be an important source for CF_4 (Rasmussen et al., 1979; Cicerone, 1979). Elevated concentrations of CF_4 and C_2F_6 have been observed in aluminum plant plumes (Penkett et al., 1981). The atmospheric lifetime of CF_4 is expected to be extremely long (>10,000 years). The major loss process for the gas is photodissociation at 121.6 nm in the mesosphere (Cicerone, 1979).

Global rates for release of $CHClF_2$ are given by Jesson (1980). The lifetime of the gas should be determined by reaction with HO in the troposphere (Atkinson et al., 1979). Rassmussen et al. (1980b) used the release data to estimate that the global burden of $CHClF_2$ should be ~35 pptv if the atmospheric lifetime of the gas were infinite. They conclude from their measurements of ~45 pptv that the release rate has been underestimated.

Measurements by Penkett et al. (1980) using a gas chromatograph/mass spectrometer combination indicate that $CHCl_2F$ in the clean troposphere is virtually unmeasurable (<1 pptv). Concentrations of CH_3Br and CH_3I are extremely low (a few pptv). Methyl iodide is thought to be produced by marine organisms (Lovelock et al., 1973). Chameides and Davis (1980) recently reviewed the budget for CH_3I, and estimate that the source strength for the gas is about $1\text{-}2\times10^{12}$ g yr^{-1}.

Halocarbon Budgets

The halocarbon budget for the troposphere may be estimated from the data presented above. These data indicate that the organic chlorine content of the troposphere was ~3.0 ppb in late 1979, while the organic fluorine content was ~1.25 ppb (see Tables 1-4 and 1-5). The temporal trends in organic Cl and F derived from the major halocarbons are shown in Figure 1-12. Contributions from minor halocarbons are omitted because of lack of information concerning their time history.

Berg and Winchester (1977) measured gas phase organic chlorine concentrations of ~1.9 ppbv near the shore in the Gulf of Mexico. Their technique involved trapping the organic species on activated charcoal, followed by spectrophotometric analysis for Cl. This method was developed further by Berg et al. (1980) to measure the total halogen content of the lower stratosphere. Neutron activation analysis was used to detect Cl and Br, which were found at concentrations of 2.7±0.9 to 3.2±0.7 ppbv and 7±4 to 40±11 pptv, respectively. No iodine was observed, but an upper limit of <3 pptv was calculated. The total chlorine data are consistent with the Cl content derived from the individual species, given the uncertainties in each estimate.

Table 1-4
Concentrations of Major Halocarbons in Late 1979. [a]

	N.H.	S.H.	Global
CH_3Cl	620±20		620
CF_2Cl_2	315±6	282±6	300
$CFCl_3$	184±5	164±5	175
CCl_4[b]	136±18	125±6	130
CH_3CCl_3	125±20	94±12	110

[a] Concentrations are given in pptv, and are taken from Figures 1-8 to 1-11.

[b] Average concentration for 1976-1980, from Figure 1-11.

Table 1-5
Tropospheric Budgets for Organic Halogens in 1979[a]

	F	Cl	Br	I
CH_3Cl		.62		
CF_2Cl_2	.60	.60		
$CFCl_3$	.17	.52		
CCl_4		.52		
CH_3CCl_3		.33		
Other CH_xX_y[b]	.49	.38	<0.02	<0.005
TOTAL (ppb)	1.26	2.97	<0.02	<0.005

[a]Concentrations are given in ppbv.

[b]Calculated from Table 1-2.

A temporal trend in the F content of the atmosphere may be inferred from measurements of HF above 30 km (Zander, 1981). These data are presented in Figure 1-12. The concentration of HF calculated from a time dependent 1-D model (Sze, 1978) is shown also. The trends in organic fluorine in the troposphere and HF in the stratosphere are similar.

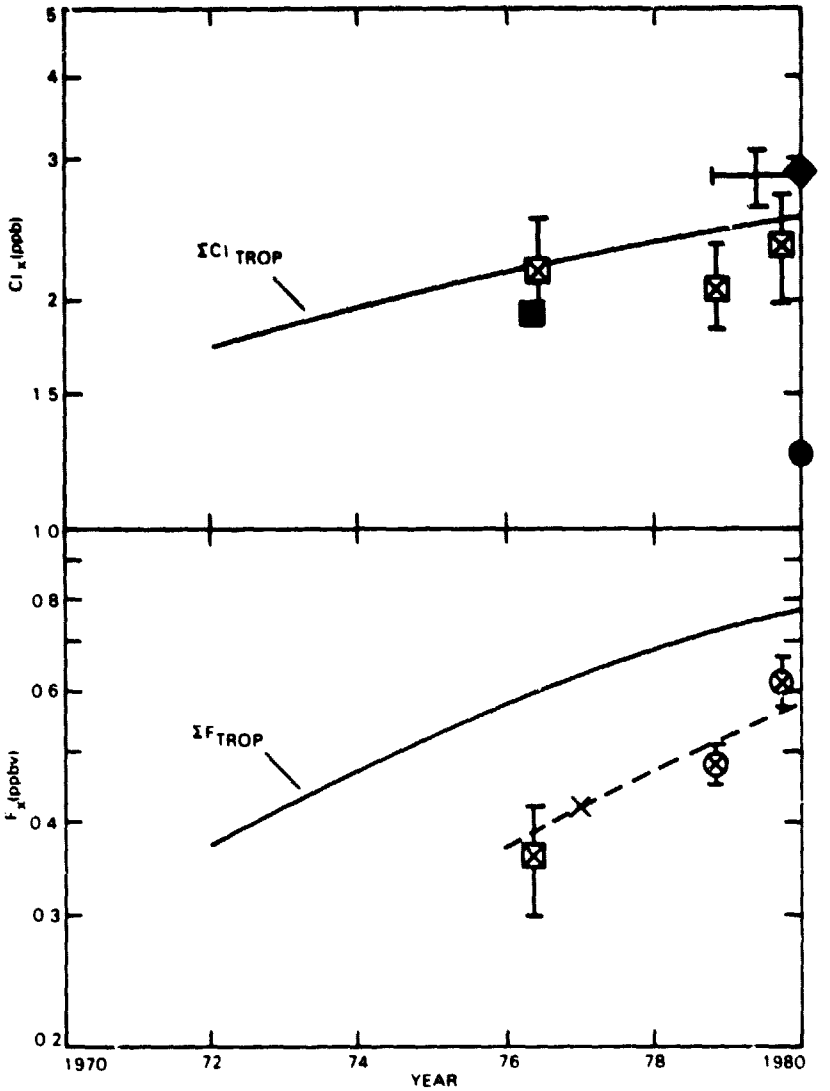

Figure 1-12. Temporal trends in chlorine and fluorine species. The solid lines show the time history of Cl and F present as major halocarbons in the troposphere of the Northern Hemisphere. Methyl chloride and CCl_4 were assumed constant, at concentrations of 620 pptv and 125 pptv respectively. Average values for CH_3CCl_3 were deduced from the data in Figure 1-10. Values for $CFCl_3$ and CF_2Cl_2 were taken from the model results in Figures 1-8 and 1-9, which provide a good representation of the data after 1975. Concentrations of Ci (◆) and F (●) from minor and major halocarbons are shown (See Tables 1-4 and 1-5). Other symbols are as follows: ■ totoal organic Cl near sea level (Berg and Winchester, 1977); ✢ total organic Cl in the lower stratosphere (Berg et al., 1980); ⊠ HCl, ⊛ HF above 30 km (Zander, 1981); ╳ model calculation for HF (Sze, 1978). The dashed line is drawn parallel to the solid line for organic F, as an aid to the eye.

HYDROCARBONS, CO AND H_2

The atmospheric data on selected hydrocarbons, CO and H_2 are listed in Table 1-2. Limited data suggests that at about 40°N, the background concentration of C_2H_6 , C_2H_2 , and C_2H_4 is about 1.6 ppb, 0.2 ppb, and 0.06 ppb respectively (Singh et al., 1979; Harrison et al., 1979; Cronn and Robinson, 1979). Because of the high reactivities of C_2H_2 and C_2H_4 , atmospheric gradients at least as large as those due to C_2H_6 can be expected. As an example, the C_2H_2 concentration is reported to be 0.23 ppb at 37°N; 0.03 ppb at 9° and 0.02 ppb at 90°S.

The global sources of CH_4 were reassessed by Ehhalt (1979) to be of the order of 590 to 930 Mt CH_4/yr. The lower boundary of this estimate is in good agreement with the sink provided by HO radicals based on recent estimates by Singh (1977a) and Volz et al. (1981b). The resulting turnover time of CH_4 is around 7 years. Recent measurements by Rasmussen and Khalil (1981) indicate that the tropospheric CH_4 concentration increased in 1979 and 1980 at a rate of 2% per year. The series of measurements performed at NCAR since 1965 (e.g., Ehhalt and Heidt, 1973a,b, 1974; Ehhalt, 1974; Heidt et al., 1980) with proper corrections to the old measurements (Heidt and Ehhalt, 1980) indicates that this increase does not constitute a long term trend but must be considered either a medium scale fluctuation or a very recent disturbance of the CH_4 cycle.

The natural sources of CO appear to be much greater than previously believed (Hanst et al., 1980). This is largely because of a higher than expected yield of CO from oxidation of terpenoid materials. Hanst et al. (1980) estimate that nearly 50% of the atmospheric CO in both hemispheres arises from oxidation of non-methane organic matter. The asymmetry of this CO source (5.1×10^{14} g/year in NH; 2.5×10^{14} g/year in SH) is comparable to the asymmetry in the CO levels in the NH and SH. There is now an increasing awareness that the hemispheric gradients of CO are only partly the result of man-made sources. The asymmetries in natural sources are significant but remain poorly characterized.

Molecular Hydrogen, H_2, is one of the most abundant trace gases, in both the troposphere and the stratosphere. Its tropospheric distribution is rather uniform. The observations showed no significant vertical gradients, except for a few regional perturbations (Ehhalt et al., 1977). There is, however, a slight interhemispheric difference: The average mixing ratio in the Northern Hemisphere is 0.576 ppmv, that in the Southern Hemisphere 0.552 ppmv (Schmidt, 1978).

It appears that most of the major sources and sinks have been identified. According to Schmidt et al. (1980a) global tropospheric H_2 sources and sinks are in balance. The present agreement is based on (1) a substantially reduced estimate of the main sink, microbial uptake by soils; (2) more recent measurements of the deposition velocity of H_2 on various soils by Schmidt et al. (1980) which give lower values than previously measured by Liebl and Seiler (1976). Obviously the errors are still sufficiently large to accommodate further substantial sources or sinks. It is noted that both production and destruction of H_2 are higher in the Northern Hemisphere which provides two-thirds of the total budget. The total amount of H_2 in the troposphere is 170×0^{12} g, with a turnover rate of about 2 years.

TROPOSPHERIC MEASUREMENTS OF HO RADICAL

The hydroxyl radical plays a key role in the chemistry of the troposphere (Levy, 1971). Because of low concentrations and potential interferences as discussed below, absolute measurements are difficult and subject to considerable uncertainty.

Four methods have been employed for the detection of tropospheric HO:

- Aircraft-borne laser induced fluorescence wherein a contained atmosphere sample is passed through an enclosed detection chamber and is probed by a pulsed laser tuned to the (1-0) band of the A-X transition at 282 nm. Fluorescence is observed at 309 nm (Davis et al., 1976 and 1979).

- Aircraft-borne laser induced fluorescence using an "open" optical arrangement in which a telescope is used to observe the backscattered fluorescence outside the boundary layer of the fuselage but in the near vicinity of the aircraft (Wang et al., 1980a).

- Measurements of carbon 14 labelled CO oxidation rates by HO in which the sample is drawn into a teflon coated vessel of 10 liter volume. All reported observations were taken in the boundary layer (Campbell et al., 1979).

- Long path (7.8 km) absorption of laser radiation of 308 nm (the Q(2) line of the $A^2\Sigma^+$, V'= 0, $X^2\Pi$ V'' = 0 transition). The experiment employs a double pass (3.9 km per degree) optical arrangement in which the beam is returned by a spherical mirror to a double monochromator located at the laser (Perner et al.,1976, 1981; Wang et al., 1981b).

Table 1-6 summarizes the recent tropospheric measurements of the HO radical. With the exception of the data from Wang et al. (1981) and one data point from the 1977 GAMETAG flight (Davis et al. 1981a), all the data presented are within the Earth's boundary layer. The majority of data presented was taken using the technique of laser induced fluorescence. These data have been questioned by Ortgies et al., 1980, who contend that in a region of high water vapor and ozone concentrations, the production of HO within the time duration of the laser pulse can dominate the HO in ambient air. Their calculations, however, make the assumption that at least one of the HO radicals, formed from the reaction of H_2O and $O(^1D)$ is rotationally thermalized within the laser pulsewidth. There are, however, no measurements as yet of the rotational relaxation rates within the ground state. Davis et al. (1981b) have recently published experimental results measuring directly the interference due to laser generation of HO. Their results indicate very little thermalization of the rotational levels during the pulse even at atmospheric pressures. They have measured the interference due to the artificial production of HO within the boundary layer to be on the order of 25 to 50% depending on the atmospheric conditions. Theoretical calculations are consistent with these values (Davis et al., 1981c). Wang et al. (1981) report that under their experimental conditions artificial HO was lower than the detection limit of their instrument. Davis et al. (personal communication) also report that there is little interference under the conditions of the free troposphere. It is clear, however, that this is a problem that must be considered carefully in all measurements of HO by laser induced fluorescence.

The GAMETAG results represent the first effort at a simultaneous measurement of most of the parameters which affect the steady-state concentration of HO in the troposphere. In addition to HO, solar UV flux, CO, H_2O, O_3 , HNO_3 and temperature were also measured. Modeling of these results showed good agreement with the measured HO, which would indicate that the model is not substantially in error, but the uncertainties in the HO measurements as well as the input parameters in the model are large enough that significant changes can be made in the model and still obtain agreement with the measurements.

It is also worth noting that the measurements of Campbell et al. (1979) are in general lower than the GAMETAG and other measurements but a comparison of isolated measurements separated by time and location without information about the different photochemical conditions is not particularly fruitful.

Table 1-6
Recent Measurements of HO in the Troposphere

Location	Date	Time	Altitude (km)	HO Molecules/(10^{-6}cm^{-3})	Estimated Uncertainty
Davis et al. (1979) - Laser induced fluorescence					
Rocky Mtns.	7/16/76	1000-1020	6.9	2.9	40%
Four Corners, NM		1030-1115	2.1	4.7	40%
Davis et al. (1981a) - Laser induced fluorescence					
2.5°N, 170°W	8/26/77	1136-1148	.465	8.0	44%
8°S, 169°W	8/28/77	1116-1146	.334	9.1	33%
24.5°S, 172°W	8/31/77	1218-1336	.430	10	29%
2.5°S, 170°W	9/1/77	1026-1040	.532	13	32%
13°N, 161°W	9/2/77	1056-1110	.300	7.5	45%
15.5°N, 169°W	5/2/78	1341-1359	.334	4.1	51%
9°N, 171°W	5/3/78	1043-1120	.340	7.5	35%
1°S, 172°W	5/3/78	1424-1456	.342	1.7	53%
30°S, 174°E	5/6/78	1258-1311	.270	3.1	71%
33°S, 173°E	5/11/78	1233-1249	.280	3.4	65%
14.5°S, 177°E	5/12/78	1050-1108	.207	4.8	54%
Campbell et al. (1979) - ^{14}CO oxidation					
46.7°N	10/11/79	1350	Ground	.3	--
46.7°N	1/27/78	1458	Ground	3.3	24%
46.7°	7/25/78	1244	Ground	3.4	18%
44°S	4/2/78	1409	Ground (1.0 km)	0.5	60%
44°S	4/4/78	1248	Ground (1.0 km)	0.6	--
35°N	8/13/78	1325	Ground	2.0	--
35°N	8/13/78	1421	Ground	3.4	3%
Wang et al. - Laser induced fluorescence					
San Bernadino, California	3/27/79	1350-1430	10	20	30%
San Diego, California	3/28/79	1030-1130	10.6	10	40%

TROPOSPHERIC PHOTOCHEMISTRY

An understanding of the processes which control the composition of the troposphere is necessary for analysis of many problems in stratospheric chemistry. Firstly, the troposphere serves as a source region for a large number of gases that play important roles in the photochemistry of the stratosphere. Since the concentrations of several of these gases are controlled by chemical sources and sinks in the troposphere (e.g., N_2O, CH_3Cl, CH_3CCl_3, CO, CH_4 and other hydrocarbons), global changes in the chemical composition of the troposphere may alter the fluxes of these species to the stratosphere. The most important sink for many of these species is reaction with HO. Any large-scale changes in tropospheric HO densities may therefore affect fluxes to the stratosphere. Secondly, changes in tropospheric chemistry may alter the tropospheric burden of radiatively active gases (e.g., O_3, CH_4, SO_2) and thereby affect tropospheric and stratospheric climate. Finally, increases in tropospheric ozone would contribute to changes in the total column of ozone. It is therefore essential to understand the processes which control ozone and hydroxyl distributions, and how they might respond to changes in sources of gases such as CO, NO_x, or CH_4.

The hydroxyl radical is produced by the photolysis of ozone:

$$O_3 + h\nu \rightarrow O(^1D) + O_2 \quad (\lambda < 310 \text{ nm}) \tag{1}$$

followed by $$O(^1D) + H_2O \rightarrow HO + HO \tag{2}$$

HO is removed by reaction with CO and CH_4

$$CO + HO \rightarrow H + CO_2 \tag{3}$$

$$H + O_2 + M \rightarrow HO_2 + M \tag{4}$$

$$HO + CH_4 \rightarrow CH_3 + H_2O \tag{5}$$

with reaction (3) dominant over (5).

HO may be regenerated through the following reactions,

$$HO_2 + NO \rightarrow HO + NO_2 \tag{6}$$

$$HO_2 + O_3 \rightarrow HO + 2O_2 \tag{7}$$

or H_2O_2 may be formed through the reaction:

$$HO_2 + HO_2 \rightarrow H_2O_2 + O_2 \tag{8}$$

Photodissociation of H_2O_2 reforms HO

$$H_2O_2 + h\nu \rightarrow 2HO \tag{9}$$

while the reactions

$$H_2O_2 + HO \rightarrow H_2O + HO_2 \tag{10}$$

$$H_2O_2 + \text{rain} \rightarrow \text{washout} \tag{11}$$

act as sinks for tropospheric odd hydrogen (H, HO, HO_2 , H_2O_2). H_2O_2 has a high solubility in water and should therefore be removed efficiently by rainfall. Logan et al. (1981) estimate reactions (10) and (11) to be the main tropospheric sinks for odd hydrogen, the gas phase reaction (10) being the more important of the two. This reduces the dependency of HO concentration on the removal rate of H_2O_2 by heterogeneous processes. The removal rate of soluble gases by precipitation is one of the more uncertain parameters in current models of tropospheric chemistry. Similarly, the effects of chemical reactions occurring in droplets or aerosols on the gas phase composition of the troposphere is not well understood.

Another major uncertainty in analyses of tropospheric problems results from the lack of data for NO_x ($NO+NO_2$). Recent measurements of NO_x indicate that concentrations in the remote troposphere may be extremely low, ranging from a few to a few hundred parts per trillion (Noxon, 1978; McFarland et al., 1979; Kley et al., 1981; Helas and Warneck, 1981). Production of HO occurs mainly by reactions (2), (6), (7) and (9) in the lower troposphere (e.g., Logan et al., 1981). Reactions (6) and (7) occur at comparable rates for concentrations of NO of ~10 pptv. The concentration of HO is independent of NO for NO at 10 pptv and is an increasing function of NO for NO between about 10 pptv and 500 pptv (Fishman et al., 1979a). Production of odd oxygen in the troposphere is also a sensitive function of NO (see below).

Odd hydrogen production from the oxidation of hydrocarbons (HC) in the atmosphere may also play a significant role for the HO distribution, particularly in the lower troposphere over continents. This production is usually initiated by a reaction of the type:

$$HO + HC \quad \ldots\ldots \alpha \cdot HO_2 + \text{products} \qquad (12)$$

where α denotes the number of odd hydrogen released in the subsequent reactions. A large number of primary hydrocarbons, some of human, some of biogenic origin, are released to the atmosphere. Odd hydrogen production depends on the type of hydrocarbons, and on the concentrations of species like NO. Hence, considerable uncertainty is attached to the calculations of odd hydrogen production from these species.

Uncertainties in the current understanding of the chemistry of HO are discussed in more detail in recent papers by Chameides and Tan (1981) and Logan et al. (1981). These papers and others (Rodhe and Isaksen, 1980; Volz et al., 1981a) present recent calculations for the distribution of HO as a function of latitude, altitude and season.

Analysis of the budget for CH_3CCl_3 has been used to test models for the global distribution of HO. Earlier estimates of globally averaged HO concentrations ($3\text{-}10\times10^5$ molecules cm^{-3}, Singh 1977a, b; Lovelock 1977; Chang and Penner, 1978; Neely and Plonka, 1978) must be revised upward by a factor of about 1.7 to take account of recent kinetic data for the reaction of HO with CH_3CCl_3 (Kurylo et al., 1979; Jeong and Kaufman, 1979). Two recent calculations of the global distribution of HO give a lifetime for methyl chloroform of 5 years (Derwent and Eggleton, 1981; Logan et al., 1981). However both models underestimate concentrations of CH_3CCl_3 after 1975 (see Figure 1-10), suggesting that calculated concentrations of HO are somewhat high. The usefulness of the CH_3CCl_3 budget as a test for models of HO is hampered by discrepancies in absolute concentrations of CH_3CCl_3 and uncertainties in the emission rate. The measurements of CH_3CCl_3 are consistent with lifetimes in the range 5 to 10 years, and globally averaged HO concentrations of $5\text{-}10\times10^5$ molecule cm^{-3}.

A reliable model for tropospheric HO provides useful information on the magnitude of the loss rate for other trace gases such as CO and CH_4, whose sources are extremely difficult to quantify. Recent studies of the budget of CO in the context of models for HO (Logan et al., 1981; Volz et al, 1981a; Pinto et al., 1981) indicate that there are large sources for the gas other

than combustion of fossil fuels and oxidation of CH_4. Likely candidates are sources from oxidation of non-methane hydrocarbons and biomass burning, as proposed by Zimmerman et al. (1978), Hanst et al. (1980), and Crutzen et al. (1979). Measurements of CO in the literature before 1981 are reviewed by Logan et al. (1981), while Seiler and Fishman (1981) present a detailed analysis of tropospheric profiles for CO.

Volz et al. (1981a) have modeled the distributions of ^{14}CO and ^{12}CO by using a 2-D model. They showed that in order to balance the sources and sinks for both species, an "average" tropospheric HO concentration of $(6.5 \pm 2.3) \times 10^5$ cm^{-3} is required, in agreement with the values deduced from the CH_3CCl_3 budget. The definition of this "average" HO is different from the "average" HO inferred from CH_3CCl_3 because of the different reaction rate constants and tropospheric distributions of the two tracers. Volz et al. (1981a) deduced a biological ^{14}CO source (excluding CH_4 oxidation) of about 1250×10^{12} g CO/yr. This is consistent with conclusions reached by considering the global CO budget (Logan et al., 1981). The 2-D model study of Isaksen (1980) required such a source to give agreement between observed and calculated CO concentrations at low latitudes. Pinto et al. (1981) have modeled the distribution of ^{12}CO by using a 3-D general circulation model. They derived an "averaged" tropospheric HO concentration equal to 7×10^5 cm^{-3} and a biological source of ^{12}CO equal to 1300×10^{12} g CO/yr (excluding CH_4 source) in excellent agreement with the above mentioned studies.

TROPOSPHERIC OZONE

The origin of tropospheric ozone has been a controversial subject for some time. From earlier analyses of the ozone distribution, Junge (1962) accepted the classical view that ozone is transported from the stratosphere and destroyed at the surface. This "dynamical control" view continues to be favored by Pruchniewicz (1973), Junge and Czeplak (1969), Fabian and Pruchniewicz (1977), Chatfield and Harrison (1977), Singh et al. (1978), Hussain et al. (1979) and Routheir and Davis (1980). On the other hand, Chameides and Walker (1973), Crutzen (1974), Fishman and Crutzen (1977), Liu (1977), Stewart et al. (1977), Chameides (1978), and Fishman et al. (1979b) have argued that gas phase photochemical production and destruction of ozone in the troposphere may be more important than injection of ozone from the stratosphere.

Ozone may be generated in the troposphere by the oxidation of CO:

$$CO + HO \rightarrow H + CO_2 \quad (3)$$

$$H + O_2 + M \rightarrow HO_2 + M \quad (4)$$

$$HO_2 + NO \rightarrow HO + NO_2 \quad (6)$$

$$NO_2 + h\nu \rightarrow NO + O \quad (13)$$

$$O + O_2 + M \rightarrow O_3 + M \quad (14)$$

$$\text{Net: } CO + 2O_2 + h\nu \rightarrow CO_2 + O_3 \quad (15)$$

Odd hydrogen (H, HO, HO_2, and H_2O_2) and NO_x act as catalysts in producing ozone from CO and O_2. The efficiency of this cycle depends on the concentrations of these species in the atmosphere. However, low concentrations of NO allow competition for the HO_2 radical by reaction (7). Thus the efficiency of ozone production depends critically on the amount of NO in the atmosphere.

Below a certain critical value of the ratio of $[NO]/[O_3]$, ozone loss through the sequence:

$$HO_2 + O_3 \rightarrow HO + 2O_2 \quad (7)$$

$$CO + HO \rightarrow H + CO_2 \quad (3)$$

$$H + O_2 + M \rightarrow HO_2 + M \quad (4)$$

$$\text{Net: } O_3 + CO \rightarrow CO_2 + O_2 \quad (16)$$

dominates over the production discussed above. For typical background ozone concentrations photochemical loss by (16) dominates the production by (15) when NO concentrations are below approximately 10 ppt. Ozone may be produced also in the photo-oxidation of CH_4 (Crutzen, 1974). The key steps are conversion of NO to NO_2

$$CH_3OO + NO \rightarrow CH_3O + NO_2 \quad (17)$$

followed by reactions (13) and (14). The dominant sinks for odd oxygen ($O+O_3$) in the troposphere are reactions (2) and (7). Current models indicate that photochemical production of ozone by (6) and (7) and loss by (2) and (7) (and other minor processes) are in approximate balance for NO ≈ 30 pptv (Fishman et al., 1979; Logan et al., 1981).

To assess the impact of tropospheric chemistry on the ozone distribution, it is essential to determine the global distribution of nitrogen oxides, and in particular the distribution of NO. The data mentioned earlier indicate that concentrations of NO_x in the remote troposphere be in the range of 10 to 200 pptv. NO concentrations are related to NO_x (the sum: $NO + NO_2$) through reaction (13) and the reverse reaction (6), (17) and (18):

$$NO + O_3 \rightarrow NO_2 + O_2 \quad . \quad (18)$$

The ratio NO/NO_x is larger in the upper troposphere than in the lower troposphere, a consequence of the signficant temperature dependence of (18). The major loss mechanism for NO_x is through reaction (19)

$$NO_2 + HO + M \rightarrow HNO_3 + M \quad (19)$$

followed by heterogeneous loss of HNO_3.

$$HNO_3 + \text{rain} \rightarrow \text{Loss} \quad (20)$$

The lifetime of NO_x with respect to reaction (19) is about a day in the lower troposphere. It is probably somewhat longer in the upper troposphere and at all altitudes in winter and mid- and high-latitudes. Concentrations of NO_x are highly variable, depending on both the source distribution and the rates of reactions (19) and (20).

Levy et al. (1980) argue that injection from the stratosphere could provide a dominant source for NO_x in the upper troposphere. Kley et al. (1981) derive global distributions for NO_x from a 1-D photochemical model and the tracer distributions of Levy et al. (1980). Based on these results, and low concentrations of NO over the Pacific Ocean (≈ 4 pptv, McFarland et al., 1979) Liu et al. (1980) conclude that the upper troposphere is the dominant region for photochemical production of ozone. Fishman (1981) on the other hand points to several other observations which indicate

considerably higher NO_x concentrations in the lower troposphere than suggested by Liu et al. (1980). Fishman (1981) finds ozone production in the lower troposphere ($Z<5$ km) to be significant.

Model estimates of tropospheric ozone production depend critically on profiles adopted for NO_x. Logan et al. (1981) estimate NO_x production from natural sources to be of the order of 10 Tg (N)/year. This is considerably higher than the <1 Tg (N)/year which is estimated to be transported downward from the stratosphere (Levy et al., 1980). It should be noted that there are large uncertainties in the production rate of NO_x in the lower troposphere, and in the removal rate of HNO_3 by heterogeneous processes. Production by lightning, possibly an important source of NO_x above the planetary boundary layer is known only within an order of magnitude. Present estimates suggest that it is in the range 2 to 15 Tg (N)/year (Dawson 1980; Hill et al., 1980). Another controversial question is the contribution of anthropogenic NO_x released at ground level to the free tropospheric NO_x burden. Releases from fossil fuel combustion are rather well known (~20 Tg (N)/year). Sources of NO_x from biomass burning are very uncertain (Crutzen et al., 1979). It is likely that a large fraction of NO_x from combustion sources is oxidized to HNO_3 within the planetary boundary layer (reaction 19), making its contribution to free tropospheric NO_x very difficult to assess at the moment.

Some of the uncertainties in the budgeted tropospheric NO_x and ozone would be resolved by measurements of the distribution of NO_x in different environments. Although photochemical production of ozone depends critically on NO, photochemical loss of ozone is almost independent of NO (Fishman, 1979). Current estimates indicate that photochemical loss of ozone is comparable to ozone transport from the stratosphere and ozone destruction at the ground (Fishman et al., 1979; Liu et al., 1980; Chameides and Tan, 1981; Logan et al., 1981).

The foregoing discussion reveals several important areas where improvements are necessary before tropospheric chemistry can be understood to the point where reliable estimates of human influences can be made.

Some of the key areas of uncertainty caused by limitations in atmospheric measurements and in the treatment of radiation, dynamics, and chemistry are listed below:

1. Measurements of the global distribution of species which show large spatial and temporal variations such as NO_x, non-methane hydrocarbons (NMHC) and H_2O are lacking.

2. Budgets of important gases such as NO_x, CO, CH_4, O_3 and NMHC are not well understood. We note that the production of NO_x by lightning, release of NMHC and CH_4 from biogenic sources and production of CO and NO_x by biomass burning are very uncertain.

3. Liquid phase removal rates of water soluble gases, as well as surface removal rates are poorly known. These processes are very important for H_2O_2, CH_3O_2H, SO_2, NO_x, CH_2O and HNO_3.

4. The effects of clouds and surface albedo on the UV fluxes need to be studied.

5. Large-scale tropospheric distributions of key species like ozone and CO are strongly influenced by dynamical processes. Realistic representation of these processes in the troposphere is likely to require a fully coupled three-dimensional dynamical-chemical model.

6. Tropospheric effects of anthropogenic and biogenic species (NO_x NMHC, SO_2) in the planetary boundary layer depend strongly on the efficiency of exchange processes. A realistic representation of the exchange of gases between the boundary layer and the free troposphere has not yet been applied to global studies in the troposphere.

STRATOSPHERIC DISTRIBUTION OF SOURCE GASES

NITROUS OXIDE, FC-11, FC-12, AND METHYL CHLORIDE (N_2O, CCl_3F, CCl_2F_2 AND CH_3Cl)

Since 1975 a number of measurements have been made of the stratospheric concentrations of N_2O, CCl_3F and CCl_2F_2. Four field programs have been particularly extensive, all involving laboratory analysis by gas chromatography of air samples collected by balloon-borne samplers. The few measurements made by in situ balloon-borne infrared techniques (Farmer et al., 1980) are consistent with these data. The four research groups are:

NOAA Goldan et al. (1980, 1981). Balloon-borne evacuated grab samples.

NCAR Heidt et al. (1975). Balloon-borne cryosampler.

KFA Volz et al. (1981b). Balloon-borne cryosampler.

Ames Tyson et al. (1978); Vedder et al. (1978); Inn et al. (1979); Vedder et al. (1981); Balloon and aircraft-borne cryosampler.

The results obtained by grab-sampling with evacuated containers and by cryosampling give consistent results, although the potential sources of error are appreciably different for the two methods. The evacuated grab sample technique collects relatively small amounts of air in a period of 20 to 30 seconds. Altitude resolution is good because of the short collection time. However, surface contamination or reactions can be important because of the low pressures in the vessels.

The cryosampling technique on the other hand provides much larger air samples but periods as long as 20 to 30 minutes are required for collection. Altitude resolution can only be maintained through slow changes in balloon altitude, carrying with it the possibility of sample contamination from the outgassing of the balloon. These problems are more severe for CCl_2F_2 and CCl_3F and for collections made during the balloon-ascent and float phases, and such contamination is clearly present in a number of samples. For this reason, all data collected during ascent and float have been excluded from consideration. Most of the errors in the laboratory measurements themselves are essentially the same as those for tropospheric air samples. The mixing ratios found in mid-stratospheric air are lower than those in the troposphere, so that the percentage errors increase with increasing altitude. The observed concentrations fall below the available sensitivity only for CCl_3F at altitudes in the region above 30 km.

The results from three of these groups, compared over narrow latitude bands, are shown for equatorial latitudes in Figures 1-13, 1-14, 1-15 and mid-latitudes in Figures 1-16 through 1-21. They are in good agreement with one another. The grab-sample data of Heidt et al. at 32°N provide altitude profiles which are consistent with the latitude differences in the troposphere shown in Figures 1-4, 1-8, and 1-9 but no data for these latitudes exist from any of the other grab sample experiments. The two single altitude profiles obtained by infrared techniques at 32°N and 30°S also fall in between the trends shown in Figures 1-16 through 1-21. The data for CCl_3F and CCl_2F_2 have been corrected for the well-established secular increase in each using the tropospheric measurements described in Figures 1-8 and 1-9.

A common feature of the data in Figures 1-16 through 1-21 is the increased scatter of data at higher altitudes. The high degree of correlation among all three components in individual samples at these altitudes demonstrates that much of this variability arises because of transport.

With each of the three molecules the concentrations fall off more rapidly in mid-latitudes than in the tropics. This behavior is expected from the known meteorological patterns through which upward mixing into the stratosphere occurs preferentially in tropical latitudes, followed by poleward mixing within the stratosphere itself. The change in mixing ratio with altitude is more rapid at both latitudes for CCl_3F than for either CCl_2F_2 or N_2O. This difference in relative concentration is indicative of more rapid decomposition of CCl_3F, consistent with higher absorption cross sections for solar ultraviolet radiation in the 190 to 230 nm wavelength range.

The vertical profile of CH_3Cl as obtained from gas chromatographic measurements on cryogenic samples from balloon flights over Southern France (44°N) is shown in Figure 1-22. The data, although largely scattered, clearly show a very rapid decrease from 600 ppt at the tropopause to about 20 to 40 ppt at 30 km indicating the short lifetime of CH_3Cl.

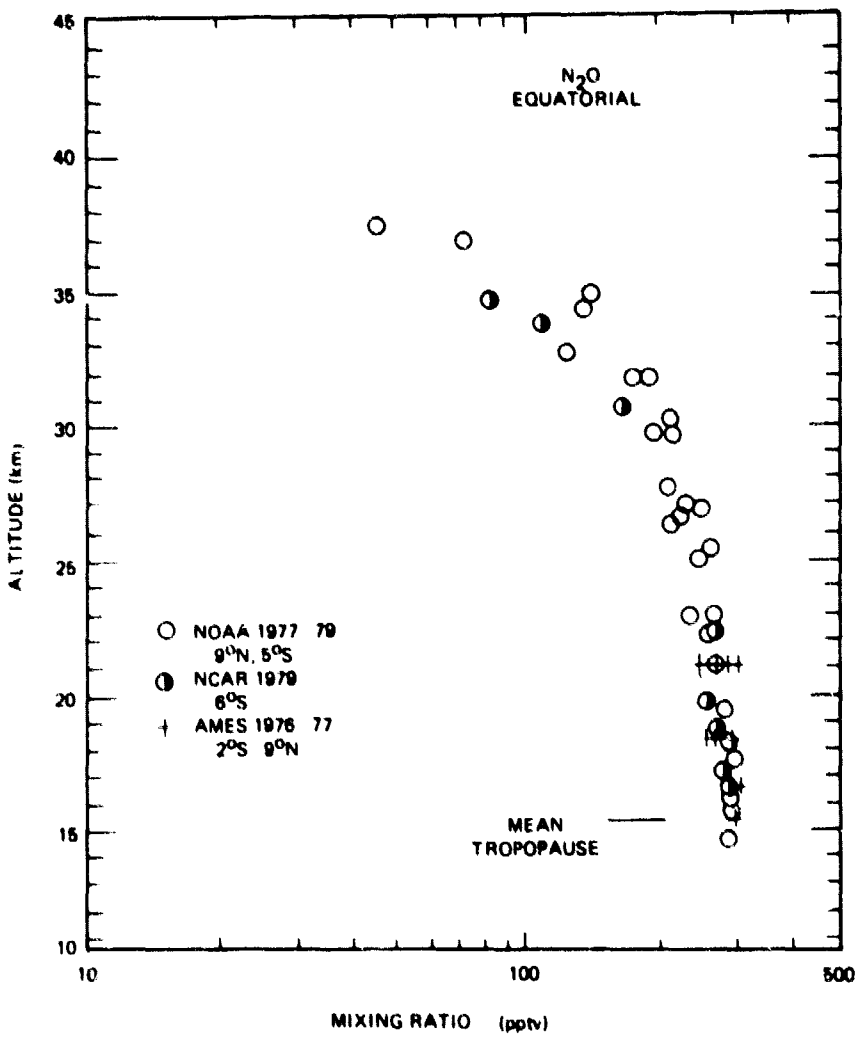

Figure 1-13. Measurements of N_2O as a function of altitude in the equatorial region.

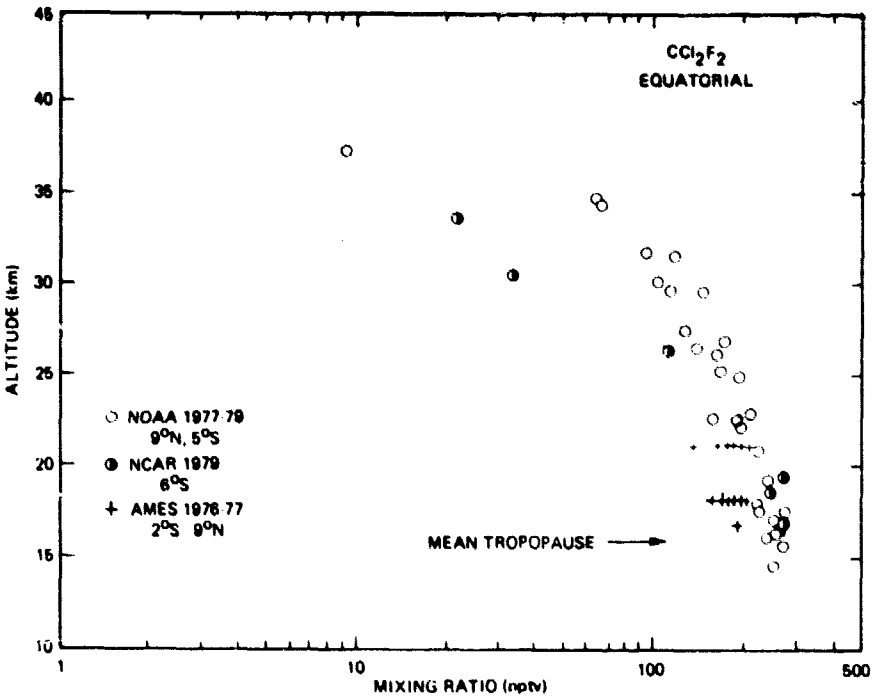

Figure 1-14. Measurements of CF_2Cl_2 (FC-12) as a function of altitude in the equatorial region.

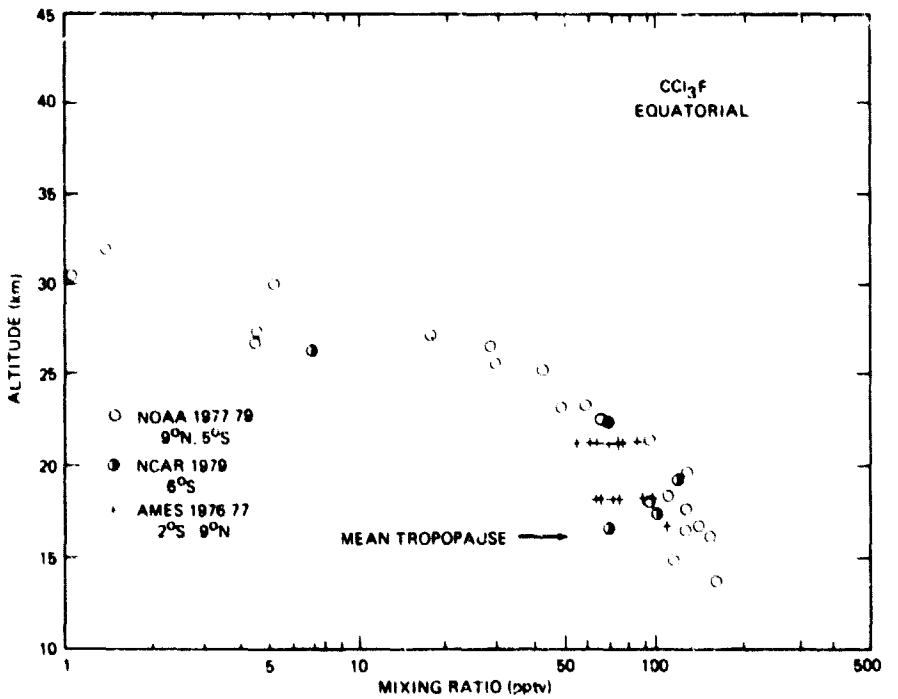

Figure 1-15. Measurements of CCl_3F (FC-11) as a function of altitude in the equatorial region.

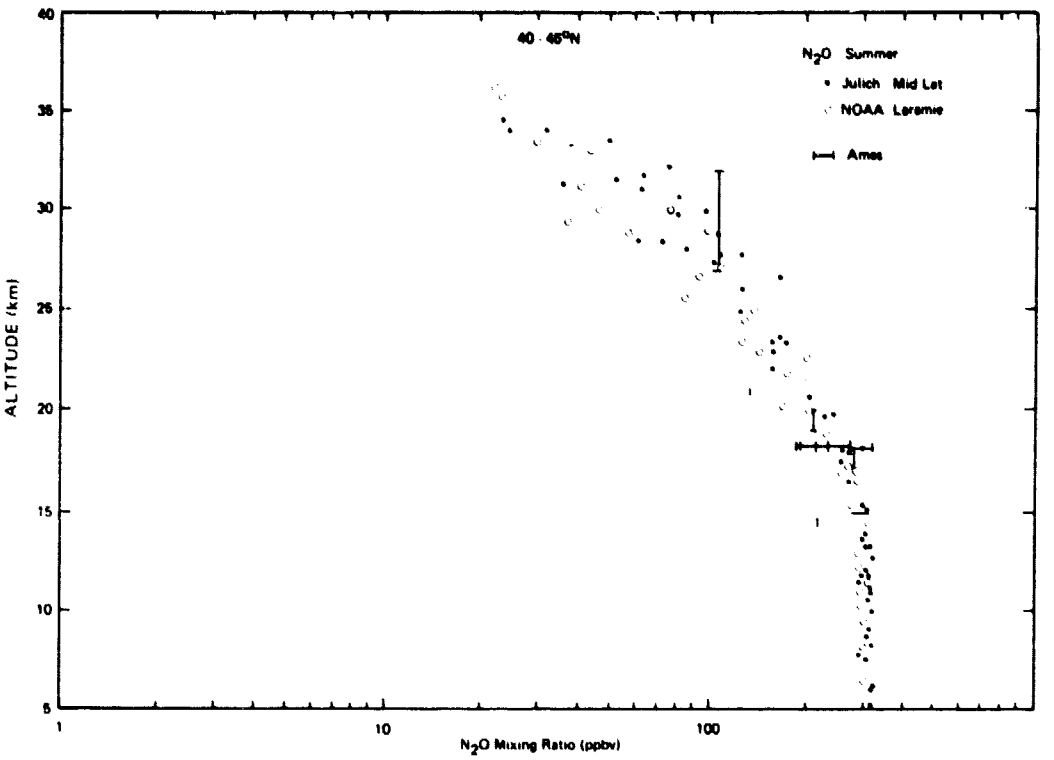

Figure 1-16. Mid-latitude Summer vertical profile of N_2O.

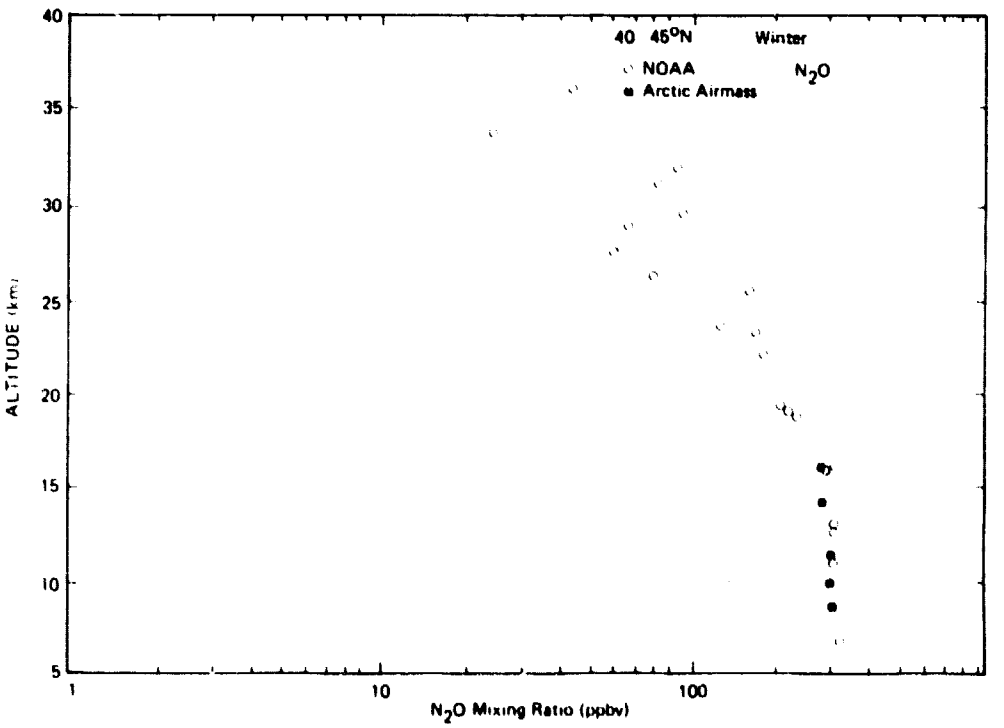

Figure 1-17. Mid-Latitude winter vertical profile of N_2O.

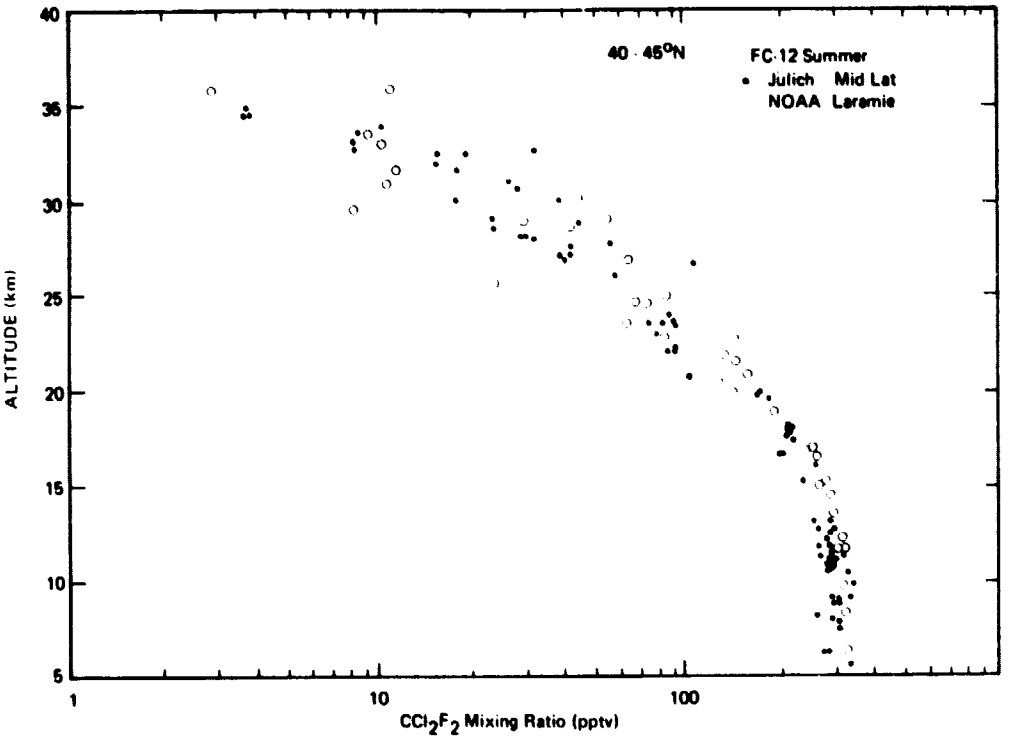

Figure 1-18. Mid-latitude summer vertical profile of CCl_2F_2 (FC-12).

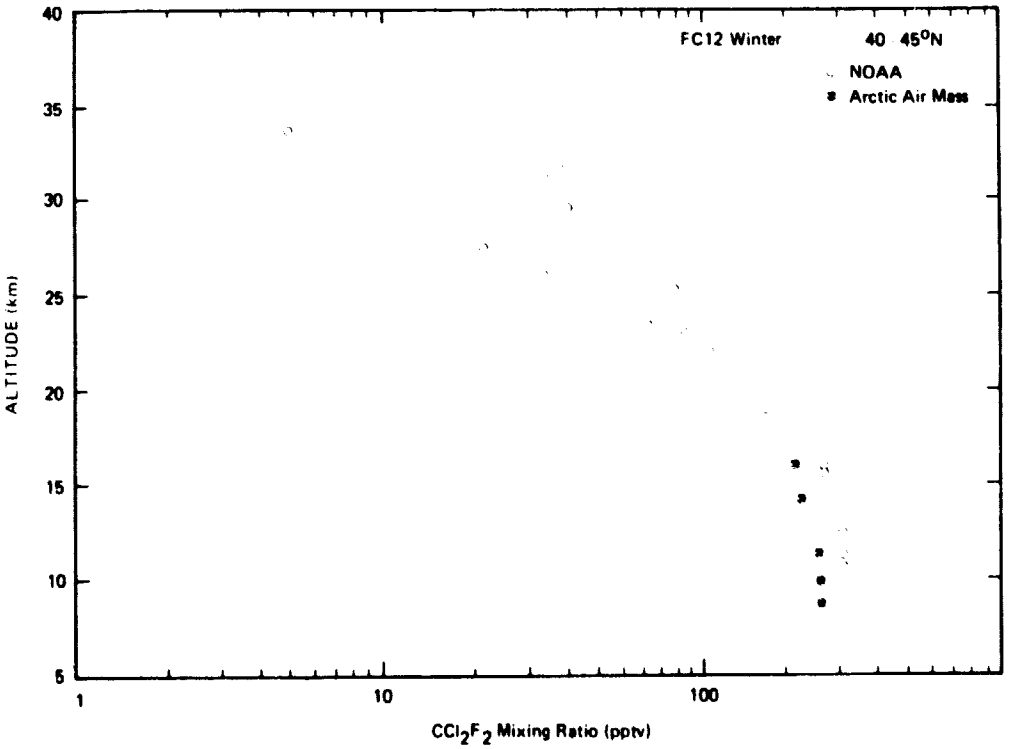

Figure 1-19. Mid-latitude winter vertical profile of CCl_2F_2 (FC-12).

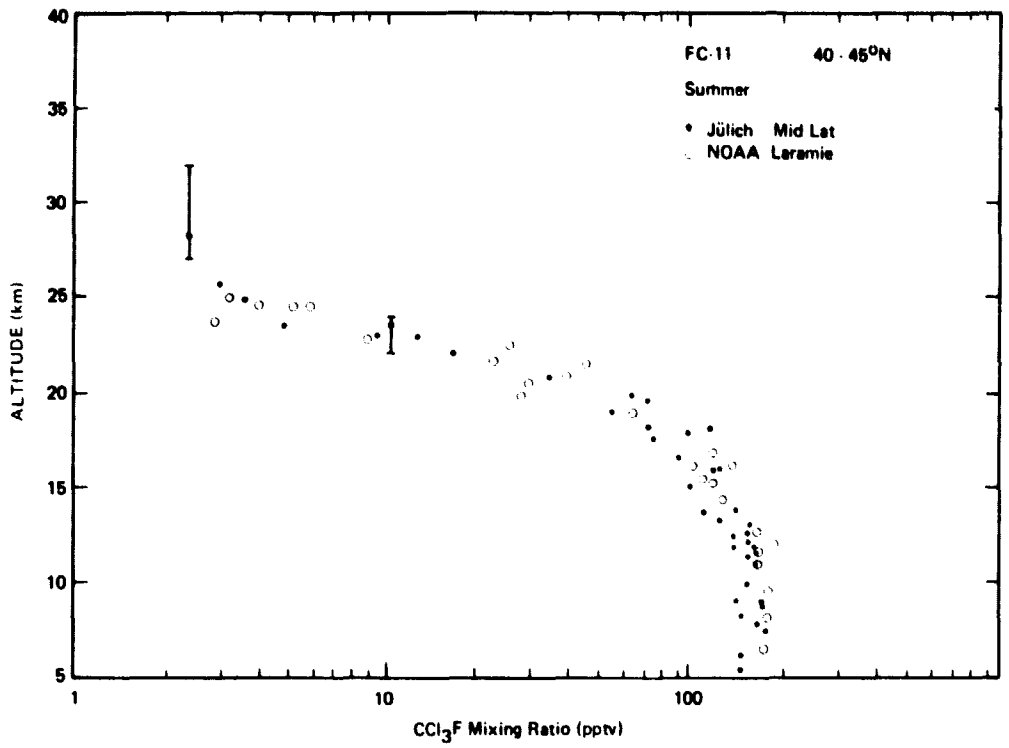

Figure 1-20. Mid-latitude summer vertical profile of CCl_3F (FC-11).

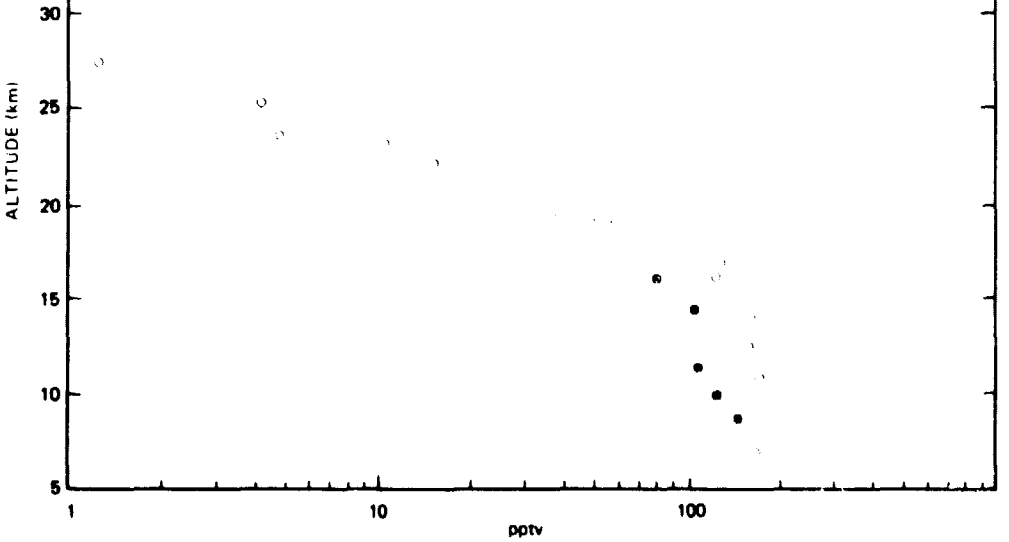

Figure 1-21. Mid-latitude winter vertical profile of CCl_3F (FC-11).

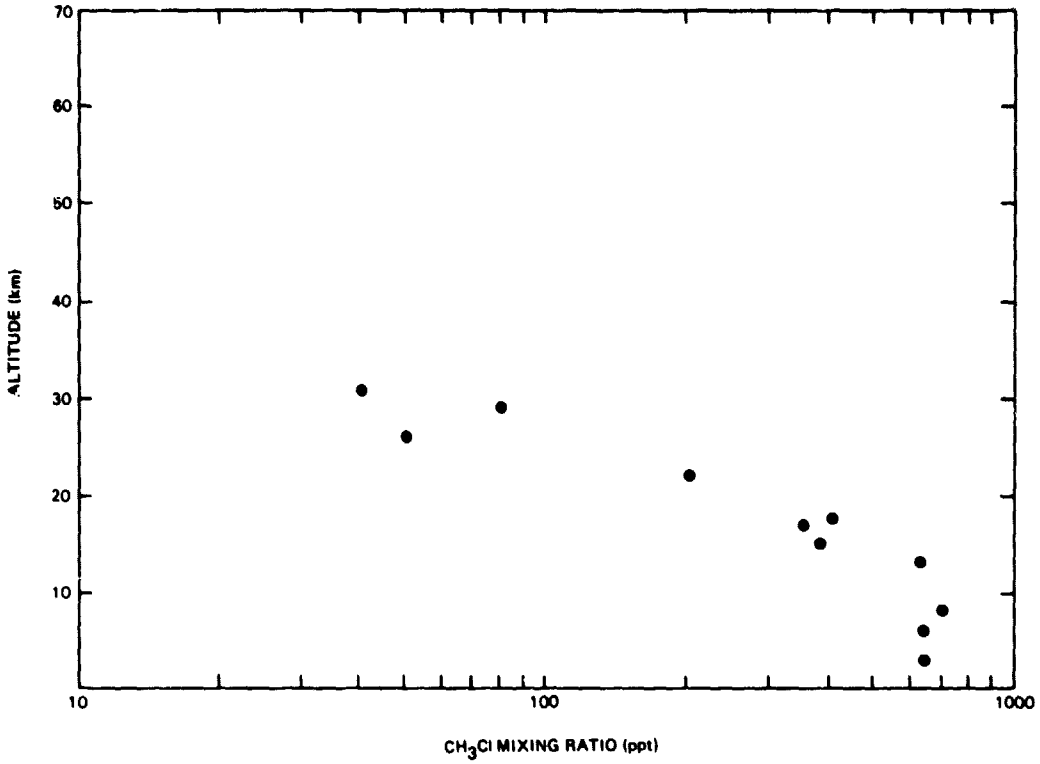

Figure 1-22. Vertical profile of CH_3Cl at 44° northern latitude. The data were measued by GC-FID and GC-MS (Penkett et al., 1979) from samples collected cryogenically during a joint balloon program (Fabian et al., 1979).

CARBON-CONTAINING SPECIES

Carbon Dioxide (CO_2)

Vertical profiles of CO_2 have been measured routinely at NCAR using a volumetric technique, achieving a precision of ±3 ppm. About the same precision has been achieved at the KFA using gas-chromatography. The precision of the gas-chromatographic measurements has recently been improved to ±0.5 ppm (Volz et al., 1981b). Additional measurements have been made by Bischof et al. (1980) using the infrared absorption technique, and by Mauersberger and Finstad (1980) using a balloon-borne mass spectrometric method.

The individual profiles of CO_2 are plotted in Figure 1-23. As can be seen, the older volumetric and GC-data show a large scatter but no significant gradients of the CO_2 mixing ratio in the stratosphere. However, from the more recent data (Volz et al., 1981b) and from the measurements by Bischof et al. (1980), a weak but significant gradient is observed in the lower stratosphere, namely the CO_2 mixing ratio is found to decrease by about 6 to 7 ppm between the tropopause and 20 km altitude. From a time series analyses of CO_2 profiles measured over the past decade, Volz et al. (1980) found approximately the same temporal increase of CO_2 in the upper stratosphere as is observed for the troposphere.

The measurements by Mauersberger and Finstad (1980) show the mixing ratio of CO_2 to increase rapidly with altitude in the upper stratosphere in contradiction to all other measurements, a finding which cannot be explained within our present knowledge.

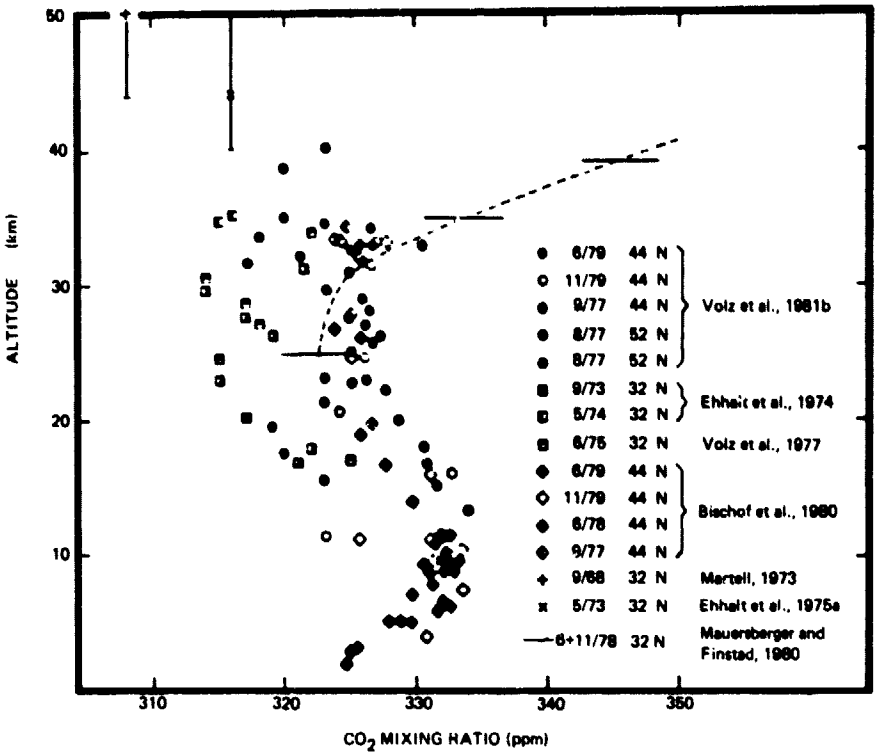

Figure 1-23. Vertical profiles of CO_2 at mid-latitudes. Some of the scatter is due to the observed secular increase of CO_2 in the stratosphere (Volz et al., 1981b) during the time the different profiles were measured.

Carbon Monoxide (CO)

Since the appearance of NASA RP 1049, little progress has been made in establishing the vertical profile of CO in the mid-stratosphere. The sampling techniques are suspect as CO could be produced in the sampler in the presence of high O_3 concentrations (Fabian et al., 1981). Some effort has been made by the MPI-Lindau, MPI-Mainz, and KFA-Julich groups to overcome this problem by destroying O_3 at the intake of the sampler using copper and silver catalysts. Laboratory tests show that O_3 can be destroyed efficiently without production or destruction of CO. However, more laboratory tests are required to prove beyond doubt that the contamination problem caused by O_3 can be solved completely. Due to this contamination problem, only CO data from in situ sampling below 22 km and above 40 km where the O_3 concentration is sufficiently low have been included in Figure 1-24. In addition to this very limited data set, two sets of remote measurements are included, one from Farmer et al. (1980) between 22 and 30 km, and three total column measurements made by Zander et al. (1981) above 30 km.

Although the experimental data are extremely limited, the measurements cover the vertical profile of CO between the tropopause and 50 km. The combined data in Figure 1-24 suggest a decrease of CO across the tropopause and in the lower stratosphere up to 20 km. Above this altitude the CO mixing ratio is constant, at 10 ppb, up to 30 km. It then increases to 40 ppb around 40 to 50 km altitude. More reliable measurements of CO in the middle and upper stratosphere are required to establish the vertical profile.

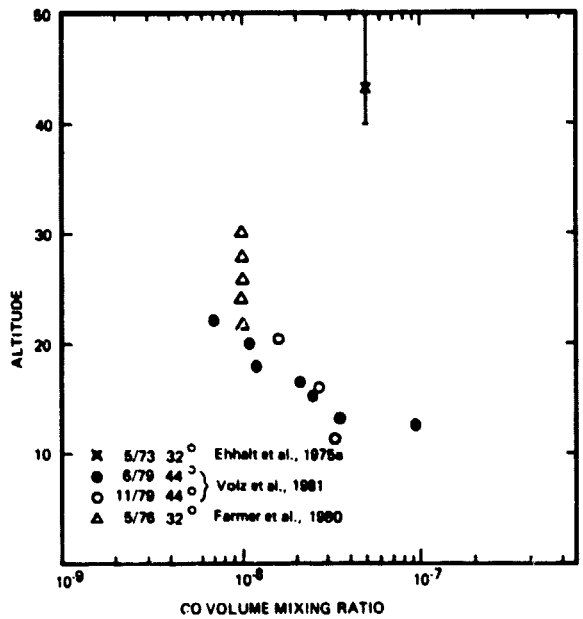

Figure 1-24. Vertical profile of CO at mid-latitudes.

HYDROGEN-CONTAINING SPECIES

Molecular Hydrogen (H_2)

Recent stratospheric measurements of H_2 are summarized in Figure 1-25. The profiles obtained at three latitudes show little vertical and latitudinal variation.

The data at 40 to 60°N show a clear decrease with altitude, from 0.55 ppm at the tropopause to 0.45 ppm at 35 km altitude (Ehhalt, 1978; Fabian et al., 1979). A similar trend although with a much larger uncertainty can be deduced from the data at 60°N. No significant trend is found for the data at 32°N over Palestine, Texas. It should be noted that the absolute calibration of the NCAR data is about 10% lower than that of the KFA. It has been shown by Ehhalt and Tonnissen (1980) in a qualitative way that elevated levels of stratospheric H_2 are associated with, and probably caused by, increased concentrations of CH_4.

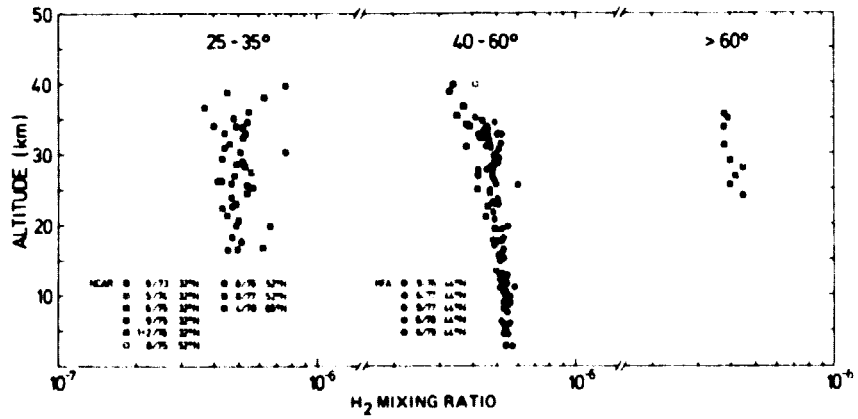

Figure 1-25. Vertical profiles of H_2 at different latitudes. The NCAR data are published by Pollock et al. (1980) and Ehhalt et al. (1975a, b), the KFA data by Volz et al. (1981b), and Fabian et al. (1979, 1981).

Methane (CH_4)

Vertical profiles of CH_4 have been measured since 1965. Most of the sampling flights were performed at 32°N, 44°N, and 52°N. Only data from two flights exist for latitudes >60° (NAS) and only one profile for the tropics. Measurements were performed either by gas chromatography on grab samples and cryogenic samples collected in situ during balloon and aircraft flights or by using long path infrared absorption from balloons. In Figure 1-26 the results are plotted separately in four latitude bands. All NCAR measurements made prior to 1974 were multiplied by a factor of 1.2 (Heidt and Ehhalt, 1980).

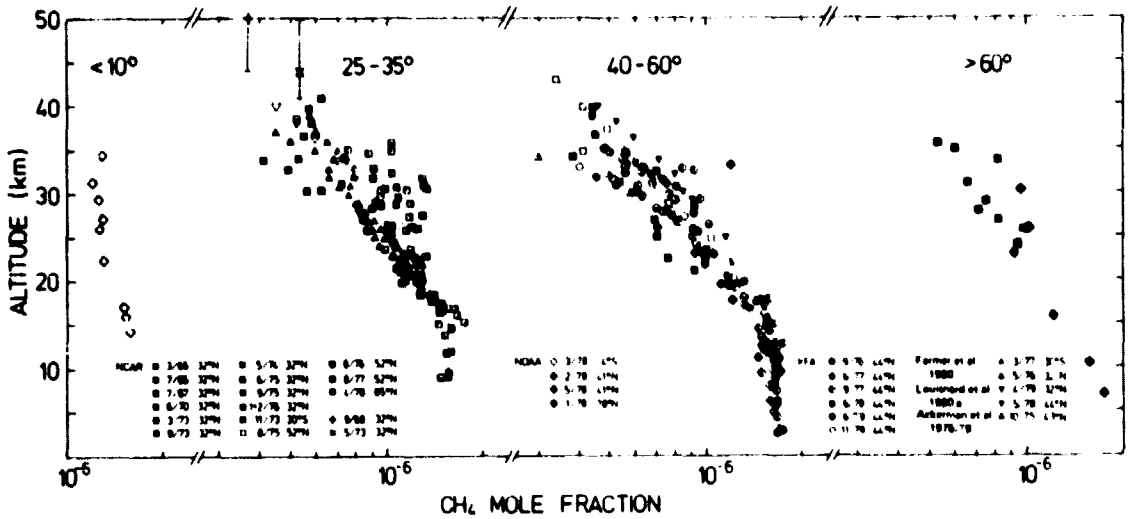

Figure 1-26. Vertical profiles of CH_4 at different latitudes. The NCAR data by Pollock et al. (1980), Ehhalt and Heidt (1973a,b), Ehhalt et al. (1974, 1975a, b); the NOAA data by Bush et al. (1978); and the KFA data by Volz et al. (1981b), Fabian et al. (1979, 1981). The NCAR data prior to 1975 were corrected by a factor of 1.2 (Heidt and Ehhalt, 1980).

At first glance, only the tropical profile deviates significantly from the others, showing a much weaker gradient in the stratosphere. This behavior, which is also confirmed by the profiles of other long-lived trace gases such as N_2O and FC-12, signifies a considerably stronger upward transport in the tropics than in mid-latitudes. A closer investigation shows some minor but still significant differences among the mid-latitude profiles. The average profile at 32°N shows only a very weak gradient between 20 and 30 km, and on several occasions, profiles with a well-mixed layer in this altitude range were observed. This behavior can be explained by the stratospheric branch of the tropical Hadley circulation displacing air from the tropical mid-stratosphere with a weak CH_4 gradient into the lower stratosphere at 30°N, (Ehhalt and Tonnissen, 1980). On some occasions, layers of almost constant mixing ratio were also observed at 44°N. In addition, from the individual profiles collected at 44°N, there is a slight hint of a seasonal variation of the stratospheric CH_4 concentration, especially above 25 km, where the average profile shows a relatively large variability compared to lower altitudes. At higher latitudes, the data though sparse indicate a more or less linear decrease of the CH_4 mixing ratio with altitude above the tropopause.

In principle there is good agreement between the remote and the in situ measurements, except for one profile by Ackerman et al. (1978) obtained in October 1975 over Southern France (43°N). This profile shows a much steeper gradient of CH_4 than is found by both in situ and the other IR observations. A similarly steep gradient was also observed during a flight over Texas (32°N) in June 1975 (Pollock et al., 1980).

Ethane, Propane and Acetylene (C_2H_6, C_3H_8, and C_2H_2)

Only three of the hydrocarbons present in the troposphere have been observed in the stratosphere; ethane, C_2H_6, propane, C_3H_8, and acetylene, C_2H_2. The tropospheric background mixing ratios of these species are quite low; around 1 to 2 ppb for C_2H_6 and up to several hundred ppt for C_3H_8. In addition, they show a strong latitudinal gradient with even lower values at the Equator. The C_2H_6 mixing ratio at the Equator is lower by about a factor of five; C_3H_8 and C_2H_2 decrease by a factor of ten (Rudolph et al., 1979; Singh et al., 1979; Harrison et al., 1979; Cronn and Robinson, 1979). Because of their low tropospheric concentrations the fluxes of these gases into the stratosphere are small and their impact on the stratosphereic carbon and hydrogen budgets is negligible. Singh and Hanst (1981) have proposed that oxidation products of ethane and propane are important carriers of reactive nitrogen.

C_2H_6 and C_3H_8 react rapidly with atomic chlorine, Cl, and can decrease the Cl concentration significantly in the lower stratosphere (Aikin et al., 1980; Rudolph et al., 1981). Measured profiles of C_2H_6 have been used to deduce the vertical profile of Cl atoms in the lower stratosphere, where direct observation of Cl atoms is not yet feasible (Rudolph et al., 1981).

The measured vertical profiles of C_2H_6, C_2H_2, C_3H_8 are shown in Figures 1-27 through 1-30. All of these gases exhibit a strong decrease in the mixing ratio with altitude. The measured profiles of C_2H_2 and C_3H_8 agree reasonably well with those predicted from a one-dimensional steady-state model. In contrast C_2H_6, which is destroyed by reaction with Cl, decreases less steeply than predicted. This has been interpreted to indicate substantially lower Cl-atom concentrations in the lower stratosphere than predicted by models (Rudolph et al., 1981).

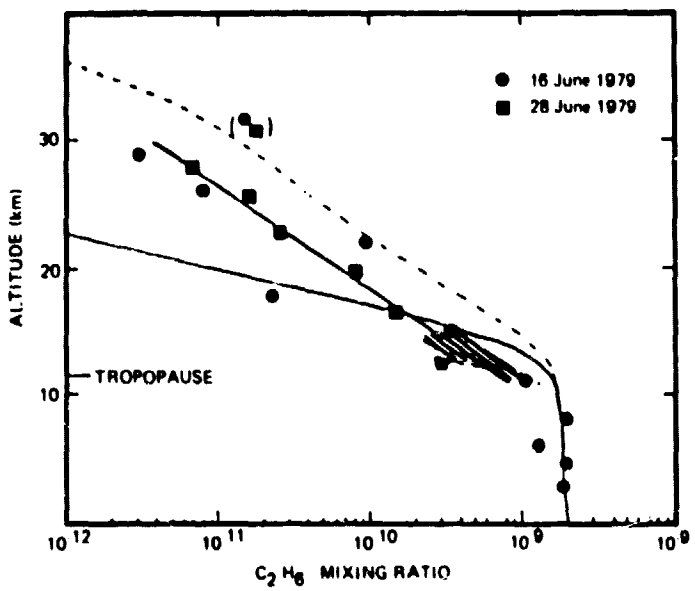

Figure 1-27. Vertical profiles of the C_2H_6 mixing ratio in the stratosphere over Southern France 44°N latitude (Rudolph et al., 1981). The stippled area shows the range of data by Cronn and Robinson (1979) over San Francisco Bay area (37°N) in April 1977.

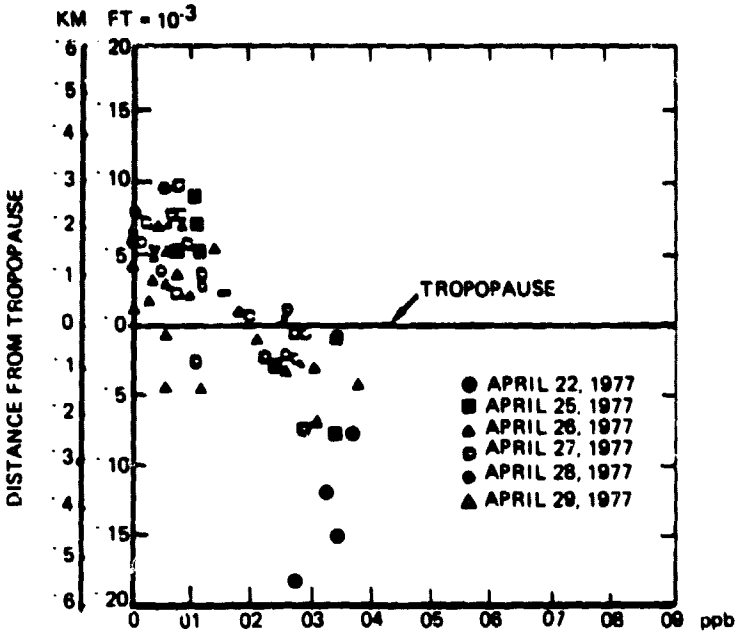

Figure 1-28. Distribution of acetylene relative tc tropopause height. The latitude range of the samples from the first flight were 36 to 47°N and 36 to 38°N for the remaining flights.

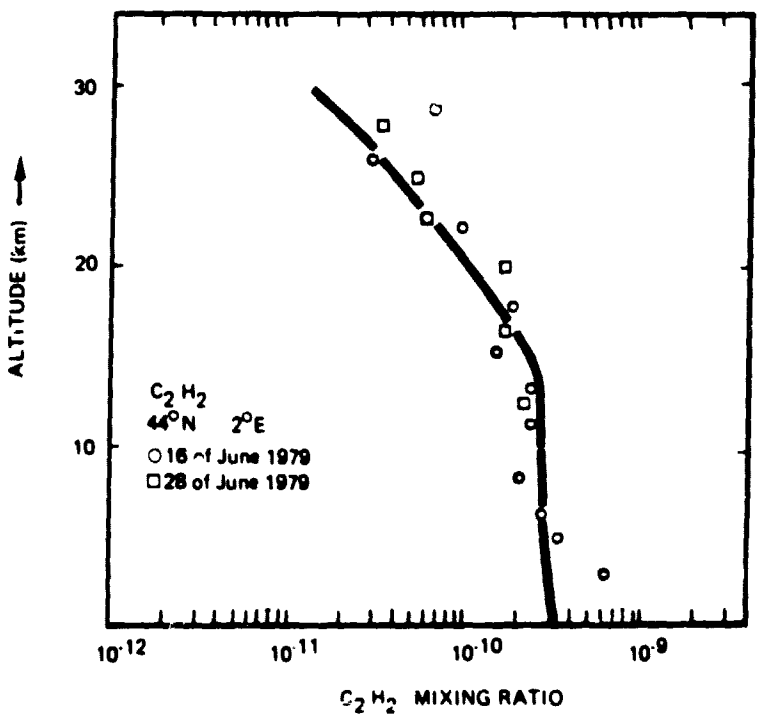

Figure 1-29. Vertical profiles of the C_2H_2 mixing ratio in the stratosphere over Southern France, 44°N latitude (Rudolph et al., 1981).

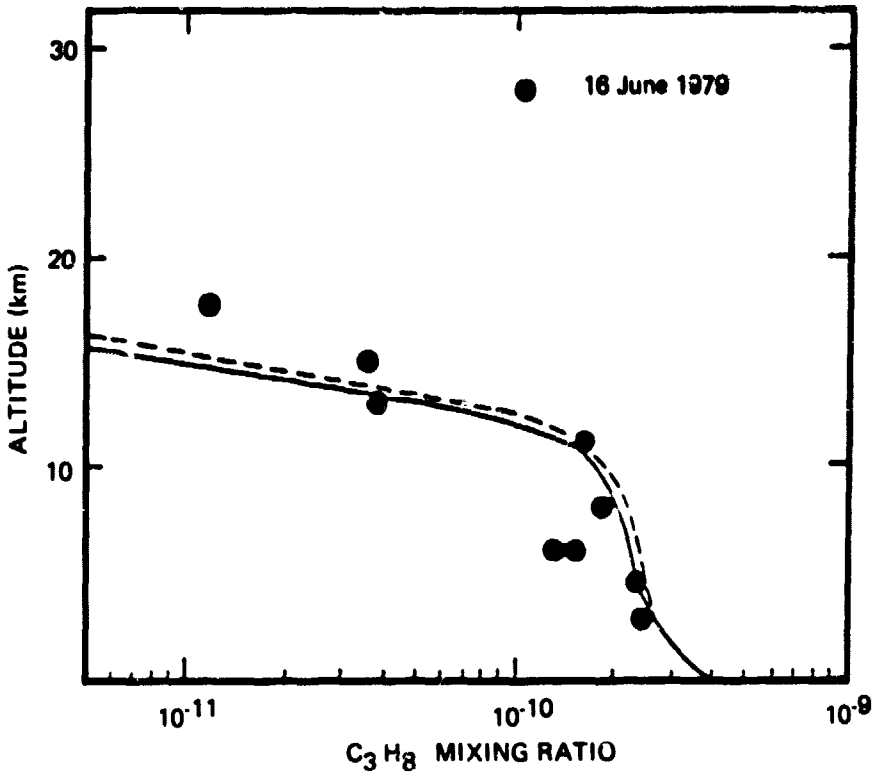

Figure 1-30. Vertical profiles of the C_3H_8 mixing ratio in the stratosphere over Southern France, 44°N latitude (Rudolph et al., 1981).

STRATOSPHERIC WATER VAPOR (H_2O)

Introduction

Ellsaesser et al. (1980) discussed the knowledge of the physical and chemical properties of stratospheric H_2O in 1979. In that work, a compilation of measured profiles was given in graphical form and a number of conclusions were drawn. In general, the basic Brewer theory of tropical "freeze drying" within the rising equatorial branch of the Hadley cell was thought to be valid. However, a number of questions remained.

- Are there significant long-period trends in lower stratospheric mixing ratio, suggesting changes in circulation or tropical tropopause temperatures?
- Is the decrease in mixing ratio with height just above the tropical tropopause as identified by Kley et al. (1979) during their only tropical sounding a regular feature of the stratosphere?
- Are there latitudinal gradients of the mixing ratio? If so, are they poleward-directed or equator-directed?
- Are there increases in mixing ratio with height? If so, can the increase be fully accounted for by CH_4 oxidation.

Although only 2 years have elapsed since that survey, some progress has been made in the measurements and the conceptual aspects of water vapor exchange between troposphere and stratosphere. The H_2O mixing ratios are graphically represented in Figures 1-31 through 1-35. An attempt has been made to separate the data according to latitude. A shaded band indicates the range of experimental results obtained from several flights.

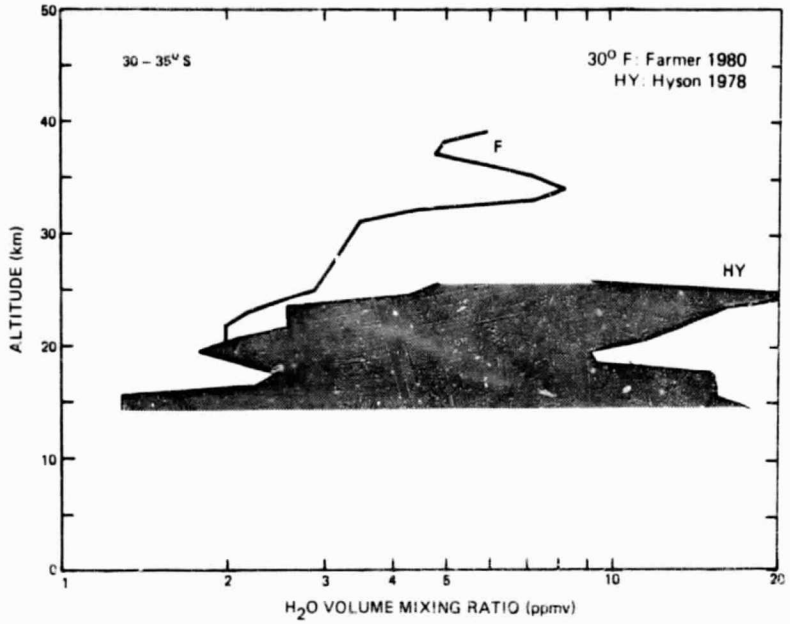

Figure 1-31. Altitude profile of H_2O between 30 and 35°S latitude. If more than one flight was made by a certain group, the stippled area represents the range of their measurement.

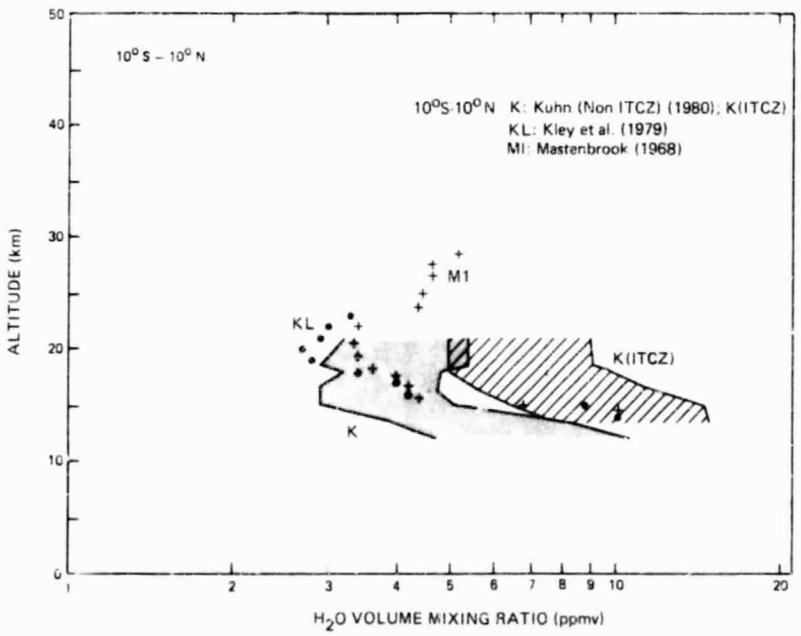

Figure 1-32. Altitude profile of H_2O between 10°S and 10°N latitude. If more than one flight was made by a certain group, the shaded area represents the range of their measurement.

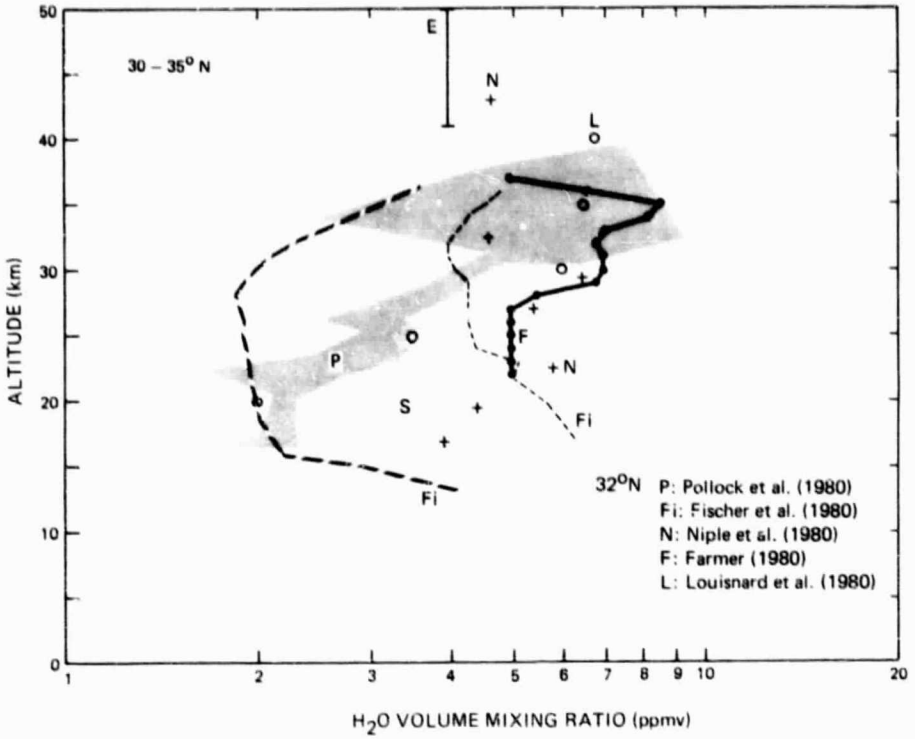

Figure 1-33. Altitude profile of H_2O between 30 and 35°N latitude.

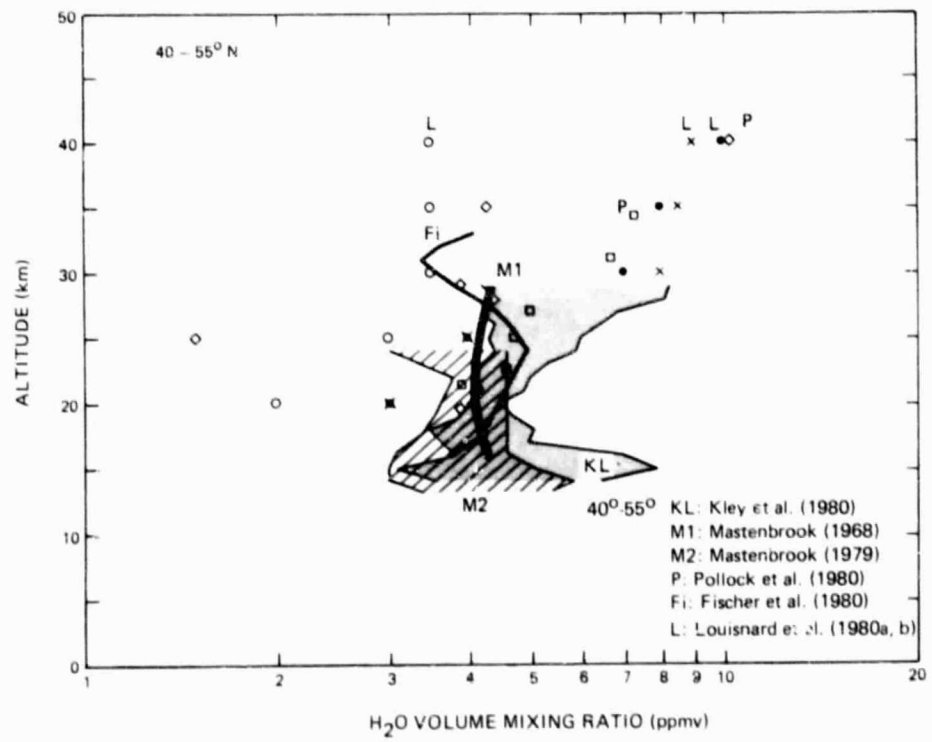

Figure 1-34. Altitude profile of H_2O between 40 and 55°N latitude. If more than one flight was made by a certain group, the banded area represents the range of their measurement.

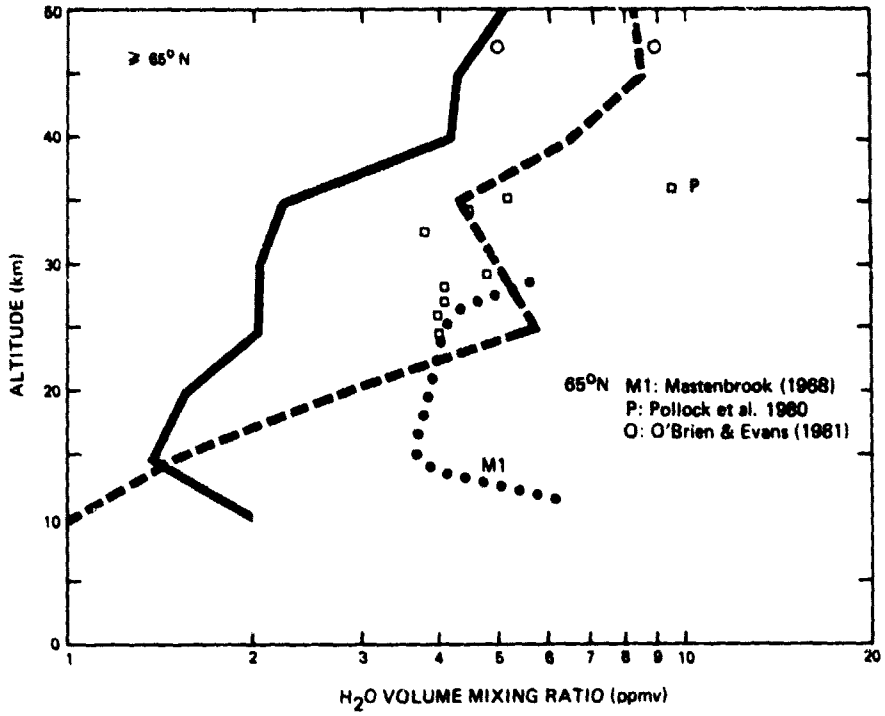

Figure 1-35. Altitude profile of H_2O for altitudes greater than 65°N.

Satellite Measurements

Water vapor profiles have been obtained by the LIMS instrument, extending from the tropopause up to ~50 km, for a number of specific occasions, and generally show a fairly gradual increase of mixing ratio with height over this range. An example of this data is compared in Figure 1-36 with profiles obtained simultaneously by two balloon-borne instruments: an infrared radiometer from the Atmospheric Environment Service (labelled AES), and the WIRS instrument of the National Physical Laboratory. The data agree closely giving encouragement that at least in the lower stratosphere, the LIMS data appears to agree well with independent observations.

In the case of SAMS, full-scale processing has also yet to commence. However, recent work (Colbeck, personal communication) has produced the vertical profile shown in Figure 1-37, which is the average of about five orbits of data. The most interesting feature is the increase of mixing ratio with height, up to a peak at about 50 km. In addition, a poleward-directed gradient of mixing ratio is observed in the limited SAMS data set so far studied.

Other Measurements

Virtually all the observations shown in Figures 1-31 through 1-35 show an increase in H_2O mixing ratio between the tropopause, or in some cases a somewhat higher level, and 30 or 40 km altitude. The satellite observations and some of the earlier measurements (O'Brien and Evans, personal communication; Radford, 1977) seem to indicate a marked peak in the H_2O mixing ratio at the 55 to 60 km level. However, Rogers et al. (1977) and Waters et al. (1980) have reported constant mixing ratios, centered around 4 ppmv at these altitudes. Since there are no theoretical arguments for large mixing ratios peaking around 55 to 60 km, confirming measurements are needed before those results can be considered real.

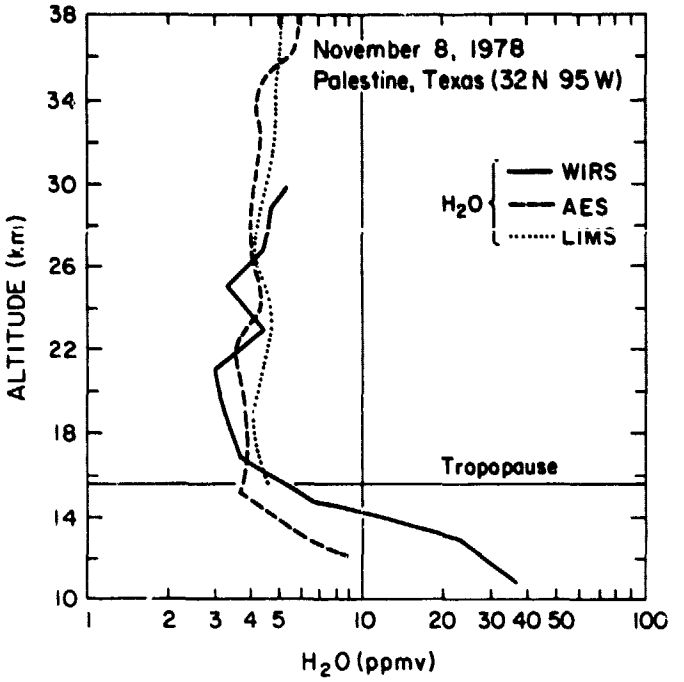

Figure 1-36. Measurements of H_2O mixing ratio over Palestine, Texas on November 8, 1978 by two balloon-borne in situ instruments (WIRS and AES) compared to the LIMS profile retrieved with the operational algorithm (Gille and Russell, personal communication).

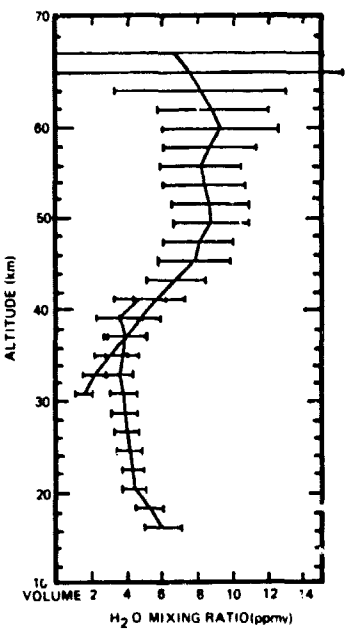

Figure 1-37. A preliminary retrieval from two of the five water vapor channels of the Nimbus 7 SAMS instrument (after Colbeck, personal communication). Data in a latitude band from 55 to 5 N are averaged together for April 4, 1979. The error bars increase at the higher levels due to the lack of information in these channels.

A search of Figures 1-31 through 1-35 for latitudinal gradients of water vapor does not provide valuable information. If the Brewer mechanism is conceptually valid, none would be expected. However, since in this concept other constituents enter the stratosphere (together with water) at the tropical tropopause, methane would be injected and slowly oxidized on its poleward transport so that the stratospheric column density of water vapor would be expected to increase toward the poles. The increase of the mixing ratio with altitudes shown on all of the Figures 1-31 through 1-35 is not sufficient proof that the methane oxidation mechanism has been detected. It is probably safe to assume that any latitudinal effect due to CH_4 oxidation is masked by errors, relative and absolute. We must wait for more latitudinal surveys, preferably done with the same instrument. As already stressed (Ellsaesser 1980) those surveys must be made from platforms operating well above the tropopause, such as satellites.

Louisnard et al. (1980a,b) have measured H_2O and CH_4 simulataneously using IR absorption spectroscopy and obtained values of the ratio CH_4/H_2O shown in Figure 1-38. They conclude that the slight increase in H_2O observed above 28 km is compatible with the CH_4 source, but that the faster increase between 20 and 28 km cannot be attributed to this source. Pollock et al. (1980) report measurements of CH_4 and H_2O as did Farmer et al. (1980), and these results are also shown in Figure 1-38. Figure 1-38b shows the ratio R, where R is given by:

$$R = 2\ \Delta[CH_4]/\ \Delta[H_2O]$$

where the differences, Δ, are calculated from the value at the lowest level of observation.

This ratio, R, should equal unity if CH_4 oxidation is the only source of H_2O in this height interval. Figure 1-38a indicates reasonably good agreement in the ratio CH_4/H_2O between observers giving values of ~0.2 to 0.3 at 25 km to ~0.08 to 0.15 at 35 km. Although the scatter in the ratio, R, (Figure 1-38b) is much worse, the values are universally <1.0; this implies that the increase in H_2O with height is larger than would be expected from CH_4 oxidation alone.

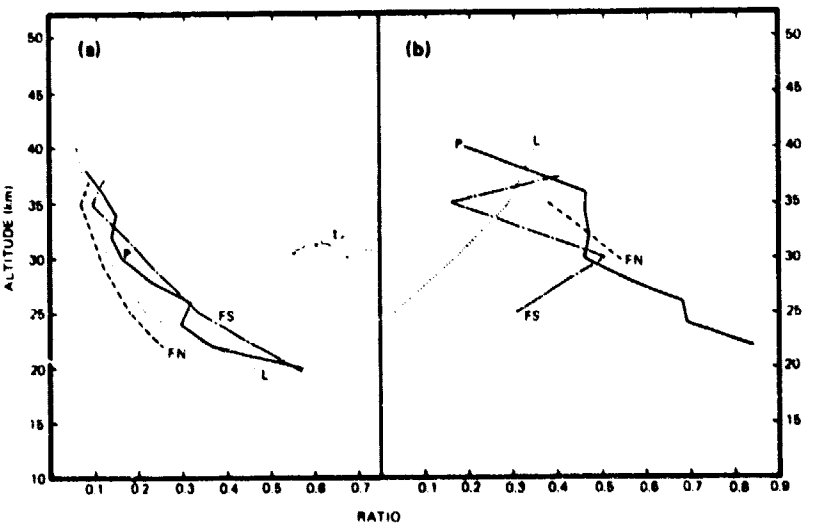

Figure 1-38. (a) The ratio $[CH_4]/[H_2O]$ taken from Farmer et al. (1980), Pollock et al. (1980), and Louisnard et al. (1980b).

(b) The ratio, R, (see text) formed from the same data. The differences were obtained by subtracting the mixing ratio at the lower level at which both H_2O and CH_4 were observed, from the values at higher levels. In the case of Pollock et al., a single average of many measurements is shown.

A new in situ device, developed by Kley and his associates (Kley et al., 1979; Kley and McFarland, 1980) has now evolved as a powerful technique. These authors have built a sensitive instrument with a fast response time for balloons and aircraft which can resolve tens of meters in the vertical. Measurements of H_2O and temperature in mid-latitudes (Wyoming) generally show undersaturation in the upper troposphere although on one flight in Brazil (Kley et al., 1979) saturation was observed at the tropical tropopause. The results of the Brazil flight are shown in Figure 1-39. However, previous observations by Dobson and coworkers (Brewer, 1949; Dobson et al., 1946) over southern England (~52°N) have shown cases of both saturation and undersaturation below the tropopause. Saturation would indicate a contradiction to the Brewer model. Even super-saturation has been observed (Dobson et al., 1946; Kley et al., 1980). It was pointed out by Kley et al. (1979) that tropical stratospheric air has a minimum mixing ratio at about 60 mb or 19 km (see Figure 1-38). This is well above the tropopause. Robinson (1980) has found more examples from literature studies. These observations indicate that the simple Brewer mechanism needs to be refined.

The second aspect of the work of Kley et al. is the structure observed in more recent soundings (Kley et al., 1980). Larger structure (the "fine structure") on a 1 to 2 km width and structure on a scale of 200 to 400 m (the "micro-structure") were observed (Figure 1-40, Kley et al., 1980). This layering should be confirmed by other groups, however, since fine-structure and micro-structure was repeated on ascent and descent it suggests that the structure was real. Other soundings (Kley et al., unpublished results) gave micro-structure that was different on ascent and descent. It is possible that, due to swinging of the payload, extraneous water from other parts of the payload could have contributed to the observed micro structure on those occasions. Kley et al. also find a significant correlation between water and ozone in the lower stratosphere. This is discussed in detail in Chapter 2.

Another set of water vapor data are the frost point measurements of Mastenbrook that are being continued by NOAA. In a recent paper (Mastenbrook and Daniels, 1980) data from four flights over Washington, D.C. during the early part of 1979 are reported. A map of annual variations of stratospheric H_2O over Washington, D.C., based on 12 years of data, is presented here in Figure 1-41.

The composite water vapor profile of Figure 1-41 is recommended for chemical modeling purposes in the lower stratosphere at mid-latitudes ($z < 20$ km). In the higher stratosphere, up to the stratopause, no such recommendation can be given at this time. Mastenbrook's instrument tends to produce altitude independent mixing ratios whereas Kley's instrument normally gives a moderate increase of 1 to 3 ppmv between tropopause and 32 km at mid-latitudes. The issue is unresolved and, therefore, most of the data collected in Figures 1-31 through 1-35 should be considered of equal weight at this time.

For the equatorial lower stratosphere it is suggested that Figure 1-39 be used. This profile is similar to earlier ones by Mastenbrook (1968) but shows the hygropause clearly. It should be noted that it is the minimum in water vapor some 3 km above tropical tropopause that was referred to as hygropause by Kley et al. (1979).

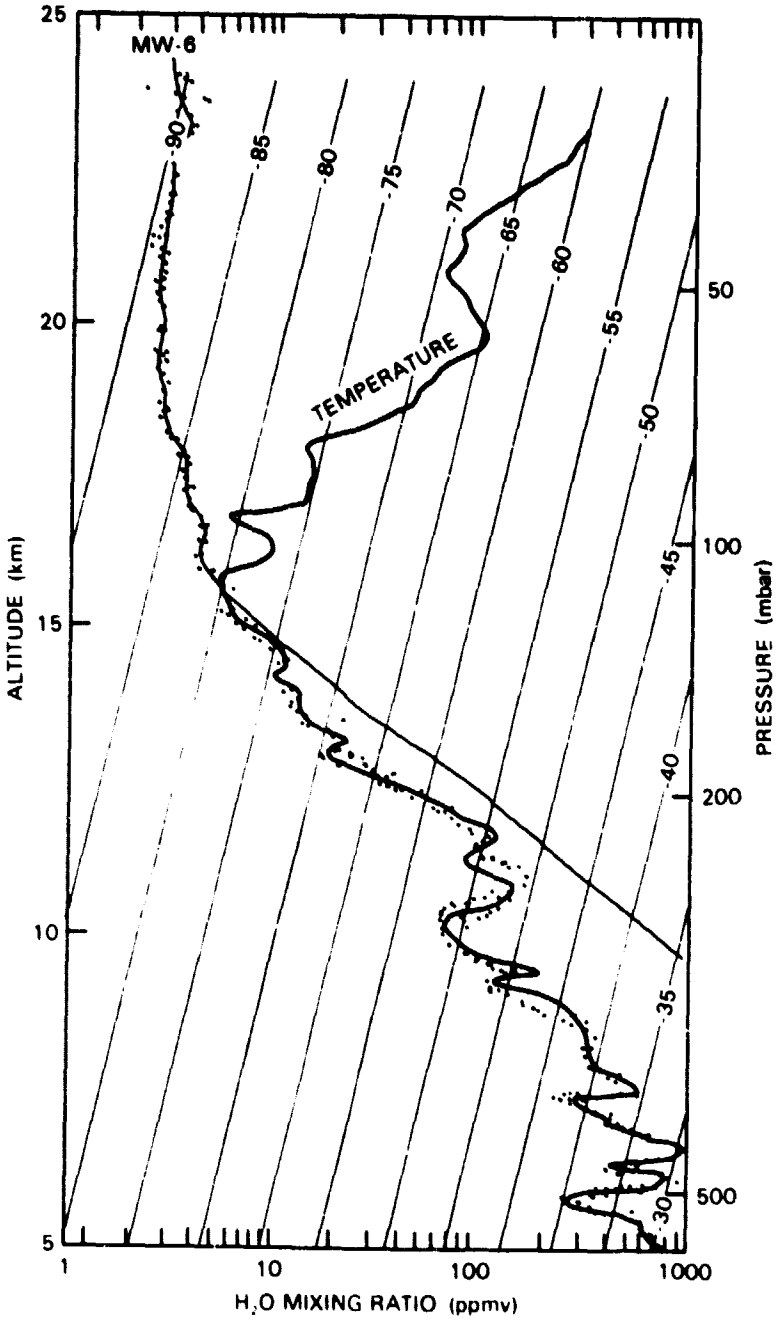

Figure 1-39. The water vapor mixing ratio measured over Quixeramobim, Brazil, on September 27, 1978, (Kley et al., 1979).

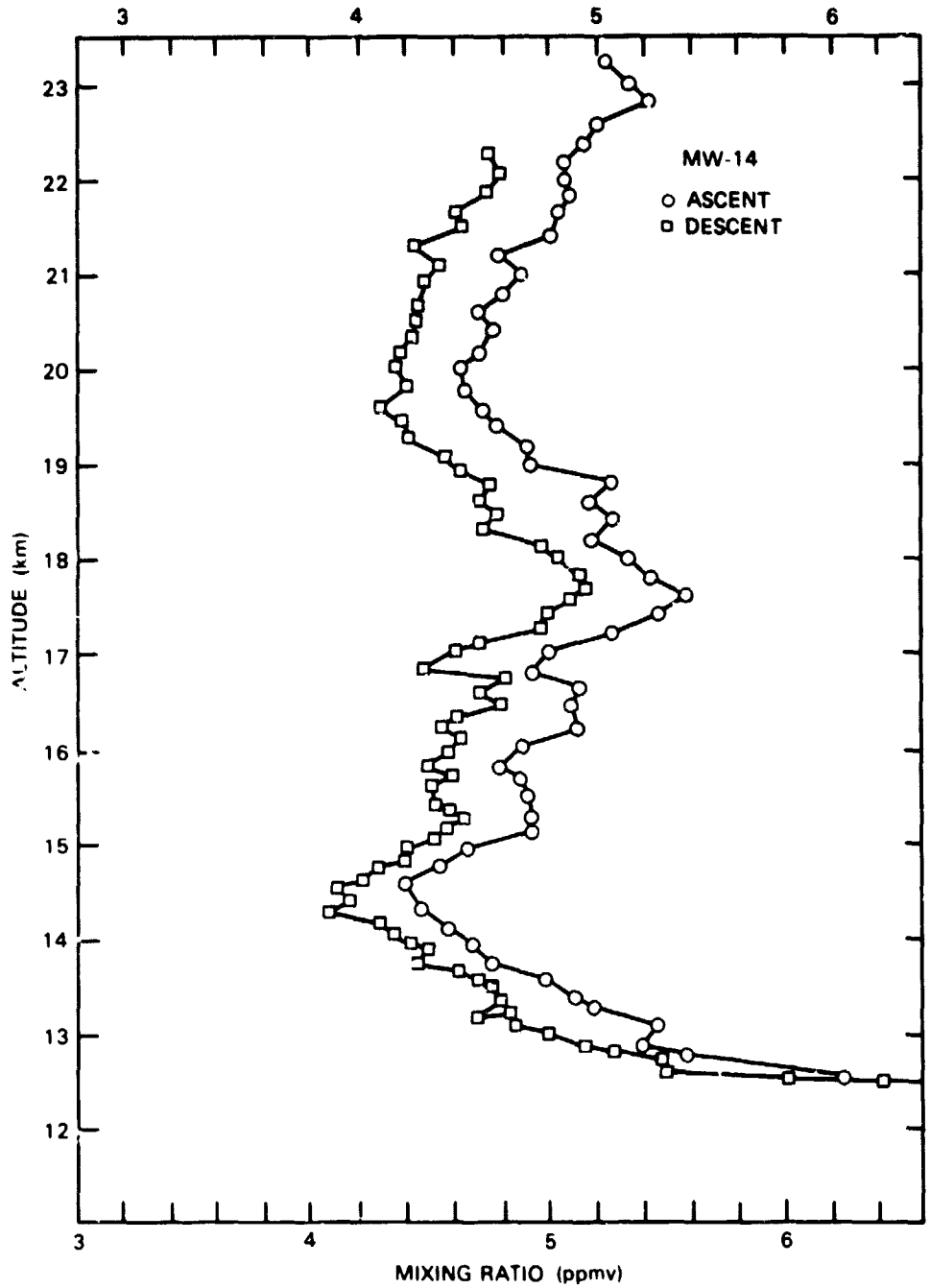

Figure 1-40. Measurements of water vapor on January 5, 1981 over Wyoming, during ascent and descent, illustrating the reproducibility of the observed structure, (Kley et al., 1981 unpublished). Note the offset of 0.2 ppm between the horizontal scales.

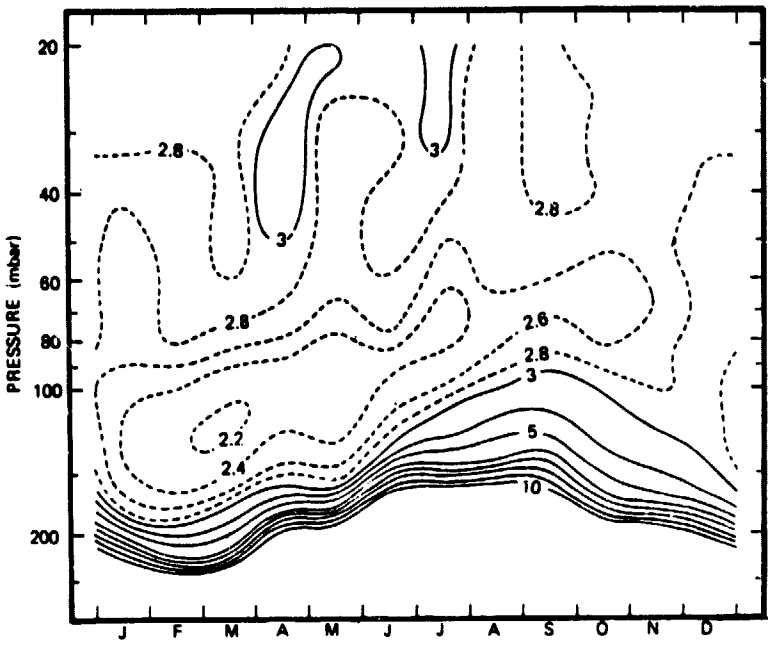

Figure 1-41. The mean annual variation of stratospheric water vapor at Washington, D.C., based on 12 years of data by Mastenbrook and Daniels (1980).

COMPARISON OF MEASUREMENTS AND MODEL CALCULATIONS FOR STRATOSPHERIC SOURCE GASES

During the last 2 years, considerable progress has been made in the development of two-dimensional (altitude plus latitude) chemical models of the stratosphere. The 2-D models are approaching the completeness of 1-D models, with complete chemical species, diurnal effects, multiple Rayleigh scattering, etc. A description of the structure of many of the existing 2-D atmospheric models is given in Table 2-14 of Chapter 2. Since measurements of long-lived source species are available for several latitude regions, only 2-D models will be used for comparison with the observations.

Several two-dimensional modeling groups participated in the Workshop (Oxford, NASA Ames, Canada AES, Univ. of Oslo). In this report calculations obtained using the AER (Ko et al., 1981) and the Du Pont (Miller et al., 1981) 2-D models will be given as examples of the current 2-D results. These two models differ considerably in their model structure and transport data base (see Table 2-14), so their use allows a first-order assessment of the sensitivity of results to these features of the model formulation. Both models used the most recent NASA/CODATA (1981) chemical reaction rate set.

Several long lived trace species, such as N_2O, CH_4, H_2, CFCs, CH_3Cl, and CO, are primarily of tropospheric origin. These species are the sources of the free radicals and other relatively short-lived species in the stratosphere. Since the photochemistry of these source species is relatively simple and thought to be fairly well characterized, the latitudinal and vertical distributions of these species are strongly dependent on the parameterization of transport processes. Because of this, these species (particularly N_2O) are often used to derive the vertical diffusion coefficient K_{zz} in 1-D models or to tune the transport parameterization.

Atmospheric measurement programs have led to a significant increase in our knowledge of the variation of the vertical distributions of these long-lived trace species with latitude. It is now possible to make detailed comparisons between the measured and calculated latitudinal variations. These comparisons can test the 2-D models' ability to reproduce the important features of atmospheric transport. Although such comparisons clearly cannot "validate" the models, they provide the first step in assessing the utility of the 2-D models as diagnostic and predictive tools.

NITROUS OXIDE (N_2O)

The observed N_2O vertical profile for the equatorial region is shown in Figure 1-42, along with the calculations. The Du Pont calculations include a band giving the range of the modeled results over the latitude band in question and the seasons of the year, while the AER calculations are for July and are shown as the dashed profiles.

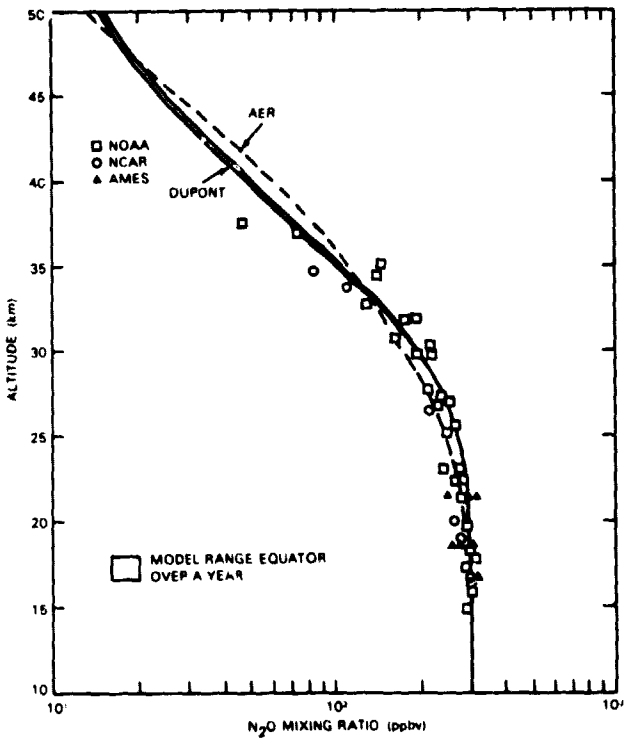

Figure 1-42. N_2O vertical mixing ratio profiles in the tropics. Points are observations. Solid lines give the range of values over seasons from the Du Pont 2-D model (C. Miller et al., 1981). Dashed curve gives results of AER 2-D model (Ko et al., 1981) for summer.

Figure 1-43 gives a similar compilation for mid-latitude observations. The N_2O concentration falls off with altitude much more rapidly at mid-latitudes than at the Equator, with values at 30 km of 60 ppb and 200 ppb, respectively. The mid-latitude observations also seem to show considerably more variability, perhaps due to seasonal changes in transport. Both of these features are qualitatively reproduced by the models. The smaller vertical gradient in the tropics is a manifestation of the rising mean circulation, which carries tropospheric air up into the stratosphere. The seasonal variations are enhanced at mid-latitudes due to both greater seasonal differences in the mean transport and to seasonal changes in the N_2O photolysis rate.

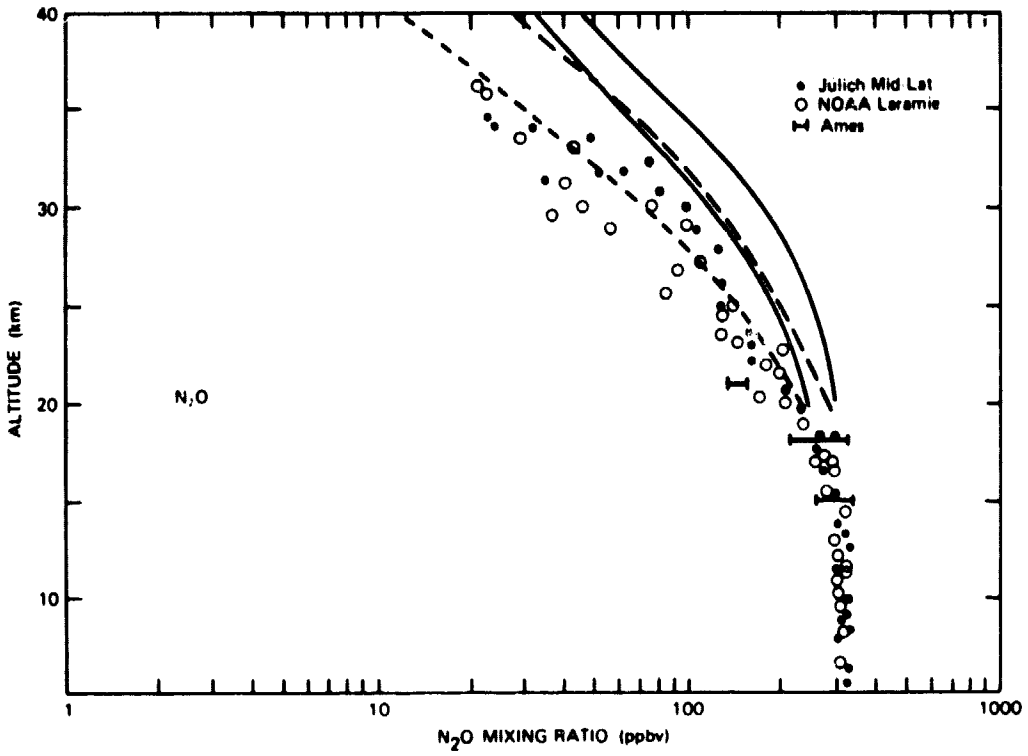

Figure 1-43. N_2O vertical mixing ratio profiles near 45°N latitude. Points are the summer observations. Solid lines are range of seasonal variations in the Du Pont model. Dashed lines give AER profiles for July; upper curve = 30°N, lower curve = 50°N.

The AER model exhibits somewhat better agreement with the measurements at mid-latitudes, with calculated mixing ratios in the 30 to 40 km region about a factor of two lower than that in the Du Pont model. This is probably due to a slower effective vertical transport rate at mid-latitudes in the AER model.

METHANE (CH_4)

The observations and model calculations for methane are shown in Figure 1-44. Most of the observations are from 25°N to 60°N. In this region, the Du Pont model fits the data quite well, while the AER model is somewhat lower than the mean. The differences between the various measurements are somewhat larger than the 2-D models would calculate on the basis of annual variations, particularly around 30 km in the 25°N to 35°N band.

As with the 1-D models, it is difficult for a 2-D model to simultaneously fit mid-latitude vertical profiles for both N_2O and CH_4 with the same transport parameterization. This may be due either to an inaccurate description of the photochemistry of these two species or to the inability to accurately parameterize the eddy diffusion of all species using the same diffusion coefficients. (See the discussion in Chapter 2).

There unfortunately exist few high-latitude or low-latitude CH_4 measurements. The only measured vertical profile in the tropics shows no gradient between 25 and 35 km, while the models calculate a decrease by a factor of four.

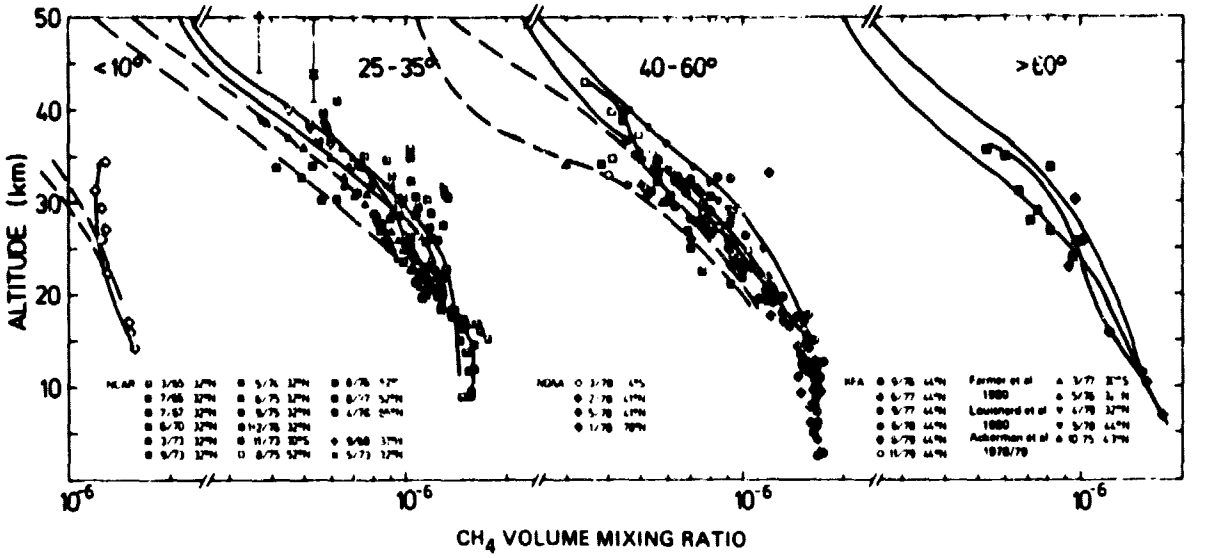

Figure 1-44. CH_4 vertical mixing ratio profiles for selected latitude bands. Observations are the points. Solid and dashed curves give seasonal variations in the latitudinal regions obtained with the Du Pont and AER models, respectively.

MOLECULAR HYDROGEN (H_2)

Measurements of H_2 are essentially limited to mid-latitudes. As shown in Figure 1-45, the measurements are characterized by a constant mixing ratio from ground level up to 30 km, with a decrease above that altitude. Data above 40 km are needed to verify this decrease. The spread in the observations is greater than calculated by seasonal variations in the model, particularly near 30°N.

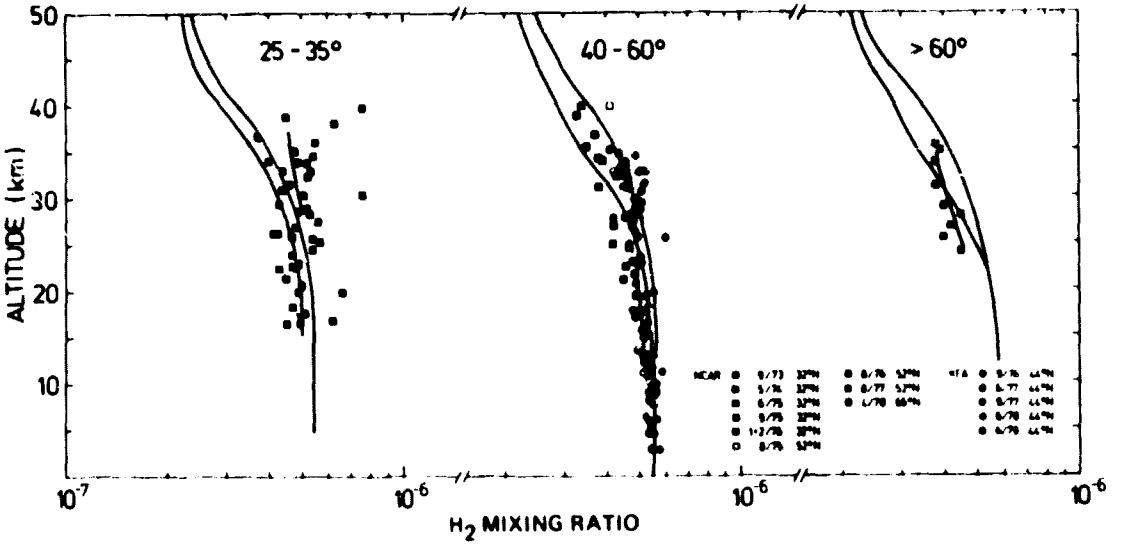

Figure 1-45. H_2 vertical mixing ratio profiles for selected latitude bands. Observations are the points. Solid curves give seasonal variations calculated with the Du Pont model.

As is the case with 1-D models, the 2-D models seem to show a slightly more rapid decrease with altitude above 30 km than the observations suggest. This is most evident in the comparison with data at 30°N, where a discrepancy is implied if the measurements are correct. Since H_2 has a photochemical source throughout the atmosphere, it is possible that the differences between the models and the observations may be due to a remaining inaccuracy in the chemical scheme.

MONOFLUOROTRICHLOROMETHANE (CCl_3F, FC-11)

The atmospheric measurements discussed in this section were obtained by several groups during the years 1976-1979. During this 3-year period, the tropospheric concentrations of the chlorine species CCl_3F and CCl_2F_2 increased by about 30%. In this section, the vertical profile measurements presented earlier in this chapter for FC-11 and FC-12 have been temporally scaled to represent mid-1980 values.

The equatorial measurements and calculations for CCl_3F are shown in Figure 1-46. The observations are characterized by a decrease in the mixing ratio between 20 and 30 km by a factor of about 30. The calculations also show a rapid decrease, but at 30 km they fall somewhat above the observations. The mid-latitude comparison is shown in Figure 1-47. Here the models overestimate the CCl_3F mixing ratio by about an order of magnitude at 30 km, as do the 1-D models.

A possible cause of this discrepancy may be an underestimate of the photolysis rate of CCl_3F. FC-11 photolysis depends sensitively on the penetration of radiation through the Schumann-Runge region of the molecular oxygen spectrum. Frederick and Hudson (1980) obtained more penetration of UV in the Schumann-Runge region than previously calculated. Observations obtained on a balloon flight indicate that the penetration is even greater than calculated by Frederick and Hudson (Hudson, personal communication, 1981).

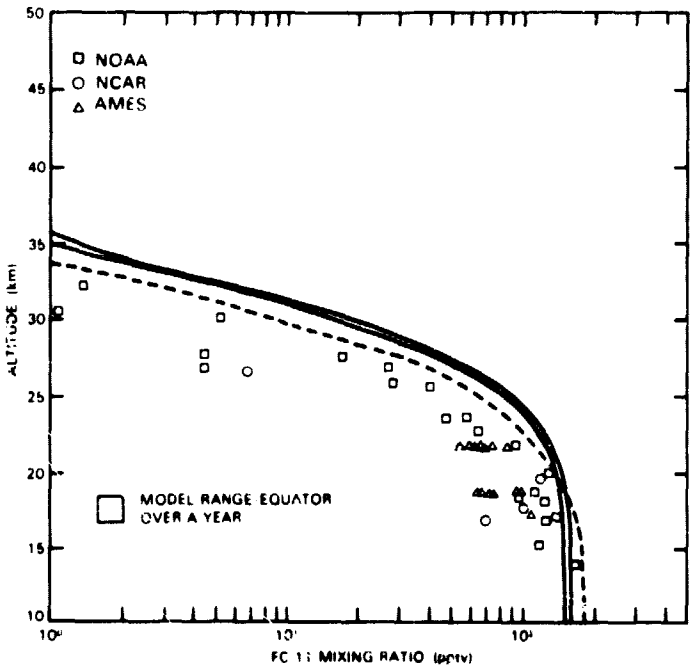

Figure 1-46. FC-11 vertical mixing ratio profiles in the tropics. Points are the observations, scaled to mid-1980. Solid lines give range of seasonal variations in the Du Pont model. Dashed curve gives summer profile from the AER model. Model calculations are for the year 1980.

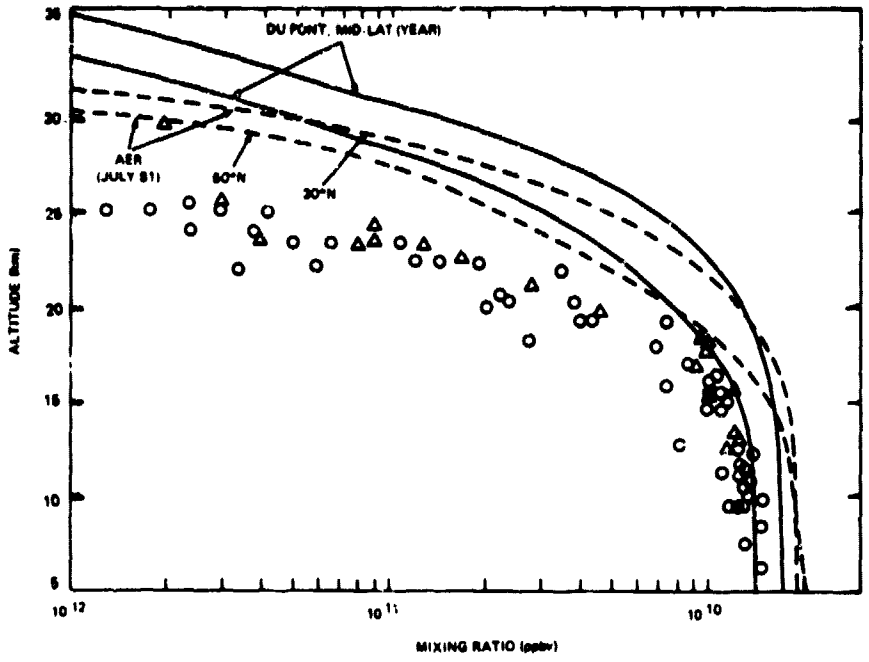

Figure 1-47. FC-11 vertical mixing ratio profiles for mid-latitudes. Similar to Figure 1-46. The upper and lower AER curves are for 30°N and 50°N, respectively.

An alternate suggestion is that the mid-latitude discrepancy for FC-11 may be due to an inaccuracy in the transport parameterization. If K_{yy} in the lower stratosphere were reduced, the mid-latitude vertical gradient for FC-11 would increase. It is possible that such an adjustment could decrease the discrepancy for FC-11, which has a relatively short atmospheric lifetime (~60 years), without adversely affecting the currently better agreement between models and observations for longer-lived species like N_2O and FC-12.

DIFLUORODICHLOROMETHANE (CCl_2F_2, FC-12)

Figure 1-48 gives the comparison between the calculations and the observations for FC-12 in the equatorial region. The agreement between the different experimental groups and the models below 30 km is quite good. Above 30 km, the few measurements cover a large range of values, with the model calculations falling at the upper end of the observations.

At mid-latitudes, (see Figure 1-49), the observations exhibit a spread by a factor of five above 30 km. This is somewhat greater than the factor of two variation calculated to occur over the latitude range from 30°N to 50°N. Both models predict too much FC-12 above 25 km, with the discrepancy apparently increasing monotonically with altitude. The AER model, due to its slower vertical transport, seems to fit the observations somewhat better.

The contribution to FC-12 photolysis from the Schumann-Runge region is important. Some of the discrepancy between models and measurements for FC-12 may be due to an inaccurate calculation of Schumann-Runge penetration.

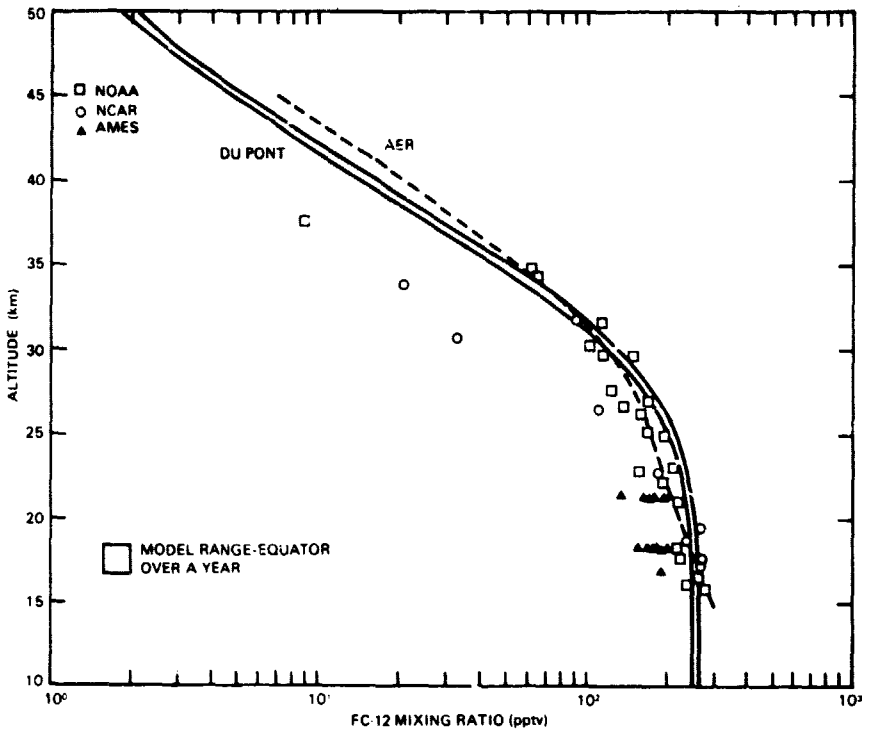

Figure 1-48. FC-12 vertical mixing ratio profiles in the tropics. Similar to Figure 1-46.

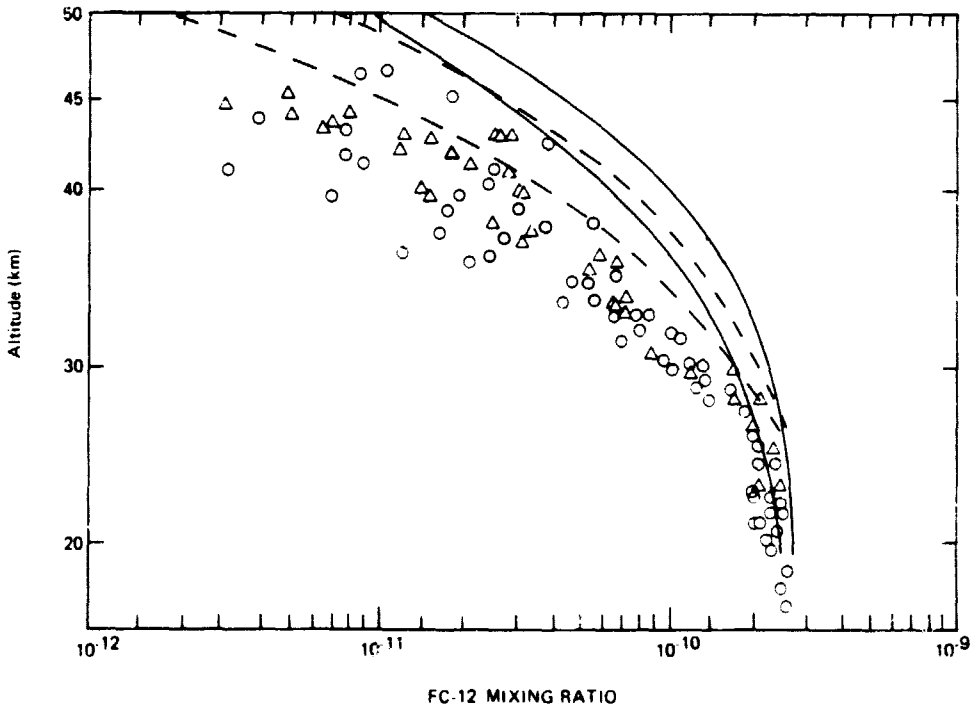

Figure 1-49. FC-12 vertical mixing ratio profiles for mid-latitudes. Similar to Figure 1-47.

METHYL CHLORIDE (CH_3Cl)

Methyl chloride (CH_3Cl), like CH_4, is removed from the stratosphere primarily through reaction with the HO radical, although photolysis accounts for about 30% of the destruction rate above 30 km. Since the HO concentration is sensitive to changes in the chemical data base, the calculations for this species are somewhat uncertain. As shown in Figure 1-50, the models predict about three times as much CH_3Cl at 25 km as the limited observations.

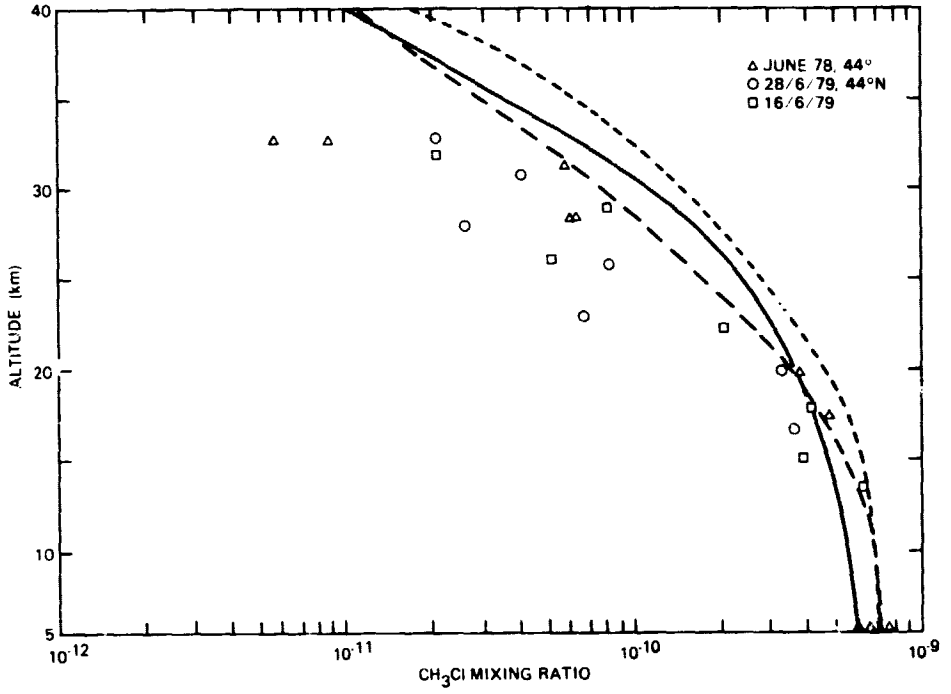

Figure 1-50. CH_3Cl vertical mixing ratio profiles near 45°N. Points are the observations, taken in June. Solid curve is Du Pont profile for 44°N June. Dashed curves are AER model results (upper curve = 30°N, lower curve = 50°N) for summer.

WATER VAPOR (H_2O)

Water vapor is a highly variable constituent of the lower stratosphere, with the complex dynamics of troposphere/stratosphere exchange being important. Most current models fix the H_2O concentration in the troposphere, and some fix it throughout the stratosphere as well. Latitudinal variations are small. Both the 1-D and 2-D models that calculate stratospheric water vapor show an increase of a few ppm from an altitude of 20 km to 50 km, due to methane oxidation, consistent with the mean of the observations.

CARBON MONOXIDE (CO)

Carbon monoxide is distributed nonuniformly through the troposphere, and its lower-tropospheric removal is primarily through reaction with the HO radical. Figure 1-51 compares the limited set of observations presented earlier in this chapter with the calculations. The calculations, which have a specified ground-level CO distribution with latitude, give the qualitative shape of the vertical profile at mid-latitudes and fall near the upper end of the observations. The calculated increase of CO in the upper stratosphere is due to photolysis of CO_2.

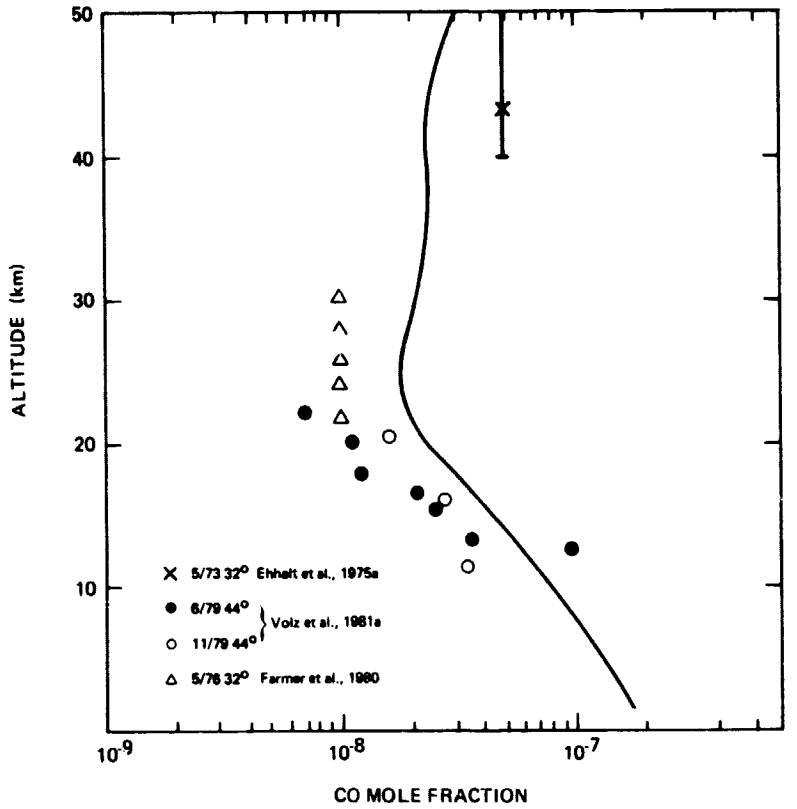

Figure 1-51. CO vertical mixing ratio profiles for mid-latitudes. Points are observations. Solid curve is calculated with the Du Pont model for 30°N latitude, spring/fall.

SUMMARY

The long-lived trace species can be divided into two categories: those which are destroyed primarily by reaction with the HO radical (CH_4, CH_3Cl) and those which are destroyed by photolysis (N_2O, FC-11, FC-12). Although it may be fortuitous, due to transport tuning in many models to fit N_2O, the agreement between models and observations is better for longer-lived trace gases than for shorter-lived species. Of the species destroyed by HO, methane is better modeled than methyl chloride.

For the species destroyed by photolysis, the agreement clearly is worse for the shorter-lived FC-11 than for FC-12 or N_2O. FC-11, especially at mid-latitudes, is the source species which exhibits the largest and best established discrepancy, with the models overpredicting the mixing ratio by an order of magnitude at 30 km altitude. If, as suggested above, this is due to an inadequate parameterization of the Schumann-Runge band absorption, then a more accurate treatment of UV penetration may improve both the 1-D and 2-D model calculations for FC-11.

The two-dimensional models reproduce the qualitative features of the latitudinal changes in the vertical profiles of long-lived trace gases, e.g., the slower vertical decrease at the equator and more rapid decrease at higher latitudes. They have not yet solved the problem, also evident in 1-D models, of fitting the mid-latitude profiles of N_2O, CH_4, and H_2 with the same parameters.

STRATOSPHERIC DISTRIBUTION OF REACTIVE TRACE SPECIES

ODD OXYGEN

The principal oxygen radicals are $O(^3P)$, $O(^1D)$, $O_2(^1\Delta)$, $O_2(^1\Sigma)$, O_2 (other excited states) and O_3. While it is feasible in this section to critically analyze all of the available data on the first five species, a thorough discussion of O_3 is obviously of such magnitude that it warrants special treatment (see Ozone Section). Given that the intention of this document is to describe the current state of our understanding of global ozone this group is obviously unique. Atomic oxygen in the ^1D level is of critical importance for establishing the oxidation rate of source molecules which enter the stratosphere such as CH_4, N_2O etc., but there currently are no observations of (O^1D) in the stratosphere. The electronically excited states, $O_2(^1\Delta)$ and $O_2(^1\Sigma)$, have been observed but the data base is small. The remaining electronically excited states of O_2 ($A^3\Sigma_u^+$, $C^3\Delta_u$, $C\Sigma_u^-$) have not been observed.

Atomic Oxygen ($O(^3P)$)

There are six observations of $O(^3P)$ in the stratosphere, all obtained using a parachute-borne, in situ atomic resonance fluorescence instrument, the results of which are shown in Figure 1-52. Experimental accuracy is ±30% and experimental precision ±10% for each measurement (Anderson, 1975).

Several points are apparent from Figure 1-52. First, there is both local structure within and absolute displacement among observed distributions which exceed respectively the precision and accuracy of the measurements. It should also be noted that the local structure does not appear consistently. For example the profiles observed on October 25, 1977 and December 2, 1977 display a small degree of local structure, typically less than ±20% variation over an interval of ±1 km above approximately 34 km. Below that altitude significantly greater local structure is apparent, though seldom more than ±50%. On the other hand, the remaining four observations exhibit at least one example of major (factor of two) variation over a ±2 km interval with an increasing structural development below the 33 to 35 km interval.

For one observation of atomic oxygen, the ozone concentration was obtained simultaneously, using a modified Dasibi instrument (see Robbins and Carnes, 1978). The two instruments were mounted approximately one meter apart on the descent platform. The results of that observation, which encompass the altitude interval 28 to 42 km, are shown in Figure 1-53. Observations were made with a solar zenith angle of 50° at Palestine, Texas, 32°N latitude on 2 December 1977.

The atomic oxygen-ozone ratio was determined from those observations for each 0.5 km interval and the results are compared in Figure 1-54 with the calculated ratio from the diurnal model of Logan et al. (1978) for a solar zenith angle of 50°. The accuracy of the $(O(^3P))$ and (O_3) observations is ±25%. An inspection of Figure 1-54 indicates that with the exception of the two lowest points at 28 km, the calculated and observed ratios lie well within the experimental uncertainty. Although obviously a single observation cannot be offered as proof, the measurement strongly suggests that O and O_3 are in photochemical steady state and that the photodissociation of O_3 and the three body recombination dominates the exchange between the major odd oxygen species. The question of the atomic oxygen-ozone concentration ratio is currently being addressed using instruments of significantly improved sensitivities and accuracy since a careful examination of this question must precede use of satellite observed ozone profiles to deduce local atomic oxygen concentrations and thus global O_x destruction rates.

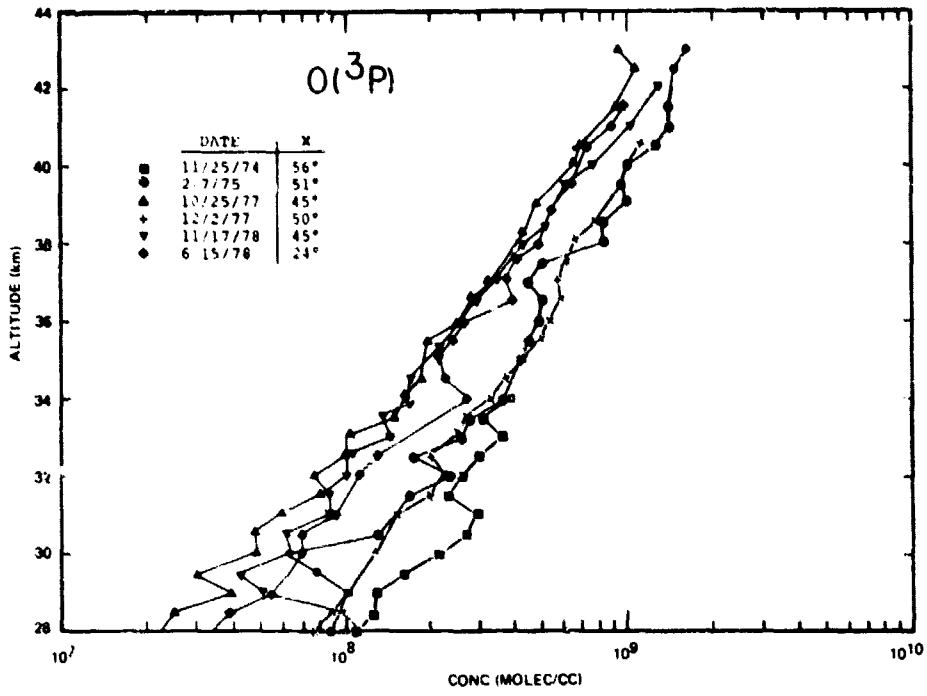

Figure 1-52. Observed concentration of $O(^3P)$ between 28 and 43 km in the stratosphere. All data determined in situ using atomic resonance fluorescence.

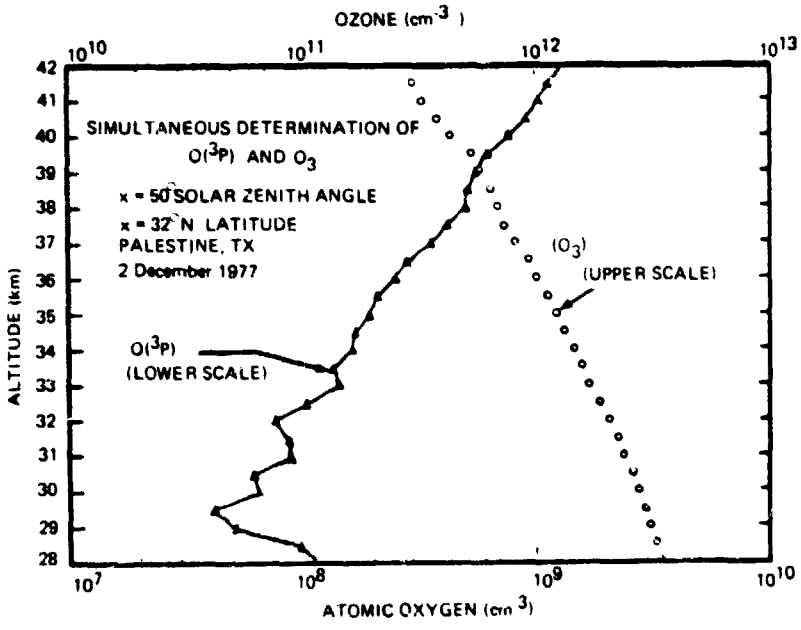

Figure 1-53. Observed concentration of $O(^3P)$ and O_3 determined simultaneously within the same volume element of the stratosphere.

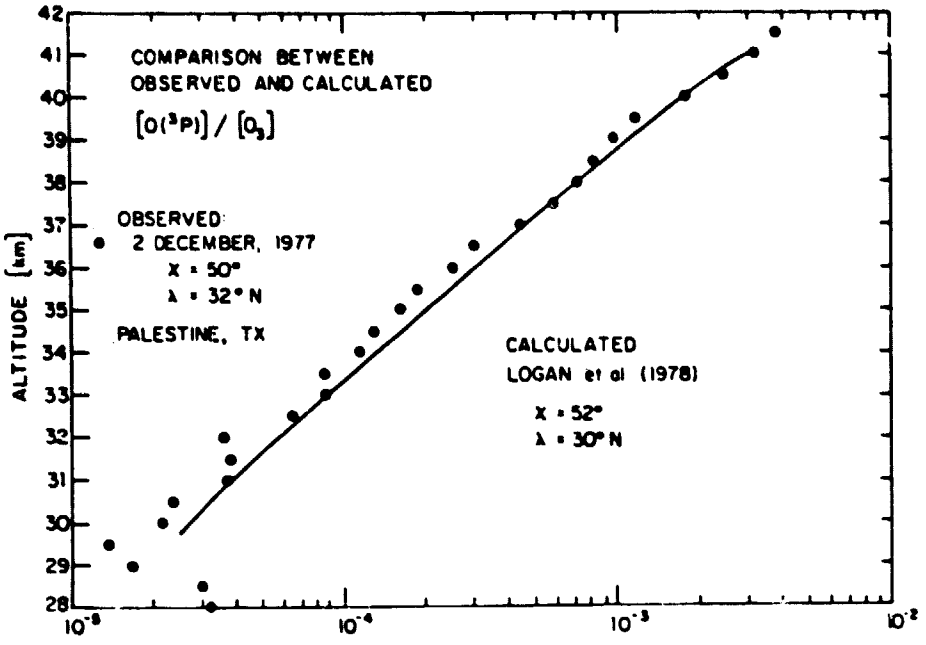

Figure 1-54. Comparison between the measured ratio, $[O(^3P)]/O_3$, and the calculated ratio of Logan et al. (1978).

Ozone (O_3)

This section will discuss in situ profile measurements; satellite and Umkehr measurements are discussed in Chapter 2. Ozone profiles are obtained routinely from Dobson spectrophotometer observations of the blue zenith sky as the solar zenith angle varies between 36° and 90° (sunrise or sunset). A discussion of errors is found in Chapter 2; a list of stations making such observations is found in Appendix C. Ozone profiles are being obtained by instruments on small meteorological balloons up to 30 to 35 km, by more complex instruments on research balloons up to about 40 km, and by means of rocket-borne instruments up to about 60 km. Each year there are several hundred small balloon ozonesondes, 10 to 30 ozone sensors on research balloon flights, and on the order of 30 to 50 ozone rocket flights. Profiles from the small balloon flights are reported routinely to the center for Ozone Data for the World, maintained by the Canadian Meteorological Service (Toronto, Ontario, Canada) in cooperation with the World Meterological Organization. Reporting of profiles from the research balloons and rockets tends to be sporadic and informal. The International Ozone Rocket Intercomparison group, sponsored by WMO, has collected a comprehensive set of rocket profiles from individual experimenters. Hilsenrath (personal communication) and Mateer et al. (1980) have recently analyzed balloon and rocketsonde profiles for use as a "first guess" in BUV and Umkehr retrievals.

Small Balloon Ozonesondes

The small balloon ozonesondes consist of an ozone sensor attached to a standard radiosonde for air pressure, temperature, and tropospheric humidity. They provide ozone density as a function of pressure altitude; potential altitude may be inferred from the hypsometric integration of the observed pressure and temperature. Dobson observations of total ozone are usually available for each flight and are sometimes used to normalize the balloon data.

Most ozonesondes use a bubble sensor conceived by Dr. A. W. Brewer (U.S. Patent no. 3,329,599) of the University of Toronto and licensed to the Mast Development Company. It is based on the electrochemical reaction which takes place when air containing ozone is bubbled into a potassium iodide solution. The resulting exchange of electrons is directly proportional to the quantity of ozone introduced by the air supplied to the sensor by a constant-volume reciprocating piston pump.

The Electrochemical Concentration Cell (ECC) was developed by W. D. Komhyr and T. B. Harris (1971) and is based on an iodine/iodide redox cell in which ozone is consumed in the oxidation of iodide ions to molecular iodine. The latter is quickly converted back to the iodide form in a reaction driven by the iodide concentration differential that exists between the cell anode and cathode. The cell is made of two bright platinum electrodes immersed in potassium iodide solutions of different concentrations contained in separate cathode and anode chambers, linked together with an ion bridge. Again air is bubbled through the system by a small constant volume pump. An earlier version is based on a carbon-iodine system (Komhyr, 1964).

In all of these instruments, the sensor is placed in an insulating box (expanded polystyrene) and attached to the train of a standard meteorological radiosonde; the signal from the cell is inserted into the radiosonde's telemetry through a sequencer.

Five variations of these two basic sondes (Brewer-Mast sonde and the Komhyr-ECC sonde) are presently used. Observations made with each method are adjusted to the simultaneously measured total column ozone (Dobson measurement) by using a single correction factor. For this purpose the ozone amount above the balloon burst level is calculated by assuming a constant mixing ratio above the top of the flight if it reaches 18 mbar (27 km). If the burst is at a lower altitude the ozone amount to be added to the flight's integrated total is obtained from climatological means. (It should be noted that this latter procedure distorts the profile information used for trend computations). The correction factor is, in the mean, 1.1 to 1.2 for the Brewer-Mast sonde and about 1.0 for the Komhyr-ECC sonde and similar instruments. The variance of the correction factor, however, is about the same for both instrument types. Although ozonesonde intercomparisons (Attmannspacher and Dütsch, 1970) have shown that the one-factor correction yields, on the whole, good agreement between different sonde types, it is nevertheless a source of uncertainty because it propagates measurement errors from one layer to the other. An alternative procedure being evaluated at NASA-Wallops Flight Center is to calibrate each sonde prior to flight by comparison with a Dasibi Ozone Monitor.

Another source of error is a change in pump efficiency with decreasing pressure, especially above 20 mbar, (~25 km), for which only a mean correction is available. In addition to the uncertainty in single soundings introduced by this problem, a bias in the mean values around 10 mbar (~30 km) and above may be introduced. Comparisons with rocket ozonesonde data indicate that at the top of the soundings (30 to 35 km) the balloonsondes yield values which are too low, an error which would be connected with smaller errors of opposite sign at lower levels due to the single-factor correction.

For the above reasons, the expected random error of the small balloon ozonesondes is about ±8 to 10% in the troposphere; is least (±4%) between the tropopause and 20 mbar (26 km); and increases upward to about ±8% at 10 mbar (31 km) and above. As indicated, there is also the possibility of a systematic negative error of around 10% at 10 mbar and above.

In the two intercomparisons at Hohenpeissenberg (Attmannspacher and Dütsch, 1970), the ECC-sonde gave ozone concentrations in the lower troposphere which were about 10% higher than those obtained with the other instruments. This was probably due to the higher concentration of the iodine solution which was used in the sonde. Since the recommendation regarding solution concentration in the ECC-instrument has changed from time to time, care

must be applied in trend calculations using such data. In the case of the Brewer-Mast sonde a change in launch time could simulate a change in tropospheric ozone because of the diurnal variation of the pollution effect at certain stations (highest pollution in the morning).

Ozone Sensors on Research Balloons

Some large research balloon payloads include ozone sensors, sometimes as a piggy-back experiment, sometimes as a desirable correlative observation needed to attain the primary objectives, and, occasionally, in conjunction with other ozone sensors for intercomparison purposes. The large balloons (generally larger than 4,000 m^3 volume) permit inclusion of ozone sensors of considerable complexity and weight (up to 50 kg and more). These sensors (see Table 1-7) are still under development in that changes are made from flight to flight with corresponding changes in precision and accuracy.

The Dasibi instrument, first flown on a balloon by Hilsenrath and Ashenfelter (1976), uses UV absorption photometry. The ozone concentration is determined by measuring the amount of light absorbed at 254 nm by an air sample flowing through an absorption cell. The absorption can be measured with an accuracy of about 0.2% for ozone densities encountered near 25 km altitude. Errors in measurement of cell and ambient temperatures and pressures, path length, and ozone cross section add an uncertainty of 2 to 3% to the value of the corresponding atmospheric ozone number density or mixing ratio. Loss of ozone to the walls of the inlet system are known to be small (tenths of a percent) at atmospheric pressures, but are expected to have a $P^{-2/3}$ pressure dependence and may be a substantial source of error at 40 km (Ainsworth et al., 1981).

Table 1-7
Ozone Sensors for Large Balloon Payloads

Type	Experimenter
Dasibi	Ainsworth (and Hagemeyer, 1980; Maier et al., 1978)
	Robbins (1980; ... and Carnes, 1978; Mauersberger et al., 1981)
UV solar spectrometer	Simon (and Peetermans, 1981)
	Mentall (et al., 1980)
Lidar	Heaps (et al., 1981)
Mass spectrometer	Mauersberger (et al., 1981)
Chemiluminescent (NO)	Drummond (1977; et al., 1979)
Chemiluminescent (methyl-2-butane-2)	Aimedieu (et al., 1980, 1981)

The Dasibi instrument from NASA-JSC (Robbins) has the most extensive flight experience, having measured 20 profiles in the stratosphere since 1978. Three of these flights were made with the mass spectrometer of Mauersberger et al. (1981). Data from the two instruments agreed over the altitude range of 20 to 35 km, with the Dasibi data being lower above 35 km. (Mauersberger et al., 1981).

Four of the recent multi-sensor intercomparisons have been based on the use of a large balloon; also included were ground-based sensors, small balloonsondes, rocketsondes, and aircraft-borne sensors.

The last flight of the Stratcom series, organized by the Atmospheric Sciences Laboratory at the White Sands Missile Range, New Mexico, was in September 1977. A summary from the Stratcom VIII report (Reed, 1980) is given in Table 1-8. It is perhaps significant that ozone values derived from the UV solar absorption instruments are consistently larger than those derived from the various in situ measurements.

The LIP (LIMS Instrument Package) series (five flights between June 1978 and April 1979) was organized by the Nimbus Experiment Team for the LIMS instrument on Nimbus 7 (Lee et al., 1982; Remsberg et al., 1980). Data from one of the flights is shown in Figure 1-55. From the data given in the report it is not possible to separate errors in the ozone sensors from errors in the pressure sensors. Each of the ozone sensors had a pressure sensor associated with it. For the ECCs, altitude is inferred from the associated pressure and temperature data, for the JSC Dasibi instrument, altitude is inferred from the measured pressure and the U.S. Standard Atmosphere, 1976. Figure 1-55 is typical in that for all of the five flights, ozone values from the JSC Dasibi instrument were generally less than those from the ECC-type sensors.

The SABE (Solar Absorption Balloon Experiment) series consisted of three flights (September 1978 - April 1980) and was primarily for a study of the detailed relationships between UV energy fluxes and atmospheric ozone densities (Reed et al., 1981). To be certain of the ozone content several types of ozone sensors were included in the second and third payloads; ECC sondes were flown independently; Dobson and other spectrophotometers were used for observations from the ground. On the large balloon payload were the GSFC and JSC Dasibi instruments, a modified Rocoz photometer, a modified ECC sonde, Drummond's NO chemiluminescent sensor, and a solar-pointed Fastie-Ebert spectrometer. Ozone data from one of these efforts are given in Figure 1-56 and Table 1-9. Again, the atmospheric pressure is measured independently by each ozone sensing system; the differences in these profiles reflect errors in both ozone and pressure values. The Rocoz profile used the same pressure profile as did the GSFC Dasibi.

An extensive campaign for intercomparison of various techniques for ozone profiles was coordinated by M. L. Chanin (Service d'Aeronomie du CNRS) and was conducted June 9-26, 1981 in southern France. A number of ground-based and balloon-borne techniques were included as can be seen from Table 1-10.

Ozone Sensors on Aircraft

Several types of instruments have been used on aircraft to obtain information related to stratospheric ozone, namely, UV absorption photometry (Dasibi), solar UV absorption, NO-chemiluminescence, and ethylene-chemiluminescence.

The Global Air Sampling Program (GASP) was conducted by NASA-Lewis Research Center (Cleveland, Ohio, USA) from March 1975 through June 1979. A package including a Dasibi ozone monitor and instruments for CO, particles, clouds, condensation nuclei, water vapor, and filter

Table 1-8
Ozone Data from the Stratcom VIII Effort (Reed, 1980)

Source	Total O_3 (atm-cm)	Ozone Density (molecules/m^3)				
		20 km	25 km	30 km	35 km	40 km
Dobson (No. 86 at ASL)	0.279					
SenTran (Simeth)	0.282					
ECC (NASA-WFC)	0.280	3.95(18)	4.30(18)	2.74(18)	1.40(18)	
MAST (ASL)		2.3 (18)	4.0 (18)	2.6 (18)		
Dasibi (Ainsworth)						5.4 (17)*
Chemilum (A-balloon) Ascent (Randhawa) Descent (Randhawa)		3.7 (18)	4.0 (18)	2.6 (18)	1.3 (18) 0.92(18)	5.0 (17) 6.3 (17)
Chemilum (Arcas) (Randhawa)		2.8 (18)	4.0 (18)	2.0 (18)	1.3 (18)	6.7 (17)
UV spectrometer (Mentall)					1.3 (18)	6.2 (17)
UV spectroirradiometer (Sellers)		2.8 (18)	5.4 (18)	2.9 (18)	1.5 (18)	8.0 (17)
ROCOZ (Super-Loki) (Krueger)		3.14(18)	5.19(18)	3.84(18)	1.91(18)	6.77(17)
SAS-II (Loewenstein)		3.0 (18)				
Average	0.280	3.1 (18)	4.5 (18)	2.8 (18)	1.4 (18)	6.3 (17)
Std. Dev. %	1	18	14	22	21	16

*Corrected for wall losses (J. Ainsworth, personal communciation)

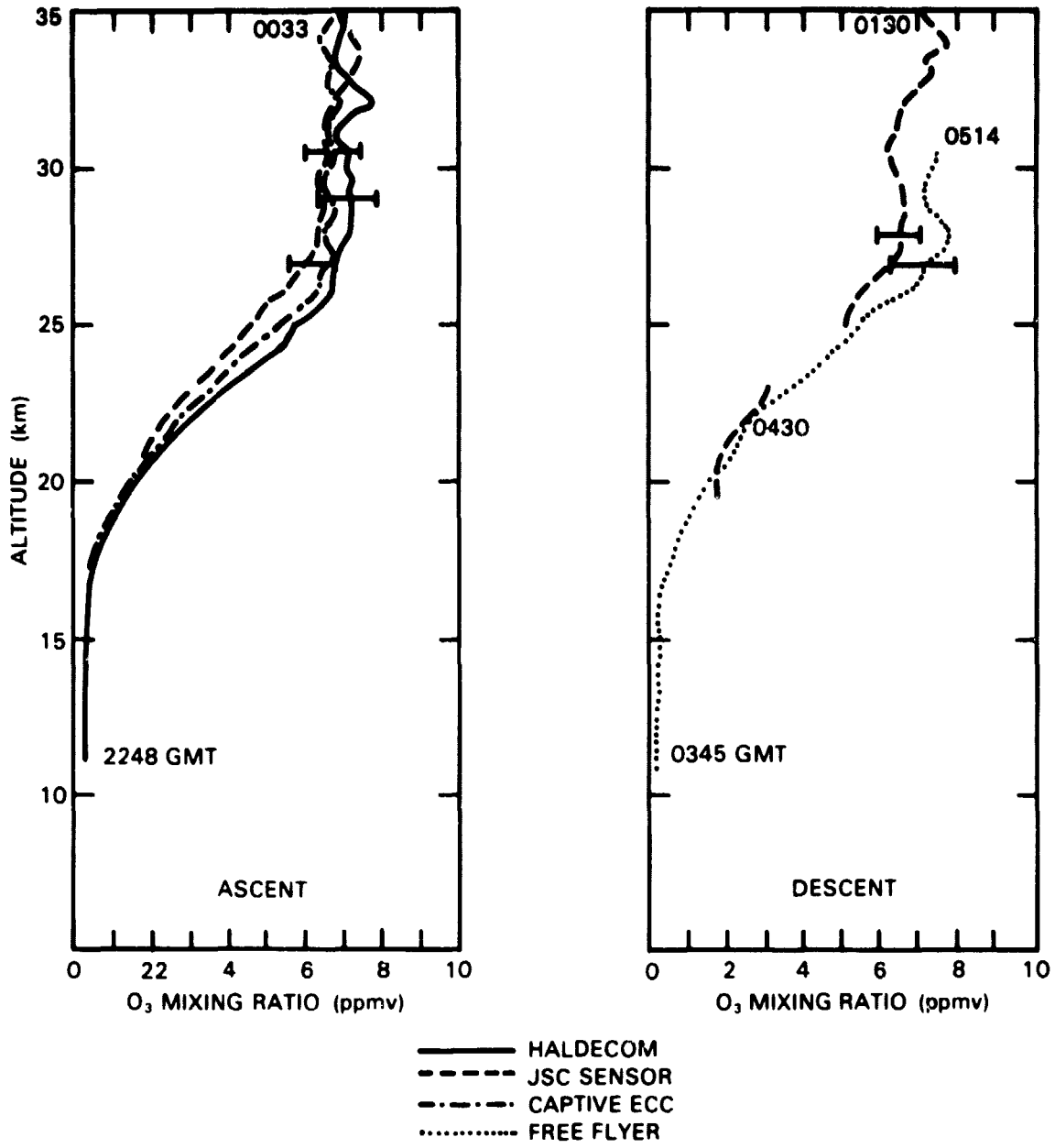

Figure 1-55. Data from the LIP flight of October 30, 1978 from Palestine, Texas. HALDECOM is an ECC sonde with enlarged anode and cathode reservoirs; JSC Sensor is the Robbins Dasibi instrument; Captive ECC is a standard ECC sonde; these three were on the large balloon payload. Free Flyer is an ECC sonde on a standard meteorological balloon released at 0345 GMT (Lee et al., 1982).

samples was placed on the NASA-ARC Convair 990 research aircraft and on four Boeing 747s in commercial passenger service. Correlative data regarding flight and meteorological parameters, including tropopause levels have been interleaved with data from the GASP package and the resulting tapes are archived at the National Climatic Center in Asheville, North Carolina. Detailed reports are available as NASA documents (e.g., Papathakos and Briehl, 1981). The data have been used primarily in studies of stratosphere-troposphere ozone transport (Nastrom, 1977; Husain et al., 1977) and in the evaluation of the aircraft cabin ozone problem (Holdeman and Nastrom, 1981; Nastrom et al., 1980).

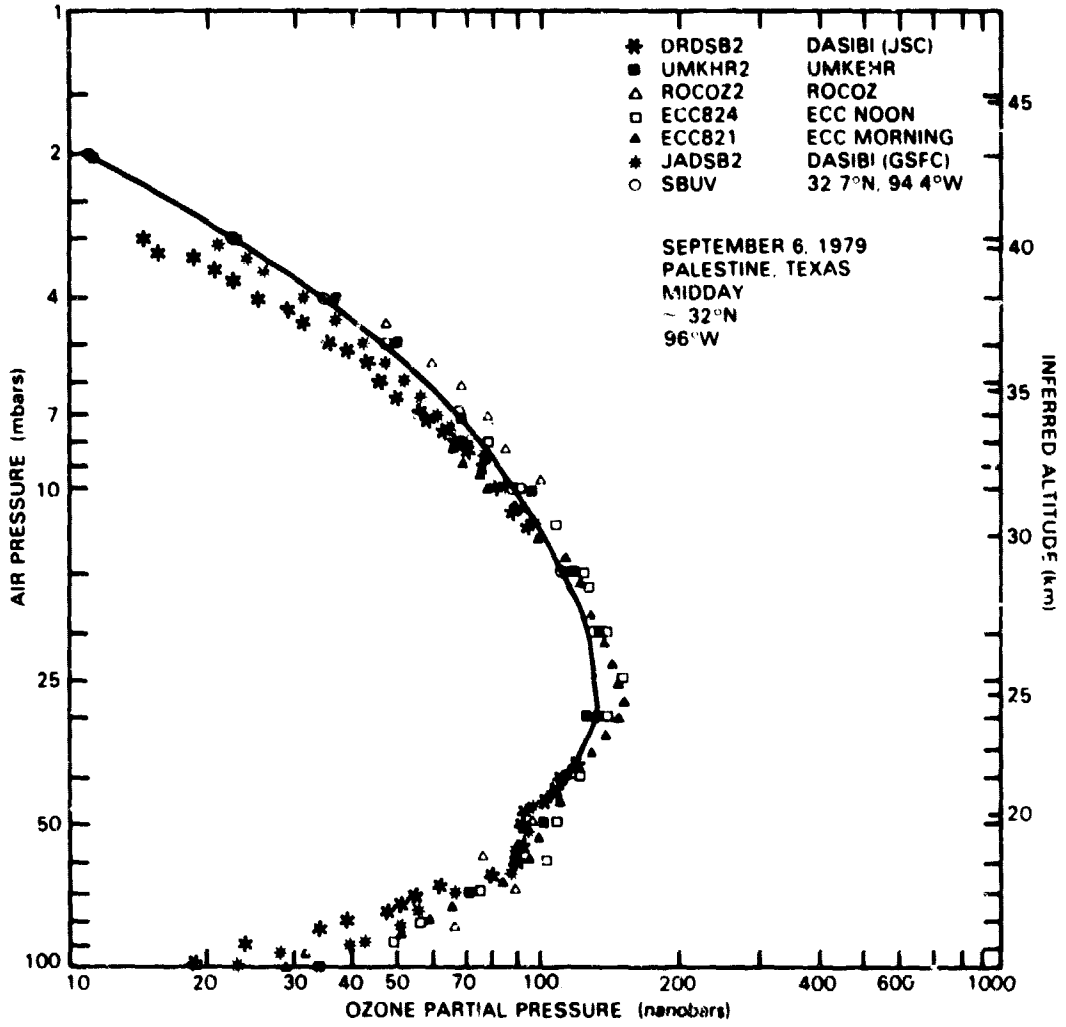

Figure 1-56. Ozone profiles from instruments on the SABE-2 balloon, independently flown ECC sondes, a Dobson spectrophotometer, and the SBUV instrument on Nimbus 7.

Table 1-9
Ozone Profiles - September 6, 1979, Palestine, Texas

Instrument	Pressure Level (mbar)/Altitude (km)													
	100/16.7	70/18.8	50/20.9	40/22.1	30/24.2	20/26.9	15/28.8	10/31.2	7/33.5	5/35.7	4/37.3	3/39.4	2/42.7	1.5/45.0
ECC No. 821	28.7	70.4	101.9	119.0	148.7	136.5	119.2	79.4						
ECC No. 824	33.9	74.8	109.0	122.4	140.5	142.8	124.1	92.1						
Dasibi-GSFC	23.5	68.8	93.7	117.5				83.8	61.2	42.6	31.4	19.6		
Dasibi-JSC	22.	62.	95.	112.				80.5	57.5	38.2	25.6	15.		
ROCOZ		77.7	97.4						77.6	53.4				
Umkehr	40.1	71.3	102.	117.	130.	133.	117.	94.8	68.1	48.3	35.3	22.3	11.7	6.7
SBUV				116.9	134.4	130.2	112.6	88.2	67.6	46.8	34.7	22.3	11.0	6.6
Average	29.6	70.8	99.8	117.	138.	135.	118.	86.5	66.4	45.9	31.7	19.8	11.4	6.6
Std. Dev. %	25	8	6	3	6	4	4	7	12	13	14	17	4	0

(Dasibi-GSFC values are preliminary, pending definitive determination of wall loss effects.)

Table 1-10
Ozone Sensors Used June 9-26, 1981, Southern France and Vicinity

Sensor	Location	Responsible Individual
Laser - differential absorption	Observatorie de Haute Provence	G. Megie
Infrared Spectrometer (S.I.S.A.M.)	Chiran (O.H.P.)	P. Jouve
Dobson Spectrophotometer	Chiran (O.H.P.)	P. Jouve
High Resolution UV Spectrometer	Chiran (O.H.P.)	P. Jouve
Microwave Spectrometer	Chiran (O.H.P.)	Max Planck Institute, Lindau
Microwave Spectrometer	Observatoire de Bordeaux	P. Dierich
Dobson Spectrophotometer	Arosa, Switzerland	
Chemiluminescent Sonde	Large Balloon	P. Aimedieu
Brewer Mast Sonde (EERM)	Large Balloon	P. Aimedieu
Dasibi (NASA-JSC)	Large Balloon	D. Robbins
UV Solar Absorption	Large Balloon	P. Simon
UV Solar Absorption (Rocoz)	Large Balloon	A. Krueger
ECC Ozone Sondes (NASA-WFC)	Small Balloons, O.H.P. and Gap	L. Troast
Brewer Mast Sondes (EERM)	Small Balloons, Biscarosse	
TOMS	Nimbus 7	A. Krueger
SBUV	Nimbus 7	A. Krueger
TOVS	Tiros-N	Cayla, Muller, Chedin

The ARC (Ames Research Center) stratospheric air sampler (SAS) for nitric oxide and ozone has been flown frequently on the U-2 high altitude aircraft. The ozone measurements, based on NO chemiluminescence, are generally between 18 and 21 km altitude. The data have been used in studies of seasonal variations (Loewenstein et al., 1975, 1978a, b), in a study of the effects of a total solar eclipse (Starr et al., 1980), compared with other ozone sensors (see Table 1-8), and used in the 1977 Intertropical Convergence Zone Experiment (Starr et al., 1979).

During the CIAP program, Hanser et al. (1978) constructed a UV spectrophotometer with a 12-position filter wheel for the measurement of overhead solar fluxes. When flown on a large balloon, the altitude changes in fluxes are interpreted in terms of an ozone profile (see Table 1-8). When flown on aircraft (WB-57, CV-990, NCAR's Electra), the fluxes are interpreted in terms of total overhead ozone (Hanser et al., 1978, Hanser and Sellers, 1980).

Two Dasibi instruments and a Columbia Scientific Industries ethylene-chemiluminescence analyzer were mounted in the NCAR Electra during the Gametag flights during 1977-1978 (Davis, 1980; Routhier et al., 1980). Large-scale anomalies of the ozone content at tropospheric altitudes have been related to a folded tropopause (Danielsen and Hipskind, 1980).

In a joint program between the Institute of Applied Physics at the University of Berne, Switzerland, and the Max-Planck-Institute for Aeronomy at Katlenburg-Lindau, Germany, Hartmann et al. (1981) used a microwave sensor on board a German research aircraft tuned to the strong resonance of ozone at 142 GHz to obtain an ozone mixing ratio profile between 25 and 60 km. Measurements of an O_2 resonance at 53.6 GHz provide a simultaneous temperature profile.

Ozone Sensors on Rockets

Although ozone sensors have been flown on small rockets for more than two decades, there is no one system that can be considered as "operational", i.e., procured, deployed, analyzed and reported according to detailed and well established procedures, as are the meteorological data sondes. Each of the various rocket ozonesondes requires continuing scientific and engineering oversight and intervention to improve and maintain reliability and data quality. In Table 1-11 are listed groups that have been active in recent years.

Rocketsondes employing chemiluminescent dyes have proven to be useful when the surfaces are prepared and calibrated with sufficient care, providing ozone profiles between 60 and 20 km with an absolute accuracy of about ±12% and a precision of about ±6% (Hilsenrath and Kirschner, 1980). They are especially useful for studies of diurnal variation and during the polar winter (Hilsenrath, 1971; Heath et al., 1974; Hilsenrath, 1980).

In the daytime, between about 60 and 100 km, the photolysis of ozone in the Hartley band is the primary source of $O_2(^1\Delta g)$, which then emits at 1.27 μm. Ozone profiles may then be deduced from the altitude profile of the overhead intensity as measured by a rocket-borne infrared photometer. Errors of the resulting ozone profile approach 20%, increasing towards the end of the altitude range, but entirely adequate to show the layered structure of ozone in this region (Llewellyn and Witt, 1977).

Solar ultraviolet absorption has long been used by rocket-borne ozone sensors. Filter photometers are often used because of their simplicity and relatively low cost. Limitations to the accuracy include: knowledge of the filter transmission, especially in the long-wavelength wing; measurement of and compensation for changes of the direction of the optical axis with respect to the Sun; correction for the scattered light contributions at altitudes below about 30 km; and adjustment of the ozone absorption coefficient for air temperature for wavelengths near 300 nm.

Table 1-11
Ozone Sensors for Small Rockets

Principle	Responsible Group	References
Solar UV Absorption Filter Photometer	B. Horton and J. Lean Physics Dept. U. Adelaide Adelaide, Australia	Lean (1981) Ilyas (1980)
1.27μm from $O_2(^1\Delta g)$ Infrared Photometer	E. Llewellyn, B. Solheim, W. Evans University of Saskatchewan, Saskatoon York University Atmospheric Environment Service Downsview, Canada	Llewellyn and Witt (1977)
Solar UV Absorption Filter Photometer	B. H. Subbaraya and S. Lal Physical Research Laboratory Navrangpura, Ahmedabad India	Acharya et al. (1979) Subbaraya et al. (1981)
Solar UV Absorpiton Filter Photometer	T. Ogawa and T. Watanabe University of Tokyo Tokyo, Japan	Ogawa and Watanabe (1980) Tohmatsu (1977)
Chemiluminescence on Rhodamine-B Surface	E. Hilsenrath Goddard Space Flight Center Greenbelt, Maryland, USA	Hilsenrath (1980) Hilsenrath and Kirschner (1980)
Solar UV Absorption Filter Photometer	A. Krueger Goddard Space Flight Center Greenbelt, Maryland, USA	Wright et al. (1979)
Chemiluminescence	V. Konkov, V. Kononkov and S. Perov State Committee for Hydrometeorology and Control of Natural Environment USSR	Konkov, et al. (1981)
Optical	N. Brezgin, A Chizhov, and O. Shtyrkov State Committee for Hydrometeorology and Control of Natural Environment USSR	Brezgin et al. (1981)
Optical Filter Photometer	Y. V. Somayajulu, S. Sampath, and K. S. Zalpuri National Physical Laboratory New Delhi, India	Somayajulu et al. (1980)

A scanning UV spectrometer would be more costly, but exchanges the problem of internally scattered light for the problem of the measurement and stability of interference filters. Under the best conditions, the change of column content over an altitude interval of 1 km can be measured with an uncertainty smaller than 5%. At the extremes in the altitude range, errors can easily approach 20%. When these ozone profiles are expressed in terms of mixing ratio versus pressure altitude, the errors in estimating the relevant air temperature and pressure must be included in the associated estimated error.

The first six of these groups listed in Table 1-11 participated in an International Ozone Rocket Intercomparison (IORI) October 21 to November 4, 1979, sponsored by the World Meteorological Organization. (Sundararaman et al., 1980, Sundararaman, 1981). In this effort, each type of sensor was flown several times over a short period of time such that both the repeatability of the instrument and its bias with respect to other types of instruments could be determined. A detailed report is expected shortly, but preliminary data are given in Table 1-12.

Table 1-12
Preliminary Mixing Ratios (ppmv) for Three Midday Flights
IORI - October 21, 1979

Sensor Type	Altitude (km)							
	25	30	35	40	45	50	55	60
			8.77	7.66	4.85	2.70	1.35	0.77
Optical			9.02	7.89	4.71	2.9		
Horton and Lean			8.4	6.88	4.56	2.47	1.83	0.46
							1.45	0.9
Infrared							1.03	
Llewellyn et al.							1.29	0.78
		6.87	6.40	5.87	4.13	2.84	1.85	
Optical		5.63	5.6	4.85	3.83			
Subbaraya and Lal		5.98	5.68	5.27	3.81	2.51		
				8.97	4.38	2.61	1.71	
Optical			11.05	9.95	5.82	3.32	2.13	
Ogawa and Watanabe			9.87	7.61	4.82	2.89	1.92	
	8.06	9.72	9.59	7.56	4.8	2.57	1.53	0.89
Chemiluminscent	7.06	9.43	9.71	7.72	5.33	2.5	1.19	
Hilsenrath	7.5	9.24	9.2	7.78	5.04	3.14	1.62	0.83
	5.51	8.71	9.98	8.49	5.02	2.2		
Optical	5.39	8.71	9.58	8.45	5.18	2.42		
Krueger	5.24	8.93	9.58	8.79	5.2	2.79	1.59	
Average	6.46	8.14	8.75	7.58	4.77	2.70	1.58	0.77
Std. Dev. %	19	19	19	18	12	11	20	21
ECC-911	5.62							
ECC-1017	5.57	8.80						

Systematic Differences

From the intercomparisons mentioned thus far and from some other studies the following points can be made:

- When compared with profiles of better altitude resolution, Umkehr profiles tend to underestimate the ozone densities at the main maximum, especially if it is situated within layer 4 (20 to 24 km), e.g., see Figure 1-56. The Umkehr profile compensates for this by giving values that are too high in the lower stratosphere (layer 2, 10 to 16 km) and, to some extent, around 10 mbar (layer 6, 28 to 33 km). This compensation is evident in a comparison of Umkehr measurements at Arosa (about 20 profiles per month) with ozonesonde (small balloons) measurements from Payerne about 200 km away (about 10 flights per month). The annual variations computed for each station are given in Figure 1-57; comparisons of concurrent observations are given in Table 1-13.

- Profiles from small balloonsondes tend to cross over profiles from rocketsondes (mostly Krueger optical sondes and Hilsenrath chemiluminescent sondes) near 30 mbar (24 km), with the balloons giving larger values below 24 km and smaller values above. A study of coincident rocket and balloon soundings from Wallops Island, Virginia, showed that at 5 mbar (36 km), the average rocket ozone profile was 30% higher than the average balloon profile (Hilsenrath, personal communication, Mateer, 1980). However the mean rocket and balloon profiles used in mid-latitude ozone models (Krueger and Minzner, 1976) agreed within 5% between 28 and 34 km.

- The Krueger optical sonde provides larger values above about 35 km than does the Hilsenrath chemiluminescent sonde; at lower altitudes the reverse is observed (see Hilsenrath et al., 1979 and Table 1-12). In other comparisons (e.g., Tables 1-8 and 1-9) solar UV absorption methods tend to give larger values for ozone than do in situ methods.

In the lower stratosphere, the best profiles available are generally from small balloonsondes. Above the ozone density maximum, (~25 km) errors due to pump efficiency, wall losses, and pressure sensors become increasingly important. Above the ozone density maximum (~25 km) the chemiluminescent and the optical (solar UV absorption) measurements are probably comparable in validity. The systematic bias with balloons is not as yet explained. Above ~60 km one must resort to the indirect method using the 1.27 μm emission from ozone photolysis by solar ultraviolet fluxes. It is to be noted, however, that only in situ methods are effective at night unless one uses faint UV sources such as the moon, stars, or air glow. Umkehr profiles, being of such low altitude resolution, are not really comparable to balloon and rocket profiles except as noted above; they should be classed with profiles from such systems as mm-wave receivers (e.g., Wilson and Schwartz, 1981).

Model and Reference Ozone Profiles

A mid-latitude ozone profile based on data prior to 1972 is included in the U.S. Standard Atmosphere, 1976 (also see Krueger and Minzner, 1976). Seventeen carefully selected rocket profiles (12 day and 5 twilight) from sites between 30° and 60°N and a number of balloon profiles from sites between 41° and 47°N were used. The rocket profiles were from several different experimenters with the majority based on Solar UV absorption.

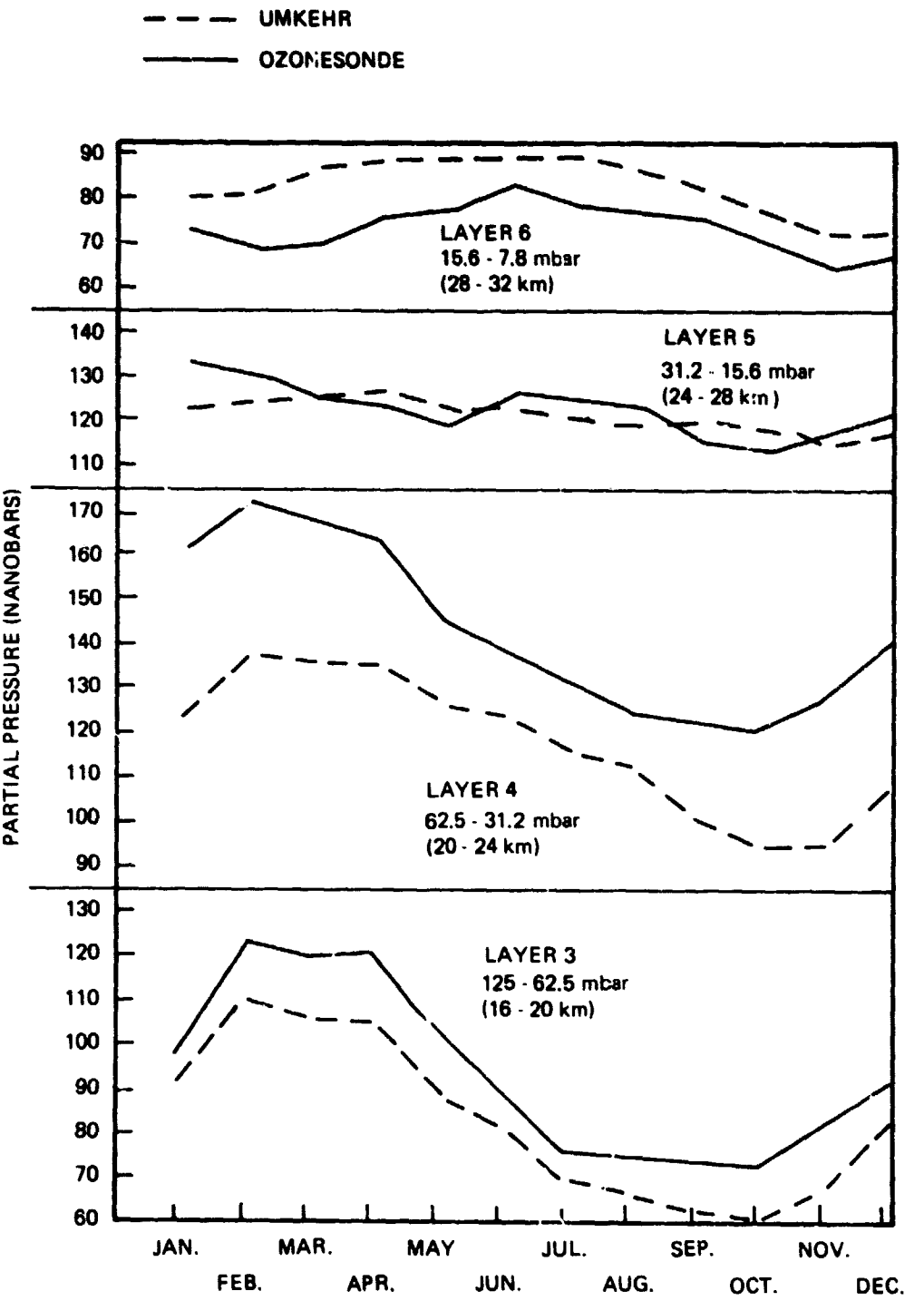

Figure 1-57. Intercomparison of mean annual variation of the ozone partial pressure, Arosa/Payerne, as derived from Umkehr and Ozonesonde observations.

Table 1-13

Comparison of Concurrent Umkehr-Ozonesonde Observations over Arosa/Payerne (WMO, 1981).

Umkehr Layer Number	Umkehr Ozonesonde (241 points) (nbar)	Ozonesonde (nbar)	Difference (%)	Lower Boundary Atm Pressure (mbar)	Lower Boundary Approx. Altitude (km)
9				1.96	43
8				3.9	38
7				7.8	33
6	83.5	73.8	13.1	15.6	28
5	120.4	122.3	-1.6	31.25	24
4	116.6	139.7	-16.5	62.5	20
3	82.4	85.5	-3.6	125	16
2	62.4	37.6	66.5	250	10.4
1	27.9	24.0	16.3	1000	0

Because the algorithms for the inversion of BUV and Dobson (Umkehr) radiance data require a "first guess" ozone profile, existing balloon and rocket profiles have been analyzed for these purposes. Total ozone and latitude zones (30° wide) are used as keys for selection of a specific profile. Initial analyses were by Hilsenrath (1979) for use in the BUV algorithm. Mateer et al. (1980) have recently repeated this for use with Umkehr data (see Table 1-14 and Figure 1-58). It is to be noted that these data are significantly primarily for altitudes below about 40 km; total ozone and latitude are not proven predictors for ozone values in the upper stratosphere and mesosphere.

Diurnal Variations

The diurnal variations of the ozone profile have been observed by various methods: Aimedieu et al. (1981) analyzed balloon observations for a change in ozone immediately after sunrise (see Table 1-15) and found consistent evidence of a decrease in ozone column content about 40 km, with a 5% local depletion at 42 km. At higher altitudes, the diurnal variations become much larger. Observations of the mm-wave ozone emission line at 101.737 GHz show more than a factor of two daytime decrease in the ozone column above about 76 km (Wilson and Schwartz, 1981). Data from the Australian optical rockets launched during the IORI are summarized in Figure 1-59, comparing the daytime and nighttime flights (Lean, 1981). These are consistent with earlier rocketsonde day-night comparisons, e.g. a daytime increase near 42 km and a large nighttime increase above 60 km (Hilsenrath, 1971; Heath et al., 1974). The balloon data (Aimedieu et al., 1981) do not compare midday with midnight, but show the transient occurring at sunrise, which theoretical studies show to be negative, e.g., Herman (1979), Groves and Tuck (1980), and Prather (1981).

Table 1-14
Standard Profiles (Bottom-Side) (Hilsenrath, 1979)

LAT.	TOTAL OZONE (D.U.)	OZONE PARTIAL PRESSURE IN NBAR AT ATMOSPHERIC PRESSURE IN MBAR															
		1000	700	500	300	200	150	100	70	50	40	30	20	15	10	7	5
LOW	200	11	12.7	11.7	8.66	7.23	7.35	12.5	27.1	52.8	75.8	99.4	110	103	76.7	51.4	34.3
	250	13.1	15	13.8	10.3	8.57	8.60	16	41.9	78.8	103	125	135	124	90.7	61.1	40.8
	300	14.9	17.1	15.8	11.7	9.79	9.67	19.6	58.9	109	132	152	160	143	103	69.8	46.6
MID	200	18.2	19.5	16.7	8.74	8.29	11.5	25.1	51.4	76.8	87.8	93.9	88.8	79.7	59.9	42.6	30
	250	20.8	22.4	19.4	13.6	18.4	24	41.2	71.7	99.3	110	114	105	92	68.7	48.9	34.5
	300	22.6	24.2	21.2	20.1	33.7	42.6	62.9	95.6	123	131	130	116	100	74.3	53	37.4
	350	23.4	25.1	22.4	29.1	55.3	68.2	90.9	123	146	150	143	123	104	76.9	55	38.7
	400	23.7	25.4	23.2	40.3	81.2	99.2	124	151	167	165	152	126	106	77.8	55.6	39.2
	450	23.8	25.4	24.2	53	108	133	161	180	186	178	159	128	106	78	55.8	39.3
	500	23.9	25.4	25.4	66.1	134	167	201	209	203	189	165	131	107	78.3	56.1	39.5
	550	24.2	25.7	26.7	78.4	159	199	240	236	219	200	172	134	109	79.2	56.8	40
	600	24.9	26.3	28.1	89.3	182	231	278	263	235	212	180	139	112	81.3	58.3	41.1
HIGH	200	13.8	12.7	11	16.6	35.4	55.5	91	101	94.3	75.7	54.3	37.3	32.9	29.5	27.4	23.3
	250	15.9	15.7	14.2	23.3	49	70.6	109	130	115	94.8	71.5	51.4	44	37.6	33.4	27.2
	300	17.4	18.5	17.5	31.6	65.2	87.1	126	147	134	114	89.9	66.6	55.4	45.3	38.7	30.1
	350	18.3	20.8	20.6	41.9	84.3	106	144	165	153	134	109	80.8	65.5	51.9	42.8	31.9
	400	18.7	22.3	23.3	54	105	129	165	184	173	154	126	92.5	73.2	56.9	45.7	32.9
	450	18.9	23.3	25.9	67.7	127	154	191	205	191	171	141	101	78.7	60.4	47.7	33.4
	500	19.1	23.9	28.9	82.6	147	181	224	228	208	185	152	108	82.7	62.8	49	33.8
	550	19.4	24.3	32.4	98.3	167	211	263	254	223	195	160	113	85.5	64.4	49.9	34.3
	600	19.8	24.8	36.2	114	185	241	305	289	237	203	165	116	87.5	65.2	50.5	35
	650	20.5	25.3	39.8	130	204	271	349	310	251	210	170	119	89.1	65.7	51.1	36

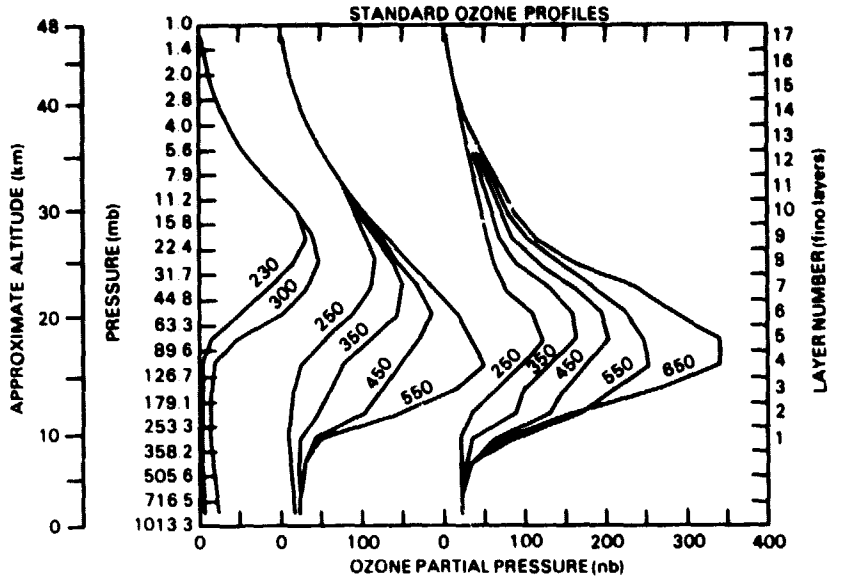

Figure 1-58. Standard ozone profiles for low latitudes (left) middle latitudes (center), and high latitudes (right). The ticks on the ordinate axes indiate the upper and lower bounds of the layers. Layer-mean ozone partial pressure (nanobars) is plotted at the mid-point of each layer (Mateer et al., 1980).

ODD NITROGEN

Nitric Oxide (NO)

Introduction

NO has been the most extensively studied stratospheric odd-nitrogen species. The last decade has seen numerous measurement programs apply a variety of experimental techniques at many different altitudes, locations, and seasons. Thus, the problem in establishing a picture of our best current experimental understanding of stratospheric NO is not a scarcity of data, but rather of making a proper assessment and selection of the data.

Altitude Profile

There have been a large number of measurements by many different groups of the NO mixing ratio as a function of altitude. The techniques employed in these measurements fall into two classes: in situ and remote. While the long-path, vertical-column measurements from the latter technique have provided some of the best information regarding the seasonal and latitudinal variations for NO, the determination of a detailed height profile from long-path data involves deconvolution at solar zenith angles near 90° in order to obtain the maximum number of absorbing molecules along the sight path. The rapid $NO \rightarrow NO_2$ and $NO_2 \rightarrow NO$ conversions at sunset or sunrise complicate the comparison of these data with model predictions.

As a consequence, in situ measurements are used here to establish the NO height profile. A limited number of midday long-path measurements are also included. The result is a more nearly homogeneous, relatively high Sun profile that should afford a better defined comparison between observations and theory. The exclusion of the results of the remote techniques does not unduly

Table 1-15
Published Results on Sunrise Ozone Changes (Aimedieu et al., 1981).

Authors and Year of Publication	Platform	Measurement Technique	Measurement Instant	Duration of the Analyzed Variation	Quoted variation in Ozone concentration
Randhawa 1971	Balloon at 46 km	Chemiluminescence in situ	Sunrise	50 seconds	Factor 3 local depletion
[illegible]d [illegible]74	Balloon at 35 km	Stellar UV absorption	Sunrise	A few minutes	Decrease of 2.5 10^{16} molecules cm^{-2} in integrated thickness above 38 km
Rigaud et al. 1974	Balloon at 38 km	Stellar UV absorption	Sunrise	A few minutes	Decrease of 1.6 10^{16} molecules cm^{-2} in integrated thickness above 38 km.
Penfield et al. 1976	Ground level	Microwave emission	Sunrise	50 minutes	Decrease of 1.0 10^{16} molecules cm^{-2} in integrated thickness above 50 km.
Randhawa and Izquierdo 1976/77	Balloon at 48 km	Chemiluminescence in situ	Morning	2 hours	Factor 1.5 local depletion
Robbins and Carnes 1978	Balloon at 37 km	UV cell absorption in situ	Astronomical twilight	20 minutes	3.6% local increase Reanalysis by Aimedieu et al: 2-5% local depletion
Aimedieu et al. 1979	Balloon at 42 km	Gas phase chemiluminescence, in situ	Sunrise	15 minutes	5% local depletion

restrict the size of the data set on which the present height profiles can be based, since there are a sizable number of in situ measurements made by several groups using a variety of techniques: chemiluminescence deployed with balloons (Ridley and Howlett, 1974; Drummond et al., 1977), aircraft (Loewenstein et al., 1975), and rockets (Mason and Horvath, 1976); photoionization mass spectrometer (Aikin and Maier, 1978), spin-flip laser absorption (Patel et al., 1974). A balloon-borne pressure-modulated radiometer (Chaloner et al., 1978) has been used to obtain midday long-path information.

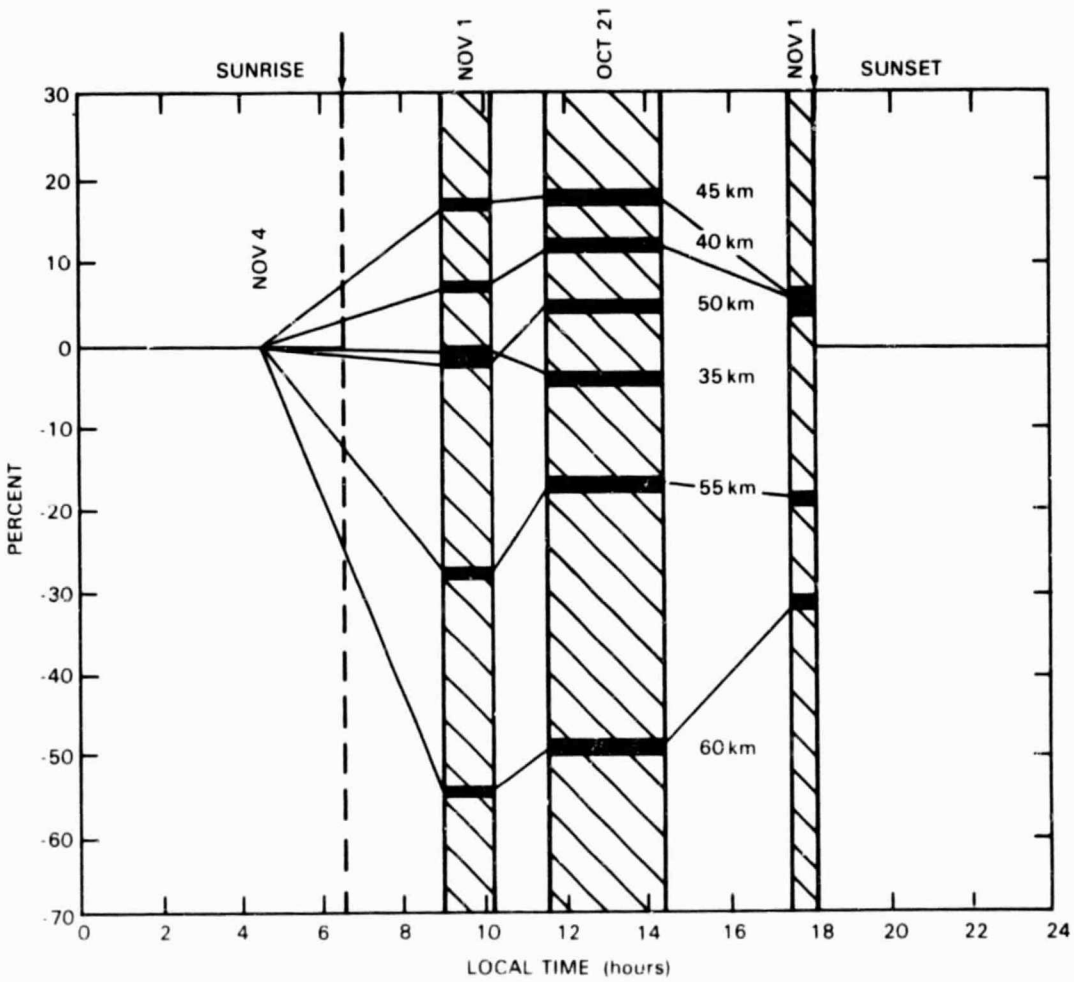

Figure 1-59. Data from the Australian optical sonde flights during the International Ozone Rocket Intercomparison at Wallops Island, Virginia, in 1979, related to the nighttime flight at 0427 local time (Lean, 1981).

Assuming instrumental reproducibility, the variations in the results from a series of flights employing the same instrument are the best indicator of natural seasonal and geographic trends, since it is likely that differences between the results of different research groups and/or instrument packages can be dominated by unknown systematic instrumental discrepancies. Consequently, the approach used is (a) to examine separately the data of each group that has accrued sizeable sets for possible seasonal and geographic effects, and (b) then to combine the data of all of the groups into an appropriate profile.

Figure 1-60 shows the balloon-borne measurements of Ridley and coworkers (Roy et al., 1980; Ridley and Schiff, 1981; Ridley and Hastie, 1981) made in October, 1977 and thereafter. All six of these flights were made with a chemiluminescence instrument that incorporated an improved inlet and in-flight calibration procedure (Ridley and Schiff, 1981). The internal consistency of the data set in Figure 1-60 strongly suggests that a sizable part of the much larger variation that this group observed earlier from flight-to-flight was instrumental. For example, the nearly coincident, half-filled symbols represent data gathered from three flights at the same place and season (32°N, fall), but in two different years. In addition, the data taken on two flights at the corresponding Southern Hemispheric latitude, but different equivalent season (SH, summer), are only slightly lower than the NH results. Lastly, measurements from the summer flight at 51°N lie wholly within the 32° data set. Since the differences between the results of the flights are very nearly equal to the variations within any one of the flights, these data present no evidence of systematic patterns over the given parameter ranges: summer and fall, 50° to 30°N and 30°S, solar zenith angle 37 to 75°. Therefore, they present no reason not to take a factor-of-three-wide band of NO mixing ratios as representative for these parameter ranges and for the indicated altitudes.

Figure 1-61 shows the rocket-borne chemiluminescence measurements made by Horvath and Mason over a five-year period at one location, 39°N, and four seasons, (Mason and Horvath, 1976; Horvath and Mason, 1978; Horvath, personal communication, 1981). There is good agreement within the data set. The later measurements (1980 and 1981) have better precision because they were taken on parachute descent, rather than rocket ascent. No clear seasonal trend emerges from this data set. The data set's homogeneity does, however, establish a factor-of-three band of NO mixing ratios at these altitudes, which are generally higher than those reached by Ridley and coworkers. The chemiluminescence data sets of Drummond et al. (1977) and Weiler and Fabian (1980) are not sufficiently large to permit internal consistency tests and are not included.

The measurement bands corresponding to the two extensive NO mixing ratio data sets are reproduced in Figure 1-62. The width of the indicated ranges includes essentially all of the individual measurements and their estimated uncertainties. The results of four other measurement series are shown. The first is that of Loewenstein and coworkers, whose chemiluminescence instrument has been flown extensively at two altitudes aboard U-2 aircraft (Loewenstein and Savage, 1975; Loewenstein et al., 1975, 1977, 1978a, b). The rectangles in Figure 1-62 represent the range of NO mixing ratios found in spring, summer, and fall and over latitudes from 5° to 50°N. Measurements were also made in winter at mid-latitudes and above 50°N. A pronounced winter variation was found and is discussed in detail below. The winter variation is excluded from the data in Figure 1-62. The second measurement series represented in Figure 1-62 is a short one, namely, two flights by Patel and coworkers, who used a spin-flip Raman laser to detect NO in absorption in a multipass cell (Patel et al., 1974; Burkhardt et al., 1975). Although only two flights were performed, the results, taken in the fall of 1973 and the spring of 1974, are in remarkably good agreement for several hours at float altitude. A single data point, representing the noontime mean, is given in Figure 1-62.

Figure 1-62 also includes the mass spectrometer data of Maier et al. (1978). Unfortunately, the instrument was used only on this one flight. Also given in Figure 1-62 are the pressure-modulated radiometer data of Roscoe et al. (1981). An earlier flight (Drummond and Jarnot, 1978) produced consistent results of considerably less precision and these are not used here. The data of Roscoe and coworkers are the only daytime long-path NO height-profile information. The uppermost datum is particularly valuable since it is at an altitude where there is only one other set of measurements.

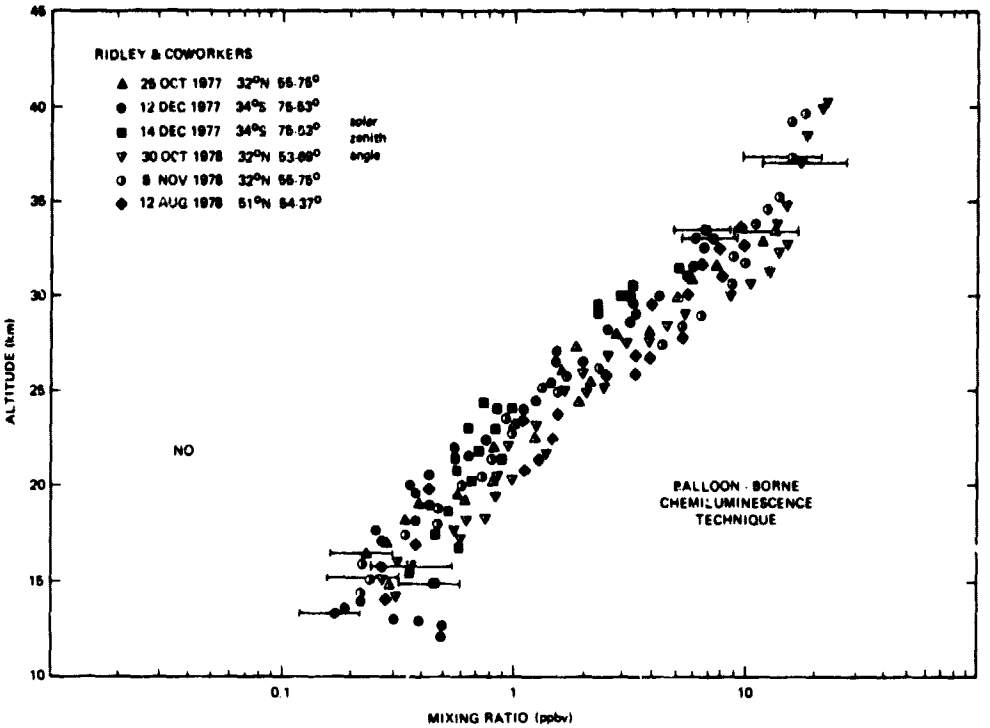

Figure 1-60. In situ NO mixing ratio measurements of Ridley and coworkers. All of the flights were made with instrumentation that incorporated a new inlet and flight calibration procedures.

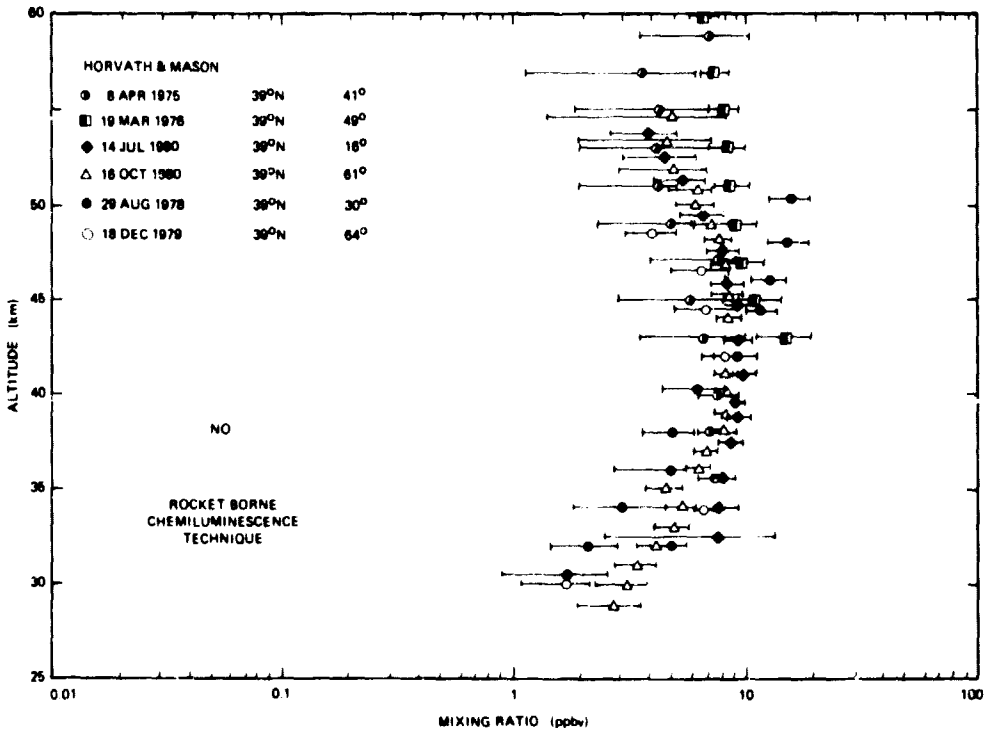

Figure 1-61. In situ NO mixing ratio measurements of Horvath and Mason. The 1980 measurements were made on parachute descent.

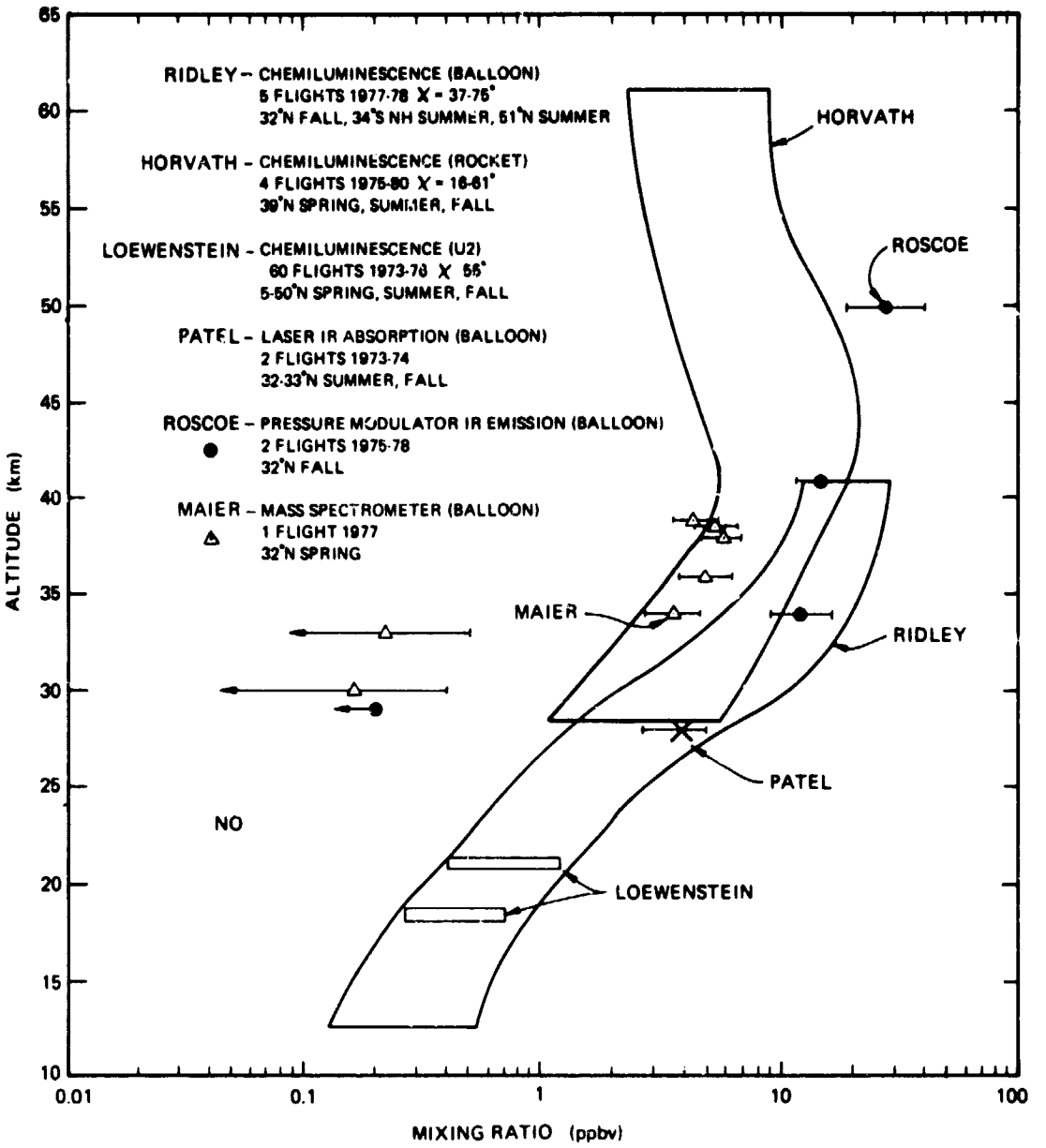

Figure 1-62. In situ NO mixing ratio measurements of several series of flight yielding self-consistent results.

As Figure 1-62 shows, the data sets are in good agreement. Even though there are some discrepancies, there is nevertheless substantial overlap. There are, of course, some in situ and remote measurements that have been excluded from this comparison and that conflict with the data in Figure 1-62. It is worth stressing here that these exclusions were based on the reasons given above and not on the fact that they conflict. Furthermore, some of the excluded measurements agree with those in Figure 1-62.

The lowest altitude mass spectrometer and pressure modulated radiometer data have been excluded. This seemed justified on the basis of the relatively large uncertainties attributed to these data and the fact that they are significantly different from a well-established body of data obtained with various techniques. While one cannot rule out the possibility that mixing ratios outside of the individual range may indeed occur, one can say that there is no compelling experimental evidence at the present that contradicts the range given in Figure 1-63. As a consequence, this area is thought to represent the best current experimental status of the NO altitude profile for northern (and perhaps southern) mid-latitudes (the equatorial zone is excluded) and all seasons except winter. The variation between extremes is typically a factor of three at the lower altitudes. However, the uncertainty is considerably larger above 40 km. Furthermore, because of the substantial difference between the results of Horvath and Roscoe at 50 km and since the latter has only one data point at these altitudes, the uppermost limit on the observed NO mixing ratios is quite uncertain above 50 km. The profile in Figure 1-63 is the one against which the predictions of 1-D models can be best compared at the present. The equatorial exclusion arises because of the paucity of data and the possibility of significant differences from the equatorial latitudes. The winter and the high-latitude exclusions arise because measurements have indicated that there are substantial differences in the profiles at this season and location, as described below.

Diurnal Variation

Observations have confirmed all of the major NO diurnal variations expected from the stratospheric odd-nitrogen chemistry: essentially no NO at night, a rapid increase at sunrise, a slow increase during the daytime, and a rapid decrease at sunset. All of these features have been observed in detail with both in situ and remote techniques.

The most extensive set of observations are from the in situ studies of Ridley and coworkers, who used their balloon-borne chemiluminescence instrument. Figures 1-64 and 1-65 show sunrise and sunset data, respectively. The sunrise 1975 flight employed two separate chemiluminescence instruments (Ridley et al., 1977), neither of which had the improved inlet calibration procedures adopted in 1977 (Ridley and Schiff, 1981). Although it might be fortuitous, the NO mixing ratios are, however, in accord with those from their later flights (see Figure 1-60). Figure 1-65 shows this group's sunset measurements (Ridley and Schiff, 1981). Both sets of data reveal these rapidly changing events in remarkable detail and Figure 1-64 clearly shows a slow NO increase during the daytime.

Patel and coworkers have also examined these variations in situ, as is shown in Figure 1-66 (Burkhardt et al., 1975). The detail is less and no one flight covered the whole period, but the use of an entirely different technique, spin-flip laser absorption, provides valuable corroboration of the chemiluminescence results.

Long-path remote studies of the total column density of NO, thus far limited to sunrise and sunset observations, show the early-morning and late-afternoon difference. Mankin and coworkers have used Fourier transform absorption spectroscopy aboard an aircraft to measure the daytime column density of NO above 12 km (Coffey et al., 1981). Their extensive measurements, which are presented in detail below, show a factor of two larger NO column density near sunset when compared to that observed after sunrise. However, Girard and coworkers, using an IR spectrometer in a similar fashion, failed to find such a daytime variation (Fontanella et al., 1975; Girard et al., 1978/79). The reason for the discrepancy is not clear and further comparisons of the result of Girard and coworkers with those of other groups are made below.

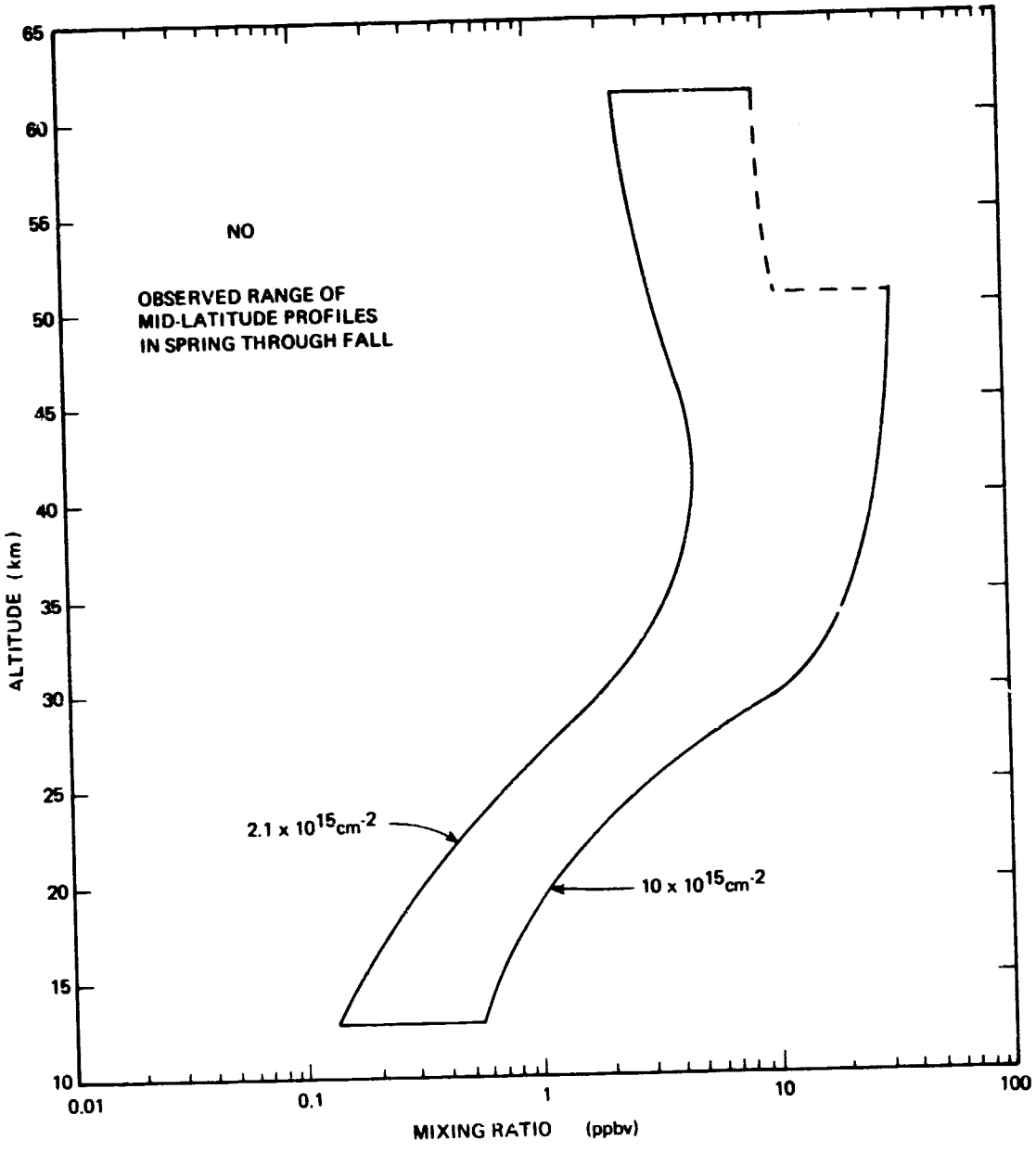

Figure 1-63. Current best observed NO mixing ratios in the northern and southern mid-latitudes in spring through fall. The width of the indicated range includes essentially all of the measurements and their estimated uncertainties. The vertical column values correspond to the left and right edges of the mixing ratio range.

C-2

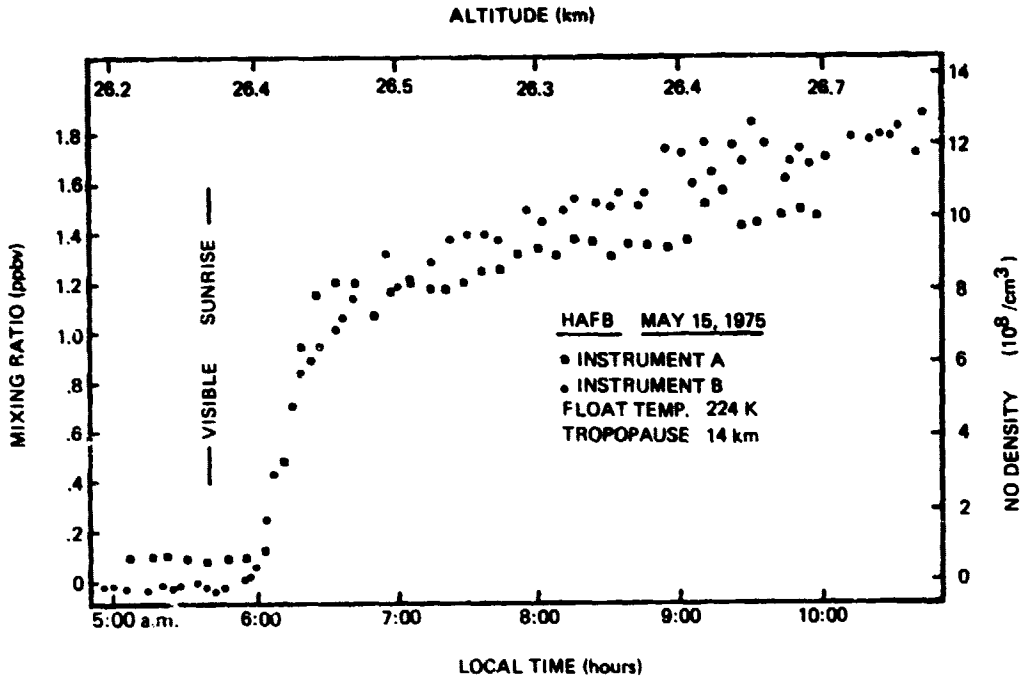

Figure 1-64. The sunrise in situ NO measurements of Ridley et al. (1977) obtained using two chemiluminescence instruments simultaneously flown on May 15,1979 near 33°N, 106°W.

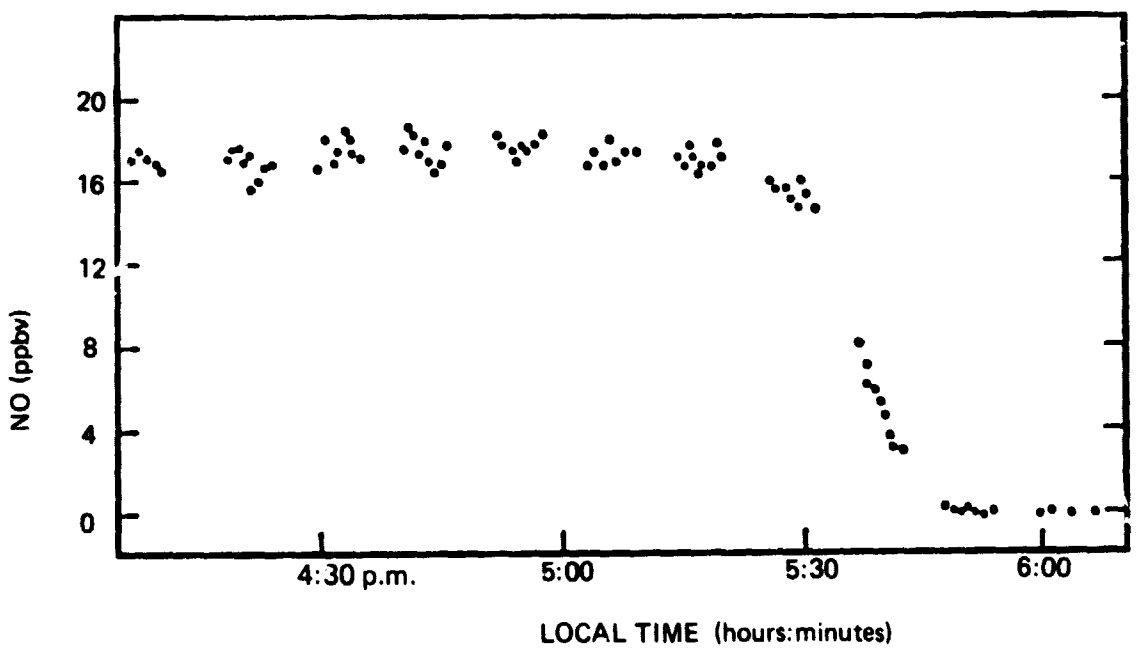

Figure 1-65. The sunset in situ measurements of Ridley and Schiff (1981) obtained with a chemiluminescence instrument flown on November 8, 1978 near 32°N, 96°W.

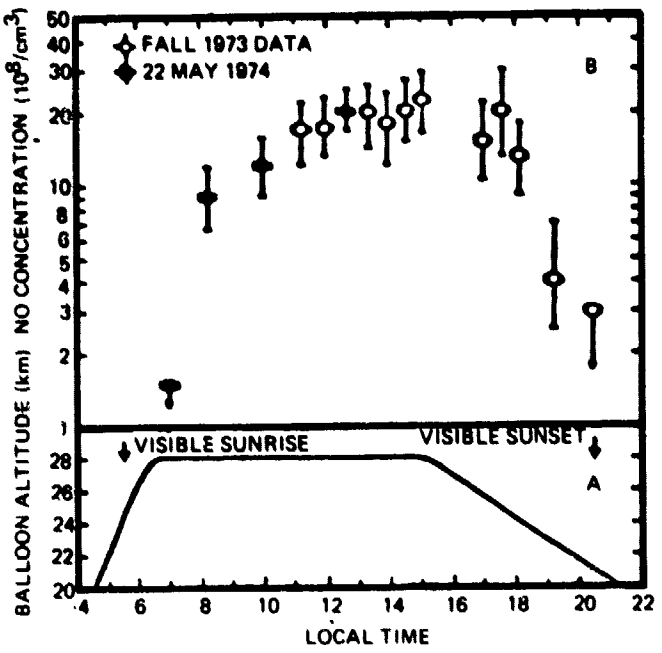

Figure 1-66. The sunrise and sunset in situ NO measurements of Burkhardt et al. (1975) obtained with a spin-flip infrared absorption instrument flown at 32°N, 96-106°W.

Loewenstein and coworkers have used their U-2-borne chemiluminescence instrument to study the "diurnal" behavior of NO at 20 km during the 26 February 1979 total solar eclipse (Starr et al., 1980). Figure 1-67 shows the results. During the eclipse maximum, the NO mixing ratio was at or below the 0.003-ppbv detection limit. Although it is not related to this "diurnal" behavior, the equilibrium NO mixing ratios before and after the eclipse were about 0.1 ppbv, which, for the 20 km flight altitude, are lower than the spring-through-fall profile in Figure 1-67. Whether this is a winter pattern or a dynamics-controlled "event" is not certain.

Seasonal Variation

The variation of NO with season necessarily requires an extensive measurement program. Fortunately, several such studies have been conducted with different techniques. The various results are in reasonable harmony.

The most extensive of such investigations are those of Loewenstein and coworkers using a U-2 chemiluminescence instrument. The studies have revealed two major seasonal effects. The first of these stems from a 4-year flight series at 21.3 km during all months of the year. The results are shown in Figure 1-68 (Loewenstein et al., 1977). A rather sharp winter minimum and a broader summer maximum is apparent. The ratio of the maximum and minimum concentrations is about six. The reproducibility of the pattern over 4 years makes it difficult to doubt its reality.

Furthermore, the same trend, although defined by less data, has been found at 18.3 km. Apparently, there are no other in situ or remote NO measurements that have been made at mid-latitudes in December or January that could offer corroboration of the magnitude of this effect. Although not directly comparable, vertical-column measurements do show slightly more NO in the summer than in the winter in mid-latitudes, but the ratio is only 1.4 (Coffey et al.,

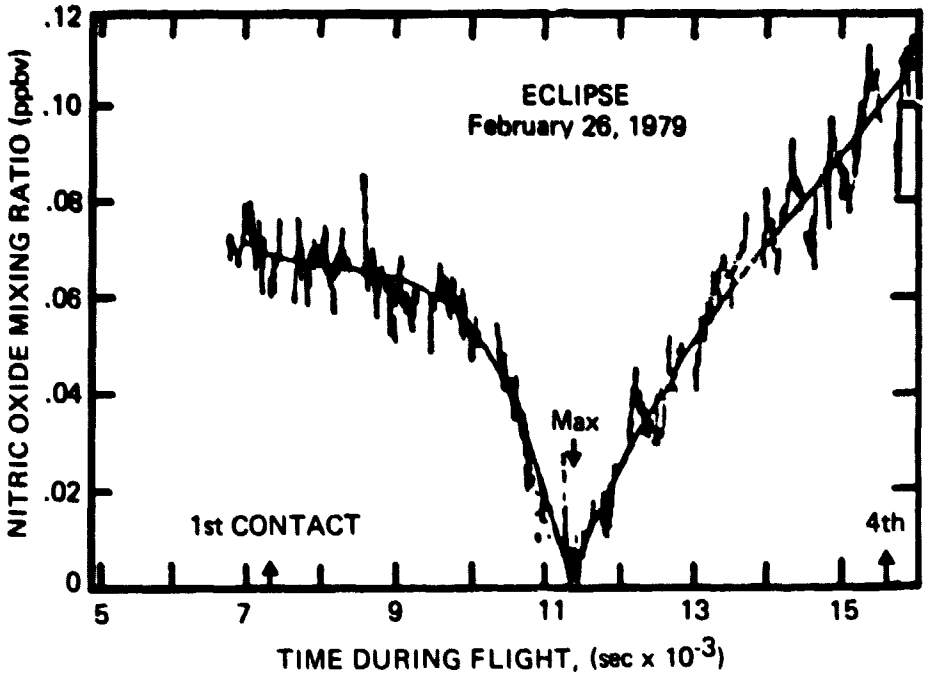

Figure 1-67. The in situ measurements of Starr et al. (1980) obtained with a chemiluminescence instrument flown during a total solar eclipse at 20 km and 47°N, 112°W. The solid line is a smooth representation of the data.

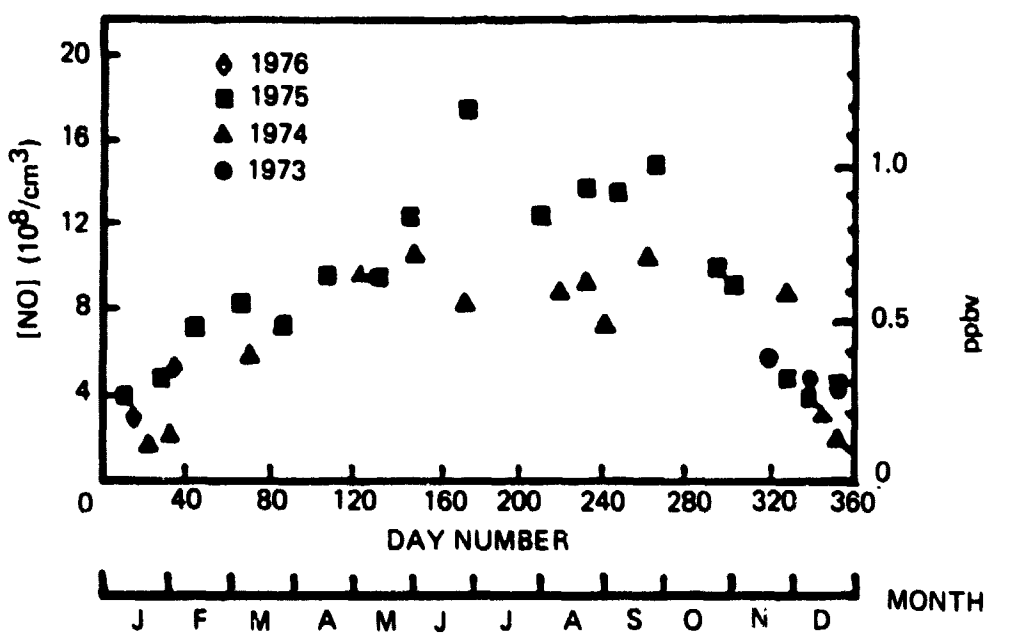

Figure 1-68. Nitric oxide seasonal data (122°W, 40°N) summary at 21.3 km. The in situ NO measurements of Loewenstein et al. (1977) obtained with a chemiluminescence instrument.

1981). However, as noted in more detail below, these winter measurements were in mid-February, which is somewhat later than the time at which the U-2 flights indicate the minimum NO concentrations.

The second striking seasonal variation discovered by Loewenstein and coworkers is shown in Figure 1-69. The data are from several summer and fall flights at 18 km altitude and from 5°N to 80°N latitude. North of about 50° or 60°, the NO concentration exhibits a marked seasonal variation; the summer values are an order of magnitude larger than the fall values. There were no winter or spring high-latitude flights, so only a summer-fall comparison is possible. The fall high-latitude values are nearly zero; therefore, the winter values cannot be much lower. At 21 km, the high-latitude data are sparse; hence, the spring-fall difference seen at 18 km could not be investigated.

Remote measurements have shown some of these seasonal features, but to a lesser magnitude. Figure 1-70 gives the vertical-column values of Coffey et al. (1981), made by Fourier transform infrared absorption spectroscopy from an aircraft platform. The summer values are somewhat higher than the winter values. Furthermore, there is a distinct reduction in the NO column at 50°N in the winter, much like that found in the in situ data. The more limited measurements by Girard et al. (1978/79), who used a similar absorption technique, do show a winter, high-latitude reduction, but these observations were made in an earlier month. The values for the NO vertical column above about 11 km obtained by Coffey et al. (1981) and Girard et al. (1978/79) are about 3.5×10^{15} cm^{-2} and 5.0×10^{15} cm^{-2}, respectively. The difference is about equal to the combined uncertainties.

Latitudinal Variations

Between 5°N and about 50°N, there is substantial evidence that the latitudinal variation of NO is not large. Figure 1-69 shows the north-south variation for summer at 18 and 21 km altitude measured by Loewenstein et al. (1978a). These data are typical of those obtained from their other north-south transects. The largest 5°N-to-50°N difference is about 2.5, the values increasing in a northern direction. Figure 1-70 has shown that the vertical-column data of Mankin and coworkers (Coffey et al., 1981) exhibit only a small latitudinal variation between 5°N to 45°N, approximately 1.3 at most. Moreover, the studies of Girard and coworkers (Girard et al., 1978/79), which employed similar absorption techniques, found the same trends.

Other Variations

Although the height profiles of Ridley and coworkers have shown little change from one year to another, there is some evidence that suggests that NO can vary considerably. Ackerman et al. (1975) have reported order-of-magnitude differences between height profiles inverted from long-path absorption data. No lengthy series of remote measurements of NO have been made, however, and it is difficult to assess whether large changes occasionally occur in the stratospheric NO mixing ratios.

Nitrogen Dioxide (NO_2)

Introduction

Several extensive flight and ground-based measurement programs have established a better picture of stratospheric NO_2 in recent years. NO_2 is a rather variable constituent, both in time and in location, and some of its now recognized variations, such as the winter minimum at high latitudes, are an unanswered challenge to theory.

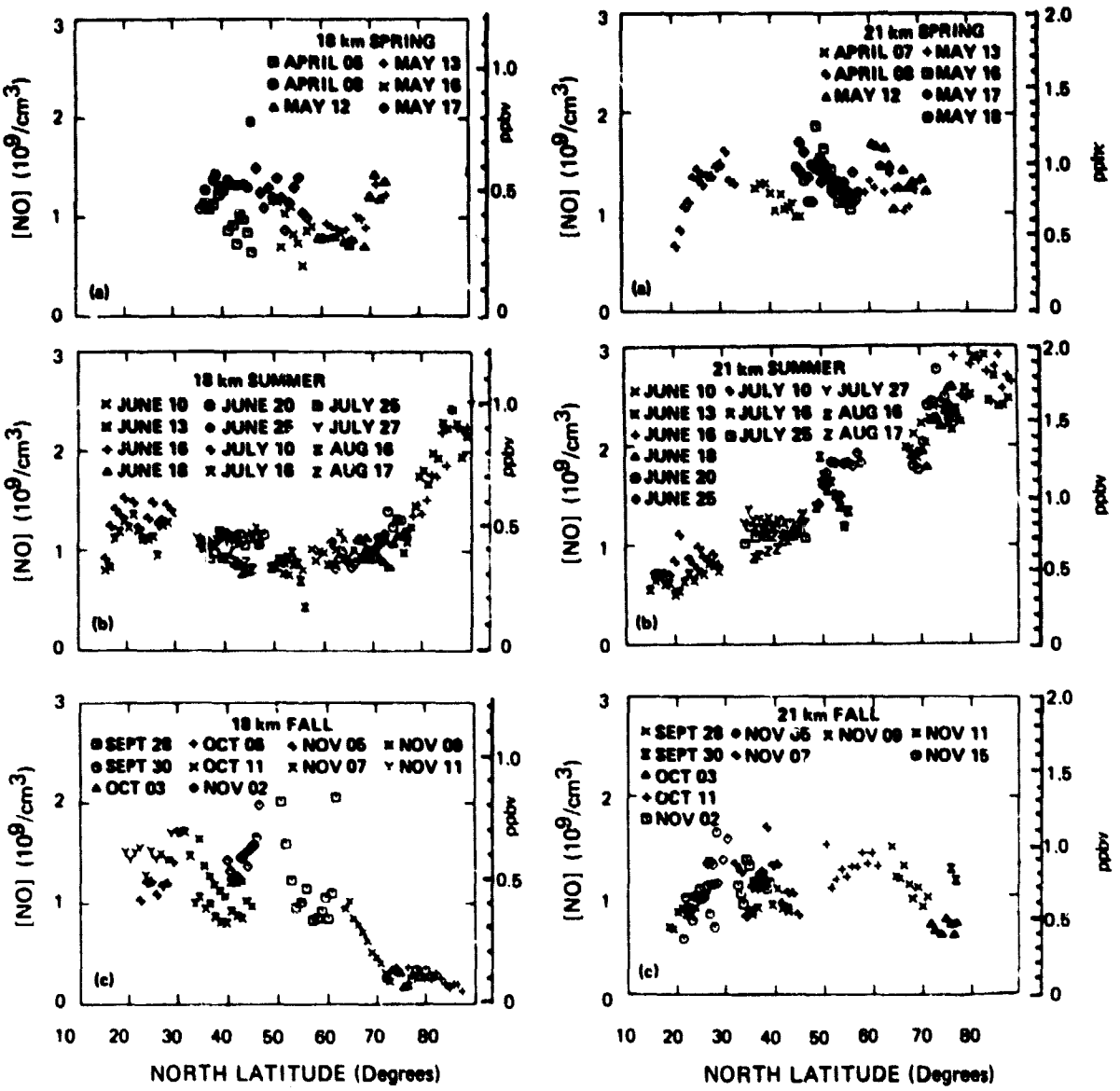

Figure 1-69. The in situ NO measurements of Loewenstein et al. (1978a) obtained with a chemiluminescence instrument in 1975 and April-May, 1976.

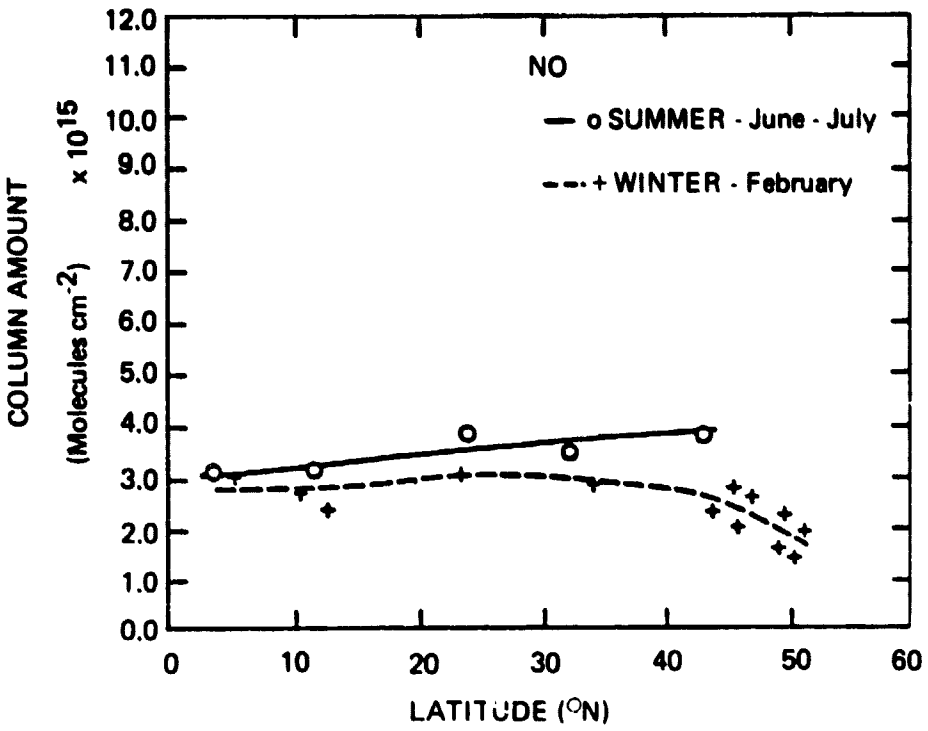

Figure 1-70. The vertical-column measurements of NO above 12 km made by Coffey et al. (1981) with a Fourier transform infrared absorption instrument in 1978, 1979, and 1980 at west longitude 80 to 119 degrees.

Altitude Profile

There are virtually no in situ measurements of NO_2 in the stratosphere; hence, essentially all of the information about the NO_2 altitude profile has come from remote techniques. Most of these methods have required the long path associated with the rising or setting Sun, obtaining the vertical variation of the NO_2 mixing ratio by unfolding it from the change of the slant column density as a function of the viewing angle. Thus, the majority of the NO_2 altitude profile measurements are grouped into either sunrise or sunset profiles. The sunset mixing ratios of NO_2 are larger than those at sunrise, the increased NO_2 having been formed from the photolysis of N_2O_5. In addition to this sunrise/sunset difference, there are marked seasonal and latitudinal variations in the vertical column of NO_2. As noted in detail below, the NO_2 vertical-column values increase with increasing latitude and are larger in the summer than winter. Therefore, the large number of profile observations must be gathered into subgroups of certain times, places, and seasons, in order to have a well-defined, homogeneous profile. The largest of these is the subset of sunset profiles. This subset is examined here to see if they also show latitudinal or seasonal trends.

Figures 1-71, 1-72 and 1-73 show observed sunset profiles at approximately 32°, 48°, and 55°N, respectively. Each profile is made up of at least two flights. The error bars reflect the reported uncertainties.

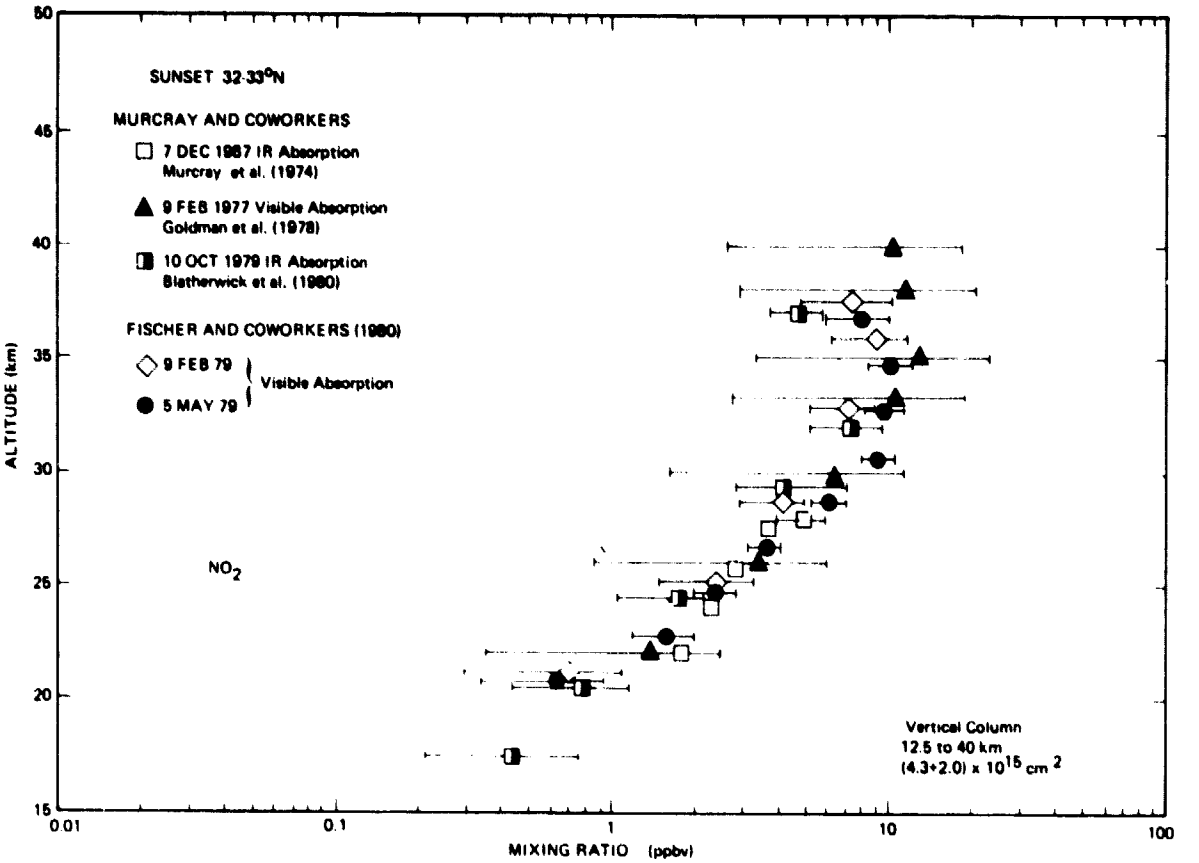

Figure 1-71. Remote measurements of the sunset altitude profile of NO_2 made at 32 to 33°N latitude.

Figure 1-71 contains the results of the extensive flight series of Murcray and coworkers, who employed infrared (Murcray et al., 1974; Blatherwick et al., 1980) and visible (Goldman et al., 1978) absorption techniques from a balloon platform launched in the southern United States. Accompanying these data are the results of the two recent flights of Fischer and coworkers (personal communication, 1981). The data set includes winter, spring, and fall flights, but there are no obvious seasonal differences between the profiles. This lack of variation is in accord with the vertical-column observations, which (see Figure 1-78 below) find little seasonal variation at latitudes below 35°N. However, the lack of a summer flight precludes the most sensitive test, namely, a summer/winter comparison.

Figure 1-72 gives the results of flights that were made in the early 1970s using infrared absorption on balloon (Ackerman and Muller, 1973; Ackerman et al., 1975) and aircraft (Fontanella et al., 1975) platforms in France. The 16×10^{-9} value of Rigaud et al. (1977) at 37 km in May of 1976 seemed too large to warrant inclusion. Three seasons are represented (winter is missing), but the small data set and the experimental uncertainties complicate the examination for seasonal trends.

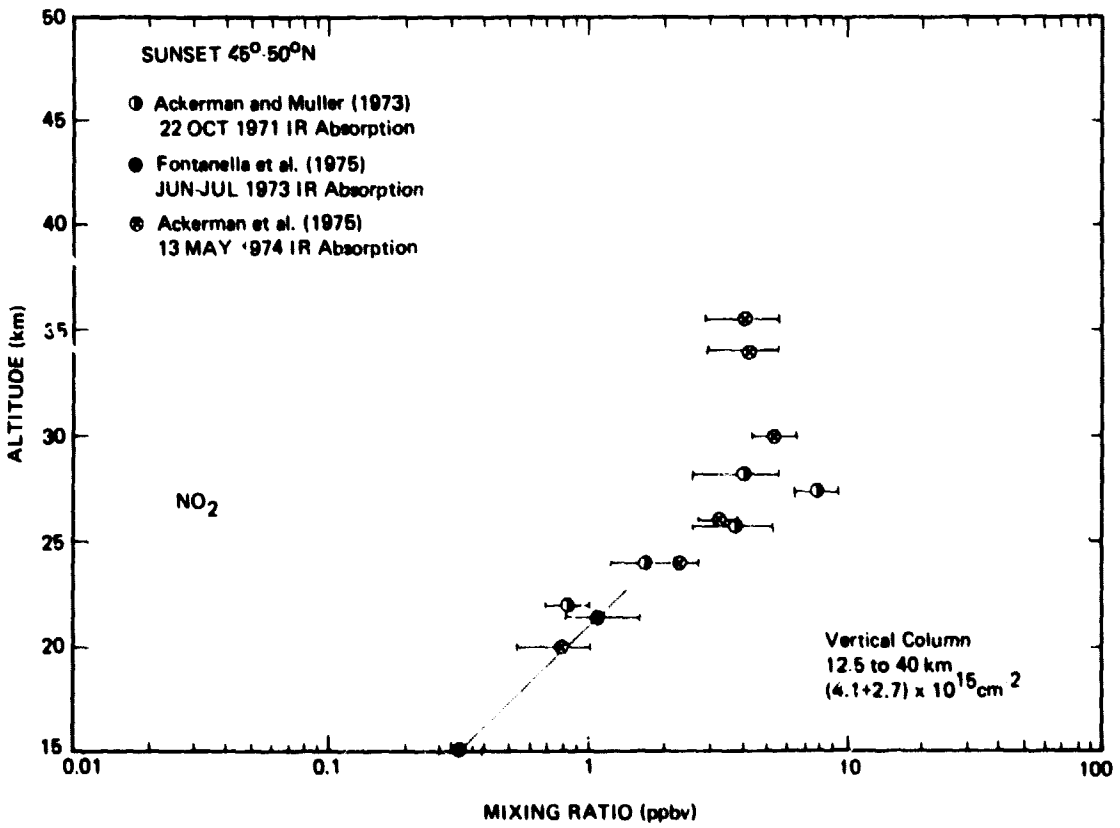

Figure 1-72. Remote measurements of the sunset altitude profile of NO_2 made at 45 to 50°N latitudes.

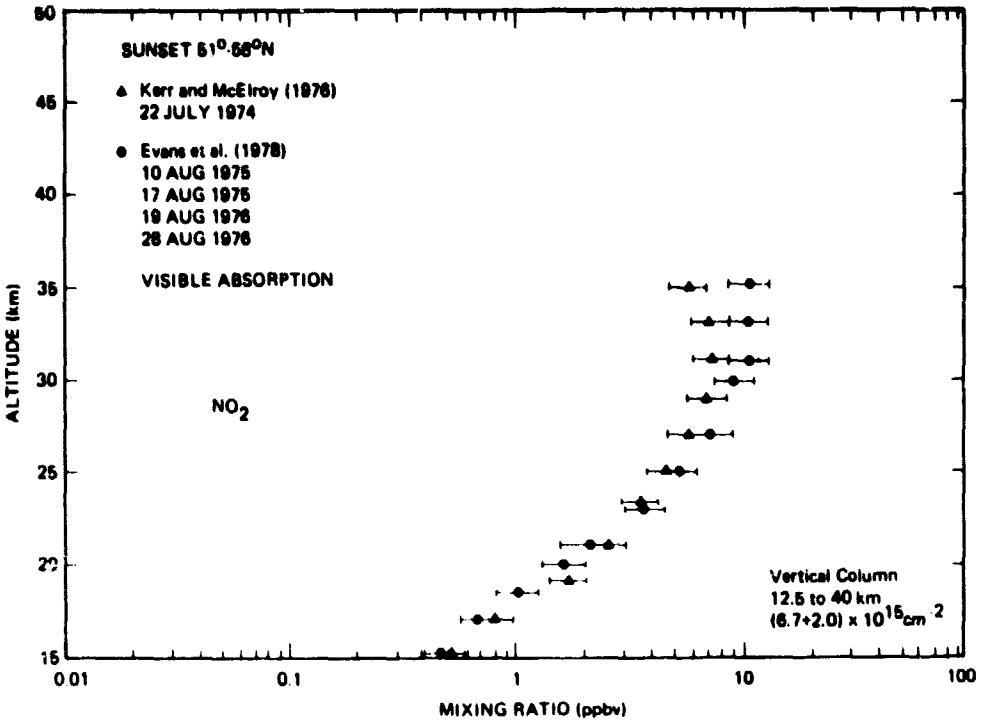

Figure 1-73. Remote measurements of the sunset altitude profile of NO_2 made at 51 to 58°N latitudes.

Figure 1-73 shows the results from flights made over a 3-year period in Canada using visible absorption techniques (Kerr and McElroy, 1976; Evans et al., 1978). Two sets of results are shown. The data of Evans et al. (1978) summarize the results of four flights. All five flights occurred in the summer.

The data in Figures 1-71, 1-72, and 1-73 are in good agreement within each latitude range. The high-latitude mixing ratios are up to a factor of two larger than the mid-latitude values in the range from 15 to 30 km, as a comparison of Figures 1-71 and 1-73 shows. Since the concentrations associated with such profiles reach a maximum value at about 25 km, these larger high-latitude values cause the associated vertical-column value to be larger. Although the uncertainties are relatively large, this 2.4×10^{15} cm^{-2} difference, which is a 50% increase corresponding to a 20° change in latitude in the summer, is in good agreement with the change that has been observed in vertical-column studies of the latitudinal dependence of NO_2 in the summer. Unfortunately, no one research group has data represented in two or more of Figures 1-71 through 1-73. Therefore, it remains possible that the agreement may be fortuituous, particularly since the 45° to 50°N vertical-column datum does not fit very well into the trend. It is nevertheless reassuring that the associated vertical-column values determined from these profiles agree fairly well with those directly measured (see Figures 1-78 and 1-79 below). Furthermore, the forthcoming SAGE satellite results (McCormick, personal communication, 1981) are quite consistent with these data.

One-dimensional model and observations can probably best be compared using the 32 to 33°N profile in Figure 1-71. However, the large zenith angle associated with these sunset measurements implies that a meaningful comparison will not be straightforward.

Figure 1-74 contains the results of measurements that were made in full daytime and nighttime. The daytime studies are from the long-path pressure-modulated infrared radiometer of Roscoe et al. (1981) and the in situ matrix isolation collector of Mihelcic et al. (1978). Earlier daytime long-path studies (Harries et al., 1976; Drummond and Jarnot, 1978) had considerably less precision and are not included here. The nighttime study is the long-path absorption investigation of Naudet et al. (1980), who used a star as light source.

Diurnal Variations

Both vertical-profile and vertical-column measurements have defined the diurnal variation of NO_2. Figure 1-75 shows the morning-evening difference reported by Evans et al. (1978), who averaged the results of four flights. The decrease from evening to morning is about a factor of two, which agrees with vertical-column measurements. Figure 1-76 shows the results of Mankin and coworkers (Coffey et al., 1981), who used infrared absorption spectroscopy aboard an aircraft. Noxon's ground-based absorption spectroscopic technique (Noxon et al., 1979; Noxon, 1980) shows a factor of two larger NO_2 vertical column density at night when compared to daytime values, which is consistent with the above studes. Girard et al. (1978/1979), using similar techniques, did not initially find a sunrise-sunset difference; however, recent, more precise measurements (Girard, personal communication, 1981) have found this difference.

Seasonal Variations

The seasonal variations of NO_2 are best illustrated by the extensive ground-based measurements of Noxon (1979). Figure 1-77 shows the results of 4 years of vertical-column measurements at various northern latitudes. The winter minimum and summer maximum is extremely regular and the ratio is as large as a factor of five at the higher latitude. Girard et al. (1978/79) report the same seasonal trend, but it is less well defined in their smaller data set. Other vertical column measurements have also been less extensive and some unusually large values have been reported (Pommereau and Hauchecorne, 1979).

Latitudinal Variations

Vertical column measurements have demonstrated that NO_2 increases with northward latitudes. Figure 1-78, which gives the airborne measurements of Mankin and coworkers, shows an increase of 50% between 5°N and 30°N, independent of season (Coffey et al., 1981). This lack of a strong seasonal variation at 30°N is consistent with the profile data in Figure 1-71. The vertical column value of Ogawa et al. (1981), 7×10^{15} cm^{-2}, from a 40°N, May, balloon flight is in good agreement with the summer data of Coffey et al. (1981).

At the higher latitudes, however, there is a pronounced seasonal effect. This is best illustrated in Figure 1-79, which gives the measurements of Noxon (1979), who first noted this unusual effect. In the summer, the NO_2 continues to increase with increasing latitude. However, in the winter, the polar NO_2 is very low, changing abruptly at about 45°N. The Southern Hemisphere is found to mirror the Northern in this regard (Noxon, 1978).

Other Variations

Noxon et al. (1979) have found that the vertical column density of NO_2 can change a factor of two within the time span of a few days. Figure 1-80 illustrates this phenomenon. On 26 April 1976, the NO_2 abundance increased sharply, only to fall within a day or so. The effect has been related to transport. This obviously implies that a single NO_2 profile cannot always be associated with a given location and season.

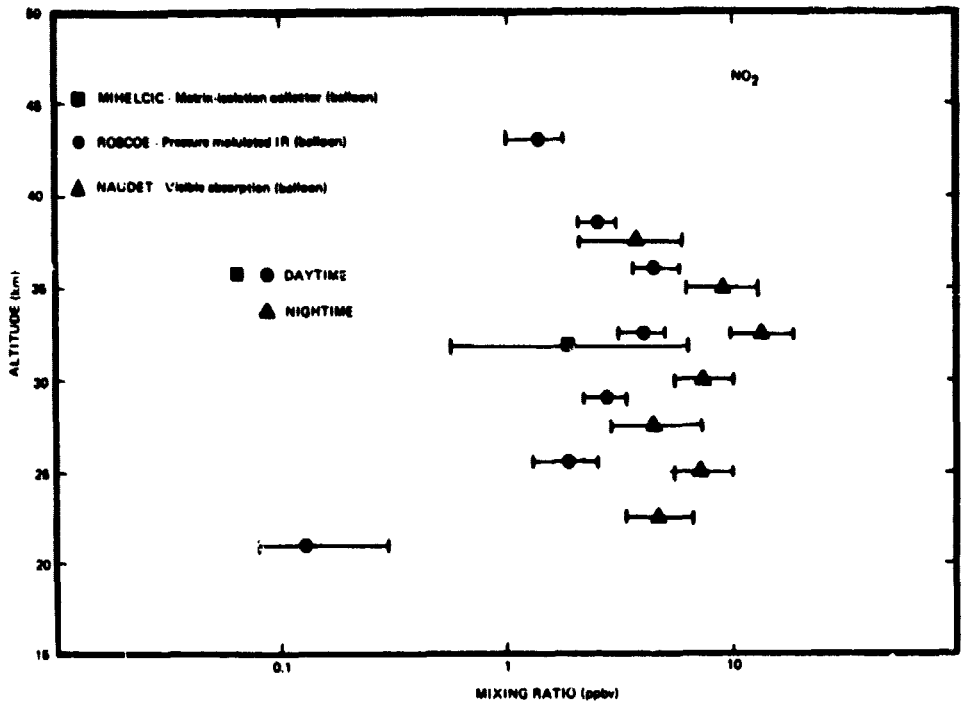

Figure 1-74. Results of full daytime and full nightime measurements of NO_2. The data of Roscoe et al. (1981) (daytime) and Naudet et al. (1980) (nighttime) were obtained using long pathlength techniques, while the daytime data of Mihelcic et al. (1978) were collected in situ.

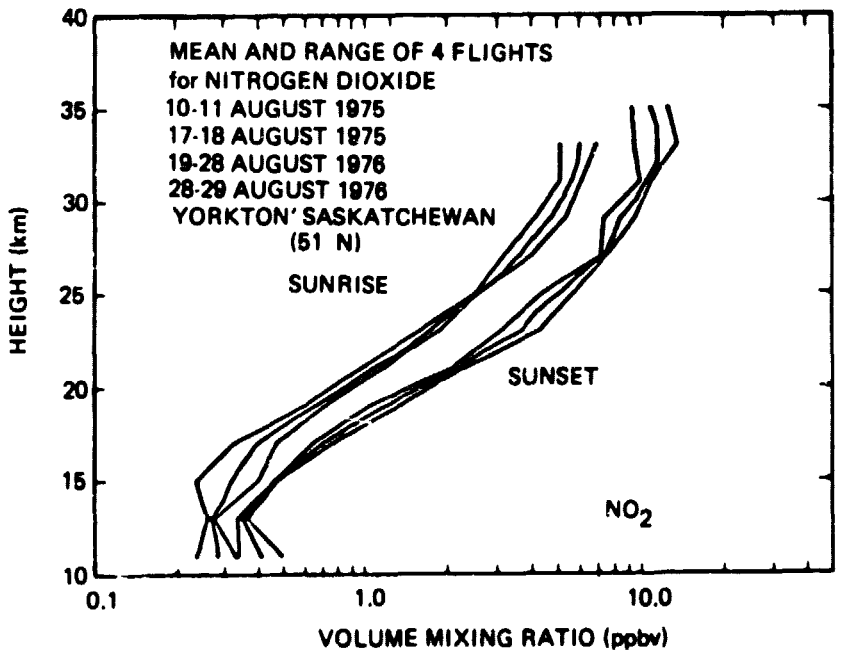

Figure 1-75. The sunrise and sunset altitude profiles of NO_2 reported by Evans et al. (1978) from the Canadian stratoprobe flight series. The upper and lower limits indicate the maximum observed deviations from the mean. The measurements were made using a balloon-borne visible absorption apparatus.

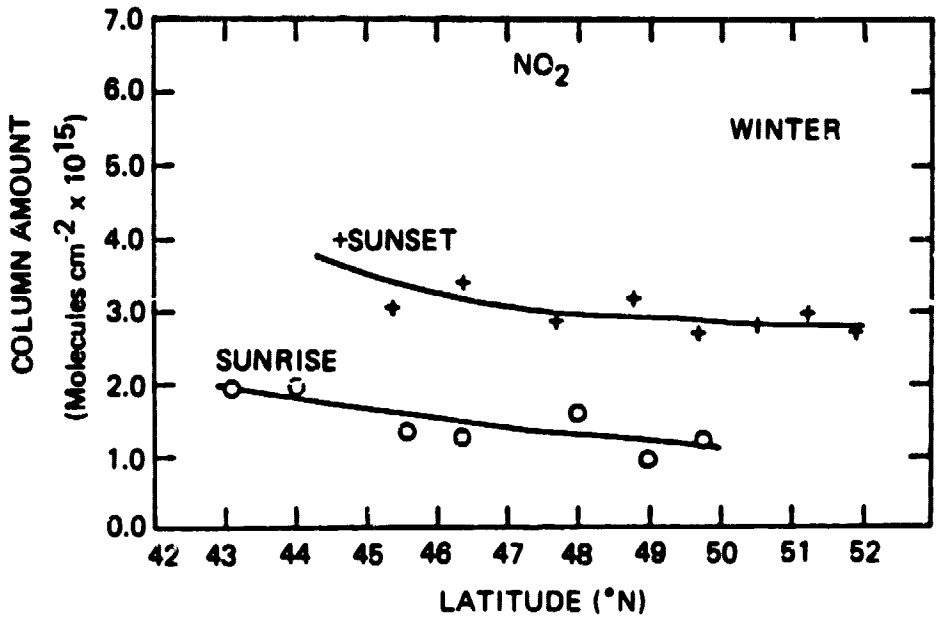

Figure 1-76. Sunrise and sunset vertical-column measurements of Mankin and coworkers, who used an infrared absorption apparatus on an aircraft platform (Coffey et al., 1981).

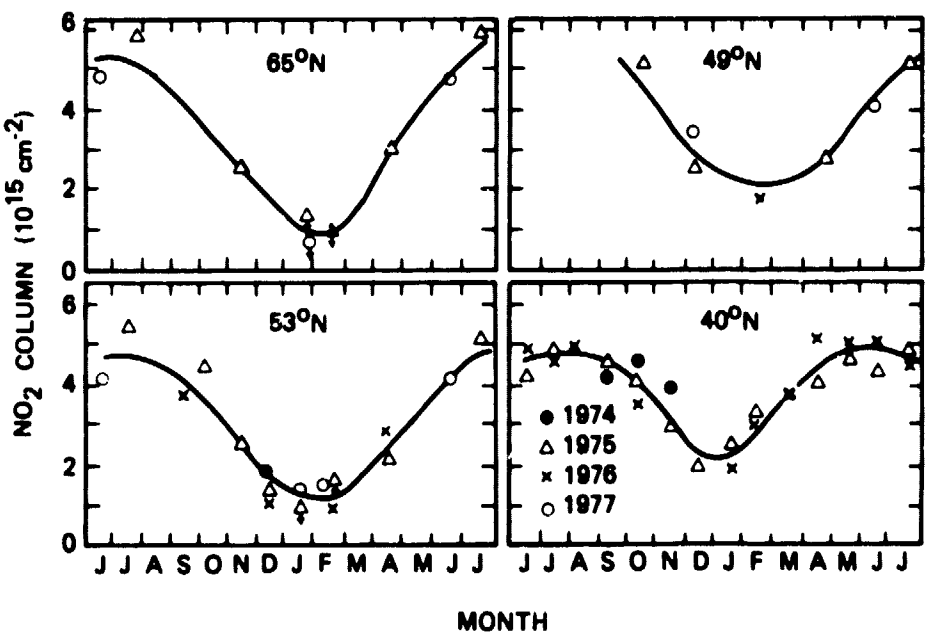

Figure 1-77. Seasonal variation of late-afternoon NO_2 at four latitudes, as given by the ground-based visible absorption spectroscopic measurements of Noxon (1979). The abundance should be multiplied by 1.25 (Noxon, 1980).

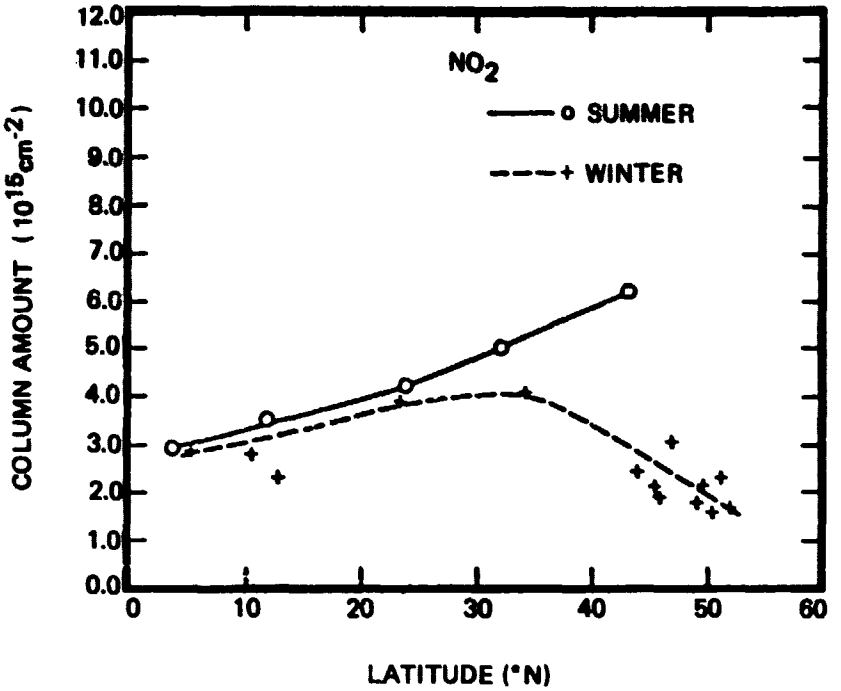

Figure 1-78. Latitudinal and seasonal variations of the late-afternoon vertical column of NO_2, as measured by Mankin and coworkers using aircraft-borne infrared absorption techniques (Coffey et al., 1981).

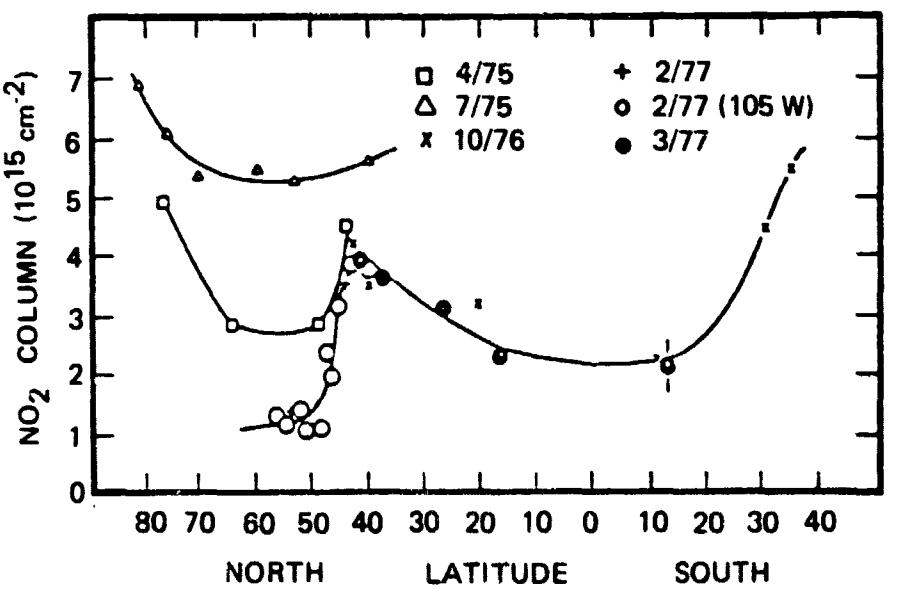

Figure 1-79. Latitudinal and seasonal variations of the late-afternoon vertical column of NO_2, as measured by Noxon (1979) using ground-based visible absorption techniques. The values represented by the open and filled circles should be multiplied by 1.6, all others by 1.25 (Noxon 1980).

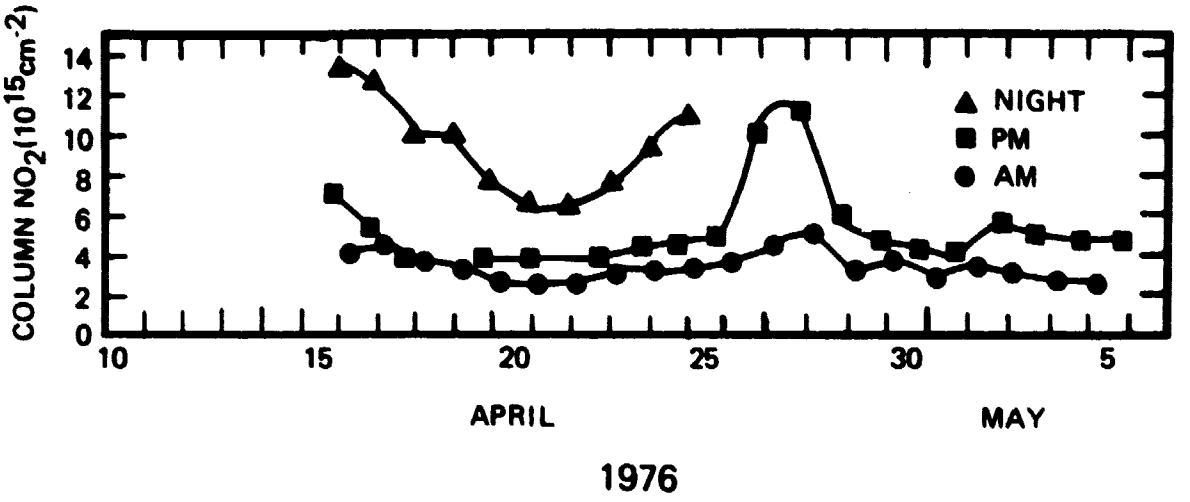

Figure 1-80. The daily variation of the vertical column of the nighttime, late-afternoon, and early morning NO_2 at 40°N in April and May 1976, as seen by Noxon et al. (1979), using ground-based visible absorption spectroscopy. The abundances should be multiplied by 1.25 (Noxon, 1980).

Nitric Acid (HNO_3)

Introduction

HNO_3 has been studied with a variety of in situ and remote techniques. The main features of the height profile have been established and much of the latitudinal variation is now well established. The current status is summarized in the section below and the details are contained in the remaining sections.

Altitude Profile

The altitude profile of nitric acid in the stratosphere has been established experimentally by in situ and remote techniques at Northern Hemispheric mid-latitudes and is shown in Figure 1-81.

Two in situ methods are represented. The first is that of Lazrus and Gandrud (1974b), who used a filter collection technique on balloon and aircraft platforms. The second in situ method is the rocket-borne ion-sampling technique of Arnold and coworkers (1980), with which the HNO_3 mixing ratio is deduced from the observed ion concentrations and the ion chemistry leading to their formation from the ambient HNO_3.

The remote measurements have employed the long path associated with the rising or setting Sun. Since HNO_3 has a long lifetime, the time of the day at which the measurement was made is not as critical a parameter as it is for NO and NO_2. Thus, both in situ and remote measurements can be meaningfully intercompared in Figure 1-81. Both infrared emission (Evans et al., 1978; Harries et al., 1976; Murcray, personal communication, 1980) and absorption (Fontanella et al., 1975; and Fischer, personal communication, 1980) have been used. The data of Evans et al. (1978) represent the mean of the results of four flights. All of the data in Figure 1-81 are in good agreement, with

the exception of the lower-altitude results of Lazrus and Gandrud (1974b) which tend to be lower than the other measurements.

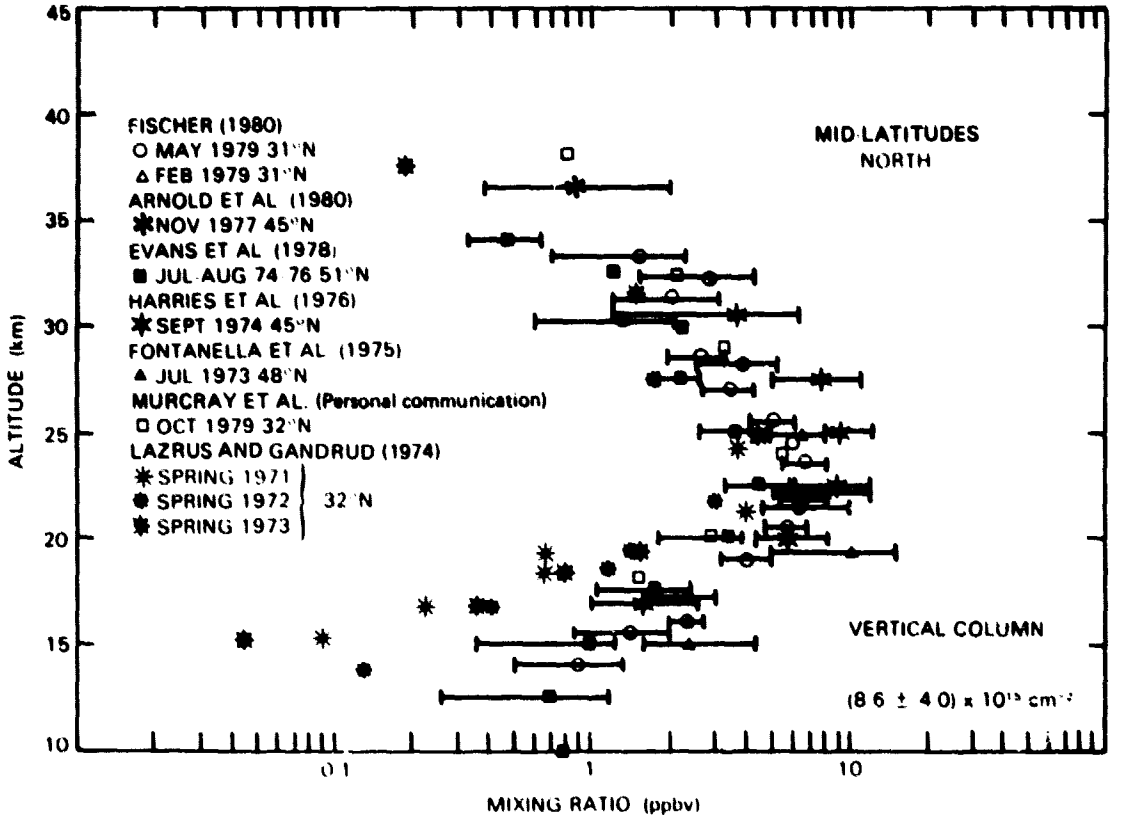

Figure 1-81. In situ and remote measurements of the HNO_3 mixing ratio at northern mid-latitudes.

There is no obvious seasonal trend in these profile data. Lazrus and Gandrud (1974b) reported that their winter and spring measurements showed higher HNO_3 concentrations than did their summer and fall measurements, but the data were too sparse to be able to make a more positive statement. The vertical column density associated with these profile measurements in Figure 1-81 is $(8.6 \pm 4.0) \times 10^{15}$ cm^{-2}, which is in fair agreement with the vertical-column measurements discussed below.

Diurnal Variation

No change in the HNO_3 abundance as a function of the time of the day has been observed.

Seasonal Variation

At latitudes less than about 40°N, there is no strong evidence to support a large seasonal variation. The vertical-column measurements of Mankin and coworkers, who used an aircraft-borne infrared absorption instrument (Coffey et al., 1981), found essentially no summer-to-winter change, as Figure 1-82 shows. Lippens and Muller (1981) found the slightly higher value $(1.8 \pm 0.4) \times 10^{16}$ cm^{-2} at 40°N in April.

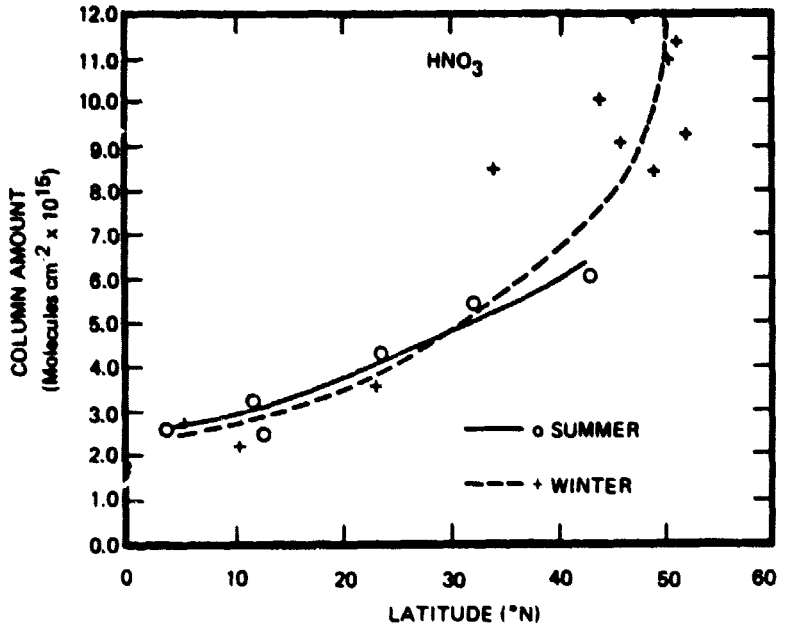

Figure 1-82. Evidence for the lack of seasonal variation in the vertical column density of HNO_3 at latitudes less than 40° as measured by Coffey et al. (1981) using infrared absorption.

Latitudinal Variation

The latitudinal variation of the vertical column of HNO_3 is well documented (Murcray et al., 1975, Coffey et al., 1981). There is a strong increase in the vertical-column density with increasing latitude, both in the Northern and Southern Hemispheres. Figure 1-83 shows the data of Murcray et al. (1975). Above about 50 to 60°N latitude, there appears to be a pronounced seasonal variation. At these high latitudes, the winter HNO_3 concentration is high (see Figure 1-82) and in the early summer, it seems to be much lower, as the data of Murcray et al. (1978) in Figure 1-84 show.

Other Variations

The observational program of Murcray and coworkers has also found that the vertical column of HNO_3 has short-term variability, as Figure 1-85 indicates. Within a few days, changes of 60% occurred, presumably due to atmospheric dynamics.

Nitrogen Trioxide (NO_3)

A single height profile is available for nighttime NO_3 (Naudet et al., 1981). The measurements were made at 43°N in September from a balloon. They are based on absorption in the visible region using Venus as the light source. The derived profile and stated uncertainties are shown in Figure 1-86.

The corresponding column abundance between 20 and 39 km is $(3.5 \pm 1.2)\times10^{13}$ cm^{-2}. This appears to be consistent with Noxon's estimate of about 10^{14} cm^{-2} in the spring and an upper limit of 4×10^{13} cm^{-2} in the summer.

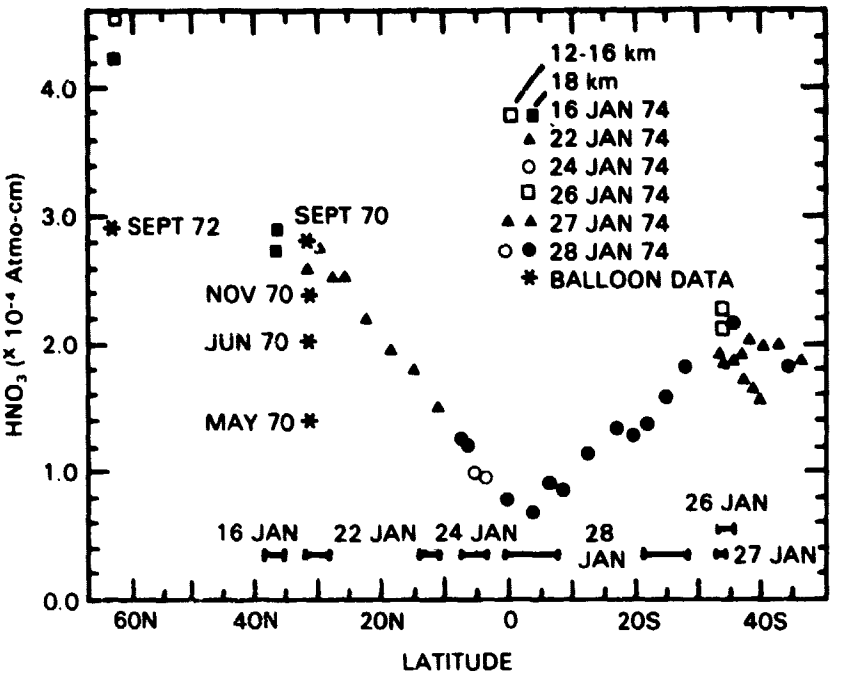

Figure 1-83. The latitudinal variation in the vertical column density of HNO_3, as measured by Murcray et al. (1975) using infrared emission. (1 atmos-cm = 2.7×10^{19} molecules/cm^2).

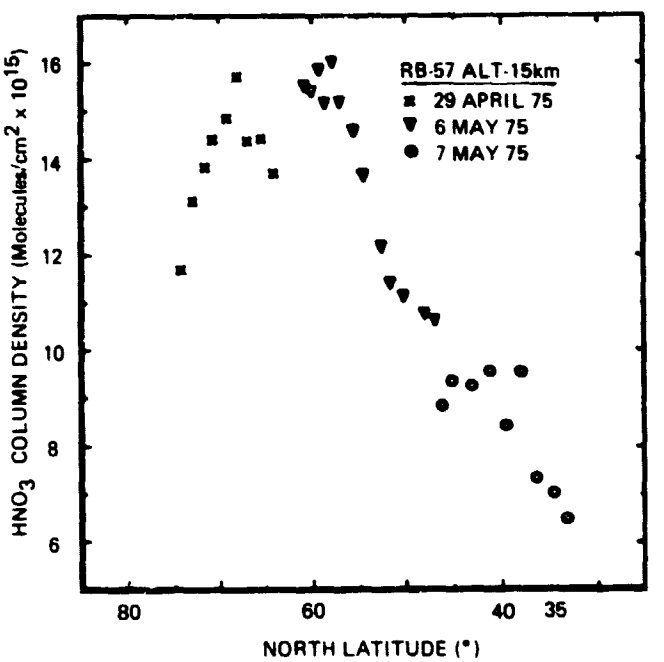

Figure 1-84. The decline of the HNO_3 vertical column density at high latitudes in the spring north of 70° as seen by Murcray et al. (1978) using infrared emission.

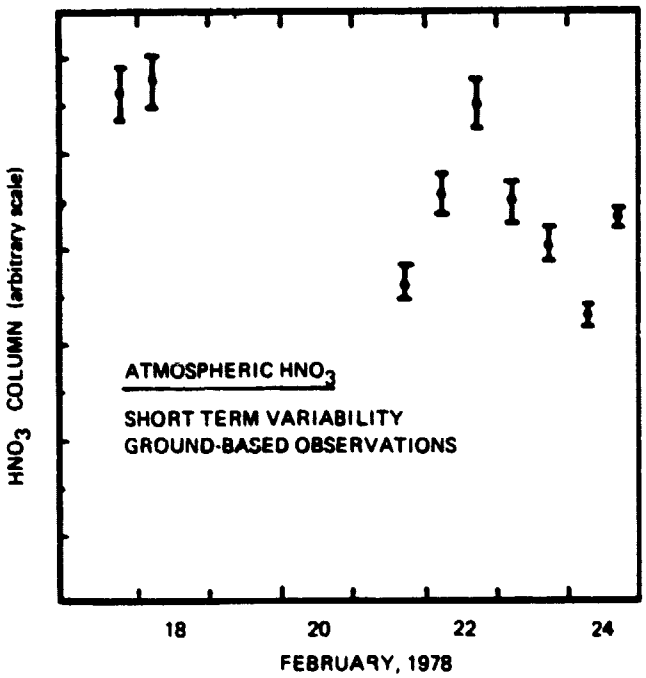

Figure 1-85. Short-term variability of the vertical column density of HNO_3, as seen by Murcray et al. (1978) using infrared emission.

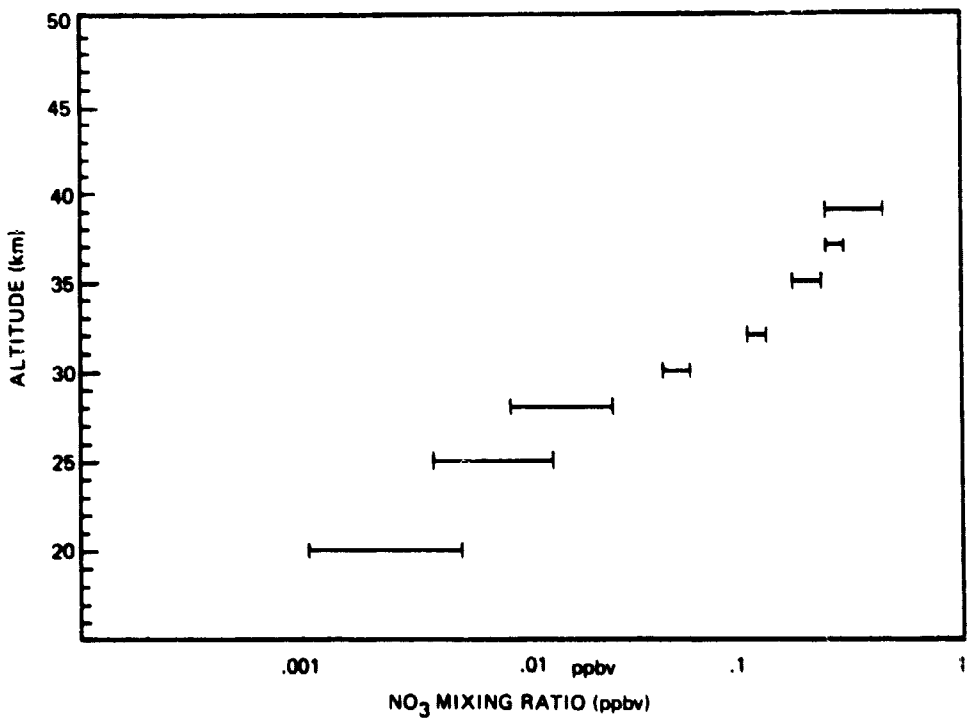

Figure 1-86. Vertical nighttime profile of NO_3 (Naudet et al., 1981) measured using visible absorption with Venus as a light source.

Nitrogen Pentoxide (N_2O_5)

There have been no new measurements of N_2O_5. This situation remains as reported in NASA RP 1049: A tentative detection of 2 ppbv at 30 km a few hours after sunrise by Evans et al. and an upper limit of 1.2×10^{15} cm^{-2} above 18 km in February by Murcray.

Peroxynitric Acid (HO_2NO_2)

Despite the recent interest in this species no detection of its presence has been reported. The upper limit remains at 0.4 ppbv as reported in NASA RP 1049.

ODD HYDROGEN

Hydroxyl Radical (HO)

Hydroxyl has been observed in the stratosphere by four independent techniques:

- Solar flux induced resonance fluorescence observed by a rocket-borne spectrophotometer (Anderson, 1971a; Anderson, 1971b) which provides a local concentration measurement by determining the change in total column emission rate as a function of altitude.

- Balloon-borne in situ molecular resonance fluorescence using a plasma discharge resonance lamp to induce fluorescence. The fluorescence chamber is lowered through the stratosphere on a parachute to control the altitude and velocity of the probe (Anderson, 1976; Anderson, 1980).

- Ground-based high resolution solar absorption by a PEPSIOS (Poly-Etalon Pressure Scanned Interferometer) instrument which resolves a single rotational line in the (0-0) band of HO at 309 nm. The total column density of terrestrial HO between the instrument and the Sun is observed, dominated by the altitude interval 25 to 65 km (Burnett 1976, 1977; Burnett and Burnett, 1981).

- Balloon-borne laser induced detection and ranging (LIDAR) in which a pulsed laser system coupled to a telescope is used to observe the backscattered fluorescence from HO. The laser is tuned to the 1-0 band of the A-X transition at 282 nm and the fluorescence at 309 nm (the 0-0 band) is observed as a function of time following the laser pulse (Heaps and McGee, 1981).

Rocket-Borne Solar Induced Fluorescence

A single rocket-borne HO observation (Anderson, 1971b) constitutes the only observation of this radical above the stratopause and because of the importance of this region to the interpretation of ground-based data, we must treat the accuracy and precision of the method.

The technique employs a high resolution scanning spectrophotometer mounted in the nose of the rocket, looking vertically as the rocket ascends. The spectrometer is polarized and rotated about the roll axis of the rocket to discriminate against Rayleigh scattered light from N_2 and O_2 (which is polarized) that otherwise masks the fluorescence emission from HO (which is not polarized). As the instrument ascends, the total column emission above the rocket is measured. That column brightness, $4\pi J$, is related to the HO column concentration, N, by the expression:

$$4\pi J = \pi F \frac{\pi e^2}{mc^2} \lambda f N \beta$$

where π F is the solar flux at each rotational line of the (O-O) band of the A-X transition of HO, λ is the wavelength, f is the oscillator strength of the transition and e, m, and c have their customary definitions. Collisional deactivation is expressed by β, the ratio of the radiative rate to the sum of the radiative rate and the rate of collisional deactivation. Experimental uncertainties are summarized in the table below:

Quantity	Uncertainties
Solar Flux, π F	±30%
Oscillator strength, f	±20%
Quenching coefficient, β	±15%
Background subtraction	±30%

A root mean square uncertainty of ±20% is adopted in this report.

Balloon-Borne In Situ Resonance Fluorescence

This method employs the allowed transition between the $A^2\Sigma$ and the $X^2\Pi$ state of HO at 309 nm. HO resonance radiation is obtained from a low pressure plasma discharge in helium and a trace amount of H_2O vapor. This radiation is collimated and passed across a flowing sample of stratosphere air created by lowering the instrument through the stratosphere on a stabilized parachute. Photons resonantly scattered from the beam by HO are counted by a photomultiplier observing the axial region of the flow which is passed through the core of an aerodynamically shaped vessel. The vessel both contains the flow, to allow controlled chemical conversion to be carried out, and isolates the detector from the radiation environment of the stratosphere.

The instrument is calibrated in a laboratory flow reactor which is capable of forming a known concentration of HO at pressures and flow velocities appropriate to the stratosphere observations. Because the instrument is removed from the laboratory system and flown without change, it is necessary only to determine the proportionality factor relating observed count rate to the absolute HO concentration for a given photon flux. Thus, the accuracy of the calibration depends only on uncertainties in the absolute HO concentration in the laboratory system.

A detailed account of experimental uncertainties (see Anderson, 1975) implies an overall experimental uncertainty of ±30%.

Ground-Based High Resolution Ultraviolet Absorption

The Poly-Etalon Pressure Scanned Interferometer (PEPSIOS) instrument developed by Burnett and Burnett (1981) for the detection of total HO column density uses a single rotational line in the (0-0) band at 309 nm. Given that the rotational line is fully resolved by the instrument, and the absorption cross section is a carefully measured and well known quantity, the major experimental uncertainty results from the proper subtraction of the background radiation. While this process is complicated to some degree by stray light in the instrument a careful analysis by Burnett and Burnett (1981) implies an accuracy of ±25% for the reported results.

Balloon-Borne Lidar Detection of HO

The Lidar technique for the measurement of HO radicals in the stratosphere consists of a laser tuned to excite the radicals, and a telescope to detect the resonance fluoresence. The laser is a frequency doubled tunable dye laser which is pumped by the second harmonic of a Nd-YAG laser. The laser is tuned so that the UV output is coincident with either the $P_1(2)$ or $Q_1(2)$ lines

(at 281.9 nm or 282.06 nm respectively) of the (1, 0) manifold of the A-X transition in HO. The laser has a bandwidth of 0.0025 nm and a temporal pulsewidth of 9 to 10 nsec, with an energy of 1.0 to 1.5 mJ/pulse. Because of collisions, fluorescence from the radical originates from both the v' = 1 and v' = 0 and a band of fluorescence 10 nm wide centered at 310.0 nm is detected. This includes both the (0,0) and (1,1) emission manifolds. Photon counting electronics are used to collect the signal. Time gating of the detectors allows for measurements at various distances away from the package. The photon return can be expressed as follows:

$$P = I_T N_{OH} \frac{A\gamma}{4\pi} \sigma_{abs} \beta \varepsilon_{fl} \int_{R_1}^{R_2} e^{-\alpha R} dR$$

Where I_T is the transmitted flux in photons/pulse (±50% uncertainty)

A is the area of the receiver (<1%)

γ is the efficiency of the receiver and electronics (±10%)

σ_{abs} is the absorption cross section of the transition taking into account the laser and absorption lineshapes and widths (±25%)

β is the HO population in the appropriate rotational level in the ground state (±5%)

ε_{fl} is fluorescence efficiency term (±5%)

R is the range from the balloon (<1%)

$e^{-\alpha R}$ is attenuation of the transmitted beam due to O_3 absorption (±1%).

This term is measured simultaneously using a differential absorption Lidar technique.

The estimated contribution to the uncertainty of the extracted HO concentration by each parameter is included in parentheses. It should also be noted that in the instance where the signal is collected near to the balloon, an additional term taking the lifetime of the excited state into account is required (Heaps, 1980).

The ranging capability of the Lidar system enables uncontaminated air to be sampled. But this fact also renders calibration more difficult since absolute quantitative spectroscopic data are required to interpret the returned signal. Errors are therefore introduced from uncertainties in absorption cross section (McGee and McIlrath, 1982) and collisional transfer and deactivation rates (German, 1975, 1976; Lengel and Crosley, 1975). The efficiency of the detector chain (telescope, spectrograph, photomultiplier tubes and counting electronics) is determined using a calibrated star source with 10.0 nm bandpasses centered at the detection wavelengths of the system. The total systematic error in the HO concentration from all the above sources is estimated to be ±57% (RMS).

Figures 1-87 to 1-90 present data from (a) the upper stratosphere-mesosphere rocket data from Anderson (1975) (Figure 1-87); (b) the stratosphere balloon data using in situ resonance fluorescence (Anderson, 1980), and LIDAR (Heaps and McGee 1981) (Figure 1-88); and (c) a composite of the two data sets with an upper limit on the mean tropospheric HO concentration taken from the methyl chloroform lifetime studies and the tropospheric laser experiments (Figure 1-90).

Figure 1-89 presents the diurnal data taken with the LIDAR instrument on October 20, 1980. The data from the figure is summarized in Table 1-16. It should be noted that the midday values are 2 to 3 times lower than Anderson's values and the evening values do not drop as rapidly as might be expected. A simplistic model based on $HO-HO_2$ chemistry predicts HO values in the neighborhood of $2\text{-}4 \times 10^5$ molecules/cc which is somewhat lower than measured, but due to the large errors associated with the measurements, they do not appear to be totally inconsistent with the model. Artificially produced HO (initiated by the dissociation of O_3 by the laser pulse), appears to be insignificant.

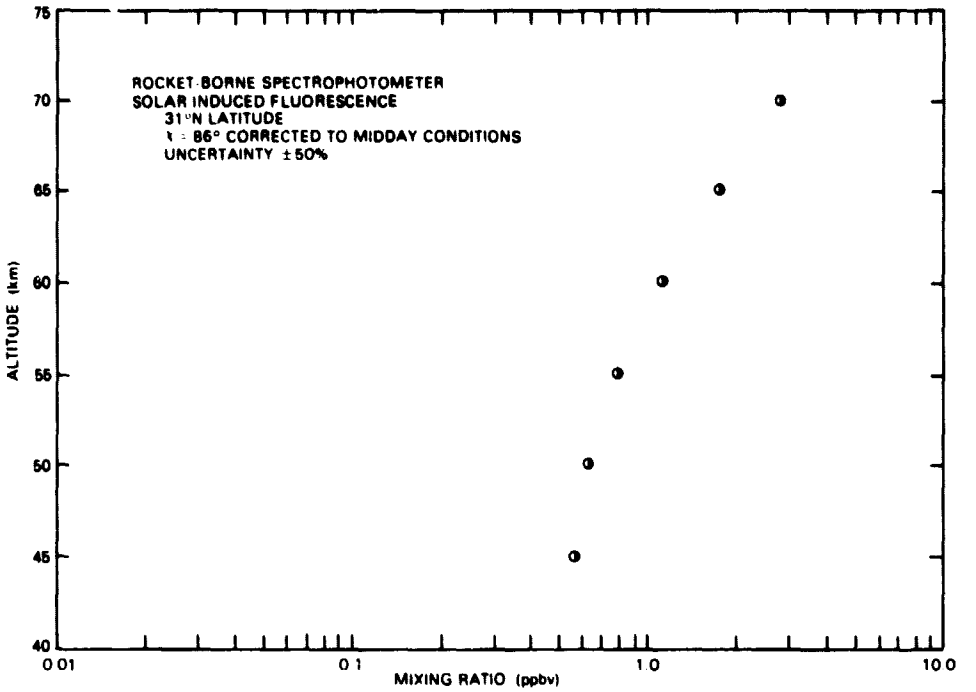

Figure 1-87. Rocket-borne measurements of HO radical in the mesosphere and upper stratosphere (Anderson, 1971b).

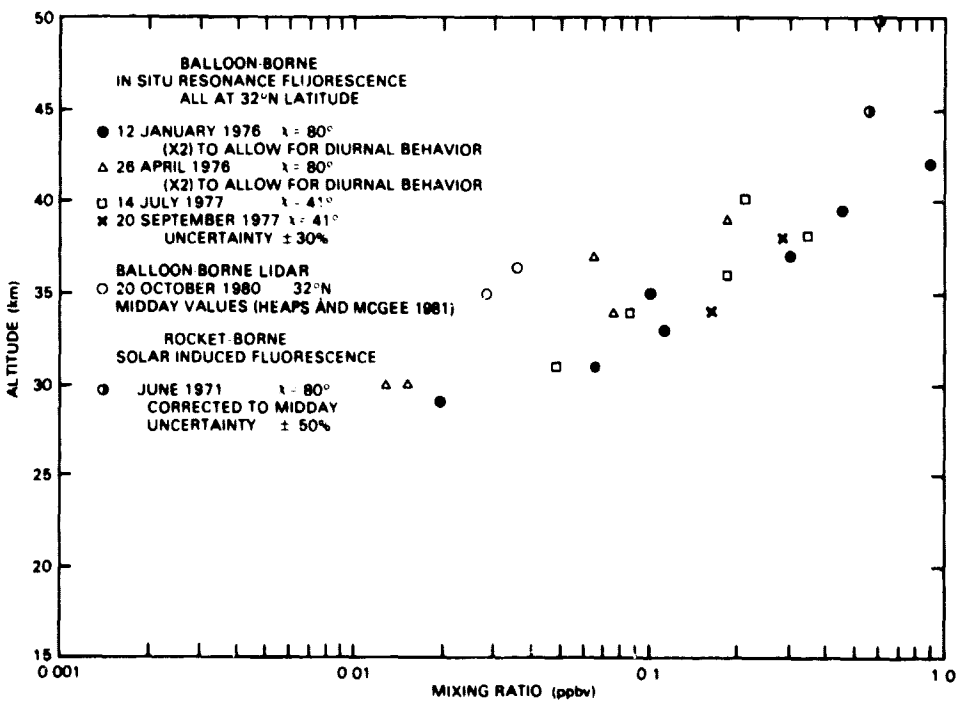

Figure 1-88. Balloon-borne, stratospheric in situ measurements of HO radical (Anderson, 1976, 1980); Heaps and McGee, 1981).

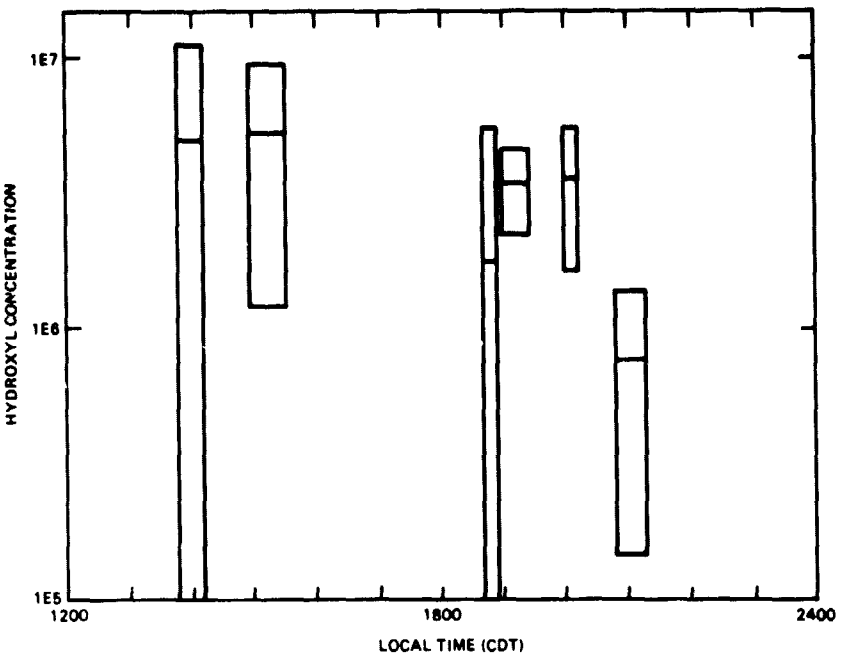

Figure 1-89. Diurnal vatiation of HO radical at 34 to 36 km. Vertical error bars are one standard deviation due to counting statistics (Heaps and McGee 1981).

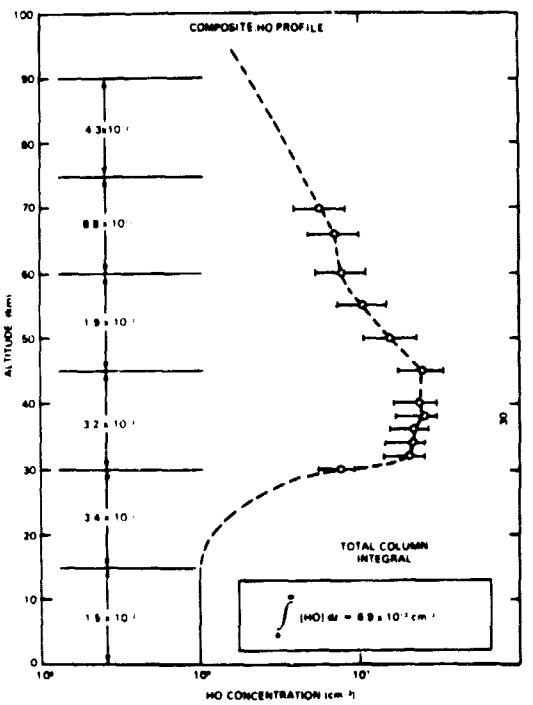

Figure 1-90. A composite HO profile based on the rocket and balloon data. The tropopsheric concentration is estimated from methyl chloroform studies and the tropospheric laser experiments.

Table 1-16
Balloon LIDAR Hydroxyl Measurements at 34-36 km

Local Time (CDT)	[HO] in Molecules/cc
1347-1410	4.9(6)±6.4(6)
1459-1534	5.2(6)±4.1(6)
1841-1853	2.9(6)±3.8(6)
1856-1926	3.5(6)±1.2(6)
2005-2015	3.6(6)±1.9(6)
2050-2119	7.8(5)±6.3(5)

Several features of the profile will be referred to throughout this section. First the total column concentration of HO determined from an integral of the in situ observations and an estimate of the upper mesospheric profile is 6.9×10^{13} cm^{-2}. The fractional contribution for each 15 km interval between 0 and 90 km is given in Table 1-17.

Second, the altitude interval over which the balloon and rocket data extend from 30 to 70 km, encompasses all but 13% of the total column concentration. Thus the ground-based observations provide an excellent cross check on the absolute concentration determined by the in situ techniques.

The total column density of HO has been observed by the PEPSIOS and reported in Burnett and Burnett (1981). Based upon a total of 270 observing days extending from December 1976 to December 1979, the midday abundance of HO averaged over all seasons is 5.7×10^{13} cm^{-2}. All reported PEPSIOS observations were made at Fritz Peak Colorado, 40°N latitude. Given the cited uncertainty of the in situ observations of ±40% and of the total column observations of ±25%, the observed absolute concentrations are consistent and are summarized in Table 1-18.

All observations by PEPSIOS were taken between a solar zenith angle of 70° following sunrise through noon to a zenith angle of 70° prior to sunset. The period of observation was from 1976-1979 with a total of 270 observing days which yielded 900 data sets with equal to or less than one hour time resolution. The diurnal behavior of the column density was fit to a curve in sec X which is characterized by an overhead Sun maximum of 7.1×10^{13} cm^{-2} decreasing to 4.9×10^{13} cm^{-2} at sec X =2 (solar zenith angle 60°). The following systematic departures from the mean were observed:

1. An annual increase of 1×10^{13} cm^{-2} in total column.
2. A gradual decrease of about 25 to 30% between spring and fall.
3. Diurnal oscillation observed with systematic changes of 30 to 40% which show a clear solar flux dependence on both a diurnal and annual basis.

Table 1-17
Contribution of Each Altitude Interval to the Integrated Column

Altitude Interval	Contribution To Total Integral	Fraction Of Total Integral	Integrated Column Density
0-5	1.5×10^{12}	0.02	
15-30	3.4×10^{12}	0.05	
30-45	3.2×10^{13}	0.46	$6.9 \times 10^{13} cm^{-2}$
45-60	1.9×10^{13}	0.28	
60-75	8.8×10^{12}	0.13	
75-90	4.3×10^{12}	0.06	

Table 1-18
Summary of the Comparison Between the Integrated In Situ Results from Balloon and Rocket Data and the Ground-Based Total Column Observation

Composite of the In Situ HO Data	Ground-Based Total Column HO
$6.9 \times 10^{13} cm^{-2}$	$5.7 \times 10^{13} cm^{-2}$
Uncertainty ± 40% Conditions: Midday, 32°N	Uncertainty ± 25% Conditions: Midday, 40°N

The observed and predicted diurnal behavior of total column HO is summarized in Figure 1-91. A representative data set is shown in Figure 1-92, indicating the scatter about the mean.

A reanalysis of the December 1976 data (from Burnett, 1977), using more advanced methods for baseline determination established a mean of $3.1 \pm 0.6 \times 10^{13}$ cm^{-2} for midday. Figure 1-93 shows the evolution of the monthly mean from December 1976 to December 1979. There is an apparent increase of approximately 1×10^{13} cm^{-2} per year during that 3-year interval. Correlating such an increase to the 11 year solar cycle was suggested by Burnett and Burnett (1981) but such a dramatic change seems difficult to rationalize and will require more extensive data coverage and a far more thorough analysis of solar cycle flux variations with an associated mechanistic hypothesis before it can be accepted.

The seasonal behavior in the total column of HO is a recurring and extremely interesting feature of the data in Figure 1-93. There is a clear suggestion of a springtime maximum in HO and a fall minimum. One very important advantage to be gained from a more extensive geographic coverage with such ground-based observations would be an examination of this seasonal behavior as a function of latitude. The correlation of this dependence with other constituents such as O_3, H_2O, NO_2 and ClO would be significant.

An unexpected and as yet unexplained aspect of the ground-based observations involves the appearance, particularly in the 1978 summer data set, of a zenith angle dependence (Figure 1-94). There is a distinct minimum in the observed column following local noon. The early afternoon decrease shows an abrupt drop of $4\text{-}5 \times 10^{13}$ cm^{-2} with a subsequent increase of 3.5×10^{13} cm^{-2} followed by the conventional decrease toward sunset. The authors believe that it is not an artifact of the data reduction or of instrumental performance. The oscillatory behavior shown in Figure 1-94 persisted into the late summer of 1978 but was not apparent in the 1979 data set which was taken with the same instrument at the same site using the same data reduction method. There was also a systematic progression of the position of the maximum and minimum through the 1978 season.

In summary, an analysis of balloon and rocket data of HO in the stratosphere and ground-based total column observations leads to the following conclusions:

1. There is substantial agreement among the three techniques; the in situ data provides a consistent picture of the altitude dependence of HO between 30 and 70 km implying a peak concentration at 40 km of 2.4×10^{7} cm^{-3} and a total column density at midday of 6.9×10^{13} cm^{-2}. The midday total column abundance determined from the ground is 5.7×10^{13} cm^{-2} as summarized in Table 1-18.

2. There is a systematic increase of approximately 1×10^{13} cm^{-2} per year between December 1976 and December 1979 and a suggestion of a yearly spring maximum and fall minimum. The spring to fall decrease is approximately 30%.

3. It is clear that a knowledge of the HO distribution between 15 and 30 km is of the highest priority. This need results not only from the fact that HO_x becomes an increasingly important component of the odd oxygen destruction rate below 30 km but also because the photochemical partitioning of chlorine and nitrogen depend on the HO concentration.

Hydroperoxyl Radical (HO_2)

Two techniques have thus far been used for the detection of HO_2 in the stratosphere:

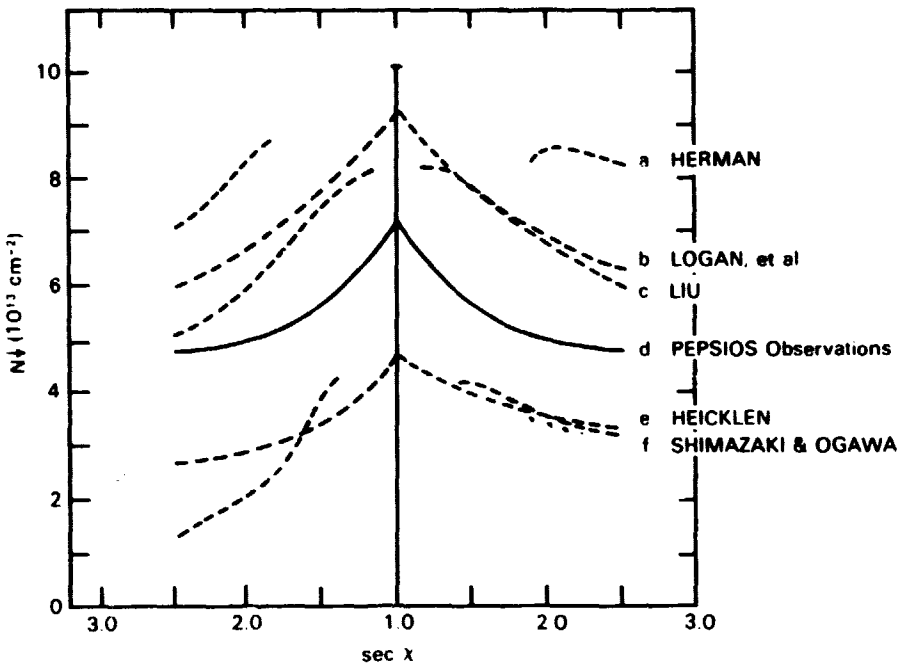

Figure 1-91. The correlation between HO total column density and solar zenith angle expressed as sec X comparing the observed and modeled behavior from Burnett and Burnett (1981).

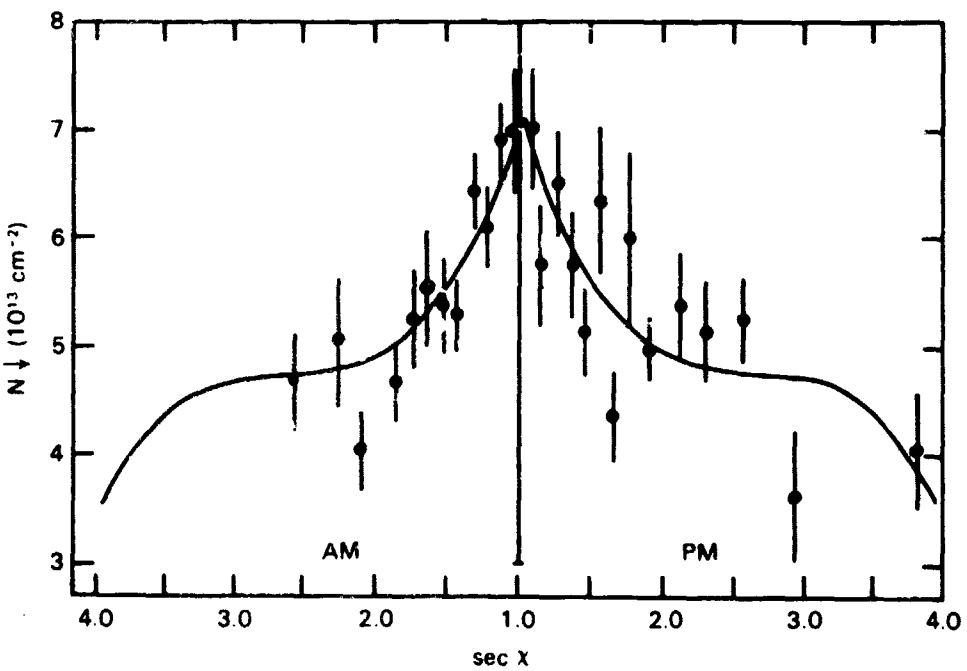

Figure 1-92. An indication of the scatter about the mean of individual observations taken with the ground-based PEPSIOS, from Burnett and Burnett (1981).

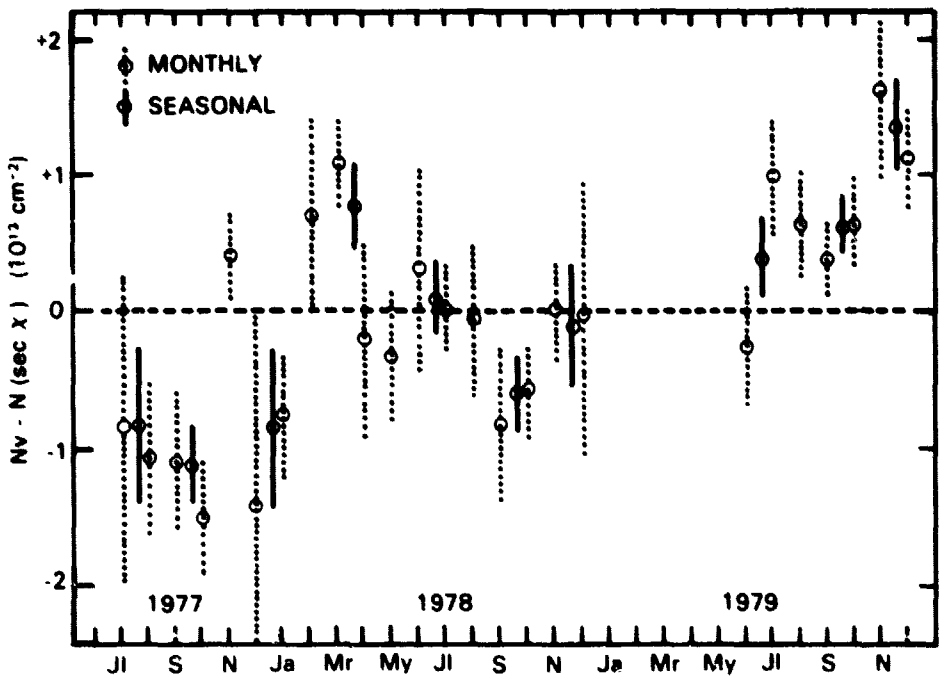

Figure 1-93. Summary of the observed fluctuations in HO total column measured from the ground.

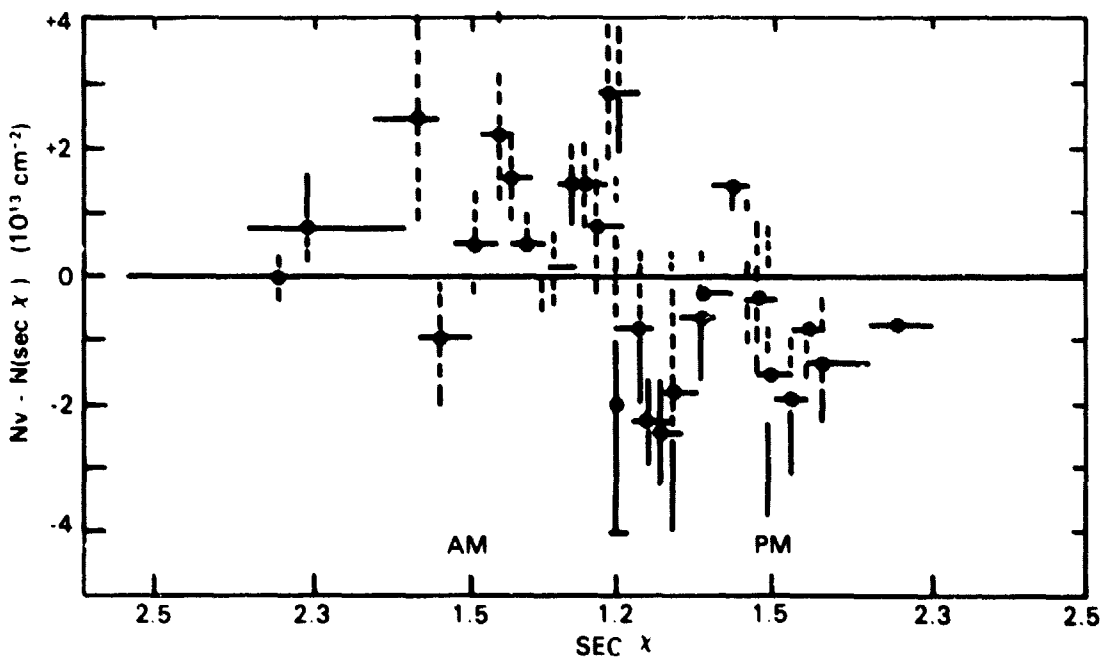

Figure 1-94. Typical example of the oscillatory diurnal behavior of the HO total column which was a characteristic signature of the summer 1978 data and does not appear to be an instrumental artifact. Data from Burnett and Burnett (1981).

- Balloon-borne cryogenic matrix isolation followed by laboratory detection of HO_2 by Electron Paramagnetic Resonance methods. The experiment is carried out by drawing a stratospheric sample into an evacuated flask, collecting the sample on a "cold finger" at a given balloon float altitude, closing the flask and returning it to the laboratory for analysis (Mihelcic et al., 1978).

- Balloon-borne chemical conversion followed by molecular resonance fluorescence detection. HO_2 is converted to HO by the rapid bimolecular reaction $HO_2 + NO \rightarrow HO + NO_2$. The product HO is then detected by molecular resonance fluorescence using a microwave sustained plasma discharge lamp to induce fluorescence in the (0-0) band of the $A^2\Sigma - x^2\Pi$ transition at 309 nm. Chemical conversion and detection is done within a chamber lowered through the stratosphere at a controlled velocity on a parachute (Anderson, 1980; Anderson et al., 1981).

A total of four HO_2 observations have appeared in the literature, one by the matrix isolation technique and three by the resonance fluorescence method. Those observations are summarized in Table 1-19 in chronological order.

As noted in Table 1-19, the sample collection of Mihelcic et al. (1978) was initiated immediately following sunrise at a solar zenith angle of 85°. The conversion to midday for comparison with models and other observations was carried out using the diurnal calculation of Logan et al. 1978. That correction factor is significant - a factor of two - and attempts to account for the period over which the sample was collected.

The data summarized in Table 1-19 are presented graphically in Figure 1-95. There is significant scatter evident in those observations which should not be attributed to atmospheric variability until:

- The signal-to-noise ratio of the observations is improved;
- Simultaneous observations of photochemically related species such as HO or H_2O demonstrates a correlation in concentration fluctuations.

Atomic Hydrogen (H)

There are no reported observations of atomic hydrogen in the stratosphere either direct or indirect, nor have any upper limits been reported.

Hydrogen Peroxide (H_2O_2)

The only reported observation of H_2O_2 is the tentative result reported by Waters et al. (1981) using the Balloon-Borne Microwave Limb Sounder (BMLS) to observe the purely rotational emission of H_2O_2 at 204 GHz. All aspects of the experimental hardware and uncertainties analysis are identical to that discussed in the BMLS section of the ClO discussion.

ODD CHLORINE

Chlorine Oxide (ClO)

Four methods have been successfully applied to the detection of stratospheric ClO:

1. Balloon-borne in situ resonance fluorescence methods (Anderson et al., 1977; Anderson et al., 1980; Weinstock et al., 1981).

Table 1-19.
Summary of Experimental Parameters for the HO_2 Observations

Launch Date/ Latitude	Solar Zenith Angle	Reference/ Experimental Uncertainty	Observed Data					
8/8/76 53°N	85°	Mihelcic et al., 1978 Factor of three	Altitude(km)				31.8	
			Observed HO_2 mixing ratio				$1x10^{-10}$	
			Corrected to midday					
9/20/77	41°	Anderson et al., 1980 ± 45%	Altitude(km)	37	35	33	31	29
			Observed resonance fluorescence S_{HO_2}	17	9	13	8	2
			HO_2 mixing ratio $[HO_2]/[M]$	$7.1x10^{-10}$	$1.84x10^{-10}$	$8.5x10^{-11}$	$\leq 8x10^{-11}$	$<7x10^{-11}$
			Detection threshold	$1.1x10^{-10}$	$8.2x10^{-11}$	$7.0x10^{-11}$	$7.6x10^{-11}$	$6.4x10^{-11}$
10/25/77 32°N	45°	Anderson et al., 1980 ± 45%	Altitude(km)	37	35	33	31	29
			Observed resonance fluorescence S_{HO_2}	3	3	9	5	–
			HO_2 mixing ratio $[HO_2]/[M]$	$3.6x10^{-10}$	$3.7x10^{-10}$	$6.9x10^{-10}$	$2.1x10^{-10}$	$<1.0x10^{-10}$
			Detection threshold	$1.6x10^{-10}$	$1.5x10^{-10}$	$1.5x10^{-10}$	$1.0x10^{-10}$	$1.0x10^{-10}$
12/2/77 32°N	50°	Anderson et al., 1980 ± 45%	Altitude(km)	37	35	33	31	29
			Observed resonance fluorescence S_{HO_2}	33	25	20	22	16
			HO_2 mixing ratio $[HO_2]/[M]$	$3.4x10^{-10}$	$2.3x10^{-10}$	$4.2x10^{-10}$	$3.4x10^{-10}$	$1.7x10^{-10}$
			Detection threshold	$8.1x10^{-11}$	$6.0x10^{-11}$	$4.6x10^{-11}$	$8.8x10^{-11}$	$8.7x10^{-11}$

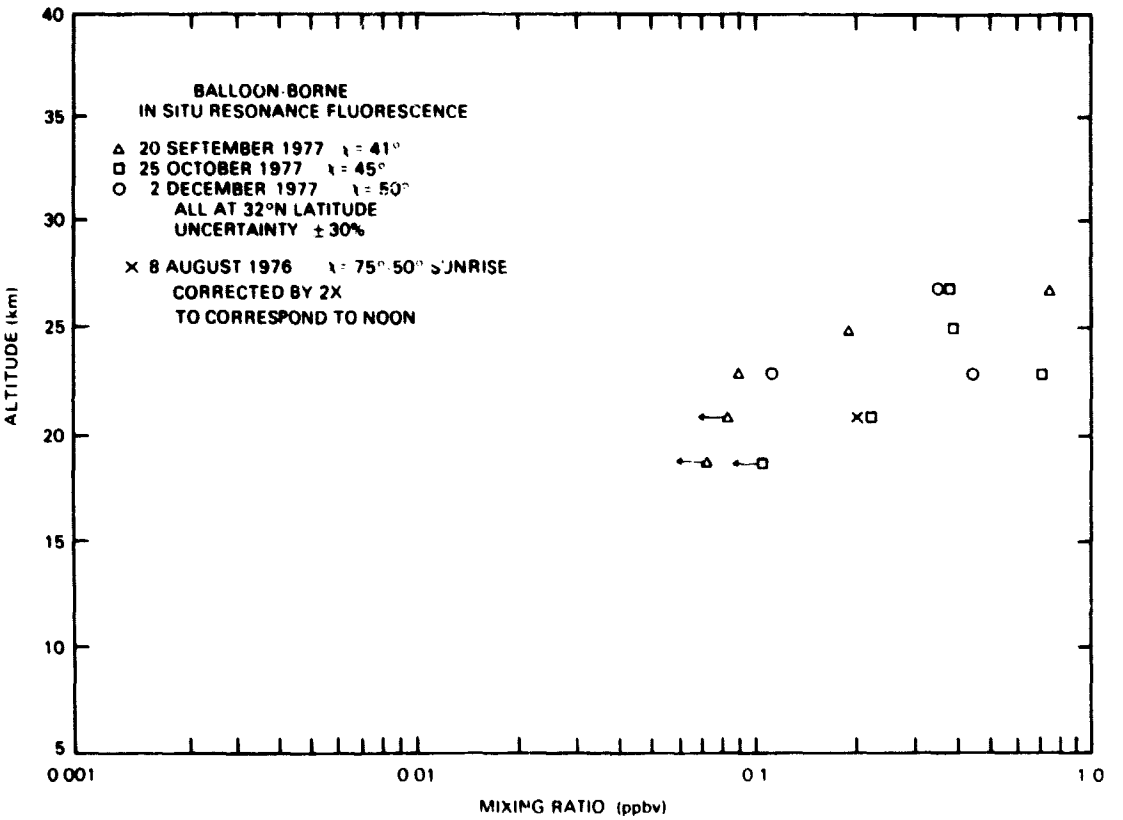

Figure 1-95. Vertical profile of HO_2 from balloon-borne resonance fluorescence measurements (Anderson et al., 1981).

2. Balloon-borne laser heterodyne radiometry for the remote observation of ClO at, and immediately following, sunset (Menzies, 1979; Menzies et al., 1981).

3. Ground-based mm-wave emission spectroscopy of the ClO total column at 204 GHz (Parrish et al., 1981).

4. Balloon-borne mm-wave emission spectroscopy of ClO at 204 GHz (Waters et al., 1981).

Although a clear consensus has yet to emerge on many crucial aspects of stratospheric chlorine chemistry, significant advances in our perception of several first order questions has evolved from the comparison of results obtained with the techniques cited above. In the following sections, results from those independent investigations are reviewed in order to first isolate those points upon which agreement has been reached and second, to identify the key questions which remain unanswered.

Discussion of Analytical Techniques

Balloon-borne in situ resonance fluoresence. The in situ ClO results reported here employed the detection of atomic chlorine using $^2D_{5/2} - {}^2P_{3/2}$ transition of atomic chlorine at 118.9 nm following the conversion of ClO to Cl using the rapid bimolecular reaction:

$$ClO + NO \rightarrow Cl + NO_2$$

Detection is accomplished within a hollow, aerodynamically shaped "pod" lowered through the stratosphere at a controlled rate (40-100m/min) by a stabilized parachute deployed from a balloon over the stratopause (44 km). The high velocity flow thus passes unrestricted through a detection chamber within the pod. This isolates the detector from the beam of resonant photons used to induce fluorescence and from the radiation environment of the stratosphere and contains the flow so that controlled, chemical conversion can be effected within the flowing sample.

The observed detector count rate from Cl atom fluorescence, under optically thin conditions appropriate to these experiments, is given by the expression

$$S_{Cl} = \left\{\int F(\lambda)\sigma(\lambda)\, d\lambda\right\}\left\{\varepsilon T \eta\right\} \ell\, [Cl] \qquad (21)$$

where the integral is the convolution of the lamp flux and the atomic absorption cross section; ε is the detector collection efficiency, equal to the ratio of the photons collected to the total number scattered from a point within the region defined by the intersection of the lamp beam and the detector field of view; T is the optical transmission of the detection optics; η is the quantum efficiency of the detector; ℓ is the length of the lamp beam intercepted by the detector field-of-view; and [Cl] is the atomic chlorine density. For a more detailed discussion of the optical geometry see Anderson et al. (1980). Note that for a given lamp flux F the right-hand side of (21) is a constant

$$C(F) = \left\{\int F(\lambda)\sigma(\lambda)\ d\lambda\right\}\left\{\varepsilon T \eta\right\} \ell \qquad (22)$$

times the Cl atom density, so that

$$S_{Cl} = C(F)[Cl] \qquad (23)$$

Three independent methods are used to determine C(F):

1. A chemical technique in which a known Cl atom density is formed in a flowing sample and $C_{chem}(F)$ is determined from (23) given the count rate S_{Cl} resulting from that Cl concentration.

2. A photometric technique in which each quantity on the right-hand side of (22) is measured and the product then calculated to determine $C_{phot}(F)$.

3. An absorption technique in which the fractional absorption of radiation at 134.7 nm ($^2P_{3/2}$ - $^2P_{3/2}$) is measured across a flowing sample which is simultaneously probed with the flight instrument so that (23) can be used to determine directly the proportionality factor $C_{abs}(F) = \Delta S_{Cl}/[Cl]$, where ΔS_{Cl} is the difference in the count rate determined in the absence and presence of a measured amount of Cl in the flowing sample.

A brief summary of the individual quantities contributing to the experimental uncertainties for each method is given in Table 1-20:

Table 1-20
Summary of the Major Experimental Uncertainties in the Determination of C_{chem}, C_{photo}, and C_{abs}.

Method	Value for C(F)	Quantity and (Measured Value) When Appropriate	Uncertainty U_i, %	$(\Sigma U_i^2)^{1/2}$ %
Chemical	$C_{chem}(F) = 1.4\times10^{-7}$ (c/s)/(atm/cm^3)	Concentration of injected NO (variable)	±10	±25
		Effect of uncertainty in concentration of residual O_3 (see text)	±15	
		Ratio of pressure to total flow in calibration (4×10^{-3} to 4×10^{-4} mbar/(scc/s)	±10	
		Variation in Doppler temperature of lamp emission line (800±200K)	±12	
Photometric	$C_{photo}(F) = 2.1\times10^{-7}$ (c/s)/(atm/cm^3)	Line center absorption cross section at 118.9 nm ($\sigma_o = 3.9\times10^{-13}$ cm^2)	±30	±50
		Absolute lamp flux ($F(^2D5/2) = 7.3\times10^{10}$ phot/s)	±20	
		Overlap of lamp emission line and absorption cross section of atom (800±200K)	±12	
		Detector quantum efficiency ($\eta = 0.17$)	±15	
		Detector collection efficiency ($\epsilon = 1.2\times10^{-3}$)	±20	
		Optical transmission (T = 0.08)	±10	
		Scattering length (l = 1.0 cm)	±20	
Absorption	$C_{abs}(F) = 1.5\times10^{-7}$ (c/s)/(atm/cm^3)	Absorption cross section at 134.7 nm ($\sigma_o = 5.2\times10^{-13}$ cm^2)	±25	±28
		Doppler width of lamp emission line	±12	

C is the calibration factor
c is counts from the detector

While the uncertainty associated with the photometric technique is clearly the largest, that determination provides an extremely important upper limit to the absolute sensitivity of the experiment so that while the method is not used on a flight-by-flight basis to establish the absolute calibration, it is a key piece of evidence linking observed count rates to absolute sensitivities based on "first principles." The reason C_{phot} is somewhat larger than C_{chem} and C_{abs} is that the Doppler width of the lamp emission line is somewhat greater than the Doppler width of the atomic absorption cross section at stratospheric temperatures.

In summary, the uncertainty in the absolute ClO concentrations cited in this document is ±30%.

Balloon-Borne Microwave Limb Sounder (BMLS)

This instrument is tuned to measure thermal emission from the 11/2-9/2 ClO rotational transition at 204.352 GHz. Multiple filter banks perform special analysis of the signal over an interval of about 300 MHz. The interval is encompassed by nine 32 MHz resolution filters, thirteen 8 MHz resolution filters and thirteen 2 MHz resolution filters. Within the bank, the set of filters with a given resolution is centered at the line frequency; adjacent filters have curves which overlap at approximately their half power points. This filter arrangement provides much greater detail close to line center while simultaneously detecting the emission background over a significant spectral interval to either side of line center. The first heterodyne down conversion is to 4 GHz intermediate frequency.

The antenna system is an offset Cassegrain with a 50 cm diameter main reflector and measured beamwidth (full angular width between half power points) of 0.3°. The antenna beamwidth corresponds to a vertical range of less than 3 km at the tangent point of the observations. A flat mirror in front of the main reflector scans the antenna beam through the atmospheric limb for profile measurements. This mirror is programmably stepped through 64 discrete positions during the measurements. A mirror near the antenna system focus chops the input to the radiometer at 4 Hz between the limb radiation recovered by the antenna and a 50° elevation sky reference. The switching mirror also chops the radiometer input between a black body target and sky reference for inflight absolute calibration. The absolute calibration accuracy is 5% or better.

Pointing of the instrument in the vertical plane (which determines the accuracy of the reported altitudes) was checked by measuring the abrupt increase in emission (due to wings of the water vapor lines) at the tropopause whose height was obtained from measurements of nearby radiosonde. The pointing determined in this way agreed within ±0.1° of the absolute pointing to which the BLMS had been prealigned. This uncertainty is due to uncertainties in the water vapor distribution at the tropopause and corresponds to less than 1 km vertical uncertainty in the stratospheric layers to which the instrument points for profile measurements.

Waters et al. (1981) cite an overall experimental uncertainty of ±25% for their reported observations, a number based on the above considerations, background subtraction and experimental signal to noise ratio.

Ground-Based Microwave

Total column emission results of Parrish et al. 1981 employed a super heterodyne receiver (Carlson et al., 1978) in conjunction with a filterbank spectrometer of 256 channels, each with 1 MHz passband. The receiving antenna limits the sky view to a symmetric cone with a full angular width of 6.3° measured at the 0.5 power point and 15° at the 10^{-2} power level. The observing procedure used a beam deflecting mirror which causes rapid, repetitive switching of the antenna beam between (a) the low elevation, long stratospheric path length, and (b) the reference, high elevation input to the detector. The difference between those two quantities normalized to the

reference signal(s), is determined for each channel on every cycle of the chopper and accumulated as data stored in 10 minute blocks. The signal strength is expressed as a brightness temperature. The relation between radiated intensity per unit band width I and temperature T is given in the Rayleigh-Jeans Limit by $I_\nu = 2kT/\lambda^2$ where λ is the wavelength and k is Boltzmann's constant.

Parrish et al. (1981) chose to present their intensity results in the form of the antenna temperature T_z which is the Rayleigh-Jeans temperature, corresponding to the intensity that would be observed if the antenna were pointing toward the zenith with no attenuation of the line resulting from tropospheric H_2O. The key transformation, the conversion from the observed dimensionless quantity described above, $2e\{(a) - (b)\}/(b)$, to $T_z x$ in temperature units follows from an analysis of the observing procedure, the geometry of the experiment, and frequent measurements of instrumental noise temperature and atmospheric opacity.

The spectral line shape is the final critical parameter needed to infer absolute concentrations from the observed brightness. For rotational transitions in ClO, the spectral line shape is dominated by pressure-broadening below an altitude of 70 km. Since pressure broadening is a (reasonably) well known function of altitude, an observed peak intensity and line shape contains information about the total quantity and vertical distribution of ClO.

In the Parrish results, temperature and pressure profiles from the 1976 U.S. Standard Atmosphere were used and the measured collisional parameters (Brinza et al., 1980) of 3.5 MHz/mbar and $T^{-0.75}$ for the 204 GHz ClO line were used. Hyperfine splitting has been included in the line shapes and the amplitude takes into account the 75% isotopic abundance of ^{35}ClO.

Parrish et al. (1981) report a systematic calibration error of 25%.

Data Presentation and Comparison of Results

There are 10 in situ observations at 32°N latitude. The altitude resolution of those experiments is equal to or better than 1 km and the observations are reported with that resolution. Figure 1-96 reveals that the in situ data falls in two classes: eight of the ten observations fall within a well defined envelope with excursions of ±50% about the observed mean. There is no clear trend with season but there is a clearly defined gradient with altitude.

At 40 km the observed range is $4\text{-}15\times10^{-10}$, at 35 km $1.5\text{-}7\times10^{10}$, at 30 km $5.8\text{-}28\times10^{-11}$, at 25 km $8\text{-}56\times10^{-12}$. Given the cited experimental uncertainty of ±30%, the observed variations among the individual profiles implies an element of atmospheric variability. There is no distinctive trend with season although the summer and early fall data are above the mean defined by the "envelope" containing the eight observations in Class 1 while the winter observations tend to fall below that mean. The second class of observations includes the two July profiles which clearly fall outside the envelope; the first on July 28, 1976 which reached a peak mixing ratio of 1.3 ppb in a broad altitude interval between 32 and 38 km, the second of which, observed on July 14, 1977, recorded a peak mixing ratio of 8 ppb at 40 km. While the observation of July 28, 1976 is not seriously in conflict with the other observations, the July 14, 1977 measurement is.

Also shown in Figure 1-96 are the microwave emission data of Waters et al. (1981) who report values at 36 and 31 km and an upper limit at 23 km. Those data were obtained in February at the same latitude as the in situ data. The initial comparison of these independent techniques implies agreement both with respect to absolute concentration and with respect to mixing ratio gradient.

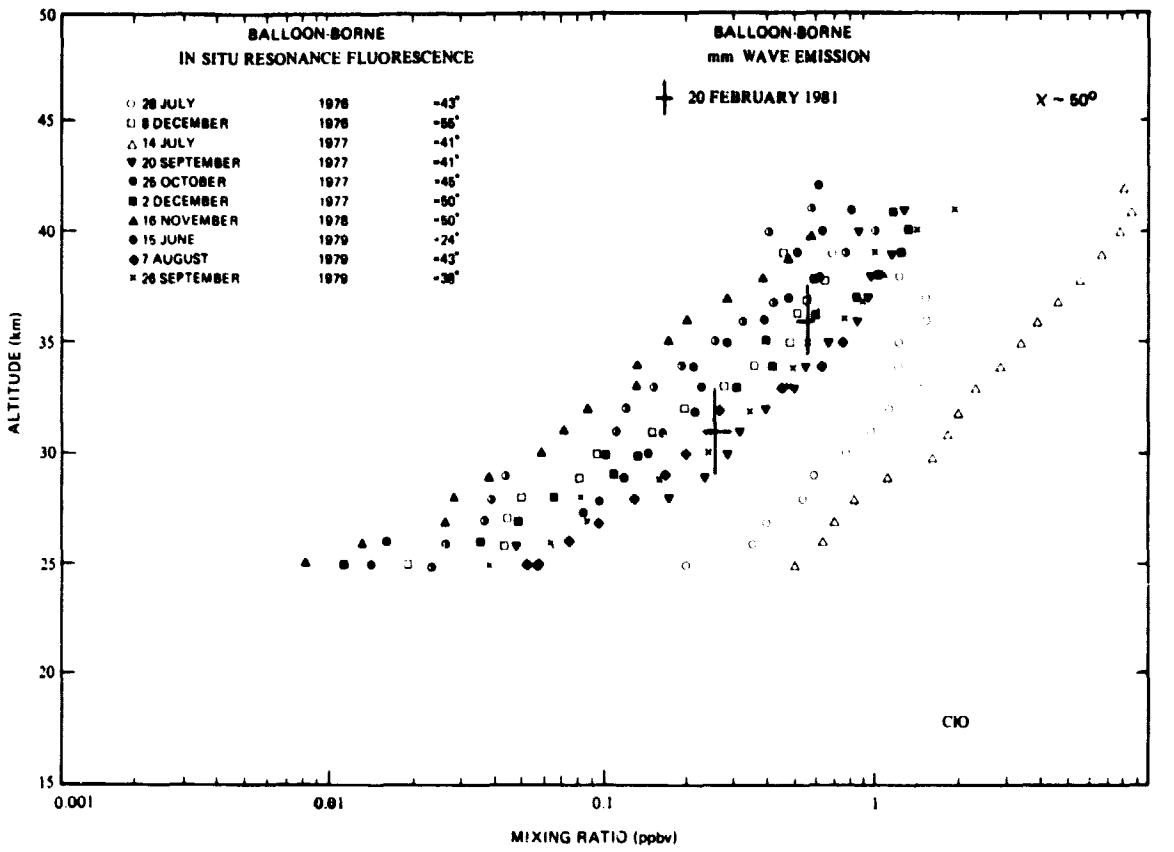

Figure 1-96. Stratospheric measurements of the vertical profile of ClO (Weinstock et al., 1981).

The recently reported ground-based microwave emission data (Parrish et al., 1981) were obtained between 10 a.m. and 4 p.m. on 17 separate days (between January 10, 1980 and February 18, 1980) at 43°N latitude from the Five College Radio Astronomy Observatory, Amherst, Mass. Such ground-based observations, which employ purely rotational transitions, are affected by collisional (pressure) broadening of approximately 4 MHz/mbar at stratospheric pressures. Low resolution altitude information can be extracted from the emission line shape, however, one must have a first order estimate of the shape of the emitting layer in order to obtain the absolute column concentration for the observed-brightness temperature as a function of frequency. In practice however, the balloon-borne observations have provided the information on the layer shape and thus absolute column measurements can be extracted. It should be noted, however, that even without knowledge of the shape of the emitting layer, some information on absolute concentration can be extracted.

Parrish et al. (1981) have taken the mean of seven in situ profiles, excluding the last profile obtained on September 26, 1979, scaled those results by 0.8, integrated the signal which would have resulted, and then overlayed that profile with the observed brightness as a function of frequency. The results are shown in Figure 1-97.

The first conclusion to be drawn is that substantial agreement exists with respect to absolute magnitude since both techniques quote uncertainties of ±25%. However, it must be noted that the ground-based observations were done at a latitude 10° northward of the balloon measurements and are confined to a relatively short period of time in mid-winter. A broader data base and observations done in the same latitude band are clearly needed. Parrish et al. (1981) report that no single day of observation exceeded the average by more than a factor of 2.5 and tentative evidence for variations on the order of a factor of two in total ClO column density occurred on a time scale of a few days.

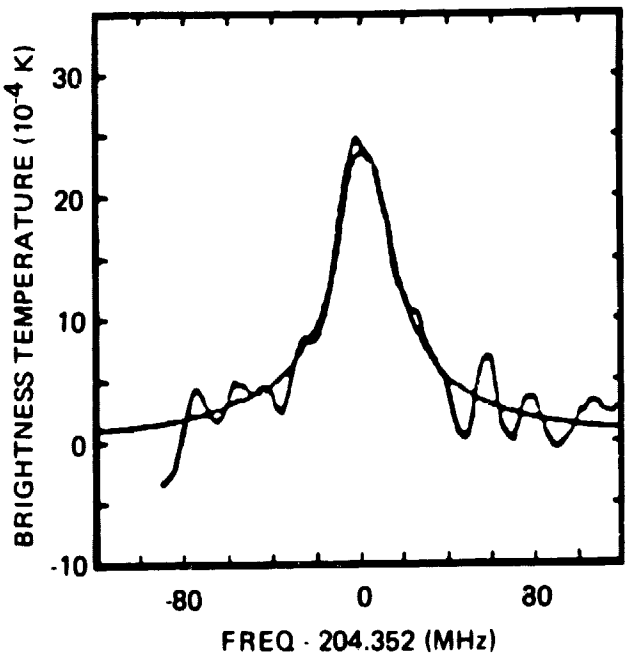

Figure 1-97. An overlay of the ground-based mm-wave emission data of Parrish et al. (1981) and the signal which would result from an integral of the mean of the balloon-borne in situ observations multiplied by 0.8. The mean was taken excluding the 28 July 1976 and 14 July 1977 data.

An inspection of Figure 1-97 indicates that the millimeter wave, emission line shape is consistent with the distribution determined in situ.

It is instructive to compare the ground-based microwave emission data with the mean of the in situ data including the 28 July 1976 observation which is shown in Figure 1-98. No scaling factor is included.

The ground-based measurements clearly contribute to the question of uncertainties in absolute calibration and the occurrence of localized enhancements as indicated in Figures 1-97 and 1-98. A significant impediment to the general deployment of this method is the severe attenuation at 204 GHz resulting from atmospheric water vapor, restricting the observing period to winter conditions at northern latitudes, whereas the large excursions reported in ClO have been observed only at mid-latitudes in summer.

In summary the following points can be made:

Altitude Profile

1. At 32°N latitude the mean of the balloon-borne in situ resonance fluorescence technique and the balloon-borne millimeter wave emission data are in substantial agreement with respect to both the shape and absolute magnitude of ClO concentration throughout the entire region of observation (25 to 36 km).

2. The ground-based millimeter wave data, although obtained at a latitude 10° northward of the balloon observations and during the winter, is not inconsistent with the shape of the in situ observation and, although approximately 20% lower in absolute concentration, falls within the cited uncertainty of the observational technique.

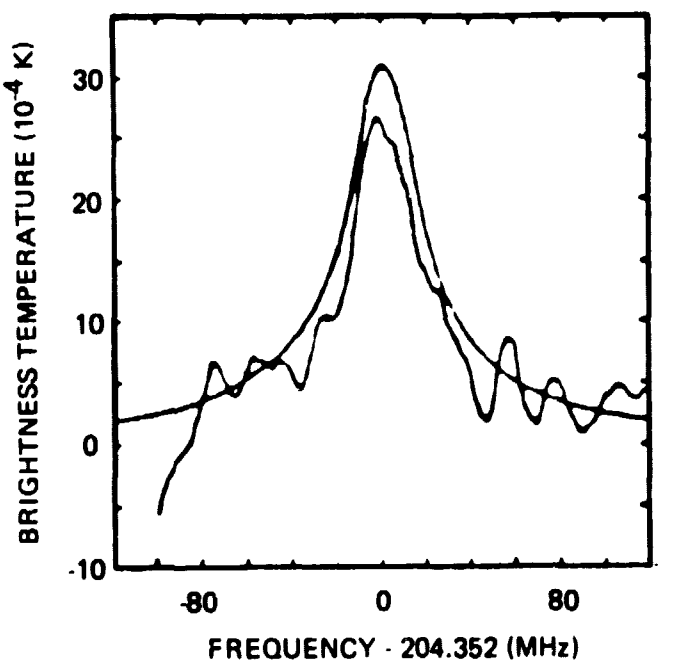

Figure 1-98. Comparison between the microwave total column emission and the in situ data excluding the July 14, 1977 observation.

Problems

1. A cross comparison of the balloon-borne methods simultaneously observing the same air mass is of highest priority to eliminate any questions about intercalibration.

2. A continuous data set on ClO taken from the ground in the vicinity of 32°N would provide crucially important continuity in the ClO total column density and would define any significant excursion from the mean such as those reported by the in situ method in July 1976/1977.

3. Extension of the ClO profile, with good altitude resolution (1 to 2 km) and signal-to-noise (S/N > 10), down to the tropopause would firmly establish the gradient. It is also essential to decrease the experimental uncertainty of the in situ measurements to ±10 to 15%.

Seasonal Variation

Although there is an indication of some seasonal dependence in ClO, the data base is clearly inadequate to draw any clear conclusions. This question should be addressed both by an improvement in the accuracy and precision of the balloon-borne methods and by the more extensive deployment of ground-based methods. Only when those are done in concert will an adequate definition of this important point emerge.

Latitude Variation

There is virtually no information on the critical question of latitude variation. The balloon-borne observations are all carried out at 32°N and the ground based data at 42°N. As will be noted in the subsequent sections, if the steep gradient in ClO below the peak is characteristic of both mid-and low-latitude conditions, the interpretation of chlorine induced depletion will be significantly simpler.

Hydrogen Chloride (HCl)

Introduction

HCl in the stratosphere has been observed by three different remote sensing techniques and one in situ method. Most of the presently available data on the vertical profile of concentration come from balloon-borne observations made at ~32°N latitude (Texas and New Mexico); there are, in addition, single profiles taken at 30°S (Australia) and 65°N latitude (Alaska). The profile measurements cover the altitude range from 14 to 40 km, and are supplemented by values for the total column abundance in the upper stratosphere. There is insufficient data from which to discern any seasonal variability, and the location of the altitude of peak relative abundance is not clearly established. The available data cover the period from 1975 to 1980.

Discussion of Remote Sensing Techniques

The remote sensing methods include several quite different techniques: spectroscopy at visible and infrared wavelengths, by absorption and emission; broadband and correlation filter radiometry (IR, principally in emission); laser heterodyne radiometry and Lidar; microwave sounding. The observations are made from the ground, from aircraft, balloon and rocket platforms, and from satellites.

The fixed-frequency, very high resolution methods (which include microwave sounding and laser heterodyne techniques) are able to measure the detailed line shape of a constituent of interest;

by appropriate deconvolution methods the distribution of the constituent above the observation base can be determined, with vertical resolution approximately equal to the scale height. The distribution can be obtained even from a single observation at a zenith angle of less than 90°. By contrast, the "incoherent" methods (e.g., high-resolution spectroscopy, correlation radiometry) derive the required altitude weighting by recording sequences of measurements at angles greater than 90° (limb techniques) and deconvolving the data using a variety of inversion procedures (often referred to as "onion-peel" methods). For these methods, therefore, the maximum altitude to which the concentration profile can be determined is the altitude of the observation platform.

A second important distinction among the remote sensing techniques can be made between emission and absorption measurements. Most of the high-resolution spectroscopic observations, which have provided data for a large number of the infrared active constituents of the upper atmosphere, have been made in the absorption mode; such measurements use the Sun as the radiation source, the geometric weighting being obtained by recording spectra during sunrise or sunset. A major disadvantage of absorption spectroscopic or radiometric methods is thus the fact that measurements can only be made at two rather restricted times of day. This aspect presents serious difficulties in the case of the diurnally varying species, especially those whose concentrations vary rapidly in response to solar insolation changes. The latter restriction does not apply of course, to measurements of the total column, and its variation with latitude and season, (i.e., where the vertical distribution is not required). Against this, the absorption measurements are not dependent (to first order) on the detailed knowledge of the temperature distribution along the line-of-sight of the observation, as is the case for measurements made in emission. In the latter (emission) case, the errors resulting from uncertainty in temperature depend on detailed factors related to the distribution of the species being measured, and can become large under circumstances where the thermal contrast is small over the region of the atmosphere where the spectral lines are formed.

All of the remote methods are subject to some degree to errors arising from uncertainty in the observational geometry, but this is more particularly the case for the limb techniques. As a result of the strong dependence of the line-of-sight airmass on zenith angle for angles greater than 90°, errors in the observation altitude and zenith angle can introduce errors in the deduced molecular column density of as much as 30%. The effects of finite beam size and uncertainty in the detailed instrumental field-of-view further contribute to this source of error. A second factor common to all of the remote methods is the error introduced by errors in the intrinsic molecular line or band parameters for the transitions being observed. For the better-studied molecules (CH_4, N_2O, H_2O for example) such errors should not now exceed 5%. However, the more recently emerging species of interest, and particularly those that are reactive under laboratory conditions (e.g., HOCl), may not be quantitatively understood to better than 50%. A related potential source of systematic differences that may arise between in situ and remote measurements of a given molecular constituent is lack of knowledge of the detailed line shapes under collision-broadened conditions. Depending on the size of the departures from ideal "pure-Lorentz" shape, an error from this source can introduce a skew towards high or low concentrations with respect to the true values of progressively lower tangent height altitudes of observation. In most cases systematic errors arising from such factors related to radiative transfer assumptions in the data reduction process should not exceed 5%.

A characteristic of remote sensing spectroscopic methods is their high specificity; provided adequate laboratory calibration has been carried out, there is usually no ambiguity associated with the identification and measurement of species. Against this, the spatial resolution of remote sensing techniques is very coarse (kilometer) in comparison with in situ sampling methods (meters). Limb observations, for example, typically sample a volume of atmosphere which is weighted towards the tangent point at a distance of hundreds of kilometers from the observation platform, and with a height (thickness) of 1 or 2 km at the limb. Thus, the effects

of spatial and temporal variability must be carefully considered when comparing in situ and remotely measured profiles. The remote methods all determine the line-of-sight column density under one or more geometric path conditions, and these values are then converted by geometric and spectral models to average local concentrations at a number of altitudes corresponding to the number of independent measurements acquired. The result is a particular approximate representation of the vertical distribution of the species, which should not be expected to match closely a profile determined by in situ sampling. The latter (in the absence of errors) is an exact profile, while the remote data give a large scale average representation.

Finally, several internal checks are available when evaluating and intercomparing the results of remote observations. For example, a sensitive verification of the geometric factors and algorithms involved in the reduction of spectroscopic data is the ability to reproduce the correct CO_2 concentration over wide spectral intervals. In addition, the many solar lines available provide a direct calibration of the qualitative reliability of the data, and are especially valuable in intercomparing spectra from several different measurements or instruments.

Altitude Profile

Balloon-borne near-infrared absorption spectroscopy has been used to obtain vertical profiles, covering the 14 to 40 km altitude range (Figure 1-99). Several groups of investigators have made measurements by this method, and obtained results which are in fairly good agreement. In addition there have been observations made by pressure-modulation radiometry, by emission spectroscopy and (recently) by absorption spectroscopy from the ground (Figure 1-100). In situ data from base-impregnated filter collection method, which determines total acidic chloride vapor, are also available; while these measurements are not specific to HCl, they should provide an independent upper limit check on the remote sensing results. The sources and pertinent observational conditions for the currently available measurement results are summarized in Table 1-21.

The measurements made by near-IR absorption spectroscopy (five different experimenters) are in sufficiently good agreement that a mean profile from 14 to 40 km can be derived from them, having a probable maximum uncertainty of ±50%. At 25 km altitude, all of the balloon-borne absorption spectroscopy results agree to within ±15% (at 0.7 ppbv), regardless of season and latitude, or experimental factors which might introduce systematic biases such as the individual balloon float altitudes. The height at which the maximum relative concentration of HCl occurs is not evident from the published spectroscopic data. The correlation radiometry (pressure modulator) results, while somewhat higher than the other absorption values over the 25 to 30 km range, are nevertheless in agreement when the combined errors are taken into account. These results (Eyre and Roscoe, 1977) show a maximum in the vertical profile between 30 and 35 km.

The IR emission results (in preliminary form at the time of writing) agree with the absorption data only at the top of the profile, but fall off much more rapidly with decreasing height. The quoted error limits do not accommodate this difference, but this comparison may well become more favorable when the first-order approximations made in the preliminary analysis of the emission spectra are removed.

The in situ data are in quantitative agreement with the shortwave IR results at the lower altitudes, but the overall profile derived from the filter sampling method is quite different in shape from the profile obtained from the remote sensing instruments (and from theory). The in situ data show a minimum at 30 to 32 km in all of the published profiles; since the filter collection results refer to all "inorganic chlorides", and in general give smaller mixing ratio values than the spectroscopic measurements (which are specific to HCl), there is a clear discrepancy between the two separate techniques.

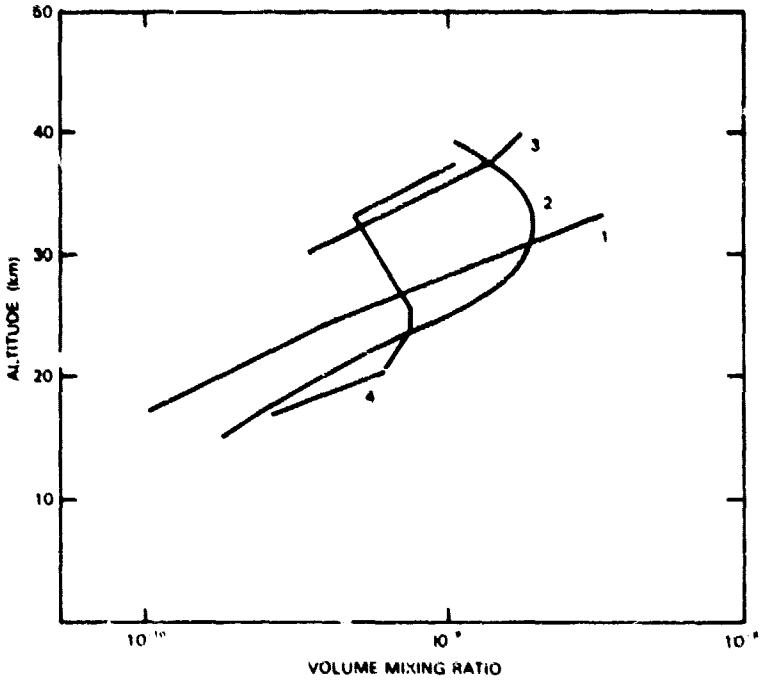

Figure 1-99. HCl measurements by (1) ground-based spectroscopy (June 79 profile), (2) pressure modulator radiometry, (3) far IR emission, and (4) in situ filter collection.

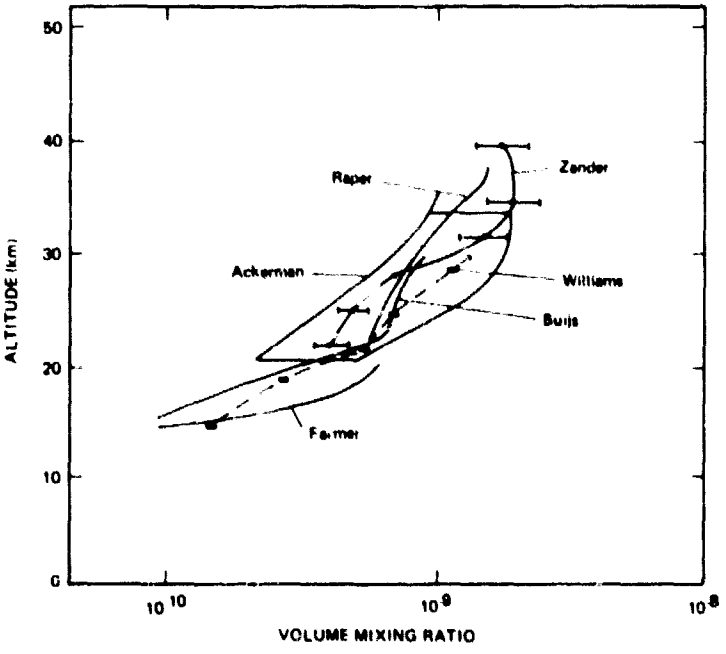

Figure 1-100. HCl distribution from balloon-borne IR absorption spectroscopy.

Table 1-21
Summary of HCl Measurements

Experimenter	Obs. Date	Latitude	Alt. Range	Method	Reference
Farmer	May/June 75	40°N	14 - 21 km	IR absorption	Farmer et al. (1976)
Ackerman	Oct. 75	42°N	18 - 35 km	IR absorption	Ackerman et al. (1976)
Williams	Dec. 75	33°N	13 - 30 km	IR absorption	Williams et al. (1976)
Eyre	March 76	33°N	16 - 39 km	IR absorption (radiometry)	Eyre and Roscoe (1977)
Bulja	May 76	65°N	20 - 29 km	IR absorption	Bulja et al. (1980)
Raper	May 76	32°N	22 - 38 km	IR absorption	Raper et al. (1977)
Zander	May 76	32°N	above 30 km*	IR absorption	Zander (1981b)
Lazrus	Mean for 76	33°N	14 - 37 km	In situ (filter)	Lazrus et al. (1977)
Farmer	March 77	30°S	22 - 37 km	IR absorption	Farmer et al. (1980)
Zander	Oct. 78	32°N	21 - 38 km	IR absorption	Zander (1980)
Carli	Apr. 79	32°N	30 - 40 km	IR emission	Bangham et al. (1980)
Zander	Sept. 79	32°N	above 37 km*	IR absorption	Zander (1980)
Marche	Dec. 78-Nov 79	49°N	0- 33 km	IR absorption (ground)	Marche et al. (1980)

*Reports total column abundance above stated altitude

From consideration of the quality of the data, the number of independent measurement sets and the agreement between them, the near-IR results are judged to be the most reliable at the present time. The suggested mean vertical profile and its associated 3σ confidence limits are shown in Figure 1-101.

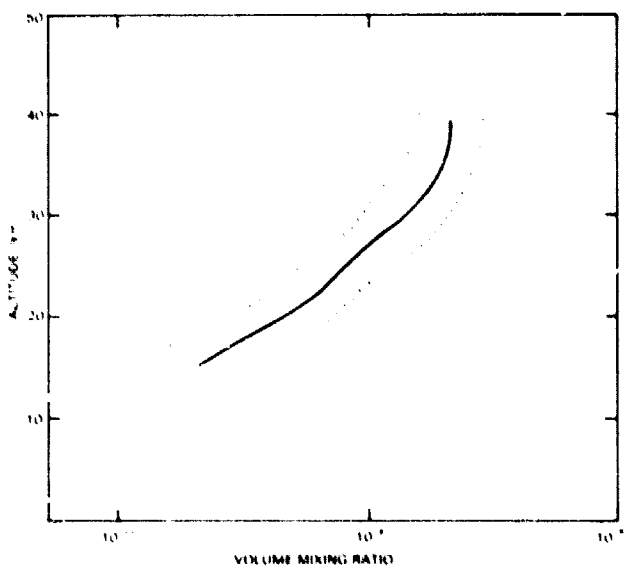

Figure 1-101. Mean HCl profile from absorption spectroscopy measurements. The dotted curves are the 3σ error estimates.

Seasonal Variation

Since many of the IR absorption measurements of HCl were made at the same latitude (32° and 33°N), it might be expected that any seasonal trend would be seen in this subset of the data. The results, however, do not show any variation greater than the quoted uncertainties associated with each measurement. (It should be mentioned also that the same conclusion regarding the absence of a seasonal variation was reached by Lazrus et al. from the base-impregnated filter measurements of total acidic chloride vapor.) With the currently improved precision of the remote spectroscopic instrumentation, profiles with associated uncertainties of perhaps less than 10% can be anticipated for the near future; thus, more sensitive tests of the seasonal variability of HCl could be made, provided sufficiently frequent observational opportunities are available.

Chlorine Nitrate ($ClONO_2$)

The only specific detection claimed for $ClONO_2$ to date is that of Murcray et al. (1979) by IR absorption. The accuracy of the result is affected both by modeling assumptions and by uncertainties in the intrinsic spectroscopic parameters involved in the analysis of the data (see below). The in situ sampling method, collection on base impregnated filters (Lazrus et al., 1977), is sensitive to all acidic chloride (see HCl) so that its results can only be used to provide an upper limit estimate for $ClONO_2$. Since the filter data are not compatible with the IR data for HCl ($q_1 v_1$), they cannot aid in evaluating the available remote sensing data for $ClONO_2$.

The published values from Murcray's observations, an October 1978 balloon flight (see Figure 1-102), differ from the preliminary values given in NASA RP 1049. The measurements were made by the limb absorption method, that is, by observing the Sun through the atmosphere at sunrise or sunset from a stratospheric balloon platform. The strong infrared absorption by $ClONO_2$ at 1292 cm^{-1} was used by Murcray and his coworkers in their analysis; this band coincides in the stratospheric spectrum with strong absorptions by the natural gases, N_2O, CH_4, and H_2O. As the absorptions due to these constituents increase (i.e., at the lower tangents heights of observation), the superimposed $ClONO_2$ absorption is completely masked. However, even at the higher altitudes, where the $ClONO_2$ absorption might be discernible against the spectral background, the maximum expected effect does not exceed 5% or 6% depression of the HCl continuum. Thus the quantitative analysis is dependent both on the spectral model and on the quality of the experimental data. With these considerations in mind, the published data may at best indicate a possible specific identification of $ClONO_2$: the deduction of a profile of concentration with associated experimental errors of ±25% does not seem justified. An upper limit concentration of 10^{-9} by volume, between 25 and 35 km altitude is consistent with the observational data.

OTHER HALOGENS

Hydrogen Fluoride (HF)

Stratospheric HF has been measured by several different groups using both remote sensing and in situ techniques. The measurements for the most part have been made at different locations and seasons and do not include a sub-set of observations similar to those for HCl from which a most probable profile can be derived. The measurements that have been made to date are summarized in Table 1-22 and Figure 1-103.

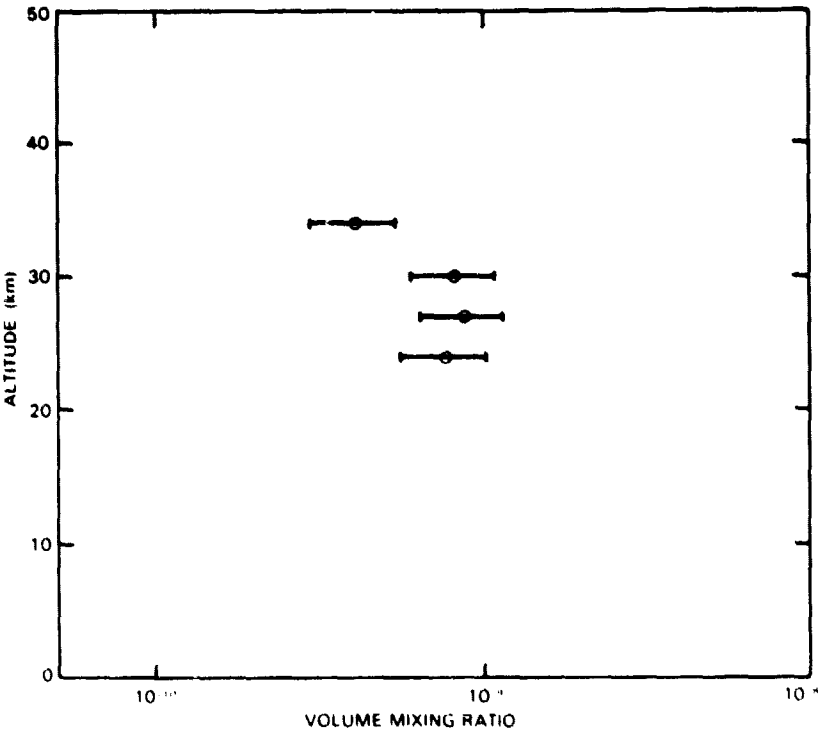

Figure 1-102. Distribution of $ClONO_2$, from Murcray et al. (1980).

Table 1-22
Summary of HF Measurements

Experimenter	Obs. Date	Latitude	Alt. Range	Method	Reference
Zander	Sept. 74		above 27 km	IR absorption	Zander (1975)
Zander	May 76	32°N	above 27 km	IR absorption	Zander (1981b)
Buijs	May 76	65°N	15 - 30 km	IR absorption	Buijs et al. (1980)
Mroz	Feb. - Nov. 76	30° - 33°N	15 - 37 km	In situ (filter)	Mroz (1977)
Farmer	March 77	30°S	14 - 40 km	IR absorption	Farmer et al. (1980)
Zander	Oct. 78	32°N	above 30 km	IR absorption	Zander (1980)
Carli	April 79	32°N	30 - 40 km	IR emission	Bangham et al. (1980)
Marche	May 79	49°N	20 - 30 km	IR abs. (ground-based)	Marche et al. (1980b)
Zander	Sept. 79	32°N	above 36 km	IR absorption	Zander (1980)

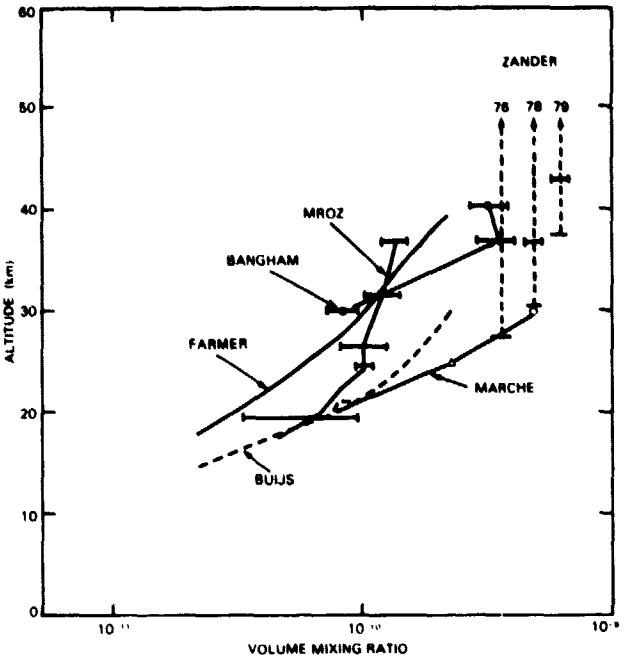

Figure 1-103. Stratospheric HF profile measurements.

The two most directly comparable measurements in terms of experimental technique, both of which yield a profile for HF, are those of Farmer et al. (1980) and Buijs et al. (1980). Both were made from balloon platforms, using infrared absorption spectroscopy to establish the profile below the float altitude of the balloon. While these two give profiles of similar slope, they differ in magnitude by a factor of two (see figure). However, these also represent the extremes of latitude at which HF observations have been made (30°S vs. 65°N) and must be compared with caution. Both sets of data are presented in terms of geometric altitude rather than effective stratospheric altitude. Given that HF is the sink term for anthropogenic halocarbons which are emitted primarily in the Northern Hemisphere, interhemispheric differences may be partially responsible for the consistently higher results obtained by all of the remote sensing measurements in the north. More measurements are needed in the Southern Hemisphere to determine if this difference is real.

Two additional profiles for HF have been obtained by Bangham et al. and Marche, the former from balllon-borne observations at 32°N in emission and the latter from ground-based absorption measurements at 42°N. These two profiles cover different altitude regions in the stratosphere, but at the one common altitude of 30 km differ by about a factor of five (see Figure 1-104).

The remaining remote sensing measurements are those of Zander (1980) who reports total column abundances above three different float altitudes from balloon flights made over a period of 4 years. These measurements were made at successively higher altitudes and yield increasingly larger values for the total HF burden above the balloon, which, if interpreted as a profile, produce the result shown in Figure 1-104. They may also be indicative of a long-term increase in the stratospheric HF which Zander has observed in the course of the IR absorption studies. The possibility of such an increase renders intercomparisons between measurements in a data base acquired over a period of 6 years even more difficult, and demonstrates the need to establish a reliable baseline profile for HF against which future measurements can be assessed.

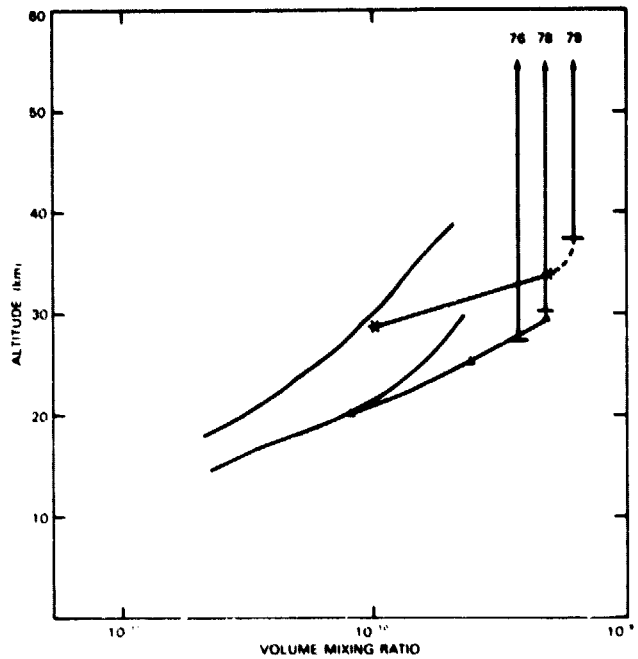

Figure 1-104. Zander's (1981b) total column measurements interpreted as the profile of HF below the highest float altitude (x-x), shown with Marche's May 1979 ground-based measurement (Δ) and Farmer and Buijs' profiles for comparison.

The in situ data of Mroz et al. shown in Figure 1-103, is the average of four seasonal sets of measurements made in 1976. Although the shapes of the profiles are different, the total stratospheric burdens for HF which can be deduced from the Mroz et al. data and that of Farmer et al. appear to be in good agreement. However, the sampling technique used by Mroz et al. is stated to be sensitive to total fluoride, including COF_2 and COFCl: depending on the model used, this implies that as much as one-third of the collected material could have been in the form of these two gases. Thus, the HF in situ results are similar to those for HCl in that they are generally lower than the results obtained using remote sensing techniques.

SATELLITE MEASUREMENTS OF TRACE GASES

Satellite observations of trace gases other than ozone did not begin in earnest until the launch of Nimbus 7 in October 1978. There were attempts to measure upper atmosphere water vapor profiles using the Selective Chopper Radiometer (SCR) on Nimbus 5 and LRIR on Nimbus 6 but for various reasons, it has not been possible to obtain much water vapor information from these experiments. TOVS and several other NOAA satellite instruments measured water vapor only below the tropopause and, therefore, they will not be discussed here. The LIMS experiment on Nimbus 7 measured the profiles of H_2O, NO_2, and HNO_3, in addition to temperature and ozone. The LIMS data set covers slightly more than 7 months of the Northern Hemisphere winter and spring periods. The SAMS experiment on Nimbus 7 measured, in addition to temperature, the concentrations of CO, CH_4, H_2O, N_2O, and NO. This instrument is still operating and returning data daily on all of these species except NO. A summary of coverage, time periods and data availability is given in Tables 1-23, 1-24, 1-25, and 1-26 for minor atmospheric constituents other than ozone.

Measurements of other trace gases are just being produced and validated, so there is not yet a large body of findings. Among the preliminary findings which may be noted are the observations

Table 1-23

Satellite Measurements of Atmospheric H_2O, NO_x and Related Species Concentration Profiles - Measurement Parameters

Instrument (Species)	Satellite	Time Period	Lat. Range (Deg.)	Spatial Resolution				Duty Cycle	Estimated Measurement Uncertainty	Comments
				Altitude Range(km)	Vertical (km)	Along Track (km)	Cross Track (km)			
SAMS	Nimbus 7	10/78 to present	50 S to 70 N		10	100 based on vert. scan rate	Orbit spacing — no cross track scan	75% (3 days on in a 4-day cycle)	100 ppb	*Uncertain due to unresolved water vapor line shape problems
(N_2O)				20-45			—			
(NO)				20-150			Data interpolated to a latitude grid of 10° zonal mean		50%	
(H_2O)				15-65					2 ppmv	
LIMS	Nimbus 7	10/78-5/79	64 S to			84	Orbit spacing (~2500) (~1300) by combining ascending and descending node data	75%		*Effective duty cycle including ERB interference effects
(NO_2)				10-50	4				25%	
(HNO_3)				10-50	2				15%	
(H_2O)				10-50	4				15%	

Table 1-24
NOAA Satellite Measurements of Atmospheric H_2O, NO_x, and Related Species Concentration Profiles - Data Information

Instrument (Species)	Satellite	Data Availability	Data Products	Format	Investigator, Institution	Comments
SAMS (N_2O) (NO)	Nimbus 7	NOPS/NSSDC	Radiances and inverted profiles	Magnetic tape	F.W. Taylor Univsity of Oxford	
LIMS (NO_2) (HNO_3) (H_2O)	Nimbus 7	Anticipate archival at NSSDC early 1982	Vertical profiles orbital/ latitudinal cross sections Maps on constant pressure surfaces, radiance vertical profiles	Magnetic tape, microfilm hard copy	J. Russell NASA/LaRC J. Gille, NCAR	

Table 1-25
Satellite Measurements of Aerosols, CO and CH_4 Concentration Profiles - Measurement Parameters

Instrument (Species)	Satellite	Time Period	Lat. Range (Deg.)	Altitude Range(km)	Spatial Resolution			Duty Cycle	Estimated Measurement Uncertainty	Comments
					Vertical (km)	Along Track (km)	Cross Track (km)			
SAMS	Nimbus 7	10/78 to present	50 S to 70 N		10	100 based on vertical scan rate	Orbit spacing —— no cross track scan — Data interpreted to a latitude grid of 30° zonal mean	75% (3 days on in a 4-day cycle)		
(CO)				35-100						
(CH_4)				20-55			10° Zonal mean		250 ppb	
SAM II (Aerosol)	Nimbus 7	10/78 to present	64-80 N 64-80 S	Cloud top to 50 km	1 km below 35 km; 5 km above 35 km	200	Orbit spacing		2-5%	
SAGE (Aerosol)	AEM-B	2/79 to present	72 N to 72 S	Cloud top to 50 km	1 km below 35 km; 5 km above 35 km	200	Orbit spacing		2-5%	

Table 1-26
Satellite Measurements of Aerosols, CO and CH_4 Concentration Profiles - Data Information

Instrument	Satellite	Data Availability	Data Products	Format	Investigator, Institution	Comments
SAMS (CO and CH_4)	Nimbus 7	NOPS/NSSDC	Radiances and inverted profiles	CH_4 on magnetic tape; CO on paper	F.W. Taylor University of Oxford	
SAM II	Nimbus 7	Available from NSSDC summer 1981	Aerosol extinction at wavelength vs. alt.	Extinction isopleths altitude vs. latitude and longitude; global maps of total burden	M.P. McCormick NASA/LARC	
SAGE	AEM-2	Available from NSSDC late 1981	Aerosol extinction at 2 wavelengths vs. altitude	Extinction isopleths altitude vs. latitude and longitude, global maps of total burden	M.P. McCormick NASA/LARC	

of the diurnal variation of NO_2, and of the downward and poleward slope of the maximum HNO_3 concentration by LIMS (Gille and Russell, private communication). Similarly, SAMS (Taylor, personal communication) has observed the diurnal variation of NO, and the rapid decrease in water vapor mixing ratio above 70 km.

COMPARISON OF MEASUREMENTS AND 1-D MODEL CALCULATIONS FOR TRACE REACTIVE SPECIES

In the previous section the data base from field measurements has been critically examined, and those observations which comprise the empirical picture of reactive trace species in the stratosphere have been identified. In this section the observations are compared with the current theoretical picture of the stratosphere expressed through a typical one-dimensional model (Wuebbles, 1981).

For each of the families which contribute to the catalytic destruction of odd oxygen (e.g., nitrogen, chlorine, hydrogen, etc.), the following questions will be answered before the differences between observed and calculated profiles are interpreted:

- Which catalytic cycles (i.e., which reaction sets taken together) dominate the destruction of odd oxygen at each altitude interval in the stratosphere?
- Which reaction in each catalytic cycle is rate limiting for that cycle?
- Given the identification of that rate limiting reaction, and thus the identification of the rate limiting reactive species, which reactions determine the fractional amount of that rate limiting species?

In order not to invalidate the discussion because of changes in laboratory rate data, six different sets of reaction rates have been used as input to the model calculations. These six cases cover the four most important rate constant uncertainties currently confronting stratospheric chemistry. The first is the reaction of the hydroxyl radical with nitric acid for which there are two current alternatives. The second is the reaction of hydroxyl with pernitric acid for which there remains a serious lack of strong experimental evidence. The third is the reaction of hydroxyl with hydrogen dioxide for which a fast and a slow rate exist. The final reaction is the formation of chlorine nitrate, from chlorine oxide and nitrogen dioxide. Two choices are identified: A "fast" chlorine nitrate formation rate which uses the observed loss coefficient for $ClO + NO_2$ and assigns the product channel entirely to $ClONO_2$; and a "slow" chlorine nitrate formation rate based on the thermal decomposition rate-equilibrium constant approach which ascribes one-third of the reaction to the $ClONO_2$ channel and two-thirds to rapidly dissociated isomeric form(s).

The six cases are:

Case 1: The rate constant set as recommended in NASA RP 1049. This set is later referred to in Chapter 3 as Case A. The significant reactions in this set are given in Table 1-27.

Case 2: The rate constant set as recommended by the NASA Panel for Data Evaluation in January 1981 (JPL 81-3) except the rate for the reaction

$$HO + HNO_3 \rightarrow \text{Products}$$

which is set equal to the rate in Case 1. The significant reactions in this set are also given in Table 1-27.

Table 1-27
Reaction Rate Constants Used in 1-D Model Calculations

Reaction	Case 1 - NASA RP 1049	Case 2
$HO + H_2O_2 \rightarrow H_2O + HO_2$	$1.0 \times 10^{-11} \exp(\frac{-750}{T})$	$2.7 \times 10^{-12} \exp(\frac{-145}{T})$
$HO + O \rightarrow H + O_2$	4.0×10^{-11}	$2.3 \times 10^{-11} \exp(\frac{+110}{T})$
$HO_2 + O \rightarrow HO + O_2$	3.5×10^{-11}	4.0×10^{-11}
$ClO + NO \rightarrow NO_2 + Cl$	$7.8 \times 10^{-12} \exp(\frac{+250}{T})$	$6.5 \times 10^{-12} \exp(\frac{+280}{T})$
$O(^1D) + \begin{matrix} N_2O \\ H_2O \\ CH_4 \\ N_2 \\ O_2 \\ CO_2 \end{matrix} \rightarrow$ Product	See NASA RP 1049	See JPL Publication 81-3
$HO_2 + HO_2 \rightarrow H_2O_2 + O_2$	2.5×10^{-12}	2.5×10^{-12} cm^3/sec
$HO_2 + NO \rightarrow HO + NO_2$	$4.3 \times 10^{-12} \exp(\frac{200}{T})$	$3.5 \times 10^{-12} \exp(\frac{+250}{T})$
$HO + HO \rightarrow H_2O + O_2$	$1.0 \times 10^{-11} \exp(\frac{500}{T})$	$4.5 \times 10^{-12} \exp(\frac{-275}{T})$
$HO + HOCl \rightarrow H_2O + ClO$	$3.0 \times 10^{-12} \exp(\frac{-600}{T})$	$3.0 \times 10^{-12} \exp(\frac{-150}{T})$
$Cl + CH_4 \rightarrow HCl + CH_3$	$9.9 \times 10^{-12} \exp(\frac{-1359}{T})$	$9.6 \times 10^{-12} \exp(\frac{-1350}{T})$
$Cl + HO_2 \rightarrow HCl + O_2$	4.5×10^{-11}	4.8×10^{-11}
$ClO + HO_2 \rightarrow HOCl + O_2$	5.2×10^{-12}	$4.6 \times 10^{-13} \exp(\frac{+710}{T})$
$NO_3 + h\nu \rightarrow \begin{matrix} NO + O_2 \\ NO_2 + O \end{matrix}$	See NASA RP 1049, page 23	JPL Publication 81-3
$HO + HONO_2 \rightarrow$ Products	8.5×10^{-14}	Same as Case 1
$HO + HO_2NO_2 \rightarrow$ Products	5.0×10^{-13}	8×10^{-13}
$HO + HO_2 \rightarrow H_2O + O_2$	4×10^{-11}	Same as Case 1

Case 3: The complete rate constant set given in JPL 81-3 (1981). This set is referred to in Chapter 3 as Case B. This set includes the fast rate for the reaction:

$$HO + HNO_3 \rightarrow \text{Products}$$

Case 4: The rate constant set for Case 3 except for the reaction

$$HO + HO_2NO_2 \rightarrow H_2O + NO_2 + O_2$$

for which a faster rate of $4x10^{-12}cm^3sec^{-1}$ is used.

Case 5: The rate constant set for Case 4 except for the reaction

$$HO + HO_2 \rightarrow H_2O + O_2$$

for which a faster rate of $8x10^{-11}cm^3sec^{-1}$ is used. This set corresponds to Case C in Chapter 3.

Case 6: The rate constant set given in Appendix A of this report. This corresponds to Case D in Chapter 3. This data set uses the slow rate for the formation of $ClONO_2$. Cases 1 through 5 use the fast $ClONO_2$ formation rate.

All the calculations shown are for noon and unless stated otherwise are for Case 6.

ATOMIC OXYGEN

Although there are relatively few atomic oxygen profiles, all of which were obtained at mid-latitude (Palestine, Texas, 32°N) corresponding to midday conditions, they form a rather consistent picture when compared with model calculations for corresponding conditions. Figure 1-105 correlates the six available atomic oxygen observations with the 1-D profile using the rate constant set six. Given the cited experimental uncertainty of ±30%, the observations are in agreement, both in absolute magnitude and the gradient with the model calculations. A critical test of the theory is the ratio of the atomic oxygen concentration to the ozone concentration. As shown in Figure 1-54 the agreement between theory and measurements for this ratio is good.

THE HYDROGEN SPECIES

Catalytic Cycles Affecting Odd Oxygen

The major hydrogen-oxygen free radicals, HO and HO_2, play a critical part in every stratospheric chemical mechanism either directly as a reactant or through control of the partitioning between free radical and stable forms within each of the chemical groups (i.e., nitrogen, chlorine, etc.)

Four major catalytic cycles involve HO_x radicals directly in an odd oxygen rate limiting process:

Cycle 1:
$$O + HO \rightarrow O_2 + H$$
$$H + O_2 + M \rightarrow HO_2 + M$$
$$O + HO_2 \rightarrow HO + O_2$$

Net
$$O + O \rightarrow O_2$$

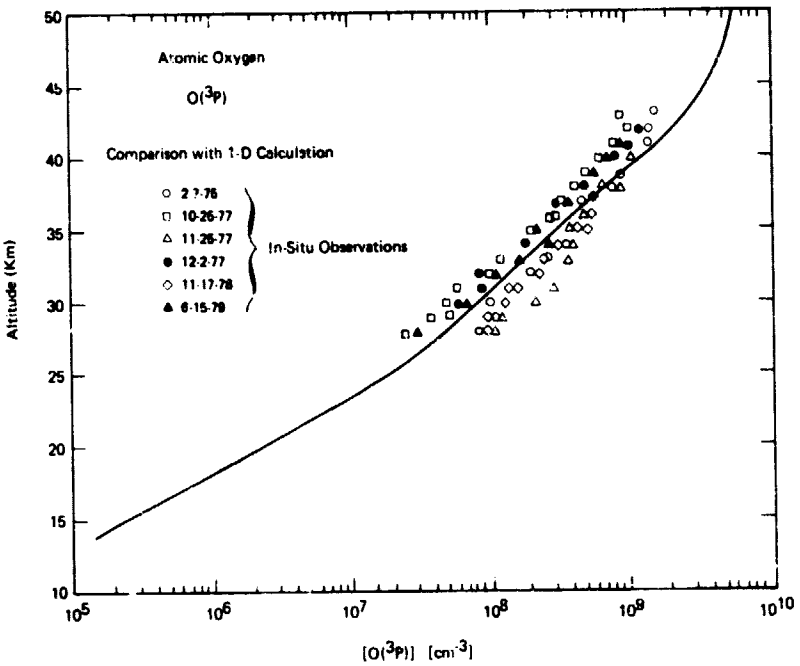

Figure 1-105. Comparison of atomic oxygen measurements with a one-dimensional calculation.

Cycle 2:
$$O + HO \rightarrow O_2 + H$$
$$H + O_3 \rightarrow HO + O_2$$
Net
$$O + O_3 \rightarrow 2O_2$$

Cycle 3:
$$HO + O_3 \rightarrow HO_2 + O_2$$
$$HO_2 + O \rightarrow HO + O_2$$
Net:
$$O + O_3 \rightarrow 2O_2$$

Cycle 4:
$$HO + O_3 \rightarrow HO_2 + O_2$$
$$HO_2 + O_3 \rightarrow HO + 2O_2$$
Net:
$$O_3 + O_3 \rightarrow 3O_2$$

Above 40 km HO_x cycles 1 and 2 are of major importance to the destruction of odd oxygen and are dominated by important pathways for cycling HO_x between HO and HO_2. Below 40 km cycle 3 begins to dominate as the O to O_3 ratio decreases and by 30 km cycle 4, which does not utilize O atoms becomes the most important. In both of these cycles the HO_2 reaction with either O or O_3 is rate limiting in that it competes with $HO_2 + NO \rightarrow HO + NO_2$ which returns HO_2 to HO without net destruction of odd oxygen.

Budget and Partitioning of Odd Hydrogen (HO_2 and HO)

Budget

The dominant source of HO_x radicals throughout the stratosphere is the reaction of $O(^1D)$ with H_2O to form HO

$$H_2O + O(^1D) \rightarrow HO + HO$$

Production of HO_x from H_2O and methane oxidation is balanced by recombination to H_2O by the bimolecular reaction

$$HO + HO_2 \rightarrow H_2O + O_2$$

and reaction cycles:

$$HO + NO_2 \rightarrow HONO_2$$

$$HO + HONO_2 \rightarrow H_2O + NO_3$$

Net $\quad 2HO + NO_2 \rightarrow H_2O + NO_3$

$$HO_2 + NO_2 \rightarrow HO_2NO_2$$

$$HO_2NO_2 + HO \rightarrow H_2O + O_2 + NO_2$$

Net $\quad HO + HO_2 \rightarrow H_2O + O_2$

However, HO_2NO_2 has not been observed in the concentrations predicted by the models. Figure 1-106 displays the altitude dependence of HO_x recombination rates, selecting the rate limiting process in each of the cycles:

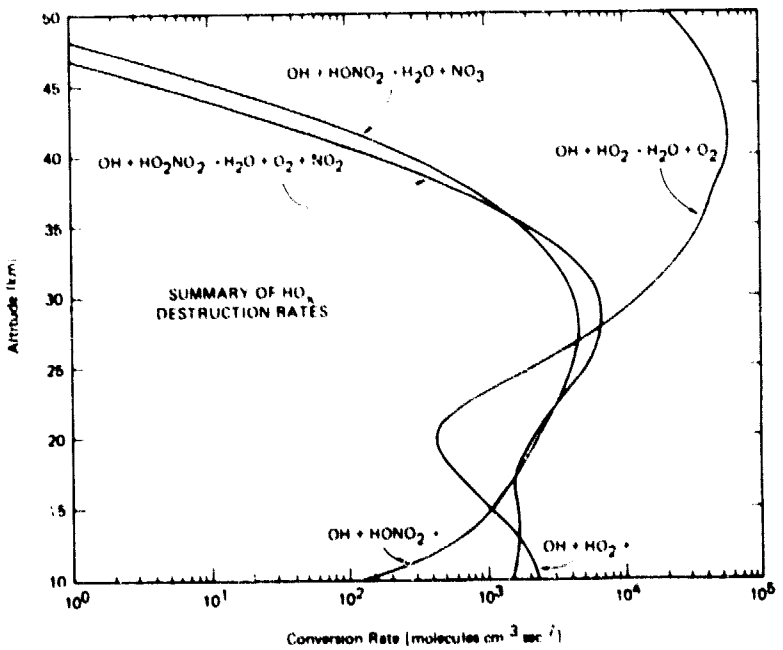

Figure 1-106. Recombination rates for HO_x.

Above 35 km, the direct recombination to H_2O through $HO + HO_2$ dominates the destruction of HO_x, while near 30 km the two catalytic cycles are closely competitive with direct recombination. At 25 km and below, the catalytic cycles rapidly (and approximately equally) dominate direct recombination down to 15 km. The quantitative details of the conversion rates displayed in Figure 1-107 depend critically upon the choice made for the corresponding rate constants. The values recommended in this document have been adopted but, as will be discussed subsequently in this section, there is considerable uncertainty regarding the appropriate rate constant choice.

Partitioning

Partitioning between HO and HO_2 is controlled by the following reactions:

$$HO + O \rightarrow H + O_2$$

$$H + O_3 \rightarrow HO + O_2$$

$$H + O_2 + M \rightarrow HO_2 + M$$

$$HO_2 + NO \rightarrow HO + NO_2$$

$$HO_2 + O_3 \rightarrow HO + 2O_2$$

$$HO_2 + O \rightarrow HO + O_2$$

$$HO + O_3 \rightarrow HO_2 + O_2$$

$$HO + CO \rightarrow CO_2 + H$$

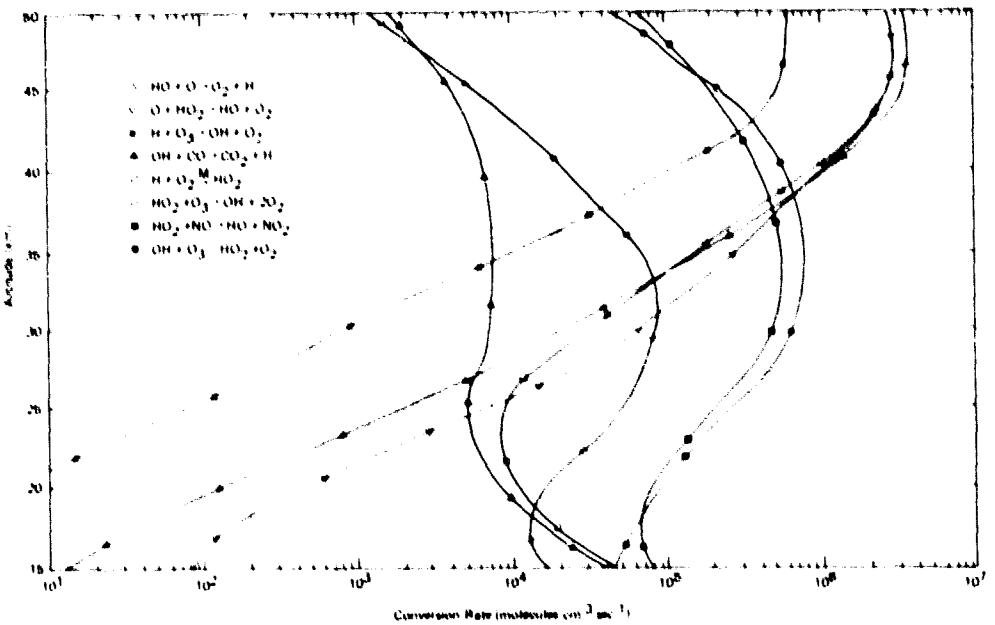

Figure 1-107. Conversion rates between HO and HO_2 as a function of altitude.

The altitude dependence of each reaction is displayed in Figure 1-107. Of particular concern are the reactions which control the fraction of HO_x partitioned into the rate limiting radical, i.e., into HO above approximately 40 km and into HO_2 below approximately 40 km. Since atomic hydrogen constitutes an immeasurably small fraction of the HO_x budget in the stratosphere and is not rate limiting at any altitude, it serves only as an intermediate, and will not be discussed explicitly.

In the altitude region from 50 to 40 km, the conversion of HO to HO_2 occurs primarily through atomic hydrogen with the rate of $HO + O \rightarrow H + O_2$ nearly balancing the subsequent three-body reaction, $H + O_2 + M \rightarrow HO_2 + M$. Approximately 20% of the H formation rate is balanced by the $H + O_3 \rightarrow HO + O_2$ reaction forming HO. Conversion of HO_2 to HO is dominated by the reaction $HO_2 + O \rightarrow HO + O_2$. Thus, the partitioning between HO and HO_2 is a photochemical steady state with $HO + O \rightarrow H + O_2$ balanced by $HO_2 + O \rightarrow HO + O_2$ such that $[HO]/[HO_2]$ depends, to first order, only on the ratio of rate constants and not upon any other constituent concentration.

Between 40 and 30 km there is a distinct shift from conversion of HO to HO_2 through atomic hydrogen via $HO + O \rightarrow H + O_2$ to direct chemical conversion by reaction of HO with O_3. Conversion of HO_2 to HO near 30 km is dominated by direct reaction

$$HO_2 + NO \rightarrow HO + NO_2$$

Thus, near 40 km the ratio $[HO]/[HO_2]$ depends to first order upon four reactions

$$HO + O \rightarrow H + O_2$$

$$HO + O_3 \rightarrow HO_2 + O_2$$

$$HO_2 + O \rightarrow HO + O_2$$

$$HO_2 + NO \rightarrow HO + NO_2$$

while near 30 km the ratio $[HO]/[HO_2]$ depends to first order on but two reactions,

$$HO + O_3 \rightarrow HO_2 + O_2$$

and

$$HO_2 + NO \rightarrow HO + NO_2$$

In the region of 30 km to the tropopause the same reactions dominate the exchange of HO and HO_2 as at 30 km.

Dependence of Odd Hydrogen Budget and Partitioning on Rate Constants

An inspection of the reactions for which major uncertainties exist regarding corresponding rate constants reveals that it is primarily those processes which recombine (directly or catalytically) HO_x to reform H_2O that are in doubt. This fact is summarized in Figure 1-108 which presents the altitude dependence of the sum $[HO] + [HO_2]$ for each of the five cases.

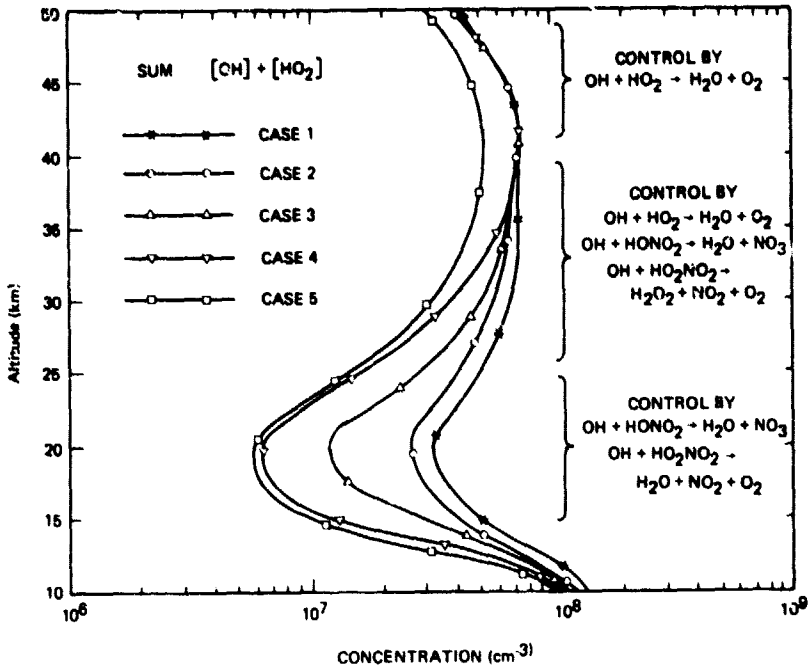

Figure 1-108. The altitude dependence of [HO] + [HO_2] for the five chemical data sets.

Between 50 and 40 km the most important uncertainty for HO_x recombination is HO + $HO_2 \rightarrow H_2O$ + O_2. Thus, all of the cases yield identical results, except that in going from case 4 to case 5, where the rate for HO + HO_2 changes from 4×10^{-11} $cm^3 sec^{-1}$ to 8×10^{-11} $cm^{-3} sec^{-1}$, the sum decreases by a factor of $\sqrt{2}$ as it should for a second order reaction.

In the interval 40 to 25 km, the rate of HO_x recombination is increasingly controlled with decreasing altitude by catalytic cycles which are rate limited by reaction between HO and nitric/pernitric acid. Thus, cases 4 and 5 converge with decreasing altitude, while cases 2, 3 and 4 diverge. Changes in the other 19 reactions define the difference between case 1 and 2, changing the sum only slightly.

Below 25 km: HO_x recombination is predicted to be controlled entirely by the catalytic cycles involving $HONO_2$ and HO_2NO_2. The uncertainties in the sum for these six chemistry data sets approaches a factor of six at 20 km and, as will become apparent in the subsequent discussion, represents a spread in concentrations which prevents a quantitative analysis of ozone photochemistry in the lower stratosphere.

Figure 1-109 shows the calculated ratio of [HO]/[HO_2] for the six cases. The difference between case 1 and case 2 results from a combination of small changes in the oxygen-hydrogen reaction rate constants, listed in Table 1-27. The divergence between cases 2, 3 and 4 below 30 km is a reflection of changes in [NO], coupled with the dominant control by

$$HO_2 + NO \rightarrow HO + NO_2$$

in converting HO_2 to HO.

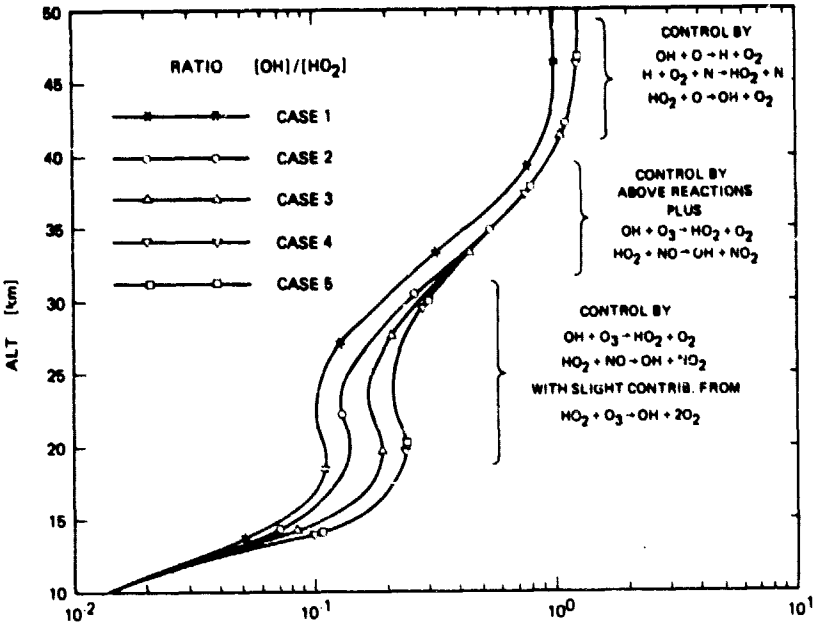

Figure 1-109. Altitude dependence of $[HO]/[HO_2]$ for the five chemical cases.

Comparison Between Calculated and Observed [HO]

Figure 1-110 summarizes the correlation between (a) the balloon and rocket-borne in situ data critiqued earlier, and (b) five of the cases representing the current range in calculated [HO]. Case 6 is not shown as it is essentially identical to case 5. The experiments demonstrate the existence of HO in the stratosphere and they provide a crude picture of the absolute concentration and altitude dependence of the hydroxyl radical down to 30 km. In the region above 30 km, the in situ data are of insufficient absolute accuracy and are too few in number. Below 30 km, where the reactions

$$HO + HONO_2 \rightarrow H_2O + NO_3$$

and

$$HO + HO_2NO_2 \rightarrow H_2O + O_2 + NO_2$$

dominate, there are no data available. It should be noted that some of the discrepancy could be in the choice of the water vapor profile used in the model. The divergence of the profiles represented by cases 2, 3 and 4 maximizes at approximately 20 km, and represents a factor of three uncertainty in lower stratospheric HO.

From the point of view of understanding the photochemical structure of the stratosphere, the absence of data on HO below 30 km (and the scarcity of empirical information above 30 km) is the single most serious shortcoming in our knowledge of the chemical composition of the stratosphere. As will become evident in the subsequent discussion of NO_x and ClO_x, without detailed knowledge of HO throughout the stratosphere, crucial aspects of current computer models cannot be tested. Rectifying this critical shortcoming is essential.

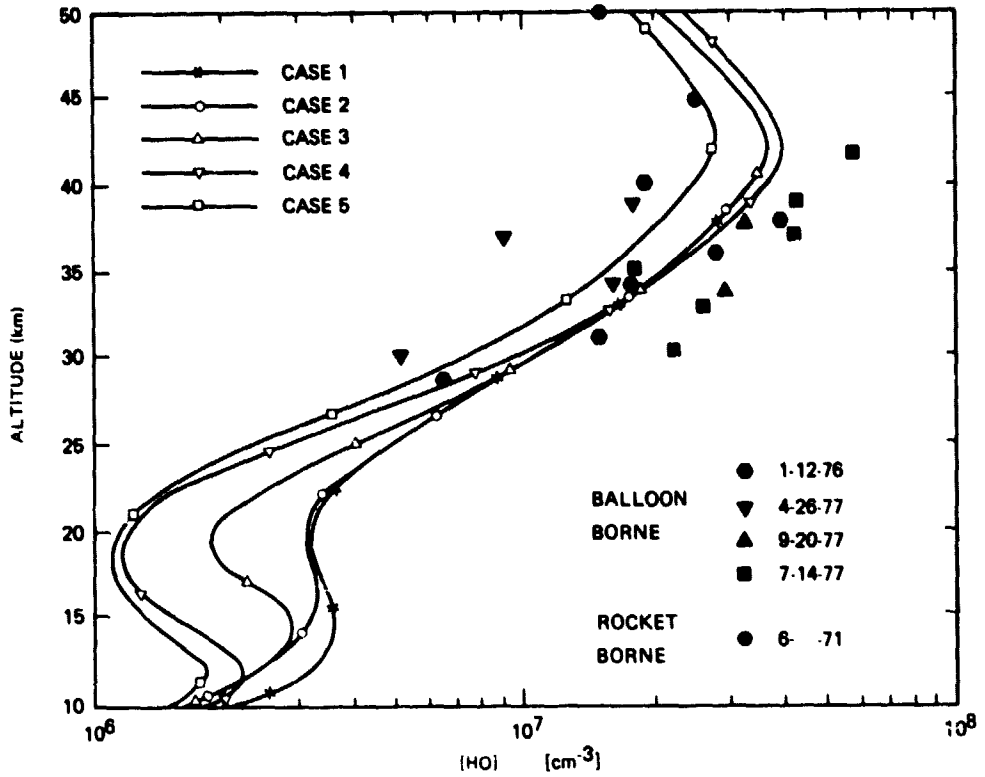

Figure 1-110. Comparison of HO measurements and 1-D model calculations for each of the five cases.

Comparison Between Calculated and Observed [HO_2]

Figure 1-111 gives a comparison between the reported observations of HO_2 and the five cases encompassing the range of calculated [HO_2].

The scatter of the observations is such that the only conclusion that can be drawn is that at noon HO_2 exists in the middle stratosphere with a concentration between 10^7 and $10^8 cm^{-3}$. An accurate characterization of the absolute concentration of HO_2 as a function of altitude is beyond the currently available data base and it is impossible to distinguish among the cases represented by the calculations.

Given that HO_2 is the major rate limiting radical in the HO_x catalyzed destruction of O_x in the lower stratosphere, the extremely large range encompassed by current calculations, coupled with the complete absence of data on HO_2 below 30 km, represents a significant shortcoming in the stratospheric data base.

THE REACTIVE TRACE NITROGEN SPECIES

Catalytic Cycles Affecting Odd Oxygen

There are two catalytic cycles involving nitrogen which reform O_2 from odd oxygen:

$$\underline{\text{Cycle 1}} - \quad NO + O_3 \rightarrow NO_2 + O_2$$

$$NO_2 + O \rightarrow NO + O_2$$

$$\text{Net} \quad O + O_3 \rightarrow 2O_2$$

and

$$\underline{\text{Cycle 2}} - \quad NO + O_3 \rightarrow NO_2 + O_2$$

$$NO_2 + O_3 \rightarrow NO_3 + O_2$$

$$NO_3 + h\nu \rightarrow NO + O_2$$

$$\text{Net} \quad 2O_3 \rightarrow 3O_2$$

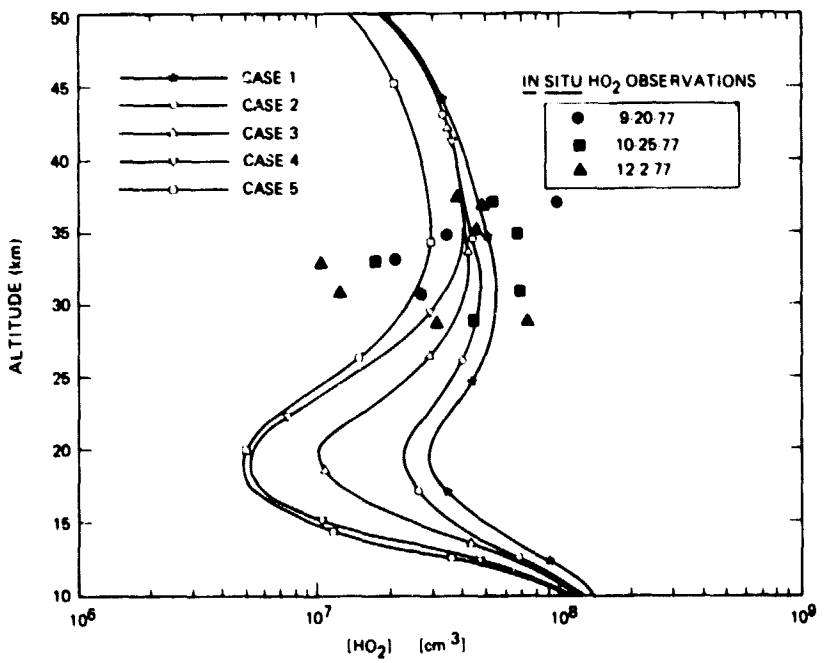

Figure 1-111. Comparison of HO_2 observations with the 1-D model predictions for each of the five cases.

The conversion rates for the reactions in these two cycles are shown in Figure 1-112. It can be seen that there is a single, dominant cycle linking the reactive trace nitrogen species to the destruction of odd oxygen which is rate limited by the reaction

$$NO_2 + O \rightarrow NO + O_2.$$

Partitioning of Reactive Nitrogen into the Rate Limiting NO_2 Radical

The principal source of reactive nitrogen in the stratosphere is the reaction of excited oxygen, $O(^1D)$, with N_2O which forms nitric oxide

$$N_2O + O(^1D) \rightarrow 2NO$$

The rate of reactive nitrogen formation from this source is small. Production peaks in the vicinity of 30 km at approximately 10^2 molecules $cm^{-3}sec^{-1}$. The only reason for the existence of significant amount of reactive nitrogen in the stratosphere is that there is no efficient chemical loss process.

It is convenient to distinguish between all reactive forms of nitrogen which include,

$$N + NO + NO_2 + NO_3 + N_2O_5 + HONO + HONO_2 + HO_2NO_2 + ClONO_2$$

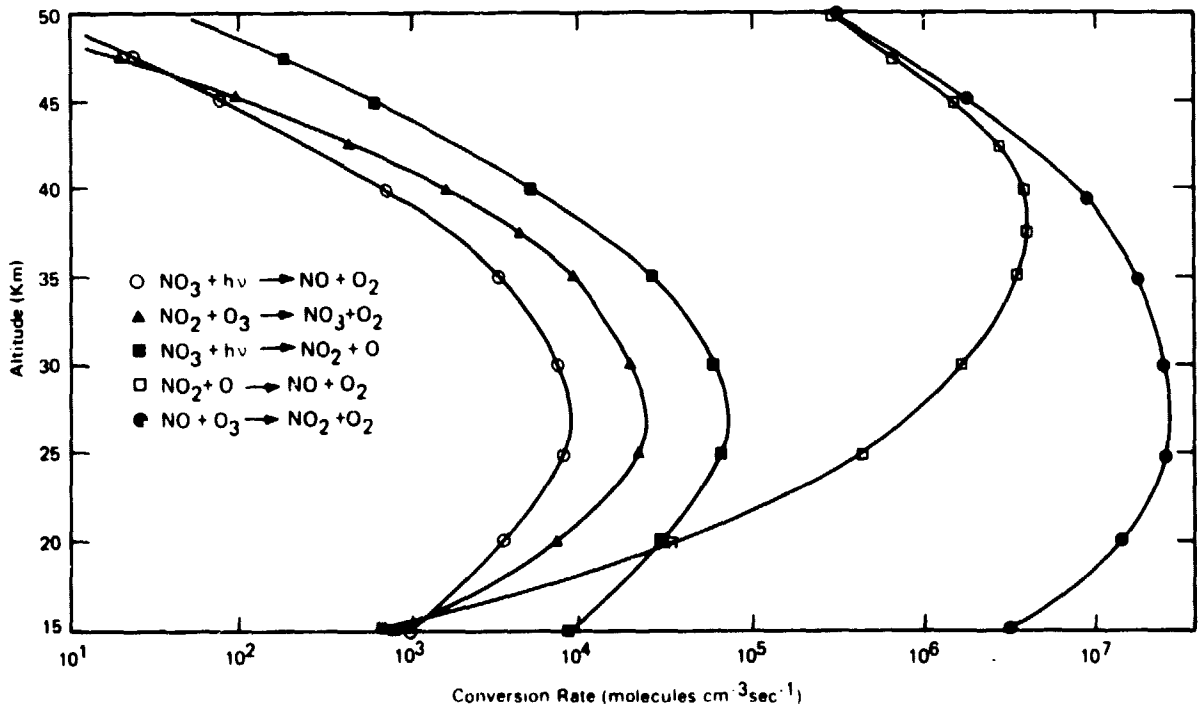

Figure 1-112. Conversion rates of odd nitrogen.

and those reactive forms which enter directly into odd oxygen catalytic destruction cycles,

$$NO_x = NO + NO_2$$

The reactions which link these forms of nitrogen are shown diagrammatically in Figure 1-113.

Figure 1-114 displays the altitude dependence of the conversion rates for these reactions. There are four significant reservoirs for reactive nitrogen: $HONO_2$, HO_2NO_2, $ClONO_2$ and N_2O_5. The proportion tied up in each and in NO_x as a function of altitude is shown in Figure 1-115.

The key points to be extracted from Figure 1-115 are that NO_x and $HONO_2$ constitute the major fraction of all reactive nitrogen throughout the stratosphere with a small but significant fraction present as N_2O_5 between 25 and 35 km. Note, however, that N_2O_5 comprises a maximum of approximately 10% of the reactive nitrogen compounds averaged over 24 hours. This partitioning will be an important part of the following discussion on the comparison between calculated and observed reactive nitrogen.

The conversion rates for reactions which partition NO_x into NO and NO_2 are shown in Figure 1-112. The ratio $[NO]/[NO_2]$ is established to within a few percent by a balance between NO + O_3 converting NO to NO_2, and the direct photolysis of NO_2 reforming NO from the tropopause to 30 km. In the vicinity of 40 km and above, the reaction,

$$NO_2 + O \rightarrow NO + O_2$$

becomes increasingly important such that at the stratopause NO + O_3 is balanced by NO_2 + O, rather than by photolysis.

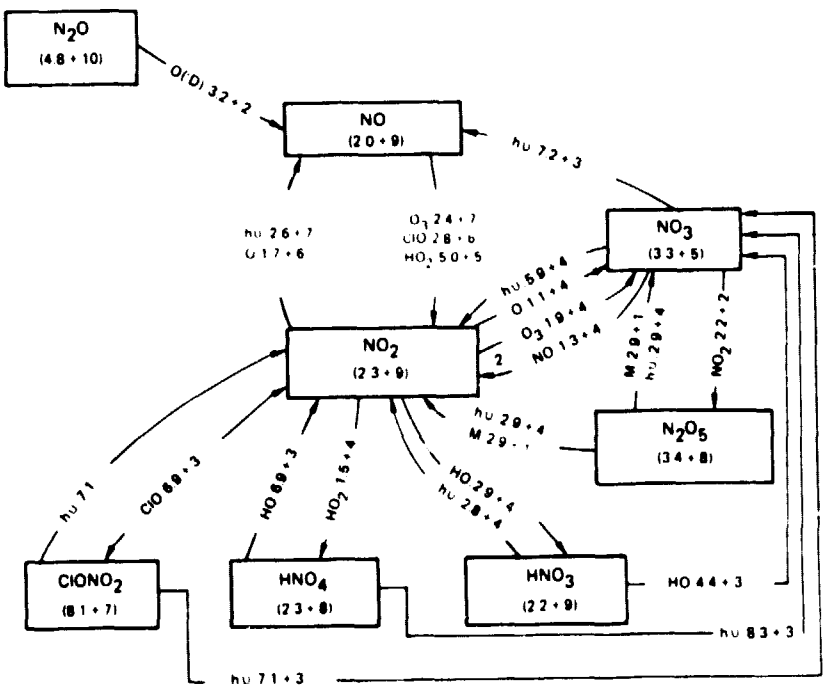

Figure 1-113. Noontime chemical life cycles of NO_x species at 30 km using case 6 chemistry.

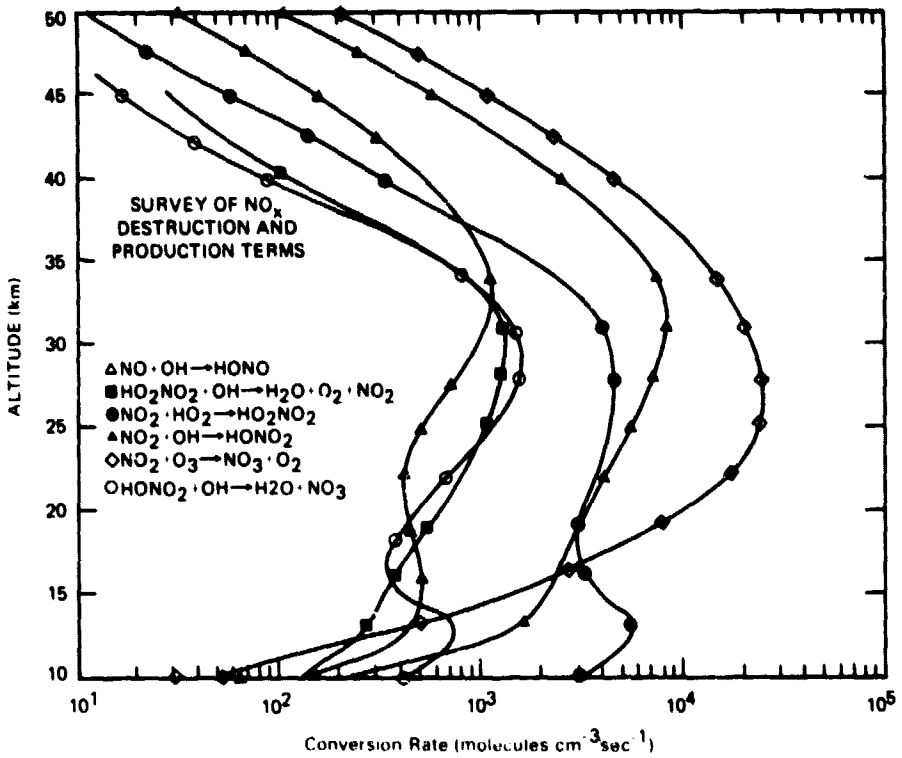

Figure 1-114. Conversion rates between NO_x and temporary reservoirs.

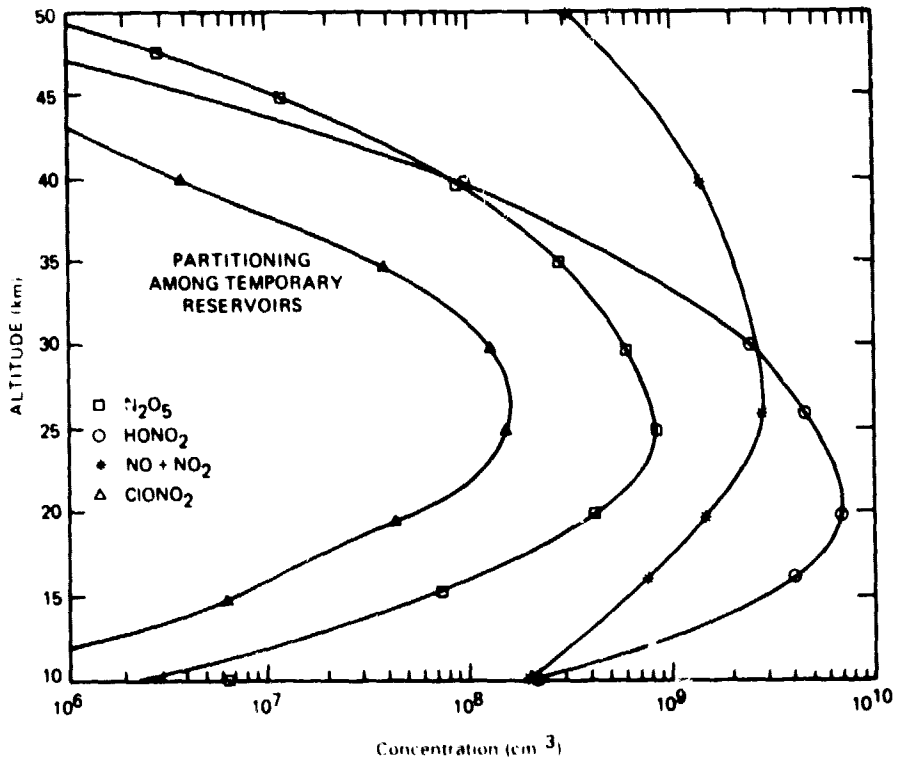

Figure 1-115. Altitude dependence of the partitioning among temporary reservoirs (24 hour average).

In addition, in today's atmosphere, the reaction $NO + ClO \rightarrow NO_2 + Cl$ constitutes 10% of the NO NO_2 conversion in the 35 to 30 km region - a cross linking between NO_x and ClO_x, which is not insignificant for some questions.

The $[NO]/[NO_2]$ ratio depends dramatically on the solar flux such that following sunset NO is rapidly converted to NO_2, thus while the ratio of NO to NO_2 is close to one at noon, the 24 hour mean shifts significantly toward NO_2.

Dependence of Nitrogen Partitioning on Rate Constant Assumptions

As NO_2 is the rate limiting radical in the nitrogen catalytic cycle, the discussion will concentrate on this molecule. Figure 1-116 summarizes the model calculations of the altitude dependence of $[NO_2]$ throughout the stratosphere. Above 35 km the differences between individual cases are insignificant, but below 30 km there is a major divergence such that at 20 km there is a factor of three disparity in calculated $[NO_2]$. The behavior of NO_2 for each of the reaction rate cases can be understood by considering the altitude dependence of the processes that (1) partition NO_x and the sum of all reactive nitrogen, and (2) partition NO and NO_2.

The displacement between case 1 and case 2 represents slight differences in the rate constants for the reactions:

$$NO_2 + HO_2 \xrightarrow{M} HO_2NO_2$$

$$NO_2 + O_3 \rightarrow NO_3 + O_2$$

and

$$NO_2 + HO \rightarrow HONO_2$$

which shift the partitioning between NO_x and reactive nitrogen as a whole.

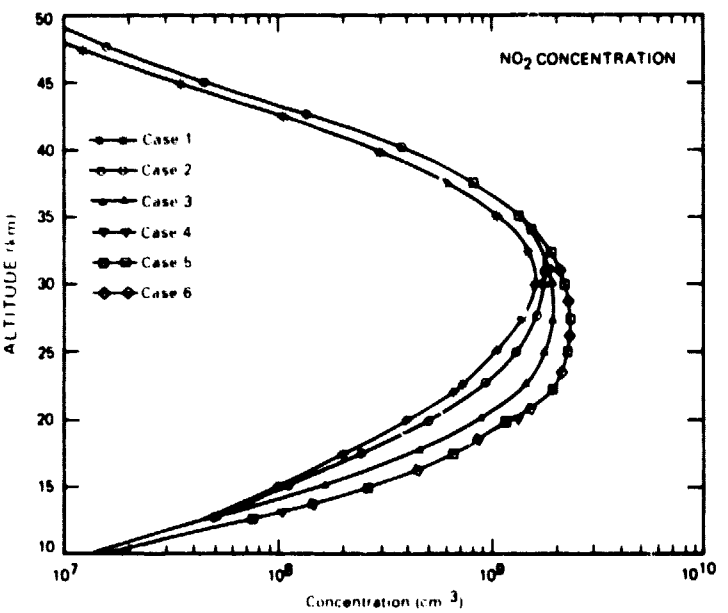

Figure 1-116. Altitude dependence of $[HO_2]$ for each of the six chemical cases.

The strong divergence between cases 2, 3 and the grouping 4-5-6 simply represents the shift from $HONO_2$ to NO_x as a result of correspondingly lower [HO] for cases 2, 3 and 4-5-6 below 30 km. The concentration of NO_2 does not respond to changes in the HO + HO_2 rate constant (represented by case 4 vs. case 5) because in the altitude interval where that reaction affects the partitioning between HO_x and H_2O only a small fraction of the sum NO + NO_2 + $HONO_2$ is tied up as $HONO_2$.

Comparison Between Calculated and Observed [NO_2]

The absence of height resolved NO_2 data for noontime conditions is a serious shortcoming for a detailed quantitative comparison. Most of the NO_2 data correspond to sunrise or sunset conditions, and were measured remotely. There is first the question of asymmetry between sunrise and sunset resulting from N_2O_5 photolysis and second the uncertainty associated with sunrise/sunset conversion of NO to NO_2.

Qualitatively the observed sunrise/sunset ratio of NO_2 follows that expected from theory, i.e., sunset concentrations are decidedly larger than those at sunrise, resulting, it is believed, from the conversion of N_2O_5 to NO_x. Table 1-28 compares the observed and calculated sunrise/sunset ratios as a function of altitude for the reaction rate set of case 6. The only concerted sunrise/sunset study was carried out at 50°N. It is now clear that low latitude studies should be carried out since there is little seasonal variation of NO_2 below 30° latitude.

The concentration of NO_2 does not change rapidly with solar zenith angle until within 5° either side of sunset. The ratio of midday to post sunset (e.g., solar zenith angle of 95°) is extremely altitude dependent.

The available [NO_2] sunset data are summarized in Figure 1-117. Each point between 20 and 36 km is corrected by a factor of 1.5 to compare those data with the theoretical calculations using the six cases of reaction rate data.

Table 1-28
Observed and Calculated Sunrise/Sunset Ratios of NO_2 as a Function of Altitude

Altitude	Observed Sunrise/Sunset Ratio	Calculated Sunrise/Sunset Ratio
50		
45		0.6
40		0.6
35	0.5	0.5
30	0.5	0.5
25	0.5	0.5
20	0.5	0.5
15	0.7	
10	0.7	

The following conclusions can be drawn from an analysis of Figure 1-117:

- Given the cited uncertainties of the observations, there exists reasonable consistency among the techniques.
- The observations fall below the calculations for cases 4, 5, and 6.

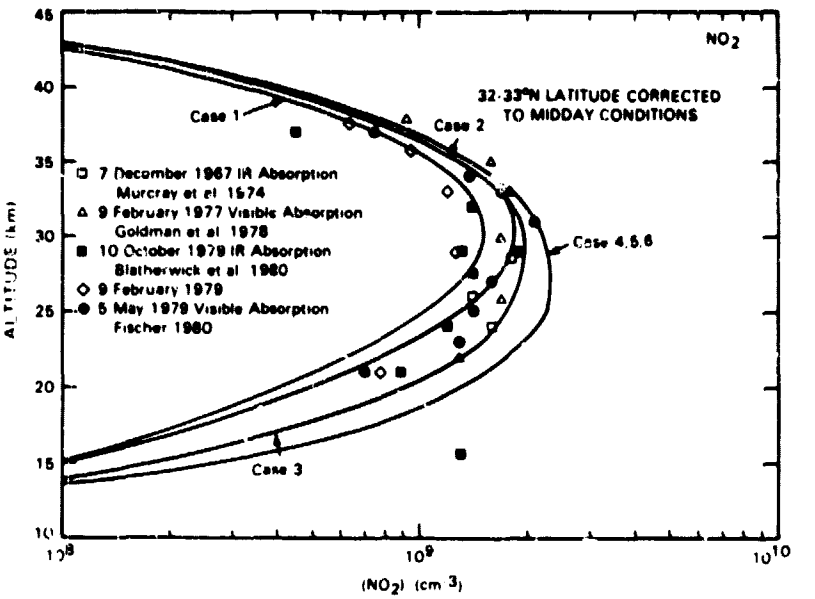

Figure 1-117. Comparison between calculated and observed $[NO_2]$.

Comparison Between Calculated and Observed [NO]

Figure 1-118 displays the internally consistent data set reported by Ridley and coworkers (Roy et al., 1980; Ridley and Schiff, 1981; and Ridley and Hastie, 1981) and calculations using the six sets of reaction rate data. The measurements were obtained in situ under conditions corresponding to midday and can thus be compared directly with the model distributions. Before such measurements can be used to test models, it will be necessary to develop methods which can simultaneously measure NO_2, NO, $HONO_2$ and HO to ±10% in the same volume of space. In short, although the observations clearly demonstrate the existence and concentrations to within a factor of three of NO in the stratosphere, they cannot be used to select among the six chemistry cases used in this report.

Comparison Between Calculated and Observed $[HONO_2]$

A comparison between the measurements obtained at mid-latitude, and the model calculations for the six cases of reaction rate data are given in Figure 1-119. Above 30 km, there is a divergence between the trend in the observations with increasing altitude and all of the cases represented. In the current understanding of the stratosphere, the $HONO_2$ concentration is determined by exchange with the reactive nitrogen system dictated by the formation reaction,

$$NO_2 + HO \rightarrow HONO_2$$

and the destruction by the photolytic decomposition step, $HONO_2 + h\nu \rightarrow HO + NO_2$

The photolysis cross section in the wavelength interval of importance above 30 km is well characterized and data exist for both [NO_2] and [HO]. Thus the divergence above 30 km could imply that there exists a mechanism which enhances the removal rate of $HONO_2$ which is not included in the current models. However the recent observation of larger ultraviolet fluxes at this altitude than predicted (Frederick and Mentall 1981) could resolve this discrepancy. The consistency in the data base below 20 km is poor. At 15 km, the observations encompass a range of 100 in mixing ratio, and it is impossible to draw any conclusion from the overlap in the range of calculated cases (all of which converge in the lower stratosphere).

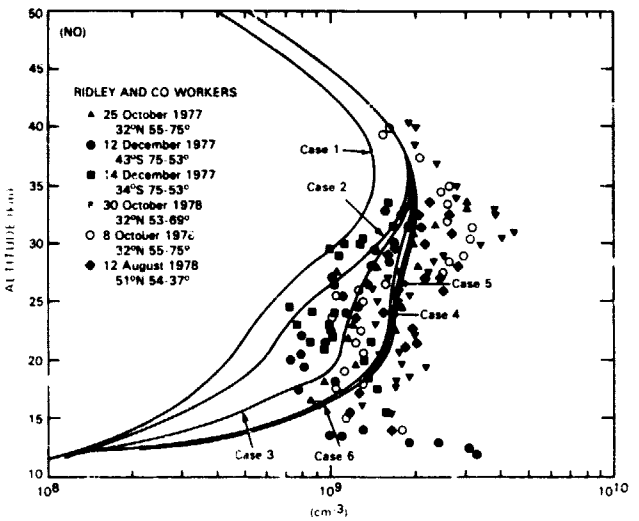

Figure 1-118. Comparison between calculated NO and measurements of Roy et al. (1981), Ridley and Schiff (1981), and Ridley and Hastie (1981).

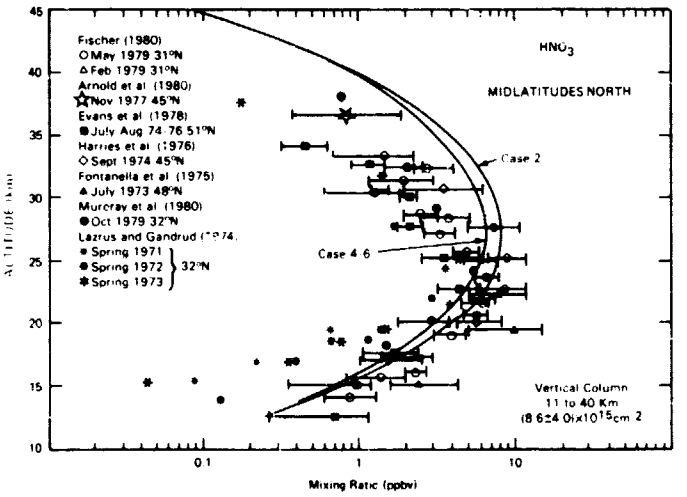

Figure 1-119. Comparison of in situ and remote measurements of the HNO_3 mixing ratio at northern mid-latitudes with 1-D calculations.

THE REACTIVE TRACE CHLORINE SPECIES

Catalytic Cycles Affecting Odd Oxygen

There are three major catalytic cycles involving chlorine

Cycle 1

$$Cl + O_3 \rightarrow ClO + O_2$$
$$ClO + O \rightarrow Cl + O_2$$
$$\text{Net} \quad O + O_3 \rightarrow 2O_2$$

Cycle 2

$$Cl + O_3 \rightarrow ClO + O_2$$
$$ClO + HO_2 \rightarrow HOCl + O_2$$
$$HO + O_3 \rightarrow HO_2 + O_2$$
$$HOCl + h\nu \rightarrow HO + Cl$$
$$\text{Net} \quad O_3 + O_3 \rightarrow 3O_2$$

Cycle 3

$$Cl + O_3 \rightarrow ClO + O_2$$
$$ClO + NO_2 \rightarrow ClONO_2$$
$$NO + O_3 \rightarrow NO_2 + O_2$$
$$ClONO_2 + h\nu \rightarrow Cl + NO_3$$
$$NO_3 + h\nu \rightarrow NO + O_2$$
$$\text{Net} \quad O_3 + O_3 \rightarrow 3O_2$$

Figure 1-120 presents a plot of the conversion rates for the reactions in these three cycles using case 6 reaction rates. At altitudes above 25 km, cycle 1 is dominant, with a contribution from cycle 2 approaching 25% at 25 km altitude diminishing to <1 % at 40 km. Between 15 and 25 km, the three cycles are competitive. However, at these altitudes odd oxygen destruction is dominated by catalytic cycles which do not invoke chlorine. Thus, for the restricted purpose of determining ozone destruction rates, a determination of which cycle dominates is academic.

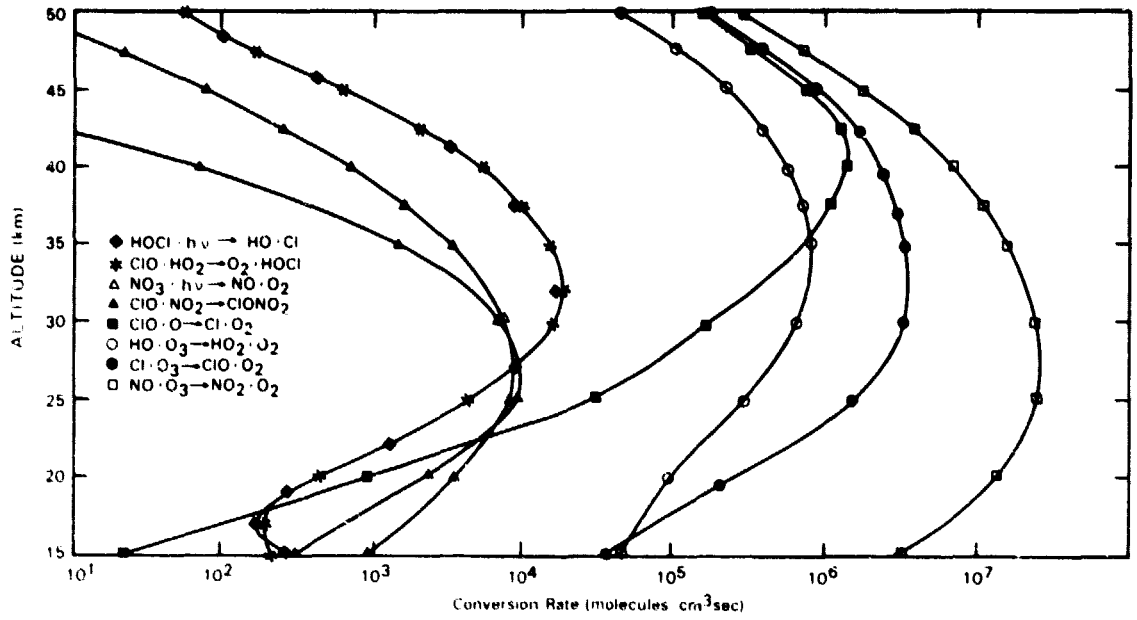

Figure 1-120. Conversion rates for the Cl_x catalytic cycles.

Given that the production rate of NO_3 is not controlled by the photolysis rate of chlorine nitrate there is only one member of the chlorine family involved in a rate limiting odd oxygen step, namely ClO.

Partitioning of Chlorine into the Rate Limiting Radical ClO

HCl is believed to be the major inorganic chlorine compound in the stratosphere. There are six major reactions involved in the partitioning of HCl into ClO, three of which exchange Cl with HCl, the magnitude of which are indicated in Figure 1-121 as a function of altitude, and three of which exchange Cl and ClO as indicated in Figure 1-122. The functional distinction between the reactions in Figures 1-121 and 1-122 is that those in the former control the ratio of $[ClO_x]$ to [HCl] (and thus to the concentration of total chlorine), while those in the latter control the ratio of [ClO] to [Cl]. It should be noted that the ratio of [ClO] to total chlorine concentration depends sensitively on the HO concentration below 40 km (above 50 km, only on the ratio of [HO] to $[HO_2]$) and the ratio of [ClO] to [Cl] depends upon [NO] below 30 km.

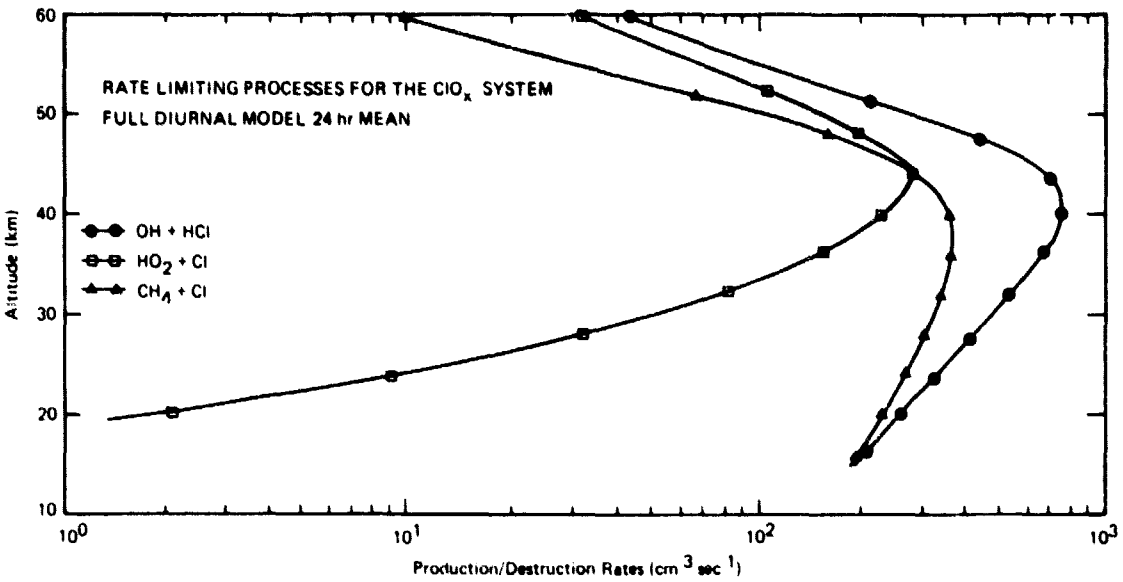

Figure 1-121. Altitude dependence of the conversion rates between Cl and HCl.

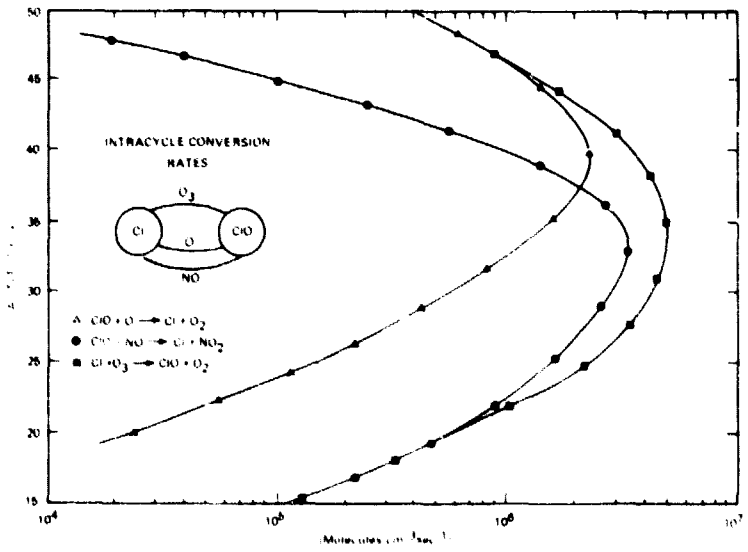

Figure 1-122. Altitude dependence of the interconversion rates between Cl and ClO.

Dependence of Chlorine Partitioning on Rate Constant Assumptions

Figure 1-123 shows the dependence of the calculated ClO concentration on the rate constant set assumed. In the altitude interval between 40 to 50 km, the ClO concentration is virtually independent of the rate constant sets used. Partitioning between ClO and HCl is controlled by the reaction set,

$$HCl + HO \rightarrow H_2O + Cl \quad .....1 \ (k_1)$$

$$Cl + CH_4 \rightarrow HCl + CH_3 \quad .....2 \ (k_2)$$

$$Cl + HO_2 \rightarrow HCl + O_2 \quad .....3 \ (k_3)$$

$$Cl + O_3 \rightarrow ClO + O_2 \quad .....4 \ (k_4)$$

$$ClO + NO \rightarrow Cl + NO_2 \quad .....5 \ (k_5)$$

$$ClO + O \rightarrow Cl + O_2 \quad .....6 \ (k_6)$$

The relationship between the concentrations of ClO and HCl can be expressed as follows:

$$\frac{[ClO]}{[HCl]} = \frac{[Cl]}{[HCl]} \cdot \frac{[ClO]}{[Cl]} = \frac{k_1[OH]}{k_2[CH_4] + k_3[HO_2]} \cdot \frac{k_4[O_3]}{k_5[NO] + k_6[O]}$$

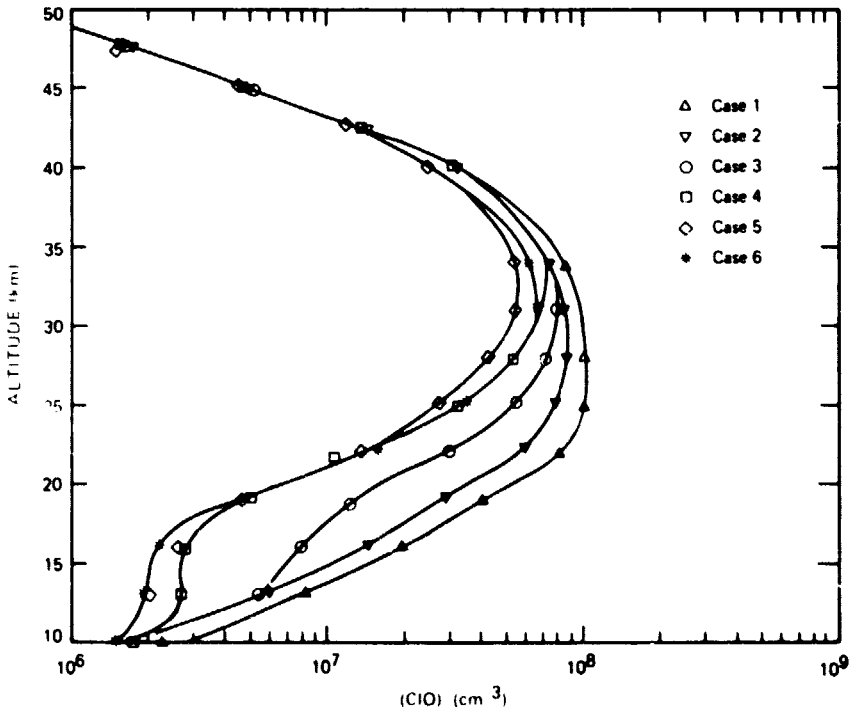

Figure 1-123. Calculated vertical profiles of ClO for each of the six chemical cases.

At and above 40 km, however, $k_6[O] >> k_5[NO]$, and in addition, $k_3[HO_2]$ becomes comparable to or larger than $k_2[CH_4]$. Thus, the expression becomes,

$$\frac{[ClO]}{[HCl]} = \frac{k_1[OH]}{k_3[HO_2]\left[1+\frac{k_2[CH_4]}{k_3[HO_2]}\right]} \cdot \frac{k_4[O_3]}{k_6[O]}$$

Because both $[O_3]/[O]$ and $[HO]/[HO_2]$ are independent of the six rate constant sets (reactions of HO with $HONO_2$, HO_2NO_2, and HO_2 only affect the sum $[HO] + [HO_2]$, not the ratio), there is a weak dependence of [ClO] on [HO] above 40 km. The hydroxyl concentration is in turn only a weak function of the rate for $HO + HO_2 \rightarrow H_2O + O_2$. The result is that partitioning of chlorine into the rate limiting form, ClO, is almost independent of the rate constant set above 40 km.

In the altitude interval 30 to 40 km, the ClO concentration becomes increasingly sensitive to the concentration of [HO] both because methane dominates the conversion of Cl to HCl and because HO_2 no longer buffers the chlorine partitioning against changes in the HO_x ($HO + HO_2$) concentration. In addition, reaction 5 dominates in the conversion of ClO to Cl below 35 km. Thus, the general expression becomes

$$\frac{[ClO]}{[HCl]} = \frac{k_1[HO]}{k_2[CH_4]} \cdot \frac{k_4[O_3]}{k_5[NO]}$$

Above 30 km, the NO concentration is independent of HO_x because NO and NO_2 dominate the reactive forms of nitrogen, so only those reactions controlling the ratio of NO to NO_2 are relevant.

In the altitude interval 30 to 10 km, the ClO concentration has almost a quadratic dependence on [HO] because in addition to the dependence expressed above, [NO] is (approximately) inversely proportional to [HO]. The key point is that [ClO] is an extremely sensitive function of [HO] below 30 km, and unfortunately this is precisely the altitude interval for which no observations of [HO] exist.

The dependence of [ClO] on assumptions regarding the formation rate for chlorine nitrate, represented by the difference between case 5 and 6 is shown in Figure 1-124. The effect of assuming a factor of three reduction in the $ClONO_2$ formation rate (and the corollary assumption that the isomer(s) formed in other channels photolyze rapidly following sunrise) is most prevalent in the altitude interval 25 to 35 km; [ClO] is increased by 30% when a slow $ClONO_2$ formation is assumed, all other factors held equal.

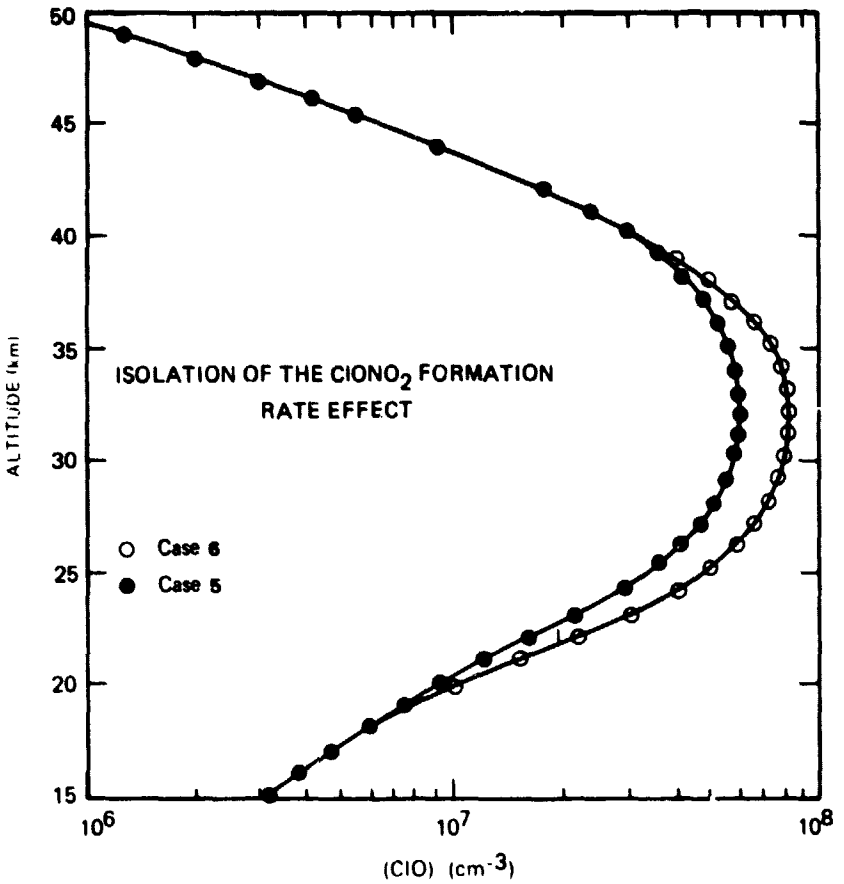

Figure 1-124. Calculated [ClO] for the fast and slow $ClONO_2$ formation cases.

Comparison Between Calculated and Observed [ClO]

Figure 1-125 gives a comparison between the experimental data obtained at mid-latitudes and calculations for reaction rate sets used in cases 1 to 5. At the upper altitude extreme of the observations, there appears to be a strong divergence; the calculated distributions (all of which converge for the reasons cited in the preceding section) decreases rapidly with height above 37 km, while the observations show no evidence for such a decrease. This general behavior of the in situ observations is substantiated by the ground based mm-wave emission data which strongly imply, via the emission line width, that there is significantly more ClO in the vicinity of 50 km than that calculated by current models.

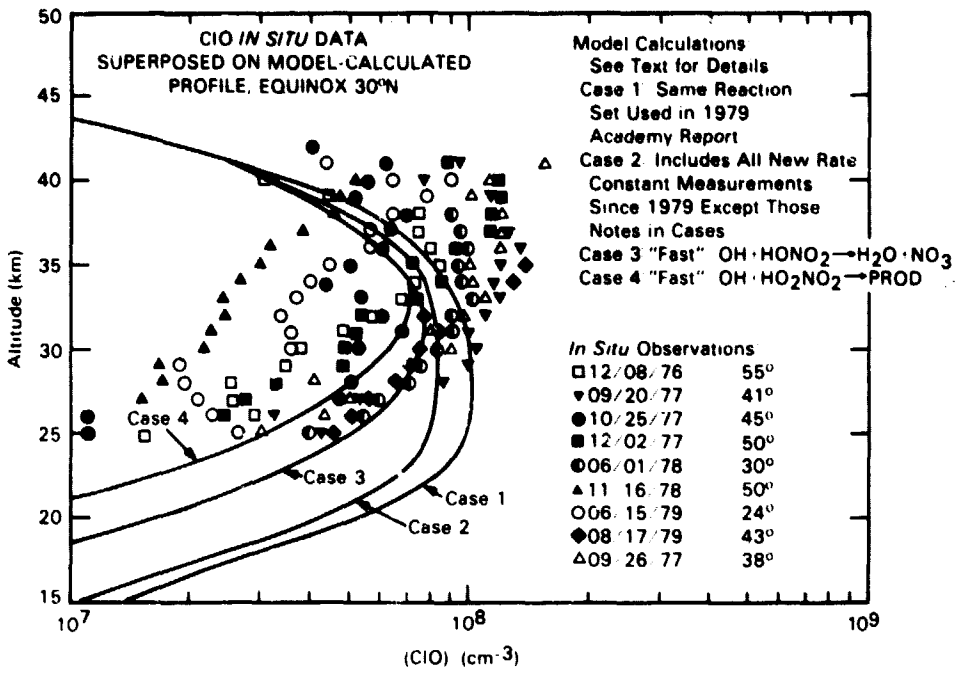

Figure 1-125. Comparison between observed and calculated [ClO]

The model which assumes the maximum rate of HO_x recombination to H_2O, case 5, exhibits the best agreement with the observed distribution of [ClO]. Below 30 km, however, the observations lie decidedly below the predicted ClO concentration. Inclusion of the fast rates for

$$HO + HO_2 \rightarrow H_2O + O_2$$

$$HO + HONO_2 \rightarrow H_2O + NO_3$$

and

$$HO + HO_2NO_2 \rightarrow H_2O + NO_2 + O_2$$

significantly improve the agreement between the calculated and observed distributions (compare, for example, case 1 and case 5). Both the in situ resonance fluorescence data and the balloon-borne mm-wave emission data suggest that less ClO exists in the stratosphere below 30 km than is predicted by the models.

The result of changing the rate data for chlorine nitrate formation is shown in Figure 1-126, where the ClO concentration is plotted for cases 5 and 6. A better agreement between calculated and measured profiles is achieved in the middle and lower stratosphere for the case of "fast" chlorine nitrate formation, but in the critical region above 33 km, where the modeled distribution decreases much more rapidly with altitude than the observations, "slow" $ClONO_2$ formation improves the correlation (though clearly the mechanism of chlorine nitrate formation is not the solution to the top side divergence). Figure 1-126 also serves to point out that the choice of chlorine nitrate formation rates does not rectify the more rapid decrease in [ClO] below 30 km. Nevertheless, the question of the products formed in the reaction of ClO and NO_2 remains serious both from the point of view of understanding the photochemistry of the chlorine/nitrogen system, and for the restricted question of ozone depletion.

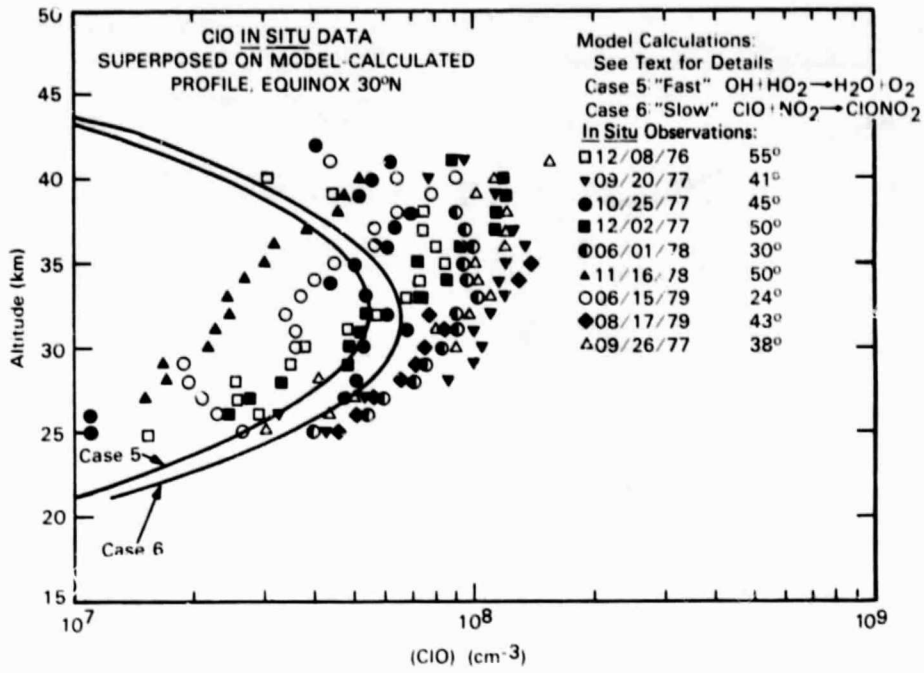

Figure 1-126. Comparison of observed [ClO] with the fast and slow $ClONO_2$ formation calculations (cases 5 and 6).

The altitude interval 50 to 35 km exhibits the largest difference between observed and calculated ClO distributions. In this altitude interval, the measurements indicate that the chlorine budget is dominated by HCl and ClO. Figure 1-127 compares, for case 6, the observed, mean, mid-latitude profiles, and the calculated profiles for HCl and ClO. An implication of Figure 1-127 is that either the HO concentration at 35 km and above is significantly greater than that used in the model, or there is a mechanism absent from the model which converts HCl to ClO_x.

In the altitude interval 35 to 25 km there exists the closest agreement between calculated and observed [ClO], although differences between the mean of the observations and the minimum modeled distribution (case 5) approaches a factor of two at 25 km. There are important consequences of the fact that less ClO is observed at altitudes below 30 km than is calculated. First, the most difficult region of the stratosphere to model with quantitative accuracy is the lower stratosphere. The characteristic times for chemical production/destruction are of the same magnitude as the transport times and thus details of the physical transport become critical to the quantitative conclusions. The minimization of chlorine induced ozone destruction below 30 km shifts the emphasis to purely chemical questions, thus solidifying and simplifying the conclusions. Second, the low ClO_x (Cl + ClO) concentration reduces the chemical coupling with other systems. For example, changes in [ClO], given the observed levels, have a negligible effect on the nitrogen system through the reaction $ClO + NO_2 \xrightarrow{M} ClONO_2$ because insufficient $ClONO_2$ is formed to constitute a significant portion of the NO_x budget.

In the altitude interval 25 to 10 km there is clearly a need to extend the experimental methods applied at higher altitudes. The recently observed upper limit of 10 ppt reported by Waters et al. (1981) at 23 km and the results from numerous in situ resonance fluorescence experiments, substantiate the general conclusion that ClO concentrations, at least down to 20 km, fall below predicted levels.

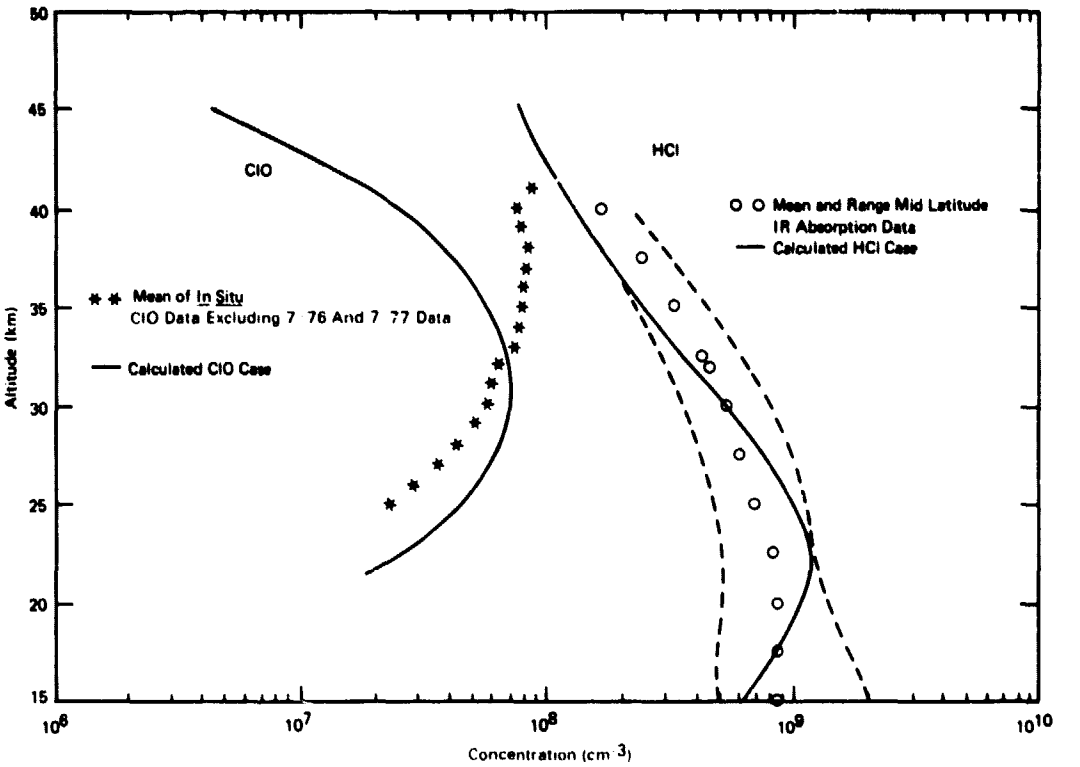

Figure 1-127. Comparison of the mean observed [ClO] and [HCl] profiles with calculated profiles using case 6 chemistry.

In this altitude regime, it is important to consider the effect of the choice of rate constants on the HCl concentration and the $ClONO_2$ and HOCl concentrations. The disagreement between observed and calculated [HCl] which peaks between 20 and 25 km is, in large measure, eliminated by the selection of the "fast" rate constant for $ClONO_2$ formation, i.e., case 5. At altitudes between 25 and 30 km, however, inclusion of the fast $ClONO_2$ formation rate significantly worsens the correlation between the mean of the [HCl] data and the calculated distribution.

COMPARISON OF MEASUREMENTS AND 2-D MODEL CALCULATIONS FOR TRACE REACTIVE SPECIES

ODD OXYGEN SPECIES (O_x)

The odd oxygen species [O_3, $O(^3P)$, and $O(^1D)$] are in photochemical equilibrium with each other throughout the stratosphere. Thus the latitudinal and seasonal variations of $O(^3P)$ and $O(^1D)$ can be inferred from the calculated ozone distribution, and a discussion of ozone alone captures the features of the 2-D model calculations.

Ozone

For most species the observational data base for testing models of stratospheric chemistry is sufficient only to determine whether the models produce observed concentrations within a

factor of approximately two and whether observed tendencies as a function of altitude can be simulated. For ozone, on the other hand, the data base is sufficiently large that more sophisticated tests of the models can be made. Because predictions of long term changes in ozone are based upon results from one- and two-dimensional models, it is essential that the ability of these models to simulate observed ozone variations on the longest possible time scales be assessed. The largest and most well-established variation of ozone occurs on a seasonal time scale. It is natural therefore that two-dimensional models should be designed to emphasize seasonal variations and that an important test of such models is their ability to simulate seasonal variations of ozone (and other long-lived species). This will be the focus of the ozone comparisons of this section.

The most temporally extensive part of the ozone data base is the historical record of columnar ozone from the Dobson station network. The seasonal and latitudinal variability of columnar ozone based on these observations is shown in Figure 1-128 (from Dütsch, 1971). Although data coverage from this network is not truly global because observations have been predominantly made at mid-latitudes of the Northern Hemisphere, the first 2 years of BUV satellite data analyzed by Hilsenrath et al. (1979) suggest that the principal features of Figure 1-128 are realistic. Figure 1-129 contains a comparison of the two-dimensional model calculation of C. Miller et al. (1981) with the observations. This model exhibits a qualitatively excellent agreement with the observed seasonal and latitudinal variation of columnar ozone in the Northern Hemisphere.

There is a general tendency for two-dimensional models to yield smaller diurnal and seasonal variations in columnar ozone than those observed. At 60°N, for example, the observations indicate an annual maximum 100 Dobson units larger than the minimum, while the modeled variation is only ~50 Dobson units. Similar results are obtained with other 2-D (Whitten, et al., 1977) and 3-D (Cunnold et al., 1980) simulations. The degree of agreement with the observations of Figure 1-128 depend primarily on the parameters used to describe horizontal and vertical transport. Since these have been obtained in an ad hoc manner from available meteorological and composition data, agreement in Figures 1-128 and 1-129 (and Figures 1-130 and 1-131) indicate that the transport parameterization, which lacks a strong physical basis, is capable of being adjusted within reasonable limits to give adequate agreement with the observed distribution of ozone (and other trace species).

Simulation of Northern Hemisphere-Southern Hemisphere ozone differences has been attempted in only a few two-dimensional models (e.g., Ko et al., 1981; Pyle, 1980). It seems inappropriate to test the capability of two-dimensional models to simulate interhemispheric differences, since, at this time, differences between the various two-dimensional models in simulating Northern Hemisphere ozone variations are substantially larger than the observed interhemispheric differences.

The data base for two-dimensional model parameterizations depend primarily on Northern Hemispheric input data, since the observational data (potential temperature, wind fields, etc.) are more readily available there. Most 2-D models use a data base that is essentially symmetric north/south, with a 6-month phase lag. Thus it is most appropriate to consider the current 2-D models as "Northern Hemisphere" models, rather than global models. Since most observations of short-lived species were obtained in the Northern Hemisphere, adopting this view does not significantly restrict the utility of the models in interpreting the measurements.

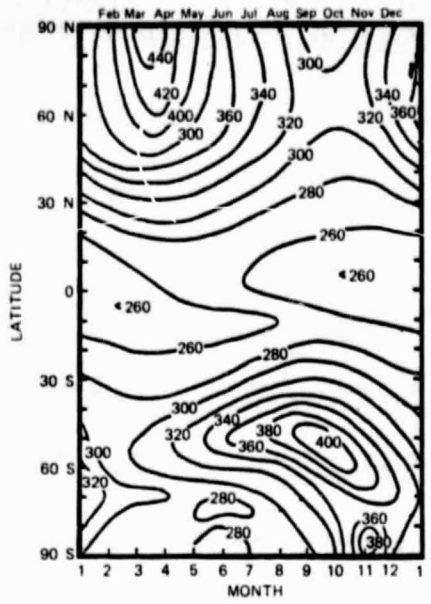

Figure 1-128. The observed behavior of columnar ozone (Dobson units) as a function of latitude and season (from Dütsch, 1971).

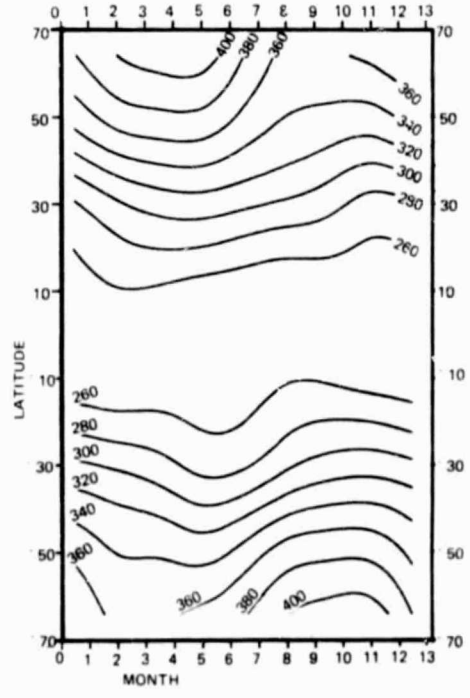

Figure 1-129. Calculated behavior of column ozone (in Dobson units) from the two-dimensional model of C. Miller et al. (1981).

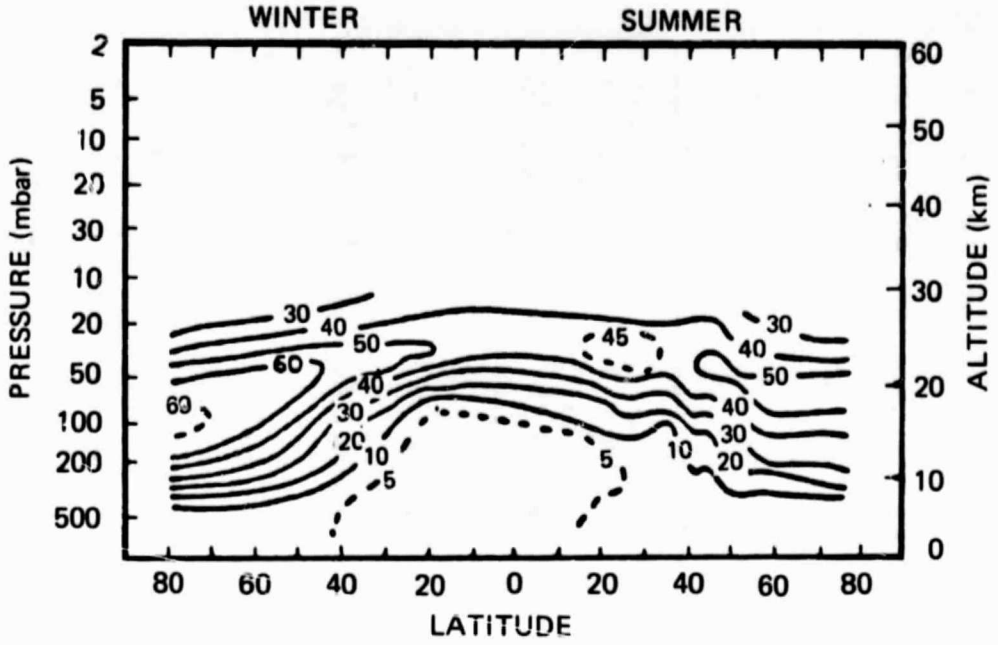

Figure 1-130. The observed distribution of ozone (units 10^{11} mol/cm^3) as a function of latitude and height for Northern Hemisphere summer and winter based on Hering and Borden (1964) and Wu (1973).

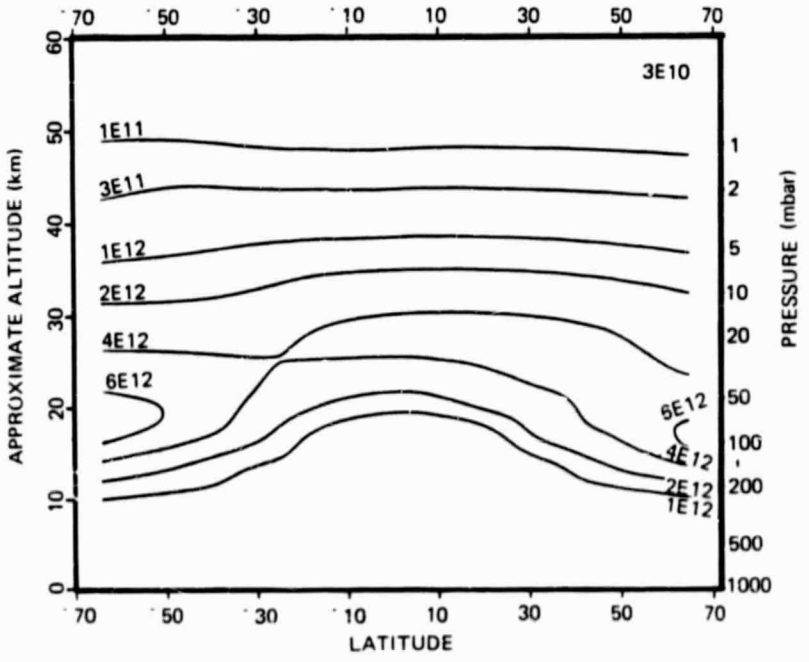

Figure 1-131. The calculated ozone distribution of July 15 (mol/cm^3) from the two-dimensional model of C. Miller et al. (1981).

The variation of ozone with altitude in the lower stratosphere has been well-characterized by ozonesonde observations. Figure 1-130 shows the seasonally-averaged distributions obtained by Hering and Borden (1964). The vertical structure calculated by the two-dimensional model of C. Miller et al. (1981) is shown in Figure 1-131. The largest seasonal changes of ozone occur between 100 and 33 mbar and are associated with ozone transport. Again the degree of agreement with the observations is excellent for this particular model. The only noticeable disagreement occurs at approximately tropopause heights where the model underestimates the ozone. This model deficiency is not expected to have serious consequences since it occurs at heights substantially below where chlorine affects ozone.

Figures 1-132 and 1-133 show a comparison of the two-dimensional model calculations by Sze et al. (1981) with a supposedly typical observed distribution between 1 and 10 mbar. OGO observations (London et al., 1977), SAGE observations (McCormick, personal communication, 1980), and rocket and Umkehr observations indicate that the principal features seen in the observation shown in Figures 1-132 and 1-133 are realistic, and that the calculated distribution is not significantly different. It is however possible that this model (and that of C. Miller et al., 1981) may overpredict the latitudinal gradient between 5 and 10 mbar in winter perhaps indicating that temporary reservoir of NO_x may not yet have been fully accounted for.

In order to assess the relative roles of transport and chemistry in the two-dimensional models, it is helpful to compare the phase of the seasonal cycle at various altitudes with that observed over Arosa (Dütsch, 1974) (See Figure 1-134). In both the observations and the two-dimensional model results, below 40 mbar ozone possesses a spring maximum associated with the poleward and downward transport of ozone. Between 5 and 10 mbar on the other hand where ozone appears to be under chemical control (e.g., Cunnold et al., 1980) the ozone maximum occurs in summer. The relative roles of transport and chemistry in the zonal-mean budget suggested by Figures 1-134 and 1-135 are approximately consistent with those calculated in the three-dimensional photochemical dynamical model of Cunnold et al. (1980).

A potentially important test of multi-dimensional models which should be applied shortly, consists of superposing (almost) simultaneous global observations of ozone and temperature in the middle and upper stratosphere. The observed covariances should provide an important test of the chemistry and of the relative importance of transport in this region. Where ozone is controlled by chemistry, the temperature-dependent chemical loss processes produce a negative correlation between ozone and temperature, while in those regions where transport dominates a positive correlation has not only been observed (see, for example, Gille et al., 1980b) but has been simulated in models (see for example, Cunnold et al., 1980). Furthermore, between 1 and 110 mbar, ozone destruction is believed to contain contributions from odd hydrogen, odd chlorine, and odd nitrogen species in addition to odd oxygen. Each of these destruction processes is associated with a different temperature-dependent loss rate which suggests that the ozone temperature covariance should help to elucidate the relative roles of radical families in ozone destruction. Barnett et al. (1975a) were the first to use this approach and suggested a temperature coefficient consistent with a combined HO_x Chapman mechanism chemistry at 50°S at approximately 1 mbar.

ODD HYDROGEN SPECIES (HO_x)

The comparison of observed HO and HO_2 with a 1-D model has been discussed previously. The 1-D and 2-D calculated vertical profiles of HO and HO_2, appropriate for mid-latitude conditions (30°N) are very similar. Since latitudinal and seasonal data for HO_x are lacking, validation of 2-D model results are not yet possible. Nevertheless, it is instructive to show the meridional cross sections of HO, HO_2 and H_2O_2 (Figures 1-136, 137 and 138) calculated by the AER 2-D model. The species that shows the largest variation with latitude is H_2O_2 and the least is HO.

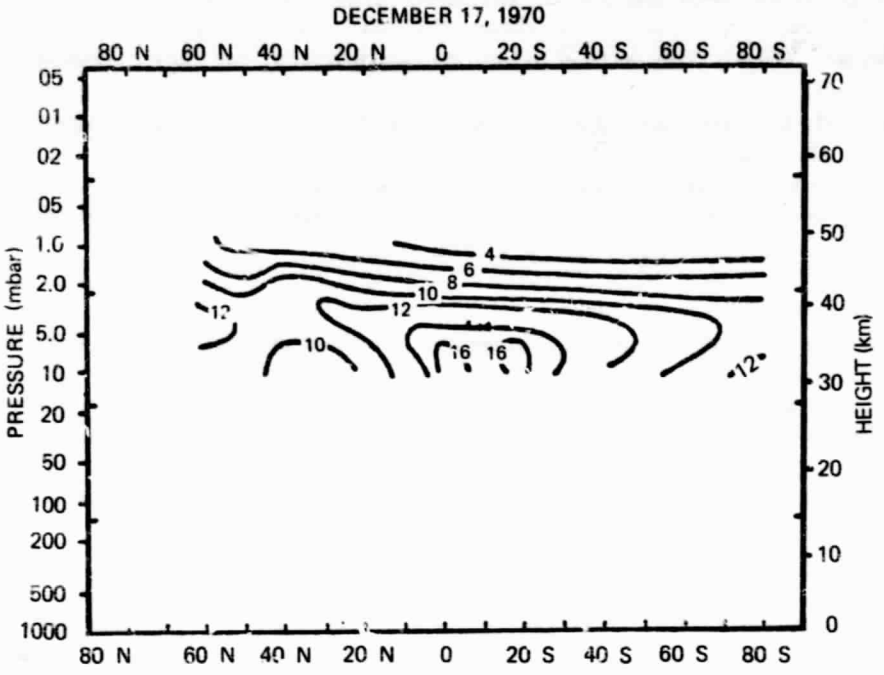

Figure 1-132. Observed ozone mixing ratios (µgm/gm) BUV observations by Krueger et al. (1973) for 17 December 1970 (supposedly typical of the ozone distribution during the solsticial seasons).

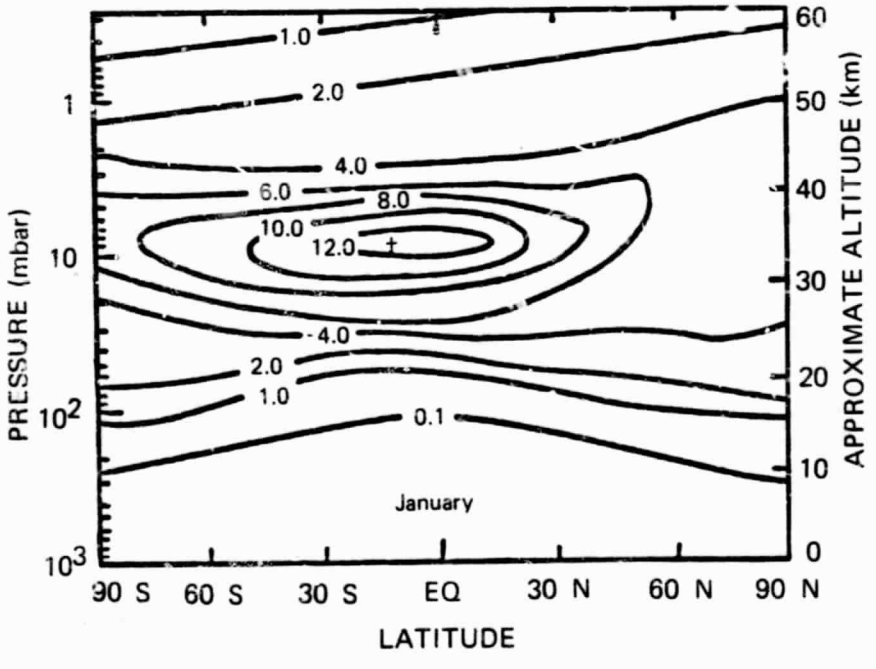

Figure 1-133. Calculated ozone mixing ratios (ppmv) for January from the two-dimensional model of Ko et al. (1981).

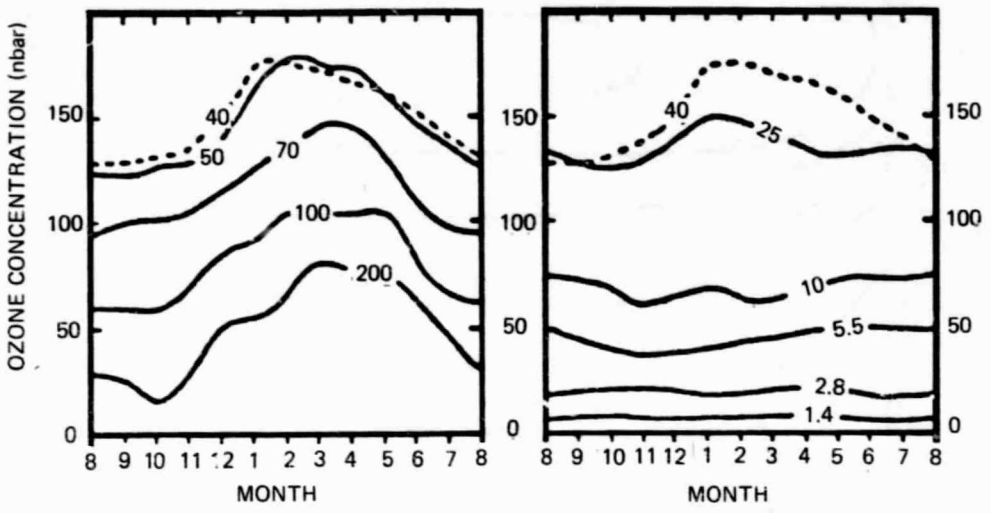

Figure 1-134. Monthly variations in ozone concentration in nanobars at various pressue levels (mbar) from observations at Arosa, Switzerland, 47°N (Dütsch, 1974).

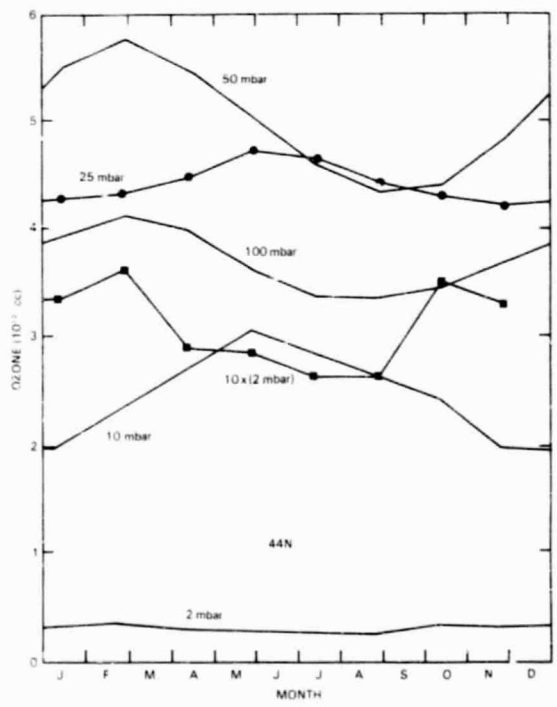

Figure 1-135. Monthly variations in ozone concentration at various pressure levels as calculated by C. Miller et al. (1981).

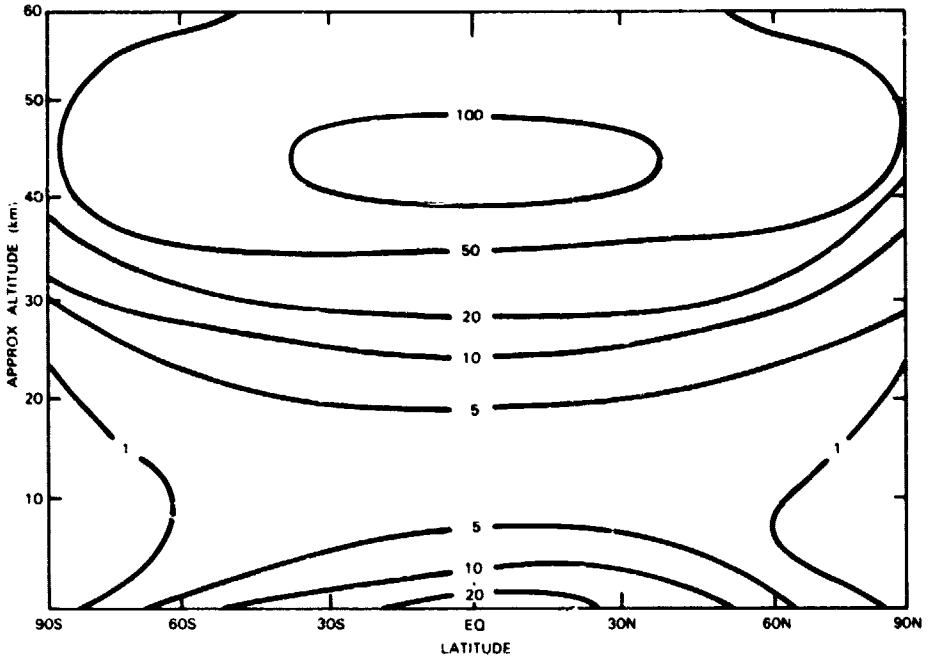

Figure 1-136. Calculated meridional cross section of HO (Ko et al., 1981).

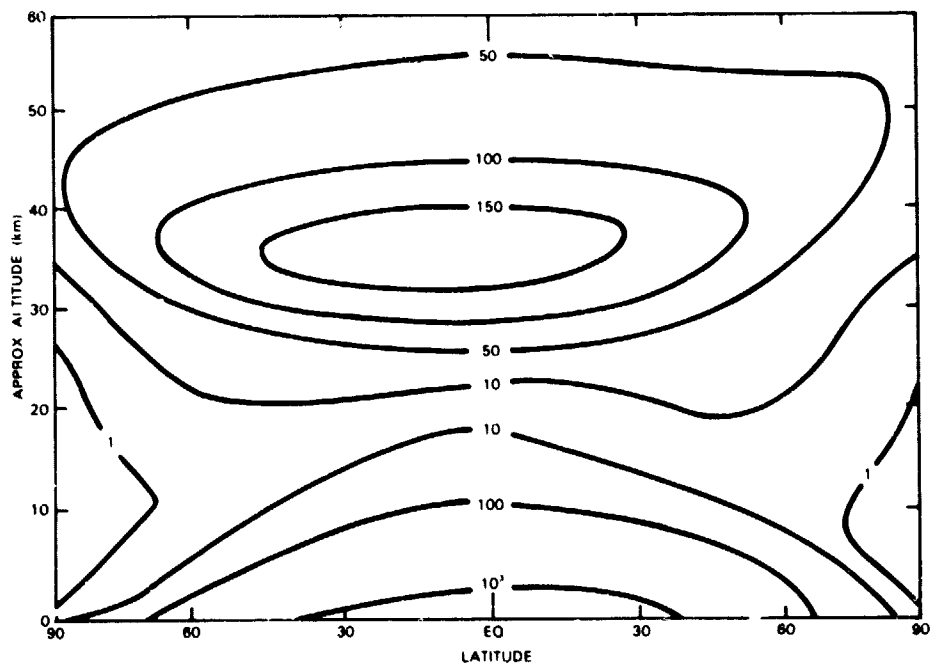

Figure 1-137. Calculated meridional cross section of HO_2 (Ko et al., 1981).

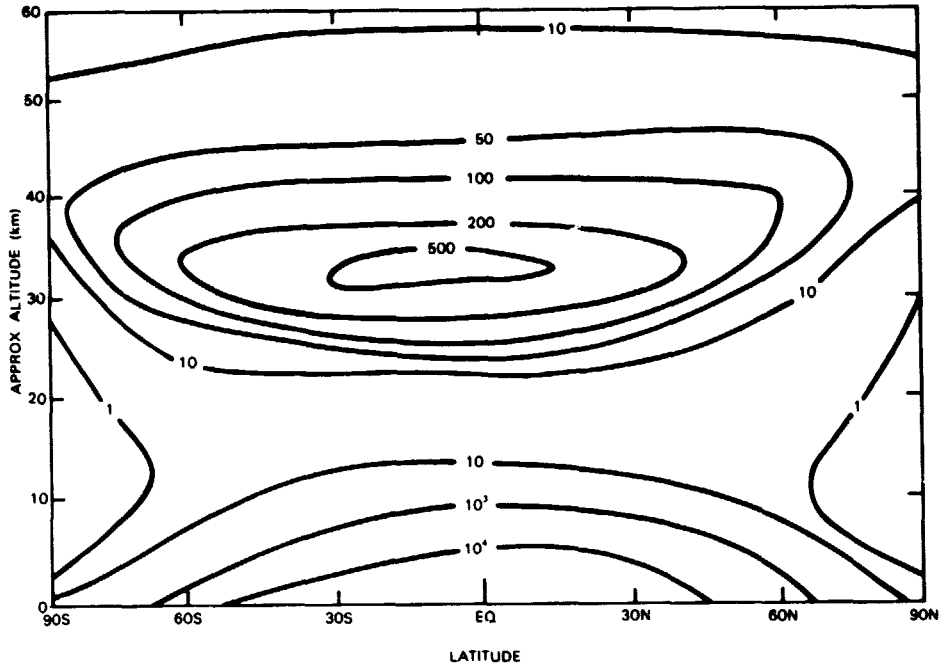

Figure 1-138. Calculated meridional cross section of H_2O_2 (Ko et al., 1981).

ODD NITROGEN SPECIES (NO_x)

Introduction

The section on 1-D modeling in this chapter details the changes in the NO_x species mid-latitude vertical profiles due to the chemical rate set updates since NASA RP 1049. Both the total amount of NO_x and the partitioning of that amount into the various species have changed considerably in the models. These chemistry changes have in general significantly improved the model comparisons with the observational data, particularly for the seasonal and latitudinal variations of the major species (NO, NO_2, and HNO_3), so that today a fairly consistent picture is emerging.

In these discussions, the Du Pont 2-D model calculations give a band corresponding to the seasonal variations of the daytime average mixing ratio for each species. The AER calculations are the approximate noontime values for July.

Nitric Oxide (NO)

Altitude Profile

The measured mid-latitude vertical mixing ratio profile of nitric oxide and the theoretical calculations are shown in Figure 1-139. The measurements are characterized by a range of approximately a factor of four from the tropopause to 30 km, increasing to about a factor of 10 at 50 km. The calculations fall entirely within this broad range of observations throughout the stratosphere. The calculations lie toward the higher end of the measurements above 20 km, with a mixing ratio at 50 km of about 20 ppb.

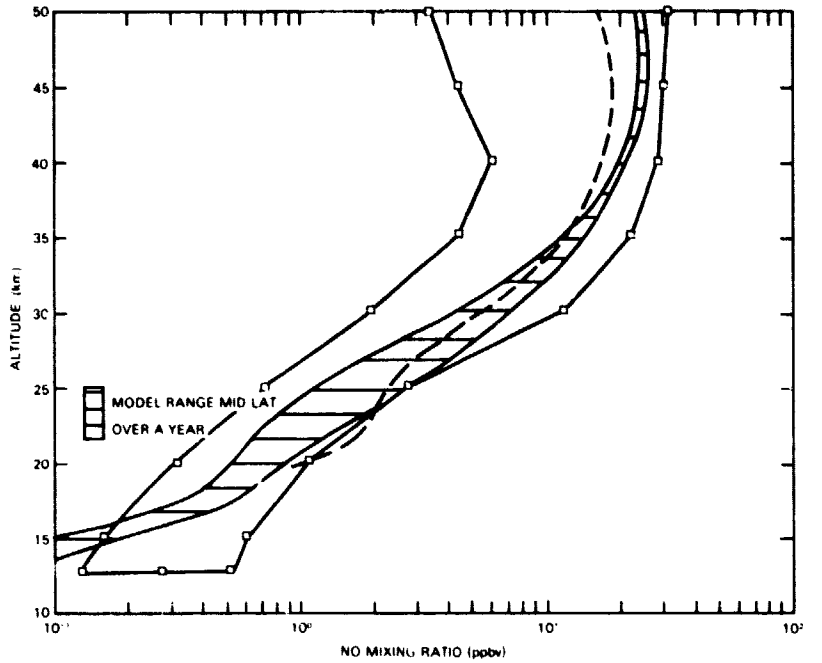

Figure 1-139. NO vertical mixing ratio profiles. Observations at mid-latitudes indicated by the band with square points. Horizontally striped region gives the seasonal range of daytime average values from the Du Pont 2-D model (C. Miller et al., 1981). Dashed line gives values from the AER 2-D model (Ko et al., 1981) for July noontime.

Recently Solomon (1980) has shown that a thermospheric source of NO may contribute a significant downward flux of NO into the upper stratosphere. The present models, which neglect this flux, may thus underestimate the NO concentration at 50 km.

Some measurements indicate a wintertime variation in the mid-latitude vertical profile. The calculations do not show large seasonal or latitudinal gradients at mid-latitudes, with only a factor of ~ 2 such variability predicted in the 20 to 30 km altitude range.

Latitudinal and Seasonal Variations

Loewenstein and coworkers, using a chemiluminescent instrument, have measured the seasonal and the latitudinal variations of NO at 18 and 21 km. These observations are reproduced in Figure 1-140 along with the calculations (daytime average) from the Du Pont model. The gross features of the observations are reproduced by the model. At both 18 and 21 km, the NO concentration increases with latitude during the summer and decreases rapidly above 50°N during the fall. The model gives similar features, with the only significant discrepancies being the underestimate of NO in the tropics at 18 km (during all seasons) and the underestimate for high latitudes at 21 km (particularly for summer).

The current chemistry and transport parameterization gives a good representation of the sharp falloff of NO during the fall above 50°N, and a reasonable simulation of the spring observations. This feature could not be reproduced using previous chemical reaction rates.

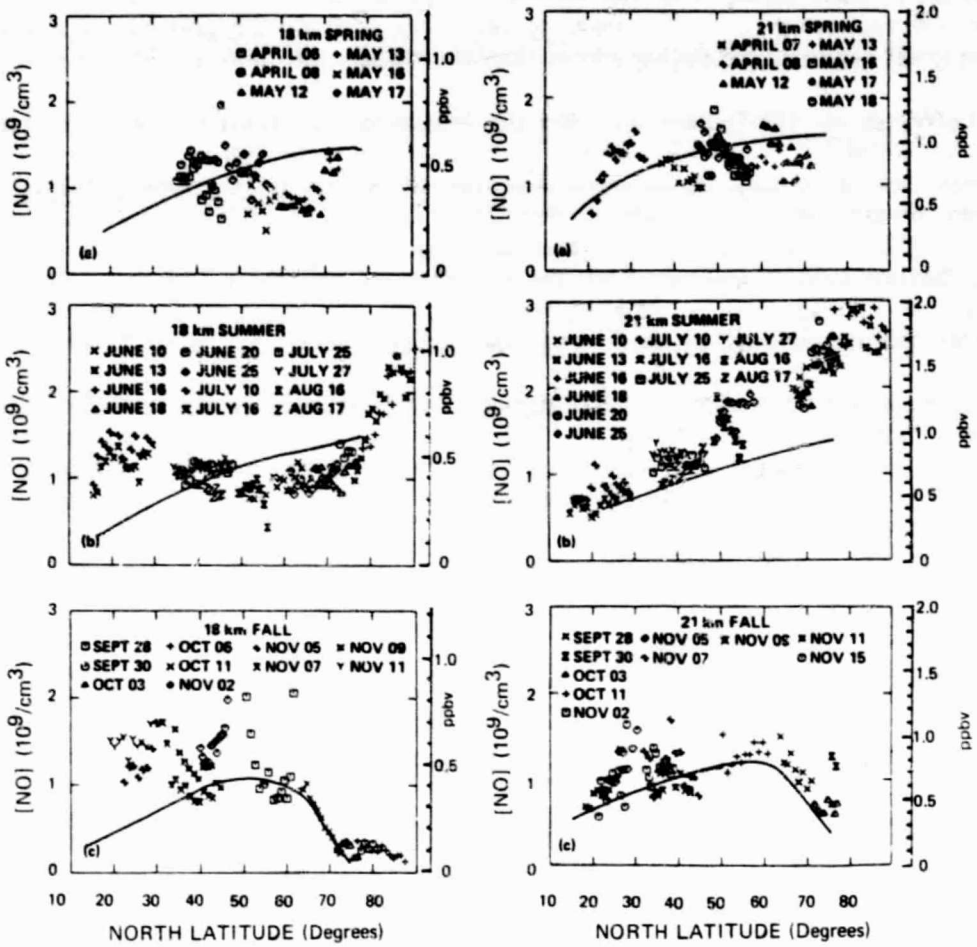

Figure 1-140. NO seasonal and latitudinal variations at 18 and 21 km. Points are observations of Loewenstein et al. (1977). Solid curves are results from the Du Pont model.

The seasonal variations of NO at an altitude of 21.3 km, obtained by Loewenstein and co-workers, for 40°N latitude are shown in Figure 1-141, along with Du Pont model calculations for 44°N and 64°N. The agreement with the calculated variation at 44°N is poor, although the 64°N graph indicates that a similar seasonal variation is calculated at higher latitudes. This apparent discrepancy, if supported by further measurements, may indicate the presence of a stronger NO_x sink in the lower stratosphere during winter than the models calculate.

Recently Coffey et al. (1981) have obtained the latitudinal variations of the NO column density above 12 km during summer and winter. The mid-stratospheric region from 20 to 40 km contributes most to the NO column, although stratospheric models (as the two discussed here) with their upper boundaries at ~55 km neglect the mesospheric NO concentration, which may contribute ~20% to the column. The observations are shown in Figure 1-142, along with the calculated daytime average column. Both the observations and the model show little latitudinal gradient in the summer, with a sharp decrease beginning at about 45°N in the winter. This is similar to the feature obtained by the in situ measurements shown in Figures 1-140 and 1-141.

The calculated shape of the NO column density versus latitude is qualitatively similar to the observations, but the predictions are too high by a factor of 1.3 in the tropics increasing to about two for high latitudes in winter. The more limited measurements by Girard et al. (1978) are higher than those of Coffey et al. (1981) by about 40%, so the overprediction may be less than suggested in Figure 1-142.

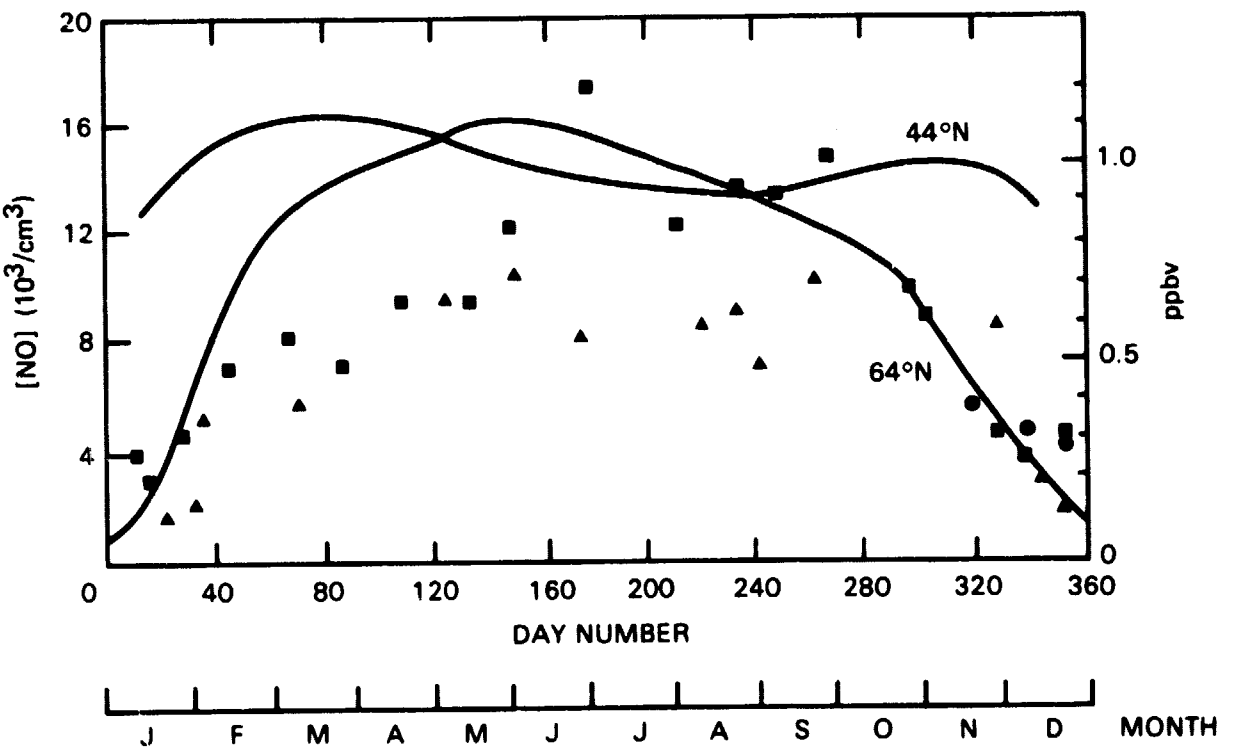

Figure 1-141. NO seasonal variations at 21 km, 40°N latitude. Points are observations of Loewenstein et al. (1977). Labeled solid curves are Du Pont model calculations for 44°N and 64°N.

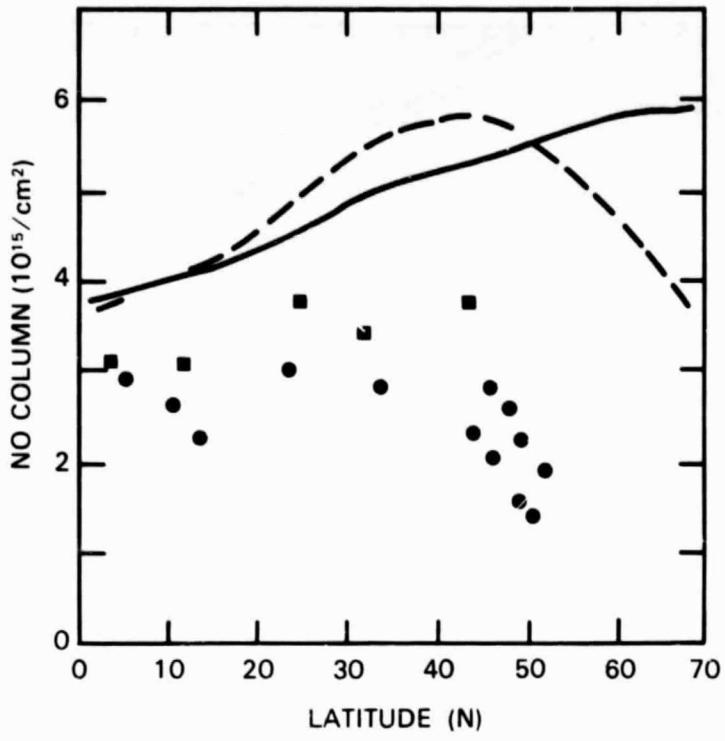

Figure 1-142. NO column densities above 12 km. Points are observations of Coffey et al. (1981): ■ = summer, ● = winter. Curves are calculations from the Du Pont 2-D model: solid = summer, dashed = winter.

Nitrogen Dioxide (NO_2)

Altitude Profile

The measured vertical mixing ratio profile for NO_2 at 30°N latitude is shown in Figure 1-143, along with the model calculations. Nitrogen dioxide exhibits considerable diurnal variation during the daytime, with sunset values (shown in Figure 1-143) about twice those at sunrise. Allowing for diurnal corrections, one concludes that the modeled shape fits the observations and that quantitative agreement to within about 50% is evident from 20 to 40 km.

Latitudinal and Seasonal Variations

The seasonal variations of NO_2 are best characterized by the column measurements of Noxon (1979), which indicate a strong winter minimum at 65°N. Figure 1-144 gives Noxon's data for 65°N and 40°N, along with 2-D model calculations for the appropriate latitudes. The model reproduces the winter minimum, with approximately the right amplitude, at 65°N. The model significantly understimates the seasonal variations for NO_2 at 40°N, however, just as was the case for the NO seasonal variations at 21.3 km altitude (see Figure 1-141). It is apparent that there is a process operating in the real atmosphere, leading to a sharp winter minimum in both NO and NO_2 at ~45°N, which the 2-D models do not adequately reproduce.

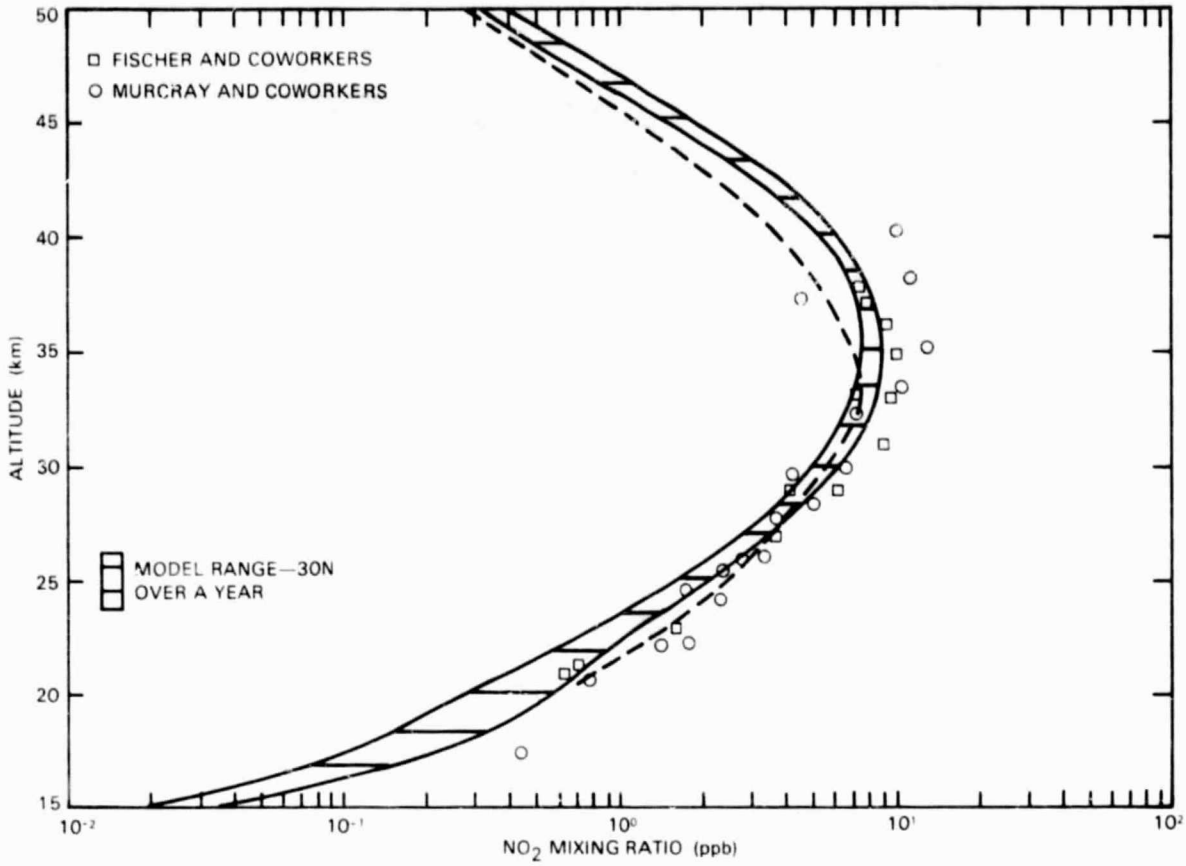

Figure 1-143. NO_2 vertical mixing ratio profiles near 30°N. Points are observations. Striped region gives seasonal range of calculated daytime average mixing ratios from the Du Pont model. Dashed curve is AER model profile for July noontime.

Figure 1-145 illustrates the column partitioning of the important daytime NO_x species. HNO_3 dominates toward the poles, especially in the winter. The conversion of NO and NO_2 to other NO_x species in the real atmosphere evidently takes place at mid-latitudes more completely during the winter than the models calculate. This may represent a transport parameterization inadequacy or a remaining inaccuracy in the model chemistry. Since the same qualitative features occur in several models, with quite different transport schemes, an inadequacy in the chemical scheme may be indicated.

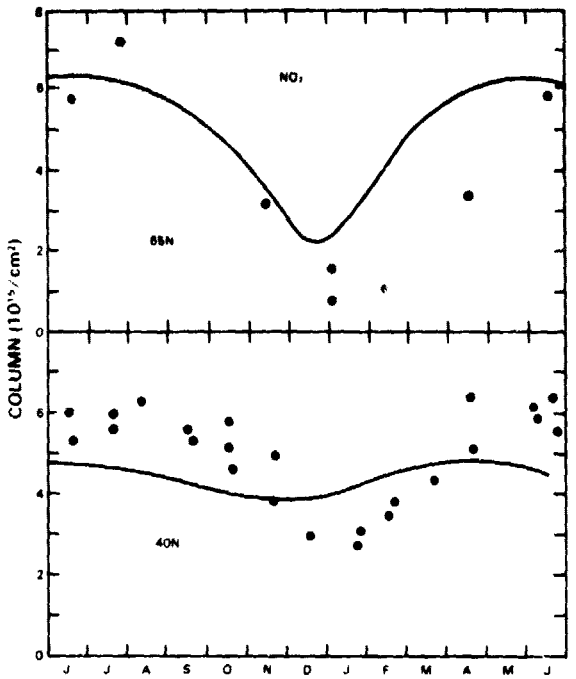

Figure 1-144. Seasonal variations of NO_2 column densities above 15 km. Points are observations of Noxon (1979, 1980). Solid curves are Du Pont model calculations.

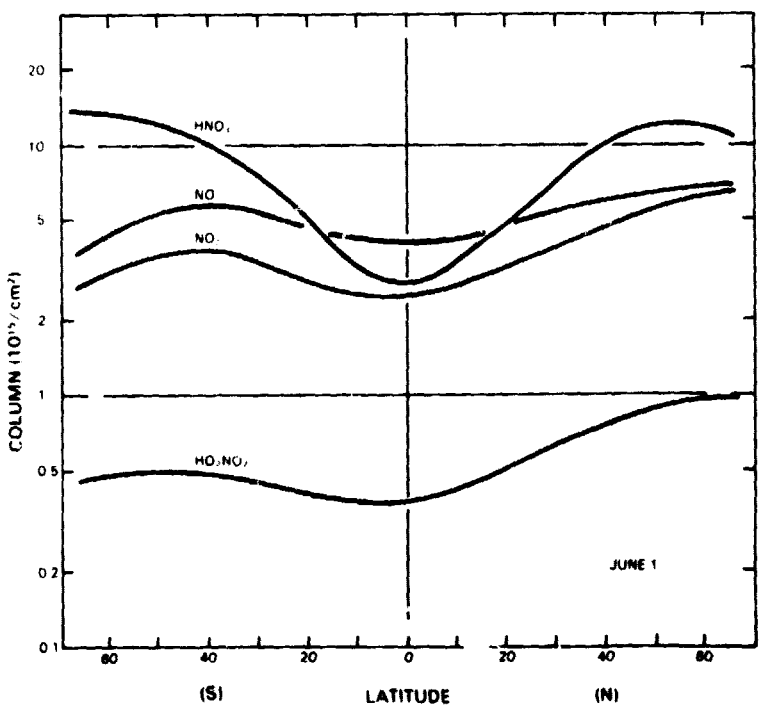

Figure 1-145. Variation of NO_x column densities with latitude. Calculated daytime average vertical columns (above 15 km) for the major NO_x species (C. Miller et al., 1981).

Both Noxon and coworkers and Coffey et al. (1981) have measured the NO_2 column abundance as a function of latitude for several seasons. All these groups' published results are collected in Figure 1-146. The summer measurements show a monotonic increase with latitude, by about a factor of two from the Equator to 60°N. The winter measurements show a rapid decrease between 45° and 50°N, sometimes called the "Noxon cliff". As discussed above, the model is best interpreted as a Northern Hemisphere model, so the (symmetric) continuation of the calculated column to the Southern Hemisphere is not shown.

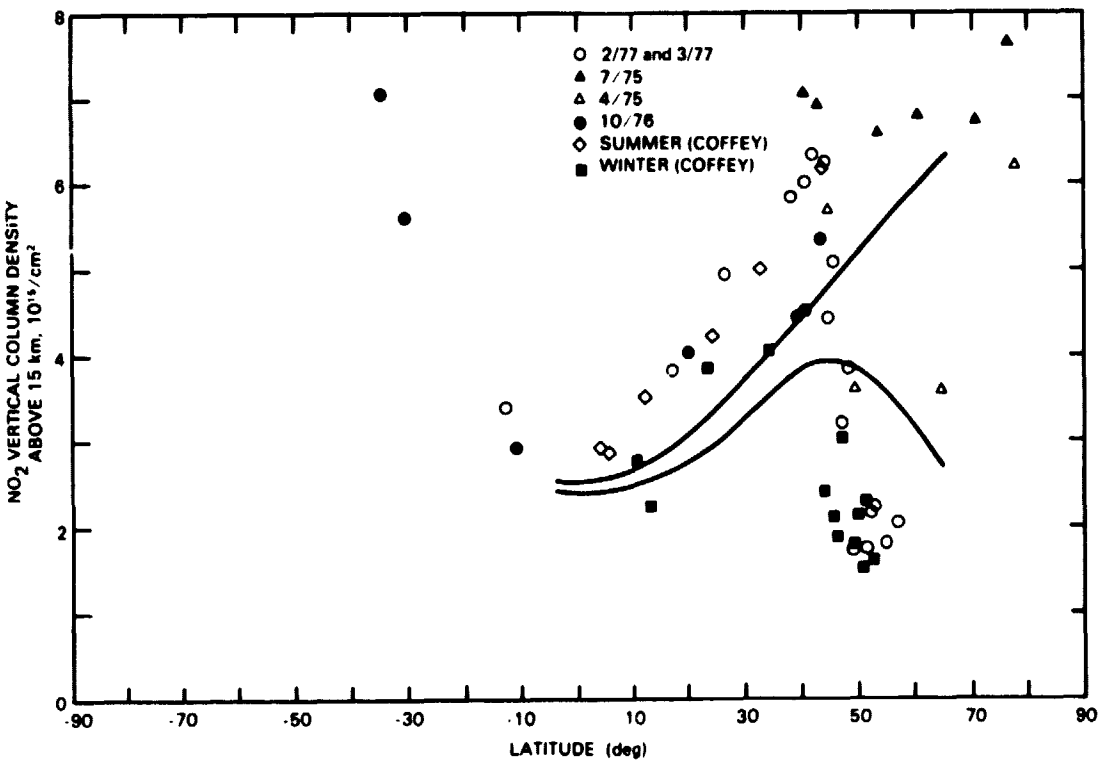

Figure 1-146. NO_2 vertical column densities versus latitude. Collected data by Noxon and coworkers and Mankin and coworkers given as points. Solid lines are Du Pont 2-D model calculations for summer (upper curve) and winter (lower curve).

The calculations shown in Figure 1-146 reproduce the qualitative features of these column variations. The upper curve is the summer variation, and the lower curve is for winter. The small seasonal variation for low latitudes is apparent, as well as a monotonically increasing column with latitude in summer and a sharply decreasing one (at ~45°) in the early winter. The model's latitudinal resolution is not sufficient to calculate sharp features like the Noxon cliff. However, a significant decrease in NO_2 at high latitudes in winter is, for the first time, clearly indicated by the calculations.

The species NO_2 participates in several key rate-limiting steps, including the reaction

$$NO_2 + O \rightarrow NO + O_2$$

which determines the rate of nitrogen-catalyzed ozone destruction. Figure 1-147 gives an altitude-latitude contour plot of the daytime average NO_2 concentration for the Northern Hemisphere's late winter season. (The nighttime average values are 50% higher.) Calculated values exceed 2×10^9 cm^3 at ~30 km everywhere except near the Equator. Very steep vertical gradients are evident in the lower stratosphere, especially at high latitudes.

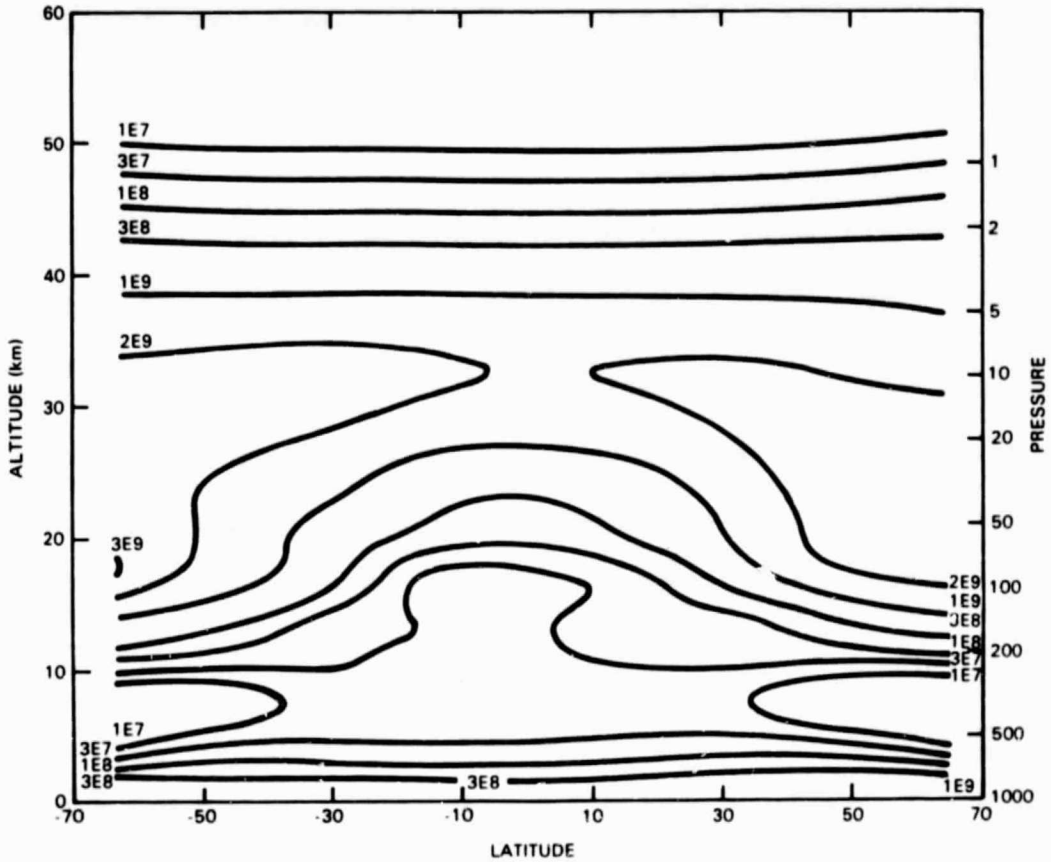

Figure 1-147. NO_2 concentrations versus altitude and latitude. Contour labels give the daytime average NO_2 concentration (molecules/cm) calculated with the Du Pont model, for March 1.

Model calculations made with the chemical reaction rate set of NASA RP 1049 could not simulate the seasonal and latitudinal variations of NO, NO_2, and (as discussed below) HNO_3. The improvement documented here has occurred with the subsequent chemical reaction rate updates. The single most important change was the large increase in the rate for HO + HNO_3, which reduced the HNO_3 concentration near the poles and significantly altered NO_x partitioning in the lower stratosphere.

Nitric Acid (HNO_3)

Altitude Profile

The observed mid-latitude vertical mixing ratio profile of HNO_3 is shown in Figure 1-148, along with the 2-D model calculations. Below 25 km, theory and observations are now in reasonable agreement. The current calculations, using the faster reaction rate for HO + HNO_3 of Wine et al. (1981b), are significantly improved over results using NASA RP 1049 chemistry below 25 km altitude and are in agreement with 1-D model calculations.

Above 25 km, the calculations significantly overestimate the measured amount of HNO_3. This overestimate, which is about a factor of three at 30 to 35 km, cannot easily be explained on the basis of the current chemical scheme. The discrepancy is also noted in the 1-D models and persists from the previous chemical rate sets.

Latitudinal and Seasonal Variations

Minimal seasonal variations are observed for the HNO_3 column below 30°N latitude, while at high latitudes the seasonal variations become more pronounced, with a winter maximum. These qualitative features of the seasonal variations in the total HNO_3 column are reproduced by the models with the current chemical rate data (see Figure 1-145)

The latitudinal variations of HNO_3 obtained by Murcray and coworkers, and Coffey et al. (1981), are shown in Figure 1-149. A consistent picture is clearly indicated, with the column increasing from a minimum of 2 to $3 \times 10^{+15}$ cm^{-2} at the Equator to about $16 \times 10^{+15}$ cm^{-2} at 60°N. This rapid variation is simulated by the calculations, including the seasonal variations from summer (bottom solid curve) to winter (top solid curve). The dominant contribution to the column comes from the 15 to 25 km region of the lower stratosphere where transport effects are significant.

The improved comparison between the calculations and observations is due both to the addition of new measurements and to improvements in the chemical reaction rate set. The models' overestimate by a factor of ~3 noted in the mid-latitude vertical HNO_3 profiles above 30 km remains a significant discrepancy.

Nitrogen Trioxide (NO_3)

Recently Naudet et al. (1981) obtained a vertical mixing ratio profile for NO_3 at night, from latitude 43°N in September. Figure 1-150 gives the measured concentration profile, along with two profiles of nighttime averaged NO_3 obtained with the Du Pont 2-D model. Because of the rapid variation of the solar zenith angle with time during September, the calculated NO_3 profile changes quite rapidly. The model does not predict a minimum for the nighttime column NO_3 during the summer, as indicated in a limited number of measurements by Noxon.

Peroxynitric Acid and Nitrogen Pentoxide (HO_2NO_2 and N_2O_5)

Peroxynitric acid (HO_2NO_2) has not been detected in the stratosphere. The current 2-D model calculations indicate that the HO_2NO_2 mixing ratio peaks at ~0.4 ppb, at about 25 km altitude, for mid-latitudes.

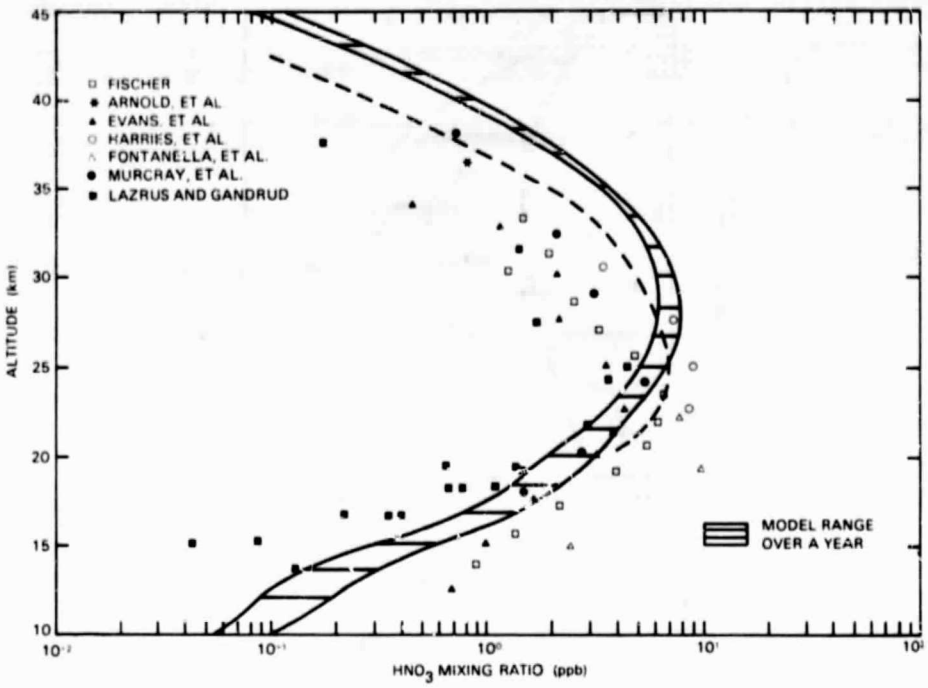

Figure 1-148. HNO_3 vertical mixing ratio profiles near 30°N. Observations given by points. Banded region gives seasonal range of daytime average mixing ratio from the Du Pont model. Dashed curve gives AER model results for July noontime.

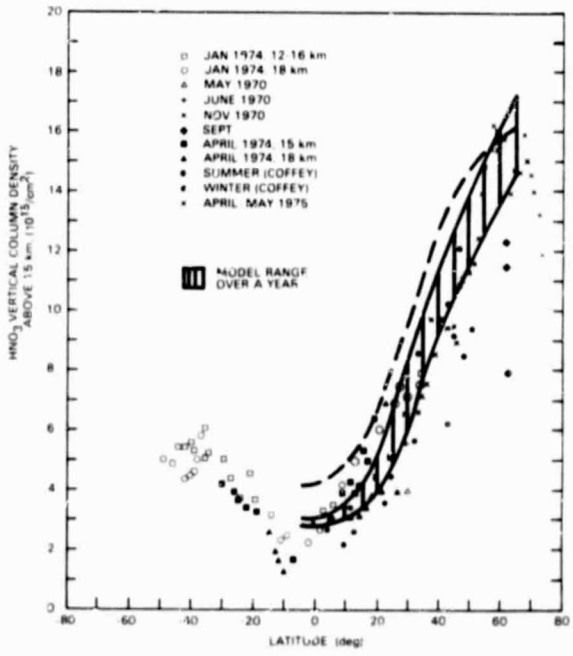

Figure 1-149. HNO_3 vertical column densities. Points give data of Murcray and coworkers and Mankin and coworkers. Vertical banded region gives seasonal variations (upper = winter, lower = summer) of daytime average column from Du Pont model. Dashed curve gives AER model results for July.

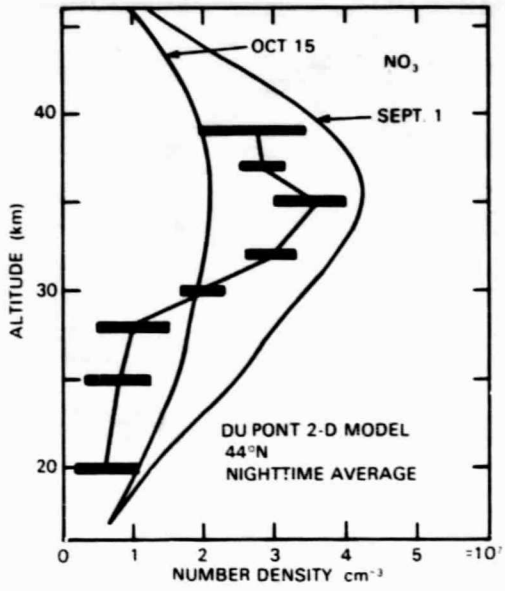

Figure 1-150. Nighttime NO_3 vertical profiles. Bars give observations of Naudet et al. (1981). Solid curves give Du Pont model calculations of the nighttime average concentration for the two nearest "seasons."

No positive detection of N_2O_5 in the stratosphere has been reported. Its calculated peak nighttime mixing ratio at mid-latitudes is ~3ppb, near 32 km altitude, with much larger values near the winter pole.

Summary for NO_x

Significant changes in several important reaction rates involving NO_x species have occurred since the publication of NASA RP 1049. These changes have improved the comparison between the model predictions and observations for the odd nitrogen species. The calculated mid-latitude NO vertical profile and the qualitative features of the NO seasonal variations now agree with observations below 35 km. The calculated NO_2 mid-latitude vertical profile agrees with the observations, especially those at the higher end of the observed range. The NO and NO_2 vertical column abundances in the 2-D models vary with latitude and season in a manner qualitatively similar to the observations, with a feature analogous to the Noxon "cliff".

The predicted HNO_3 mid-latitude vertical profile in the lower stratosphere has been improved with the chemistry updates and now agrees quite well with the observations, although a factor of three overprediction of HNO_3 at ~30 km persists. The column abundance of HNO_3 in the 2-D models varies with latitude and season consistent with the observations.

Although the gross features of the latitudinal and seasonal NO_x variations are simulated by the models, several quantitative disagreements persist. The seasonal variations are not well modeled, especially in the 40°N to 50°N region during the winter. The observed columns of NO and NO_2 show sharp variations at high latitudes in winter that are not reporduced, indicating either that the 2-D models are not properly simulating some feature of NO_x chemistry or else that they do not adequately describe "local" (i.e., occurring over $\lesssim 10°$ in latitude) transport properties in this region.

C-3

ODD CHLORINE SPECIES (Cl_x)

Stratospheric levels of Cl_x are expected to be increasing with time as a result of anthropogenic emissions at the ground. In both sets of model calculations presented here, estimates are given for the Cl_x species concentrations in the stratosphere for the present day (mid-1980), corresponding to an upper stratospheric mixing ratio of 2.0 to 2.2 ppb total Cl_x. The sources of the Cl_x in the models are CH_3Cl and CCl_4, with fixed ground-level mixing ratios, and the anthropogenic species CH_3CCl_3, CCl_3F, and CCl_2F_2 based on historical estimates of the ground-level release fluxes.

Hydrogen Chloride (HCl)

Figure 1-151 gives a comparison between the observed HCl profiles measured by high resolution absorption spectroscopy (at mid-latitudes) and the calculated results from two 2-D models. The range of variations over the year 1980 at 30°N latitude is shown for the Du Pont model, while the AER model gives the noontime profile for July 1980. The calculations fall toward the middle to high end of the observations from the lower stratosphere up to 30 km. However, the data at 35 to 40 km possibly indicate an HCl mixing ratio (~2 ppb) somewhat larger than the calculated values (~1.5 ppb). These calculated vertical profiles for HCl at mid-latitudes are very similar to those obtained with 1-D models.

Figure 1-152 presents the latitudinal variations in the column abundance of HCl measured by Girard et al. (1981) above 11 km during the spring. These are the only available observations of column HCl latitudinal variations. They are clearly characterized by a minimum at the Equator and an increase toward the poles. Also shown in the figure is the daytime average column calculated with the Du Pont 2-D model. The calculations show Northern Hemisphere variations similar to those observed except near the Equator, where the calculated values are a factor of two higher than the upper limit of the observations.

Chlorine Oxide (ClO)

The calculated altitude/latitude contour plot of the daytime average ClO concentration is shown in Figure 1-153. Above 10 km in the winter hemisphere, the calculated [ClO] decreases with latitude from the Equator to the poles, while latitudinal gradients in the summer hemisphere are less pronounced. At a fixed altitude, the calculated concentration is higher in summer than in winter. These seasonal variations directly follow those of the HO radical, which affects Cl_x partitioning.

The largest calculated daytime average ClO concentrations (~6×10^7 cm^3) occur at ~30 km altitude for latitudes from 0° to 50° in the summer hemisphere. In the winter hemisphere, the altitude giving the largest concentration increases with latitude, reaching ~40 km at 65°. The concentration at a given altitude is larger during summer than winter, with a factor of two seasonal variation near 30 km at 50° latitude.

The in situ ClO measurements at 30°N latitude are compared with the model calculations in Figure 1-154. If one excludes the two high ClO profiles as being not representative of the "normal" range for this species, the calculated profiles fall at the high end of the measurements at ~25 km and deviate toward the low end at ~40 km. The mid-latitude calculations are similar to those obtained with 1-D models.

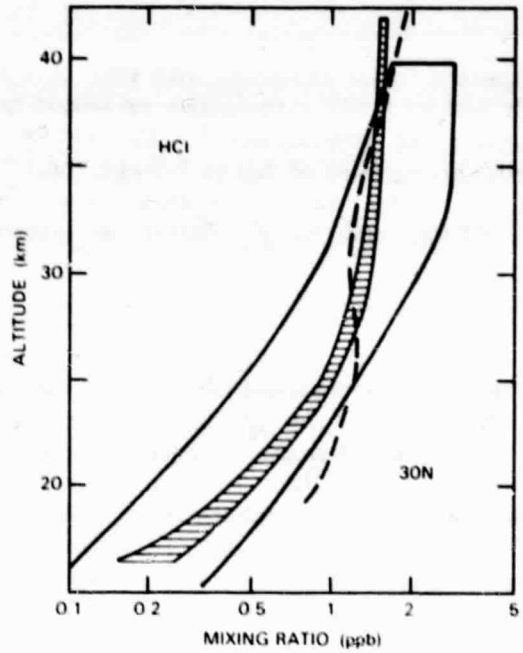

Figure 1-151. HCl vertical mixing ratio profiles near 30°N. Outer curves give range of observations from IR absorption spectroscopy. Horizontal banded region gives seasonal range of Du Pont model calculations (C. Miller et al., 1981) for daytime average HCl mixing ratio. Dashed curve gives AER model profile (Ko et al., 1981) for July noon.

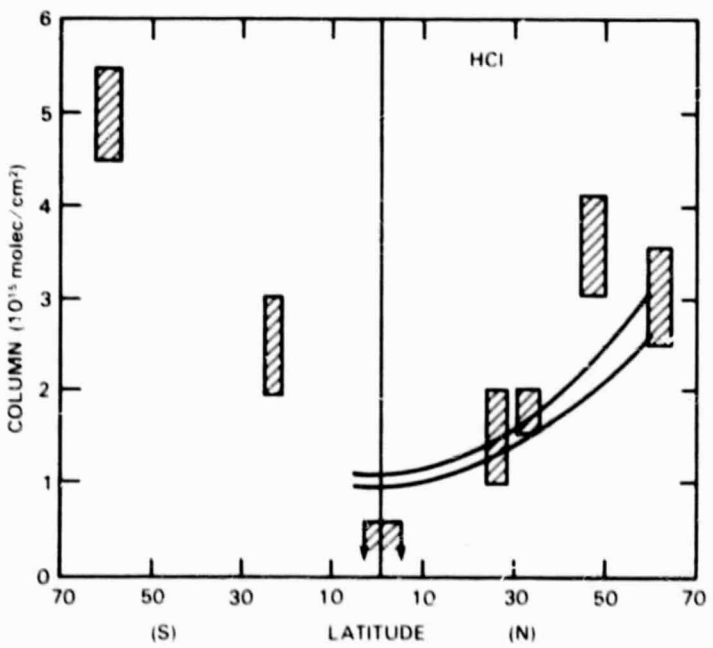

Figure 1-152. Vertical HCl column densities versus latitude. Banded regions are observational data of Girard et al. (1978). Solid curves give the seasonal range of daytime average columns from the Du Pont model.

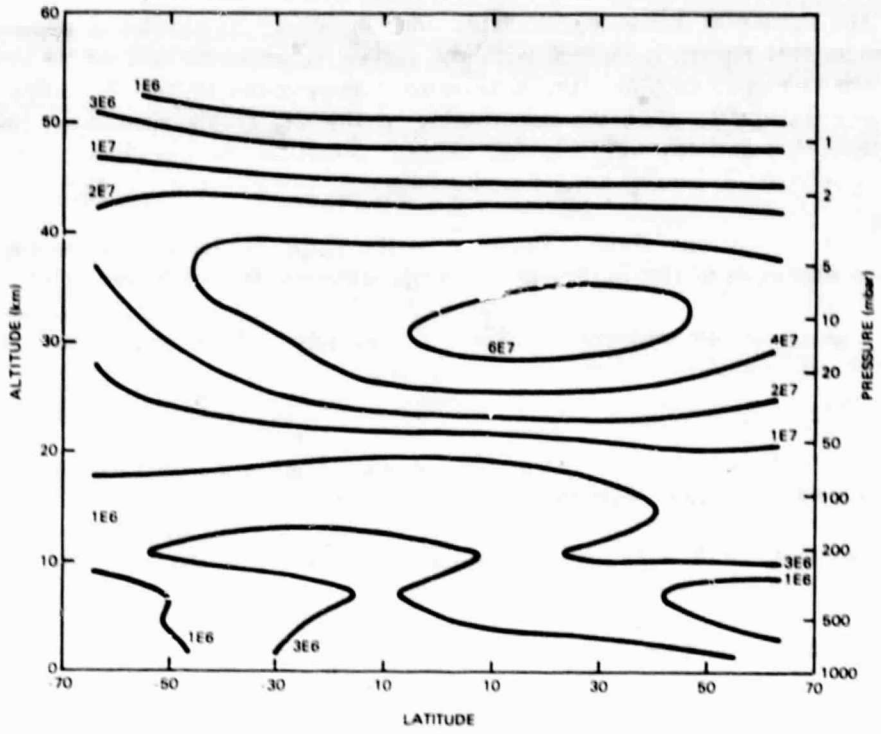

Figure 1-153. ClO concentration versus altitude and latitude. Contour labels give ClO concentration in molecules/cm^3, calculated with the Du Pont model, for July 1980.

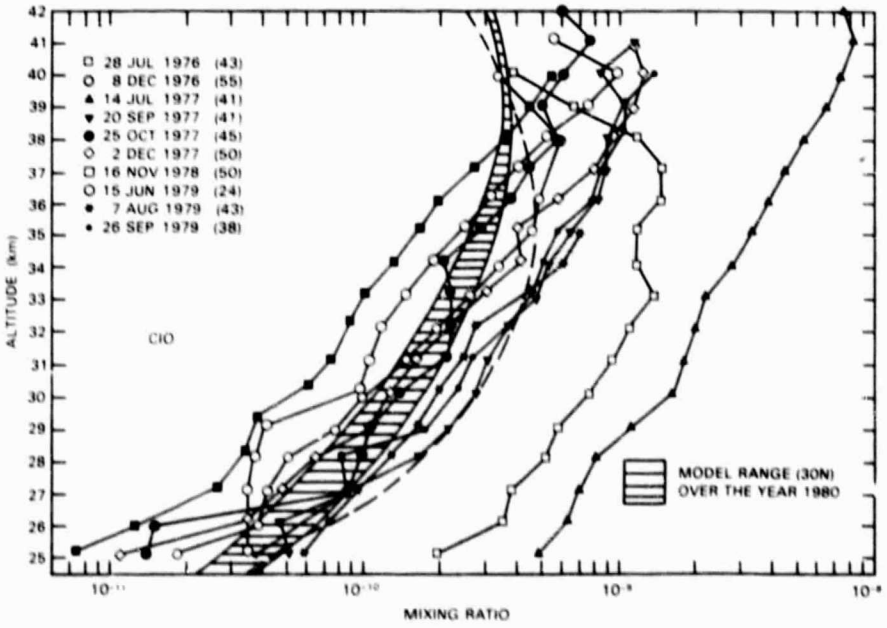

Figure 1-154. ClO vertical mixing ratio profiles near 30°N. Connected points are observational data of Anderson and coworkers. Banded region gives seasonal range of daytime average values from the Du Pont model. Dashed curve gives AER model calculations for July noontime. (C. Miller et al., 1980b)

Below 35 km, the agreement between calculated and observed ClO profiles is improved using the chemistry given in this report, compared with the earlier recommendations of NASA RP 1049. The net result of the changed reaction rates is to reduce abundances of the HO radical in the lower stratosphere and thereby to shift the partitioning of the Cl_x family away from the catalytically active forms (ClO, Cl) and toward HCl. The average slopes of the calculated and observed ClO vertical profiles between 25 and 30 km are now similar.

Above 35 km, the calculations show a decrease in the slope of the vertical profile of ClO with altitude, with a maximum in the mixing ratio profile between 35 and 40 km. This feature is not found in the envelope of the observations, although some of the individual profiles exhibit such behavior. The agreement between both 1-D and 2-D models and the observations for ClO above 35 km is not good, suggesting a remaining inaccuracy or an unknown mechanism in the current chemistry scheme.

Parrish et al. (1981) have measured ClO at 42°N in winter using a mm-wave emission technique, and their results are consistent with the vertical profile of the in situ measurements. The winter 1980 vertical column density of ClO above 24 km altitude obtained by Parrish et al. (1981) was $1 \times 10^{+14}$ molecules cm^{-2}, while a 2-D model calculation (C. Miller et al., 1981) for the same season and latitude gives a daytime average value ~40% lower.

Cl Atom, Chlorine Nitrate and Hypochlorous Acid ($ClONO_2$ and HOCl)

The calculated latitudinal variations of the daytime atomic chlorine concentration above 35 km are small (~20%) except toward the winter pole. The calculations for mid-latitudes show little seasonal variation and vertical profiles similar to those of 1-D models in the ~35 to 45 km region for which the only observations exist.

The calculated $ClONO_2$ mixing ratio using the chemistry recommended in this report is a factor of about three lower than that obtained with the chemistry given in NASA RP 1049. The vertical profiles of $ClONO_2$, in both the 1-D and 2-D models, exhibit a sharp maximum at ~30 km altitude, with a daytime average mixing ratio of ~0.2 ppb there. These calculations are well below the measurements of Murcray et al. (1980), which are interpreted above as giving a tentative upper limit of 1 ppb in the altitude range 25 to 35 km.

The maximum HOCl mixing ratio (daytime and nighttime averages ~0.1 and 0.3 ppb, respectively) is calculated to occur at ~35 km altitude in the summer hemisphere, with the altitude of the maximum increasing significantly with latitude toward the winter pole. No stratospheric measurements of HOCl have been reported.

Total Chlorine

Both sets of 2-D model calculations discussed in this section are for the year 1980, based on historical ground level release rates for CCl_3F, CCl_2F_2, and CH_3CCl_3, and fixed ground level mixing ratios of CH_3Cl and CCl_4. They calculate 2.0 to 2.2 ppb total Cl_x in the upper stratosphere. By comparison, the total chlorine measurements of Berg et al. (1980) indicate the presence of ~3 ppb Cl_x for the late 1970s. The in situ measurements of HCl and ClO at ~40 km, while showing a large range of values, give a mean totai Cl_x amount of ~3 ppb.

Adjustments to the existing ground level organic Cl_x sources in the models, within the uncertainty range of the observations, could be made to obtain ~3 ppb Cl_x at high altitudes. The size of the additional source would be similar to that due to FC-11 and FC-12. However, an increased ground level Cl_x source would also cause an increase in lower stratospheric HCl and ClO. Since the calculations for both these species currently fall at the high end of the observations near 25 km, an upward adjustment in Cl_x would weaken the agreement with HCl and ClO measurements in the lower stratosphere.

Summary for Chlorine Species

The chemical reaction rate changes since NASA RP 1049 have improved the agreement between models and measurements for HCl and ClO in the lower stratosphere. However, the models now appear to predict too little HCl (by ~50%) and ClO (by about a factor of two) at 40 km. These observations and total chlorine measurements suggest an upper stratospheric Cl_x mixing ratio (in 1980) of ~3 ppb, about 50% larger than obtained with the models.

Measurements of the Cl_x species have generally been restricted to mid-latitudes. The only extensive observational data on latitudinal variations of chlorine species are Girard et al.'s recent HCl column measurements. The 2-D models give qualitatively the same features as these HCl measurements, with a minimum near the Equator and a column increasing rapidly toward the poles.

CHAPTER 2

MULTIDIMENSIONAL ASPECTS: OZONE, TEMPERATURE AND TRANSPORT

INTRODUCTION

Our understanding of the photochemistry of the ozone layer has been increasing steadily over the past several years. Many types of studies including laboratory chemical kinetics, remote and in situ measurements of trace species, and photochemical modeling have provided essential information. However, without doubt, it is the one-dimensional photochemical model which has played the central role in the scientific assessment of possible anthropogenic threats to the ozone layer. Such models, which parameterize the entire effects of atmospheric motions by use of a vertical eddy diffusion coefficient, reduce the complex three-dimensional interplay of atmospheric motions and trace constituent budgets to rather simple budget equations for the (globally and annually averaged) vertical profiles of the various constituents. The limited number of degrees of freedom in these models makes it feasible to carry out a wide variety of perturbation studies with rather complete chemistry. However, the global and temporal averaging implicit in such models introduces uncertainties which are difficult to evaluate in a precise manner. Thus, for example, the National Academy of Sciences (NAS) panel on Atmospheric Chemistry stated that their estimate of the steady-state ozone depletion due to release of chlorofluoromethanes was uncertain by a factor of two due to the crude treatment of atmospheric transport in one-dimensional models apart from all other uncertainties.

For some purposes, these uncertainties perhaps can be tolerated. However, it is clear that for a completely safisfactory scientific understanding of the ozone layer it is necessary to consider the full three-dimensional spatial variability as well as the temporal variability of all the trace species relevant to the ozone budget. Such an approach demands explicit understanding and modeling of the three-dimensional transport and dispersion due to atmospheric motions together with continuing comparison of model results with the observed three-dimensional (four-dimensional including time) temperature, wind, and composition structure.

Recent work on the photochemistry of ozone as reviewed by Cicerone (1981) as well as in other chapters of this report indicates that there are still important uncertainties in the chemistry, primarily involving the roles of the hydroxyl radical and certain intermediate storage molecules (e.g., $ClONO_2$) in the lower stratosphere. Since, in the lower stratosphere, chemical and dynamical time scales are comparable, chemical composition must depend crucially on atmospheric transport and dispersion. Significant further reduction of the uncertainty in ozone perturbation predictions may thus require multidimensional models which incorporate the effects of temporal and spatial variability in the lower stratosphere (below~35 km). The purpose of this chapter is to review our capability for obtaining four-dimensional data on stratospheric structure, dynamics, and ozone; to review some of our advances in knowledge that have come from analyses of these data sets; and to review progress in the development of multidimensional models of the stratosphere. Ozone is singled out in this chapter as a stratospheric constituent, not only because of its importance but also because multidimensional ozone observations are in a far more advanced state than is the case for any other stratospheric constituent.

A major theme of this chapter is the interplay of observational and theoretical (modeling) work. Global observations are clearly necessary to establish a data base for validating results from multidimensional models. Clever analysis of data can reveal processes and phenomena which may demand new modeling strategies (e.g., vertical momentum transfer by small-scale gravity waves). Equally important, but less appreciated, is the potential role of models in guiding our observing strategies. A proper understanding of the four-dimensional variability of the stratosphere is necessary in order to begin to view in their proper framework the measured one-dimensional

vertical profiles discussed in the previous chapter. Local vertical profiles obviously cannot be used indiscriminately for validating one-dimensional (globally averaged) photochemical models. Such profiles, however, can play an important role in delineating the vertical distribution of various trace species, and may also implicitly contain information on the effects of transport and dispersion. However, in the absence of proper three-dimensional observations there has been a tendency in some quarters to overinterpret local vertical profiles. One role which multi-dimensional modeling can play is in helping experimenters to interpret local vertical profiles.

The discussion of multidimensional aspects of the stratosphere is divided into four major sections: observations, analysis and interpretation, modeling, and transport of trace species. In the first section there are discussions of global observations of ozone by both ground-based and satellite techniques and observation of stratospheric temperature by satellite techniques. This section includes a summary of the temporal and spatial coverage of these data as well as a discussion of the accuracy and limitations of these data. Since routine in situ meteorological soundings (radiosonde and meteorological rockets) have been summarized thoroughly in NASA RP 1049, such measurements will not be discussed in any detail here. However, this section does discuss the potential of ground-based wind measurements utilizing the so-called MST radar systems for studying short period dynamics, and the importance of research aircraft for studying small-scale horizontal variability.

In the second major section, progress in the analysis and interpretation of global data sets is reviewed with emphasis on satellite data. Progress and problems in defining the momentum, heat and energy budgets of the stratosphere as well as mechanisms of tracer transport and some information on chemistry are discussed. This section includes a discussion of interannual variability in the stratosphere and its implications for interpretation of the data. In addition, the role of future satellites, e.g., the Upper Atmosphere Research Satellites (UARS), in elucidating various unsolved problems is discussed.

The third major section of the chapter summarizes the current status of multidimensional modeling and the role of such modeling in stratospheric research. We first consider the area of two-dimensional photochemical and dynamical models. Recently, important theoretical advances have been made in our understanding of the transport-dispersion processes in the atmosphere. These advances promise to place two-dimensional transport models on a firmer theoretical basis. However, a three-dimensional initial value approach is still required if one is to really "simulate" the complete radiative-dynamical-chemical system and is very useful in diagnosing the treatment of processes in two-dimensional models. We have attempted to summarize the current work of all groups having active two- and three-dimensional models of the stratosphere. Information on the technical aspects as well as the scientific goals of the various projects is provided.

This section also reviews current thinking on the importance of various radiative-chemical-dynamical coupling processes; the role of models in assessing perturbations in climate due to such couplings; coupling of observations and models; the possible role of models in the design of observational strategies; and the crucial role of global observations in validating models.

In the final section of this chapter, a number of facets of our understanding of the global transport of stratospheric trace species are synthesized. This section begins with a discussion of trace constituent distributions and their implications for stratospheric dynamics and continues with a conceptual view of the mechanisms responsible for producing tracer transport and variability. This section then discusses the important special problems associated with the exchange of trace species between the stratosphere and troposphere. The section ends with an analysis of the water vapor budget as an example of the multidisciplinary problems encountered in trying to understand the distribution of a single important trace constituent.

GLOBAL OBSERVATIONS OF OZONE AND TEMPERATURE

INTRODUCTION

Two crucial parameters to be measured in the stratosphere are ozone and temperature. Ozone is important not only because of its importance in shielding biological systems from harmful ultraviolet radiation but also because it plays a very important role in absorbing solar radiation and absorbing and reemitting infrared radiation. Since ozone plays a crucial role in determining the distribution of stratospheric heat sources and sinks, its distribution helps to determine the stratosphere's temperature and wind structure. Measuring the distribution of stratospheric temperature is important for many reasons. If one knows the distribution of temperature in the stratosphere, one can use the hydrostatic relation together with information on the tropospheric structure to derive the distribution of geopotential height of pressure surfaces, or equivalently the distribution of pressure as a function of altitude, latitude, and longitude. Then, using the geostrophic wind relations, one can obtain the distribution of the geostrophic wind, which is a close approximation to the prevailing wind at stratospheric levels in the extratropics. Thus, from a measured stratospheric temperature field it is possible to approximate the dynamics structure of the extratropical stratosphere. Also, many important stratospheric chemical reaction rates are quite temperature-dependent so that the temperature must be known before one can determine the chemical production and loss rates of several stratosphere constituents. Finally, the stratospheric temperature field is important in determing the stratosphere's exchange of infrared radiation with the troposphere below, with the atmospheric regions above, and with space.

Both ground-based and satellite techniques exist for measuring stratospheric ozone and temperatures. It is the purpose of this section to briefly discuss some of these measurement techniques along with the availability and quality of the data. These subjects were also previously discussed in NASA RP 1049.

Brief descriptions of various satellite instruments are included in Appendix C to aid in understanding some of the limitations of the data. A listing of the measurement errors and physical parameters, such as field-of-view, sampling, and coverage, is presented within the chapter to describe the character of the various satellite data sets. Pertinent data on error sources were obtained from the experimenters for each experiment; in most instances, errors were estimated from ground simulations and testing. It is recognized that validation of satellite data depends heavily on comparisons with measurements made by independent techniques from ground, balloon, aircraft, and rocket platforms. These measurement techniques have their own errors and data reduction problems which must also be considered. Despite such problems, these "correlative measurements" are important since they provide the only truly independent comparison set.

Some of the barriers to the use of stratospheric satellite data are the lack of convenient access to the data in machine readable form and difficulties in assimilating these very large data sets. We have tried to address these and other problems in this section with the goal of stimulating the use of large satellite data sets in the study of key stratospheric problems. A later section summarizes some of the analyses that have been done with these data by reference to some published works.

OBSERVATIONS OF OZONE

In the following section, measurements of total ozone column amounts are discussed separately from measurements of ozone profiles in the stratosphere. Both measurements are, of course, important. For instance, in addressing concerns of increased exposure to harmful solar ultraviolet radiation it is very important that we understand whether changes in vertically integrated

ozone amounts are occurring. On the other hand, changes in the vertical distribution of ozone, even if the total amounts are unchanged, can lead to changes in stratospheric structure and thus possibly even to changes in tropospheric climate.

Measurement Techniques for Total Ozone

Two different ground-based techniques are used for routine observations of total ozone: the Dobson spectrophotometer and the M-83 filter photometer. In addition, a number of satellite-based systems have been (and are being) used for total ozone measurements. The principal satellite systems that have provided total ozone data are the Backscattered Ultraviolet (BUV), Solar Backscattered Ultraviolet (SBUV), and the Total Ozone Mapping Spectrometer (TOMS) techniques. Other satellite methods involve the Infrared Interferometer Spectrometer (IRIS), the High Resolution Infrared Radiometer (HIRS) systems and the Multichannel Filter Radiometer (MFR). A more detailed description of these different total ozone observing techniques is given in NASA RP 1049 and WMO (1981).

For the purposes of analysis of long-term ozone variations, Dobson observations provide the longest continuous series of measurements, having started as early as 1925 at some stations. Currently operating ground-based total ozone stations with 15 or more years of observations are shown in Figure 2-1. The stations marked "other" in most cases use the M-83 type instrument (see Appendix C). The geographic distribution of ozone observations in the global observing network is quite limited as can be seen in Figure 2-1. Satellite systems reduce this limitation. Past and planned future total ozone satellite measurement programs are depicted in Figure 2-2. As shown, only the Nimbus 4 satellite has thus far yielded continuous data covering more than 1 or 2 years. However, the use of the data from Nimbus 4 is limited due to concerns having to do with instrumental drift and uneven sampling (see following discussions). All data from the Nimbus 4 BUV experiment have been processed and the total ozone data are now available from the National Space Science Data Center (NSSDC), Goddard Space Flight Center. In addition, monthly average global synoptic analyses of total ozone have been completed and are available from NSSDC.

Ground Based: Dobson Spectrophotometer

Estimated ranges of various types of measurement errors for the Dobson spectrophotometer are given in NASA RP 1049, (Table 6-2) reproduced here as Table 2-1. (See that report for a discussion of how these estimates were derived.)

Significant recent developments concerning our understanding of Dobson spectrophotometer total ozone measurements errors are the following:

- Some experimental evidence suggests that Dobson total ozone measurements may be systematically biased by as much as 5 to 7% (Komhyr, 1980). A redetermination of the Huggins band ozone absorption coefficients is currently in progress at the National Bureau of Standards, Gaithersburg, Maryland (A.M. Bass, personal communication). If the redetermination confirms the validity of the presently used absorption coefficients, then other possible error sources will need to be explored, e.g., the presence in clean air of anomalous absorbers other than ozone (see below). Such an absorber might affect ozone trend determinations if its atmospheric abundance gradually changes with time.

- Komhyr et al. (1980) have recently applied corrections to Bismarck, North Dakota, total ozone data for 1963 through 1979. Data collected in the 1960s needed a bias correction of about 2.5%, while the 1970s data did not require correction. Unfortunately no other similar studies are available for other stations.

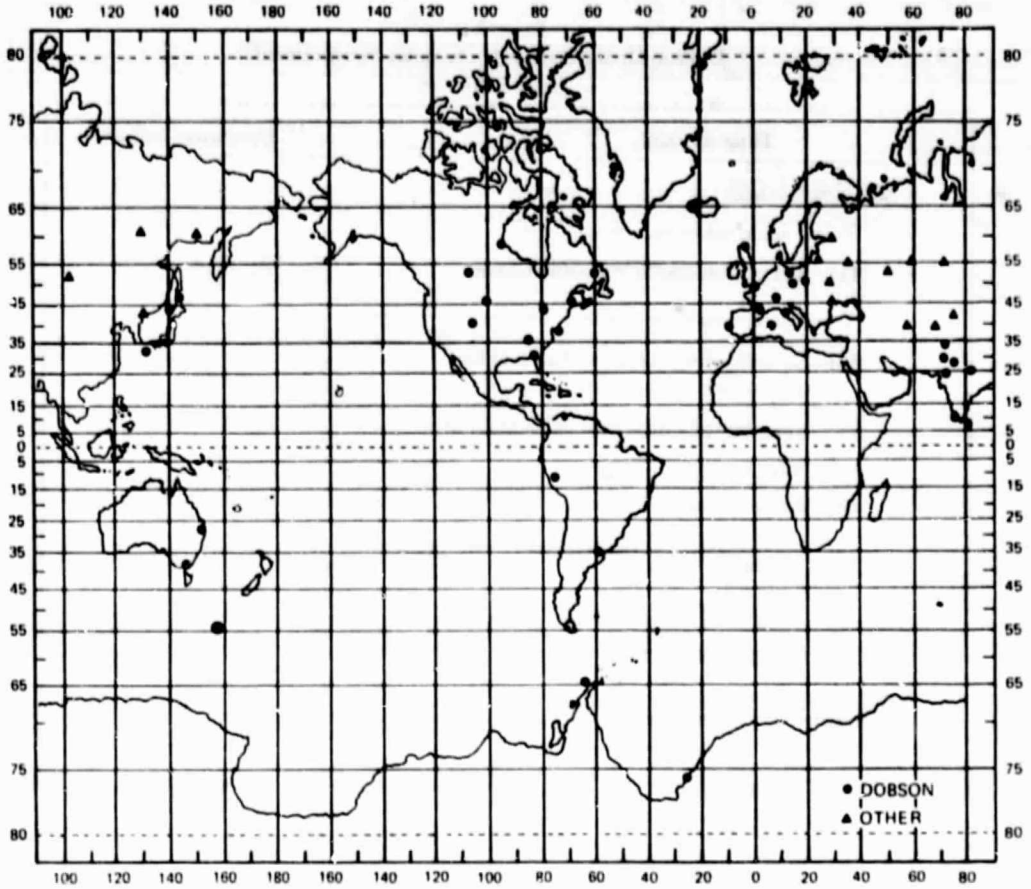

Figure 2-1. Current total ozone observing stations with 15 or more years of observations.

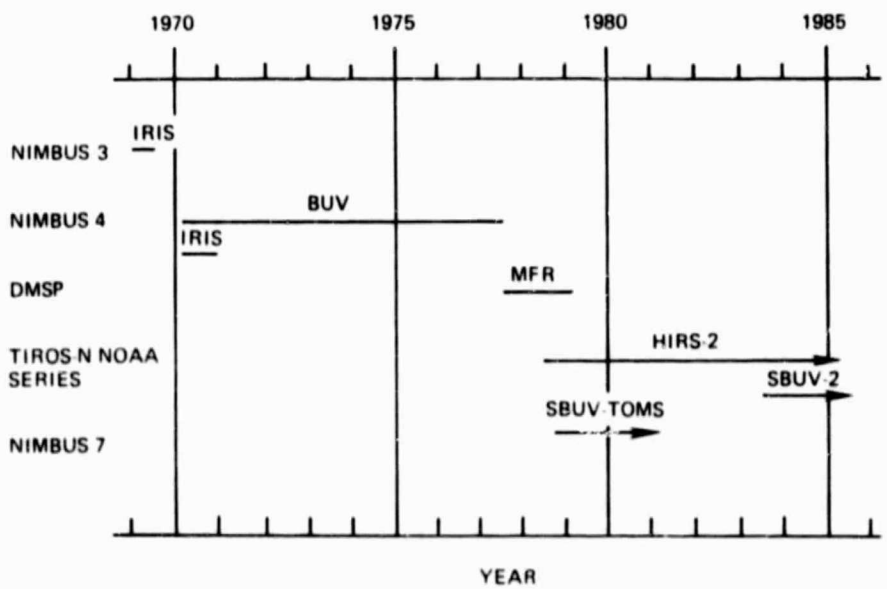

Figure 2-2. Schedule of satellite systems for total ozone (Miller, personal communication).

Table 2-1
Dobson Ozone Spectrophotometer Measurement Error Estimates

Type of Error	Estimated Value*
Systematic Errors	
1. Trend determinations not affected:	
(a) Absorption coefficient uncertainties	(0, +7)%
2. Trend determinations affected (change per decade):	
(a) O_3 absorption coefficient affected by stratospheric temperature changes	± 0.5%
(b) Uncorrected instrument calibration drift	± 3%
(c) Solar spectrum changes	± 0.3%
(d) Aerosol changes	± 1%
** (e) Tropospheric pollution changes with time	
– ozone	± 1%
– other absorbers (e.g., SO_2)	± 2%
(f) Change in cloudiness	± 1%
Random Standard Errors	
3. AD direct sun observations	
– optimal	± 1.5%
– average	± 3%
4. Zenith sky observations	
– optimal	± 2.5%
– average	± 5%

* Using the usual convention ±0.5% means that the % error from this source lies between the limits -0.5 and +0.5, that is, in the interval (-0.5, +0.5)%.
**This is not really an error, but can affect interpretation of stratospheric ozone trends.

- The question of whether variations related to solar activity affect Dobson spectrophotometer A-, B-, C-, and D-wavelength extra-terrestrial constants, L_o, is of interest since a Dobson instrument calibrated on an absolute scale at a time of a minimum in sunspot number might yield erroneous data as solar activity gradually increased to a sunspot number maximum. However, some preliminary evidence exists (Komhyr, personal communication) to indicate that significant Dobson instrument extra-terrestrial constant variations do not occur during the course of a sunspot cycle, at least for the double pair wavelengths such as the AD and CD.

- No new information about the effect of aerosols on the accuracy of Dobson spectrophotometer total ozone is available, except confirmation by Mateer and Asbridge (1981), using Toronto Dobson spectrophotometer total ozone data, that the simple haze formulation proposed by Dobson is consistent with observations, and that the observational evidence supports not only the internal consistency of the present A, C, and D wavelength absorption coefficients but, also, confirms the recommended use of the AD double pair wavelengths as the standard for total ozone measurements.

- While the traditional view has been that ozone originates in the stratosphere and diffuses downward into the troposphere to be destroyed at the Earth's surface, the possibility has been suggested of local synthesis of ozone in clean tropospheric air (see, for example, Crutzen, 1974; Chameides and Walker, 1976; Fishman et al., 1979b; Liu et al., 1980). This raises the possibility that tropospheric ozone concentrations are being subtly perturbed by man-made pollution sources. It is well known that ozone is produced photochemically in highly polluted air. Indeed, under conditions of high insolation and extreme pollution, the near-ground photochemically produced ozone can approach an amount equal to 10% of the total ozone column.

At remote sites, it does not appear that the surface ozone concentration is changing with time. This is shown by the NOAA/GMCC surface ozone measurements made at various nonurban locations during 1973 through 1979 (see Figure 2-3). Some available ozonesonde and Umkehr data, on the other hand, suggest that tropospheric ozone amounts at mid-latitudes of the Northern Hemisphere have increased during the past decade (see discussion that follows). However, measurements of tropospheric ozone using ozonesondes or by the Umkehr method are, in general, not sufficiently accurate to insure that these measured increases are real. Also, some of the "observed" changes in ozone may reflect secular changes in local or regional pollution rather than global pollution.

At most operating Dobson spectrophotometer stations throughout the world, the effect of ozone produced in polluted tropospheric air on background total ozone measurements is believed to be small. Definitive data are, however, not available. Research in this area is needed, particularly at stations subjected to frequent episodes of high local pollution.

Dobson spectrophotometer ozone measurement errors also occur when observations are made in polluted air containing trace gases that absorb UV radiation at the Dobson instrument wavelengths (Komhyr and Evans, 1980). Among such trace gases are SO_2, NO_2, N_2O_5, H_2O_2, HNO_3, acetaldeyde (CH_3CHO), acetone ($(CH_3)_2CO$) and acrolein (CH_2CHCHO). Of these, the interference caused by N_2O_5, H_2O_2, HNO_3, acetaldeyde, acetone and acrolein is negligible (see Table 2-2). SO_2 and NO_2, however, are potentially capable of causing errors that approach 25% and 5%, respectively, in instances of extreme pollution and for ozone observations on AD wavelengths. At most Dobson instrument stations throughout the world such interference is believed to be small, but recent observations indicate that it might not be negligible. Research in this area is needed at the few Dobson instrument stations where SO_2 pollution may be increasing. We note that the estimates for the effect of SO_2 were made using absorption coefficients given by Thompson et al. (1963). More recent measurements of these coefficients, when used with the Dobson or Brewer ozone spectrophotometers, yield SO_2 amounts about twice as large as when the Thompson-Komhyr coefficients are used (Evans et al., 1980). For Dobson AD measurements, 0.001 atm-cm of SO_2 causes an apparent increase in ozone of 0.001 atm-cm.

Ground Based: M-83 Photometer

The M-83 makes use of two relatively broad band filters for determination of total ozone by direct Sun or zenith sky observations. The major errors associated with ozone measurements using the M-83 are:

- Instrument errors involving the standardization and stabilization of the filters used in the instrument.

- Strong air mass (along column) bias because of the large bandwidth of the filters.

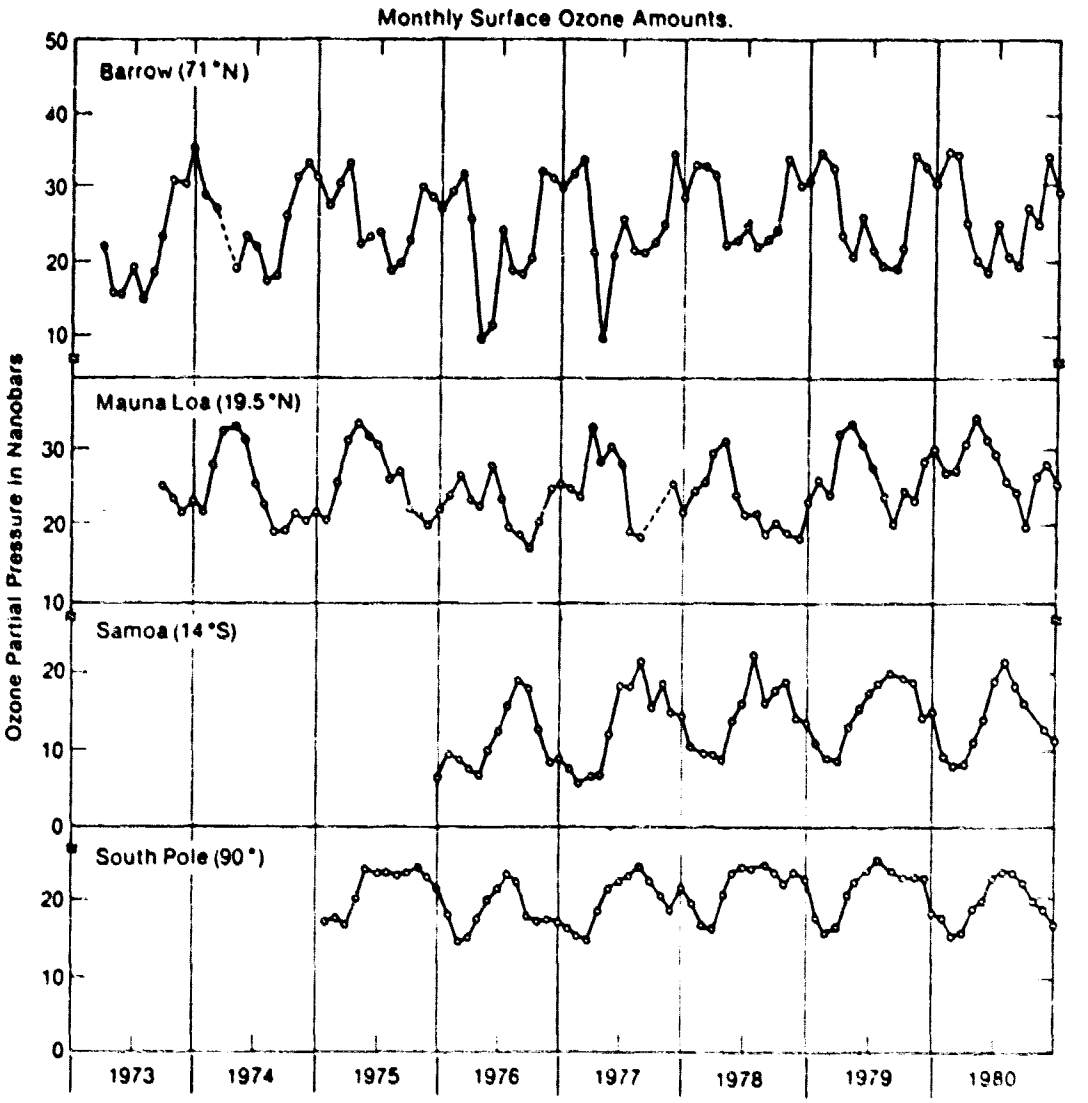

Figure 2-3. Monthly mean surface ozone (1973-1980) (from Oltmans, 1981).

Table 2-2

Dobson Spectrophotometer Ozone and Other Trace Gas Species Effective Absorption Coefficients (Values in brackets are Dobson instrument percent ozone measurement errors for an assumed background ozone amount of 0.300 atm-cm, an assumed one km thick mixing layer, and the indicated maximum trace gas amounts that may occasionally be present in extremely polluted air.) (Komhyr and Evans, 1980)

Mean Wavelength (nm)	Abs. Coeff. Designator	Decimal Absorption Coeff. cm^{-1}								
		O_3*	SO_2	NO_2	N_2O_5	H_2O_2	HNO_3	Acetaldehyde	Acetone	Acrolein
λ = 305.5	a		3.24	2.07	0.18	0.065	0.044	0.64	0.25	0.39
A	a'		0.14	3.59	0.03	0.025	0.011	0.17	--	0.67
λ' = 325.4	$a_A = a - a'$	1.748	3.10	-1.52	0.12	0.040	0.033	0.47	0.25	-0.38
λ = 308.8	a		4.75	2.20	0.16	0.056	0.038	0.58	0.21	0.44
B	a'		0.06	3.90	0.05	0.021	0.007	0.11	--	0.70
λ' = 325.1	$a_B = a - a'$	1.140	4.69	-1.70	0.11	0.035	0.031	0.47	0.21	-0.26
λ = 311.45	a		2.18	2.46	0.13	0.049	0.033	0.52	0.18	0.48
C	a'		0.04	4.14	0.04	0.018	0.003	0.07	--	0.73
λ' = 332.4	$a_C = a - a'$	0.800	2.14	-1.68	0.11	0.031	0.030	0.45	0.18	-0.25
λ = 317.6	a		0.99	2.92	0.09	0.036	0.022	0.34	0.10	0.58
D	a'		0.02	4.89	0.03	0.012	--	0.03	--	0.71
λ' = 339.8	$a_D = a - a'$	0.360	0.97	-1.97	0.06	0.024	0.022	0.31	0.10	-0.13
AD	$a_{AD} = a_A a_D$	1.388 (8.3%)	2.13 (25.6%)	0.45 (5.4%)	0.06 (0.01%)	0.016 (0.01%)	0.011 (0.01%)	0.15 (0.04%)	0.15 (0.07%)	-0.25 (-0.30%)
AC	$a_{AC} = a_A a_C$	0.948 (8.3%)	0.96 (16.9%)	0.16 (2.8%)	0.01 (0.01%)	0.009 (0.01%)	0.003 (0.01%)	0.02 (0.04%)	0.07 (0.05%)	-0.13 (-0.23%)
AB	$a_{AB} = a_A a_B$	0.608 (8.3%)	1.59 (43.6%)	0.18 (4.9%)	0.01 (0.01%)	0.005 (0.01%)	0.002 (0.01%)	0.0 (0.0%)	0.04 (0.04%)	-0.12 (-0.33%)
BD	$a_{BD} = a_B a_D$	0.780 (8.3%)	3.72 (79.5%)	0.27 (5.8%)	0.05 (0.02%)	0.011 (0.01%)	0.009 (0.02%)	0.16 (0.34%)	0.11 (0.09%)	-0.13 (-0.28%)
BC	$a_{BC} = a_B a_C$	0.340 (8.3%)	2.55 (125.0%)	-0.02 (-1.0%)	0.0 (0.0%)	0.004 (0.01%)	0.001 (0.01%)	0.02 (0.10%)	0.03 (0.06%)	-0.01 (-0.05%)
CD	$a_{CD} = a_C a_D$	0.440 (8.3%)	1.17 (44.3%)	0.29 (11.0%)	0.05 (0.04%)	0.007 (0.01%)	0.008 (0.03%)	0.14 (0.53%)	0.08 (0.12%)	-0.12 (-0.45%)
Estimated Maximum Trace Gas Mixing Ratios in Polluted Air, ppm		0.250	0.500	0.500	0.010	0.010	0.050	0.050	0.020	0.050

*Ozone absorption coefficients are values adopted for use by IAMAP in 1968.

- Errors arising from the use of empirical charts for ozone determination from the instrument measurement.

M-83 observations are currently taken at about 30 stations mostly in the U.S.S.R. and some Eastern European countries. Of these, about 15 stations have data for the past 15 or more years.

Changes in the optical system (improved light filters) and calibration procedures used with the M-83 were made starting in 1971. As a result, the data variances have been reduced by a factor of about three but are still somewhat larger than variances derived from ozone observations taken at the same latitude with Dobson instruments.

The root mean square difference (RMSD) between satellite and Dobson measurements, and satellite and M-83 measurements, are shown in Figure 2-4(a). The correlations between the satellite/Dobson data and between the satellite/M-83 data are shown in Figure 2-4(b). Both sets of calculations are given for the period of useful BUV observations. (The BUV observations will be discussed separately below.)

For the BUV/Dobson comparison, the RMSD is seen to be reasonably constant through this period at about 20 Dobson units with the correlation between the two sets of data pairs better than 0.90. For the BUV/M-83 comparison, the results before 1974 show an uncomfortably large RMSD difference of the order of 50 Dobson units but is reduced to a value only slightly larger than that for the BUV/Dobson set after 1974. The correlation coefficient between the BUV/M-83 data pairs also is quite low (~0.7) until 1974 after which it is only slightly lower than that for the BUV/Dobson set. This rather dramatic improvement of the M-83 total ozone observations after 1974 will be of considerable help in evaluating realistic long term ozone variations over a large area of the Northern Hemisphere.

The measurement precision for the improved M-83 for observations taken in relatively clear air and for solar zenith angle less than 60° is of the order of ±5% for monthly average amounts.

Satellite Measurements

Satellite measurements of total ozone have been made continuously since the launch of the Infrared Interferometer Spectrometer (IRIS) and Backscatter Ultraviolet (BUV) instruments on Nimbus 4 in 1970. (There was an 8-month interval between the end of IRIS observations on Nimbus 3 and the launch of Nimbus 4.) IRIS provided data for approximately 10 months, and the BUV provided data for more than 7 years before being turned off in 1977. The SBUV and TOMS instruments were launched on Nimbus 7 in 1978 and are still functioning. Beginning in early 1977, four Air Force Block 5-D satellites carrying the Multifilter Radiometer (MFR) instrument with a single infrared ozone channel (1022 cm^{-1}) were flown and provided data between early 1977 and early 1980. The NOAA operational satellites with the TOVS instrument, which includes a single channel for measurement of total ozone, began flying in early 1979. Thus, there is a continuous record of total ozone measurements beginning in 1970, and even though there have been instrument changes, there have also been overlaps in time so that efforts can be made to reconcile the data and produce a continuous global ozone history over 11 years in length.

Tables 2-3 and 2-4 provide more details on available satellite total ozone measurements, together with some characteristics of the measurements, such as accuracy, precision, field-of-view, coverage, sampling, and data availability. More detailed estimates of random and systematic errors for each experiment are given in Table 2-5. These data sets are not archived at a common location; therefore, those desiring the data must contact the individual archive or, in some cases, the investigator for each experiment.

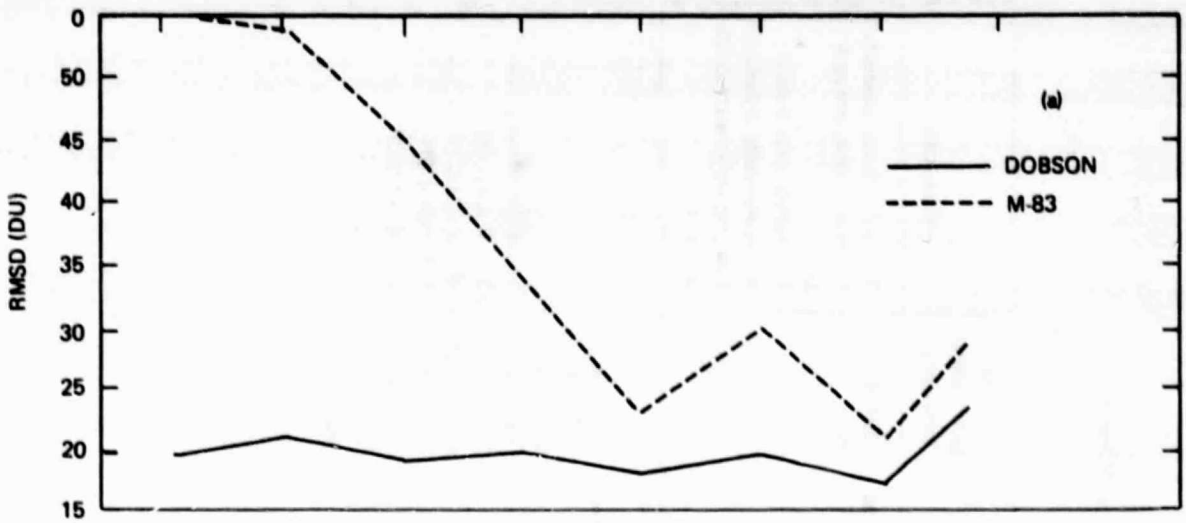

Figure 2-4a. RMS difference between BUV/M-83 and between BUV/Dobson total ozone observations.

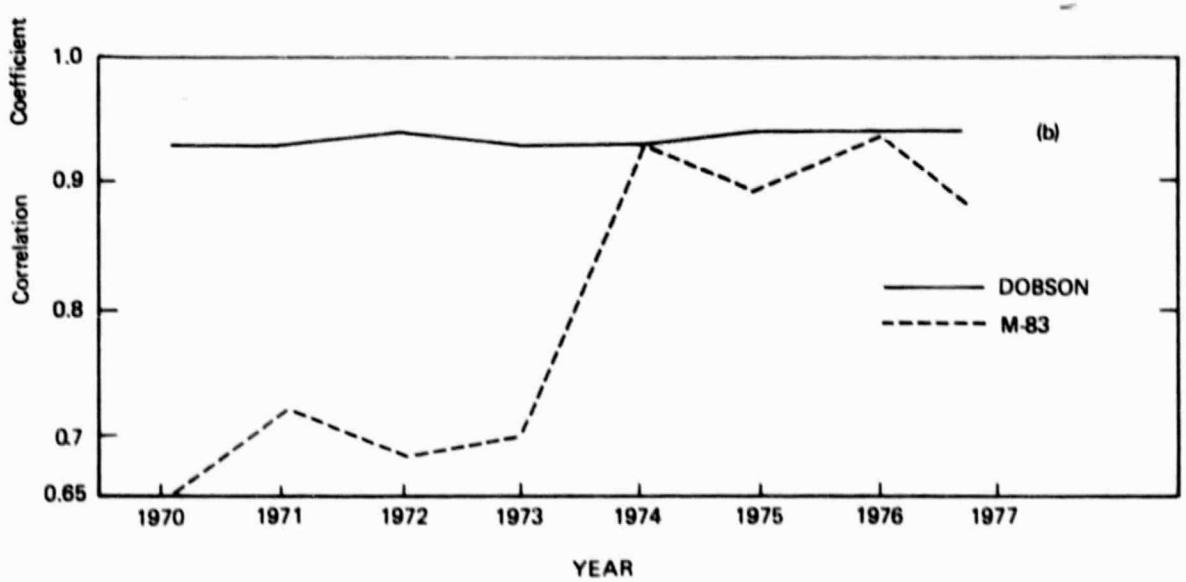

Figure 2-4b. Correlation for BUV/Dobson and BUV/M-83 total ozone observations.

Table 2-3
Satellite Measurements of Total Ozone - Measurement Parameters (continued)

Instrument	Satellite	Time Period	Lat. Range (Deg.)	Spatial Resolution (km)		Duty Cycle	Estimated Measurement Uncertainty	Comments
				Along Track	Cross Track			
IRIS	Nimbus 3 Nimbus 4	4/69-7/69 4/70-1/71	80 S to 80 N	Nadir IFOV = 96 km Near contiguous FOV along track	2500 km Instrument is nadir looking	Continuous	5-20% A 5% P	Thermal emission measurements at ~noon and midnight Comparison with Dobson shows seasonally dependent bias, greatest in winter, high latitudes
MFR	DMSP Block 5D F-1 F-2 F-3 F-4	 3/77-7/77 7/77-2/80 8/78-1/80 6/79-1/80	All Lat. (98° polar Orbit)	Nadir, circular dia = 39 km 207 km between nadir soundings	IFOV Instrument is nadir looking with cross track scan capability of 1021 km on each side of nadir; 58 km to 157 km between cross track IFOV centers	Continuous	There is a 3-5% bias when compared with Dobson spectrophotometers (MFR <Dobson) No estimate of precision.	Equatorial crossing times F-1 12 AM & PM F-2 10 AM & 10 PM F-3 7 AM & PM F-4 10 AM & PM

NOTE: IFOV denotes instantaneous field-of-view
A denotes accuracy
P denotes precision

Table 2-3
Satellite Measurements of Total Ozone - Measurement Parameters

Instrument	Satellite	Time Period	Lat. Range (Deg.)	Spatial Resolution (km)		Duty Cycle	Estimated Measurement Uncertainty	Comments
				Along Track	Cross Track			
TOVS	TIROS-N NOAA 6 and subsequent NOAA spacecraft	5/79 to Present	All Lat. (Polar Orbit)	Circular IFOV Dia = 15 km Retrieval FOV Dia = 200 km 100 km between nadir soundings	Instrument is nadir looking with cross track scan capability of ±1120 km	Continuous after 5/79	With Dobson A Approximate 6% P	
BUV	Nimbus 4	4/70-5/77	80 S to 80 N	200 km	Orbit spacing	Continuous	2% P	Daytime Only
SBUV	Nimbus 7	11/78 to Present	80 S to 80 N	200 km	Orbit spacing	Continuous	2% P	Daytime Only
TOMS	Nimbus 7	11/78 to Present	90 S to 90 N	50 km	Following orbit to preceding orbit. Instrument has track scan capability.	Continuous	2% P	Daytime Only

NOTE: IFOV denotes instantaneous field-of-view
A denotes accuracy
P denotes precision

Table 2-4.
Satellite Measurements of Total Ozone - Data Information

Instrument	Satellite	Data Availability	Data Products	Format	Investigator, Institution	Comments
TOVS	TIROS-N NOAA 6 and subsequent spacecraft	Data reduced before 6/81 available from investigator. Data reduced after 6/81 archived at NCC Asheville, N.C.	Individual retrievals of total O_3	Magnetic tape	(a) W. G. Planet NOAA/NESS (b) A. J. Miller NOAA/NWS	Data have not been validated to date. Daylight data only have been reduced. Current regression schemes limit data reduction to latitude range 30°S to 60°N. Regression schemes being improved to cover other latitude ranges.
BUV	Nimbus 4	NSSDC	Reduced data (total O_3) zonal means, gridded total ozone)	Magnetic tape	D. F. Heath NASA/GSFC	
SBUV	Nimbus 7	Anticipate archived at NSSDC of first year's data late 1981	Total O_3, UV albedo, atmospheric radiance, solar irradiance	Magnetic tape	D. F. Heath NASA/GSFC	Data being validated by Nimbus experiment team prior to archival
TOMS	Nimbus 7	Anticipate archival at NSSDC of first year's data late 1981	Total O_3, UV albedo	Magnetic tape	A. J. Krueger NASA/GSFC	Data being validated by Nimbus experiment team prior to archival

Table 2-4
Satellite Measurements of Total Ozone - Data Information (continued)

Instrument	Satellite	Data Availability	Data Products	Format	Investigator, Institution	Comments
IRIS	Nimbus 4	Total O_3 from investigator, calibrated radiances from NSSDC	Reduced data (Total O_3)	Magnetic Tape	B. J. Conrath, NASA/GSFC	
MFR	DMSP Block 5D F-1 F-2 F-3 F-4	Reduced data archived at LLNL during 1981	Reduced data (total O_3)	Reduced data on magnetic tape	F. M. Luther LLNL	

Table 2-5
Total Ozone Measurement Errors

TYPE OF ERROR	INSTRUMENT					
	IRIS	BUV	MFR	SBUV	TOMS	TOVS
SYSTEMATIC						
- Spectroscopic Parameters	5%	*	5%	*	*	N/A
- Instrument Calibration	1%	2%	1%	1%	1%	1%
- Solar Flux Changes	N/A	unknown	N/A	1%	1%	N/A
- Temperature Measurements	1%	N/A	1%	N/A	N/A	N/A
- Long Term Verification/Calibration	---	1%	1%	1%	1%	1%
RANDOM						
- Spectroscopic Parameters	1%	1%	1%	1%	1%	N/A
- Cloud Errors	2%	1%	Unknown	1%	1%	**
- Surface Reflectance Errors	---	1%	1%	1%	1%	N/A
- Aerosol Contamination	2%	0.5%	Unknown	0.5%	0.5%	unknown
- Instrument Noise	4%	1%	1%	0.5%	0.5%	1%
- Algorithm Sensitivity	unknown	2%	unknown	2%	2%	6%

*Uncertainty in knowing cross sections gives error ≤5%
**Ozone derived from "clear" or cloud-free observations

Since the SBUV-type and NOAA infrared instruments are, and will become increasingly important for the purpose of total ozone trend determination, a few remarks about their use for this purpose are made in the following paragraphs.

Principal error sources (see Table 2-5) for BUV type experiments (including BUV, SBUV and TOMS) involve instrument calibration, uncertainty of the relevant absorption cross sections, and the algorithm used in deriving total ozone data from the radiance measurements. Other errors in the BUV technique are associated with instrument noise, and underlying cloud and aerosol effects. In addition, the Nimbus 4 BUV experiment encountered two serious problems that limit use of the data in ozone trend determinations. The first is that the diffuser plate, which allows the solar flux measurements to be made at precisely preset wavelengths, degraded within several months after launch in a possibly wavelength dependent manner. Thus, variations in derived ozone amounts depend on the relative accuracy of the assumed solar fluxes compared to the actual solar fluxes. This could cause a time-dependent drift of the "observed" ozone that could be a function of the solar zenith angle.

The effect of the degradation of the instrument diffuser plate on the reported total ozone has been studied by Fleig et al. (1980), A. Miller et al. (1981), Reinsel et al. (1981b), and Keating et al. (1981), on the basis of comparison of the BUV data and the quasi-synchronous Dobson observations. To the extent that there are no time-dependent instrumental errors in the Dobson measurements, the average difference as a function of time between the two data sets should indicate the effect of the BUV instrument drift. This is shown in Figure 2-5 (after A. Miller et al., 1981) for the period of the Nimbus 4 BUV observations. There is an indicated global average Dobson-BUV bias change of about 8 Dobson units, a drift of approximately 2.7% over 81 months of observations. Using a different averaging method, Keating et al. (1981) determined a similar drift but also found a latitudinal dependence in the bias. It is still not clear, however, how the bias affects the seasonal satellite-derived total ozone values.

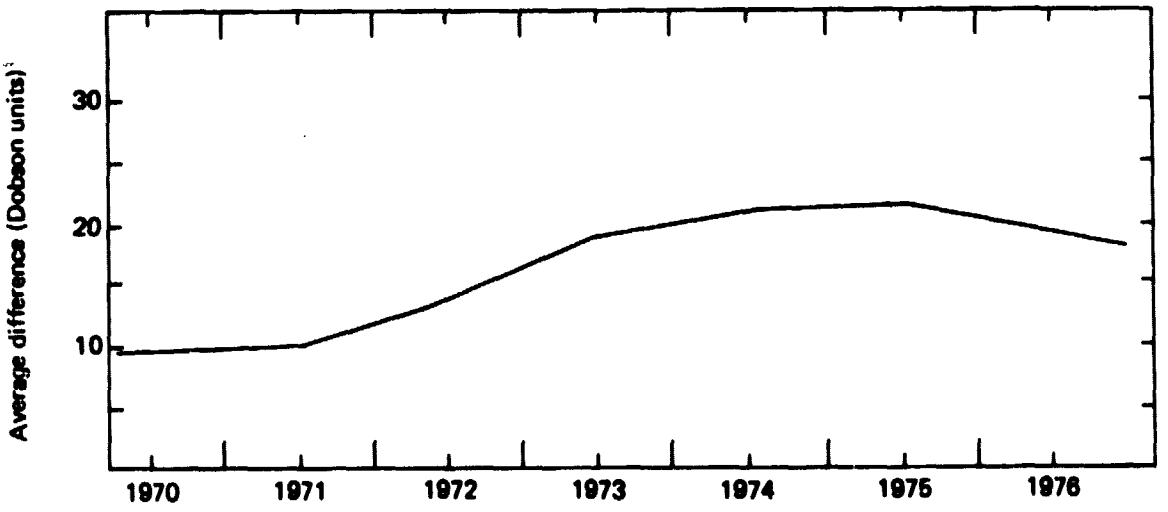

Figure 2-5. Average difference - BUV/Dobson total ozone observations (after A. Miller et al., 1981).

A second problem, potentially more serious for analysis of global ozone changes, is that the solar panels on the Nimbus 4 also suffered degradation in time. This limited the time the experiment could be operating and therefore limited the spatial coverage of the data. The BUV data-point coverage is shown in Figure 2-6 as a function of latitude and time. From the time of the satellite launch in April 1970 to June 1972, when one of the solar panels of the spacecraft failed, there were more than 500 observations per month in each latitude band except during the winter months at high latitudes. After June 1972, the number of data points subsequently decreased, particularly at high latitudes, with some latitude zones having fewer than 500 observations per month over extended time periods. Consequently, care must be taken that the data be considered for appropriate representativeness in any particular analysis, especially when applied to the later years of the observations.

The major problems involving total ozone data from the Nimbus 4 BUV instrument, discussed above, have been corrected in the SBUV instrument on Nimbus 7 which became operational in November 1978.

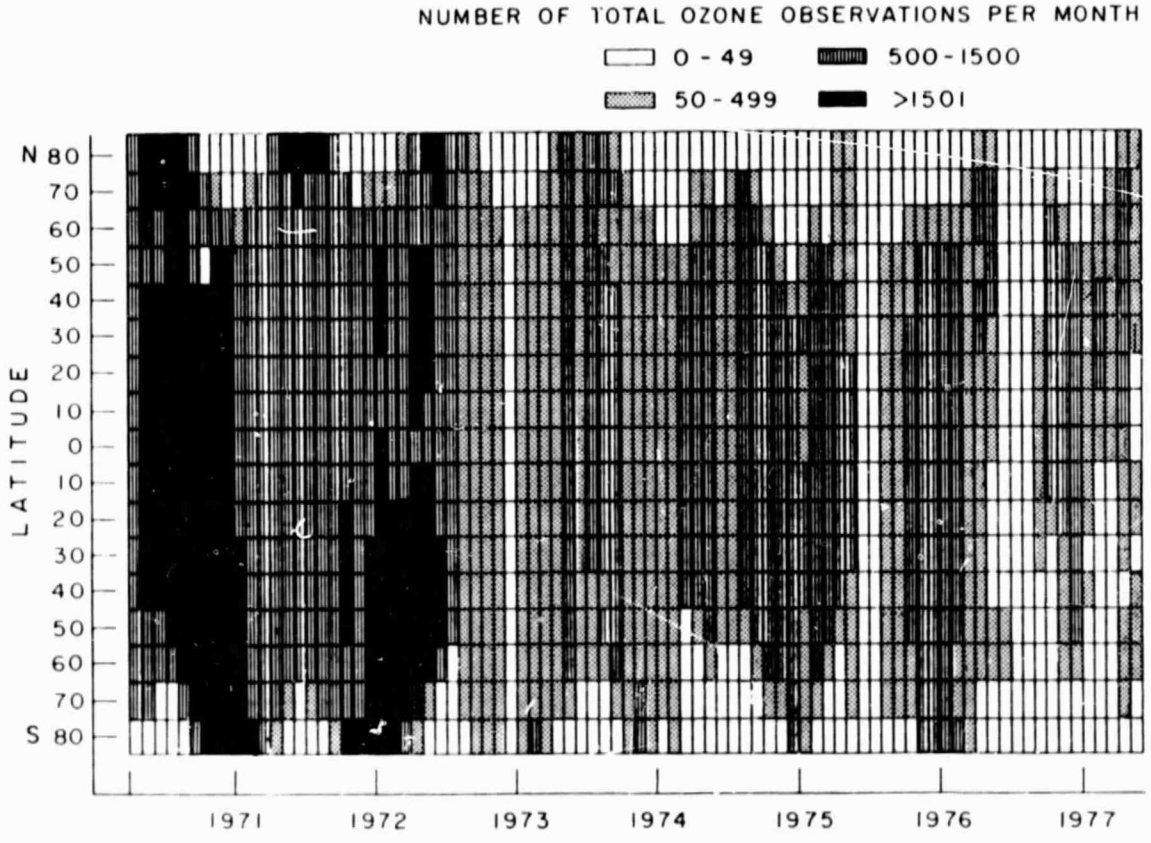

Figure 2-6. BUV data point coverage (Hilsenrath and Schlesinger, 1981).

The principal infrared satellite measurement technique is the TOVS operating on the TIROS-N operational satellite system. 'Reliable' observations using the TOVS instrument started in April 1979 and are expected to continue through 1985. The major errors of the TOVS (Crosby et al., 1980) due to algorithm sensitivity may be relatively large, and the dependence on regression analysis against Dobson data introduces potentially large uncertainties in the derived ozone amounts. The retrieval accuracy of TOVS is about 7% of the mean total amount from 30° to 60°N and about 4.5% in the region 30°S to 30°N. Comparison of the TOVS retrievals with those from SBUV showed an RMS difference of almost 10% of the average total ozone. The present configuration of sounding instruments on the TIROS-N series should be operational until 1984 or 1985. However, the retrieval procedure was designed so that the new instrument configuration would have no negative effects on the accuracy of the retrievals. This should provide a continuous and consistent record of the global distribution of total ozone starting from April 1979 and continuing beyond 1985. Point estimates of total ozone are being archived and will be available from the National Earth Satellite Service. Synoptic analyses of the TOVS data are being constructed on a daily basis and will be available from the National Weather Service.

Infrared emission measurements of total ozone have also been made from the Nimbus 3, Nimbus 4, and U.S. Air Force DMSP satellites.

The time span for each of these measurement programs, however, has been relatively short and their usefulness in total ozone trend analysis is, therefore, quite limited.

Measurement Techniques for Ozone Profiles

Standard techniques for routine measurements of the vertical ozone profile include ground-based Umkehr observations, balloon-borne ozonesondes and satellite measurements. Rocketsonde observations have provided additional information on the ozone distribution, particularly in the 30 to 55 km region. Although there are relatively few rocketsonde observations, these data can be used for cross-validation of the measurements obtained by the other techniques.

Umkehr Observations

Umkehr observations may be taken at any station with a Dobson spectrophotometer. These observations consist of spectrophotometer observations taken on the blue zenith sky while the Sun is between the horizon and an elevation of 30°, during morning or afternoon. Umkehr observations are taken under cloudy sky conditions only at Arosa. Thus, Umkehr observations have a strong fair-weather bias and, therefore, may not be representative of average atmospheric conditions. This may not be important for derivation of ozone trends in the upper stratosphere, but may be a drawback for their use for lower stratosphere trends because ozone in the lower stratosphere is highly correlated with day-to-day weather changes. In addition, random errors in Umkehr profiles are greatest in the troposphere (layer 1) and lower stratosphere (layers 2, 3). (See Table 2-6 for pressure intervals for different layers).

Umkehr observations share most, but not all, of the errors associated with Dobson total ozone measurements. However, Umkehr observations suffer some additional errors which do not significantly influence total ozone measurements. A slight error in wavelength setting can distort profiles obtained from Umkehr measurements. Changes in calibration could thus introduce spurious trend information. Apart from strictly instrument calibration problems, the major sources of uncertainty in the ozone profiles derived from Umkehr observations are those involving the inversion algorithm, the temperature dependence of the absorption cross sections, and the optical effects of both stratospheric and tropospheric aerosols.

Table 2-6
Adopted from WMO, 1981

Aerosol and Temperature Errors for Umkehr Profiles for Moderate Climatological Variations in Aerosol Optical Depth* and Vertical Temperature Profiles

Umkehr Layer No.	Pressure Intervals (mbar)	Error due to temperature variation (%)		Error due to aerosols (%)	
		Winter	Summer	Tropospheric $\tau_d = 0.17$	Stratospheric $\tau_d = 0.017$
9	2.0 - 1.0	10	5	-5 < e < -10	-20 < e < -15
8	3.9 - 2.0	7	4	-4 < e < -7	-10 < e < -5
7	7.8 - 3.9	7	2	-2 < e < -4	-8 < e < -3
6	15.6 - 7.8	2	-1	0 < e < -2	-4 < e < -1
5	31.3 - 15.6	1	-3	0 < e < -2	-3 < e < 0
4	62.5 - 31.3	0	4	-2 < e < +1	-2 < e < +1
3	125 - 62.5	2	-19	-5 < e < 0	-2 < e < +5
2	250 - 125	2	-15	-1 < e < +10	+5 < e < +8
1	1000 - 250	33	-4	-1 < e < +20	+5 < e < +25

* Note: Aerosol optical depth ranges considerably with location. For example, at Mauna Loa it can be an order of magnitude less than 0.17 while it could be double 0 17 during summer in Eastern USA. Occasionally, highly stagnant conditions in Eastern USA cause the aerosol optical depth to become extremely high.

The effects of temperature variations and of aerosols have been calculated, and the associated errors are discussed in WMO (1981) and shown in Table 2-6. While these effects introduce both a systematic bias and random noise into the Umkehr profiles, the single effect with greatest impact on the use of these profiles for determination of long-term upper stratospheric trends is the error introduced by aerosols. Increases in both tropospheric and stratospheric aerosols cause decreases in Umkehr-derived ozone concentrations in the upper stratosphere. This effect is vividly illustrated in the Umkehr record for Aspendale, Australia, where in June 1963, an apparent 50% decrease in Umkehr layer 9 (1 to 2 mbar) occurred between two Umkehr observations which were separated by a few days. Presumably, this decrease was associated with the overhead passage of the stratospheric dust cloud from the Agung volcanic eruption on Bali. These effects may persist for months, or even years, before there is a recovery to normal stratospheric dust levels (DeLuisi, 1979). Similar effects from the dust veils of other volcanoes have also been observed. It must be understood that these apparent results arise because of optical effects of the dust on the Umkehr measurements and do not represent an effect of the dust on the ozone itself (in fact, the dust layer is far removed in altitude from the upper stratosphere). Therefore, analyses of Umkehr profile data for upper stratospheric trends should take special note of dips in the record which follow volcanic events. An attempt is now under way to use dust optical depth measurements at Mauna Loa to establish a table of approximate corrections to Umkehr profiles for these effects (DeLuisi, 1979).

Umkehr measurements provide the longest data set for analysis of extended period variations of ozone in the upper stratosphere. As many as 50 different Dobson stations have reported Umkehr observations since 1956. However, only about 20 are taking Umkehr observations at the present time and, of these, only about 10 stations have observations over the past 15 years or more. Because of their fair weather bias, the frequency of observations may be quite uneven during the various months of the year. A list of stations currently active and with moderately long records is given in Appendix C.

Balloon Soundings

About 20 to 25 ozonesonde stations are presently operational but the observations for varying time periods are very unevenly distributed over the globe. As a result, any worldwide climatology of the vertical ozone distribution (e.g., Dütsch, 1978) is based on an inhomogeneous space and time data set. This has to be kept in mind when such data are compared with satellite results. The certainty in the presently available knowledge of the global vertical ozone distribution is the sum of the instrumental uncertainties quoted above and of inhomogeneity of the available observational material. Ozonesonde stations currently taking ozone profile measurements and with relatively long periods of observations are listed in Appendix C.

There are only 11 stations with continuous soundings for the last 10 to 15 years. Trend analysis may thus be considerably biased by the very inadequate spatial coverage, although observations from the five stations in mid-latitudes of the Northern Hemisphere could be used for comparison with model results for this latitude zone. Global mean values in fixed layers may not be too meaningful, at least below about 35 km, (i.e., at the levels reached by balloons) because of the big differences in vertical distribution with latitude and with season caused by the interaction of chemistry and transport.

The distribution of Umkehr and ozonesonde stations with 10 or more years of observations is shown in Figure 2-7. Seven of these stations take both Umkehr and ozonesonde profile measurements. For discussion of techniques see Chapter 1.

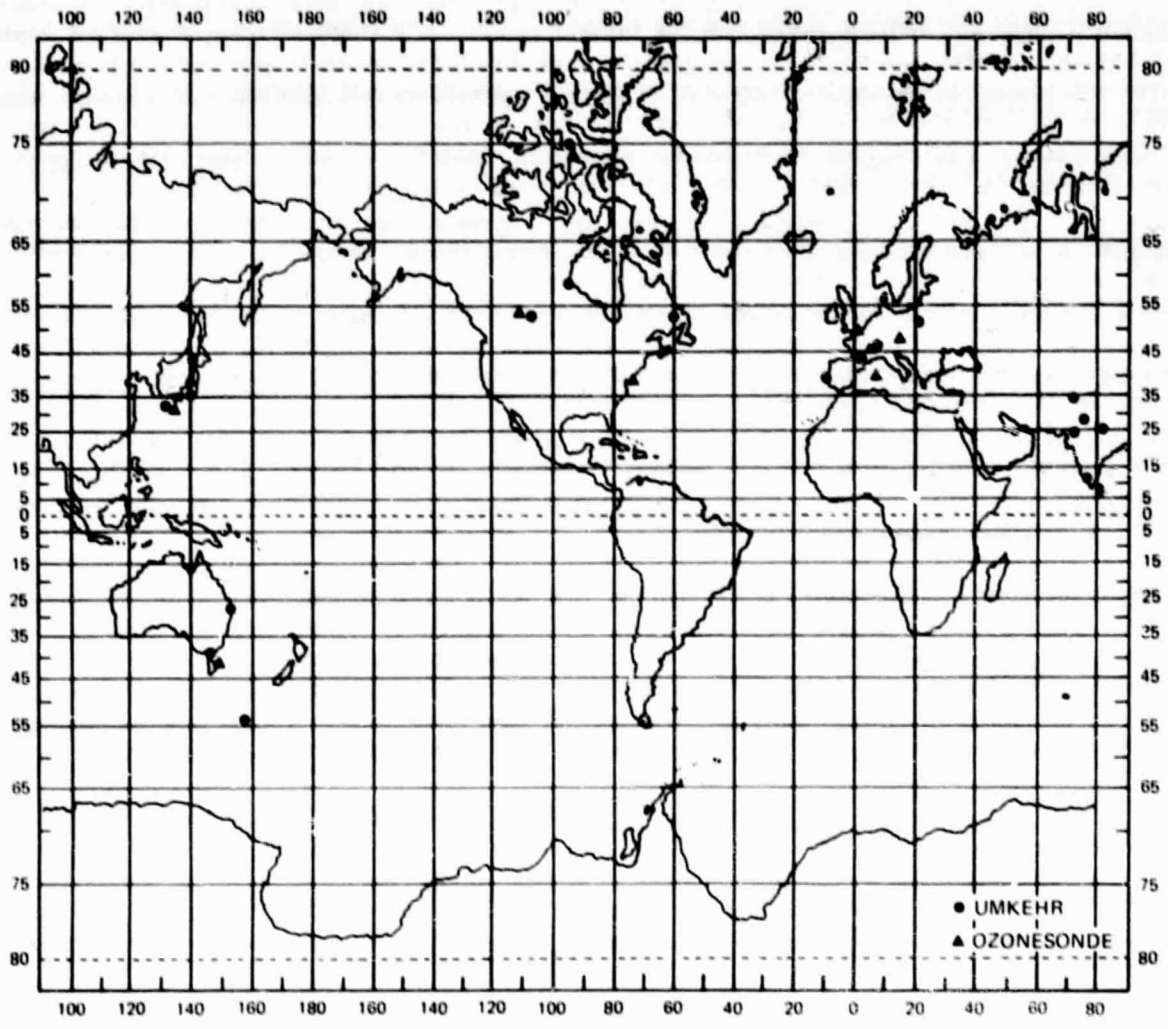

Figure 2-7. Geographic distribution of current Umkehr and Ozonesonde observations with 10 or more years of observations.

Satellite Observations

Satellite observations of ozone vertical profiles starting from the region of peak ozone density and extending to higher altitudes have been made almost continuously since the launch of the BUV on Nimbus 4. (Ozone profile measurements were also measured on OGO-4 by a BUV-type instrument during the period September 1967 to January 1969. Analysis of this data is not presently complete, however.) Figure 2-8 illustrates the measurement periods for ozone profiles that have been made over the last decade by satellite. The Limb Radiance Inversion Radiometer (LRIR) experiment, launched in June 1975 on Nimbus 6, can provide ozone profiles with 3 km vertical resolution from the tropopause to 60 km. There was a period of approximately 18 months (May 1977-October 1978) when no satellite observations of ozone profiles were made because suitable instruments were not available. (Actually, there were BUV measurements at low latitudes on AE-5, but these data have not been reduced to ozone profiles.) The significance of

this break in the data record needs to be evaluated. Nimbus 7, launched in October 1978 carried the Limb Infrared Monitor of the Stratosphere (LIMS) and SBUV experiments which represented updated versions of the earlier LRIR and BUV experiments. The Stratospheric Gas and Aerosol Experiment (SAGE), launched on the AEM-2 satellite in February 1979, can measure ozone profiles with a vertical resolution of better than 1 km above the troposphere. Since this is a solar occultation experiment, only two profiles per orbit are obtained. In the future, the data base from past experiments will be supplemented and updated by data from new instruments: SBUV II, the operational SBUV which the National Oceanographic and Atmospheric Administration (NOAA) will fly on the TIROS-N series of satellites, and SAGE II which will fly on the Earth Radiation Budget Satellite (ERBS). These instruments will continue making ozone profile measurements at least through the 1980s. Also, near the end of the 1980s the Upper Atmosphere Research Satellites (UARS) will carry limb emission sounders to provide ozone profile data over a broad altitude range from about 70 km down into the upper troposphere.

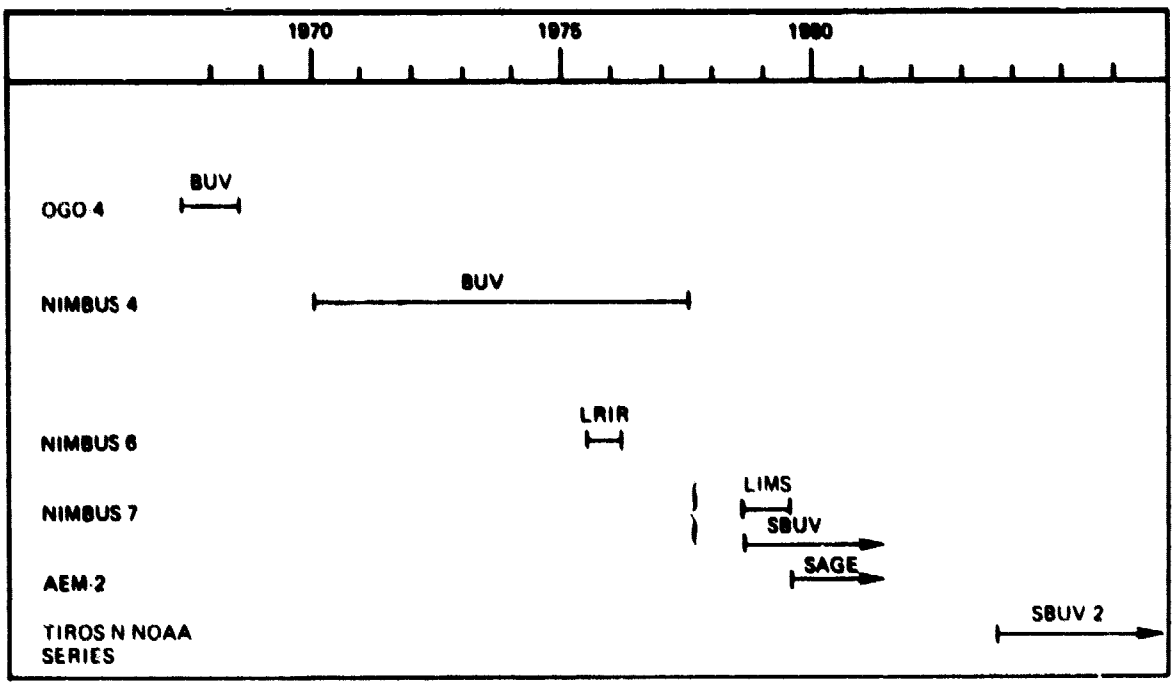

Figure 2-8. Summary of temporal coverage of satellite ozone profile data (Miller, personal communication).

Tables 2-7 and 2-8 provide more details on the available satellite ozone concentration profile measurements together with some characteristics of the measurements and information on the data products and their availability. All of these data sets are, or soon will be, archived at the National Space Sciences Data Center (NSSDC) in Greenbelt, Maryland. Table 2-7 also gives estimated accuracies and precisions associated with each of the available satellite data sets for ozone concentration profiles. These represent the investigators' best estimates of these parameters. In addition, all of the investigators evaluated the systematic and random measurement errors associated with their particular instrument. This information is given in Table 2-9. It is assumed that the Nimbus 6 Limb Radiance Inversion Radiometer (LRIR) and the Nimbus 7 LIMS measurement errors are similar (Gille and Russell, personal communication) and as a result these errors have been combined into single "Limb-IR" data set.

Table 2-7
Satellite Measurements of Atmospheric Ozone Concentration Profiles - Measurement Parameters

Instrument	Satellite	Time Period	Lat. Range (Deg.)	Altitude Range	Spatial Resolution			Duty Cycle	Estimated Measurement Uncertainty	Comments
					Vertical	Along Track	Cross Track			
BUV	Nimbus 4	4/70-5/77	80 S to 80 N	25 to 60 km	6-8 km	200 km	200 km separated by orbit spacing	100%	5% P	Daytime Only
LRIR	Nimbus 6	6/75-1/76	64 S to 84 N	15 to 65 km	3 km	12 km	300 km separated by 26° orbital spacing (one-half orbital spacing by combining ascending/descending nodes)	75%	0.3-1 ppmv	Measurement uncertainty is altitude dependent
SBUV	Nimbus 7	11/78 to Present	80 S to 80 N	25 to 60 km	6-8 km	200 km	200 km Separated by orbit spacing	100%	5%	Daytime only
LIMS	Nimbus 7	10/78-5/79	64 S to 84 N	10 to 65 km	3 km	84 km	300 km separted by orbit spacing (one-half orbit spacing by combining ascending/descending nodes)	75%	0.1-0.3 ppmv	Effective duty cycle includes ERB interference effects. Measurement uncertainty is altitude dependent
SAGE	AEM-2	2/79 to Present	72 N to 72 S	Cloud top to 50 km	1 km below 35 km 5 km above 35 km	200 km	300 km separated by orbit spacing	100%	2-5%	Solar occultation measurement. Fifteen profiles/day (Every 24° longitude). Repeat latitude every 6 weeks.

NOTE: P denotes precision

Table 2-8
Satellite Measurements of Atmospheric Ozone Concentration Profiles - Data Information

Instrument	Satellite	Data Availability	Data Products	Format	Investigator, Institution	Comments
BUV	Nimbus 4	NSSDC	O_3 Profiles	Magnetic tape	D. F. Heath NASA/GSFC	
LRIR	Nimbus 6	Anticipate archival at NSSDC during 1982	Inverted O_3 profiles, coefficients for mapping	Magnetic tape	J. Gille, NCAR	
SBUV	Nimbus 7	Anticipate archival at NSSDC of first year's data late 1981	O_3 profiles, UV albedo, atmospheric radiance, solar irradiance	Magnetic tape	D. F. Heath NASA/CSFC	Data being validated by Nimbus experiment team prior to archival.
LIMS	Nimbus 7	Anticipate archival at NSSDC during 1982	Vertical profiles, coefficients for mapping, latitudinal cross sections, maps on constant pressure surfaces, radiance vertical profiles	Magnetic tape Microfilm	J. Gille, NCAR J. Russell NASA/LaRC	Data being validated by Nimbus experiment team prior to archival.
SAGE	AEM-2	Aerosol in NSSDC late 1981; ozone in 1982, also to AES World Ozone Data Center.	O_3 extinction and number density vs. extinction isopleths altitude vs. latitude and longitude.	Magnetic tape	M. P. McCormick NASA/LaRC	

Table 2-9
Ozone Profile Measurement Errors

TYPE OF ERROR	INSTRUMENTS			
	BUV	SBUV	LIMB-IR	SAGE
SYSTEMATIC				
- Spectroscopic Parameters	Cross Section Error 5%	Cross Section Error 5%	3%	2%
- Calibration	3%	3%	1%	2%
- Temperature Pressure Determination	---	---	0.5%	---
- Aerosol Parameters	---	---	---	---
- Algorithm	1%	1%	---	---
- Solar Flux Changes	5%	1%	N/A	---
- Long Term Verification/Calibration	5%	5%	---	---
RANDOM				
-Spectroscopic Parameters	---	---	---	---
-Instrument Noise	2%	0.5%	1.5-3%*	2%-5%
-Aerosol Contamination	unknown	unknown	---	1%-4%
-Clouds/Background	0%(upper)-1%(lower)	0%(upper)-1%(lower)	---	---
-Pointing Errors	---	---	T	---
-Temperature Determination	---	---	--- **	1%-3%
-Algorithm	3%(upper)-6%(lower)	3%(upper)-6%(lower)	T	---

* = End to end precision based on orbital results 0.3 ppmv on LRIR and 0.15 ppmv on LIMS at O_3 max (32 km),
**Effect included under instrument noise.
T = Small effects predicted theoretically but not explicitly evaluated.

The use of satellite derived ozone profile measurements for the determination of slowly varying changes in upper stratospheric ozone fields places very stringent requirements on the continuity and self consistency of ozone data derived with various experimental techniques by different instruments on different satellites at various intervals in time. To date the most extensive data sets in space and time have been obtained with the backscattered ultraviolet (BUV), solar backscattered ultraviolet (SBUV), and the infrared limb emission (LRIR and LIMS) techniques.

In the investigation of slowly varying changes in the upper stratospheric ozone fields, data sets should be evaluated on the basis of the following criteria:

1. Greatest interval of temporal coverage
2. Similarity of observational technique
3. Similarity of inversion algorithms
4. Continuing assessment/instrument performance from ground truth measurements
5. Observational continuity
6. Independence from recalibration in orbit by indirect methods
7. Availability of the data sets.

As can be seen by referring to Figure 2-6, the only two satellite data sets that come close to meeting these criteria at the present time are the BUV and SBUV experiments. This is due to the duration of the BUV experiments and the similarity between the BUV and SBUV instruments and data reduction algorithms. Because of this, we will briefly discuss some of the factors that need to be considered when using these data sets to infer trends in ozone concentrations.

There are several sources of error with the Nimbus 4 BUV which may introduce long term drifts into the inferred ozone profiles. The two principal unknowns are the effect of the assumption of constant solar spectral irradiance in the region of 250 to 340 nm over the 7-year data record and the wavelength dependent changes in the instrument sensitivity. The most probable consequence of either of the effects is a slowly varying monotonic change with wavelength or a similar change in the ozone profile which most likely would increase with decreasing wavelengths. This would produce the greatest bias at the highest altitudes. Indeed, as was already discussed, a slowly varying drift in the Nimbus 4 measurements was noted when the satellite observations were compared with synchronous collocated total ozone observations taken at Dobson stations (see Figure 2-5).

In addition, the coverage for vertical profile retrievals was compromised by interference from the Van Allen radiation belt in the vicinity of the South Atlantic off the northeast quadrant of South America. Furthermore, the BUV system is dependent upon Umkehr, rocket and balloonsondes for validation assessment of instrument performance, but there has been an insufficient amount of ground truth ozone profile data which can be relied upon to be free from either slowly varying biases or step function changes such as could be introduced when shifting from one system to another as happened to the rocket optical ozonesonde between Nimbus 4 and Nimbus 7. Trend prediction from satellite data could be greatly improved if the absolute accuracy or the long term precision were improved significantly.

The SBUV instrument incorporated three principal changes to overcome the major shortcomings in the Nimbus 4 BUV instrument. The first was that an optical chopper was introduced which eliminates the interference due to the South Atlantic anomaly. Secondly, the diffuser plate is stowed and protected when solar observations are not being made. Hence, degradation of the diffuser plate is no longer a serious problem. Finally, a special observational mode was added which makes it possible to measure either the solar spectral irradiance between 160 to 400 nm or the atmospheric radiances from 190 to 400 nm for investigating variations in the ultraviolet solar flux as well as possible time dependent changes in the scattering properties.

OBSERVATIONS OF TEMPERATURE PROFILES

Satellite measurements of stratospheric temperature profiles have been made on a continuous basis since April 1969 when the Satellite IR Spectrometer (SIRS-A) flew on Nimbus 3. The data have been gathered from several instruments flown on a number of satellites sponsored by NOAA, NASA, and DoD. The NOAA satellites have provided operational temperature data for meteorological purposes. DoD also collects operational temperature data for defense purposes. These data are not available except that the radiance data from the four satellites (F-1 through F-4) which carried the MFR have been made available for analysis along with ozone channel data.

Tables 2-10 through 2-13 provide more details on the available temperature measurements together with information on their characteristics and availability. For convenience, the tables have been divided into two parts: Tables 2-10 and 2-11 list the NASA and DoD (MFR) data, while Tables 2-12 and 2-13 list the NOAA operational data. With the exception of the IRIS and MFR data, all of the temperature results in Tables 2-10 and 2-11 are, or will be available from NSSDC. All of the data in Tables 2-12 and 2-13 are, or will be, available from the NOAA Data Center at Asheville, North Carolina.

ANALYSIS AND INTERPRETATION OF SATELLITE DATA

INTRODUCTION

The characteristics and current status of satellite data sets for ozone and temperature in the upper atmosphere were described in the preceding section. The analysis of these data and subsequent interpretation of results are still at an early stage in most instances. The reasons for the often considerable time between satellite observation and data archival and use are not widely appreciated and hence will be briefly discussed here. Remote sounding of the atmosphere requires highly accurate and precise radiometry or photometry, typically better than 3% accuracy with even better precision. It takes time to demonstrate that these stringent instrument requirements are being met in orbit. Processing algorithms generally must be revised to account for unexpected atmospheric and instrumental effects. Comparative data from in situ measurements often entail further delays. Finally the manipulation of huge data sets -- typically 10^{11} bits/year with large increments arriving daily -- represents a logistics problem that should not be underestimated.

There is no doubt that the existing data hold high potential for addressing key scientific questions. This has already occurred in the case of some data (e.g., BUV results during a solar proton event; dynamics studies using SCR, PMR, and LRIR data). Our ability to study the atmosphere and to understand important problems will accelerate as the Nimbus 7 LIMS, SAMS, SBUV/TOMS, SAM II and SAGE experiment data become more fully analyzed.

In this section, we will first discuss some of the ways in which satellite data may be utilized for global studies with particular emphasis on some of the limitations of such studies. An extensive, but not complete, bibliography of upper atmosphere studies that have been reported to date, is given in Appendix C. This is organized in tabular form by instrument and parameter measured to provide a convenient reference to such studies. This list of references was compiled by questionnaire to the satellite instrument investigators, and should not be taken to be all inclusive. Then, there is a discussion of some of our progress in understanding large-scale dynamics and transport that has come from the analysis of satellite data. Finally, there is a brief discussion of some remaining problems for which the analysis of past, present, and future satellite data should be most important in increasing our understanding.

Table 2-10
NASA and DoD Satellite Measurements of Atmospheric Temperature Profiles - Measurement Parameters

Instrument	Satellite	Time Period	Lat. Range (Deg.)	Altitude Range	Spatial Resolution			Duty Cycle	Estimated Measurement Uncertainty	Comments
					Vertical	Along Track	Cross Track			
IRIS	Nimbus 4	4/70-1/71	80 S to 80 N	10-35 km	~6 km	96 km	Orbit spacing	Continuous	1.5 K	Thermal emission measurements at noon and midnight local time.
SCR 6 Channel	Nimbus 4	4/70-12/72	80 S to 80 N	0-40 km	~7 km		Orbit spacing	Continuous	1 K	
SCR 16 Channel	Nimbus 5	12/72-6/76	80 S to 80 N	0-45 km	~7 km		Orbit spacing	Alternate days to alternate weeks	1 K	
LRIR	Nimbus 6	6/75-1/76	64 S to 84 N	15-65 km	3 km	12 km	Orbit spacing (~2500 km) (~1300 km by combining ascending and descending node data)	75%	1 K A 1 K P	Vertical resolution, accuracy, and precision are somewhat altitude dependent
PMR	Nimbus 6	6/76 - 6/81	80 S to 80 N	40-90 km	~10 km		Orbit spacing	Continuous	1 K	

NOTE: A denotes accuracy
P denotes precision

Table 2-10
NASA and DoD Satellite Measurements of Atmospheric Temperature Profiles - Measurement Parameters (continued)

Instrument	Satellite	Time Period	Lat. Range (Deg.)	Altitude Range	Spatial Resolution			Duty Cycle	Estimated Measurement Uncertainty	Comments
					Vertical	Along Track	Cross Track			
SAMS	Nimbus 7	10/78 to Present	50 S to 70 N	15-90 km	10	100 km based on vertical scan	Orbit spacing Data interpolated to a grid 2.5° latitude x 10° longitude	75% (3 days on, 1 day off)	3 K A 1 K P	Accuracy is a function of height. It is expected to improve somewhat with further processing.
LIMS	Nimbus 7	10/78 to 5/79	64 S to 84 N	10-70 km	~3 km	84 km	Orbit spacing (~2500 km) (~1300 km by combining ascending and descending node data)	75%	3 K A 1 K P	Effective duty cycle including ERB interference effects. Vertical resolution, accuracy, and precision are somewhat altitude dependent
MFR	DMSP Block 5D F-1 F-2 F-3 F-4	 3/77-7/77 7/77-2/80 8/78-1/80 6/79-1/80	All latitude (98° polar orbit)	Upper Trop. to upper strat.		Nadir circular IFOV DIA = 39 km, 207 km between soundings	Instrument is nadir looking with cross track scan capability of 1021 km on each side of nadir. 58 km to 157 km between cross track IFOV centers	100% of orbit	Temperatures have not been retrieved from radiance data	

NOTE: A denotes accuracy
P denotes precision

Table 2-11
NASA and DoD Satellite Measurements of Atmospheric Temperature Profiles - Data Information

Instrument	Satellite	Data Availability	Data Products	Format	Investigator, Institution	Comments
IRIS	Nimbus 4	From investigator	Reduced data T(p)	Magnetic tape	B. J. Conrath, NASA/GSFC	
SCR 6 Channel	Nimbus 4	NSSDC*	Calibrated radiances (from investigator)	Magnetic tape	J. T. Houghton University of Oxford	*Raw data retained by investigator. Contact investigator about availability of retrieved and analyzed data products.
SCR 16 Channel	Nimbus 5	NSSDC	Calibrated radiances (from investigator)	Magnetic tape.	J. T. Houghton University of Oxford	
LRIR	Nimbus 6	Anticipate archival at NSSDC during 1982	Inverted profiles, coefficients for mapping	Magnetic tape	J. Gille, NCAR	
PMR	Nimbus 6	NSSDC	calibrated radiances	Magnetic tape	J. T. Houghton University of Oxford	
SAMS	Nimbus 7	NSSDC	Radiances and gridded temperatures	Magnetic tape	F. W. Taylor University of Oxford	
LIMS	Nimbus 7	Anticipate archival at NSSDC during 1982	Vertical profiles, coefficients for mapping, latitudinal cross sections, maps on constant pressure surfaces, radiance vertical profiles	Magnetic tape, microfilm	J. Gille, NCAR J. Russell, NASA/LaRC	
MFR	DMSP Block 5 F-1 F-2 F-3 F-4	Radiance data available from NOAA or LLNL	Radiance data	Magnetic tape	F. M. Luther LLNL	Radiance data available for temperature profiles from upper troposphere to mid-stratosphere. These data have not been reduced at the present time.

Table 2-12
NOAA Satellite Measurements of Atmospheric Temperature Profiles - Measurement Parameters

Instrument	Satellite	Time Period	Lat. Range (Deg.)	Altitude Range	Spatial Resolution			Duty Cycle	Estimated Measurement Uncertainty	Comments
					Vertical	Along Track	Cross Track			
SIRS A	Nimbus 3	4/69-9/70	80 S - 80 N	0-30 km	5-10 km	300 km	400 km	Continuous	2-3 K	
SIRS B	Nimbus 4	4/70-10/72	80 S - 80 N	0-30 km	5-10 km	400 km	400	Continuous	2-3 K	
ITPR	Nimbus 5	12/72-6/74	82 S - 82 N	0-30 km	5-10 km	400 km	50 km	Intermittent	2-3 K A 1 K P	
VTPR	NOAA 2 NOAA 3 NOAA 4 NOAA 5	10/72 3/79	90 S - 90 N	0-30 km	4-10 km	600 km	500-700 km	Continuous	2-3 K A 1 K P	
HIRS	Nimbus 6	6/75-3/76	80 S - 80 N	0-40 km	5-10 km	200 km	250 km	Intermittent	2-3 K A 1 K P	
TOVS: SSU BSU (HIRS-2) MSU	TIROS-N NOAA 6 and sub-sequent spacecraft	3/79 to Present	90 S - 90 N	0-50 km	5-10 km	210 km	220-500 km	Continuous	2-3 K A 1 K P	Two-satellite system

NOTE: A denotes accuracy
P denotes precision

Table 2-13
NOAA Satellite Measurements of Atmospheric Temperature Profiles - Data Information

Instrument	Satellite	Data Availability	Data Products	Format	Investigator, Institution	Comments
SIRS A	Nimbus 3	NSSDC	Vertical temperature soundings	Magnetic tape	D. Q. Wark NOAA/NESS	
SIRS B	Nimbus 4	NSSDC	Vertical temperature soundings	Magnetic tape	D. Q. Wark NOAA/NESS	
ITPR	Nimbus 5	NSSDC	Vertical temperature soundings	Magnetic tape	W. L. Smith NOAA/NESS	
VTPR	NOAA 2 NOAA 3 NOAA 4 NOAA 5	NCC Asheville, N. C.	Vertical temperature soundings	Magnetic tape	Operational Data No investigator	
HIRS	Nimbus 6	NCC Asheville, N. C.	Vertical temperature soundings	Magnetic tape	W. L. Smith NOAA/NESS	
TOVS: SSU BSU (HIRS-2) MSU	TIROS N NOAA 6 and subsequent spacecraft	NCC Asheville, N. C.	Vertical temperature soundings	Magnetic tape	Operational data	

DIAGNOSTIC STUDIES AND SATELLITE DATA

Satellite data have revealed the structure of phenomena in the stratosphere which could not be resolved with the current network of balloon and rocket observations. In addition to their use in phenomenological studies, satellite data can in principle be used to diagnose (i.e., to describe and understand) the manner in which various physical conservation laws are satisfied in the stratosphere. Diagnosis in terms of the conservation laws is an aid to understanding the maintenance of the properties of the atmosphere and provides an objective method of determining the "importance" of the various phenomena observed.

The conservation laws include the conservation of mass (both for individual constituents and their aggregate), conservation of momentum, and conservation of energy. The latter can be further subdivided into heat balance, kinetic energy balance, available potential energy balance, etc. The conservation laws are normally written in partial differential equation form for the purpose of diagnostic analysis. To approximate the terms in these equations, one requires the values of the variables of interest at all points in the region of interest at one instant in time. In meteorology, these instantaneous fields are often called synoptic fields.

Several steps are required to employ satellite data in diagnostic studies. These are outlined below.

- Convert Satellite Instrument Data to Physical Variables - Instrument counts must be converted to physical data such as temperature and constituent concentrations as functions of pressure at the location and time of measurement. The accuracy of this procedure can be assessed through measurement error budgets based upon the instrument model and by comparison with correlative data.

- Construct Synoptic Fields of Physical Variables - Data from satellites in all but geosynchronous orbits are asynoptic in nature. Sun-synchronous, polar-orbiting satellites generally view a particular geographical region once during the day and once during the night. If only day or only night observations are used to construct a synoptic field, then 24 hours are required to obtain one observation from all geographical regions. Thus, 24 hours may pass before adjacent longitudes are sampled. If day and night observations can be combined in a single analysis, then 12 hours are required. Rodgers (1977a) has developed a numerical filtering approach which overcomes some of the problems encountered in the construction of synoptic fields from asynoptic data. In general, however, only phenomena which are large-scale and slowly varying or very regular in time can be resolved by asynchronous measurement from a single polar orbiting satellite and then be incorporated faithfully into the synoptic fields derived therefrom.

- Approximate Unmeasured Variables - Current satellites measure only temperature and constituent concentrations. To perform budget calculations using the conservation laws, the velocity field is also required. The height of constant pressure surfaces can be obtained from profiles of temperature as a function of pressure with the hydrostatic equation if a boundary condition on the height is known. Various approximations to the fields of the horizontal wind velocity can be obtained from the height fields. The simplest and most often used of these approximations is the geostrophic approximation.

Estimates of the vertical velocity can be obtained by use of the vorticity equation, the thermodynamic equation or their combination in the form of the omega equation. These estimates of the vertical velocity build on the approximations used to obtain the horizontal wind field and also require additional information. Thermodynamic vertical velocities require the heating rates be

known, while the vorticity and omega equations also require assumptions or knowledge about the momentum damping by unresolved scales and boundary conditions on the vertical velocity.

After all of the above steps have been completed, it is clear that any diagnostic studies which we perform with these data are circumscribed by the following limitations.

- Resolution - Only those phenomena which are (1) resolved by the measurement and inversion process, and (2) preserved during the construction of synoptic fields will be represented in the data, and only their influences will appear. Only the largest horizontal and vertical scales and phenomena which are extremely regular or slowly varying in time can be properly resolved with a single polar-orbiting satellite. The effects of phenomena not resolved by the measurement and mapping process will not be explicitly incorporated in the estimated mass, momentum, and energy budgets.

- Accuracy - Even limiting consideration to those phenomena which are well resolved, only diagnostic studies which require precision consistent with the level of approximation applied in determining the basic data are sensible. For example, if the Rossby number for the waves in the stratosphere is 0.1, then, theoretically, the determined geostrophic winds should be within 10% of the true winds if the height field has been perfectly measured. With these winds it is possible to determine product terms such as the zonal mean momentum transport by the waves to within 20% (this error growth due to multiplication is probably unrealistically pessimistic, particularly after zonal averaging).

- Since the tendency term (that which expresses rate of change with time) in conservation equations is generally small compared to those terms which we can estimate only to at best 10 to 20% accuracy, we cannot estimate the terms in the equation accurately enough to determine which of them are most responsible for the tendency. The same argument can be applied to the heat and mass balances to deduce that zonal-mean temperature and constituent tendencies cannot be predicted with current satellite data as input except in those rare instances when the tendency is extremely large.

- Rewriting the conservation equations to eliminate some of the cancellation which appears in zonally averaged equations has improved the clarity of their diagnostic function (Andrews and McIntyre, 1976; Edmon et al., 1980), but it does not alleviate the problem that the wind estimates are accurate to first order, whereas the time tendencies one wishes to explain are normally second order effects.

- Domain of Applicability - Because of the breakdown of simple geostrophic balance relationships between the wind and height fields in the tropics, estimates of the horizontal velocity fields based upon the height field are very inaccurate, if not worthless, in the tropics. Thus, only diagnostic studies of the extratropical stratosphere are possible with satellite temperature data using present techniques.

Despite all of these limitations, diagnostic studies using satellite data are not only useful in increasing our understanding of the dynamics and general circulation of the stratosphere and mesosphere but constitute the principal data base for such studies of global-scale dynamics and transport.

While these limitations should be kept in mind when utilizing satellite data, such data make possible analyses of global-scale dynamics, constituent distribution, and constituent transport above the lower stratosphere that cannot be accomplished by any other means. These analyses have been, and should increase in importance as, a very active and valuable area of stratospheric research (see Gille, 1979, for a review). During the last decade there have been such great

numbers of scientific investigations of the stratosphere using satellite data that it is not practical to do a comprehensive review of these results here. Rather, in Appendix C we list by author and title some of the analyses of satellite data that have been accomplished. This list has been compiled by asking satellite instrument groups for lists of publications that have used their data and is meant to be illustrative rather than comprehensive. There is a brief discussion of some of the scientific output that has come from these satellite data analyses in the next section. Again, this discussion is meant to be illustrative rather than comprehensive.

SCIENTIFIC RESULTS

The previous sections have contained discussions of the capabilities of various satellite instruments that give global data sets from which the distribution of stratospheric parameters can be derived. In Appendix C, an indication has been given of the status of the ongoing research using these data sets. The following section contains a discussion of some of the scientific advances that have come from the analysis of global stratospheric data sets that were derived from satellite measurements. More extensive reviews on this subject are those of Gille (1979) and the discussion in Chapter 5 of NASA RP 1049. In this discussion, we will try to indicate also in what future areas of stratospheric research the diagnostic analysis of global stratospheric satellite data sets should make major contributions over the next few years and beyond.

Mean Atmospheric Temperature Distribution

The described stratospheric satellite data have added greatly to the geographical coverage that was available earlier. This is especially true over oceans, above 30 km, and in the Southern Hemisphere. These data have both confirmed many previously observed features, and added an enormous amount of detail. Differences between Northern and Southern Hemispheres are particularly apparent. The Southern Hemisphere winter polar tropopause (190 K) is colder than its Northern Hemisphere counterpart (205 K) while the Southern Hemisphere summer polar tropopause (235 K) is warmer than the Northern Hemisphere (230 K). These differences in the mean state in the two hemispheres are probably due in part to the variation in the Sun-Earth distance during the course of the year. Other interhemispherical differences can be observed at the stratopause. Labitzke (1974) discussed differences in the temperature regions between Northern Hemisphere and Southern Hemisphere, while Barnett (1974) has discussed their annual variation.

Similarly, the global mean temperature of levels in the middle and upper stratosphere show primarily an annual cycle of a few degrees amplitude (see Barnett, 1974). This is believed to be due to the ellipticity of the Earth's orbit about the Sun, the maximum temperature occurring in December when the Earth is nearest to the Sun. It is an important result because it implies that for these layers (but not for the upper mesophere as noted below), changes of insolation are balanced by changes with each layer independently, whereas such small perturbations might reasonably have been expected to be hidden by vertical heat transfers from other layers.

Hirota and Barnett (1977) have shown that zonal mean temperatures near the winter pole have an almost perfect negative correlation between stratopause and mesopause levels. This was previously well known for seasonal variations (i.e., that the mesopause is hottest during winter whereas the stratopause is hottest in summer), but the measurements show that this is also true on time scales of a few days during warming events, when peaks or dips of temperature at the stratopause are mirrored by dips or peaks respectively near the mesopause. This result together with the early satellite finding by Fritz and Soules (1970) that winter warmings at extratropical northern latitudes were accompanied by global scale decreases of temperature in the tropics and in the Southern Hemisphere clearly points to the important role of variations in meridional heat

transports for warming events. Crane (1979b) has recently studied the annual and semiannual cycles of zonal and global mean temperature in the mesosphere. The annual cycle of the global mean near the mesopause is very much like that at lower levels, having similar amplitude and phase. However, there is also a strong semiannual component near the mesopause, whereas the semiannual component is much weaker at lower levels. Further examination shows that near the mesopause, the half year wave is in phase at all latitudes, thus giving a net global component, whereas at lower levels, the tropical semiannual component is out of phase with mid- and high-latitudes, giving a fairly precise cancellation. There is currently little understanding of these variations.

The mean zonal wind may be calculated from these temperatures, using the geostrophic relationships. Leovy and Webster (1976) compared the Northern and Southern Hemisphere mean zonal winds during winters. They found similar cross sections in early winters (although the strongest winds were 5 to 10° closer to the pole in the Southern Hemisphere). Perhaps most intriguing, they found that the calculated potential vorticity gradient would sometimes satisfy the conditions for barotropic instability.

Planetary Scale Waves

Satellite observations have been very valuable in establishing the climatology and phenomenology of large-scale waves, especially of the propagation of mid-latitude Rossby waves. Planetary scale waves are easily observed, because it is possible to study spatial and temporal variations of radiances without the necessity for absolute calibrations, or for inversion of the radiances to obtain temperatures. Of course, without derived temperatures, only phenomenological studies can be carried out.

Quasi-stationary Rossby waves are particularly suitable for study with nadir viewing measurements because of the large amplitude of the temperature variations, large vertical wavelength, and their small phase motion between satellite observations. In addition, they appear to be ubiquitous, or nearly so, and have been studied by numerous authors. Such studies (e.g., Fritz, 1970) have found traveling and stationary waves with largest amplitudes in winter, as expected, by analyzing SIRS radiances. Quasi-stationary waves in the Northern Hemisphere are twice as strong as in the Southern Hemisphere.

The vertical structure of these waves has also been clarified. Hirota and Barnett (1977) showed that the temperature waves can have significant amplitude to the mesopause at least, with the maximum amplitude occurring as high as 65 km for waves 1 and 2, although Kohri (1981) found maxima at 45 km during a less active winter. He confirmed Leovy and Webster's (1976) finding of large variations in wave amplitude, with maximum amplitudes occurring at 60° in both hemispheres.

Hirota (1976) clearly showed that for wave 1, the wave axis tilts westward with height, except in the tropics. This westward tilt is consistent with our picture of vertically propagating planetary waves, and indicates poleward transport of heat (and associated vertical flux of energy). At a given altitude, the waves tilt toward the east in the poleward direction. This indicates a poleward transport of eddy momentum. Wave 2 has similar behavior, but not as pronounced. Barnett (1975a) has pointed out a previously unnoticed feature; these waves extend across the Equator in the equinoctial seasons.

Dynamical Phenomena and Satellite Data

The structure of the stationary planetary waves in the middle and upper stratosphere, as revealed by satellites generally supports the theoretical ideas of Charney and Drazin (1961), Matsuno

(1970), Dickinson (1968a, 1968b) and others on the propagation of planetary waves in the meridional plane. Kohri (1981), for example, has used LRIR data to show that the term U_{yy}, makes an important contribution to the refractive index and plays an important role in ducting the waves into the upper stratosphere. This behavior was anticipated theoretically by Simmons (1974).

Regular westward propagating waves of period 5 and 2 days have been identified as atmospheric normal modes. The characterization of the structure of the 5 day wave, Rodgers (1977), Rodgers and Prata (1981), for example, now allows the extensive development and refinement of the theory of such oscillations (Geisler and Dickinson, 1976; and Salby, 1981, for example).

In the Southern Hemisphere winter, planetary waves, particularly zonal wavenumbers 2 and 3, have been shown to propagate eastward during winter at quite regular phase speeds (Deland, 1973; Harwood, 1975; Hartmann, 1976a; Leovy and Webster, 1976; Ghazi and Barnett, 1980). A theory that these are upward extensions of long baroclinically unstable waves, has been worked out in detail, based on the idea that such ultra-long unstable waves can readily occur in the Southern Hemisphere but not in the Northern because of the unique structure of the meridionally narrow but intense Southern baroclinic zone (Hartmann, 1979; Straus, 1981). It is possible that such a mechanism occasionally operates in the Northern Hemisphere, but more weakly and largely obscured by other processes.

Diagnostic Studies with Satellite Data

With stratospheric satellite data there is the capability of defining the zonal and time mean structure as well as resolving large-scale slowly varying (with respect to a day) disturbances. It has generally been accepted that, in the stratosphere above the level where synoptic scale disturbances can propagate, there is a region in which large-scale slowly varying disturbances of the type that can be resolved by satellite data are of primary importance. It is believed that the general circulation in this region can be understood strictly in terms of the radiative forcing and the dynamical interaction between large-scale slowly varying waves and the zonal mean flow. It is also believed that at some height farther up in the stratosphere or mesosphere small-scale eddy motions become as important as large-scale eddies in determining the zonal mean climatology. These ideas can be tested by studying the heat, momentum, and energy budgets through diagnostic studies including only those phenomena resolved by the synoptic analyses derived from satellite data. One particular method of testing the consistency of these assumptions is to compare the mean meridional circulations obtained as residuals in the heat and momentum balances. Hartmann (1976b) used SCR data to show that, while these two independently derived meridional circulations agree to within the expected uncertainty in the lower and middle stratosphere, in the upper stratosphere they are qualitatively different. Subsequent analyses of PMR data by Crane et al. (1980) and of LRIR data by Gille et al. (1981) also showed large differences between mean meridional circulations in the upper stratosphere and mesosphere derived from the zonal mean heat and momentum balances respectively. These differences are too large to be explained by the errors on scales resolved by the satellite data and suggest that phenomena not resolved by the data are becoming important. While it was known that at high enough levels tides, gravity waves, and turbulence would become as important as slowly varying planetary scale waves, the diagnostic studies described above provide independent evidence on the altitudes at which these phenomena begin to become important. They suggest that unresolved phenomena are already of major importance at 50 km. The inconsistencies in the large-scale budgets can be rectified by postulating unresolved momentum sources or sinks which produce increasingly large zonal flow decelerations with height. Estimates of the effect of momentum carried upward by unresolved gravity waves seem sufficient to account for the required decelerations (Lindzen, 1981).

Crane (1979a) used Nimbus 4 SCR data to study the energy budget during the major stratospheric warming of January 1973. Energy fluxes and transformations were derived and a budget obtained for each day in a 1-month period. There were two main results: (1) the amplification of the temperature wave in the 10 to 2 mbar layer during the warming resulted from a transfer of eddy potential energy from the 50 to 10 mbar layer, thus within the stratosphere, and not from below 50 mbar, and (2) the eddy kinetic energy maxima at high latitudes were caused primarily by vertical energy flux convergence, whereas at mid-latitudes the maxima were caused by barotropic conversion.

One of the goals for the LRIR data set is to determine the components of stratospheric energetics for different seasons, Kohri (1981) and Kohri and Gille (1981) have calculated some of the components for waves 1 and 2 for December 1975. These confirm some earlier observations that indicate the energy of the eddies is maintained in the lower stratosphere by forced baroclinic conversion, whereas the convergence of upward propagating kinetic energy provides the drive in the upper stratosphere. Of particular interest is the large time variability of the balances that control stratospheric energetics observed.

Total Ozone Distribution

Satellite observations have now provided a picture of the global mean distribution of ozone and its variations with a coverage not previously possible. Two parameters are discussed: the total ozone in a vertical column, and the concentration as a function of altitude, or vertical distribution. The total ozone is of great importance, since this is what protects the Earth's surface from biologically harmful ultraviolet radiation. Corrected results for the first 2 years of Nimbus 4 operation have been presented by Hilsenrath et al. (1979b), Heath (1980), and Ghazi (1980b). They include monthly mean global maps, zonal mean values as a function of time, the annual mean values over the globe (which vary with longitude) and temporal variations of the global total ozone. This latter quantity is not constant, but varies from season to season, and from one year to the next, making a search for trends very difficult, as discussed in Chapter 3. Tolson (1981) and Hilsenrath and Schlesinger (1981) have used the entire 7-year BUV data set to determine variations in the zonal means. Tolson (1981) also investigated the longitudinal waves 1, 2, and 3 in total ozone. Prabhakara et al. (1976) have presented seasonal maps of total ozone based on IRIS results. There have also been analyses of total ozone from IRIS and BUV that suggest a relationship between global total ozone and solar activity (Blackshear and Tolson, 1978; Keating, 1978; Keating et al., 1981). These results are rather controversial (London and Reber, 1979; Reber and Huang, 1981). The satellite maps of total ozone confirm the major features found previously by ground-based measurements, and add a great deal of detail not available otherwise, particularly in the Southern Hemisphere.

Since total ozone is dominated by its concentration at levels where it is a conservative tracer, total ozone distributions are dominated by circulation processes. This is shown clearly by a comparison between TOMS maps and conventional meteorological analyses which shows a concidence between the location of the jet stream and the location of high horizontal gradients in total ozone (Shapiro et al., 1981). A high degree of correlation is found between total ozone and lower stratospheric temperatures which is indicative of their both being under dynamic control. This is especially obvious during a stratosphere warming (Ghazi, 1974).

Vertical Distribution of Ozone

Observations by OGO 4 (London et al., 1977), BUV (Krueger et al., 1973), and LRIR (Gille, 1980) have provided a much more detailed picture of the vertical and latitudinal distribution of ozone

than existed previously. High values occur somewhat above 10 mbar in the tropics, with a tongue of high values extending toward high latitudes near 5 mbar, especially in the winter hemisphere, where they can reach 2 mbar at 60°. These extensions, which may depend on the temperature dependence of the chemistry or on transport processes, were an unexpected feature first discovered in the satellite observations.

The measurements described above have been used directly to test the theories of ozone photochemistry. A variety of ozone measurements in the tropical mesosphere, including LRIR, BUV, occulation measurements by OAO-8, and rockets agree with the theoretically predicted mesospheric ozone concentration. This supports the conclusion that the theory is not fundamentally in error (Gille et al., 1980d).

Ozone Photochemistry and Transport

Simultaneous observation of temperature and ozone has allowed the study of the relation between the temperature and ozone perturbations associated with planetary waves and other dynamical phenomena in the stratosphere. With winds inferred from the temperature field, the transport of trace constituents by resolved phenomena can also be computed.

Ozone and temperature profiles as retrieved from BUV and SCR, respectively were used to calculate the vertical structure of radiative heating/cooling in the tropical stratosphere during the period of a stratospheric warming. The results show that there is a net additional radiative heating in the upper stratosphere of the tropics during the sudden warming (Ghazi, 1980b).

Barnett et al. (1975b) found a high inverse correlation between BUV ozone concentrations and SCR temperatures. From a comparison between their observed correlations and those derived from photochemical theory they deduced that odd-hydrogen chemistry had roughly three times the effect of the Chapman chemistry on ozone loss in the vicinity of the stratopause. Ghazi et al. (1976) found a similar effect.

Dickinson (1969) has shown that during periods of weak mean winds radiative damping will tend to strongly dissipate vertically propagating planetary waves. If the damping rate calculated by Ghazi et al. (1979) for the Southern Hemisphere stratopause region in October of the order of 0.35 day^{-1} is representative, then radiative damping may play an important role in the wave-mean flow interaction process which generates late winter stratospheric warmings.

Gille et al. (1981) have presented data exhibiting general agreement with the theoretical picture given by Hartmann and Garcia (1979). Their LRIR data showed that there was an underlying region in which motions dominate the ozone distribution, and an overlaying photochemically controlled region in which the temperature dependence of ozone reaction rates significantly affects the ozone distribution. The latitudinal distribution of these regions shows dynamic control extending up to only 30 km at low latitudes, but at least up to 60 km in high winter latitudes with a chemically controlled region above. The region between is characterized by the largest eddy transports. The information on the latitudinal variations of these regions should provide useful tests for numerical models in the future.

The ability to measure ozone both day and night with the limb IR technique allows a study of the diurnal variation of ozone. Initial results have been presented by Anderson et al. (1981). These show detectable diurnal variations above 50 km, with magnitudes which support present theoretical expectations. However, there appear to be some disagreement between these observations and theory on the detailed temporal variation.

OBSERVATIONAL STUDIES OF STRATOSPHERIC DYNAMICS AND TRACE CONSTITUENT TRANSPORT: FUTURE PROGRAMS

Satellite data provide a series of global temperature and ozone observations which can be used for the observational study of the dynamics of the stratosphere and mesosphere. These data can be used to approximate winds and transports of trace constituents. The present discussion is divided into the following two parts:

- The philosophy and limitations of diagnostic studies using satellite data and some recent results.
- Some of the important remaining questions.

While, as has been indicated earlier, there have been a number of advances in our knowledge based upon satellite observations, the periods for which the behavior of the middle atmosphere has been carefully and thoroughly analyzed have been short and sporadic. A unique characteristic of satellite instruments is their potential to provide relatively homogeneous spatial coverage with uniform coverage in time. This type of monitoring is by no means a routine function, but rather is an essential component of research on the fundamental problems of the middle atmosphere. Blackmon (1976), Lau and Wallace (1979) and others have indicated that we are only now beginning to learn from our troposphere experience the importance of a long homogeneous global data base for sorting out mechanisms of atmospheric variability. It is difficult, for example, to answer questions using data sets which have large gaps in space and time. Length of record and homogeneity are also obviously vital for trend analysis.

Unfortunately, uniformity in time and space coverage does not characterize all of the existing satellite data sets for temperature and ozone, two of the most fundamental variables, and the two for which the measurement techniques are best developed. It is important, therefore, that every effort be made to ensure continuity and homogeneity in future measurement programs for these variables. Furthermore, as techniques for measuring other parameters which are central to our understanding of the chemistry and dynamics of the stratosphere are proven, these should be added to our complement of monitoring tools as rapidly as resources allow.

Outstanding Questions

Let us consider some of the outstanding issues which future satellite measurements of ozone and dynamical parameters can be expected to address. Much of the interannual variability in the middle atmosphere is associated with stratospheric warmings, but despite the available data and a promising theoretical context, due mainly to Matsuno (1971), they are not yet understood at a sufficient level of detail to explain why major warmings occur in some years, but not in others. A detailed understanding of their mechanism remains to be developed. Similarly, there exists a detailed theory of the atmospheric tides and some comparisons of the predictions of tidal theory with a scattering of rocket data, but the detailed structure of the tides between 30 and 90 km is still unknown. It is not known, for example, whether the topographic components of the tides, which are dominant in most of the radiosonde data, continue to dominate above 30 km. To date, satellites have not contributed significantly to the solution of this problem but could do so.

The mechanism of the Quasi Biennial Oscillation (QBO) now seems to be fairly well understood. The semiannual oscillation, however, which has amplitude maxima near the stratopause and near the mesopause, is still not understood, although Hirota (1979) has shown that both rocket and satellite data give indications that Kelvin waves of vertical wavelength ~15 km may be responsible. Hirota's findings remain to be convincingly demonstrated with a data set more well-suited to observing waves of relatively small vertical scale.

Concerning ozone, the leading question is: are there long-term trends at any level which can be plausibly associated with photochemical factors? Although there have been attempts to answer this question for total ozone, the answers are still controversial. Since anthropogenic and natural perturbations produce much larger effects at certain levels than they do in the total ozone, vertical profiles of ozone should be relatively sensitive to such perturbations and an attempt has been made to isolate both natural and man-made perturbations in BUV, SBUV and infrared limb data. However, this question can be answered unambiguously only by long-term monitoring with instruments of adequate stability and precision. Although this question of long-term trends in ozone concentration remains unclear, there is clearly significant interannual variability in total ozone and in the vertical distribution of ozone. There is, for example, a component associated with the QBO, which in the tropics has been suggested to be consistent with Hadley cell modulation (Tolson, 1981). The mechanism for the quasi-biennial ozone variation remains rather obscure, however, especially at higher latitudes.

In the future, coordinated studies using balloon-borne grab-sample measurements of constituent profiles together with three-dimensional fields of wind, temperature, and constituents inferred from satellite measurements will provide great insight into the behavior of these constituents and will reduce somewhat the uncertainty introduced into the interpretation of grab-sample profiles by the large variability produced by motions.

Another set of questions concerns the ozone concentration in the middle and upper mesosphere. There are very large differences between measurements by different experimenters using different techniques in this region, much larger than can be accounted for by existing theory. Measurements of Hays and Roble (1973) show a secondary ozone peak above 75 km, a feature which is consistent with some photochemical models, but it is not yet clear whether this structure is a prevailing feature of the normal mesosphere. Better information on the vertical ozone concentration and its seasonal and latitudinal variation in the mesosphere is a prerequisite for improved dynamical modeling since the temperature of the mesosphere is so sensitive to ozone concentrations. Photochemically, there is some evidence of diurnal variation, but as yet a detailed comparison between data and models cannot be made.

A promising future development in satellite observation of the stratosphere is the anticipated direct measurement of the global wind field on the UARS satellites. At the present time, stratospheric winds are derived from satellite measurements by integrating the derived temperatures upward to get the geopotential height field using the hydrostatic equation. The wind field is then derived by applying the geostrophic wind relation or some variant thereof (e.g., the gradient wind). Some of the difficulties in this procedure are that measurement inaccuracies in the temperature field are reflected in the derived wind field and, more importantly, this procedure cannot be used near the Equator due to the breakdown of the geostrophic relation. It is expected that the simultaneous measurement of stratospheric winds and temperatures on UARS will lead to more consistent diagnostic analyses of the observations.

MEASUREMENT OF SMALL-SCALE STRATOSPHERIC PROCESSES

The principal emphasis of work on multidimensional dynamics and transport in the stratosphere has been on studying and modeling the global scale circulation. The global scale dynamics and composition structure of the stratosphere is known to depend on small-scale physical processes in several ways. Thus, in order to understand the global scale structure of the stratosphere in a satisfactory manner we must have a sufficient knowledge of certain small-scale processes to understand their effects on global scale stratospheric structure. Measurement of these small-scale processes cannot easily be done with satellite instrumentation, but ground-based and in situ measurement programs can be designed which, together with theoretical modeling efforts, can bring our understanding of these processes to the point where a proper treatment of their

effects on large-scale stratospheric processes can be included in multidimensional models. Two examples of this interplay between small-scale and global-scale stratospheric processes are the effects of gravity waves and turbulence in decelerating the mean zonal flow in the stratosphere and mesosphere and the role of small-scale motions in troposphere-stratosphere constituent exchange. In the following, we will give some scientific background on these topics and describe how some existing observational techniques can be used to enhance our understanding of these areas to the point where their effects on the large-scale stratosphere can be included properly in modeling.

Momentum Dissipation by Small-Scale Motions

Proper modeling of the large-scale stratospheric circulation is found to require an accurate representation of dissipation terms in the zonal momentum equation (Leovy, 1964). Recent models of Schoeberl and Strobel (1978a) and Holton and Wehrbein (1980a) have confirmed Leovy's conclusion and have tried to parameterize this effect through the specification of a height-dependent Rayleigh drag term (a linear drag term that gives rise to a deceleration proportional to the magnitude of the zonal velocity). The source of this physical effect is believed to be the vertical transfer of momentum by gravity waves that originate at the Earth's surface or in the troposphere where the zonal wind speeds are small or zero. As gravity waves propagate upward, their amplitudes tend to grow exponentially due to the upward decrease in air density. At the altitudes where these gravity waves break, they will exert a drag which will decelerate the mean flow. Thus, in this picture the momentum dissipation acting on the large-scale flow is dependent on small-scale motions that cannot be modeled practically in a global circulation model and, hence, must be parameterized. The GFDL approach in general circulation modeling of the stratosphere has been different. Rather than utilizing the "required" Rayleigh drag in their model, they have used a Richardson number dependent diffusion (Fels et al., 1980) formulation as a momentum dissipation effect. Thus, the planetary scale motions in their model generates wind shears that produce vertical momentum diffusion. One finds by this approach, that some momentum drag is required in addition to this diffusion to bring the model results into agreement with observations. The wave stresses produced by gravity waves propagating from the troposphere appear to be necessary to account for the decrease in the mean zonal wind speeds observed above about 65 km. This is particularly true in the summer hemisphere where planetary wave activity is small.

Lindzen (1981) has shown that breaking gravity waves produce both diffusion and mean flow deceleration. It is a very important problem in modeling the global stratosphere circulation to understand whether the small-scale dynamics, gravity waves and turbulence, influence the large-scale flow in the manner suggested by theory. It is not possible to address this problem observationally by satellite measurements since small-scale dynamics are not resolved. It must be addressed by a mixture of in situ measurements (balloons and rockets) and remote sensing measurements.

The newly emerging MST radar technique looks very promising for this purpose. In this technique, a high power VHF (30 to 300 MHz) or UHF (300 to 3000 MHz) radar is used to measure the Doppler shift in signals that are partially reflected from clear air irregularities in the radio refractive index. Since these irregularities are believed to be due to turbulent patches of air that move with the neutral wind, this Doppler shift gives a measure of the line-of-sight wind velocity. By using multiple radar beam directions or by scanning the beam direction, the three-dimensional wind vector can be inferred. Since wind and scattered power profiles can be measured in a period of minutes with this technique, MST radars can measure the structure of gravity waves, turbulence, and the time-average flow simultaneously. The overall objectives in using this technique include the following:

- To delineate the global morphology of gravity waves in the stratosphere and mesosphere, including geographical and seasonal variability.

- To do observational case studies of gravity wave breaking and dissipation and compare these with modeling studies to increase our understanding of gravity wave generation of turbulence and gravity wave interaction with mean winds.

- To obtain a global morphology of turbulence in the stratosphere and mesosphere.

A principal goal of these studies will be to understand the sources of gravity waves and turbulence in the stratosphere and mesosphere, and subsequently to develop proper methods to parameterize the effects of nonresolved small-scale motions for inclusion in upper atmosphere global circulation models.

Troposphere-Stratosphere Exchange Processes

The exchange of constituents between the troposphere and the stratosphere involves atmospheric motions on various scales, from the planetary scale down to turbulent scales. The mesoscale and small-scale motions appear to play a very important role in these processes. For instance, it is thought that almost all of the upward transport of mass from the troposphere to the stratosphere takes place in the rising branch of the tropical Hadley cell. The arguments for this are based on the small water vapor amounts in the lower stratosphere and have been reviewed recently by Robinson (1980). Furthermore, it has been suggested that these upward transports take place only within the rapid upward vertical motions of cumulonimbus towers, which are known to extend into the stratosphere occasionally. In this picture, there is slow downward motion filling the area between the cumulus towers. The uncompensated portion of the upward motion is what actually constitutes the rising branch of the Hadley cell. This hypothesis is known as the "hot tower" hypothesis and was first described by Riehl and Malkus (1958). It should be noted that in this view the large-scale dynamics organize the cumulus scale dynamics and the net effect of the cumulus dynamics gives the rising branch of the Hadley circulation which gives upward mass transport in the tropics from the troposphere to the stratosphere.

There is also known to be an exchange of stratospheric air with tropospheric air at middle and high latitudes as a result of "tropopause folding". Evidence for this exchange was first shown by Danielsen (1959). These exchanges appear to be mainly stratospheric air entering the upper troposphere through thin laminar intrusions in the vicinity of upper level fronts associated with the tropospheric jet stream. The dimensions of these laminae are typically 1 km in the vertical, more than 100 kilometers in the horizontal orthogonal to the wind, and more than 1,000 kilometers parallel to the wind. This stratospheric air is then mixed into the troposphere by cumulus-scale and turbulent-scale processes. Thus, the mesoscale tropopause folds are organized about the globe by planetary scale dynamics and are mixed by the smaller scale cumulus- and turbulent-scale motions. The extent to which tropospheric air can enter the stratosphere by this "tropopause folding" has yet to be determined and requires further study.

While satellite instruments may be capable of observing the results of such exchanges of air between the troposphere and stratosphere, their spatial resolution is not sufficient to quantitatively study these exchange processes themselves. Perhaps the optimal platform from which to conduct measurements on troposphere-stratosphere exchange is the research aircraft. These aircraft can be directed into the areas in the vicinity of cumulus clouds to measure the air motions and the various tracers that characterize tropospheric and stratospheric air such as potential vorticity and ozone to infer the mass exchanges taking place. They can also be directed to fly tracks perpendicular to the mean flow through tropopause folding events to characterize

the mass exchange processes occurring there. With properly designed aircraft experiments, the global scale organization of the mesoscale tropopause folding processes can be seen together with measurement of the actual fluxes of momentum, energy and trace constituents. These computations require simultaneous measurement of temperature, pressure, and trace species. At present, there exist fast responding in situ sensors for measuring the thermodynamic variables, water vapor, ozone, aerosols and hydrometeors. Many other sensors are now being designed for measuring other significant trace species. In short, only measurements from aircraft appear to provide the horizontal, vertical, and temporal resolution of meteorological variables and trace constituent concentrations necessary to resolve the small-scale and mesoscale phenomena of troposphere-stratosphere exchange. Moreover, aircraft have the flexibility to be directed into areas where significant processes are occurring along optimal trajectories.

Such aircraft investigations of troposphere-stratosphere exchanges have been, and continue to be, carried out. In the first Intertropical Convergence Zone (ITCZ) experiment, which was carried out in Panama in 1977 (Poppoff et al., 1979) under the coordination of the NASA/Ames Research Center, the goal was to determine the presence, or lack, of significant small-scale variability in this region. Aircraft were used to measure the horizontal variability, and balloons were used to measure the vertical variability. The results of this experiment showed the importance of this small-scale variability in this region of the atmosphere. In the second ITCZ experiment, which was carried out in Panama in 1980 also under the coordination of the NASA/Ames Research Center, the goal was to measure the environment of cumulonimbus clouds before and after their penetration into the stratosphere to help define their role in the water vapor budget of the stratosphere. These data are still being examined.

NUMERICAL MODELING

INTRODUCTION

The stratosphere is a very complex physical system which is governed by the interactions of various radiative, dynamical and chemical processes many of which are highly nonlinear. The only viable technique for fully developing and testing our theoretical understanding of this interactive system is numerical modeling.

Many types of numerical models can play important roles in stratospheric research. The one-dimensional photochemical models, discussed elsewhere in this report, provide a method to test photochemical theory without introducing the complexities provided by atmospheric transport and spatial/temporal variability. However, observations generally show that trace species distributions have significant spatial and temporal variability. In particular, strong latitudinal gradients appear to be a common feature of trace constituent climatology, while longitudinal gradients are usually, but not always, less dramatic. For this reason, two-dimensional (height-latitude) models are attractive for study of the photochemical problems of the stratosphere. The second part of this section reviews the status of two-dimensional models and discusses the prospects for their further development.

A crucial step in the development of a two-dimensional model is the parameterization of the net transport (horizontal and vertical) by zonally asymmetric "eddy" motions. Such eddies range in scale from global scale (so-called planetary waves) to microscale turbulent eddies.

Eddies control trace species distributions through both advective and diffusive transport processes. Parameterizations of eddy effects in two-dimensional models have often in the past been based primarily on diffusion models empirically "tuned" by fitting observed tracer distributions. Further improvement in eddy parameterizations, however, seems to demand a good theoretical understanding of the three-dimensional structure of the stratosphere. Thus, even if

two-dimensional models become the primary tool for prognostic studies of ozone perturbations, a wide variety of three-dimensional models will still be necessary to validate the two-dimensional models. More importantly, only in three-dimensional models can we include many of the dynamical and physical processes required for understanding the stratosphere as a coupled radiative/dynamical/chemical system.

The third part of this section reviews the current status of three-dimensional model development while the fourth part summarizes many of the radiative-chemical-dynamical interaction processes which make three-dimensional modeling essential. Finally, the section concludes with a discussion of the importance of coupling models with observations both in the sense of using observations to validate models and using models to guide observational strategies.

TWO-DIMENSIONAL MODELS

Approach

The study of the processes that determine the distribution of chemical species in the stratosphere is clearly a three-dimensional (four-dimensional, including time) problem. However, the complexity of stratospheric chemistry and the interactions among chemistry, radiation, and dynamics make general circulation studies of, for example, possible ozone perturbations a very expensive computation. To date, the role of General Circulation Models (GCMs) has been to study dynamical and transport processes, and only very simplified chemical schemes have been included. On the other hand, one-dimensional models can include very detailed chemistry but, by their nature, are incapable of including important meteorological processes.

Two-dimensional models, in which zonal averages are considered, are meant to bridge this gap. The motivation for two-dimensional models lies in the fact that, on a rotating planet with a homogeneous underlying surface, the value of meteorological quantities averaged over many days is expected to show no variation with longitude. In practice, latitudinal gradients in the Earth's atmosphere are generally larger than those in the longitudinal direction.

Two-dimensional models can include more detailed chemistry as well as some treatment of vertical and horizontal transport by mean and eddy motions with modest computational requirements compared to those of three-dimensional models. Inevitably, some compromise is involved. For example, the diurnal variation of species is usually treated in less detail than in one-dimensional models. Similarly, eddy transports, which are calculated consistently in the GCMs, must be specified in some manner.

For any tracer with mixing ratio, X, the zonally averaged continuity equation may be written

$$\frac{\partial \bar{X}}{\partial t} + \bar{v}\,\frac{\partial \bar{X}}{\partial y} + \bar{\omega}\,\frac{\partial \bar{X}}{\partial p} = -\frac{1}{\cos\phi}\,\frac{\partial}{\partial y}\,\overline{(v'X'\cos\phi)} - \frac{\partial}{\partial p}\,\overline{\omega'X'} + \bar{S} \qquad (1)$$

where ($\bar{}$) represents an average around a longitude circle and ( )' the departure therefrom, and v and ω represent velocities in the northward, y, and vertical, p, directions respectively. ϕ is latitude, and S represents all sources and sinks of X.

The transport terms on the left hand side of Equation (1) involve zonal means only. This is the transport by the mean circulation. On the right hand side are found products of departures from the zonal mean. These are the horizontal and vertical eddy terms, representing, in the stratosphere, transport mainly by the large-scale waves. Different types of two-dimensional models may be distinguished by the way in which the mean and eddy terms are treated.

The Mean Circulation

The majority of two-dimensional chemistry models have employed a specified meridional circulation. Generally, such a circulation might be based on the calculations of Louis (1974), Gudiksen et al. (1968), or Murgatroyd and Singleton (1961) although there now exist the newer model calculations of Schoeberl and Strobel (1978a) and Holton and Wehrbein (1980b). Alternatively, the mean circulation can be calculated self-consistently within the model. In this approach (Rao-Vupputuri, 1973; Harwood and Pyle 1975, 1977), the zonal mean dynamic and thermodynamics equations are solved for the three velocity components and the temperature field. This requires a treatment of radiative heating (and latent heat release in the troposphere) in addition to treatments of eddy heat and momentum transport. This increased complexity leads to a number of advantages over those models with specified mean circulations. Firstly, perturbation experiments which might produce large departures from the initial meteorological state must be open to question in models with a specified circulation. Allowing the mean circulation to evolve increases, to some extent, the confidence that may be placed in such calculations. Of course, even in these models, because of other parameterizations, the reliability of perturbation experiments cannot be assessed with great confidence. Secondly, a variety of feedback processes can be included when the mean circulation is calculated. For example, the impact of a change in upper stratospheric ozone on the radiative heating and hence on the temperature and wind structure (and, therefore, ozone transport) can be considered. Thirdly, perturbations affecting radiative processes can be considered quite simply in these models. For example, Haigh and Pyle (1979) have studied the impact of increasing levels of CO_2 on the stratosphere. Heating by aerosols could also be considered. It should be stressed that these models with calculated mean circulations depend critically on the treatment of the eddy heat and momentum fluxes which will either be modeled or specified from observations.

Eddy Transport

The treatment of eddy transport has generally followed the approach of Reed and German (1965), in which the horizontal and vertical fluxes are related to the mean gradients of the transported, quasi-conservative tracer by a tensor of transport coefficients. Thus

$$\overline{v'X'} = -K_{yy}\frac{\partial \bar{X}}{\partial y} - K_{yz}\frac{\partial \bar{X}}{\partial z} \qquad (2)$$

$$\overline{w'X'} = -K_{zy}\frac{\partial \bar{X}}{\partial y} - K_{zz}\frac{\partial \bar{X}}{\partial z} \qquad (3)$$

There have been several determinations of K values in the literature. The first such determinations of the K's was by Reed and German (1965). They assumed small linear displacements and thus could use mixing-length theory to derive the K's from atmospheric data. Later suggested K values were by Luther (1973) and Gudiksen et al. (1968). Recently, Danielsen (1981) has suggested a rather general formalism for deriving K values from atmospheric data.

The idea of the K approach is that these K's can then be used to compute the eddy fluxes of any quasi-conservative tracer. In practice, some modelers choose to regard the K's as adjustable parameters which can be altered to produce a good fit for a particular tracer; however, this one set of K's is then used for all species.

Some of the assumptions behind the K-theory approach are weak (or invalid, see below) and, however well the present day atmosphere is reproduced, this must reduce the credibility of perturbation experiments (just as it does for one-dimensional models).

Another limitation of K-theory for perturbation experiments arises from holding the K coefficients constant. It is well known that the propagation of waves in the atmosphere depends critically on the zonal mean state (see e.g., Schoeberl and Geller, 1976). Perturbations to the ozone layer will affect the zonal mean temperature and wind structure. (It is interesting to note, however, that the calculations of Schoeberl and Strobel (1976) indicate that the effects of changes in column ozone on the mean zonal structure of the stratosphere are less than what might be first imagined.) Thus, wave propagation also will be affected and hence the K's should change. This potentially important feedback cannot be included in two-dimensional models with parameterized eddy transport.

Despite its empiricism, the K-theory treatment is capable of reproducing some of the expected characteristics of transport by waves. Thus, the near-cancellation of the mean and eddy transports in the winter hemisphere is found for both ozone and temperature by Rao-Vupputuri (1973) and Harwood and Pyle (1975, 1977). This cancellation is expected on theoretical grounds, is seen in the GCM results, and, most importantly, is seen in the observations.

It should be mentioned that eddy terms also arise in photochemical source and sink terms. These are due to the zonal mean of products of perturbation mixing ratios (e.g., $\overline{k\,A'B'}$ where k is a rate constant). Tuck (1979) has discussed their importance. For example, the percentage difference between the true zonal mean rate $\overline{k\,O('D)\,H_2O}$ and $\overline{k\,O('D)}\;\overline{H_2O}$ can be typically between 0 and 30% (Allam et al., 1981).

Existing Two-Dimensional Models of the Stratosphere

A summary of the structure of existing two-dimensional models of the stratosphere and troposphere is given in Table 2-14 which describes the differences in those components of existing models important to representing atmospheric processes. This summary is an update of a previous comparison (Wuebbles, 1980) based on papers presented at the WMO Workshop on Two-Dimensional Models held in Toronto, Canada during Feburary 1980. Along with updating the model descriptions for changes since that meeting, several additional recently developed models have also been included.

Summary of Important Results from Two-Dimension Models with Coupling Between Dynamics and Chemistry

The results of perturbation experiments using two-dimensional models are described elsewhere and will not be repeated here. However, some salient features of two-dimensional model behavior will be discussed in the following paragraphs.

Two-dimensional models are capable of reproducing the gross features of the observed latitude-time variation of total column ozone with equatorial minima and spring, high latitude maxima. Harwood and Pyle (1977), by the use of observed asymmetric values for $\overline{u'v'}$ in the momentum equation, reproduced the observed asymmetry in total ozone with the maximum at the pole in the Northern Hemisphere and at ~60°S in the Southern Hemisphere. Published budgets of ozone from

Table 2-14
A Summary of Two-Dimensional Transport-Kinetics Models

	Du Pont Company	Oxford University	NASA-AMES	MPIC*/University of Miami
Physical domain	0-55 km 90°N-90°S	0-95 km 90°N-90°S	0-60 km (mod. 1) 0-90 km (mod. 2) 80°N-80°S	980-0.415 mbar (55 km) 90°N-90°S
Spatial variables	Pressure; sine of latitude (θ)	Pressure latitude	Altitude latitude	Pressure latitude
Grid resolution	$\Delta \ln (p_0/p)=0.43$ (~3 km) $\Delta(\sin\theta) = 0.2$	$\Delta \ln (p_0/p)=0.5$ (~3.5 km) $\Delta\theta=\pi/19$	$\Delta z = 2.5$ km $\Delta\theta = 5°$	$\Delta \ln p$ corresponds to about .5 km $\Delta\theta = 10°$
Chemical scheme	30 species (+3 inactive)	17 species (19 in diurnal model) (H_2O, CH_4, H_2, N_2O, CO, inactive; however, these were calculated in recent studies)	35 species	35 species
Atmospheric structure	T same as NASA-AMES. H_2O rel. humidity fixed below 100 mbar. Mixing ratio at 100 mbar varies from 3 ppmv at equator to 4 ppmv at high latitudes.	Radiative cooling = 1.5°C/day in troposphere, while in upper troposphere (8-12 km) the radiative cooling = 0.75°k/day; detailed radiation calculation in stratosphere, non-local thermodynamic equilibrium effects are included.	$T \leq 20$ km from Oort and Rasmussen (1971) T >20 km from Nastrom and Belmont (1975). p determined using hydrostatic relation	T based on Oort and Rasmussen (1971) and Louis (1974). (determine saturation temperature, T_s, by relating humidity to saturation humidity)
Photolysis treatment	Includes multiple scattering. Albedo = 0.25 at all latitudes and seasons. absorption by O_2 and O_3	Average photodissociation rates computed every 10 days by Gaussian integration over a number of zenith angles.	Calculate diurnal averaged photolysis rates.	Average (daytime) photolysis rates computed every 15 days Multiple scattering approximated at wavelengths larger than 300 nm.

Table 2-14. A Summary of Two-Dimensional Transport-Kinetics Models (continued)

	Du Pont Company	Oxford University	NASA-AMES	MPIC*/University of Miami
Transport treatment	Prescribed. v, w based on Murgatroyd and Singleton (1961) multiplied by 0.4. K's based on Luther (1978), but modified.	v, w, T calculated (or can be prescribed). K's prescribed based on Luther (1973) (usually unmodified). $\overline{u'v'}$ based on observations from Oxford radiometers. Some calculations use diabatically driven circulation plus calculated eddies (chemistry dependent).	Prescribed. v <20 km based on Oort and Rasmussen (1971); are extrapolated above so that no net mass flux at upper bndry. w derived using mass continuity eqn. K's derived to fit O_3 and tracers.	Prescribed. v, w based on Louis (1974) K s based on "trial and error" to fit O_3 and H_2O.
Solution methods	Family approach for odd oxygen (O, O_3). Other species solved directly. Photochemical equilibrium for H, N. Iterative solution at each time step using Newton-Raphson.	Family approach (O_x, NO_x, HO_xClO_x) Long lived species solved directly. Diurnal averaged model uses Adams-Bashford method. Diurnal model uses divided-difference formulation of Gear's method.	Family approach (O_x, HO_x, NO_x). Time split the chemistry and transport terms. The vertical and horizontal advection and diffusive terms are also time split. Chemical and horizontal terms are solved implicitly, others solved explicity.	Family approach (O_x, HO_x, NO_x, ClO_x)
Time-dependent integration	Δt = 3 days	Δt = 4 hours (5 minute for diurnal) Δt = 1 hour for diabatic calculation.	Δt = 1 day	Δt = 2 hours

Table 2-14. A Summary of Two-Dimensional Transport-Kinetics Models (continued)

	Du Pont Company	Oxford University	NASA-AMES	MPIC*/University of Miami
Boundary conditions	Upper boundary: $\phi = 0$, all species. Lower boundary: latitude dependent mixing ratio or flux prescribed (e.g. $\phi = 5 \times 10^9$ $cm^{-2}s^{-1}$ for NO_2)	Upper boundary: $\phi = 0$ or photochemical equilibrium. Lower boundary: mixing ratio or flux prescribed.	Zero flux at lateral boundary. Upper boundary: mixing equilibrium (i.e. $\phi = 0$) or flux condition Lower boundary: flux or prescribed concentrations.	Upper boundary: $\phi = 0$ for most species. Lower boundary: mixing ratio for N_2O, H_2 CH_3Cl, COS, HCl, H_2O ϕ for HNO_3 NO_x, CH_4 Cl_3CF, Cl_2CF_2, CCl_4, CCl_3, SO_2.
Heterogeneous removal	τ = 5 days below 280 mbar for HCl, HNO_3, NO_2, CH_2O, $HOCl$, H_2O_2, HNO_4.	τ = 20 days for HNO_3 HCl, H_2O_2. Constant throughout troposphere.	τ = 10 days for water soluble species	H_2O dependent on condensation and precipitation of cloud formation based on T. Removal of NO, H_2O_2 CH_3O_2H, N_2O, HNO_3 based on water vapor profile.
Surface deposition	$w_D = 0.22$ cm s^{-1} for O_3	Not included	Included	Varies over land and water: w_D(land) w_D (water) HNO_3 0.2 cm s^{-1} 1 O_3 " 0.05 NO_x " 0.5
Diurnal effects	Diurnal averaging by 2-tank approx. (ave. daytime and nighttime). (C. Miller et al., 1979)	Diurnal average. Ignores nighttime chemistry. Rate of change weighted by fraction of sunlight per day. Diurnal model also available.	Diurnal averaging used based on Turco and Whitten (1978).	Photolysis applied to sunlit hours; photochemistry "frozen" at nighttime except for NO_3, N_2O_5, ClO, $ClONO_2$.

Table 2-14. A Summary of Two-Dimensional Transport-Kinetics Models (continued)

	Du Pont Company	Oxford University	NASA-AMES	MPIC*/University of Miami
Seasonal variations	T, transport coef. constant over 1/8 year intervals.	Are calculated	Are calculated	Are calculated
References:	C. Miller et al. (1980a) C. Miller et al. (1981) C. Miller (personal communication, 1981)	Pyle (1980) Pyle & Rogers (1980) Pyle (personal communication, 1981)	Whitten et al. (1977) Whitten et al. (1981 Borucki et al. (1980)	Crutzen & Gidel (1980) P. Crutzen (personal communication, 1981)

*MPIC - Max-Planck-Institut Für Chemie

Table 2-14. A Summary of Two-Dimensional Transport-Kinetics Models (continued)

	Canada AES	Aerospace Corp.	U.K. Met. Office	Belgium Aeronomy Inst.
Physical domain	1--55 km 90°N-90°S	0-50 km 90°N-90°S	0-48 km 90°N-90°S	0-50 km 90°N-90°S
Spatial variables	$Z = \ln p/p_0$ latitude	Geometric altitude latitude	Pressure latitude	Geometric altitude latitude
Grid resolution	$\Delta Z = 0.4236$ (~3 km) $\Delta\theta = 10°$	$\Delta z = 2$ km for $z = 0$-12 km; $\Delta z = 1$ km for $z = 12$-35 km; $\Delta z = 2.5$ km for $z = 35$-50 km. $\Delta\theta = 10°$	$\Delta \log p = 0.3$ (~2 km) $\Delta\theta = 30°$ (75°N, 45°N, 15°N, 15°S 45°S, 75°S)	$\Delta z = 1$ km $\Delta\theta = 5°$
Chemical scheme	18 species H_2O, H_2, CH_4 specified.	31 species	25 species Parameterized CH_4 cycle (i.e., $CH_3 \rightarrow 3HO_2$) H_2O specified in trop.	19 species (CO, H_2, H_2O constant)
Atmospheric structure	Not available	T, based on Louis (1974). Solar flux based on Ackerman et al. (1971) and Simon (1975).	Temperature based on U.S. Standard Atmosphere (1962) interpolated sinusoidally between summer and winter. Solar flux based on Ackerman et al. (1971), Simon (1974), Broadford (1972), and Thekaekara (1972).	Temperature based on U.S. Standard Atmosphere (1962) interpolated between summer and winter. Solar flux based on Simon (1974).
Photolysis treatment	Radiative heating and photolysis rates computed at each time step.	Daylight averages Photolysis rates calculated every 3rd time step; multiple scattering included (based on Luther et al. (1978).	Photolysis rates calculated every half hour; are interpolated in between (linearly in $\cos \chi$); multiple scattering not included.	Use diurnal averaged solar flux.

Table 2-14. A Summary of Two-Dimensional Transport-Kinetics Models (continued)

	Canada AES	Aerospace Corp.	U.K. Met. Office	Belgium Aeronomy Inst.
Transport treatment	v, w, T calculated. K's prescribed based on Reed and German (1965) (Luther, 1973 used in recent sensitivity tests). Vertical K constant with altitude in most calculations. Geostrophic approximation in u-momentum eqn.	Prescribed. v, w based on Louis (1974). K's based on modified Luther (1973).	Prescribed v, w based on Newell et al. (1972) extended upward using COMESA 3-D model. K's based on Luther (1973) for Jan. & July interpolated sinusoidally over a year; have been adjusted.	3 approaches; (1) constant K's only (steady state version). (2) prescribed (time dependent version). v, w based on Cunnold et al. (1975) K's based on modified Gudiksen et al., (1968) and Luther (1973) to fit O_3. (3) v, w, T calculated (in progress).
Solution methods	Family approach (O_x, NO_x, HO_x, ClO_x). Use Adams-Bashford method for continuity eqn.	Each species determined directly. Use time-implicit finite difference scheme with leap-frog and Dufort-Frankel finite difference schemes for advective and diffusive terms. Implicit solution method for species whose chemical lifetime less than 2 days; explicit method for others.	Family approach (O_x, NO_x, ClO_x, HO_x). Time splitting, with transport terms calculated every two hours and chemistry at every time step. Use Euler backward scheme with Richardson extrapolation. When only calculating hemisphere, then values at 15°S assumed equal to those 6 months earlier at 15°N.	Family approach (O_x, NO_x, ClO_x). Alternating direction method.
Time-dependent	Δt = 6 hours	Δt = few days	$\Delta t = \begin{cases} 3 \text{ mins daytime} \\ 10 \text{ mins nightime} \\ 1 \text{ min transition} \end{cases}$	a few days

Table 2-14. A Summary of Two-Dimensional Transport-Kinetics Models (continued)

	Canada AES	Aerospace Corp.	U.K. Met. Office	Belgium Aeronomy Inst.
Boundary conditions	Not available	Upper boundary: Photochemical equilibrium or extrapolation of mixing ratios. Lower boundary: concentration or flux defined.	Upper boundary: Not available Lower boundary: defined concentrations or flux	$\Phi = 0$ at poles. Mixing ratios specified at lower and upper boundary.
Heterogeneous removal	Not available	First order rate law for rainout of H_2O, HNO_3, NO_2, NO, HO_2, H_2O_2, N_2O_5, NO_3 and ClO_x (based on Junge, 1963). NO and NO_2 removed at 1/10 rate of other species.	First order rate law for rainout is function of altitude and latitude for HNO_3, HCl, H_2O_2 (~10 days in lower troposphere).	First order rate law for rainout of HCl and HNO_3.
Surface deposition	Not available	Not available	Not available	Not included.
Diurnal effects	Diurnal averaging included by using average daytime zenith angle.	Diurnal averaging used; similar to Turco and Whitten (1978)	Normally include diurnal variations; diurnal averaging done in some calculations by averaging daytime photolysis rates.	24 hour average of solar flux.
Seasonal variations	Are calculated. K's changed each season. Sun position changed each day.	Are calculated	Are calculated	Are calculated
References:	Vupputuri (1980a) Vupputuri (1980b)	Widhopf (1980)	Clough (1980)	Brasseur (1980) Brasseur & Bertin (1978) Brasseur (personal communication, 1981)

Table 2-14. A Summary of Two-Dimensional Transport-Kinetics Models (continued)

	University of Oslo	AERE Harwell
Physical domain	0-18 km (0-50 km in stratospheric model) 85°N-85°S	0-15 km 90°N-90°S
Spatial variables	Altitude latitude	Geometric altitude sine of latitude (θ)
Grid resolution	Δz = .5 km $z < 3$ km 1 km $z > 3$ km $\Delta\theta = 10°$ (Δz = 2 km in strat. model)	Δz = 2.5 km $\Delta(\sin\theta) = 1/18$
Chemical scheme	O_x, HO_x, NO_x hydrocarbons and sulfur compounds; reactions and rates based on NASA RP 1049.	14 species
Atmospheric structure	T,p based on Louis (1974) Relative humidity calculated in troposphere.	p, T from U.S. Standard Atmos. (1976); H_2O from Newell et al., (1972)
Photolysis treatment	Includes multiple scattering. Diurnal average photo dissociation rates calculated every month.	Calculated diurnal average photolysis rates. Luther and Gelinas (1976) treatment for multiple scattering.

Table 2-14. A Summary of Two-Dimensional Transport-Kinetics Models (continued)

	University of Oslo	AERE Harwell
Transport treatment	Prescribed v, w based on Newell et al. (1972) K's based on Hidalgo and Crutzen (1977) with boundary layer partially dependent on average thermal stratification; Louis v, w, K's in stratosphere.	Prescribed v, w based on Newell et al. (1972) Kyy, Kzz based on Louis (1974)
Solution methods	Alternate treatment: v, w calculated from diabatic heating rates given by Newell et al. (1972)	All species solved implicity with Gear's method except $O(^1D)$, CH_3, H
Time-independent integration	Family approach. Semi-implicit approach solution method. Δt = 0.5 hours (Δt = 3.75 days in strat. model).	Chosen automatically by numerical method but $\leq 1 \times 10^4$ sec.
Boundary conditions	Zero horizontal transport at lateral boundaries. Vertical advection zero through upper and lower boundaries. Upper boundary vertical flux specified. Lower boundary flux specified.	Flux upper boundary conditions for CO, H_2, CH_4 and halocarbons. Lower boundary: fixed mixing rates for H_2, CH_4 Fluxes for CO, NO_x

Table 2-14. A Summary of Two-Dimensional Transport-Kinetics Models (continued)

	University of Oslo	AERE Harwell
Heterogeneous removal	Treat (a) reversible incloud scavenging (b) irreversible incloud scavenging (c) subcloud scavenging	Latitudinally dependent for HNO_3, H_2O_2 from Karol (1974).
Surface deposition	O_3 $w_D = 0.4$ cm s^{-1} SO_2 $w_D = 0.7$ HNO_3 $w_D = 0.7$ PAN $w_D = 0.2$ NO_2 $w_D = 0.2$ sulfate $w_D = 0.2$	Varies over land and sea for O_3, H_2, HNO_3, CO.
Diurnal effects	Can do diurnal calculations or diurnal averaging.	Diurnal version available.
Seasonal variations	Are included	Are calculated
References:	Isaksen & Rodhe (1978) Isaksen (1980) Horntveth & Isaksen (1981) I. Isaksen (personal communication, 1981)	Derwent & Eggleton (1978) Derwent & Eggleton (1981) R. Derwent (1981).

Table 2-14. A Summary of Two-Dimensional Transport-Kinetics Models (continued)

	Atmospheric and Environmental Research, Inc.
Physical Domain	0 - 60 km 90°N-90°S
Spatial variables	Pressure coordinates. Latitude
Grid resolution	$\Delta \ln (p_s/p) = 0.5$ (~ 3.5 km) $\Delta \theta = \pi/19$ (~ 10^3 km)
Chemical scheme	35 calculated species + H_2O as fixed species
Atmosphere structure	T ~ taken from earlier calculation of Oxford model, specified every 10 days, ρ calculated from given T, H_2O calculated from seasonal dependent relative humidity in troposphere, fixed at 5 ppmv in stratosphere
Photolysis treatment	Diurnal-averaged photo-dissociation rates using gaussian integration over zenith angles. Absorption by O_2 and O_3. Adjustment allowed for multiple scattering and surface reflection at long wavelengths
Transport treatment	Zonal-mean approach with eddy diffusion coefficients. Zonal-mean wind fields and T taken from the earlier Oxford model, specified every 10 days. Eddy diffusion coefficients from Luther (1973) input once a month
Solution methods	Family approach (O_x, HO_x, NO_x, Cl_x) Diffusion equation is solved for following species using Adam-Bashford scheme:

Table 2-14. A Summary of Two-Dimensional Transport-Kinetics Models (continued)

	Atmospheric and Environmental Research, Inc.
Solution methods (continued)	Long-lived: N_2O, FC-11, FC-12 CCl_4, CH_3Cl, CH_3CCl_3, H_2, CO, CH_4. Families: NO_x, Cl_x, O_x. The radical species concentrations obtained assuming local photochemical equilibrium
Time-dependent integration	Δt = 4 hours
Boundary condition	(B. C. on long-lived species only) Upper boundary: $\phi = 0$ all species Lower boundary: Fixed mixing ratio N_2O, CH_3Cl, CCl_4, H_2, CH_4, O_3, NO_x, Cl_x Latitude-dependent fixed mixing ratio: CO Flux B.C.: FC-11, FC-12, CH_3CCl_3
Heterogeneous removal	τ = 5 days $Z \lesssim 3.5$ km τ = 11 days 3.5 km $\lesssim Z \lesssim$ 7 km τ = 38 days 7 km $\lesssim Z \lesssim$ 10 km for HCl, HNO_3, CH_2O, H_2O_2
Surface deposition	Not used
Diurnal effect	Diurnal averaging simulated by using diurnal-averaged photolysis rates
Seasonal variation	Seasonal variations of T and wind fields are taken from Oxford model which are calculated
References	Ko et al. (1981) D. Sze (personal communication 1981)

two-dimensional models show the near cancellation between mean and eddy transports. There appears to be some ability in these models to reproduce some features of the observed latitudinal variation of the lower stratospheric long-lived gases HNO_3, N_2O, and CH_4.

Those models with calculated temperatures and winds reproduce the gross features of the temperature structure with a tropopause which varies in height with latitude and increasing temperatures up to the stratopause at about 50 km. Harwood and Pyle (1980) overestimate the zonal jet strengths at the stratopause by almost a factor of two. Their lower stratospheric vertical velocities are in good agreement with the values based on observations, derived by Vincent (1968).

The principal advantage of two-dimensional models over one-dimensional models for perturbation experiments lies in their ability to reproduce latitudinal and seasonal variations and to include more feedback processes. Rao-Vupputuri (1979), Borucki et al. (1980), and Pyle (1980) have all discussed the latitudinal variations in ozone depletion with minimum predicted depletions in equatorial latitudes increasing towards the pole. Pyle (1980) also found a seasonal variation with largest depletions in high latitudes in spring. These latitudinal and seasonal variations are produced in the model by interactions between chemical, radiative, and dynamical processes.

Some Recent Advances

Recent work has suggested improvements to two-dimensional models by using a more physically based K-theory (Danielsen, 1981) or by applying some of the ideas which have emerged from studies employing Lagrangian-mean theory (see Andrews & McIntyre 1976, McIntyre 1980a).

The limitations of some of the assumptions behind Reed and German's (1965) K-theory approach have been exposed by a number of workers. Mahlman (1975) used tracer fluxes from a GCM to show that the mean flux is not necessarily down the mean gradient. Clark and Rogers (1978) and Plumb (1979) have considered the transport by planetary wave motions and have shown that the transport by planetary waves tends to take place along the gradient of conservative tracers. In this case then, the transport tensor would take quite a different form from that of Reed and German (1965) with $K_{yy} = K_{zz} = 0$ and $K_{yz} = - K_{zy}$.

In 2-D models the eddies are not just small scale, turbulent whorls, isotropic in form. Instead, they include the complete spectrum of internal waves which contribute to both the symmetric and antisymmetric tensors. Matsuno (1980), using a simple channel model with a wave number 1 perturbation, derived analytic expressions for both tensors whose coefficients depend on the product of his proposed mixing time τ and the angular frequency of the wave ω. When $\omega\tau<1$, the symmetric sensor dominates in agreement with Reed and German's (1965) assumption of linear displacements (linearly polarized waves). Conversely, when $\omega\tau>1$ the antisymmetric tensor dominates in agreement with Clark and Rogers' (1978) elliptically polarized planetary waves. Compatible with his modeling assumptions, Matsuno (1980) assumed $\omega\tau>>1$, which effectively eliminated the symmetric tensor.

Danielsen (1981), taking full advantage of Eulerian coordinates, extended Matsuno's mixing time concept to include all waves. A complete asymmetric transport tensor, whose antisymmetric components include the Eulerian mean motion corrected for elliptically polarized velocity deviation (Stokes Drift) and whose symmetric components contain all linearly polarized deviations, is shown to be determined from the solution of two equations in two unknowns. To solve these equations a representative gridpoint data set of balanced u, v, and w velocities and thermodynamic scalers is required. Appropriate sets are being derived by numerical diagnostic methods and Danielsen (1981) believes these data will show that Matsuno's (1980) estimated

mixing time τ is much too long, and that both the symmetric and antisymmetric tensors will contribute to transport, their relative importance depending on altitude.

Other recent work has suggested a new approach to studies of tracer transport using a Lagrangian mean framework in which apparently the eddy terms need not be calculated. Considering Equation (1), in practice, the mean and eddy flux terms almost cancel under steady circumstances without strong diabatic effects, so that the small residual of two large terms must be found. For steady, non-dissipating waves (the eddies), an Eulerian-mean meridional circulation is induced which just cancels the effects of the eddies on the mean state. If, however, a Lagrangian description is considered, the species continuity equation becomes particularly simple, and no eddy terms appear, thus

$$\frac{\partial \bar{X}^L}{\partial t} + \bar{v}^L \frac{\partial \bar{X}^L}{\partial y} + \bar{w}^L \frac{\partial \bar{X}^L}{\partial p} = \bar{S}^L \qquad (4)$$

where $(\ )^L$ is some Lagrangian average. (In a simple case, this could be an average following an air parcel.) Thus, in a Lagrangian description, we move with the flow; in an Eulerian description, the flow is observed from a fixed point). The problem then becomes one of finding v^L and w^L (and S^L) rather than the eddies. It should be mentioned at this point that Danielsen (1981) has argued that Equation (4) is a great oversimplification when applied to bulk parcels of air. For averages over large volumes, the deviations from either an Eulerian or Lagrangian mean will be very significant; eddy terms cannot be neglected. Their dispersion about the Lagrangian mean has also been demonstrated by Hsu (1980). Note that, for large deviatory flows, it is possible that none of the individual fluid parcels within the bulk average will have trajectories given by v^L and w^L. (For further discussion of the practical limitations of the Lagrangian approach, see McIntyre, et al. 1980b and Mahlman et al. 1981. To caution further, it should be remembered that whatever description is applied, the transport process must contain the essential physics.

Dunkerton (1978) pointed to the possible advantages of an approach based on Equation (4). He approximated the Lagrangian mean circulation with that driven by the Eulerian mean diabatic heating. In fact, the eddy diabatic heating term also will contribute to the Lagrangrian mean circulation.

The above ideas have led to the development of modified Eulerian mean models. Making the same approximations as Dunkerton (1978), Pyle and Rogers (1980) and Rogers and Pyle (1980) identify a 'residual meridional circulation' (the difference between the Eulerian circulation and that part induced by steady, non-dissipating waves (see Andrews and Mcintyre, 1976) with that circulation driven by the diabatic heating. The cancellation of the eddy terms in Equation (1) by the induced meridional circulation is only exact in the case of steady waves, with no dissipation, away from critical lines and for a conservative tracer. The chemically-induced transport, modeled by the symmetric component of the K's (see above) also must be included.

Thus, in their model, Rogers and Pyle include the diabatic circulation plus the chemical contribution to the eddy transport as well as the photochemical sources and sinks. The eddy perturbation velocities, occurring in the expression for the K's, are calculated within the model. The ozone distribution reproduced shows many satisfactory features with an equatorial minimum and high-latitude spring maxima.

Holton (1981) has also developed a modified Eulerian model in which the transport is purely advective. His definition of the residual meridional circulation is a little different from that of Pyle and Rogers, and is derived from the output of a primitive equation model. Nevertheless, the models are basically similar in approach and represent an area of activity in two-dimensional modeling. However, neither model includes diffusion which is important. It should be remembered, for example, that the spread of radioactive traces from equatorial latitudes is well represented as just a diffusion process (Feely and Spar, 1960; Reed and German, 1965).

One approach that might hold some promise in two-dimensional modeling of the stratosphere is isentropic modeling, i.e., using potential temperature as a vertical coordinate. While this technique has not been used in modeling the stratosphere, it has been used in modeling the troposphere (Bleck, 1974) and the ocean (Bleck, 1978). Mean meridional circulations in the troposphere have also been modeled in isentropic coordinates (Dutton, 1976).

The current state of affairs in two-dimensional modeling of the stratosphere is one in which both theoretical work and three-dimensional modeling results may be expected to provide treatments of the eddy and mean circulation transports that have a better physical foundation than now exists in these models. Most existing two-dimensional modeling efforts use highly empirical transport treatments, and their results must be interpreted with care taking into account these formulations.

THREE-DIMENSIONAL MODELS

Existing Models

Because the atmosphere is a three-dimensional fluid, it is clear that a complete quantitatively accurate simulation of the radiative-chemical-dynamical behavior of the stratosphere requires a three-dimensional model. Three-dimensional models need not rely as heavily on parameterization of unresolved processes as do one- and two-dimensional models. Thus, development of fully coupled three-dimensional models must be regarded as a key objective of any serious long-term research effort to understand and predict perturbations of the ozone layer and/or surface climate as a result of human activities.

The development of a credible three-dimensional simulation is a complex undertaking which cannot succeed without a firm basis in theoretical understanding of the various physical and dynamical processes which control the coupled atmospheric system. Attainment of this level of understanding requires that we utilize an arsenal of three-dimensional models of varying complexity. Although many levels of sophistication are represented by the various models summarized in Table 2-15, for classification purposes we have divided these into two major types: the general circulation model (GCM) and the mechanistic model (MM). We will define the GCM to be any model which is capable of a comprehensive treatment of the atmospheric (stratosphere-troposphere) system using the primitive equations of motion. The MM is a more limited model, simplified to study certain phenomena, such as sudden warmings. MMs classified here are usually area restrictive (e.g., no troposphere) and/or dynamically simplified (e.g., quasi-geostrophic).

A major goal of three-dimensional modeling is to provide an accurate simulation of stratospheric dynamic phenomena to (1) increase our understanding of the physics of the stratosphere, (2) guide measurement strategies, and (3) perform prognostic studies to determine the impact of various pollution scenarios on the Earth's climate. All of the models mentioned in this section achieve a measure of success in the first goal. Fewer of the models, only the most sophisticated, have made achievements along the other lines. Because three-dimensional models are time consuming, complex, and require several years of development, results from the simplest

Table 2-15

Three-Dimensional Stratospheric Models

Investigator Institution	Dynamics: Type	Dynamics: Versions of Equations, Horizont	Dynamics: Domain	Dynamics: Levels	Dynamics: Initialization	Physics: Radiation: SR	Physics: Radiation: Insolation	Physics: Stratospheric Momentum Sources/ Sinks, Diffusion	Troposphere	Chemistry	Sponsor	Level of Effects (MY)	Purpose or Goal	Most Recent Publications
C.J. Gadd British Met. Office	MM	PE/Grid 5° x 130 Km	Global	18	Climatology-spin up	NC	Climatology	Nonlinear diffusion	Moisture Cycle surface exchange, topography, crude PBL	Nonlinear O_3 and tracer	BMO	1	Study stratospheric dynamics, stratospheric tracers	O'Neill et al. (1980)
A.J. Gadd British Met. Office	MM	PE/Grid 5° x 10°	Global/ stratospheric	32	Satellite data	NC	LH	Rayleigh friction	–	Nonlinear O_3	BMO	3-1/2	Study dynamics, ozone layer, data assimilation	–
W. L. Grose NASA–Langley	MM	PE/S 23 x 23	Global	12	Spin up	NC	LH	Scale selective dissipation	Orography and surface heating no PBL, dry	Off line	NASA	3	Investigate stratospheric dynamics and transport	–
J.R. Holton Univ. of Washington	MM	PE/S6 10° x 3	Global/ stratospheric	12	Spin up from data	WL	LH	Rayleigh friction	–	–	NASA	3	Study wave mean flow interaction and wave transport	Holton and Wehrbein (1980a)
B.G. Hunt Australian	MM	PE/S5 4.5° x 40	Global	54	Climatology	Owa scheme	Owa scheme	– –	No topography, dry, surface heating, crude PBL	–	CSIRO	1	Simulate stratospheric structure 0-100 Km	Hunt (1981)
A. Kirkwood, K. Rose Free University, Berlin	MM	PE/Grid 5° x 22.5°	Hemispheric, stratospheric	24	Data set	NC	–	–	–	–	DPG	2	Sudden warmings studies	–
E. K. Kao University of Utah	MM	PE/S 24 x 4	Hemispheric	31	Data set	NC	–	ν^2 diffusion	Dry topography and PBL	–	NASA/ MSP	2.5	Sudden warmings, Troposphere-stratosphere interaction	Lundi et al.(1980)
J. D. Mahlman et al. GFDL, Princeton Univ	GCM	PE/Grid up to 5° x 3.6°	Global	40	Spin up	PS	LH	Rh-dependent diffusion S type diffusion	Prescribed clouds, O_3 or tracer full troposphere simulations	Off line	NOAA	8	3-d fully interactive model development to understand entire middle atmosphere, Tracer and pollution studies	Pyle et al. (1980)
Prinn et al* MIT GIT	MM	QG/S 20 x 20	Global	12	Spin up	R	Owa scheme interacts with chemistry	–	Topography no PBL, dry, surface heating	O_x, NO_x, HO_x ClO_x (50 reactions)	NASA	3.2	Investigate the interaction between chemistry-dynamics and radiation in stratosphere	Ou-Jaidi et al. (1980)
D. Rind GISS	GCM	PE/Grid 8° x 10°	Global	15	Data set	Owa scheme	LH	–	Topography, PBL, moist	Off line HO_x,NO_x,ClO_x	NASA	<10	Investigate stratospheric dynamics, climate studies	–
M.B. Schoeberl Naval Res. Laboratory	MM	QG/S6 5° x 5°	Global	35	Steady state winter	A	St	Rayleigh friction	Prescribed tropopause temperatures, topography	Photochemical equilibrium O_3 fixed	NASA/ ONR	1-1/2	Study dynamics, chemistry, of the stratosphere, troposphere interaction	Agnmaw et al. (198*)
R. Young NASA–Ames	MM (Under development)	PE/S 7 x 7	Global	16	Variable	–	–	$K_H \nabla^4_H$ diffusion	No topography	–	NASA	2.5	Develop general purpose model for atmospheric studies	–

NOTES
– = None or not applicable
GCM = Model capable of simulating entire stratosphere includes troposphere and mesosphere
MM = Restricted to a region of phenomena, very low resolution, or uses simplified equations of motions
* = Two versions, only most recent described
A x B = for Grid A,B = degrees (lat x long)

PE = Primitive Equations
QG = Quasigeostrophic
Grid = Grid in horizontal direction
SS = Semispectral grid in NS, harmonics in EW
S = Spectral harmonics in both directions

for SS A = degrees B = zonal harmonics

NC = Newtonian cooling
PS = Fels and Schwarzkopf (1981)
LH = Lacis and Hansen (1974)
St = Stuhlbel (1978)
S type diffusion = Isoenergetic diffusion

R = Rammathan (1976)
Crude PBL (Planetary Boundary Layer) = Either Ekman layer or surface drag
A = Agnmaw (1980)
WL = Wehrbein and Leovy (1981)

for S A,B = meridional harmonics x zonal harmonics

three-dimensional models have dominated the literature in number, at least. This section contains a brief review of the progress achieved by the three-dimensional models and a discussion of some of the anticipated future research areas to be attempted with these models.

The list of three-dimensional models (and modelers) given in Table 2-15 is based on a poll of the community. This list contains only the poll respondents and may not be complete. We have not included models which are no longer active (e.g., Schlesinger and Mintz, 1979) or models still under initial development. Only one publication is listed for the models which have published results. Additional references may be found in the listed publication.

Formulation of Three-Dimensional Models

Some extra care must be devoted to the formulation of stratospheric models since it is not immediately obvious what resolution requirements are needed to simulate stratospheric structure. It is apparent from Table 2-15 that a variety of vertical and horizontal spacing schemes are used by various modeling groups. For the "stratosphere only" models, the resolution is often dictated by the phenomona under study.

In the vertical, the resolution should be some fraction of the vertical wavelength of the eddies or depth scale of the circulation under consideration, or a fraction of the density scale height, whichever is less. These scale requirements are quite different for the mid-latitudes and the tropics. For example, some tropical stratospheric wave simulations may require vertical grid scales of 1 km or less (Plumb, 1981). On the other hand, mid-latitude planetary wave simulation may require a vertical grid of only 3 to 5 km because planetary waves are observed to have rather long vertical wavelengths in the stratosphere.

Another problem associated with stratospheric models is the upper boundary condition. Many models use a log pressure (or $\log \sigma$, where σ is the ratio of the pressure to the surface pressure) vertical coordinate which requires a boundary condition at some finite altitude. The rigid lid condition ($\dot{\sigma} = 0$ at the upper boundary) reflects upward propagating waves. To prevent such reflections some models employ enhanced damping regions below the lid. The effect of sponge layers on the dynamics of three-dimensional models is not completely known and remains a subject for future research. Nevertheless, it appears that stratospheric models should place their sponge layer and rigid lids well above the stratopause to avoid interference with the zonal mean circulation.

The lower boundary conditions, of course, vary depending on whether or not the model includes a troposphere. Many of the "stratosphere only" models make some kind of specification of the eddy fluxes into the stratosphere as well as zonal mean fields along some pressure surface in the troposphere or at the tropopause ($\sim$ 100 mbar). These models can make no attempt to study troposphere-stratosphere interaction but focus on the flow evolution in the stratosphere alone.

The models which contain a troposphere often use the implicit topographic formulation of the coordinate system which follows the topography. Thermal forcing is often utilized in the context of specified land-sea temperatures, or the more comprehensive models use fixed surface temperatures over the ocean and an energy balance condition over land.

Some models (e.g., GFDL's model) use an interface between σ and p systems at some finite pressure (Sangster, 1960; Arakawa and Lamb, 1977). While this system may provide some computational difficulties for the dynamics and may reflect some upward propagating waves, (aithough there has been no demonstration of this) it offers other distinct advantages as discussed by Fels et al. (1980). For example, the computational speed of the model is increased because the horizontal diffusion terms and other pressure determined parameterizations in the

model do not have to be interpolated from the σ to the p grid. Also, it facilitates the analysis of the modeled fields.

A variety of methods are used for the horizontal approximations of differential equations. Finite difference techniques with fourth order accuracy are known for grid point models, and enstrophy and energy conserving schemes have been clearly described (Arakawa and Lamb, 1977). Spectral methods are also quite popular since they are relatively simple to code and appear to have slightly lower computer memory requirements for equivalent resolution. Spectral models generally use an advective formulation (Bourke, 1974, for example) but a flux form has been recently developed by Gordon (1981). There does not appear to be any clear computational or formulative advantages of high resolution spectral models vs. grid methods in the long run.

Quasi-geostrophic numerical models have been used historically because the quasi-geostrophic scaling eliminates gravity waves, thus permitting a larger time step. A drawback in the quasi-geostrophic approximation is that the equatorial circulation is poorly modeled.

The development of the semi-implicit time scheme (Robert, 1969) and other specialized algorithms (Gadd, 1978) allows a large increase in the time step for the primitive equation models without a corresponding increase in the computational overhead. This technique is usually applied to spectral models (Bourke, 1974) but has also been used in grid models (Chang and Madala, 1980). The computational cost advantage of the quasi-geostrophic model has decreased relative to the primitive equation model but because of its simplicity it still remains a useful tool for stratospheric modeling.

The parameterization schemes for the physical processes in the stratosphere vary widely as Table 2-15 indicates. These schemes fall into three categories: radiation (UV insolation and IR processes); chemistry, friction or diffusion of momentum; and the inclusion of the transport and chemistry for trace constituents. How the models formulate these processes will be discussed in the next sections since these aspects of the models usually represent recent developments.

Status and Progress of Three-Dimensional Models

In principle, three-dimensional models can be made to be more internally consistent and made to include more interactive physical processes than can the lower order, more highly parameterized models. Historically, workers with three-dimensional models have been reluctant to include complicated interactive chemistry packages in them. This is partly due to considerations of computer resources, but there are also more fundamental reasons.

For example, the study of interactive transport and chemistry using a general circulation model with questionable dynamics, i.e., one in which the dynamic structure does not compare favorably with observations, does not tell one much about the Earth's atmosphere. In addition, uncertainity in chemical reaction rates and/or photochemical cross sections has caused investigators with three-dimensional models of the stratosphere to avoid incorporating on-line computation of transport and chemistry into their models for the most part. The emphasis of these three-dimensional models at the present time then is on the understanding of radiative-dynamical-chemical interactions rather than on completely simulating stratosphere conditions or predicting future states of the stratosphere.

The following sections discuss some of the recent contributions of three-dimensional modeling to understanding the stratosphere. Only recent efforts are discussed since previous efforts have been reviewed by NASA RP 1049.

The Zonal Mean Circulation

There is a significant departure from radiative equilibrium in the middle atmosphere during solstice in both the summer and winter mesosphere and at the winter stratopause (Murgatroyd and Goody, 1958). For example, radiative equilibrium computations give polar night stratospheric temperatures 40 to 50° lower than is observed (Manabe and Hunt, 1968). Leovy (1964) and later Schoeberl and Strobel (1978a) showed that dynamical heating and cooling by a vast pole-to-pole circulation cell could raise the winter stratopause and lower the summer mesopause temperatures to the observed values. To generate the pole-to-pole circulation cell, these authors required a momentum sink in the mesosphere which they parameterized by Rayleigh friction.

Holton and Wehrbein (1980a) and Mahlman and Sinclair (1980) showed that the zonally symmetric circulation in addition to warming the winter polar stratosphere could produce the easterly phase of the semiannual oscillation of the mesophere.

Upward propagating planetary waves appear to be incapable of providing the large momentum sink that is given by the Rayleigh friction parameterizations in the studies mentioned above. Furthermore, planetary waves are observed at upper stratospheric levels only in the winter hemisphere while the momentum sink must be present in both hemispheres throughout the seasons.

Lindzen (1971) and others have suggested that breaking gravity waves which originate in the troposphere might provide such a momentum sink. Lindzen (1981) has analyzed the gravity wave problem noting that breaking gravity waves would produce a momentum sink with a functional form quite unlike Rayleigh friction. However, Lindzen's model, also highly parameterized, has yet to be fully tested in a three-dimensional model. Andrews et al. (personal communication) have been able to simulate closure of the stratospheric jets in an annual mean model using a Richardson number dependent diffusion. In their calculation, the required deceleration is induced in the upper mesosphere by the mechanical dissipation of upward propagating planetary waves.

The importance of the diabatically forced mean meridional circulation in the upper stratosphere for tracer transport studies was emphasized by Dunkerton (1978). In addition to the diabatic effects of radiative heating and cooling, the momentum dissipation processes for the zonal mean flow are crucial in determining the strength of the mean meridional circulation in the upper stratosphere. The lower and middle stratosphere, however, contains large amplitude dissipating and transient waves which also contribute to the transport of tracers and the diabatic processes of lower stratosphere as will be discussed in the next section.

Another physically important aspect of the zonal mean circulation is the tropical Hadley cell. It is currently believed that the dessication of the stratosphere occurs because the minimum water vapor mixing ratio in the stratosphere is partially set by the mass of air ascending through cumulus "hot towers" in the tropics. The minimum mixing ratio provides a sink for the downward flux of water vapor (generated by methane photolysis) from the upper stratosphere. The fact that the water vapor mixing ratio varies by four orders of magnitude from the surface ($\sim 10^4$ ppm) to the lower stratosphere (~5 ppm) has important implications for the development of hydrological and transport schemes in three-dimensional stratosphere-troposphere models. For example, if the water vapor mixing ratio exceeds 15 ppm in the stratosphere through numerical error, the radiation budget will also be affected. The large variation of water vapor mixing ratio with temperature probably makes it unrealistic for a finite grid model to simulate the cold tropical tropopause trap without parameterization. Kida (1977), in a simplified general circulation model, has shown that air parcels do, on the average, follow the trajectories of a large Equator-to-pole "Hadley cell." Three-dimensional models should incorporate a fairly realistic tropical troposphere with a

moisture cycle and simulated latent heat release to simulate the Hadley cell correctly. Very few of the models listed in Table 2-15 have this capability at present.

Extratropical Waves, The Sudden Warming

The winter stratosphere is influenced by the presence of large amplitude planetary scale waves as indicated by observational studies (e.g., Van Loon et al., 1973), and predicted by numerical models (e.g., Matsuno, 1971). These waves play an important role in the transport and variability of inert and photochemically active trace species. Thus it is essential that the large scale waves and their effects on the mean flow be reasonably simulated in three-dimensional models. The most spectacular example of large scale wave-mean flow interaction in the stratosphere is the stratospheric sudden warming. This phenomena has been the focus of much recent work. Numerical simulations by Schoeberl and Strobel (1980) pointed out the differences in the development of the warming for different wavenumbers and examined the effect of dissipation on the warming. Lordi et al. (1980) and Hsu (1981) demonstrated how wave-wave interactions can greatly alter and possibly accelerate the evolution of the sudden warming. O'Neill (1980) analyzed the sudden warming which spontaneously appears in the British three-dimensional model. He noted that prior to the warming event the equatorward flux of momentum by planetary scale waves suddenly reverses. Similar results were obtained by Haggard and Grose (1981). Dunkerton et al. (1981) have diagnostically analyzed a model generated zonal wavenumber 2 sudden warming. They showed that the evolution of the mean flow as a result of wave-mean flow interaction processes could be determined by evaluating the so-called Eliassen-Palm (EP) flux (Eliassen and Palm, 1961 and Andrews and McIntyre, 1976). The EP flux can be shown to be a fundamental measure of the flux of wave activity in the meridional plane which has the property that its divergence nearly equals the net wave driven mean flow acceleration. The wavenumber 2 warming is often characterized by the poleward progression of easterlies. They found that the evolution of critical layers at low latitudes from absorbing to reflecting wave energy produce this effect. Even some fully nonlinear models show this behavior (Lordi et al., 1981), but the real atmosphere does not appear to produce sudden warmings in this manner. Considerable effort is under way to try to understand the differences between models and observations.

The significance of planetary wave dynamics on the transport of trace species was clearly demonstrated by Hsu (1980). She used a ring of marker particles to trace the Lagrangian motion of the fluid during a model generated sudden warming. Figures 2-9 and 2-10 show her results. The sudden warming was a planetary wave 2 event with a polar temperature peak occurring at day 30. In Figure 2-9 the evolution of the ring of tracer particles in the horizontal plane is shown. Figure 2-10 indicates the height-latitude cross section of a ring initially at 60°N. The Lagrangian mean motion of the fluid is also nicely illustrated in Figure 2-10 where the descent of the center of mass of the ring is clearly seen. The rotation of the ring illustrates the presence of eddy heat transport as downward displaced particles, which are compressionally heated, move northward. Upward displaced (cooler) particles move toward the Equator. Both figures show the enormous horizontal and vertical dispersion which take place for air parcels during the sudden warming. In the horizontal plane, air parcels at 30°N are displaced to nearly 60°N in 10 days. A vertical dispersion of 4 km is seen in Figure 2-10. Note that the dispersion of the particles is much larger than the Lagranglan mean displacement. Such dispersion will produce large altitude variability in tracers with an initial mean gradient and will also contribute to "mixing" of the air parcels.

The overall condition of the stratosphere-troposphere system which gives rise to the sudden warming and the mechanism by which large scale waves are forced and maintained still are not well understood. Schoeberl and Strobel (1980) have indicated that planetary scale topography seems sufficent to produce the large scale waves which force the sudden warming. The role of thermal forcing due to land-sea heating has yet to be explored fully (Dickinson, 1980).

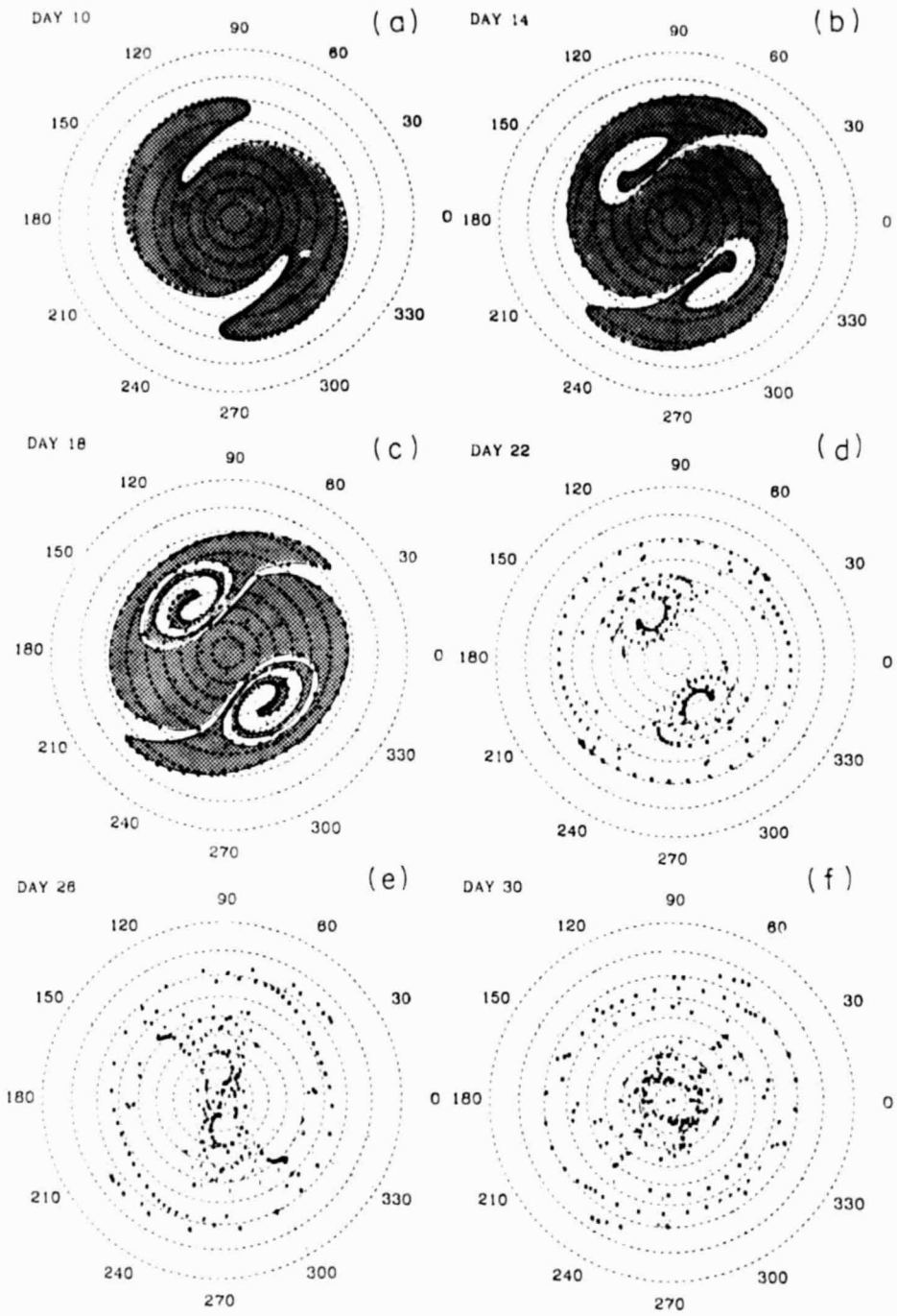

Figure 2-9. Horizontal projections of a set of particles on the indicated days. The particles are distributed uniformly around the 30°N latitude circle at 30.8 km on day 0. In (a)-(c) the area inside the thin solid line connecting the particles is shaded. This is not possible in (d)-(f) due to the complicated geometry (from Hsu, 1980).

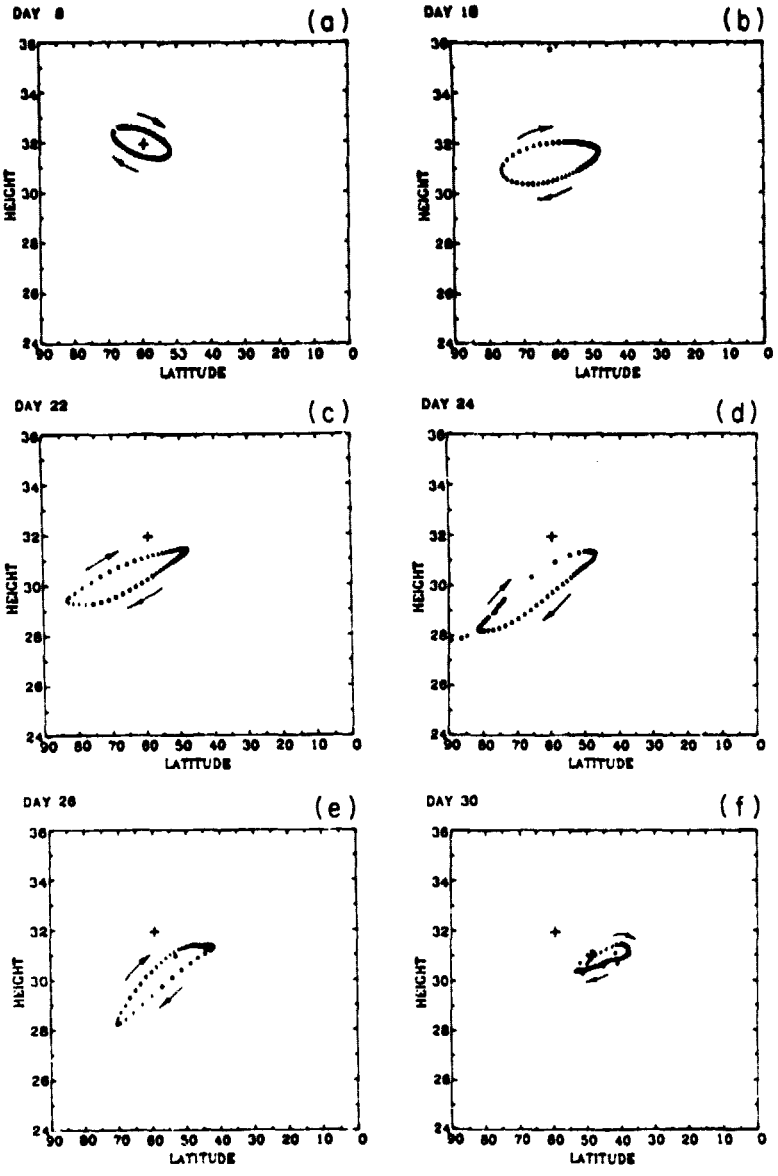

Figure 2-10. Height-latitude cross section of a ring of particles initially at 60°N (from Hsu, 1980).

Tropical Waves

Some three-dimensional models have had some success at simulating tropical wave structure in the upper stratosphere (Mahlman, personal communication), but the requirements on vertical resolution probably puts the QBO (Quasi-Biennial Oscillation) beyond the range of most models where the resolution requirements were made with the extratropics in mind. On the other hand, it is not apparent that the QBO--and simulation of the mixed Rossby-gravity and Kelvin waves which force the QBO play any significant role in tracer advection outside of the tropics. However, extratropical effects of the QBO cannot be ruled out. For example, Holton and Tan (1980) have shown that 50 mbar height deviations at high latitudes are apparently correlated with the QBO phase. Sudden warming simulations by Schoeberl and Strobel (1980) also showed different results depending on the phase of the QBO. Certainly, the BUV total ozone amounts show a quasi-biennial modulation. Thus, QBO simulation may be a necessity for a realistic simulation of the extra-tropical stratospheric environment.

Dunkerton (1979) has proposed a mechanism whereby the dissipation of a vertically propagating, zonal wavenumber 1 Kelvin wave with phase speed in excess of 50 m/s might give rise to the westerly phase of the semiannual oscillation. Observations appear too coarsely spaced in the vertical to confirm this idea (Hirota, 1978) but it is interesting to note that the westerly phase of the semiannual oscillation in the GFDL model appears to result from the same mechanism (Mahlman and Sinclair, 1980).

Radiation

A considerable effort has been made to improve the radiative transfer algorithms in three-dimensional models. Studies by Ramanathan (1977) indicated that important changes in the direct radiative interaction between the stratosphere and the surface might be possible through the downward stratospheric IR emission during sudden warmings. Because H_2O carries most of the IR load from the troposphere, tropospheric GCMs use very simple CO_2 and O_3 IR models. However, H_2O is the weakest IR emitter in the stratosphere with optically thick CO_2 taking the load. The opacity of the CO_2 line cores make careful treatment of line wings, overlap effects, hot bands, and isotopic bands important since almost no radiation escapes to space from the line core itself. A very sophisticated accurate radiation model has been developed recently by Fels and Schwartzkopf (1975, 1981). Computationally faster, but less detailed models have also been developed by Apruzese (1980) and Wehrbein and Leovy (1981) using different techniques.

The necessity of accurate sophisticated treatment of radiation has been demonstrated clearly by Fels et al. (1980) for CO_2 doubling and O_3 depletion experiments in their annually averaged model. The impact of the new radiative transfer schemes on model-simulated sudden warmings is currently being investigated.

Some new results have also been obtained in the computation of solar insolation. Most models or parameterization schemes use the measurement of UV fluxes by Broadfoot (1972) to compute the heating in the Herzberg continuum and Hartley regions; however, a new measurement by Mount et al. (1980) during solar maximum indicates that these values may be too high by 35 ± 15%.

One of the weakest points of model radiative parameterizations is the treatment of clouds and their radiative properties. Cloud emissivities are arbitrarily prescribed instead of making these depend on the water content of clouds. This is potentially a serious problem for cirrus clouds since their water content varies significantly from Equator to pole, particularly during wintertime. It is possible that the corresponding latitudinal variation in IR cooling rates, which is not accounted for in models, may help determine the wintertime zonal wind profile between the

upper troposphere and middle stratosphere. Furthermore, since the water content of cirrus clouds is largely determined by large-scale dynamics, cirrus cloud-radiative interactions may be one of the important contributors to radiative dynamical interaction.

It is well established that radiative-chemical coupling amplifies the radiative damping rates in the stratosphere, a process first postulated by Craig (1950). This effect results from the temperature sensitivity of the Chapman reactions. However, the emergence of catalytic reaction control of the photochemical equilibrium ozone mixing ratio indicates an increased time constant for photochemical acceleration of the radiative damping rate. Recent work indicates that radiative damping (Fels, 1981) and photochemically accelerated radiative damping in the atmosphere is strongly dependent on the vertical scale (Hartmann, 1978; Strobel, 1978, 1979; Ghazi et al., 1980). In the former case, if the vertical wavelength of the thermal disturbance is short (one scale height or less), IR exchange between layers enhances the radiative relaxation. In the latter situation, the vertical structure of the ozone column determines and controls the insolation changes which are important for photochemical acceleration.

Chemistry and Tracers

Long-term simulation with interactive although with highly simplified chemistry and dynamics have been performed with the MIT/GIT model (Cunnold et al., 1980). Most modelers prefer to utilize "off line" tracer chemical models in which the dynamic model advects and diffuses the tracer, but no feedback into the dynamic model is allowed. This latter type of model can fill a variety of roles. Moxim and Mahlman (1980) for example, have used the tracer model developed by Mahlman and Moxim (1978) to assess the ozone sampling network and determine the impact of new observing stations. Mahlman et al. (1980) have used the same model with 11 level GCM dynamics to examine ozone advection using chemically computed and specified ozone distributions along the upper boundary (10 mbar). They found, as is observed, poleward-downward flux of ozone during winter due to the "Lagrangian-mean" drift of the constituent as produced by transient and dissipating eddies. This process is of great importance in the irreversible transport of tracers into the polar vortex. Levy et al. (1979) have also examined the structure and variability of N_2O with their tracer model.

RADIATIVE-CHEMICAL-DYNAMIC INTERACTIONS

Introduction

The observed stratospheric climate is influenced strongly by interactions among radiative, dynamical, and chemical processes. Troposphere-stratosphere interactions also play a key role in determining stratospheric climate since the two regions of the atmosphere exchange mass, momentum, and radiative energy. The coupled nature of the problem as we understand it from modeling and observational studies is illustrated schematically in Figure 2-11. The troposphere-stratosphere radiative/mechanical coupling, of course, enables changes in stratospheric climate to be transmitted to the troposphere to some extent. Vertically propagating planetary waves and modulation of tropospheric solar absorption by stratospheric O_3 absorption are some of the possibilities. Recent one-, two- and three-dimensional model studies have examined the interactions among some of the processes and have provided valuable insights into the problem. In spite of these important recent developments, several outstanding problems need to be resolved in our understanding of these interactive processes. Here, we will focus our attention on this aspect (viz, the outstanding problems) of modeling interactive processes.

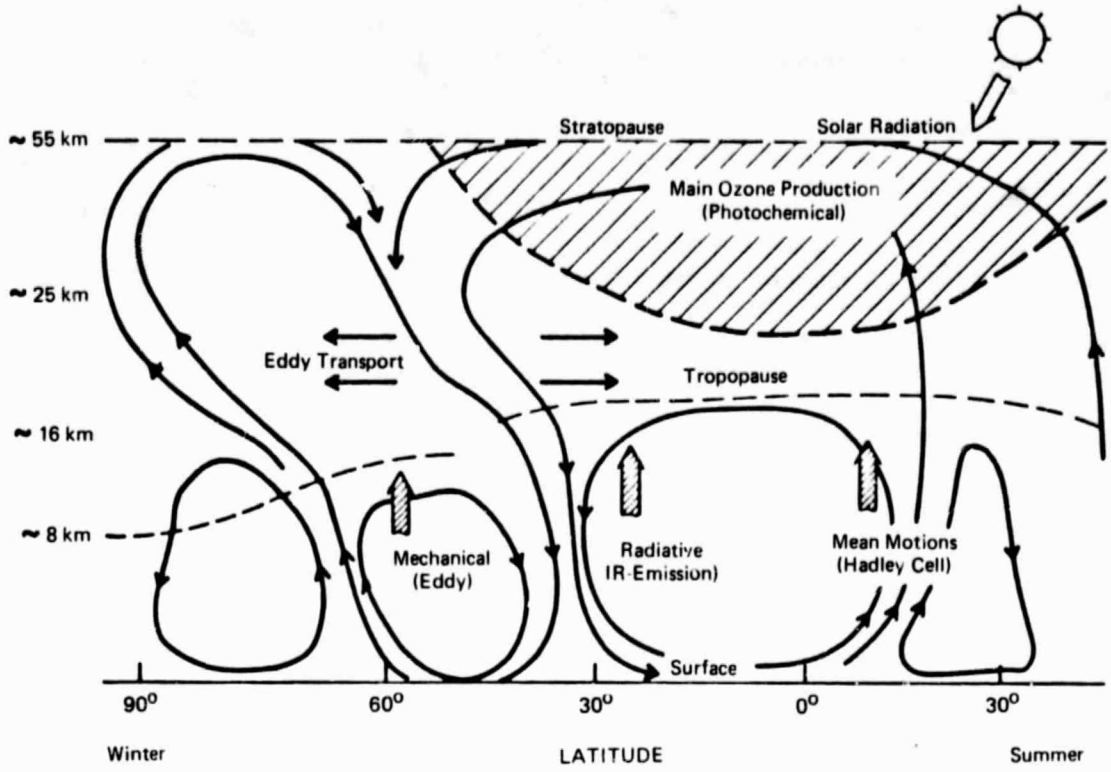

Figure 2-11. The coupled troposphere-stratosphere system (from Ramanathan, 1980a).

Modeling Interactive Processes

Radiative-Dynamical Interactions

- Wintertime Zonal Winds and Temperatures

The troposphere-stratosphere coupling through planetary wave propagation is strongest in winter and spring since planetary waves propagate mainly in the presence of westerlies. The poleward transport of heat by these waves helps to maintain wintertime middle and polar latitude temperatures against IR cooling.

Furthermore, these effects of the propagating waves are strongly influenced by the vertical and latitudinal distribution of radiative dissipation rates. As a result, the wintertime stratospheric climate is determined to a large extent by stratosphere-troposphere coupling and by radiative-dynamical interactions within the stratosphere. Hence, the simulation of the winter stratosphere is a crucial test for a model's capability to account for such coupled processes. Unfortunately, most primitive equation GCMs fare badly in this area. The winter polar temperatures predicted by the GCMs in midstratosphere are often 30 to 40 K colder than observed and the zonal winds are almost twice the observed. Improvements in several areas may be required to resolve this problem: (a) proper treatment of radiative effects: temperature dependence of CO_2 hot bands, Doppler broadening effects, a better prescription of the vertical and latitudinal distribution of H_2O and clouds (these radiation processes may introduce strong latitudinal and vertical gradients in radiative dissipation rates as well as greatly reduce polar IR cooling during wintertime); (b) proper treatment of physical

processes that excite cyclone and planetary waves in the troposphere and lower stratosphere; and (c) inclusion of the mechanical dissipation by small scale motions in the mesosphere which can indirectly warm the stratosphere through an enhancement of the mean meridional circulation.

- Interhemispheric Asymmetry

  Another observed phenomenon which may provide a test for the model's ability to simulate radiative-dynamical interactions is the interhemispheric asymmetry in the observed lower stratospheric temperatures. The difference between the observed zonally averaged mean temperatures in the two hemispheres in corresponding months is reproduced from Van Loon et al. (1972) in Figure 2-12. Several suggestions (sometimes contradictory) have been put forward to explain the very low Antarctic winter temperatures in the lower stratosphere. For example, Wexler et al.(1960) suggests weaker meridional exchange of air in the Antarctic, while Schumacher (1955) indicates the reduced 9.6 μm O_3 heating in the Antarctic (since surface emission is much lower there) as the reason for the colder Antarctic stratosphere. Note from Figure 2-12, however, that maximum interhemispheric differences in surface heating occur in fall whereas maximum interhemispheric differences at 100 mbar occur in spring. Basically, there is a significant change in the seasonal phase of the interhemispheric asymmetry from the surface to 100 mbar. The slightly warmer 100 mbar Antarctic temperature in summer can probably be attributed to stronger solar heating, since the summertime solar insolation in the Southern Hemisphere is larger by several percent than that in the Northern Hemisphere. The much colder temperatures during the rest of the season can be attributed to the smaller surface radiation. However, we must invoke dynamical interactions to explain the strong seasonal variation in the interhemispheric asymmetry. In short, it is a problem of troposphere-stratosphere radiative-dynamical interactions. GCMs (Manabe and Mahlman, 1976) are able to reproduce asymmetry to the extent that the lower stratosphere Southern Hemisphere is colder than the Northern Hemisphere but the seasonal phase of the asymmetry shown in Figure 2-12 has still not been satisfactorily simulated. Interhemispheric asymmetries in planetary wave activity (e.g., asymmetries in stationary and transient waves as well as in the structure of stratospheric warmings), radiative heating, and ozone distribution among several others probably play a crucial role in the observed stratospheric features in Figure 2-12. Since these features influence the transport of trace constituents and their interhemispheric asymmetries, it is important to simulate these features in our models (see Mahlman et al., 1980).

Coupling Between Temperature and Ozone Changes

Several of the chemical reactions that contribute to the neutral chemistry of the stratosphere are strongly temperature dependent. The net effect of this temperature dependence is to cause a negative correlation between temperature and ozone changes in regions of the stratosphere where dynamical effects on ozone distribution are not great, e.g., upper stratosphere during summer or at low latitudes. This effect is of importance in understanding the natural variability of the stratosphere. For example, changes in temperature due to natural variation would induce O_3 variations and vice versa. It is also possible that the coupling between temperature and ozone helps control the summer-to-winter temperature changes in the upper stratosphere. In order to understand the importance of this process we need a GCM simulation of O_3 and temperature distribution with and without radiative-photochemical coupling.

Radiative-Chemical-Dynamical Coupling

As can be inferred from the preceding discussions on radiative-dynamical and radiative-chemical interactions, the three processes, viz radiation, chemistry, and dynamics are mutually interactive.

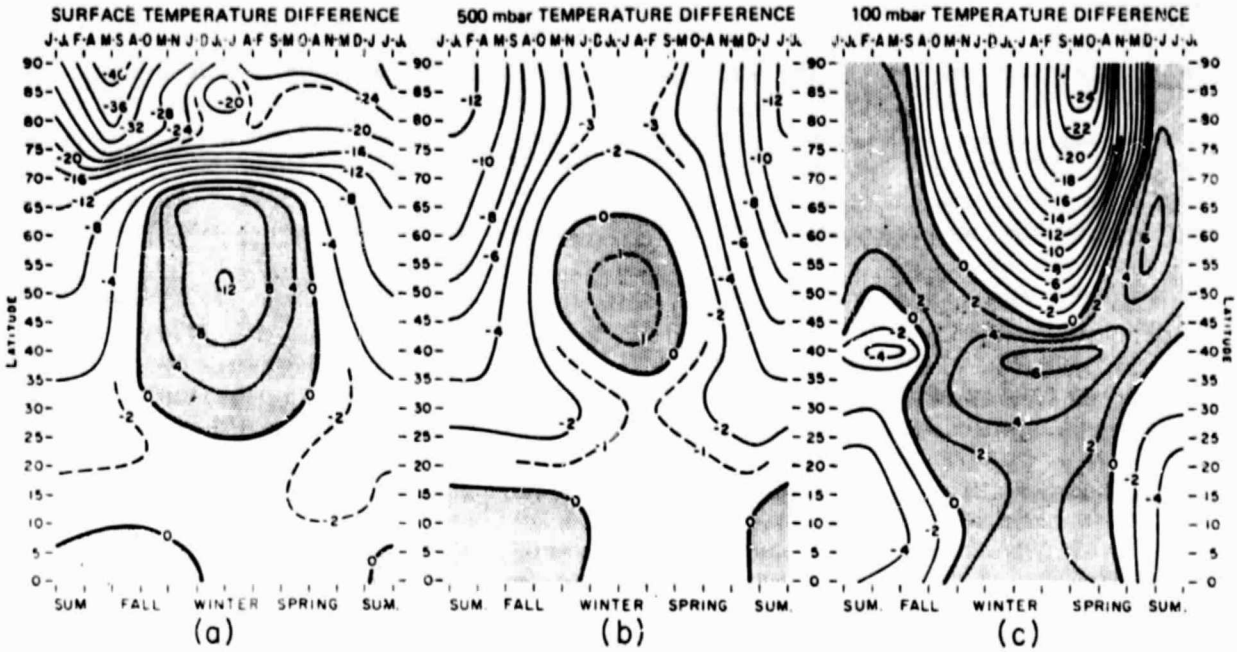

Figure 2-12. Difference (degree centigrade) between the zonally averaged mean temperature in the two hemispheres in corresponding months (shaded where SH is warmer): (a) surface air, (b) 500 mbar, and (c) 100 mbar (from Van Loon et al., 1972).

The role of these interactions on the observed stratospheric climate needs to be assessed quantitatively. We need to explore the problem with two- and three-dimensional coupled models. What is urgently needed are simplified and computationally efficient procedures for incorporating important aspects of the neutral chemistry of the stratosphere in these models.

Simulation of upper troposphere/lower stratosphere water vapor distribution, including cirrus clouds, is especially important because the H_2O distribution in this region of the atmosphere is determined by the following interactive processes: (a) troposphere-stratosphere dynamical interactions through propagating planetary waves and exchange of mass through synoptic scale events; (b) at the tropical tropopause level the IR cooling (or heating) of water vapor and cirrus clouds play a crucial role in determining the zonal mean temperatures. In turn, the stratospheric H_2O is influenced by tropical tropopause temperatures through the "cold trap" mechanism; and (c) furthermore, O_3 solar and IR heating strongly control tropopause temperatures (excepting the winter polar regions). As a result of (b) and (c) above, there is a complex interaction between the O_3 distribution and stratospheric H_2O budget.

With regards to the O_3 distribution, simulating the vertical distribution is as important as simulating the total O_3 since the level of radiative energy (both solar and IR) deposition is quite dependent on the vertical O_3 distribution.

It should be pointed out, however, that there might be several other trace constituents which are more important than the ones discussed above as indicators of a model's success in capturing the essence of atmospheric chemistry, but the constituents and processes described above are some of the best indicators of the model's ability to simulate coupled phenomenon. Models which couple radiative, dynamical and chemical processes are also valuable for estimating effects of stratospheric chemistry on tropospheric climate which is the subject of the next section.

Effects on Tropospheric Climate

The absorption of solar radiation and tropospheric IR radiation by the stratosphere as well as the downward IR emission by the stratosphere helps modulate the solar and IR radiation incident on the troposphere and thus the stratosphere influences tropospheric climate. The magnitude of the various solar and IR processes is shown in Figure 2-13 from Ramanathan and Dickinson (1978a). One of the interesting results in this figure is that the stratospheric absorption of IR radiation (emitted by the troposphere) is twice as large as its solar absorption. Furthermore, the net effect of the stratosphere on the troposphere, computed by taking the difference of downward IR emission and the reduction in solar radiation (caused by stratospheric absorption) reaching the troposphere, is to cause a radiative heating of the troposphere by about 10 W m^{-2}. Based on the sensitivity of present climate models, 10 W m^{-2} radiative heating would cause a significant global surface warming of about 5°K. The troposphere-stratosphere radiative coupling can be altered by natural as well as anthropogenic factors.

Natural Factors

We will give two examples in this category. During sudden stratospheric warming events, there is an enhancement in the downward IR emission into the polar troposphere (Ramanathan, 1977). The magnitude, of course, depends on the strength of the stratospheric warming. The enhanced IR emission not only warms the troposphere but also reduces the pole-to-Equator gradient in radiative heating.

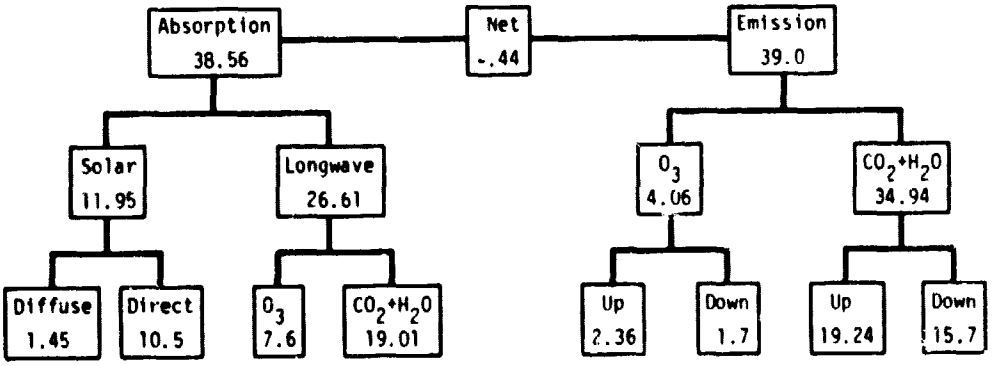

Relative Effects of O_3 and CO_2+H_2O in the Stratosphere	Stratospheric Effect on the Tropospheric Energy Balance	
	(a) Total	(b) O_3
O_3(=11.95+7.6-4.06)=15.49	Solar=-10.5x.69=-7.2	Solar= -7.2
CO_2+H_2O(=19-34.94)=-15.94	IR= 17.4	Longwave, O_3= 1.7
	Net=(17.4-7.4) 10.2	Longwave, (CO_2+H_2O)=7.8(15.7/2)
		Net 2.3

Figure 2-13. Global mean stratospheric radiative energy balance. Net = Absorption-emission. Units W m^{-2}. (from Ramanathan and Dickinson, 1978).

Changes in stratospheric O_3 due to alterations in stratospheric chemistry by events such as solar proton events, cyclical changes in solar UV output, and natural variability in the dynamics would impact tropospheric climate in several ways: the solar radiation incident on the troposphere would be altered; the downward IR emission by O_3 in the 9.6 m region would change with a change in O_3; and the resulting change in stratospheric temperatures would alter the downward IR emission by H_2O and CO_2.

In addition to this radiative coupling between troposphere and stratosphere, there is also the possibility of dynamical coupling through planetary waves as was originally suggested by Hines (1974). Since large-scale planetary waves are known to propagate some of their energy upward from the troposphere through the stratosphere in winter, Hines (1974) suggested that changes in stratospheric winds and temperatures could affect the transmission-reflection properties of the stratosphere to the planetary waves that are forced in the troposphere by airflow over surface topography and the nonuniform distribution of diabatic heating. Bates (1977) and Geller and Alpert (1980) have looked at what changes in tropospheric planetary waves might result if the forcing for these waves remains constant, but there is a change in the zonal mean wind and temperature structure in the stratosphere. Bates (1977) found that dramatic changes in the northward flux of sensible heat resulted from changes in stratospheric structure. Geller and Alpert (1980), using a somewhat more realistic model, found that the stratospheric structure had to be altered below about 35 km before any significant changes in the structure of tropospheric planetary waves were found. Their calculations did indicate, however, that changes in zonal mean stratospheric winds beneath 35 km gave rise to significant changes in tropospheric planetary wave structure given fixed forcing for these waves. It should be noted, however, that in still more realistic models by Schoeberl and Strobel (1978b) and Fels et al. (1980) in which they explored the consequences of uniform column decreases of ozone that no significant change in planetary wave structure was detected. These results appear to be consistent with the results of Geller and Alpert (1980) since the zonal wind structure did not show the necessary changes below 35 km in either of these models. Thus, planetary wave coupling from the troposphere to the stratosphere should be considered as a possible means of coupling tropospheric weather and climate to changes in the stratosphere, but only if some factor causes significant alterations in the stratospheric zonal wind structure at altitudes below 35 km.

Anthropogenic Factors

Radiatively and chemically active trace gases are being injected into the atmosphere as a result of human activities and these gases perturb the photochemical and radiative energy balance of the Earth-atmosphere system. Furthermore, the two processes, viz, photochemistry and radiation, are strongly coupled, and hence realistic estimates of the climatic effects of human activities must be made with models that account for the coupling between climate and photochemistry. The coupled nature of the problem is illustrated in Figure 2-14.

The injection of trace gases CO_2, CH_4, N_2O, and CFCs which have strong IR bands can directly warm the surface by enhancing the atmospheric "greenhouse" effect; while CO, CH_4, and NO injection can warm the climate indirectly by enhancing the production of tropospheric O_3. In addition, injection of CFC catalytically destroys O_3 in the stratosphere, and the resultant alteration in troposphere-stratosphere radiative coupling perturbs the tropospheric climate. It is important to resolve the climatic effects of these various constituents since in some cases the effect of some of the constituents is one of compensation while others are additive. For example, both CO_2 increase and the reduction in O_3 due to CFCs, cool the stratosphere by about the same magnitude. The IR absorption by the CFCs warms the troposphere which may be somewhat compensated by the accompanying O_3 reduction.

Modeling attempts at estimating the future climate changes, due to the anthropogenic emissions shown in Figure 2-14, are subjected to a large range of uncertainty resulting from: photochemical and climate modeling uncertainties; possible large errors in estimates for the natural sources and sinks for the trace species; and finally, uncertainty in the scenarios for future increase in emission rates for these trace gases. These difficulties notwithstanding, the practical importance of the problem clearly dictates that we make serious attempts at unraveling the role of various anthropogenic trace constituents on the climate. However, such attempts ultimately must be made with models that account for the coupling between radiation, chemistry and dynamics.

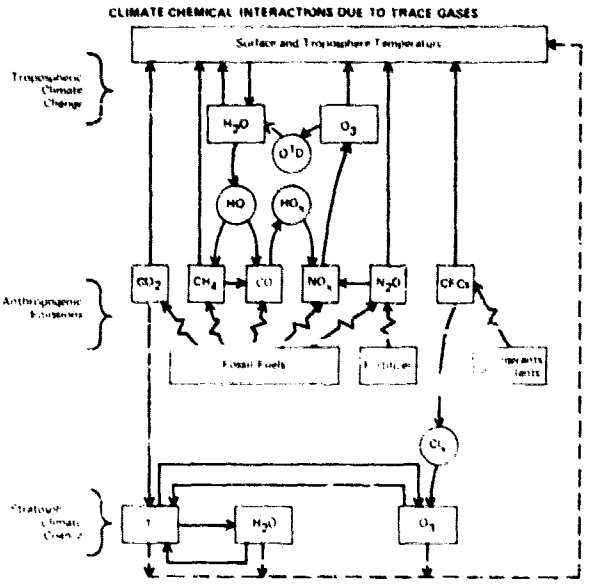

Figure 2-14. Climate-chemical interactions due to trace gases (from Ramanathan, 1981a, b).

COUPLING OF MODELS AND OBSERVATIONS

Introduction

In the past 20 years, emphasis in atmospheric modeling has increased considerably. The physically "complete" and comprehensive general circulation models have demonstrated a steady growth in reliability and sophistication. A by-product of this growth is the demand for even more complete observations to test these model simulations. Although the simulations are far from perfect, there are now a number of physical processes and regions of the atmosphere in which the "best data" available is that provided by such comprehensive models. This suggests that it is now time for the use of this type of model to play a more active role in providing information to aid in the design of various observational programs. There are at least three approaches already being explored:

1. Model output provides information on where and how often to measure. Part of the information gained is used to test the model itself. This new information leads to possible improvements in model design and input.

2. Model output is used to insert model data into real or hypothesized networks. Some of the network biases due to various errors or sampling limitations can then be evaluated. In turn, bias of the model data relative to actual network data can be evaluated.

3. In some models which forecast the short-term future atmospheric structure, observational data is injected directly into the model on a real-time basis. Thus, the model data and observational data co-exist in the model to produce a more realistic analysis.

In the following sections, examples will be presented of the applicability of various research efforts to approaches (1) and (2). To date, approach (3) has not been applied to middle atmospheric problems, although efforts to do so appear to be beginning in both England and the United States. The current status of the use of observations to evaluate comprehensive models also will be reviewed.

Model Guidance for Measurements

In this section we explore the potential for comprehensive models to indicate what might be expected to be measured for a particular quantity at a particular place. This capability is especially meaningful in situations where seldom-measured quantities are involved.

Global Structure of Trace Constituents

A good example of such a quantity is atmospheric N_2O, a substance of fundamental importance for understanding the chemistry of ozone destruction paths. Figure 2-15 shows seasonal zonal-mean cross sections of N_2O mixing ratio and longitudinal relative (percent) standard deviation taken from the 3-D model simulation of Levy et al. (1979). Note that although N_2O concentrations are relatively uniform in the troposphere, significant meridional and vertical gradients are predicted. In addition, N_2O is predicted to exhibit a longitudinal standard deviation of greater than 5% in the stratosphere. Such results thus predict the amount of sampling required to separate out the variability from the average values. (Note that, in this discussion, this 3-D model is being used as an indicator of N_2O variability. It is not being used to test against the observed distribution of N_2O.)

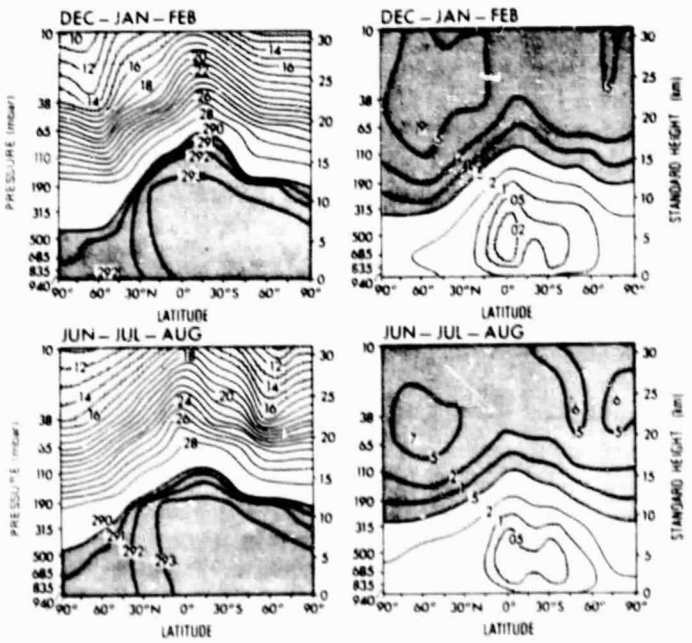

Figure 2-15. On the left are winter and summer cross sections of zonal mean N_2O mixing ratios (parts per million by volume). Note smaller contour interval in the dark shaded area. On the right are winter and summer zonal mean cross sections of N_2O longitudinal relative (percent) standard deviation. (From Levy, Mahlman, and Moxim, 1979).

Later, as more comprehensive modeling experiments become successful, such guidance will be expanded to a much wider variety of trace constituents. In the meantime, results of modeling and observation of N_2O can prove to be of value in planning measurements of other long-lived source gases.

Local Structure of Trace Constituents

It is well known that ozone is characterized by considerably stronger vertical and meridional gradients than those shown in Figure 2-15 for N_2O. Associated with this, the 3-D ozone simulation of Mahlman et al. (1980) predicts longitudinal relative standard deviations as large as 40%. This model also predicts temporal relative standard deviations of similar magnitude in the mid-latitude lower stratosphere. These predicted magnitudes are somewhat less than found in actual ozone observations in each hemisphere by Dütsch (1969, 1974) and Pittock (1977). There may be no incompatibility in these results, however, if the contributions to the variability on space and time scales below those resolved by the 3-D model were to be removed from the observational data. This is a point which must be addressed in any comparison of measured data structure against that of model data. On the other hand, the measured quantities should, if at all possible, have most of the artificial variability due to sampling or measurement error removed from the record before attempting to compare against model data. Normally, this would be accomplished by redundant sampling, at least until the known error structure is identified.

While the large variability of ozone is well appreciated, it is less recognized that other stratospheric trace constituents such as total odd nitrogen or total odd chlorine (or possibly their major "reservoir" subspecies) should exhibit similar structure and variability in the lower stratosphere. In fact, the variabilities of these heretofore unmeasured tracers probably will correlate so highly with ozone itself in the lower stratosphere that well designed programs to observe these constituents should exploit this in their planning.

A related point concerns the spatial scales over which this longitudinal tracer variability is distributed in the atmosphere. For example, in contrast to the usually available meteorological variables such as geopotential height, wind, or temperature, the GFDL 3-D tracer model predicts that lower stratospheric tracers should exhibit considerable variability on scales normally regarded to be "small" for the stratosphere. The model predicts significant power in planetary wavenumbers 6 to 10 and a relatively "flat" spectrum out in the higher wavenumbers (Mahlman, 1975). The TOMS data also shows ozone variability on spatial scales that are associated with upper tropospheric variability rather than with those of the stratosphere (Krueger, personal communication).

Instantaneous model information about horizontal spatial structure of this kind might be used to anticipate the expected structure to be encountered in an aircraft measurement program. In particular, a model prediction of the character of the data to be expected (or required) might shift attention toward a more important set of unanswered questions than would otherwise be addressed.

It should be noted also that lower stratosphere quasi-conservative tracers such as ozone and total odd nitrogen, or total odd chlorine must, in addition, exhibit high local correlations with the potential vorticity (and to a lesser degree, potential temperature). This was shown by Hering (1966) and Danielsen et al. (1970) from comparisons with ozone, and by Mahlman and Moxim

(1978) using the GFDL 3-D tracer model. This fact can aid measurement interpretation by providing a means for assessing which parts of the measured variability are real and which are due to experimental error.

Use of the Data Obtained

Finally, once model-consistent data sets have been obtained, such data should be compared against the equivalent "data" from the models. If they agree, then we might regard that portion of theory and observation to be "well understood". However, in general we can expect that such comparisons will lead to points of significant disagreement between theory and observation. Thus, observation or theory (or both) might be wrong. It is at this point that potential for further progress exists. The nature of the discrepancy may or may not immediately suggest possible avenues for improvement. Nevertheless, an "improved" version of the theory must eventually emerge and the process begins anew, either with existing or "new and improved" data.

Model Evaluation of Observational Networks

Here we summarize some examples which use models to provide evaluations of current observational networks. In these examples, model information is considered at only the locations corresponding to those of the network stations under consideration. The statistics inferred from that subset of points are then simply compared with the complete set available from all the model points. (Much of the material in this section has been adapted from Mahlman, 1979).

Surface Total Ozone Network

The first example is taken from the "Simple Ozone" experiment of Mahlman et al. (1980). In this study, model total ozone "data" are used to evaluate the capability of the active and reliable parts of the surface total ozone network for determination of global and hemispheric means and trends. A sample calculation is presented in Figure 2-16, taken from the analysis of Moxim and Mahlman (1980). This figure shows that the network underestimates the Northern Hemisphere model total ozone, while it overestimates in the Southern Hemisphere.

In that study, it was shown that global annual trends estimated from 2 months separated by a year can be several percent in error due to sampling inadequacies. Averaged over a year, the sampling bias calculated is the order of 1%. No error in long term (e.g., 10-year) trend estimates is implied, however, unless such a trend exists in tropospheric wave patterns. Also, that study addresses the possible improvements to be realized if the network density were to be increased. Such evaluations may aid in the future design of networks in a more effective manner.

Meteorological Rawinsonde Networks

In a different type of study, Oort (1978) examined the capability of the global rawinsonde network to sample various meteorological statistics of importance in the atmospheric circulation by using the general circulation model of Manabe et al. (1974) and Manabe and Mahlman (1976). Although that study indicates that the rawinsonde network gives an excellent portrayal of many quantities, in other cases significant distortions were found. Most notable are the following: serious errors in the Southern Hemisphere mean meridional circulation; a bias toward overestimation of the tropical easterlies in the upper troposphere; and a significant network underestimation (30%) of the Northern Hemisphere stationary eddy kinetic energy.

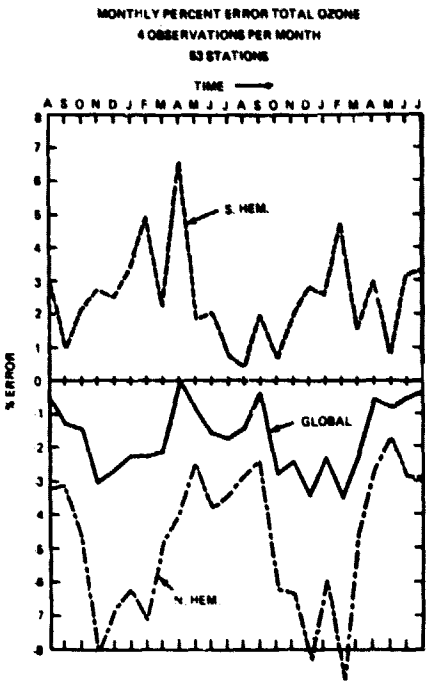

Figure 2-16. Model estimation of the percentage error in measuring global and hemispheric means of total ozone, as determined from a realistic 53 station network (from Moxim and Mahlman, 1980).

Satellite Networks

Although no studies of this type addressing satellite data have yet been performed, the value of such analyses could be extremely high. Such a model-oriented satellite network analysis could, in principle, achieve much more than just evaluation of the data "holes" due to limited longitudinal, vertical, and temporal sampling. For example, systematic analyses could be performed on the impact of the required diagnostic relationships which must be imposed to obtain a "complete" meteorological data set. These requirements, of course, arise from the unavailability of direct wind measurements with current remote sensing technology. Thus, "winds" must be inferred from geostrophic (or possibly higher order) balance relationships. By exploring the errors introduced by using these diagnostic relations of the "data" from a reasonably comprehensive GCM, we might learn in a clearer manner what important processes are being omitted or distorted by such data limitations.

Use of Observational Data to Evaluate Models

It has long been recognized that our "theoretical" understanding of atmospheric structure is strongly guided by the availability of observations. A fairly recent example of this is given by the drastic decrease in the number of competing theories about the stratospheres of our neighbor planets now that improved observations are available.

Judgements about the skill of comprehensive models are always based upon the level of agreement of model statistical properties with corresponding properties of the actual atmosphere. We, of course, are reduced to comparing statistical properties because no two instants in the atmosphere (suitably separated in time) are very much alike, let alone, say, model and actual atmosphere on a given calendar date. Such statistical comparisons are continuing to be more elaborate as our observations and models continue to improve. Here we list some of the types of atmospheric statistics which have been, or will be, useful for evaluating models.

Zonal-Time Means of Various Quantities

Traditionally, this has been the most popular way to present model and observational data. For models, the motivations for this choice is clear. On the other hand, for observational presentations, this choice is not obvious, as massive amounts of data must be assembled and reduced to provide such information. Fortunately for the basic meteorological variables (U,V,Z,T), this has been accomplished for the troposphere and lower stratosphere (e.g., Oort and Rasmussen, 1971). For the middle and upper stratosphere regions, definitive climatologies have yet to be established. However, important contributions are available (e.g., Newell, 1968). In some cases this deficiency appears to be more due to lack of sustained analysis effort than to lack of data. Clearly, the satellites hold tremendous potential for filling these data gaps.

Traditionally, the most useful zonal-mean quantities to determine have been those of the basic variables, their variances and various "eddy" covariances -- usually those related to meridional and vertical transport of various fundamental quantities. Such statistical quantities will continue to be useful as long as we can foresee into the future.

Less common zonal-mean quantities which will receive greater attention in the future are distributions and fluxes of conceptually important quantities related to energy, vorticity, potential vorticity, enstrophy, potential enstrophy, quadratic tracer properties, wave action, etc. In some cases such higher order quantities may be extremely difficult to obtain directly from observations.

Another useful way to prepare data along a latitude circle for model comparison or diagnostic understanding is to present power spectra or zonal harmonic decompositions. This gives us information about the scale of the disturbances found there. Needless to say, such spectra, in addition to the above zonal mean quantities, provide very stringent tests for a comprehensive simulation model.

Horizontal (x-y) Fields of Various Quantities

Considerable increases in our understanding of the structure of the atmosphere can be gained through presentation of various features in horizontal map form. Again, this is not only for time means of the basic quantities, but for other temporal statistical properties such as transient variances, relative standard deviations, and covariances (fluxes). Also, additional useful information can be learned simply from presentation of successive maps of instantaneous structure. This is a surprisingly useful test for a comprehensive model simulation which is not covered by any small set of statistical quantities. In other words if the model instantaneous fields do not look reasonable relative to observed instantaneous fields, the model is probably deficient even if other statistical quantities appear to match reasonably well.

Time Series Statistics

It is very well known that the atmosphere displays variations on every time scale that has been sampled. Thus, time variability provides another important observational constraint on the validity of a comprehensive model simulation.

For convenience, we normally divide this atmospheric temporal variability into regular and irregular parts. The only regular parts that can be accepted without controversy appear to be the diurnal and annual cycles. There also appear to be some regular phenomena which are parasitic on the diurnal and annual radiative forcing. Obvious examples of these are the semidiurnal tide and the semiannual oscillation.

There is an intermediate class of quasi-regular phenomena which for some time intervals appear regular, but do not exhibit sharp spectral "spikes" for complete records. Examples of this class may be the quasi-biennial oscillation, certain wave-like phenomena, and the tropospheric "index cycle". Also in this intermediate class are phenomena which are suspected to be periodic, but not conclusively demonstrated. The obvious examples of great potential relevance to understanding the stratosphere are the so-called 11- and 22-year sunspot cycles. Resolution of this controversy is essential for predicting and monitoring, as well as for modeling the stratosphere.

Finally, the observations indicate a large class of phenomena which must be classified as irregular. Examples include the lower stratospheric remnants of tropospheric cyclonic disturbances, episodic planetary waves, tropospheric blocking anticyclones, sudden warmings and coolings, spring circulation reversal, interannual variability, etc. In each case, such phenomena exhibit considerable spatial and temporal coherence in spite of their lack of predictable variability.

In view of this richness of temporal structure displayed by the atmosphere, suitably prepared time series (or time-height cross sections) provide very powerful tests for comprehensive models. This is a point that appears to have gone unrecognized and unexploited. This arose partly due to the great emphasis given to our need for global data sets and partly because our models and computing capabilities have only begun to be strong enough to focus on extended temporal behavior.

In a sense it seems unreasonable to assert that local time series can provide such powerful tests for evaluations of a global model. However the very richness of the temporal behavior exhibited by the atmosphere means that a corresponding model time series should exhibit similar behavior. Thus, in a sense, a single time series, properly obtained and properly analyzed, is sufficient to demonstrate serious inadequacies in a model simulation.

Obviously, such local information in total isolation from any other knowledge would be of severely limited use. However, these types of records, when interpreted through use of spatial information should see significantly increased application in future model evaluation.

Concluding Remarks

At the present time, it is well known that many stratospheric phenomena, both chemical and dynamical, have not yet been simulated in comprehensive models. In most cases we have reasons to believe that the simulation capability of such models will continue to improve, although perhaps at a slower pace than we would wish.

On the other hand, there are many aspects of model behavior that have neither been confirmed nor discredited by existing data analyses. In some cases the data is simply unavailable. In other cases, this is so because of fundamental limitations in our capability for analysis of observed data. Examples are: energy dissipation rates, sub-scale transfers; chemical sources and sinks, etc.

In any case, future progress seems to depend upon a closer and more productive interactive cooperation between observational and theoretical modeling approaches than we have utilized to date.

TRANSPORT OF TRACE CONSTITUENTS

INTRODUCTION

Much of the material in this section has been adapted from Mahlman et al. (1981).

Historically, attention was focused on how trace constituents are transported by the realization that the distribution of ozone could not be explained solely by photochemical mechanisms alone (e.g., Dobson and Harrison, 1926). After establishment of the Dobson ozone network, analysis of the measurements indicated that maximum ozone column amounts occurred during spring at high latitudes. Furthermore, day-to-day variability at particular stations were observed and were found to correlate with the passage of surface weather systems. For the next several decades numerous investigators devoted considerable effort in an attempt to explain observed local total ozone column variations by various advective and/or flux divergence schemes (e.g., Dobson, 1930; Haurwitz, 1938; Nicolet, 1946; Craig, 1950; Reed, 1950; and Normand, 1953).

Emphasis began to shift toward a global perspective of transport processes with the advent of nuclear weapons testing in the atmosphere. Concurrently, a number of investigators were suggesting various theories for a mean meridional circulation which would act to transport constituents. Dütsch (1946) proposed a mean meridional circulation with sinking motion in the winter hemisphere as a means of transporting ozone to high latitudes. Brewer (1949) suggested a mean circulation with rising motion in the tropics and sinking at the poles would be consistent with the observed "dry" stratosphere. Similar hypotheses for a mean meridional circulation were advanced by Dobson (1956), also the calculations of Murgatroyd and Singleton (1961) gave a consistent result.

Reed and Julius (1951) proposed a role for "eddy motions" (zonally asymmetric) in the transport process. Various other researchers contributed to the concept of eddy transport. But the work of Newell (1961, 1963a, 1936b, 1964, 1965) represented a major contribution toward an understanding of the role of eddy fluxes. For example, his work indicated that forced transient eddy motions could transport both heat and a tracer poleward in a manner consistent with the annual mean "reversed" meridional temperature gradient in the lower stratosphere. Later, it was realized that the stratospheric transport of trace constituents occurs through the combined interaction of the mean circulation and the eddies (e.g., Mahlman, 1966). Hunt and Manabe (1968) performed general circulation model simulations which showed that the net transport of a trace constituent (in the zonally-averaged budget) occurred as a residual of opposing mean cell and eddy flux convergences.

Eliassen and Palm (1961) and Charney and Drazin (1961) had previously indicated that eddy motions do not necessarily lead to a systematic acceleration of zonal mean flows. These results were successively made less restrictive by Dickinson (1969), Holton (1974), Boyd (1976) and Andrews and McIntrye (1976, 1978a, b). The generalized theorem states that steady, frictionless, adiabatic waves of small amplitude, propagating in a basically zonal flow, exert no net effects on the mean flow. Rather, such waves induce meridional circulations at second order in wave amplitude which exactly cancel the eddy flux convergences due to the waves. Further results are available for finite amplitude disturbances, but must be given in terms of "Lagrangian mean" quantities. Note that no general results of this kind are available for waves propagating in basic states which already include violations of the requisite conditions for "non-acceleration" to hold. A little later, various authors offered arguments indicating that "non-acceleration" conditions might also imply "non-transport" for suitably distributed conservative tracers (e.g., Andrews and McIntrye, 1978b; Clark and Rogers, 1978; Wallace, 1978; Plumb, 1979; Holton, 1980a; Mahlman et al., 1980; Matsu[illegible]; Pyle and Rogers, 1980).

The above developments gave a more rigorous basis for the demonstrated connection between the meridional circulation and eddy transports by showing that, under these special circumstances, the induced indirect meridional circulation is a property of the wave field itself. This helped provide an interpretation of the mutually compensating tracer transport convergences found in the numerical simulations of Hunt and Manabe (1968) as well as those found by Mahlman (1973), Newson (1974), Cunnold et al. (1975), Mahlman and Moxim (1978), Schlesinger and Mintz (1979), and Mahlman et al. (1980). The disappearance of this compensating effect when chemical sources and sinks are strong has been shown in the above studies as well as by Hunt (1969) and Clark (1970). Mechanistic interpretations of this effect are given in Hartmann and Garcia (1979) and Garcia and Hartmann (1980). In addition, Mahlman and Moxim (1978) showed that the compensation effect diminishes markedly during seasonal transitions in middle latitudes, and most of the time in lower latitudes.

Thus, even though there are many cases in which the traditional partitioning into zonal means and eddies gives straightforward results there are many others where more enlightened approaches are required. Important advances in this regard were provided in the work of Matsuno (1972), Uryu (1974), and Andrews and McIntyre (1976, 1978b) which demonstrated the power of utilizing Lagrangian displacements (from simple undisturbed states) for gaining analytical simplicity and physical understanding. Using these ideas Matsuno (1972, 1980) emphasized the zonal mean diabatic heating (Murgatroyd and Singleton, 1961) as the most fundamental portion of the meridional circulation, somewhat analogous to that suggested earlier by Danielsen et al. (1962). The utility of this idea was demonstrated by Kida (1977) in a simplified GCM which calculated extended particle trajectories. The point was clarified by Dunkerton (1978) who argued that the motion related to the zonal mean diabatic heating may serve as a good approximation to the "Lagrangian mean circulation" (the average meridional and vertical drift of a material tube of particles, see Matsuno and Nakamura, 1979). On the other hand, the results of Mahlman et al. (1980) suggest that, in the lower stratosphere at least, the effects of eddy diabatic heating are important contributors to the Lagrangian mean cicrculation, as well as to the dispersion of particles about that mean. In that study, the argument was based on the problem of determining the equilibrium structure of the meridional slopes of tracer isolines. The very significant effect of dispersion about the Lagrangian mean was demonstrated rather dramatically in a study of particle trajectories associated with a model sudden stratospheric warming (Hsu, 1980). As will be argued later, proper consideration of such dispersive effects is essential for obtaining a quantitatively correct calculation of trace constituent structure. A number of possibilities and problems associated with application of Lagrangian mean concepts to tracer transport problems have been addressed in a perceptive summary by McIntyre (1980b).

CHALLENGES TO THE UNDERSTANDING OF TRANSPORT PROCESSES IMPLIED BY THE OBSERVED BEHAVIOR OF TRACE CONSTITUENTS

With the preceding brief historical perspective of the trace constituent transport problem as a background, it is appropriate to draw attention to particular aspects of observed characteristics of tracer behavior that present a challenge to theoretical formulations of transport processes. In addition, they impose stringent demands upon comprehensive models currently being used to simulate tracer behavior.

As noted earlier, ozone develops a maximum in the spring high-latitude lower stratosphere. Numerous efforts have been made to simulate the spatial and temporal distribution of ozone. Cunnold et al. (1980) reported long-term simulations of ozone conducted with a three-dimensional quasi-geostrophic model with interactive chemistry. Although they successfully simulated some aspects of the observed ozone, the model employed a severely abbreviated chemistry and transported only ozone with the NO_x distribution specified. Mahlman et al. (1980) conducted ozone simulation experiments with a general circulation model. A

separate 'off-line' transport model was used together with a simplified ozone photochemistry at only the top level (10 mbar) of the model. No feedback from chemistry to dynamics was allowed by this procedure. This experiment demonstrated some success in simulating observed ozone behavior. Both of the above efforts have provided some insight into transport processes, but many questions cannot be answered with the various approximations and constraints imposed on models of these types. A comprehensive three-dimensional model with fully interactive radiation, chemistry, and dynamics has yet to be developed for numerous reasons, both practical and conceptual, some of which have been mentioned earlier in this chapter.

Early measurements of radioactive debris from nuclear weapons tests showed that the debris returning to the troposphere tended to be concentrated at middle latitudes in spring (Machta, 1957). Numerous measurements provided estimates of residence time for the radioactive material in the stratosphere varying between 15 months and 5 years (Libby, 1956; Machta and List, 1959; Feely et al., 1966; and Telegadas and List, 1969). Telegadas and List (1969) explained the differences in residence times inferred for particular debris from those inferred for $C^{14}O_2$ that resulted from the initial deposition of C^{14} at much higher levels by high-yield thermonuclear weapon devices. Mahlman and Moxim (1978) provided theoretical substantiation for increasing residence time with altitude from their general circulation/tracer model simulations.

A tendency for pronounced meridional sloping of zonal mean isolines is observed in the ozone cross sections presented by Hering (1966) and the radioactivity cross sections presented by Feeley et al. (1966) and Machta et al. (1970). Later compilations showed a tendency for largest winter radioactive concentrations tending to occur near 60 to 70° North (Machta and Telegadas, 1973).

The various data compilations indicate a steeper meridional slope for the radioactive tracer isolines than for the slope of zonal mean isentropic surfaces. Hering (1966) noted that zonal mean ozone correlated well with zonal mean potential vorticity in middle and high latitudes. Danielsen et al. (1970) showed that this correlation extends as well into synoptic and mesoscale features. The characteristic slope of the tracer isolines, the winter high latitude bulge, and the correlation with potential vorticity were simulated in the model experiments of Mahlman and Moxim (1978).

Other aspects of trace constituent behavior can be valuable in assessing the validity of theories of transport processes. Dütsch (1969, 1974) and Pittock (1977) have presented statistics of ozone temporal variations at individual stations. They showed that ozone relative standard deviations in the middle latitude, lower stratosphere are larger than 50% in both hemispheres. The individual O_3 profiles show a strongly layered structure which often exhibits strong time continuity (e.g., Breiland, 1967, 1968). Using special observing periods in the North American Ozonesonde Network and trajectory techniques, Berggren and Labitzke (1966, 1968) and Mahlman (1970) have derived daily synoptic maps of ozone mixing ratio. Large synoptic-scale variations of ozone are observed in the maps of the lower stratosphere with maximum values in the long wave troughs. Satellite observations have been used to develop maps of ozone in the middle and upper stratosphere (e.g., Heath et al., 1973). At these levels the variations are larger in scale because of the dual effects of decay of cyclone-scale disturbances with altitude and increasingly efficient photochemical damping.

Despite there being less ozone data for the Southern Hemisphere, significant differences from the Northern Hemisphere are observed. Dütsch (1969) showed that largest values of total ozone are found later in spring and at somewhat lower latitudes than in the Northern Hemisphere.

An intriguing aspect of ozone transport is its relationship with jet streams. Briggs and Roach (1963) noted that larger ozone mixing ratios occurred on the cyclonic shear side of the middle

latitude jet streams. Lovill (1972) noted that total ozone displayed a similar effect. Such a structure is compatible with the direct circulation about the polar front jet stream hypothesized by various researchers (e.g., Namias and Clapp, 1949; Danielsen, 1968) and subsequently calculated by Mahlman (1973).

The behavior of ozone during sudden stratospheric warmings has been noted by several researchers. Dütsch (1962) and London (1962) noted a dramatic increase in ozone at high latitudes during warming events. This has also been noted in satellite observations by Ghazi (1974). A probable interpretation is that the polar ozone increases are a result of the dynamically induced poleward and downward trajectories which produce the warming itself. Observational evidence of this was presented by Mahlman (1970) and simulated with a mechanistic model by Hsu (1980).

Measurements of the vertical and meridional distribution of long-lived trace constituents such as H_2O, N_2O, CH_4, H_2, and chlorofluoromethanes can provide valuable insight into transport processes. Various researchers have obtained such measurements, and these are documented in detail in Chapter 1. For example, the relative dryness of the lower stratosphere may indicate the predominant temperatures of air entering the stratosphere from the troposphere. These long lived constituents can provide information on vertical transport rates in the upper and middle stratosphere. Levy et al. (1979) suggest that such observations can provide extremely valuable tests for quantitative simulation models.

Obviously, observed trace constituent behavior has posed numerous challenges to our understanding of transport processes. Future improved measurements may provide further enlightenment, but undoubtedly will present further formidable challenges to our theoretical analyses and model simulations.

A CONCEPTUAL VIEW OF STRATOSPHERIC TRANSPORT

In this section, we outline some of the various considerations that can be used to construct a usable theoretical framework for understanding stratospheric transport. As will become obvious, these various theoretical arguments have yet to be merged into a single coherent structure. Nevertheless, considerable progress has been made in the past decade or so.

Perhaps the simplest conceptual framework from which to view stratospheric transport is the so-called isentropic (potential temperature) coordinate approach. In this approach, it is first noted that air parcels cannot cross the quasi-horizontal isentropic surfaces of the stratosphere unless non-adiabatic processes are occurring. Of course adiabatic events can cause the isentropic surfaces themselves to move; indeed during a sudden stratospheric warming, isentropic surfaces move comparatively rapidly. However, in the time-averaged sense, the potential temperature surfaces in the stratosphere remain in essentially the same locations from year to year. This means that, for longer term systematic vertical transports, non-adiabatic processes are essential.

These considerations make it immediately obvious that the stratosphere is a region in which the vertical transport of tracers back to the troposphere must be relatively inefficient. First the potential temperatures of the stratosphere are very high, in most cases much larger than have ever been observed as sensible temperatures in the lower troposphere. Thus, stratospheric air must experience considerable cooling before it enters the troposphere. Second, the higher the static stability of the atmosphere, the smaller is the allowed vertical displacement of an air parcel relative to an isentropic surface for a given diabatic heating rate. This again indicates the relatively large resistance to vertical transport in the stratosphere.

To increase our insights into the various mechanisms leading to irreversible transport, let us examine what qualitative understanding might be gained from some simple hypothetical situations. First, consider an almost frictionless stratosphere (say molecular diffusion only), which receives no upward propagating tropospheric disturbances and is subject to no zonally asymmetric instabilities. In the absence of seasonal or diurnal radiation cycles, such a system would be extremely close to radiative equilibrium. Accompanying this would be an intense zonal wind (westerly) of sufficient magnitude to balance the strong meridional pressure gradients necessarily present in such an atmosphere. The only transport of a conservative tracer introduced into such a system would be in the zonal direction. An air parcel injected at a particular place would essentially remain "frozen" at its original latitude, height and potential temperature.

The next obvious modification of this simple imaginary situation is to allow the solar heating to undergo its diurnal and annual cycles. This of course, allows some instantaneous net heating and thus movement of air parcels relative to isentropic surfaces. However, although this time-dependent heating would lead to transient motions in response to the resultant unbalanced pressure forces, probably relatively small net meridional or vertical displacements would occur over periods long relative to the radiative forcing interval.

Now consider what could happen if a significant amount of mechanical damping or friction is added to this hypothetical system. Initially, the frictional damping produces a reduction in the zonal wind, thus leading to an imbalance between the zonal wind and the meridional pressure gradient. This leads to a poleward acceleration of the meridional wind component. The resultant tendency to accumulate mass in higher latitudes lead to sinking there. This sinking, through adiabatic compression, acts to warm the polar region above its radiative equilibrium temperatures. Once such a system finally comes into equilibrium, it is again characterized by a nearly geostrophically balanced zonal wind. However, this hypothetical atmosphere now contains a thermally direct Hadley-type meridional circulation. The poleward flow in the upper branch of the Hadley circulation acts to restore the westerlies against frictional deceleration and maintain geostrophic balance. In addition, the polar sinking and equatorial rising motion act to keep the polar and equatorial temperatures above and below their respective local radiative equilibrium values. This means that the balancing radiative cooling and heating leads to downward and upward flux of air parcels through isentropic surfaces at higher and lower latitudes, respectively. Thus, systematic meridional and vertical air motions are a fundamental property of this simple system. Note, the crucial role of mechanical damping in this system, however.

The next levels of complexity are far more difficult to deal with and understand in terms of their implications for stratospheric transport. Suppose we now allow various motion systems produced in the troposphere to propagate into and influence the state of the above hypothetical stratosphere. Assume a steady disturbance is "switched on" at some instant. Even if the disturbance flow is adiabatic, the stratospheric isentropic surfaces themselves will move toward their new steady-state positions compatible with the steady state forcing. After this initial response, the "non-acceleration" - "non-transport" theorems tell us that little further transport would occur, as long as the crucial assumptions are nearly valid for the basic state, as well as the disturbance.

In a superficial sense, this appears to represent the quasi-stationary state of the early winter Northern Hemisphere stratosphere. However, a closer look shows that this apparently equilibrated "almost non-transport" situation can lead to significant real transport in at least three ways. First, the stratospheric basic state considered here already contains departures from "non-transport" conditions because of the impact of the assumed mechanical friction. Second, the adiabatically forced displacement of the isentropic surfaces leads to actual temperature

changes when viewed in physical space. This, in turn, excites increasing radiative damping, and hence more parcel motion across isentropic surfaces. Third, if such a stationary disturbance is induced during, say midwinter, the eventual onset of summertime radiative conditions can lead to a collapse of the effective forcing. At that time, the associated readjustment of the flow can lead to large irreversible parcel displacements (Mahlman and Moxim, 1978; Matsuno, 1980).

Realistic situations become even more complex in that the forcing is actually time dependent over a number of time scales. In addition, disturbances coming from the troposphere involve a spatial spectrum of motions from small scale gravity waves and clear air turbulence all the way to the scale of the Earth itself. The interplay of these complex motions can lead to even more radiative damping. In addition, these motion scales interact in such a manner as to increase substantially the probability of irreversible or 'turbulent' mixing on various scales (see also Dunkerton, 1980). The effect of this process is evident in various numerical experiments (e.g., Mahlman, 1975; Hsu, 1980). These arguments imply that it is the motions themselves which determine much of the degree and character of dissipation, both radiative and mechanical. Once such mechanical dissipation is induced, however, increased temperatures at the higher latitudes are implied. This is because the increased mechanical damping leads to additional poleward accelerations (at least in the Lagrangian sense), and increased adiabatic heating. Thus, zonal-mean diabatic heating and cooling can be increased in response to non-zonal processes.

The above arguments emphasize the importance of various processes leading to excitation of diabatic motions in the stratosphere. Ultimately, however, horizontal gradients in diabatic heating will lead to horizontal gradients for any trace constituent on a given isentropic surface. This implies that essentially adiabatic processes might, under some circumstances, lead to irreversible transports on the isentropic surfaces themselves. In fact, we can argue that the equilibrium meridional slopes of tracers in the stratosphere result from the competition between the above two processes. If mixing along the surfaces were the only process acting, the equilibrium tracer surfaces would exhibit the same meridional slope as the isentropic surfaces. On the other hand, if the only process acting was the meridional gradient of diabatic heating, the equilibrium tracer surfaces would tend to adopt an extremely steep meridional slope, eventually becoming vertical or even inverted and convoluted. The fact that the equilibrium tracer surfaces show a structure between these two extremes strongly suggests that a balance between these two rather different processes is indeed effected in the stratosphere.

VARIABILITY

The previous conceptual view of transport dealt with the role of transport in giving rise to climatological distributions of trace constituents. Here another role of transport, that of giving rise to variability in constituent concentrations, is briefly discussed.

There are at least two ways in which transport generated variability complicates the intepretation of observations of trace constituent concentrations. One complication arises in the chemical interpretation of instantaneous profiles of trace constituent concentrations, and the other arises when attempting to draw conclusions based upon the evaluation of trends in data records of length on the order of 10 years.

Because of the time variability of the motions in the stratosphere, air parcels at adjacent heights in an air column at a particular time, or air parcels at the same height but at different times, may have come from quite different locations. The ambient concentrations at these locations may be quite different from each other and also quite different from the average concentration at the position of the column of interest. The extent of the variability depends on the amount by which the concentration of a moving parcel of air can differ from its environment. Simplifying the situation by using a linear argument, this in turn is controlled by the size and direction of

the spatial gradient in the mean ambient distribution and the distance parallel to this gradient which a parcel can travel before losing its identity through relaxation of its concentration toward its ambient value. For a given distribution of parcel velocities, the variability of the concentration of a particular constituent will be proportional to the time a parcel can maintain its concentration. For short-lived constituents the appropriate time is the photochemical relaxation time whereas for long-lived constituents, the appropriate time is the mixing time, the time after which parcels lose their identity through purely mechanical processes. Thus conceptually, the variability should be large when parcel displacements are large, where the magnitude of the mean gradient of the constituent concentration is large and where the photochemical relaxation time of the constituent of interest is long compared to the time required to achieve the large parcel displacement. These expectations are essentially borne out for ozone which has a 50 to 75% variability in the lower stratosphere (Dütsch, 1969; Pittock 1977). Variability should be generally less in the tropics where parcel displacements are smaller. (Levy et al., 1979).

Another form of variability is the interannual variability of constituent concentrations and in particular of total ozone. This is caused by the large interannual variability in the planetary scale motions in the stratosphere which results quite directly from the interannual variability of the planetary scale circulation in the troposphere. Planetary wave activity varies greatly from one winter to the next, and in fact, during some winters there are stratospheric warmings with their attendant large increases in high latitude total ozone column and in some winters there are not. This leads to a discernable red noise component to the temporal distribution of temperature, wind, and ozone concentration in the stratosphere. This natural low frequency variability must be carefully considered when interpreting trends in stratospheric data.

TROPOSPHERE-STRATOSPHERE EXCHANGE

In order to understand how man's activities affect the stratosphere, it is necessary that we understand how tropospheric and stratospheric air are exchanged. We take as a point of departure for this discussion the hypothesis of Brewer (1949) that the extreme dryness of practically all the air in the stratosphere at any time is due to its having passed through the equatorial tropopause, the only location in the atmosphere where it could be desiccated by condensation and precipitation during cooling to below -80°C at a pressure of about 100 mbar. Brewer's hypothesis did not localize an exit region, but called for a vertical gradient of water vapor in the lowest 1 or 2 km of the stratosphere, maintained by eddy diffusion against a mean downward mass transport. This hypothesis was originally based on in situ (aircraft) observations of frost-point in a very limited geographical region around 0°E, 50°N.

It was later established, following a suggestion of R. J. Reed (1955), most convincingly by aircraft observations (Danielsen, 1968) of the radioactive products of stratospheric explosions, that the regions of exit from the stratosphere were limited in large measure to mid-latitudes, occurred mainly in spring, and were associated with jet streams. These observations were not incompatible with a reverse (troposphere to stratosphere) transport in this region, but did not establish it.

Brewer's hypothesis of a unique source of very dry air is compatible with atmospheric dynamics and energetics, which call for low level convergence in the equatorial zone, but in itself gives no clue to the physical nature of the mass flow, e.g., whether steady and widespread or localized and impulsive.

There is a seasonal variation in the mass of the Northern Hemisphere stratosphere of about 30% or 10^{17} kg, the rate of mass change being most marked in spring at the time of the observed major transfer of stratospheric radioactivity. The actual annual mass transfer was estimated by

Danielsen and Mohnen (1970), from a study of ozone transport and the phenomenon of tropopause folding to be above 3.6×10^{17} kg/yr. Robinson (1980), on the other hand, postulated that the actual hemispheric mass exchange was the minimum value of 10^{17} kg/yr, the difference between the masses of the winter and summer stratospheres. He also argued that, since H_2O contents much greater than 2 to 4×10^{-6} by mass have not been observed in the region of the sub-tropical and polar front jets above a height of about 16 km, tropospheric air did not pass upward through this level (which is normally 2 to 6 km above the conventional tropopause in these regions). This simple "one-door in, one-door out" picture allows an estimate of the stratospheric budget of minor constituents if their mixing ratio is known at the "doors", the equatorial tropopause and the 16 km level in mid-latitudes. Robinson claimed some success for estimates based on this hypothesis, particularly for CCl_4 and the CFCs, but the paucity and imprecision in the observations tend to render his estimates speculative.

In the last 2 years, two developments have complicated this simple "one-door in, one-door out" picture. The first concerns the result of two NASA/Ames observation campaigns employing U-2 aircraft in the tropical convergence zone near Panama (Poppoff et al., 1979). The second is the detailed, reproducible observations of small-scale variability in the stratospheric water content by D. Kley and his colleagues (1979 and personal communication).

Consider first, the tropical convergence zone experiments. The Brewer hypothesis calls for condensation and precipitation in the tropical ascent region. The equatorial convergence is at low levels and the major water removal must occur in cumulonimbus clouds. Radiosonde observations in the neighborhood of major cloud clusters, at least in the Panama region and the eastern tropical Atlantic (GATE), do not show the conditions required for desiccation below a mass mixing ratio of 6 to 12×10^{-6}. Furthermore, detailed examination of the H_2O vapor and particle content in and near the anvil cirrus produced in the stratosphere (as conventionally defined) indicates that the process is introducing air with a water content considerably higher than the 2 to 4×10^{-6} mass mixing ratio required.

During the 12 August 1980 mission, the U-2 pilot flew the aircraft into the outer portions of an anvil, penetrating down into it 150 to 300 meters to an altitude of about 17 km, where Kley's water vapor sensor measured a total water content of 450 ppmm at a temperature of -80°C. This large value (the sum of the in situ vapor and the evaporated ice crystals entering the probe) greatly exceeds the saturation mixing ratio of 5.8 ppmm.

Cumulonimbus (Cb) clouds in the Panama area may penetrate the conventionally defined tropopause by 2 to 3 km. When these clouds are present, there is what may be described as a transition region with water content (particulate and vapor phase) varying from the order of 10×10^{-6} by mass, to the order of 1000×10^{-6}. If this air is to enter the non-local stratosphere and propagate to non-equatorial latitudes, it must be subjected to desiccation within the transition region. Danielsen (personal communication) has suggested that waves induced by the penetrating Cb clouds, associated with the selective growth of some ice particles could provide the basis of such a mechanism. It is also conceivable that this transition zone air might be reincorporated in the troposphere. In this latter case, we would have to look elsewhere in the equatorial zone for the region of entry of stratospheric air, the most likely region being the Indonesian sector where a high frequency of Cb cloud is associated with a particularly cold conventional tropopause and frequent occurrence of temperatures -80°C to -85°C at 100 mbar. Detailed associations of high cloud and local temperature and water content structure are not available in this area.

The second recent development is illustrated in Figure 2-17. The feature significant for our present discussion is the considerable range of mixing ratios in layered structures which persist from balloon ascent to descent implying a horizontal spatial scale of order at least tens of km, and a very detailed layered vertical structure with many scales, but with major features of order

1 km thick. Danielsen (personal communication) has made an isentropic trajectory analysis (illustrated in Figure 2-18) for one major feature of the measurements. This establishes that air, in a layer of thickness hundreds of meters, moved, without significant mixing, in a few days from the tropical stratosphere in the western Pacific to a position 3 km lower over Wyoming. At the point of origin of the trajectory, the H_2O and O_3 content was appropriate to the tropopause in the Indonesian region, but the pressure and temperature implied either a forced, highly anisentropic ascent in the lower tropical stratosphere or desiccation by local isentropic ascent to a temperature of about -85°C at a pressure of about 65 mbar, well above the conventional tropopause. This work of Danielsen has implications concerning the scales on which isentropic Lagrangian trajecctory analysis may and may not be usefully employed.

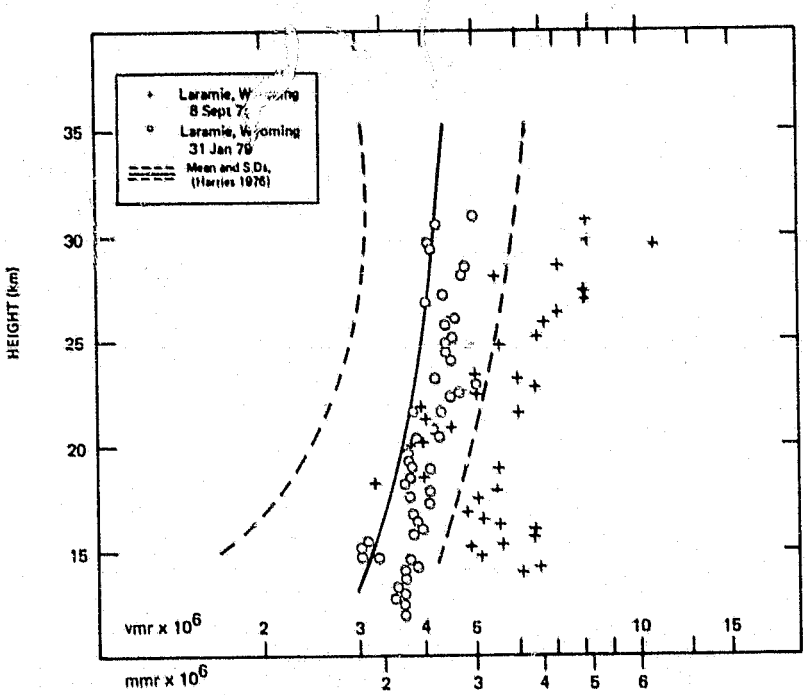

Figure 2-17. Observations of the concentration of H_2O in the stratosphere (illustrating small-scale variance).

Danielsen also suggests that the variance of Kley's observations at altitudes around 15 to 20 km in temperate latitudes suggests that tropospheric air may be entering the stratosphere above the jet core, contrary to Robinson's hypothesis. Fairly rapid mixing and a stratospheric desiccation mechanism would be called for in this case: the latter could be provided by mountain and cumulonimbus-induced waves, with condensation and precipitation. The question whether or not tropospheric air enters and remains in the stratosphere in the neighborhood of the mid-latitude jet streams is important from the point of view of the spread of anthropogenic pollutants, particularly those, such as NOx from aircraft, with a relatively short tropospheric lifetime.

Resolution of the uncertainties discussed above will require, at least, many more observations of the concentration of minor constituents, on a very small sampling scale in time and space. These are required particularly in the upper troposphere and lower stratosphere in the equatorial zone,

in the neighborhood of the mid-latitude jet streams, and near large clouds penetrating the conventional tropopause. Precisions and accuracies of 10% or better are needed. In situ observations by rocket, balloon, and aircraft are required because current, and currently conceived satellite techniques, do not have the necessary spatial resolution.

Figure 2-18. Isentropic trajectories 28 January - 1 February 1979 (Danielsen, personal communication).

STRATOSPHERIC WATER VAPOR BUDGET

INTRODUCTION

The amount of water vapor present in the lower stratosphere is important for the radiative balance and for the rate of production of HO, a key free radical in the photochemical kinetics of the stratospheric ozone distribution.

Any discussion of the stratospheric water vapor budget requires definition, over the globe, of the boundary between stratospheric and tropospheric air. Availability of data limits our discussion to the Northern Hemisphere, with the knowledge that 15 to 20% of stratospheric air is exchanged annually between the hemispheres. Budgetary discussion also requires quantification of the sources and sinks of atmospheric water vapor. The known sources are evaporation at the Earth's surface, which supplies about 5×10^{17} kg/yr to the Northern Hemisphere, and photochemical oxidation of methane which is several orders of magnitude smaller. It is estimated that not more than about 10^{12} kg/yr of H_2O enters and leaves the Northern Hemisphere stratosphere. About 10^{11} kg/yr of methane enters the Northern Hemisphere stratosphere, of which not more than 10% is oxidized with ultimate production of H_2O. There is no known significant chemical destruction of H_2O. The only viable way in which the water content of a parcel of air can be reduced is by cooling, with subsequent condensation and precipitation. The observed mass mixing ratio of air in the lower stratosphere (at heights more than about 1 to 3 km above

the tropopause) is around $3x10^{-6}$. For methane it is about $8x10^{-7}$. If all the methane in a parcel of stratospheric air were to be oxidized the mass mixing ratio of H_2O in the parcel would be increased by not more than $1.5x10^{-6}$. If as much as 10% of the yearly exchange of methane were to be oxidized there, an additional export of $2x10^{10}$ kg/yr of H_2O from stratosphere to troposphere would be required.

The outstanding problem associated with stratospheric humidity observations is to account for the very low values, ranging from 2 to 6 ppmm, with a minimum a few km above the tropopause. Such low values rule out ascending motion and condensation to ice through the generally observed global distribution of temperature minima (tropopauses), which would result in values of 30 to 50 ppmm in the extratropics and values of 5 to 15 ppmm in the tropics. The requisite thermodynamic conditions to produce 2 ppmm (temperatures -83°C and pressures 95 mbar) are to be found in the climatological record only at certain geographical locations of the equatorial tropopause, and in the rather small volume of the polar winter stratosphere between 10 and 70 mbar. Air with 2 ppmm water vapor entering the stratosphere must therefore have experienced temperatures at least as low as this; note, however, that the flow of dry air into the stratosphere need not necessarily be vertical in the sense of cumulonimbus convection. In addition studies have shown that particularly during periods of intense mid-latitude tropospheric cyclogenesis, there is often a jet stream breakdown and tropopause folding (Danielsen, 1968) with a concomitant outflow of air from the lower stratosphere into the upper and middle extratropical and tropical troposphere. This air soon loses its stratospheric characteristics through convective activity and turbulent mixing. An additional observational constraint is that injections of moist tropospheric air into the lower stratosphere through the tropopause near jet streams must be small enough, in the time averaged zonal mean, to permit dilution by dry air to a degree compatible with the observed latitudinal humidity amounts and gradients. Finally, other quasi-conservative tracers must satisfy the exchange process.

This gross picture of the stratosphere-troposphere exchange does not include the understanding of detailed mechanisms particularly as regards the dessication process and influx. Further insight requires examination in two meteorological contexts: cloud physics and atmospheric dynamical structure. The aim here will be to establish rough time and space scales for some basic processes.

CLOUD PHYSICS CONSIDERATIONS

Cloud physics is important because the primary sink for water vapor in the atmosphere is condensation to the water and ice phases, following adiabatic cooling as a result of ascent. Motions on the scale of a cumulonimbus cloud are roughly characterized by a time scale of minutes to hours with an individual cell having a lifetime of perhaps 30 minutes although some storms consisting of several cells may last for several hours. The vertical scale is 5 to 20 km, with a horizontal dimension of about the same order. The characteristic time scale of "turrets", emerging from Cb tops and collapsing, is 5 minutes.

For the desiccation process, the relevant physics includes possible hydration by evaporation of ice crystals transported into and mixed with stratospheric air; possible dehydration by ice crystal formation; and growth and sedimentation within the stratosphere. Since the temperatures are much colder than -40°C, there is no difficulty with initiation of the condensation process: it can occur homogeneously, without benefit of preexisting nuclei. For ice crystals falling from cirrus clouds, the radiative cooling and ventilation of the particle are important; crystals may survive a fall distance of up to 2 km when the relative humidity is less than 70% with respect to water (Roach 1976; Hall & Pruppacher 1976). Even in thin cirrus clouds, the humidity field should reach saturation with respect to ice in a minute or so, and observed frost points in cirrus should therefore not depart significantly from air temperature. Ice crystals small enough to have very

slow fall speeds may survive long enough to be carried a few thousand kilometers, for instance by a typical tropical easterly jet flow, if it is protected from the warm lower troposphere by thicker cirrus veils between 150 and 300 mbar (Roach, 1961). The dependence of water vapor saturation mixing ratio (with respect to ice) upon air temperature and pressure is given in Table 2-16: the data are derived from the thermodynamics of air and phase transitions of water substance.

Table 2-16
Water Vapor Saturation Mass Mixing Ratio with Respect to Ice (ppmv)

Temperature		Pressure				
°C	K	90 mbar	95 mbar	100 mbar	115 mbar	125 mbar
-77	196	6.0	5.6	5.3	4.6	4.4
-80	193	3.8	3.5	3.3	2.9	2.7
-83	190	2.3	2.1	2.0	1.7	1.7
-86	187	1.3	1.2	1.2	1.0	1.0
-89	184	0.8	0.7	0.7	0.6	0.6

Rising "turrets" from an intense cumulonimbus, on simple energetic grounds and as a matter of observation, may penetrate the stratosphere by 1 to 4 km. The updrafts needed to achieve this against the environmental stability are capable of carrying upwards sizeable numbers of ice crystals of larger dimensions than will stay suspended in still air. After collapse of the turrets some of these crystals remain in the lower stratosphere. U-2 Knollenberg aircraft measurements (Danielsen, Kirstewbreg, Kley, personal communication) support these contentions with observed total H_2O content of about 450 ppmm at -89°C (saturation mixing ratio 3.5 ppmm). Another phenomenon observed by the U-2 pilot is ejection of a jet of ice crystals some 300 to 700 m above the turret. These large crystals, falling through supersaturated air lifted by the turret will desiccate this air. The combined effect of these two phenomena could contribute to the observed decrease of water vapor mixing ratio above the tropopause. The climatological frequency of large Cb is partially available in radar climatologies and from GOES infrared satellite imagery. At both middle and low latitudes there is evidence of topographic forcing. At low latitudes there is evidence also of cloud clusters associated with both standing and propagating disturbances. In extratropical latitudes they are correlated with subtropical jet streams.

ATMOSPHERIC STRUCTURE CONSIDERATIONS

Contemporary analyses based on current radiosonde observations indicate that the mean temperature of the tropical tropopause is also not cold enough for the Brewer hypothesis to apply to a steady circulation at all longitudes. However, longitudinal variations do exist in the mean temperatures which yield the prescribed cold temperatures. Figure 2-19 (Danielsen, personal communication) shows two regions on opposite sides of the globe with monthly mean temperatures colder than -80°C at 100 mbar. The colder region (~-83°C) is located over Indonesia. Newell and Gould-Stewart (1981) using monthly mean statistics for more than 10 years show that the dual structure persists seasonally but the dominant center oscillates toward India in the summer and towards Indonesia during the winter. As Newell points out the Brewer hypothesis must be shifted from the Hadley to the Walker circulation.

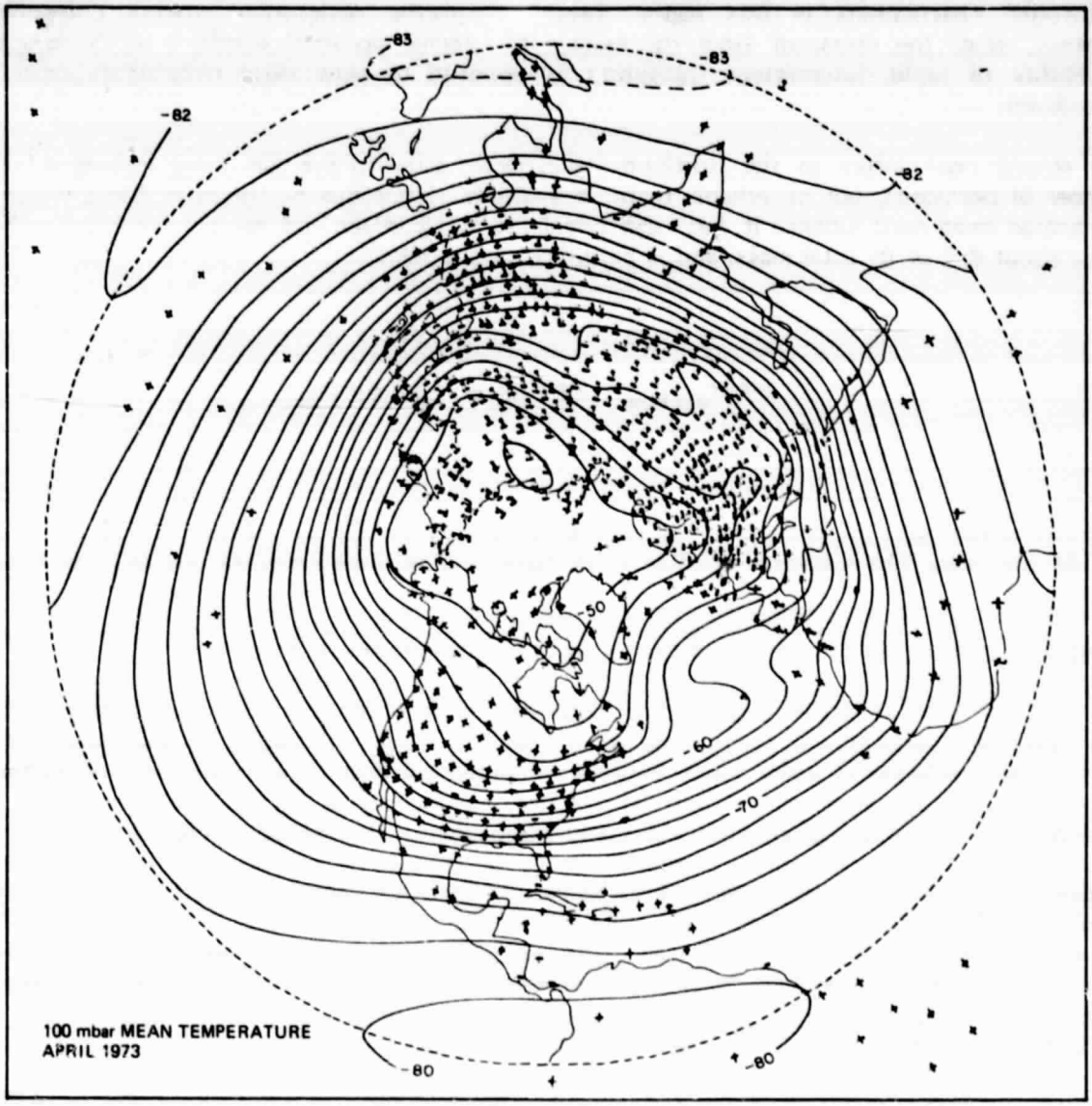

Figure 2-19. 100 mbar mean temperature April 1972. Temperature in C. (From Danielsen, personal communication)

Recently, Kley et al. (1980) have observed correlated minima in both ozone and water vapor at 15 km (θ = 405 K) in stratospheric air over Wyoming. These minima were traced back via isentropic trajectories to the area of the Philippines and Indonesia (Danielsen, personal communication). Although the trajectories trace the air back to the most probable source region, the actual radiosonde observations in this region leave the specific desiccation process unresolved. However, since the transport from the tropics to Laramie occurred within 4 or 5 days the possibility of rapid, intermittent transports as opposed to slow mean circulations must be considered.

The annual mass influx to the Northern Hemispheric stratosphere has been estimated on a number of occasions, but no reliable figure is available. The efflux on the other hand, which in the annual mean must balance it, has been calculated by Danielsen and Mohnen (1977) and others to be about 80% of its total mass, and is described by the relation:

$$dM/dt_{\text{out flow}} = \left\{3.6 + 1.8 \cos (2\pi) (t\text{-}4.5/12)\right\} \quad (5)$$

where M is the mass in units to 10^{17}kg/yr, t=0 on January 1, 1/12, on February 1 and t=1 at the end of the year. The maximum outflow is in April, and is three times as fast as it is in late autumn.

GENERAL CIRCULATION MODELS AND STRATOSPHERIC WATER VAPOR

The previous considerations suggest that large-scale wave motions in the tropical troposphere and lower stratosphere will need to be treated well in model calculations if the troposphere-stratosphere exchange of water vapor is to be computed correctly. This is also true of exchange on isentropic surfaces at extratopical jet streams, particularly as regards the question of air entering the lower stratosphere from the upper troposphere. The vertical resolutions required are approximately 1 and 2 km respectively. There is, of course, no prospect of treating cumulonimbus clouds explicitly in a general circulation model; the computational requirements for theoretical investigation of these events are themselves similar to those of general circulation models, applied on a scale of a few tens of kilometers. Their treatment of the cloud microphysics and radiative transfer is highly parameterized. Given this, deep convection itself in a general circulation model is also highly parametric, being evident often at a single column on the horizontal grid.

The main advantage that general circulation models bring to the problem is the ability to provide a consistent and uniform data set sampling the entire spatial domain over an annual cycle, rendering the computation of global fluxes and three-dimensional trajectories complete, if not necessarily accurate.

With regard to comparison with available data, this must of necessity be rather superficial at present, for two reasons: the paucity of reliable data and the rather coarse resolution of the general circulation models which have tried to simulate the stratospheric water vapor budget. At least two general circulation modeling groups have attempted this, GFDL and the British Meteorological office, but neither have published accounts of a diagnosis of the results in terms of fluxes and mass budgets, although a paper addressing the effect of water vapor-ozone covariance on the global HO distribution is available (Allam et al., 1981). The position may be

summarized briefly for the BMO model as follows (Allam and Tuck, personal communication): water vapor mixing ratios are indeed lowest (2 to 3 ppmm) in the equatorial longitudes where observed tropopause temperatures are lowest. The mid-latitude lower stratosphere has too much water vapor present, by approximately a factor of two or three, possibly as a result of too much upper tropospheric air entering the lower stratosphere near jet stream locations as a result of coarse vertical resolution. There is, however, some preliminary indication in the real atmosphere of a maximum of water vapor mixing ratio in the mid-latitude lower stratosphere (Ehhalt and Tönnissen, 1980; and Murgatroyd, personal communication), although this is not necessarily caused by intrusion of tropospheric air. Encouraging agreement as to the pattern of water vapor at 39°N exists with the 11-year mean altitude-time section obtained from the series of water vapor balloon ascents made by Mastenbrook and Daniels (1980).

The use of Newtonian cooling and the coarse vertical resolution degrade the value of this simulation at the equatorial tropopause, despite the encouraging longitudinal distribution of water vapor mixing ratio here. This is clearly shown by the work of Mahlman et al. (personal communication) who showed that accurate handling of the water vapor fluxes in the presence of large vertical gradients required resolution better than 1.5 km in the tropics, and about 1.7 km at extratropical latitudes. These vertical grid spacings, combined with fourth-order finite differencing represent considerable improvements over a previous model, but nevertheless produced a tropical tropopause which was too cold (188 K) and too dry (0.5 ppmm) compared to reality.

Further work, with improved spatial resolution, is clearly required, and should, among other things, attempt to deal with the following questions:

- Is the mid-latitude maximum of water vapor in the lower stratosphere real?
- If so, is it caused by transfer around jet streams, by the descent of methane oxidation products, or both?
- Is the decrease of water vapor mixing ratio in the 30 to 100 mbar thick layers, often observed above the extratropical tropopause, caused by intrusion of tropospheric air around jet streams?
- What causes the decrease in mixing ratio sometimes observed above the equatorial tropopause?
- What three-dimensional trajectories are followed by air entering and leaving the stratosphere?

CHAPTER 3

MODEL PREDICTIONS AND TREND ANALYSIS

INTRODUCTION

Chapter 1 has emphasized the diagnostic use of models to explain observations (e.g. the present-day distribution of trace species) and to study the relative importance of chemical processes and their mutual interactions. This chapter is concerned with the prognostic application of these models, i.e., to extend the comparison of theory and experiment in terms of possible long-term changes in stratospheric composition, especially ozone. The available types of models have been described in Chapter 2. The three-dimensional models give, in principle, the closest simulation of the real atmosphere, but are so demanding of computer time and memory that it has not yet been possible to simulate realistic chemistry. They remain diagnostic tools. Two-dimensional models are beginning to be applied to perturbation problems but there are many interesting problems with their formulations of atmospheric dynamics that are discussed in Chapter 2. One-dimensional models remain the basic diagnostic and prognostic tools in stratospheric research. The one-dimensional models used in the following discussions compute altitude-dependent concentrations that, in general, represent a hybrid between a global-seasonal average and instantaneous values. This is because the transport, represented by the diffusion coefficient, is usually determined from measurements of a long-lived tracer such as N_2O. The observed distribution of N_2O represents the results of the entire global circulation and in that sense the transport has been globally averaged. On the other hand the photodissociation coefficients which drive the rapid photochemistry are usually taken as instantaneous values at about 30° latitude during either equinox. Thus the chemical constituents that are mainly photochemically determined are calculated with instantaneous photodissociation values from globally averaged source gases. The representativeness of these models and the problems associated with their use have been discussed in many publications (e.g. UK-DOE Poll. Papers #5, 1976; #15, 1979; NAS, 1975; NAS, 1976; NAS, 1979; NASA RP-1010, 1977; NASA RP 1049, 1979). In this chapter one-dimensional models are the primary tools used for perturbation analysis. Two-dimensional models are used to illustrate some of the expected seasonal and latitudinal variations in computed perturbations.

The chapter begins with a discussion of a series of individual perturbations. These are hypothetical perturbations determined by model computation in which it is assumed that one particular input or set of inputs to the model (e.g., chlorofluorocarbon release) is changed while all others are held constant. The model then is usually integrated until a steady-state is reached and the ozone concentration is compared to a similar calculation without the perturbation. The set of hypothetical perturbation calculations considered include doubling the input flux of N_2O, doubling the CO_2 concentration, injecting a steady flux of NO_x at a specific altitude, and combinations of these. These perturbations are called hypothetical because they do not represent any experiment actually being done in the atmosphere in that it is impossible to hold all other parameters constant in the real atmosphere. The difficulty in interpretation lies with the choice of realistic scenarios. Two years ago, when calculations showed the sensitivity of stratospheric ozone to chlorine-only injections to be high and to NO_x injections to be very low, the simple CFC release scenario seemed to be adequate. As will be seen the computations now indicate an intermediate sensitivity to each thus requiring careful consideration of both, and others, in determining the expected response of the atmosphere to human influence. Nevertheless study of the effects of individual perturbations serves as the basic reference point in understanding the complex interactions of simultaneous multiple perturbations. Thus, after

consideration of the model response to individual perturbations, combinations of these perturbations are considered. As will be seen, the results for individual perturbations are changing as our understanding of the underlying chemistry changes as also are the results for the non-linear addition rules for combinations of perturbations. These combined, yet still idealized, perturbations then form the basis for analyzing and understanding the results of the more reasonable time-dependent scenarios that are considered. The time-dependent scenarios offer two types of results. The first is prediction of how ozone and other constituents should have changed up to the present time due to changes known to have occurred. These results provide potentially testable hypotheses which can be examined so as to evaluate our understanding of the mechanisms responsible for changes in atmospheric ozone. The second type of result is for possible future scenarios. These latter are, of course, highly dependent on assumptions as to the future development of various sectors of the world economy and can only be used as a guide to some of the possible directions which may become important. These future scenarios do point out the need for careful examination of the question of detection thresholds even when the current record is not sufficient to provide an observable effect.

In order to provide a framework for testing hypotheses which emerge, the ozone record is then examined. For this purpose it is necessary to identify and isolate the major "natural" processes affecting the long period ozone variations and to determine, from observations, whether or not theoretically predicted ozone changes resulting from human activities can be verified.

For any time-dependent phenomenon, its time series can be analyzed and, to within some degree of confidence, the characteristic variations of the time-dependent variable can be described, even if no specific suggested mechanism for the origin of these variations is put forward. If, on the other hand, a particular causative mechanism or set of mechanisms is hypothesized, the hypothesis could be tested with the observed time series. The questions that need to be answered in this chapter are:

- What are the best estimates of past time dependent variations of, (a) globally averaged total ozone, and (b) upper tropospheric and stratospheric ozone. Are there geographic differences in these variations?

- What are the overall uncertainties of these "observed" variations?

- Are photochemical model predictions and statistical model estimates from the ozone record consistent?

- What are the thresholds, timescales, and limitations for the detection of the effects of human influence on ozone changes when these effects are considered either separately or simultaneously?

In evaluating long-term (over 10 years) trends of ozone due possibly to historical releases of CFCs, concern is with a predicted average decrease of total ozone of about 1% over the globe most of which occurs during the last decade, and a maximum decrease of the ozone concentration at a height of 40 km of about 5% during the same period. Because of the sensitivity of the ozone vertical profile to many of the suggested possible photochemical and solar induced perturbations, it is imperative that time series analyses of the vertical ozone profile be made. Unfortunately, in the historical data, the observational precision and spatial coverage of the total ozone measurements are much better than for the vertical ozone profiles. Hence, initial analyses have concentrated on the total ozone variations. With extension of the vertical ozone profile data base, particularly through the approaching availability of long-term

satellite information, this disparity will be substantially alleviated and the problem can be investigated as a whole.

MODEL PREDICTIONS OF POTENTIAL ANTHROPOGENIC PERTURBATIONS

CHLOROFLUOROCARBONS: FC-11 AND FC-12

Of the many potential human perturbations of the stratospheric ozone layer, most current interest is in the possible effect of the chloroflurocarbons FC-11 and FC-12. As has been pointed out in many places in this report, understanding of the key chemical and photochemical processes is still evolving. These changes in stratospheric chemistry have had a clear impact on the comparisons of model predictions with observations. The changes have also affected the model predictions of the impact of chlorofluorocarbons on the stratospheric ozone concentration. The aim of this section is first to illustrate how these reevaluations have changed the steady state ozone depletion estimates with as many of the other model inputs as possible held constant. Further attention is then directed to estimates of the present-day total ozone column depletion and the variation of these depletion estimates with altitude, latitude, and season.

Table 3-1 shows model results obtained by 10 different investigators for the effect of chlorofluorocabron release on the total column amount of ozone assuming no other atmospheric changes. Two columns of results are shown: The first is the computed change in 1980 as compared to a pre-1970 level obtained by varying the CFC emission rate with time according to historical release rate estimates; the second is the computed change when steady-state is reached with continuous CFC emission at about 1976 levels. The emission levels are not exactly the same in each model but are probably not more than 10% different. Four possibilities were considered for the chemical kinetics input data. These are labeled A through D in the table and are approximately historical. They specifically are the following:

Case A: The recommendations of the NASA Panel on Chemical Kinetics in 1979 as reported in NASA RP 1049. The major features of this set of chemical reaction rate coefficients relative to the later sets are the slow rates for HO + HNO_3 and HO + HNO_4. Models with this set give large (>10^6 cm^{-3}) HO concentrations throughout the lower stratosphere.

Case B: The updated recommendations of the NASA Panel in December of 1980 as reported in JPL 81-3. A major change is the faster rate for HO + HNO_3 ($1.5x10^{-14}$ e $^{+650/T}$) and a slightly faster rate for HO + HNO_4.

Case C: The same as B with the rate coefficient for HO + HNO_4 increased to $4x10^{-12}$ cm^3 $molecule^{-1}sec^{-1}$ and HO + HO_2 increased to $8x10^{-11}$ $cm^3molecule^{-1}sec^{-1}$.

Case D: The recommendations of the combined NASA and CODATA panels as reported in Appendix 1 of this document. This set incorporates the faster HO + HNO_4 and HO + HO_2 of Case C, slower $ClONO_2$ formation and numerous small changes.

Although the photochemical input has been standardized in this sequence of runs no concerted effort was made to standardize the other model aspects such as boundary conditions, transport parameters, or solar flux.

The results for steady-state column ozone change show a consistent variation among the various models in that relatively large ozone depletions were obtained with case A, declining to significantly smaller values for B and then C, then increasing somewhat for case D. As indicated in Chapter 1 the principal driving force in the changes is the modification in the computed HO

Table 3-1
Percentage Change in Total Ozone Column for 1980 and at Steady State Resulting from the Continued Release of FC-11 and FC-12 at 1976 (or comparable) Levels

Investigator	Status of Chemistry Input Data	Change by 1980 (%)	Change at Steady State (%)
Sze (AER)	A	-1.6	-16.0
	B	-0.9	-8.2
	C	—	-4.7
	D	-0.6	-6.1
Wuebbles (LLNL)	A	—	-19.3
	B	—	-9.5
	C	—	-6.1*
	D	-0.6	-5.0
Derwent (AERE)	A	—	-17.4
	B	—	-10.7
	C	-0.7	-7.2
	D	-0.7	-6.5
Liu (NOAA)	C	-0.8	-7.0
	D	-0.5	-4.5
Miller (Du Pont) 1D	A	—	-24.**
	B	-0.7	-11.0
	D	-0.5	-7.0
	D	-0.6***	—
2D	B	-1.4***	-10.0
	D	-0.9***	-6.2
Cariolle (EERM)	A	-2.0	-16.5
	B	-0.9	-9.9
	D	-0.7	-7.0
Logan (Harvard)	A	—	-18.0
	D	—	-7.2**
Brasseur (IAS)	C	-0.9	-4.0
1D	D	-1.1	-4.8
2D	D	—	-7.0
Isaksen (U. Oslo)	B	-1.4	-11.0
Stolarski (NASA)	A	—	-15.8
	B	—	-10.2
	C	—	-6.6
	D	—	-8.7
Turco/Whitten (R&D/NASA)	A	—	-16.0
	B	-1.3	-11.0

* Has slow $ClONO_2$ formation rate.
** Indicates that a change in K_z profile has been made over and above changes in chemistry.
***Includes perturbations due to methyl chloroform as well as FC-11 and FC-12.

See text for description of Cases A through D.

concentration in the lower stratosphere where it has never been measured. The upward swing in the computed ozone depletions between cases C and D results primarily from changing from a fast formation rate for $ClONO_2$ to a slower formation rate. These correspond to the fast and slow rates shown in NASA RP 1049 and in JPL 81-3. When the slower rate is used in case D it is also assumed that the isomeric products formed when ClO and NO_2 interact at the faster rate are rapidly photodissociated with no effects on the chemistry. This progression of steady-state model results is illustrated in Figure 3-1 where the bars represent the range of model results for each of the evaluations. The 1979 evaluation for the NASA RP 1049 chemical kinetics shows the originally quoted range of 15 to 19%. The result in Table 3-1 for Miller indicates a number of 24% including a reevaluated diffusion coefficient profile. The major effect of this new slower diffusion coefficient is to increase the effective residence time of the fluorocarbons thus increasing their calculated concentrations at steady-state and hence the predicted ozone depletion. This is an illustration of the sensitivity of these depletion calculations to transport; this sensitivity is discussed in more detail later in this chapter. One point to note in Figure 3-1 is the relative constancy of the absolute value of the range of model results from evaluation to evaluation at ~3 to 4%. This is a measure of the precision of the existing models when the same chemical kinetics is assumed. The question of overall uncertainty is considered later in the chapter.

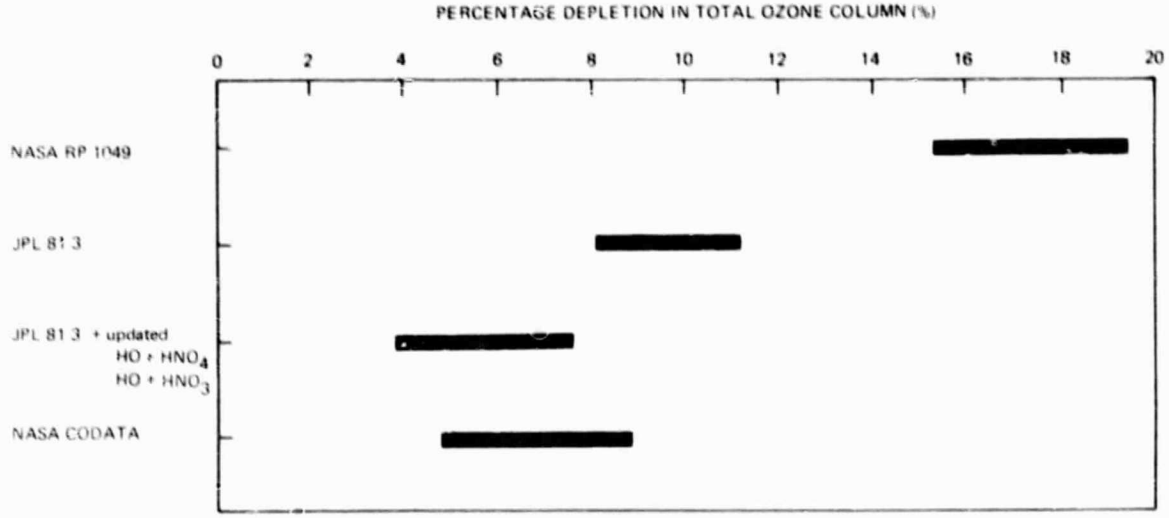

Figure 3-1. The variation in steady-state total ozone depletion estimates due to CFC release caused by the reevaluations in certain rate coefficients.

Table 3-2 shows a longer view of the history of the impact of major revisions in the chemical kinetics input data on total ozone depletion estimates for the steady-state release of FC-11 and FC-12 as determined by the LLNL 1-D model (also see Figure 3-14). Generally speaking, the magnitude of the predictions from the perturbation experiments is in the 5 to 9% range, which is about the same as was obtained during the 1976-1977 period. In the intervening period the results have risen by nearly a factor of three and then fallen back by about the same factor. Also shown in the figure are the concurrent results obtained for the perturbation experiment in which N_2O at the lower boundary is doubled. These results show almost an inverse behavior because HO affects the NO_x cycles in the opposite manner to its effect on the ClX cycles. This is discussed in more detail when NO_x perturbations are considered.

Table 3-2
Change in LLNL One-Dimensional Model Calculations Since 1975 of Expected Effect on Total Ozone From Constant Emissions of FC-11 and FC-12 (later calculations includes CH_3CCl_3 also)

Date of Evaluation	O_3(%)	Comments
mid-1975	-14. (emissions at 1973 levels)	As discussed in NAS (1976), no $ClONO_2$
early 1976	-7.5	includes $ClONO_2$ chemistry
mid-1977	-7.3 (emissions at 1975 levels)	Luther et al. (1978)
	-14.2	NASA RP 1010 (1977) chemistry, fast HO_2 + NO
mid-1978	-15.9	Luther (1978)
early 1979	-18.6 (emissions at 1976 levels)	NRC (1979) (actually used 1977 emission levels)
mid-1979	-19.3	Luther et al. (1979), NASA RP 1049 (1979) chemistry with slow $ClONO_2$ formation
	(Case A) -14.2	same with fast $ClONO_2$ formation
early 1980	-13.9	Wuebbles and Duewer (1980), same as above with Bass et al. (1980) CH_2O absorption cross sections
	-14.3	with Molina and Molina (1980) HNO_4 absorption cross section
	-13.9	with Keyser (1980) rate for $HO+H_2O_2$
mid-1980	-9.5	Wuebbles et al. (1981b), includes faster rate for $HO+HNO_3$
December 1980	(Case B) -9.1	1980 NASA chemistry recommendation (JPL 81-3, 1981)
May 1981	(Case D) -5.0	NASA/CODATA chemistry (March 1981)

These changes in the model computed response of the total column of ozone to a CFC perturbation are not simply a scaling downward of the effect at all altitudes but have been a result mainly of changes in the lower stratosphere. This is shown in Figure 3-2a for both the eventual steady-state and for the change up to present day, i.e., 1980. The major effect predicted is a decrease centered about 40 km with very small effects in the lower stratosphere. Most models in fact show a slight increase centered around 20 km as illustrated by the LLNL results in the figure. The effects of the reaction rate changes are shown by comparison to Figure 3-2b which is taken from NASA RP 1049 showing a significant decrease in the lower stratosphere. In fact the absolute decrease, also shown, has a second peak in the lower stratosphere which is larger than the upper stratospheric peak. The current calculations have a net increase in

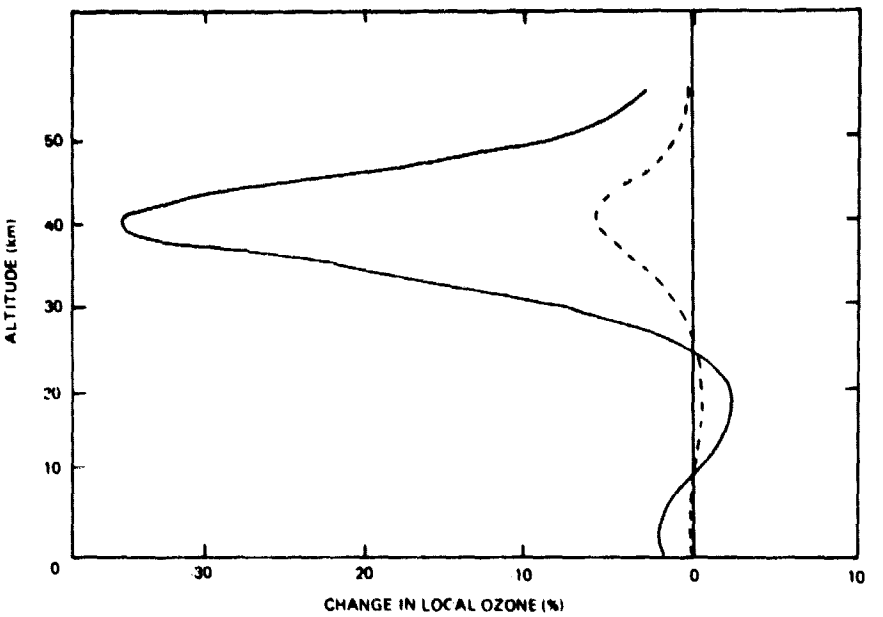

Figure 3-2a. The percentage change in the local ozone concentration at each altititude for the present day (· · ·) and steady state (—) for continuous release of FC-11 and FC-12. (LLNL 1-D Model, May 1981, NASA Chemistry, LLNL K_z).

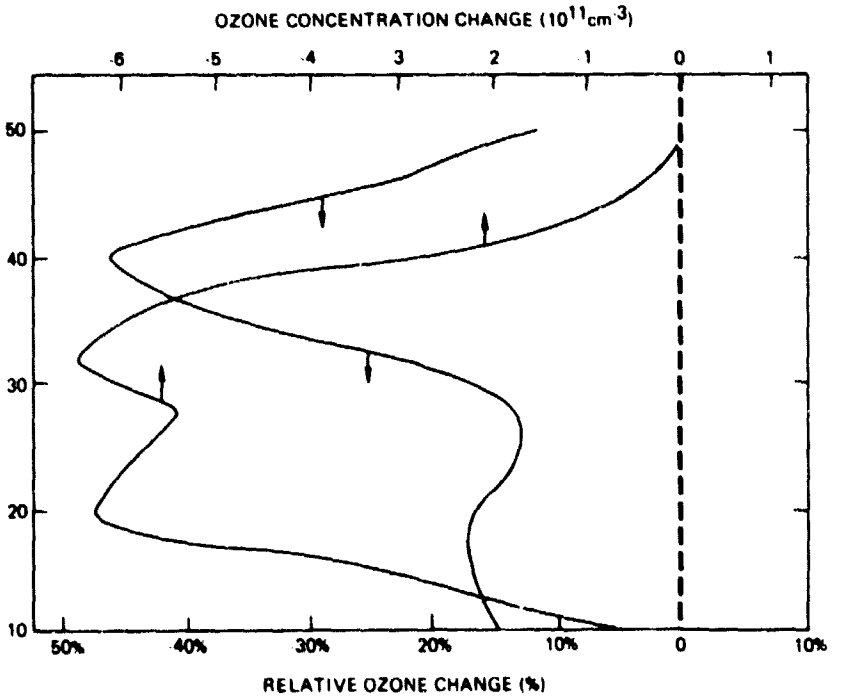

Figure 3-2b. Predicted ozone reductions as a function of altitude using case A chemistry (from NASA RP 1049, 1979).

the lower stratosphere causing some cancellation of the upper stratospheric decrease. It is worth emphasizing that the upper stratospheric predicted decrease, centered around 40 km, has been a relatively constant feature of the model calculations. The calculated decrease at steady-state is now about 35%, a value which has changed little with the recent reevaluations of HO_x chemistry. This is because most of the more drastic reevaluations have involved reactions with molecules such as HNO_3 and HNO_4 which are formed via 3-body reactions and are thus much less frequent in the upper stratosphere. The upward revision of the $HO + HO_2$ rate coefficient by a factor of 2 has had some effect but this is minimized by the fact that the HO concentration (which directly affects the ClX destruction efficiency) varies only with the square root of this rate coefficient.

As has been mentioned above the transport parameterization may contribute significantly to the uncertainty in both the steady-state value of ozone depletion and the time evolution of the approach to steady-state. The major effect of the transport coefficient on the steady-state ozone depletion is through its effect on the effective atmospheric residence times of the injected fluorocarbons. The longer the effective residence time the larger the steady-state fluorocarbon concentration which in turn leads to more ClX and more ozone destruction. Table 3-3 illustrates the effect of a number of transport parameterizations in several models. The transport coefficient profiles were derived to fit some aspect of the observed N_2O, CH_4, FC-11 or FC-12 profiles with altitude or the removal of radioactive carbon 14 formed during nuclear tests. The transport coefficient profiles, K_z, are shown in Figure 3-3.

Table 3-3
The Effect of Transport Parameterization on the Calculated Atmospheric Lifetimes of FC-11 and FC-12

Investigator	K_z Profile	Ref.	Lifetime, Years	
			FC-11	FC-12
Wuebbles	Chang (1976)	A	65	105
Derwent	N_2O-K_z	D	57	126
	Chang (1976)	A	55	107
	Hunten	B	93	169
	Meteorological Office	C	89	169
	Ehhalt	A	64	121
Miller (1-D)	Du Pont	E	75	139
(2-D)		F	60	120
Liu		G	85	140
AER (2-D)		H	62	118

A. NAS (1976)
B. Johnston et al. (1976)
C. Groves et al. (1978)
D. Derwent and Curtis (1981)
E. Miller, C. et al. (1979)
F. Miller, C. et al. (1981)
G. Liu, S. personal communication
H. Sze, D. personal communication

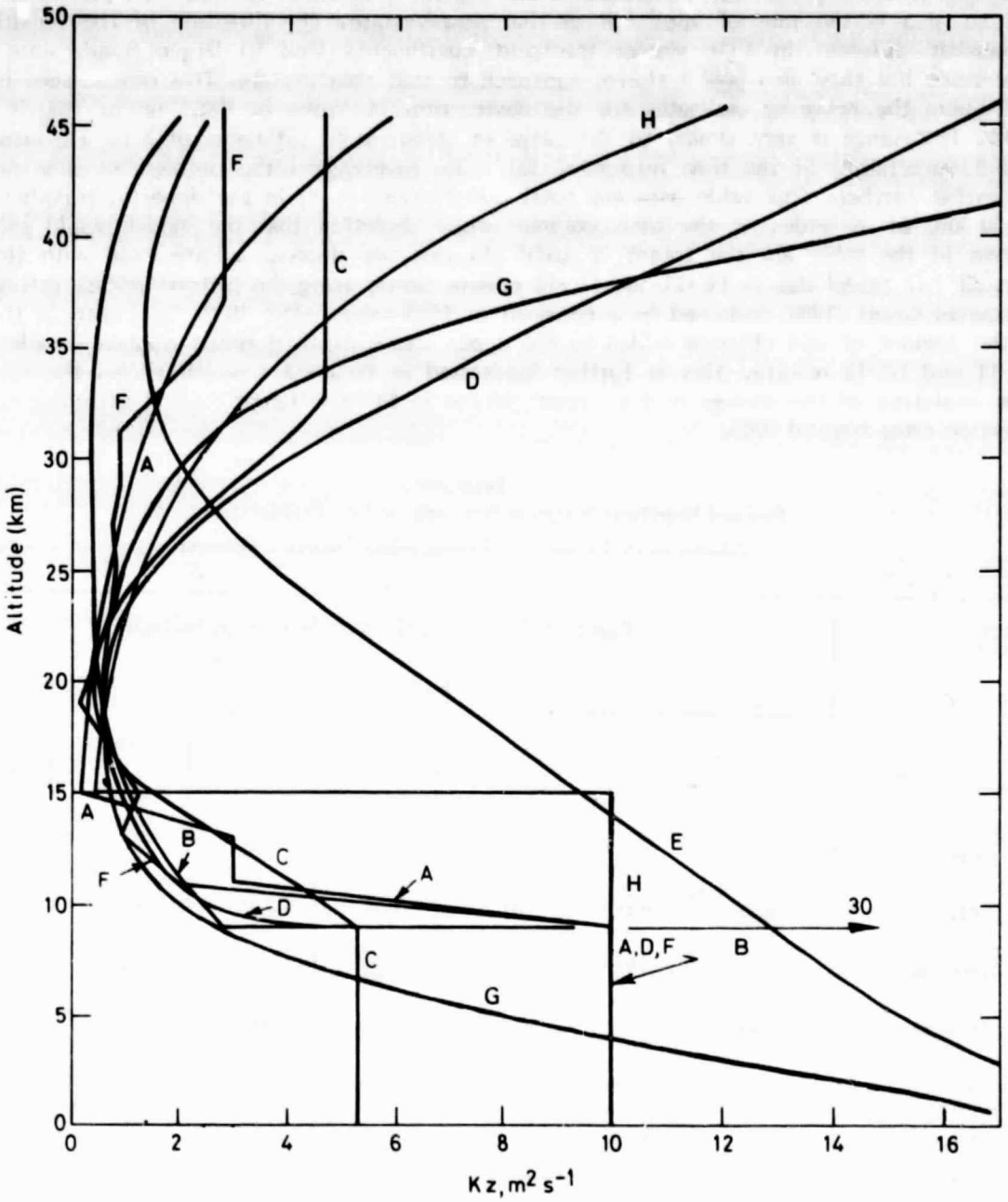

Figure 3-3. The variation of the vertical eddy diffusion coefficient, K_z, with altitude.

KEY:

A, Hunten; B, Chang (1974); C, Ehhalt; D, Chang (1976); E, Brasseur (max); F, Meteorological Office; G, from global mean observations of N_2O; H, Du Pont.

Not only is the steady-state computed ozone depletion sensitive to transport parameterization, but so also is the rate of approach to that steady-state. The direction of the sensitivity is somewhat different in that slower transport coefficients lead to larger steady-state ozone depletions but they also give a slower approach to that steady-state. This can be seen in Table 3-1 where the range of estimates for the destruction of ozone by CFCs up to 1980 is 0.5 to 0.9%. This range is very similar to the range in steady-state estimates of 5 to 9% despite the added uncertainty of the time response. Table 3-4 investigates the problem of time response somewhat further. This table uses the total odd chlorine (ClX) in the upper stratosphere, i.e., at 50 km, as an index of the total column ozone depletion that the model would calculate. Shown in the table are the trends in total chlorine per decade, as predicted with the AERE Harwell 1-D model due to FC-11 and FC-12 release alone, using the historic release estimates of Alexander Grant (1980) followed by a constant at 1979 values after 1979. Each entry in the table is the amount of odd chlorine added to the upper stratosphere during the given decade due to FC-11 and FC-12 release. This is further illustrated in Figure 3-4 which shows the calculated time evolution of the change in the ozone column in three different models assuming constant emission rates beyond 1980.

Table 3-4
Past and Near-Term Trends in Stratospheric Odd Chlorine Due to the Release of FC-11 and FC-12 Using AERE Harwell 1-D Model

Period	Change in Total Odd Chlorine at 50 km in ppb/decade						
	K_z Profile						
	N_2O	Chang	Chang	Hunten	Ehhalt	Brasseur	Met. Office
	K_z	(1976)	(1974)			(max)	
1940-1949	.003	.003	.001	.001	.003	.005	.001
1950-1959	.040	.042	.016	.025	.040	.052	.027
1960-1969	.167	.173	.086	.120	.170	.200	.126
1970-1979	.538	.545	.332	.432	.550	.565	.450
1980-1989	.538	.518	.595	.630	.574	.403	.634
1990-2000	.458	.443	.572	.576	.495	.337	.570

Another aspect of the transport parameterizations which gives rise to uncertainty in ozone depletion predictions is the representativeness of the 1-D eddy diffusion transport model. This parameterization by its nature cannot explicitly include the effects of latitude and season nor can it specifically treat advective transport. A great deal of theoretical work is currently being done on determining the proper representation of the transport in two-dimensions. Models in two dimensions are clearly the minimum required to describe the latitudinal, seasonal, and advective transport effects in the atmosphere. The recent developments and the status of such 2-D models are discussed in some detail in Chapter 2. It was originally hoped that a detailed comparison of 2-D models with each other could be done for this document, but an insufficient number were available and the similarities and differences in transport parameterizations were not well enough

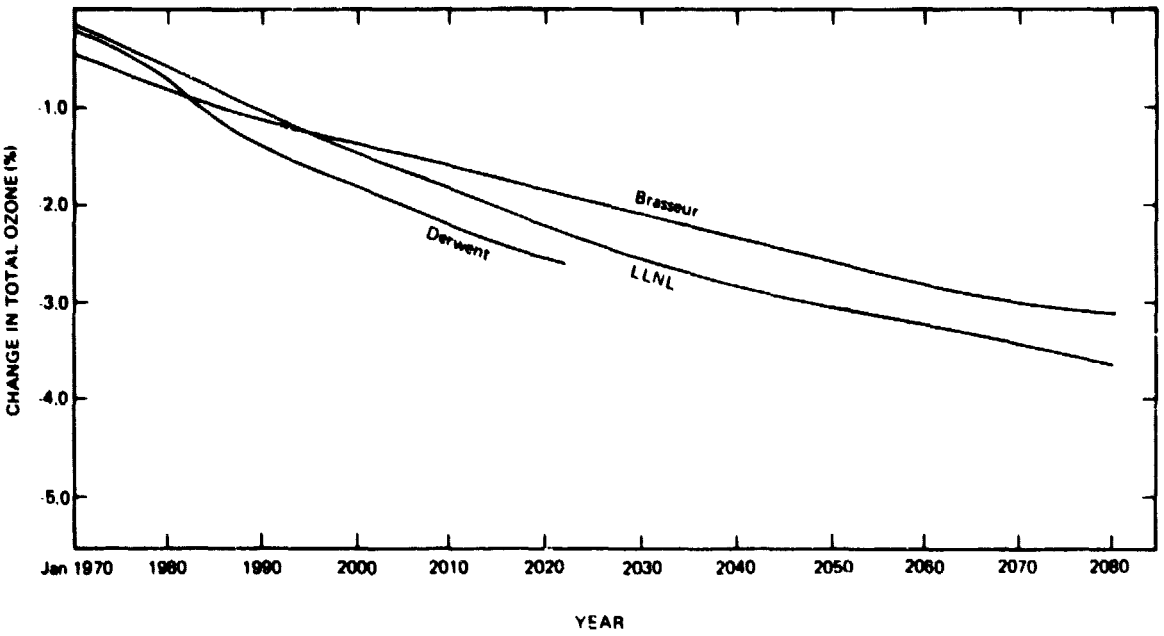

Figure 3-4. Time evolution of the percentage change in the total column ozone depletion due to FC-11 and FC-12 from 1970 onwards.

known to complete this task. The results from the models examined in this report and in the literature (e.g., Borucki et al., 1980) indicate a close similarity in the overall features between those obtained in 1-D and 2-D models. See Chapter 1 for a comparison of 2-D model calculations for the present-day atmosphere with measurements.

Figure 3-5 illustrates the seasonal and latitudinal variations of the steady-state total column ozone depletion due to FC-11 and FC-12 release with no other changes as calculated in the Du Pont model (C. Miller et al., 1981). At high latitudes the seasonal variations in column ozone depletion approach about a factor of two, from minimum in the summer to maximum in the winter. At low latitudes the seasonal variation nearly vanishes and the ozone depletion value is very near the seasonal mean of the higher latitudes. The symmetry between hemispheres is a direct consequence of the assumption of symmetric circulation. This simplifying assumption precludes the examination of the cause of the observed hemispheric asymmetry in ozone but should not significantly disturb the model's ability to determine the approximate latitudinal and seasonal gradients in ozone depletion. These latitudinal and seasonal variations are characteristically different from those reported from a previous 2-D calculation (UK-DOE Pollution Paper No. 15, 1979). The previous study showed a similar seasonal variation at high latitudes but a significantly stronger latitudinal gradient such that at low latitudes the steady-state depletion was significantly less than even the high latitude minimum. It is tempting to ascribe these differences wholly to reevaluations in the chemical kinetics parameters but it must be remembered that the transport representations of the two models are quite different and no detailed analysis of the consequences of the types of differences between these models or any others has been made. The argument for chemical nature of the differences is as follows: the principal changes were in the reactions of HNO_3 and HNO_4 with HO serving to suppress HO concentrations in the lower stratosphere thus reducing the chlorine catalytic efficiency. Since HNO_3 concentrations increase towards the poles (see Chapter 1) and so presumably do HNO_4 concentrations, the suppressing effect of the reaction rate coefficient evaluation is stronger at higher latitudes thus reducing the previously obtained latitudinal gradient.

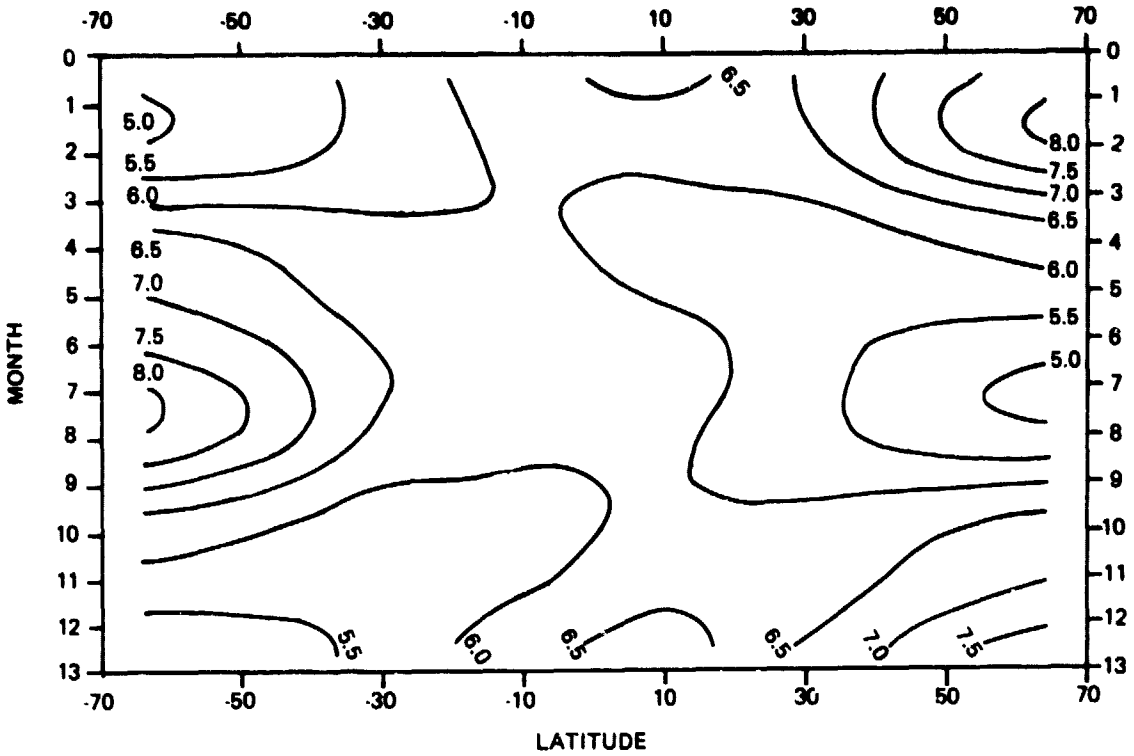

Figure 3-5. Calculated variations with latitude and season in the steady-state total ozone depletion due to FC-11 and FC-12 in terms of the percent change in column content (C. Miller et al., 1981).

OTHER HALOCARBONS

While most of the attention in the past has been directed toward the impact of fluorocarbons 11 and 12 on stratospheric ozone, other chlorine-containing trace gases have been observed in the troposphere and can potentially contribute to the stratospheric chlorine budget. Historical release rate estimates are available for such halocarbons as methyl chloroform (CH_3CCl_3), FC-113(CCl_2FCCl_2F), FC-114($CClF_2CClF_2$), FC-115(C_2ClF_5), carbon tetrachloride (CCl_4), FC-22($CHClF_2$), and tetrachloroethylene (C_2Cl_4). These can be used together with a knowledge of the loss processes for each molecule to provide a preliminary assessment of their possible impact on stratospheric ozone to determine which, if any, should be given further attention. Table 3-5 presents results from two 1-D models for the effect of the above mentioned halocarbons as well as for FC-11 and FC-12. In each case the quoted "current" (1978, 1979 or 1980) release rates were used and the model run to steady-state with and without the release of the particular halocarbon. The runs were for the JPL 81-3 chemistry (case B) but the results are not identical to the numbers in Table 3-1 for FC-11 and FC-12 because of the differences in the assumed release rates. An important general feature of the results is the relatively constant ratios of ozone depletion to release rates for the fully halogenated halocarbons, as compared to the significantly smaller ratio for the partially halogenated halocarbons which contain an H atom which can be abstracted by HO in the troposphere. These halocarbons, if released until steady-state is reached, would apparently increase the predicted column ozone depletion by about one-third. The increase would result mainly from CCl_4, CCl_2FCCl_2F(FC-113), and CH_3CCl_3.

Table 3-5
Estimated Steady-State Total Column Ozone Depletion Resulting from the Continued Injection of Nine Halocarbons at Present Release Rates

Halocarbon	Current Annual Release Rate, $x10^3$ Metric tons/yr.	Estimated Steady State Ozone Depletion, %	
		Derwent[8]	Wuebbles[9]
CCl_3F (FC-11)	272[1]	2.9	3.0
CCl_2F_2 (FC-12)	383[1]	3.2	3.3
CCl_2FCClF_2 (FC-113)	91[2]	0.7	0.8
$CClF_2CClF_2$ (FC-114)	18[2]	0.1	0.1
C_2ClF_5 (FC-115)	4.5[3]	0.01	0.02
CCl_4	82[4]	0.8	1.0
CH_3CCl_3	476[5]	0.2	0.8
C_2Cl_4	608[6]	0.02	--
$CHClF_2$ (FC-22)	71[7]	0.01	0.04
		7.9	9.1

[1] Alexander Grant and Co. (1980). 1979 release rates.

[2] Du Pont (1980).

[3] EPA (1980), Metra Gruppe (1978).

[4] Singh et al. (1979).

[5] Neely and Agin (1980).

[6] Bauer (1978).

[7] OECD (1981).

[8] These values were obtained with the modified JPL 81-3 chemistry data base and the N_2O-K_z profile, (Derwent and Curtis 1981).

[9] Wuebbles (1981)

The results in Table 3-5 are indicative of only the efficiency of ozone destruction and of the current release rate. The impact of these halocarbons on the past ozone trend or on that for the near-term future depends also on the time history of the release rate. Figure 3-6 illustrates the computed time history of ozone change for FC-11 and FC-12, CCl_4 and CH_3CCl_3. The figure shows that although CCl_4 contributes significantly to the ozone change since 1930, its contribution since 1970 is much smaller. CH_3CCl_3, on the other hand, has not yet contributed much to the computed ozone depletion but if its release rate continues to increase rapidly so will its importance. Future assessments will have to carefully consider the complete set of halocarbons in order to determine the expected overall impact on the ozone layer.

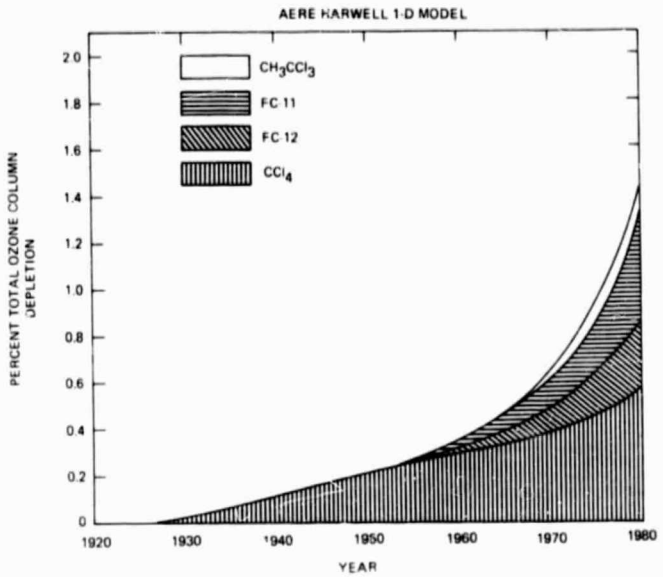

Figure 3-6. Time evolution of the cumulative total ozone depletion due to a number of halocarbons.

TROPOSPHERIC AND LOWER STRATOSPHERIC AIRCRAFT

Considerable quantities of nitrogen oxides are injected into the atmosphere, mostly in the Northern Hemisphere, by aircraft engines. The impact of these emissions has been studied in great detail during the last 10 years (see e.g., CIAP, 1975a,b; COMESA 1975; Oliver et al., 1977; Luther et al., 1979). The NO_x molecules created during combustion are dispersed in the atmosphere by several transport processes and react with other chemical species. If a continuous emission of NO_x is assumed, a steady state is reached after a few years and the equilibrium time is thus much shorter than in the case of CFC emissions.

The recent reevaluations of chemical kinetics discussed earlier in this chapter with respect to CFC emissions have also had a significant impact on the ozone change computed for NO_x injections and hence for the evaluation of the effects of aircraft. Table 3-6 shows the calculated total ozone change for steady-state NO_x emissions of $1x10^8$ and $2x10^8$ molecules $cm^{-2}sec^{-1}$ distributed over a 1 km thick layer centered at the injection altitude for a number of altitudes of injection. These cover the range of typical flight altitudes for various existing and proposed aircraft. These results continue to show ozone column increases for injections below 17 km but now give ozone decreases for injection altitudes above 17 km. This is in contrast to the results obtained with the NASA RP 1049 chemistry (case A) in which Luther et al. (1979) calculated a change of +1.3% for both 17 and 20 km injections of $1x10^8$ $cm^{-2}sec^{-1}$. The increases of local ozone in the troposphere and lower stratosphere and decreases in upper stratospheric ozone still persist, but with different relative magnitudes than before. However, the importance of HO_x

Table 3-6
The Change in Total Ozone (Percent) Resulting from NO_x Injections
Distributed Over a 1-km Thick Layer at the Injection Altitude.

Injection Altitude (km)	NO_x Injection (Δ) Rate ($cm^{-2}s^{-1}$)	LLNL K_z Chang, 1976		NOAA[1] Liu		AER Sze	IAS Brasseur
		JPL 81-3 (Case B)	NASA/CODATA (Case D)	JPL 81-3 (Case B)	NASA/CODATA (Case D)	NASA/CODATA (Case D)	NASA/CODATA (Case D)
9	2×10^8	+0.5	–	–	–	–	–
11	2×10^8	+0.8	–	–	–	–	–
13	2×10^8	+0.9	–	–	–	–	-0.7
17	1×10^8	+0.01	-0.9	–	–	–	-1.8
	2×10^8	- 0.7	-2.2	–	–	–	-2.7
20	1×10^8	- 2.0	-3.4	-6	-8	–	-3.6
	2×10^8	- 5.3	-7.1	–	–	-6.2	-6.4

(1) Lower boundary of the model is located at 10 km. No tropospheric impact in the model.

catalytic cycles has been reduced by the recent chemistry modifications, particularly due to the rate changes for HO + HO_2, HO + HNO_3, HO + H_2O_2, and HO + HNO_4, which result in reduced HO_x levels. Because of these reduced HO_x levels, the positive changes in ozone previously found in the lower stratosphere due to NO_x injections are greatly reduced. Also, the relative importance of the NO_x catalytic cycle in the upper atmosphere has increased. Figure 3-7 shows the local changes in ozone calculated corresponding to an injection of 10^8 NO_x molecules $cm^{-2}sec^{-1}$ at 17 and 20 km. Figures 3-8 and 3-9 show the change in total ozone column expected for variations of the 17 and 20 km injection amounts from zero to $2x10^8$ molecules $cm^{-2}sec^{-1}$ of NO_x. For emissions located at 17 km, the net increase which is found for the JPL 81-3 chemistry for injection rates less than 10^8 molecules $cm^{-2}sec^{-1}$ disappears with the adoption of the NASA/CODATA chemistry. The 20 km injection produces a net reduction in ozone for all injection rates and for the two chemical schemes. While the change in ozone is nonlinear for both the 17 and 20 km flight altitude at injection rates less than 10^8 molecules $cm^{-2}sec^{-1}$, both are nearly linear at injection rates higher than this.

In order to estimate the effects of current and projected aircraft fleets the above information about the effects as a function of altitude of injection and magnitude of injection must be combined with the injection rate versus altitude. As an example Table 3-7 gives the NO_x emission rates corresponding to a high estimate of a 1990 subsonic and supersonic fleet (Oliver et al., 1977) as a function of injection altitude. Adopting these emission rates, Luther et al. (1979) calculated a net increase of 2% in ozone for the 1990 fleet, using the LLNL K_z. The change in total ozone with the NASA 1980 chemistry is now found to be +1.3% with the LLNL K_z.

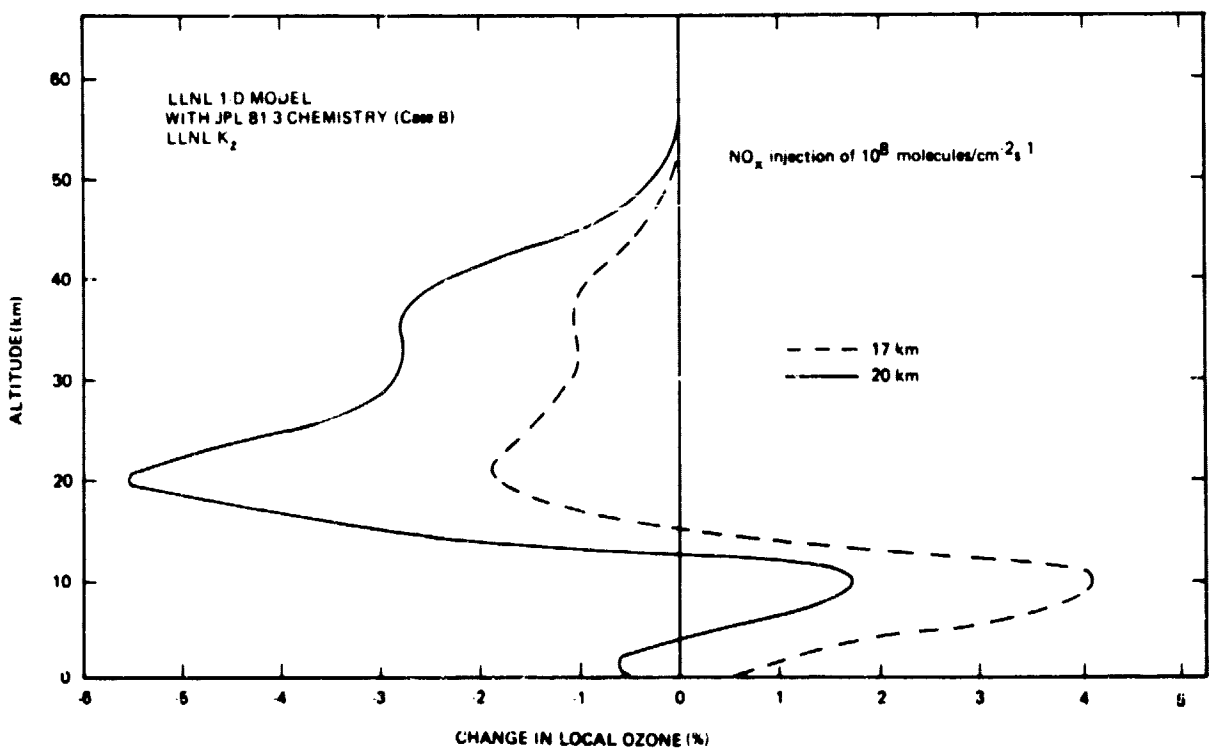

Figure 3-7. The percent change in the local ozone concentration for the steady-state NO_x injection of 10^8 molecules $cm^{-2}sec^{-1}$ in a 1 km layer at about 17 km (- - -) and 20 km (——).

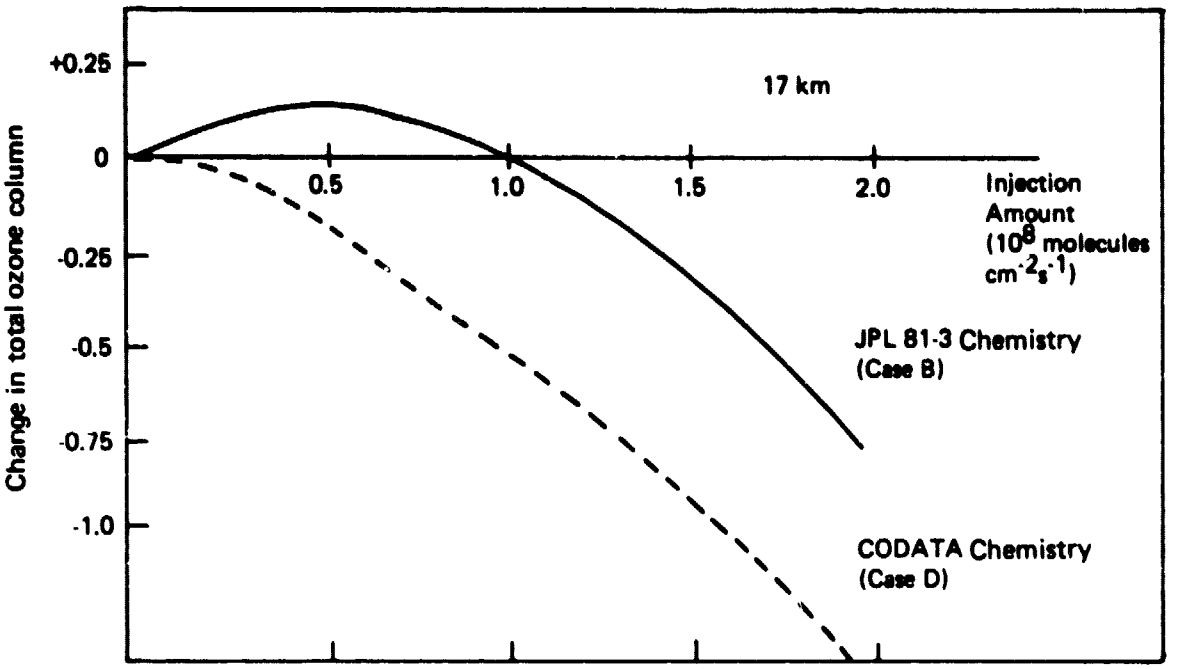

Figure 3-8. Percent change in the total ozone column for NO_x injection in a 1 km thick band centered at 17 km as a function of the magnitude of the injection in 10^8 molecules cm^{-2} s^{-1} for two chemical rate coefficient sets.

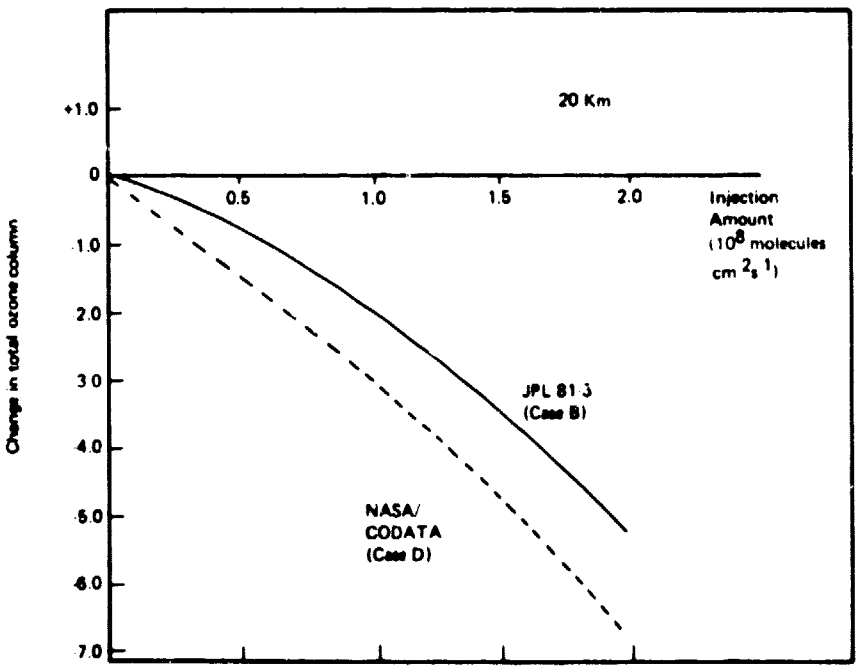

Figure 3-9. Percent change in the total ozone column for NO_x injection in a 1 km thick band at 20 km as a function of the magnitude of the injection in 10^8 molecules $cm^{-2}s^{-1}$ for two chemical rate coefficient sets.

Table 3-7
Projected 1990 Aircraft Emissions of NO_x (Oliver et al., 1977, High Estimate)

Injection Altitude (km)	NO_x Injection Rate Total Fleet (molecules $cm^{-3}s^{-1}$)
6	90
7	179
8	265
9	665
10	1167
11	1161
12	520
13	75
14	18*
15	18
16	33
17	43
18	29
19	8

*Emissions from the projected 1990 SST fleet are included at 14 km and above.

Table 3-8 summarizes the published results from a number of 1-D and 2-D models for various fleet estimates. The 1990 high estimate has already been shown in Table 3-7. The 1990 low estimate is also taken from Oliver et al. (1977). The various 1975 to 1980 fleets are explained in each of the references quoted in the table. The key result is that all of these estimates are for total ozone increases in the 1980 to 1990 period with the largest increases located in the 8 to 10 km altitude region.

Table 3-8
Summary of Various Estimates of Ozone Changes from Subsonic Aircraft

Investigation	Type of Model	Perturbation	Injection Rate, kg yr^{-1} (as NO_2)	Percentage Change in Total Column at 30°N annual mean	Percentage Change in Local Ozone at 30°N 8-10 km
Isaksen (1980)	2-D	1990 high	4.855×10^9	+1.0%	+15.0%
Liu, Kiley, McFarland Mahlman and Levy (1980)	1-D	1980 low	1.843×10^9	+1.5 - +3.0%	+15-30%
Luther, Chang, Duewer, Penner, Tarp and Wuebbles (1979)	1-D	1990 high	4.855×10^9	+1.86%	+27.0%
		1990 low	3.078×10^9	+1.29%	+18.5%
		1979	1.1×10^9	+0.5%	-
Hidalgo and Crutzen (1977)	2-D	1990	2.06×10^9	+0.63	+12.0%
Derwent (1981)	2-D	1975	4.855×10^8	+0.28%	+2.0%
		1990	4.855×10^9	+1.81%	+15.4%
Wuebbles, personal communication (1981) (NASA/CODATA Chemistry)	1-D	1990 high	4.855×10^9	+1.02%	+20.0%

Table 3-9 provides a summary of various LLNL assessments of the effects of aircraft operations based on injection of 2×10^8 molecules (NO) $cm^{-2} sec^{-1}$ distributed over a 1 km thick layer centered at 17 or 20 km. The results are based on published calculations made with the LLNL one-dimensional model since mid-1974. These results demonstrate the combined effects of the evolution of the understanding of stratospheric chemistry and evolution of the treatment of physical phenomena in the one-dimensional model. It is interesting to note that when the effect of NO_x on ozone is enhanced, the effect of chlorine is reduced and vice versa (see Figure 3-14). The balance between these two actions is related to the concentration of HO radicals in the lower stratosphere which thus plays a central role in this problem. The new rate constants which have been recently introduced in the models lead to lower concentrations of the hydroxyl radicals and therefore to a higher sensitivity of ozone to aircraft and a lower sensitivity of ozone to CFC releases.

Figure 3-10 shows the local change in ozone corresponding to the 17 km injections and obtained for several schemes dating from early 1975 to the present. Only negative changes in local ozone are found in the early 1975 results. By late 1975 the positive region in the lower atmosphere due to increased importance of HO_x had appeared. This increased importance was due to the reduction in the evaluation of the $HO + HO_2$ rate coefficient from 2×10^{-10} to 2×10^{-11} cm^3 $molecules^{-1} sec^{-1}$. The resulting larger HO concentrations then cause a higher fraction of the injected NO_x to be stored as HNO_3 and thus not available for catalytic destruction. The smog-like reactions of HO_2 generated from CH_4 oxidation are thus better able to compete with catalysis. The major change shown in the early 1980 curve is caused by the inclusion of the revised much faster $HO_2 + NO$ reaction rate coefficient. This fast rate coefficient has been used since 1977 as illustrated in Table 3-9.

This reaction further increased the lower stratospheric HO concentration and caused a significantly stronger coupling to exist between the NO_x and HO_x cycles. It was not until this time that an increase in the total ozone column was calculated. As discussed earlier, the more recent changes have somewhat reversed this trend by causing a reduction in lower stratospheric HO and a consequent enhancement in the relative importance of the NO_x catalytic cycles.

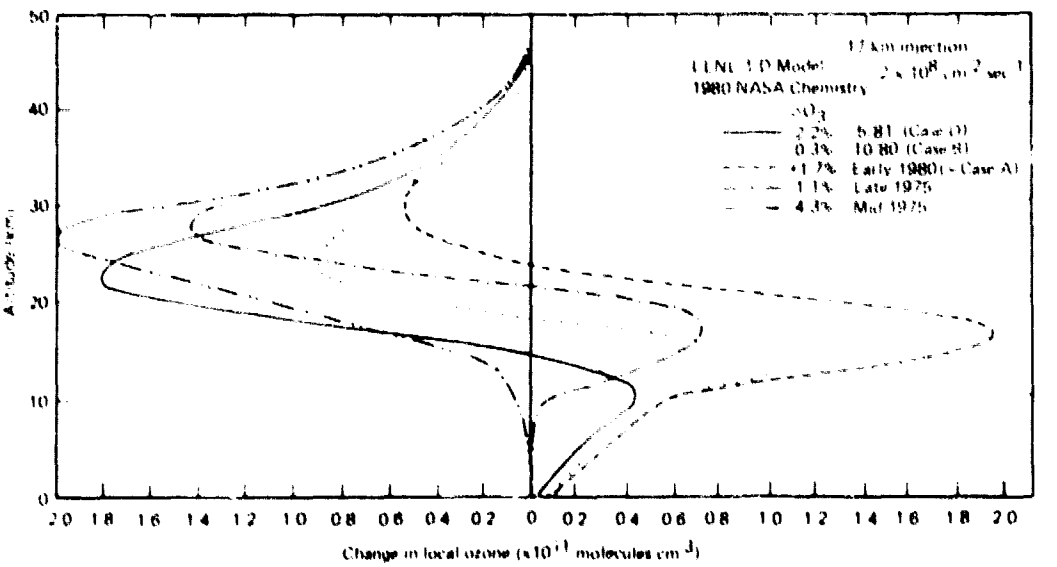

Figure 3-10. Local change in ozone corresponding to 17 km injections for several chemical schemes from early 1975 to the present.

The historical record shows that model predictions have changed significantly over the last 6 years. Although the understanding of the chemical and physical processes that determine the ozone distributions in the troposphere and stratosphere has greatly improved, it is not obvious that similar changes in model sensitivity might not occur in the future.

Table 3-9
Change in LLNL One-Dimensional Model Calculations of Expected Effect on Total Ozone from NO_x Emissions at 17 and 20 km at a Constant Emission Rate of 2×10^8 Molecules $cm^{-2} s^{-1}$.

Date of Evaluation	ΔO_3(%) for injection at 17 km	ΔO_3(%) for injection at 20 km	Comments
mid-1974	-4.8	-10.2	based on CIAP Monographs (also Chang and Johnston, 1974)
early 1975	-5.3	-11.2	based on CIAP (1975b); minor chemical changes
mid-1975	-4.3	-9.8	based on Duewer et al. (1977); used Chang (1974) K_2; NBS 866 chemistry, fast HO + HO_2
mid- to late 1975	-1.8	-5.2	same as above with slow HO + HO_2
late 1975	-1.1	-3.5	same as above with NO_3 + hν → NO_2 + O
mid-1976	-0.7	-2.9	based on Luther (1976), "old" Chang (1974) K_2, no ClO_x
	-1.2	-4.2	"new" Chang (1976) K_2; no ClO_x
mid- to late 1976	-0.7	-3.3	same with 1 ppb ClO_x
mid-1977	-1.3	-4.8	based on Luther (1977), NASA RP-1010 chemistry, slow HO_2 + NO
mid- to late 1977	+2.0	+0.5	fast HO_2 + NO
mid-1978	+3.2	+3.6	based on Luther (1978), NBS 513 chemistry except modified HO_2 + O_3, HO_2 + NO, 1.2 ppb ClO_x
early 1979	+2.6	+2.2	based on Luther et al. (1979); NASA JPL chemistry
mid-1979 (Case A)	+2.0	+1.1	NASA RP 1049 chemistry
early 1980	+1.7	+0.6	same with minor chemistry changes
October 1980	-0.3	-4.5	with new HO + HNO_3 (Wine et al., 1980)
December 1980 (Case B)	-0.7	-5.3	with new NASA chemistry
May 1981 (Case D)	-2.2	-7.1	with new NASA/CODATA Chemistry

NITROUS OXIDE (N_2O) CHANGE

Since N_2O is the principal source of stratospheric nitrogen oxides, possible perturbations in its concentration have been of great interest in understanding the possible effects of human activities on ozone. Concern has centered around the question of the intensive use of fertilizers and their impact on N_2O when this "fixed" nitrogen is returned to the atmosphere through nitrification or denitrification (see e.g., Crutzen 1974; Liu et al., 1976; McElroy et al., 1977). Another potentially increasing source of N_2O is from combustion (see e.g., Weiss and Craig, 1976; Pierotti and Rasmussen, 1976). Evidence from the variability in N_2O and its observed slow rate of increase (Weiss, 1981) indicate that its lifetime is in the 100-year range and that short-term changes in its concentration will be small.

In order to examine the possible effects of increased emission of nitrous oxide to the atmosphere, the response of ozone to a doubling of N_2O has been considered in various model calculations. Although such large increases would not be expected in the near future, the results for this arbitrary perturbation provide a benchmark for comparison as chemical rate sets are changed. Results which are given in Table 3-10 provide values of the ozone reduction which are higher than the results obtained two years ago. In 1979, Luther et al. calculated a 2.8% ozone decrease while the same model gives a value of 11.5% with the NASA/CODATA chemistry. The results of different modeling groups show a dispersion of a factor of two which could be explained partly by differences in the vertical exchange coefficient. The larger result in the NOAA model is partly due to its lower boundary at 10 km which eliminates the enhancement of the troposphere ozone concentration as computed in the other models.

Table 3-10
Percentage Change in Total Ozone for Doubling of N_2O, CFC Release, and Both Simultaneously.
1981 NASA/CODATA Chemistry

Model	Perturbation		
	2 x N_2O	CFC	2x N_2O + CFC
LLNL (Chang/Wuebbles)	-12.5	-5.0	-12.9
NOAA (Liu)	-16	-4.5	-16.5
IAS (Brasseur)	-10.7	-4.9	-12.4
AER (Sze)	-9.5	-6.1	-13

Figure 3-11 shows that the response of ozone to a uniform increase in N_2O varies considerably with latitude and is most important in the polar regions according to the model of Sze (personal communication). This model indicates a depletion of total ozone which varies by a factor of five between the Equator and the pole. Whitten et al. (1981) obtain results in their 2-D model which have the same general behavior but indicate a lower Equator-to-pole gradient. The sensitivity of total ozone change due to N_2O seems to follow the same general pattern as for fluorocarbons with a maximum depletion in the polar regions during winter or spring. The altitude distribution of ozone change shown in Figure 3-12 shows that the sensitivity of ozone to N_2O is the largest in the polar regions with a maximum between 20 and 30 km. These depletions are only partially balanced by the tropospheric increases which are in the equatorial zone.

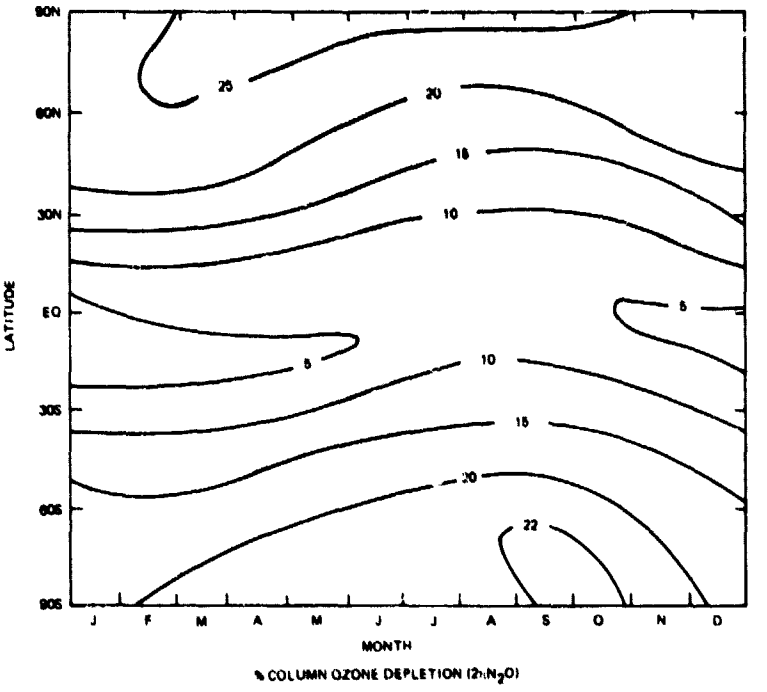

Figure 3-11. Latitude and seasonal dependence of the change in ozone column for a doubling of N_2O (after Sze, personal communication).

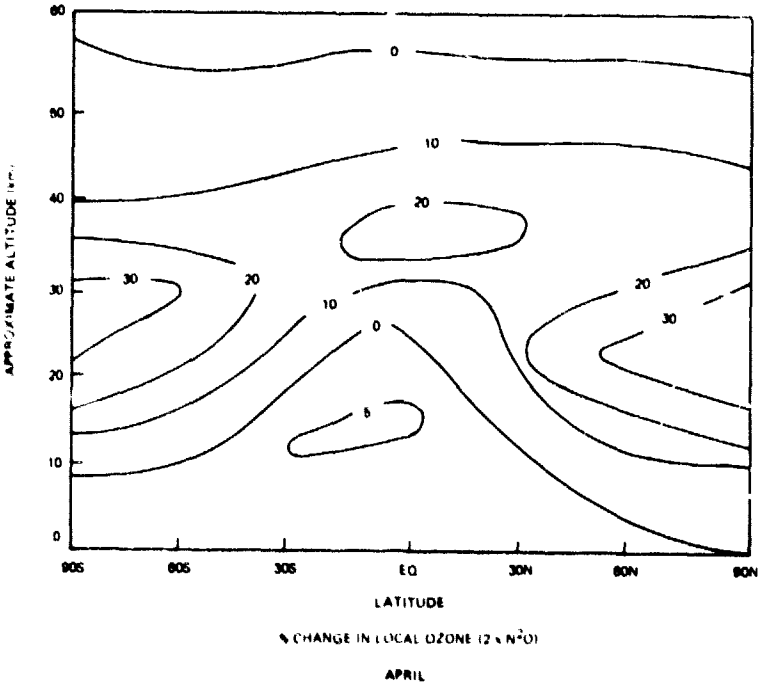

Figure 3-12. Altitude and latitude dependence of the change in local ozone in April for a doubling of N_2O (after Sze, personal communication).

Table 3-10 also shows the large nonlinear response to simultaneously doubling N_2O and including constant emission rates of chlorofluorocarbons. For instance, the ozone decrease of 12.5% calculated with the LLNL model for a doubled amount of N_2O is not considerably modified when the N_2O and CFC effects are considered simultaneously (12.9% instead of 12.5%). In fact, the results tend to show that, if one of the two perturbations is significantly dominant, the effect of the second perturbation will not appear on the total ozone amount but will modify the local behavior of ozone depletion as shown by Figure 3-13.

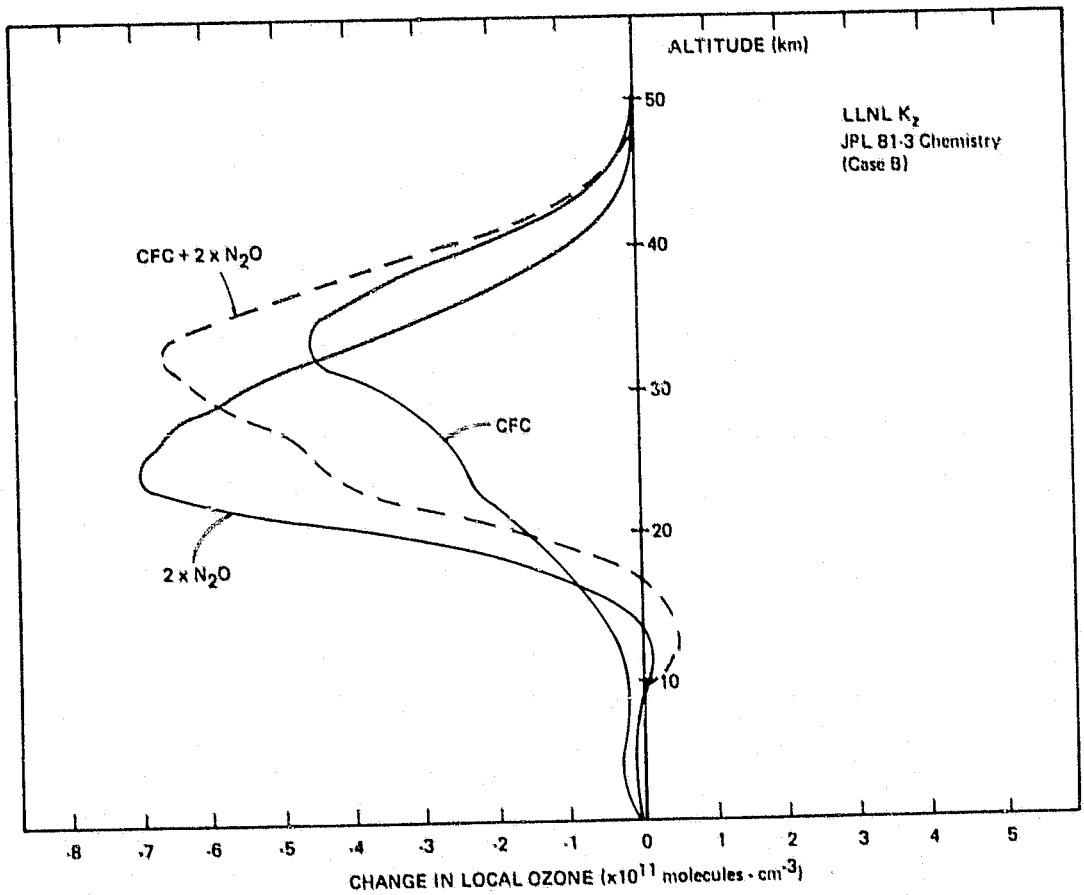

Figure 3-13. Local ozone change vs. altitude for CFC release, doubling N_2O and the combined effects in LLNL model.

CARBON DIOXIDE CHANGE

Carbon dioxide in the atmosphere is observed to be increasing (Keeling et al., 1976). Its potential effect on the global surface temperature through the greenhouse effect has been discussed extensively elsewhere (NRC 1979; CEQ, 1981). Its potential effect on ozone comes about because CO_2 is the principal constituent which contributes to stratospheric cooling via escape of infrared radiation. Thus, an increase in stratospheric CO_2, which will follow from the increase in tropospheric CO_2, will lead to a cooling of the stratosphere. The temperature dependence of the chemical reaction rate coefficients will convert this temperature decrease into an ozone increase.

Table 3-11 shows the calculated percentage change in O_3 at steady-state for a doubling of CO_2 in two different one-dimensional models. Also shown is the decrease in O_3 calculated for the combined effect of doubled CO_2 and constant CFC release. The main result is that higher levels of CO_2 slightly increase the ozone sensitivity to chlorine, but the coupled perturbation is nearly a linear combination of the results from CFC and CO_2 perturbations alone. The differences are primarily because the odd oxygen loss rates from ClX catalyzed mechanisms are a much larger percentage of the total O_3 loss rate in the CFC perturbed atmosphere than in the ambient atmosphere. Since the ClX catalyzed loss rates are not very sensitive to temperature change, the effect of increased CO_2 is lessened.

Table 3-11

Percentage Column Change in O_3 at Steady-State Using Chemistry in JPL 81-3 for Doubled CO_2, CFC Release, and the Combined Effects from 1-D Calculations.

Model	Perturbation		
	2 x CO_2	CFC	2 x CO_2 + CFC
LLNL	+6%	-9%	-4.4%
AER	+2.7%	-8.2%	-6.3%

The corresponding vertical maximum temperature decrease is of the order of 7 to 10 K near 40 km for an ozone increase of about 20 to 30%. The principal mechanism responsible for the ozone increase is the sensitivity of the oxygen reactions of the Chapman cycle (see for example Blake and Lindzen, 1973).

$$O + O_2 + M \rightarrow O_3 + M \qquad k = 1.05 \times 10^{-34} \exp(510/T) \qquad (1)$$

and

$$O + O_3 \rightarrow 2O_2 \qquad k = 1.5 \times 10^{-11} \exp(-2218/T) \qquad (2)$$

Nevertheless the temperature sensitivity of the reaction

$$N + O_2 \rightarrow NO + O \qquad k = 7.7 \times 10^{-12} \exp(-3220/T) \qquad (3)$$

is also of importance for the predicted O_3 increase.

As a result of the large activation energy for this reaction, when the temperature is decreased, the N atom concentration is increased. This increases the rate for the reaction

$$N + NO \rightarrow N_2 + O \quad . \qquad (4)$$

As discussed by Duewer et al. (1977), reaction (4) is an important NO_x sink in the stratosphere, so that the net effect of the decreased temperature is to decrease total stratospheric NO_x. As a result of this change, the NO_x catalyzed ozone loss rate is decreased and O_3 is increased. Nevertheless the magnitude of this effect is dependent upon the downward flux of NO from the mesosphere. Doubling CO_2 may have a large impact on the mesospheric temperature, thereby affecting the exchange between mesosphere and stratosphere and the NO flux.

One-dimensional model calculations can take into account radiative and photochemical feedback. Dynamical processes will also be affected by changes in the atmospheric temperature structure. Using the Oxford 2-D model (Harwood and Pyle, 1975), an attempt to characterize the importance of the dynamical feedback was made. Table 3-12 shows the percent change in O_3 for perturbations similar to the one reported in 1-D calculations.

Table 3-12
Percent Change in O_3 from Oxford 2-D Model
from Haigh and Pyle (1981).

PERTURBATION	GLOBAL O_3 CHANGE
CO_2 (from 320 to 625 ppm)	+8.8%
CFC (in 2040)	-12.8%
CFC and CO_2 (as above)	-8.1%

Conclusions pertaining to the upper stratosphere, drawn from one-dimensional calculations, are confirmed by the 2-D calculations. But changes in the zonal mean wind structure clearly influence the calculated ozone variations in the lower stratosphere especially at high latitudes. The greatest column change is indicated to occur at high latitudes, similar to the results for other perturbations.

COMBINED SCENARIOS

Many of the above studies (predictions) were based upon the assumption of single source function changes. That is, the scenario assumes that only one source of stratospheric trace species may change at any given time. This single perturbing source scenario allows a clear delineation of the details of perturbing influence and the corresponding feedback processes. However, it does not reflect reality. As is clear from the above discussions several source functions have been changing over past decades. In fact this information has been used to construct individual scenarios for analysis. If we are to understand events of the recent past we must study a likely set of combined scenarios. For example, N_2O, NO_x from subsonic aircraft and FC-11 and FC-12 have all been increasing during the past two decades. Consequently if we are to understand the long term ozone trends over the same period we must evaluate how these simultaneous changes may affect stratospheric ozone. This combined scenario is particularly important in view of the interference among various perturbing influences. Figure 3-14 illustrates one such coupling. As our understanding of stratospheric chemistry improves the theoretically predicted ozone perturbations due to NO_x from aircraft and CFCs change. It is important to note that since 1976 the estimated influences of added chlorine and NO_x are changing in opposite directions. As the influence of one increases, the other declines. Consequently if both NO_x and ClO_x are increasing either in the past or the future, it is not possible to construct the net changes by summing results from individual single scenario studies. In the following section a set of likely combined scenarios have been studied both to estimate the ultimate changes in ozone and to help to evaluate the accuracy of theoretical models by comparing with observed ozone changes in the most recent past.

To provide a framework for testing model predictions calculations must be made for the time dependence of the ozone change expected as a result of all of the influences which should have changed ozone. Figure 3-15 shows the trend predicted with the LLNL model, Penner (1981), relative to 1970 for total O_3. The solid line was calculated using the historical release rates for

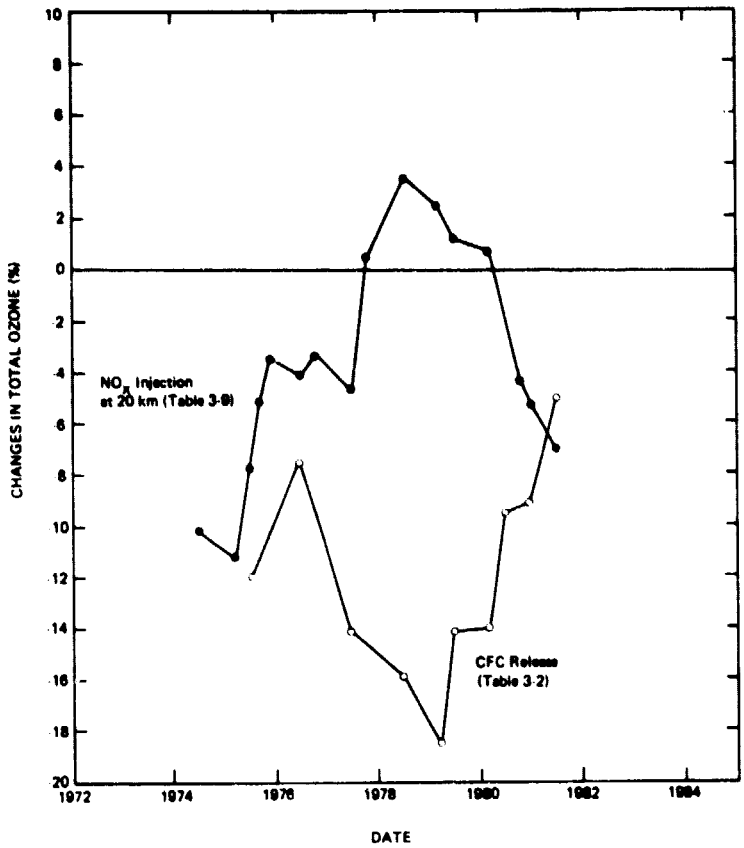

Figure 3-14. Time history of calculations of the expected change in total ozone from CFC release and from NO_x injection at 20 km.

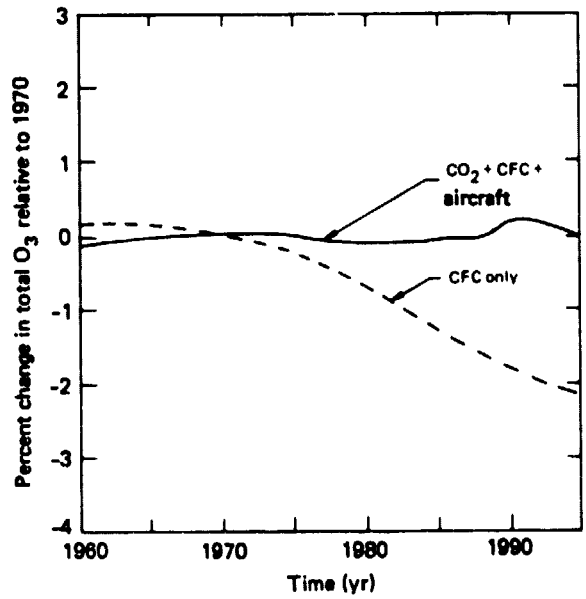

Figure 3-15. Percent change in Northern Hemisphere total ozone for time-dependent scenarios of changes in CFCs, CO_2 and aircraft emissions (Penner, 1981). Stratosphere contains 1.1 ppb of Clx initially.

CF_2Cl_2, $CFCl_3$, and CH_3CCl_3 through 1980 with a constant release rate at 1977 production levels thereafter. CO_2 followed the historical increase to 1980, then increased by 1.5 ppm/year. Subsonic aircraft emissions increased by 9.4%/year up to 1975 as indicated by Bauer (1978). Emissions increased by 8.8%/year after 1975 to reach the "low" 1990 emissions estimate of Oliver et al. (1977). Emission rates for the Northern Hemisphere were used so that the calculations give the expected change in ozone averaged over the Northern Hemisphere only. The reaction rate coefficients were taken from JPL 81-3 (Case B). The solid line represents the most probable model prediction for the resulting O_3 trend. The dashed curve is a similar calculation without CO_2 increase or aircraft emissions. Clearly, these opposing effects tend to cancel masking the individual effects of either.

The trend for the curves for the decade 1970 to 1980 is -0.13% for the "best" scenario and -0.73% for the CFC only scenario. Figure 3-16 shows a similar set of calculations for upper level O_3 (Umkehr layers 7 + 8 + 9) also from Penner (1981). The 10-year trend for the decade 1970 to 1980 is -2.6% for the "best" scenario and -3.8% for the CFC only scenario.

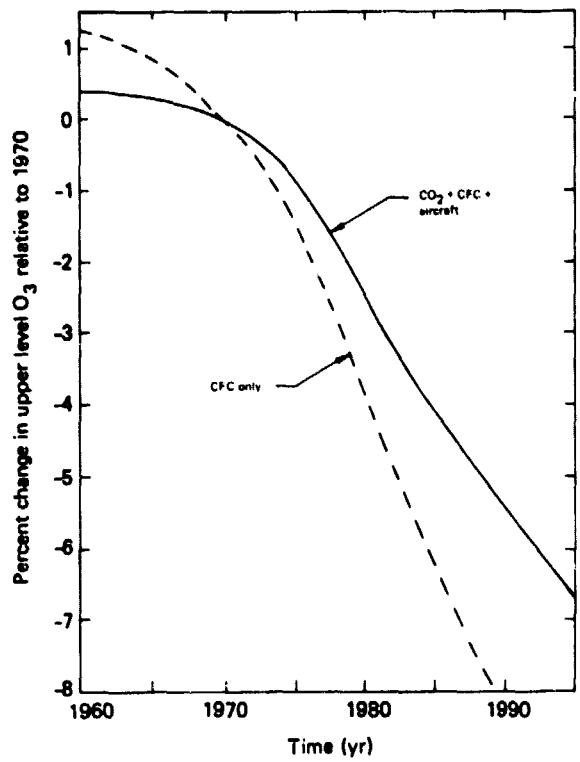

Figure 3-16. Percent change in upper level ozone (near 40 km) for time-dependent scenarios of CFC, CO_2 and aircraft emissions (Penner, 1981). Stratosphere contains 1.1 ppb of Clx initially.

Figure 3-17 shows more detail on the altitude profile of the change in ozone in the Northern Hemisphere for a combined scenario between the years 1971 and 1980. These also were run on the LLNL model by Wuebbles and Luther (1981) using the NASA/CODATA chemistry. The small change in total ozone column (+0.13%) is seen to be made up to a decrease of approximately 3.5% centered about 40 km and an almost exactly cancelling increase of about 7% centered about 10 km. Thus although the predicted change in column content is essentially zero, significant changes are predicted in the upper stratosphere and in the troposphere which can be compared with available data.

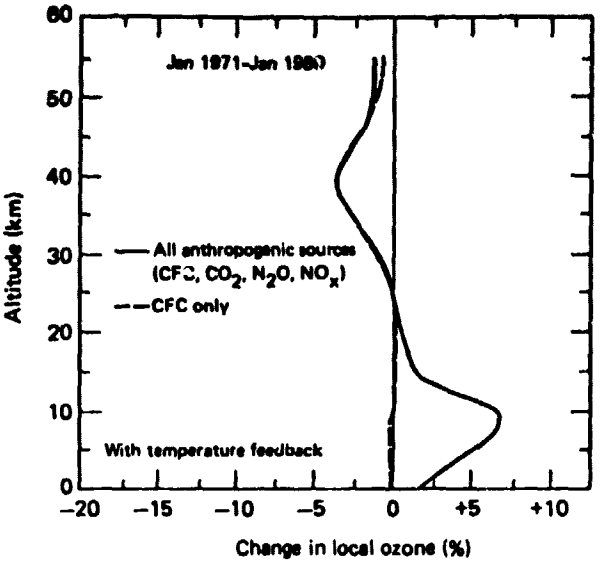

Figure 3-17. Calculated change in Northern Hemisphere local ozone from 1971 to 1980 for CFC only and for CFC plus other anthropogenic source perturbations (Wuebbles and Luther, 1981). Stratosphere contains 0.6 ppb of Clx in 1970.

Figure 3-18 extends this computation to the year 2080, illustrating the time evolution of the altitude profile of ozone change (Wuebbles and Luther, 1981). The aircraft emissions are assumed constant after 1990 and the tropospheric increase quickly becomes near a steady-state at a 20% increase. The fluorocarbon emission rate is also steady but the long residence times give rise to a continued increase in the upper stratospheric depletion.

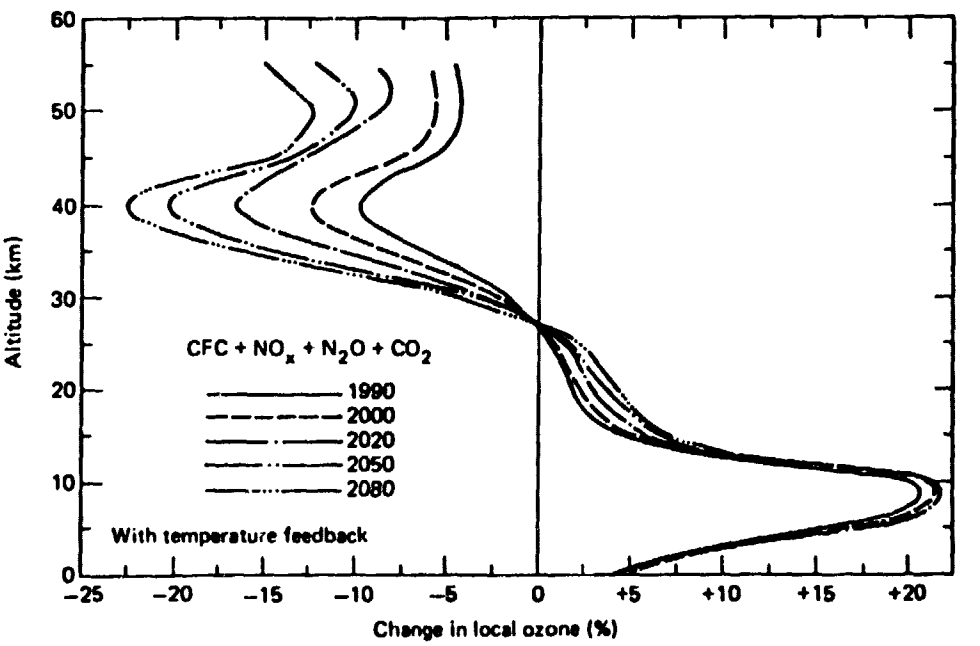

Figure 3-18. Calculated change in Northern Hemisphere local ozone at various times relative to background atmosphere for perturbation containing all anthropogenic sources (Wuebbles and Luther, 1981). Background atmosphere contains 0.6 ppb of Clx.

OZONE VARIATIONS AND TRENDS

Studies of long-period variations of different atmospheric parameters have shown that although the amplitude of such variations generally increases with the length of the period studied the slope of the change as a function of time decreases (e.g., NAS, 1975). Also, as clearly indicated by the results discussed by Birrer (1974, 1975) for variations of total ozone at Arosa, slight changes of the time period or length of the period could result in changes of sign of the ozone trend. The choice of a suitable time interval over which ozone variations are calculated is therefore normally motivated by two factors: First is the total time period for which there are suitable data; second is to attempt to test specific physical mechanisms, if known, that influence the ozone variations. Since most ozone observing programs started sometime after 1958, the longest interval that can be used to calculate representative ozone trends is (except Arosa) of the order of about 20 years.

The basic pattern of seasonal and spatial variation of total ozone and its vertical distributions are well documented and reasonably well understood. Long-term ozone variations, however, are not as evident and are not well understood. Major difficulties in establishing the existence of these long-term ozone changes stem from the requirement that the observed data series be long enough so that random fluctuations, real or due to measurement noise, do not mask the "observed" variation, and that the observations be distributed geographically to provide a representative sample for a global average. Ground-based total ozone observations are not adequately distributed over the globe and satellite observations are presently available only for relatively short periods. Nevertheless, some information is at hand to indicate apparent global ozone variations over the past 20 years. Such information can then be compared with the appropriate theoretical predictions so as to provide an assessment of the adequacy of various theoretical models in making predictions of ozone perturbations.

OBSERVED TOTAL OZONE VARIATIONS AND TRENDS

Descriptive Analysis

Earlier analyses of long term ozone trends have usually used linear regression analysis or piecewise linear least square fitting techniques, e.g., Komhyr et al. (1971); Johnston et al. (1973); Angell and Korshover (1973, 1976, 1978b); London and Oltmans (1978/1979); and Birrer (1974). Komhyr et al. first noted that there was an apparent increase in total ozone over the Northern Hemisphere during the 1960s. This has been confirmed by all later analyses. Further, London and Oltman showed that no such changes could be established for the Southern Hemisphere. Johnston et al. showed that there is more structure in the ozone record of the sixties than a general increase. Specifically their analysis supports the view that there was a decrease of a few percent in total ozone in the early sixties and a slow increase after 1963. This piecewise linear trend is consistent with the single trend for the full period seen by others.

Figure 3-19 is typical of such analysis and contains all of the observed data for the 22-year period (1958-1979) as derived from the ground-based network of Dobson and M-83 stations (WMO, 1981). In Figure 3-19 the annual average total ozone amounts expressed as the average of the percentage deviation from each station mean are plotted for different geographic regions, latitude zones, and for the globe. The vertical bars extend two standard deviations of the mean (standard deviation divided by the square root of the number of stations) either side of the mean, as determined yearly from the percentage deviation from station average of the station values within the region. There is the inference that there is only about a 5% chance that the true value of the yearly mean lies outside the extent of the vertical bars.

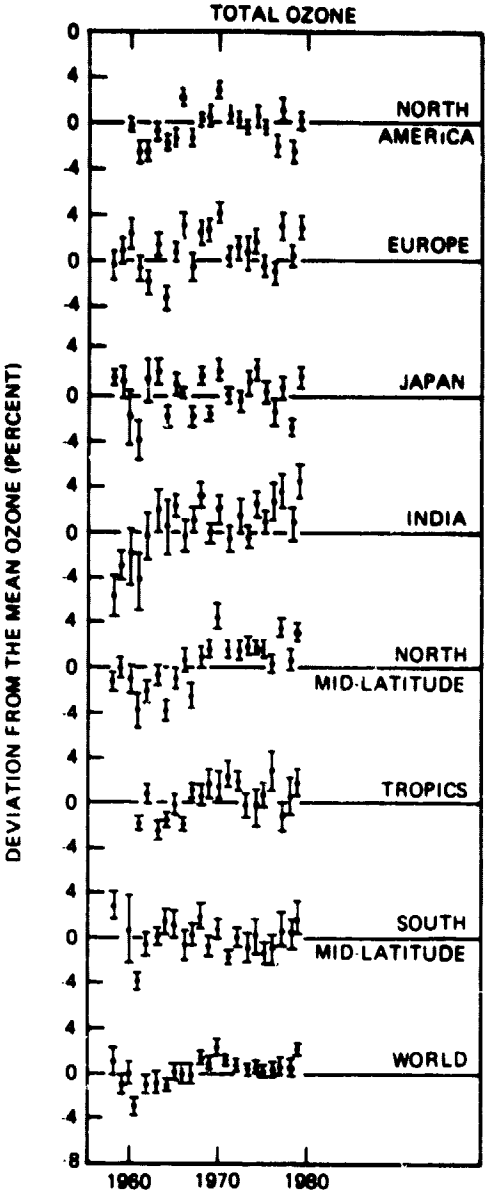

Figure 3-19. Variation of annual total ozone (WMO, 1981).

Because of the uneven distribution of Dobson stations the overall uncertainties are believed to be underestimated. It is only to a first approximation, then, that we can state that if the vertical bar does not intersect the zero axis the mean value for the year is significantly different from the long-term average. This technique only indirectly addresses the problem of the significance of a long-term trend through the aegis of non-overlapping vertical bars for different years.

The average for the Northern Hemisphere mid-latitudes, shown in Figure 3-19, was obtained from a 3, 3, 2, 1, 1, weighting of the total-ozone values for North America, Europe, Soviet Union, Japan and India, respectively. Note that the Soviet Union data are not presented in Figure 3-19 because of the space required to encompass the large deviations and broad confidence limits. The above subjective weighting is based on relative area of the region, number of stations within the region, and estimated accuracy of the data. The Soviet Union receives half the weight appropriate for its area because of the relatively poor quality of the M-83 data. This could be increased somewhat for the mid-and-later 1970s in light of the instrument improvement after 1971.

In other zones the station values are simply averaged to provide a regional mean. A hemispheric average was then obtained from an approximate area weighting, i.e., a 1, 3, 2 weighting of polar, mid-latitude, and tropical zones, respectively, while the global average has been obtained from a 1, 3, 4, 3, 1 weighting of north polar, north mid-latitude, tropical, south mid-latitude, and south polar regions, respectively. More details on the method of analysis are contained in Angell and Korshover (1978b). It is obvious from the data plotted in Figure 3-19 that there are regional differences in the year-to-year and long-term ozone variations. However, for the world average there appears to be an increase of ozone during the period 1960-1970 and a decrease from 1970-1975. Analysis shows worldwide ozone maxima in 1958, 1970, and 1979, the years of sunspot maxima. This latter result may be an artifact of the method used in the global analysis, but because of its significance in delineating and understanding "natural" mechanisms for long-period ozone trends it is necessary to see if this pattern of variations can be verified. As mentioned in Chapter 2 Keating et al. (1981) have analyzed the global mean total ozone derived from the Nimbus 4 BUV instrument and found a high correlation with solar activity. These results have been challenged by Reber and Huang (1981). Keating et al. (1981) also show that when corrected for BUV instrument drift (discussed in Chapter 2) a residual 2 to 3% decrease in ozone from solar maximum to solar minimum appears. The shortness of the satellite sampling period precludes the drawing of final conclusions from these data concerning the magnitude of solar influence on total ozone.

Observed ozone changes averaged over the Northern Hemisphere and the world suggest that a 10-year time interval is the shortest period that is meaningful for calculating ozone trends. In addition, the present diagnostic study is an attempt at assessing the effects of human influences on ozone variations. Since model predictions of some of these effects are based on the assumption that these influences have had an increasing impact on stratospheric ozone since the early 1970s it is of some interest to start with analysis of decadal ozone variations where the data permit. It should be noted, however, that as the data base increases, and other mechanisms for effecting ozone variations are tested, different time intervals need to be used for ozone slope determinations with, quite likely, somewhat different results.

The results of computed 10-year trends for Arosa, shown in Figure 3-20, are based on the homogeneous "C" wavelength Dobson observations discussed by Birrer (1975) and extended to include the 10-year interval 1970-1979. The largest decadal increase during the entire period of observations occurred during the interval 1932-1941 (~2 DU/year) followed by the largest decadal ozone decrease in the interval 1940-1949 (~2.8 DU/year). This large decrease was the result of the high ozone values during the Winter and Spring of 1940 and 1941 associated with the frequent outbreaks of cold Arctic air and strong advection of high ozone concentrations from

the north. Subsequent increasing and decreasing slopes at Arosa are much less pronounced. The pattern of variation of 10-year trends appear to be random, although this inference must be treated with caution in view of the short observational record (less than 50 years).

Linear total ozone trends at Arosa calculated for 20-year intervals are also shown in Figure 3-20. For the larger time interval, the magnitude of the trend values is smaller and the high frequency trend fluctuations are damped. There has been a continuous negative 20-year trend since the mid-1950s, although the overall change at Arosa for the period 1932-1979 is very small (-0.11 DU/year).

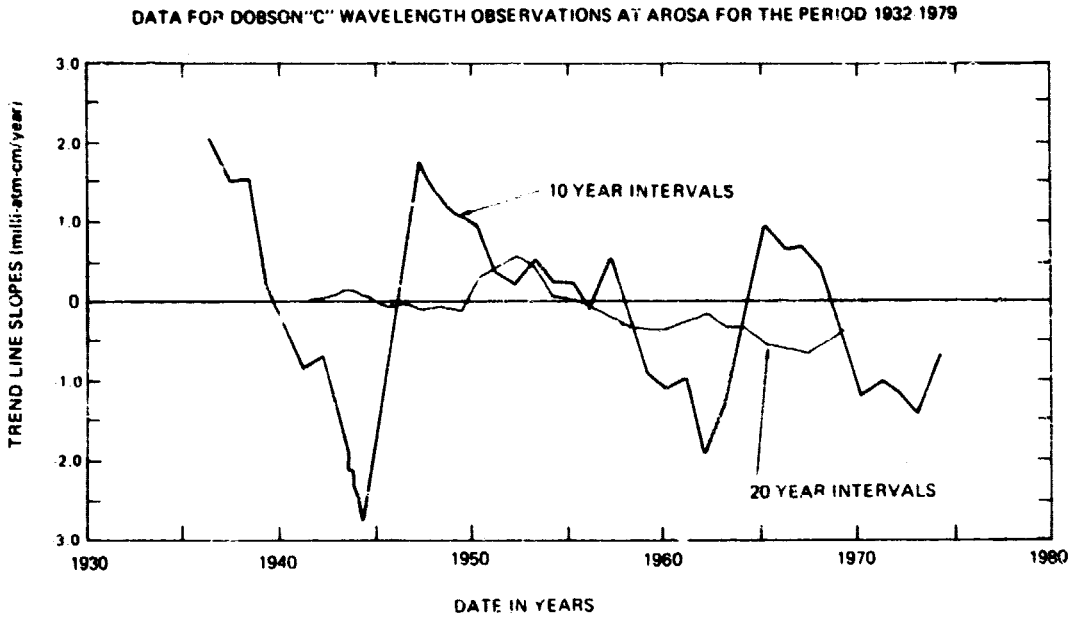

Figure 3-20. Observed 10-year and 20-year trends of total ozone for Arosa.

Trends in total ozone for successive, overlapping 10-year intervals are presented in Figure 3-21 for mid-latitude regions in the Northern Hemisphere. The solid lines denote decadal trends obtained by linear regression. The dotted line for North America represents decadal trends obtained from a least squares autoregressive model (Komhyr, personal communication). Even though the two techniques do not use exactly the same data set, the results are similar, with a strong tendency for the decadal trends to progress from positive to negative during the approximately 20-year period studied.

The progression in decadal trends is similar in Europe and North America, but Japan shows little variation in the trend with time, and the variations in India and the Soviet Union have tended to be out of phase. The very large decadal trends indicated by Soviet M-83 data must, of course, be considered with caution.

Figure 3-22 presents the derived decadal trends in total ozone for different latitude zones, hemispheres, and the world. Here the solid lines represent the 10-year trends obtained using the M-83 data, the dashed lines the trends obtained excluding the M-83 data. In north temperate latitudes the results differ by as much as a factor of two in the the two cases, but in the average for the world there is little difference in the variation in derived decadal trends if the M-83 data are excluded. The amplitude of the decadal trend variation is much larger in the

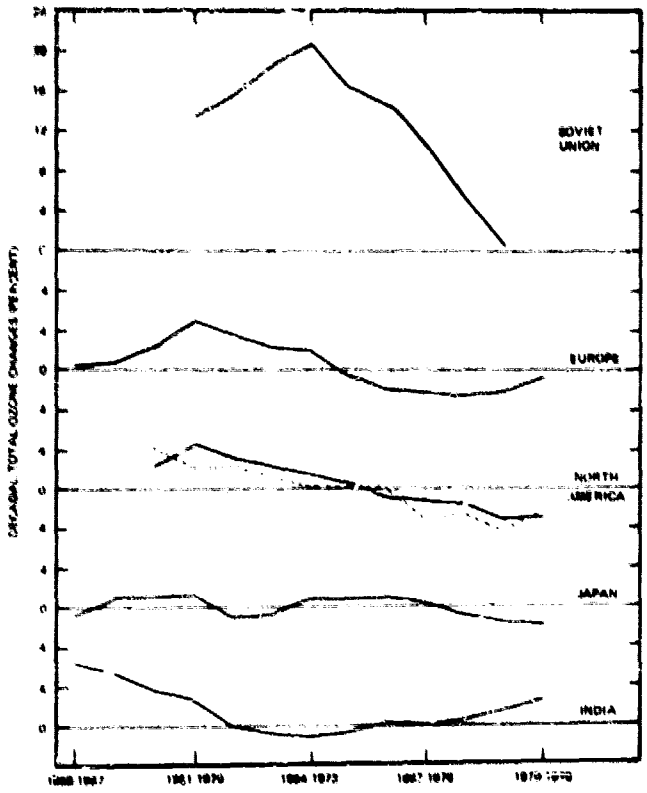

Figure 3-21. Observed decadal trends of total ozone for different geographic regions.

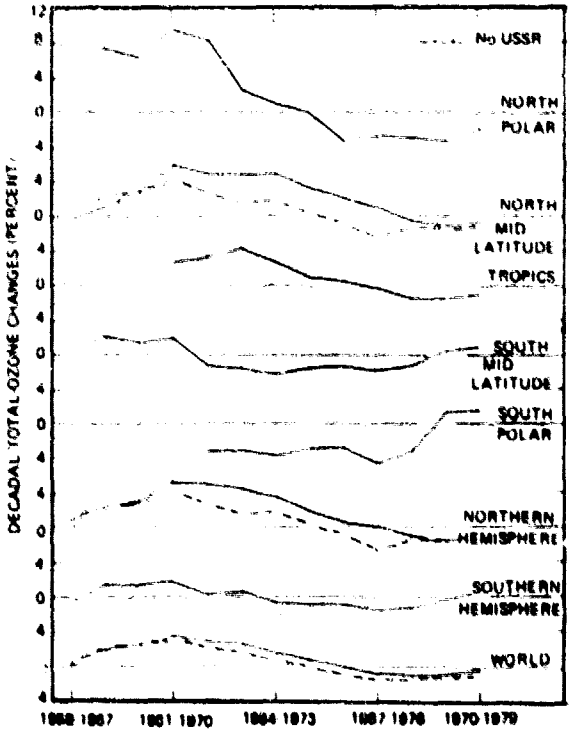

Figure 3-22. Observed decadal trends for different zones, hemispheres, and the world.

Northern than Southern Hemisphere during this period and the world variation reflects the Northern Hemisphere pattern.

An important point to consider is the difference in decadal trend at yearly intervals. Even for the world as a whole the decadal trend of -1.0% in 1969-1978 changed to only -0.3% in 1970-1979. Accordingly, the trend obtained for any particular decade should be considered in the context of the trend for adjacent decades to ensure that a representative trend is being obtained.

Time Series Models

Meteorological and environmental data for specific localities are frequently collected at equally spaced time intervals e.g., hourly observations of pressure, daily values of average temperature, monthly averages of total column ozone. Due to various natural and man-made causes, such time series often exhibit the following types of behavior: (1) regular annual or other periodic patterns, (2) slowly evolving underlying long term variation, and (3) irregular short-term noisy fluctuations. To characterize these variations, we can write a time series of, say, monthly observations Y(t), where t stands for month, as

$$Y(t) = \mu + S(t) + N(t) \tag{5}$$

where μ is the mean of the series, S(t) represents a seasonal component and N(t) a nonseasonal component. The S(t) component can often be adequately described by combinations of sinusoidal functions with period of 12 months and their harmonics, or simply 12 constants for the 12 months of the year. Variations in the N(t) components can sometimes be explained by the dynamic influences of other atmospheric related factors. However, it is frequently the case that the physical nature causing the variation is rather complex and not clearly understood, or that adequate data on the atmospheric parameters are not available. Because of the dynamic nature of these exogeneous influences, time series observations are often autocorrelated so that there is information in the series itself which could be used to make inference about its future pattern. It is for this reason that models relating N(t) to past values N(t-1), N(t-2), ... have been found useful to characterize the behavior of time series.

From the original work of Yule (1927), a useful class of time series models are the autoregressive processes

$$N(t) = \phi_1 N(t-1) + \ldots + \phi_p N(t-p) + \varepsilon(t) \tag{6}$$

where $\varepsilon(t)$ represents a series of independent random variables with zero means. As an illustration Figure 3-23 gives the deseasonalized series of monthly total column ozone at Kodaikanal from 1961 to 1979, exhibiting considerable low and high frequency variations. Employing modeling procedure described, e.g., in Box and Jenkins (1976), an adequate model for this series is

$$N(t) = 0.75\, N(t-1) + 0.16\, N(t-2) + \varepsilon(t) \tag{7}$$

Figure 3-24 shows the residual series $\varepsilon(t)$ computed from Equation (7) indicating that much of the variation in the N(t) series has been accounted for and $\varepsilon(t)$ is essentially a white noise series.

The power spectrum of time series provides an alternative to time domain autoregressive models for describing the autocorrelation structure of a time series. It describes the way in which the variance of the series is associated with different frequencies (see Figure 3-25).

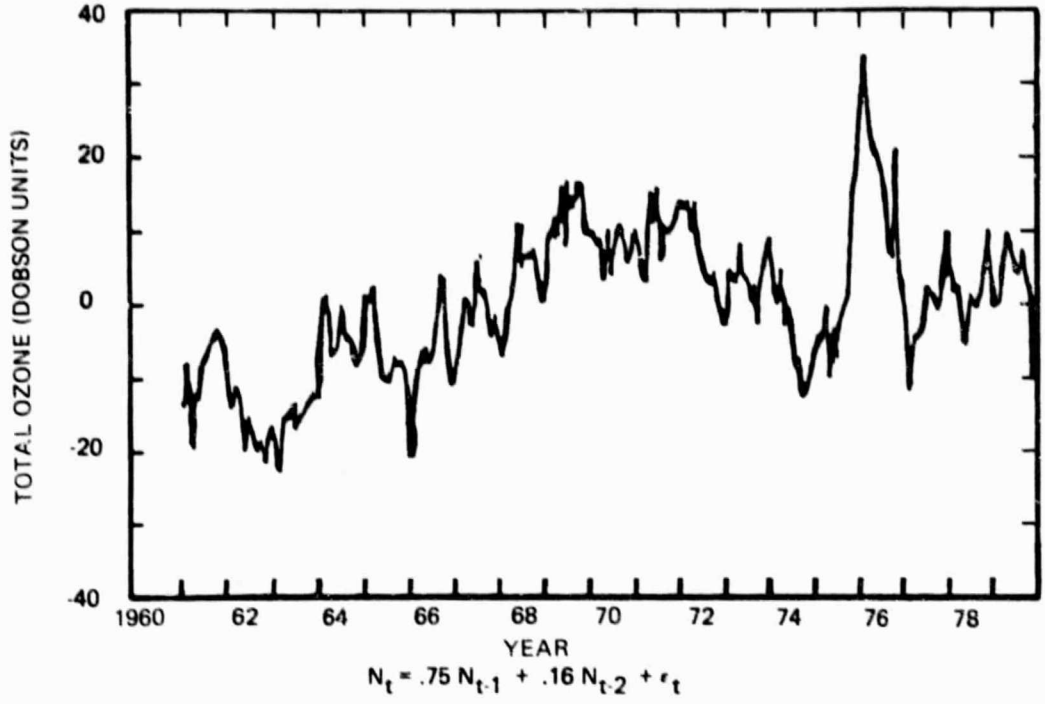

Figure 3-23. Deseasonalized monthly total ozone for Kodaikanal.

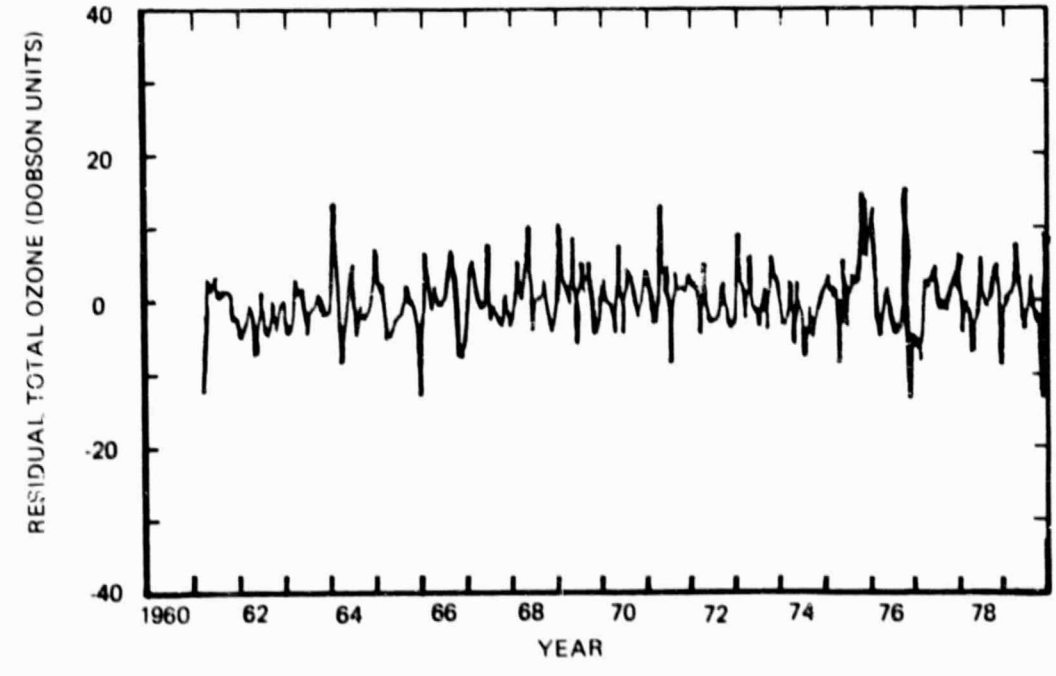

Figure 3-24. Residual total ozone series for Kodaikanal.

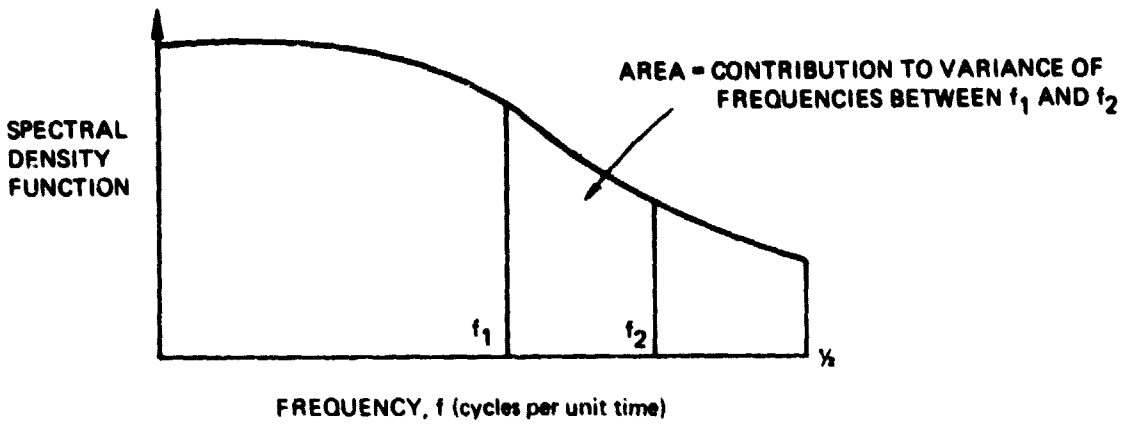

Figure 3-25. Statistical power spectrum model (schematic).

The power spectrum of a time series is the Fourier transform of its autocovariances, which are the bases for estimating time domain models. It therefore contains, in a mathematical sense, the same information as the autocovariances, although it expresses that information in a different way.

A series with no autocorrelation has a flat spectrum. It is often called "white noise," by analogy with the spectrum of white light. Geophysical series typically have "red spectra," i.e., higher spectral power at low frequencies than at high frequencies. Such series are typically smoother than white noise, and often show sustained swings above or below their long term means.

The problem of detecting changes in total ozone due to possible human influences (such as CFCs) can then be analyzed through statistical analysis of the available time series of total ozone observations. The model assumed for the monthly averages, Y(t), of total ozone collected at a particular location is

$$Y(t) = \mu + S(t) + \omega X(t) + N(t), \tag{8}$$

where as before μ is the mean long term total ozone amount, S(t) represents the annual seasonal component of variation, X(t) represents the form of any deterministic trend and N(t) represents the "noise" or error component reflecting the aggregate effect of natural, measurement, and other causes which could induce nonseasonal variation in the total ozone data. Thus N(t) may contain various low and high frequency components of variation, and hence, may be autocorrelated. To account for this autocorrelation, N(t) may be modeled by the autoregressive process as in Equation (6), where N(t) possibly has different variances for different months of the year.

Statistical Analysis

Three statistical studies for the detection of changes in ozone have been made recently based on average monthly total ozone amounts from a network of 36 or 37 Dobson observing stations for the period 1958-1979 (Bloomfield et al., 1981; Reinsel et al., 1981c; St. John et al., 1981). In the first two studies, the function X(t) representing a linear trend starting in 1970 was used in the model to estimate a global change in ozone over the period 1970-1979 that may be associated with human activities. In the third study (St. John et al.) a trend function shaped like the predicted CFC effect starting in 1960 was used. The 36 stations used in these analyses can conveniently be grouped into seven different geographical regions, North America, Europe, Japan, India, Australia, South America, and Hawaii (somewhat similar to the group used by Angell and Korshover, see WMO, 1981). It is this structure that has been used to obtain a global estimate of the change in ozone during the 1970s and an estimate of the standard error of this estimated global change by accounting for the revealed variation within individual stations, among stations within each region, and between regional averages.

In the study by Bloomfield et al. (1981), the noise component time series N(t) in Equation (8) for each of the 36 stations was assumed to consist of a global component common to all stations, a regional component common to all stations in a given region, and an individual station component. Certain assumptions concerning the nature of the spectral characteristics of these various component series were made, and their analysis was then carried out using frequency domain techniques.

In the other two studies autoregressive time domain methods were used to estimate models of the form if Equations (8) and (6), separately for each of the 36 stations' time series. This procedure results in an estimate of the rate of change parameter ω in Equation (8) and an estimate of its corresponding within-station or individual station standard error for each of the 36 stations. In Figure 3-26, a histogram of the 36 trend estimates ω (expressed as percent change per year) obtained from the analysis by Reinsel et al. (1981c) is shown. The trend estimates in the histogram seem to form a cluster about zero which suggests no overall trend during the 1970s. Since the typical estimated standard error of an estimated percentage change within an individual station is about 0.15% per year, the large spread among the 36 trend estimates in Figure 3-26 indicates that there are other sources of variation in the estimated trends in addition to the within-station uncertainty. These sources of variation may be due to any factors which can cause variations between estimates within a given region as well as those which cause variations between regions. Hence to obtain an estimate of global change, the 36 trend estimates of the rate of change can be represented as:

$$\begin{aligned}\text{individual trend estimate} = {} & \text{global trend} + \text{regional trend effect} \\ & + \text{individual station effect within region} \\ & + \text{within-station error.}\end{aligned}$$

Then assuming that the within-station, among-stations-within-region, and regional effects are random components with zero means and unknown variances to be estimated, standard variance components techniques may be applied to the individual trend estimates to obtain an estimate of the global trend ω, as well as estimates of the variances associated with the various effects. One of the main effects of the variance components formulation above is to account for the fact that the individual trend estimates of neighboring stations within each region will be (positively) correlated. Having obtained the global trend estimate we may also estimate its standard error and 'partition' this standard error into the contributions from the within-station, among-stations within-region, and between-regions sources of error. For the two time domain studies, the contribution to the standard error of the estimated change based on the analysis by Reinsel et al. (1981b), from within-station, among-station-within-region, and between-regions variations are

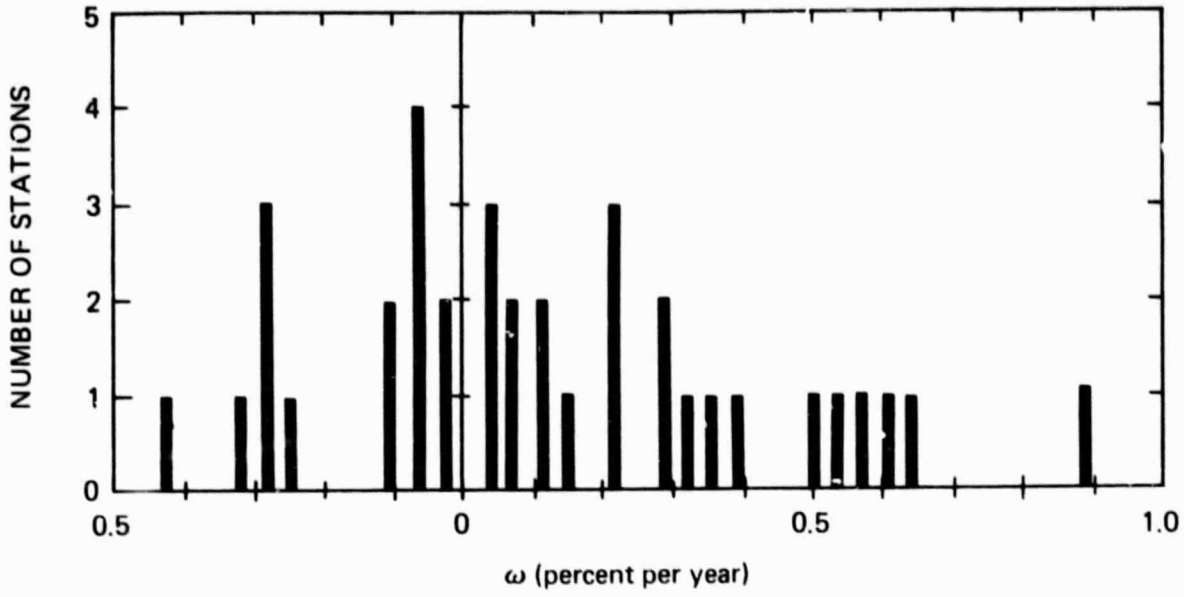

Figure 3-26. Distribution of total ozone trend estimates from time series model.

0.38%, 0.39%, and 0.40%, respectively, while the contribution to the standard error based on the work by St. John et al. (1981), due to within-station and the combined effect of among-station-within-region and between-regions variations are 0.41% and 0.43%, respectively. These values are summarized in Table 3-13 below.

Table 3-13
Revealed Total Ozone Trend Standard Errors from Dobson Stations
(Expressed as Percent Per Period Shown)

Components of Variation	Researcher	Bloomfield et al.	Reinsel et al.	St. John et al.
	Type of intervention	Linear trend	Linear trend	CFC shape curve
	Period	1970-79	1970-79	1960-79
	Number of Stations	36	36	37
(1) Within-station variation (σ_1)		0.37	0.38	0.41
(2) Among-stations-within-regions variation (σ_2)			0.39	0.43
(3) Among-regions variation (σ_3)		0.40	0.40	
Total $\pm 2\sigma_A = \pm 2\sqrt{\sigma_1^2 + \sigma_2^2 + \sigma_3^2}$		±1.1	±1.35	±1.2

In the frequency domain analysis of Bloomfield et al. (1981) the correlation structure of a time series is considerably simplified by taking its discrete Fourier transform. In fact, to a good approximation the values of the Fourier transform are uncorrelated, and have variances proportional to the power spectrum at the appropriate frequencies, provided these frequencies are separated by multiples of one cycle per record length. Thus, a model such as:

observed data = systematic part + autocorrelated errors

can be replaced by:

Fourier transform of data = Fourier transform of systematic part +

Fourier transform of errors,

in which the error term is now essentially uncorrelated from one frequency to another. The transformed model can therefore be analyzed by weighted least squares, provided the spectrum of the error term can be estimated.

To analyze cross-correlated data such as ozone records from 36 stations, the cross-spectrum of each pair of stations must be considered. The simplest way to handle these is to assume that the observed ozone measurement can be represented by:

observed data = systematic part + global component

+ regional component + station component

The three components are each autocorrelated time series, but are not necessarily cross correlated with each other. The station component represents all sources of variation that are individual to the station (within-station and among-stations-within-regions). The regional component is common to all stations in the given region, but differs from region to region. It therefore causes cross-correlation among stations in a region, but not between pairs of stations in different regions. The global component is common to all stations. It thus adds to the cross-correlation among stations within a region, and introduces cross-correlation into all other pairs.

Since there are several independent replicates of the station and region components, their spectra can be estimated by averaging their raw sample spectra (periodograms) across replications, rather than across frequencies. However, the global term is not replicated. To estimate its spectrum, we assume that it is proportional to some given function, large at low frequencies, such as $1/f$ or $1/\sqrt{f}$.

When unknown constants in the systematic part of the model are estimated by weighted least squares, their standard errors can be broken down into contributions from each type of component. The contribution from station components combines the "within-station" and "among station within region" contributions of the time-domain approach. The regional contribution has the same interpretation in both approaches. However, the global component has no counterpart in the time-domain approach.

The result when the hypothesized trend $\omega X(t)$ is fitted to the same 36 Dobson stations as used in the time-domain analysis is that the change from 1970 to 1979 is estimated to be 1.7% with a standard error of 1.0%. The station, region, and global components of this standard error are 0.37%, 0.40%, and 0.87%, respectively. In this analysis, a function similar to 1/f was used to model the global spectrum. The high power in this function at low frequencies explains the large contribution from the global component.

In summary, the three studies by Bloomfield et al. (1981), St. John et al. (1981), and Reinsel et al. (1981b) give the following 95% confidence intervals for global change in total ozone in the 10-year period 1970-1979.

Bloomfield et al.	$(1.7 \pm 2.0)\%$
St. John et al.	$(1.1 \pm 1.2)\%$
Reinsel et al.	$(0.8 \pm 1.3)\%$

ESTIMATES OF UNCERTAINTY IN TOTAL OZONE TRENDS

The above mentioned statistical analvses of time series models are based on total ozone records at 36 or 37 Dobson stations that have observations over periods ranging from 11 to 22 years. Analysis of the variations within and among stations reveal several types of uncertainty of trend estimates. These are called "revealed" estimates.

Such records by themselves cannot reveal the uncertainties due to fluctuations over long periods (more than 50 years or so) or possible biases due to the location of the Dobson stations. Some separate computations have been made to estimate the magnitudes of these uncertainties utilizing some additional ozone measurements. However, these are much less accurate ("softer") and are called "unrevealed" estimates.

Revealed Uncertainties Derived from the Dobson Network

The statistical analysis of total ozone determined from the Dobson network has led to estimates of the standard errors of the deterministic trend estimates from testing for changes in the 1970s. This "revealed" variation is quantified, but not necessarily identified as to cause. As shown in Table 3-13, the $\pm 2\sigma$ limits or trend uncertainties were derived from breaking the variation into components of error in the classical statistical variance component or random effects approach.

The within-station component (σ_1) reflects the uncertainty in any trend estimate at a station after the station time series has been fitted by an autoregressive type model. This contains the aggregate effect of random noise and some of the low frequency variations in the record captured by the autoregressive model.

The component (σ_2) refers to the variation in the trends from station-to-station within regions. This will include contributions due to station-to-station instrumental drifts, operator effects, local pollution, and meterological variations that lead to trends or drifts. Since some of the regions are large, both large-scale and mesoscale meteorological variations contribute to σ_2.

The component (σ_3) refers to the region-to-region effects that can influence trends. Here the regions considered are North America, South America, Europe, India, Japan, Australia, and Hawaii. This will include contributions from spatial sampling effects such as variations due to large scale planetary waves that are shifting over time, and region-to-region instrumental effects, e.g., possible instrumental drifts in the secondary standards.

The values for σ_1, σ_2, and σ_3 as computed by three different groups are given in Table 3-13. In some cases, as indicated, the values were not computed individually in the statistical analysis. When σ_1, σ_2, and σ_3 are combined, a measure of the ±2 standard errors ($\pm 2\sigma_A$) associated with revealed uncertainties can be calculated. Note the close agreement in $\pm 2\sigma_A$ among the three investigators using 36 or 37 stations in the analyses.

The good agreement among the three studies is not surprising because they are based on essentially the same statistical model; that is, assuming no deterministic trend in the 1960s and using either a linear trend or a function shaped like a chlorofluorocarbon (CFC) prediction curve.

In the NASA RP 1049 (1979) document, the following sources of trend variation were offered in the absence of formal statistical analyses, with the exception of the first source:

σ_{stat} = random noise and unmodeled short-term time dependencies
σ_{inst} = trend errors in Dobson instruments
σ_{spat} = spatial sampling
σ_{nat} = natural long-term variation in global zone
σ_{other} = other possible man-made changes

Although the associations that can be made between these sources of variation and those that come from statistical analyses do not have a one-to-one correspondence, the statistically calculated σs capture variability contained in σ_{stat}, σ_{inst}, σ_{spat}, and σ_{nat} plus additional contributions of variability. The variation described by σ_{stat} is captured in σ_1. The contribution of σ_{inst} can be spread across σ_1, σ_2, or σ_3, depending on whether an instrument drift varies within a station, varies from station-to-station within a region, or is common to one region but not to another. The spatial sampling variability in σ_{spat} is captured by σ_2 and σ_3. Any spatial bias, that is not corrected for, would appear in the trend estimate. However, if the mean sampling bias over long periods (say 10 or more years) is not significant, σ_{spat} would be accounted for by σ_2 and σ_3. Low frequency contributors to σ_{nat} contained in the Dobson data will appear in σ_1.

Finally, σ_{other} was introduced to account for other man-made variations if one wanted to detect and identify a CFC effect over and above other man-made effects, as discussed elsewhere in this report, and natural variations. An estimate of this does not seem appropriate from the statistical approach and would have to be done via theoretical chemical model simulations using different chemistry scenarios, assuming an estimate was needed.

Uncertainties Due to Long-Period Variations (σ_4)

Bishop and Hill (1981) inferred σ_4 from a modified 48-year total ozone record at Arosa, by considering the standard deviations of 10-year trends, and obtained $\sigma_4 = 0.75$. Probably only an extremely small fraction of this number is due to "revealed" temporal variations if the estimate given by Tiao is applicable. Although there is considerable uncertainty about the global representativeness of the Arosa data, this series is the only long-period record available and the question is still open. At any rate, it is clear from visual inspection of the curves shown in Figure (3-27) based on the 53 year data set of "C" wavelength observations at Arosa (1927-1979) (Birrer, 1975; Dütsch, personal communication) that the low frequency contribution to variations contained in the Arosa series is not negligible. Many meteorologists believe that long-period ozone variations are associated with long-period variations of meteorological variables (see, for instance, Newell and Wu, 1978). The only variable for which we have reasonably reliable information over a century or longer is surface temperature. This has a white spectrum down to

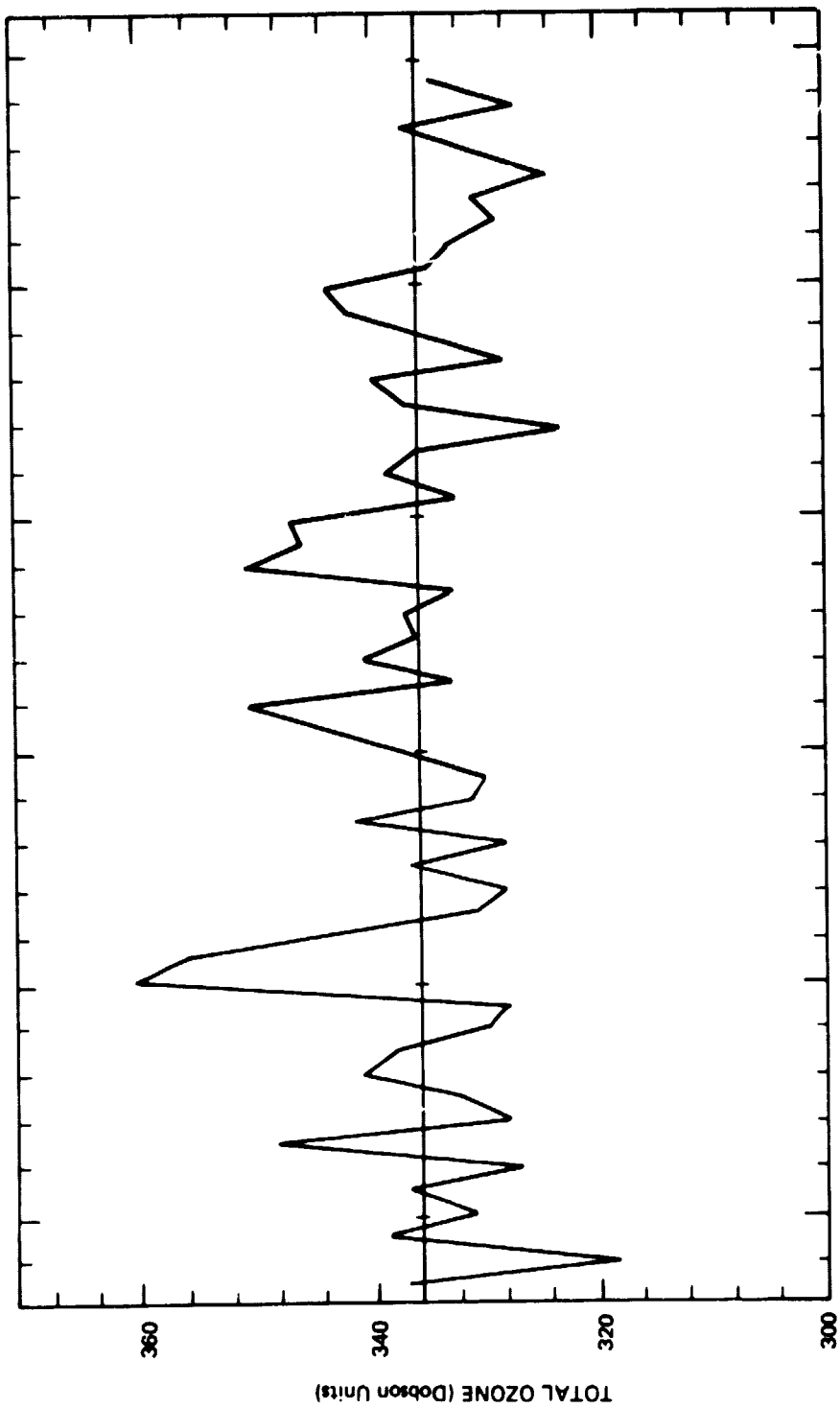

Figure 3-27. Yearly average total ozone at Arosa - "C" wavelength Dobson observations. (Dütsch, personal communication)

frequencies of order 1 cycle/century, beyond which the spectrum appears to contain an additional "red" component. Hence, it is possible that the estimate by Bishop and Hill is low.

In any case, we cannot give an exact estimate of σ_4. If, indeed, the unrevealed low frequency ozone variations are not zero, there is an added uncertainty which should be included in the value for σ_4, that due to the applicability of the statistical model chosen. Also, a component of long-term ozone variation, due to tropospheric pollution sources, discussed at this workshop (see Chapter 1) does not have the trend pattern assumed in the statistical models. Thus the range for σ_4 would be from a low of 0.75% (Bishop and Hill value) to some higher but subjectively determined value. The corresponding $2\sigma_4$ uncertainty range would begin at 1.5%.

Spatial Data Representativeness of the Dobson Network

Satellite data can be used to study the question as to whether or not the trends derived from the Dobson network are representative of global trends. Unfortunately, trends from satellite observations can be derived only over periods of about 4 years or so (see earlier discussion of satellite data). Some of the comparisons to date are discussed below.

One of the major difficulties encountered in the literature of estimating global total ozone variations is that there is no unique way to estimate such changes from the given ground-based data set. Each investigator has considerable flexibility in determining the technique of area integration and relative weight assigned to each method of observation (e.g., Dobson versus M-83).

For example, London and Oltmans (1978/1979) analyze the monthly average data in a synoptic manner, integrating the hemispheric and global values from values interpolated to a uniform latitude, longitude grid. Angell and Korshover (1978b) assign relative weights to groups of stations; this weight depending on the number of stations in the region, its relative area and the "confidence" in the quality of the data. Hasebe (1980), on the other hand, has recently developed an optimum interpolation analysis technique applicable to the monthly average data. The integral values are then determined from the gridded data. Finally, Reinsel et al. (1981a) determine the trend at each site from a 36 Dobson station network and use these determined trends to arrive at a global trend.

The relative weights assigned to the observational regions by Angell and Korshover (1976) and by Reinsel et al. (1981a) are indicated in Table 3-14.

Clearly, significantly different weights are assigned by each group and one might anticipate that different trends would be obtained for the same period.

The additional question of the impact of regions unsampled by the ground-based sites on the actual total ozone variations has been studied by using data from the Backscatter Ultraviolet Ozone Sensor on Nimbus 4.

Reinsel et al. (1981b) use BUV data for the periods April 1970 through May 1975 and through April 1977, and compare the distribution of 468 trends estimated from monthly averages of ozone gridded in 468 blocks over the globe with that determined from the 36 "trend estimates" obtained from satellite data sampled initially every third day (but with decreasing frequency through the satellite operational period) at locations near the 36 Dobson stations. (See discussion of BUV data coverage problem in Chapter 2). For both time periods, the means and standard deviations of the two sets of trend estimates were in close agreement, with the difference in means between the 468 block trends (weighted by surface area) and the 36 trend estimates equal to about 0.6% per decade (36 trend estimate value less negative).

Table 3-14
Relative Weights for Averaging Global Trends from Ground-Based Observations

Area	Reinsel et al.	Angell and Korshover
North America	4.0	3
Europe	4.4	3
India	3.5	1
Japan	2.6	1
Australia	3.0	8
South America	2.0	2
Tropics	1.2 (Hawaii only)	13
Soviet Union	0	2
North Polar	0	3
South Polar	0	3

A. Miller et al. (1981) on the other hand, examine the BUV data for the Northern Hemisphere (0-60°N) only and for the more limited time period April 1970 through mid-1976. For this case, the results indicate an approximate 2% difference in trend over the 3 years with the Angell and Korshover (ground-based) trend more negative than the BUV trend. This is consistent in sign and about 1% larger than the earlier results of A. Miller et al. (1979d) in which they used the meteorological fields at 50°N to examine the possible spatial sampling errors. The ground-based total ozone data set does not currently have adequate geographic and temporal coverage to define uniquely a representative "global" ozone trend. Judicious increase of the ground-based observing network and complementary use of satellite observations, as recommended in the WMO report (WMO, 1981), would help to ameliorate this problem.

At present it is difficult to make a quantitative estimate from this information concerning the effect of a possible bias for Dobson station locations, σ_5, on trend determinations. The "revealed" effect is captured mostly in σ_3 (Table 3-13), but also in σ_2. Thus, the total uncertainty in the trend due to spatial variation is of order 0.5%. If the results of Reinsel et al. (1981b) were completely certain, there would be no indication of a spatial bias due to the locations of the Dobson stations. In contrast, the work by Miller et al. (1981) suggests that considerable biases may exist.

In the mean, over very long periods, both global and Dobson location trends are zero. Therefore the problem is to estimate the standard deviation of such trend differences, given that, on one occasion, the difference was 0.6%. Clearly, such a standard deviation is uncertain. It is difficult to give a numerical estimate of σ_5, the effect of Dobson location bias on trend estimates. A range of $2\sigma_5$ values from 0 to 2% is suggested.

Synthesis of Uncertainties in the Trend Estimates

Thus far the revealed 2σ uncertainty of the trend estimate is estimated to be about 1.2%. The unrevealed contributions were estimated to vary between 1.5% to 3% (temporal) and 0% (spatial). Taking means to be most probable, the overall 2σ limit becomes $\sqrt{1.2^2 + (2.25)^2 + 1^2} = 2.7\%$. The lower limit is $\sqrt{1.2^2 + 1.5^2} = 1.9\%$ and the upper limit is $\sqrt{1.2^2 + 2^2 + 3^2} = 3.8\%$. The meteorologists at the workshop tended to prefer values close to this upper limit, while most of the statisticians present preferred values closer to the lower limit.

OBSERVED CHANGES IN VERTICAL OZONE PROFILES

For many reasons, the ozone concentration in particular altitude regions will experience a more rapid and larger percent response to most perturbations to the ozone system than will the total column ozone. This response, however, can be quite different at different layers in the atmosphere depending on the particular physical/chemical perturbation imposed. Purely photochemically related variations would generally be observed at levels above about 30 km. Those variations associated with interacting atmospheric chemical and transport processes would be reflected in changes below about 30 km. It is appropriate therefore to analyze long-term ozone variations as a function of altitude.

The only observations presently available for upper level long-term ozone analysis are those derived from Umkehr and ozonesonde measurements. These measurements are severely restricted as to length of the observational period, instrumental and meteorological biases, and both time and space sampling problems. Many of these problems will certainly be ameliorated in the near future as BUV and limb IR techniques provide a suitable data base for stratospheric ozone trend detection. Such observations have been made and continue. Satellite data sets are now available for analysis of temporal observations from the Nimbus 4 BUV and Nimbus 7 SBUV observations. Programs for an integrated global observing system are currently being developed (WMO, 1981).

Routine Umkehr measurements from a few stations are available for almost 20 years and ozonesonde measurements for almost 15 years. Most of these stations are located in mid-latitudes of the Northern Hemisphere and analyses of some of these data have been discussed for a few individual stations by e.g., Dütsch and Ling (1973) and Pittock (1977). Variations of the annual averaged ozone amount in different layers for a group of stations in mid-latitudes of the Northern Hemisphere are shown in Figure 3-28 as prepared by Angell and Korshover (see WMO, 1981). The annual percentage change from the long-term mean is given as an average of the observations from North America, Europe, Japan and India. The vertical bars represent two standard deviations of the mean as in the case of total ozone. Some caution must be exercised in evaluating the results shown in Figure 3-28. The data base is not homogeneous since less than half of the Umkehr and ozonesonde measurements overlap in place, time, and period of the observations. Also, it should be noted that ozonesonde observations are generally more reliable below the ozone maximum (~25 km) and less reliable above the ozone maximum than are Umkehr observations.

In the 32 to 46 km layer (heights indicated are approximate), most sensitive to the anthropogenic effects of CFCs, the Umkehr-derived ozone amount continued to increase in 1978 and 1979, with the 1979 value comparable to those prior to the eruption of Fuego in 1974. The Fuego eruption brought about an "apparent" ozone decrease in this layer because of the influence of stratospheric aerosols on Umkehr measurements. In both 16 to 24 and 24 to 32 km layers there continued to be a slight discrepancy between Umkehr-derived and ozonesonde-derived ozone trends; the ozonesonde measurements yielding a small ozone decrease (superimposed on a strong quasi-biennial oscillation), the Umkehr measurements showing essentially no ozone change. In the tropospheric 2 to 8 km layer the ozonesondes continued to indicate an ozone increase in north mid-latitude regions of about +7% per decade. Both sets of measurements also provide evidence of a recent ozone increase in the 8 to 16 km layer bracketing the tropopause.

Trends in layer-mean ozone for successive, overlapping 10-year intervals are presented in Figure 3-29 for the various height layers, as obtained by linear regression. Here the dashed line refers to results obtained from north temperate Umkehr observations, the solid line with crosses results obtained from north temperate ozonesondes, and the dotted and dash-dot lines the results obtained from north polar (Resolute) and south temperate (Aspendale) ozonesondes, respectively.

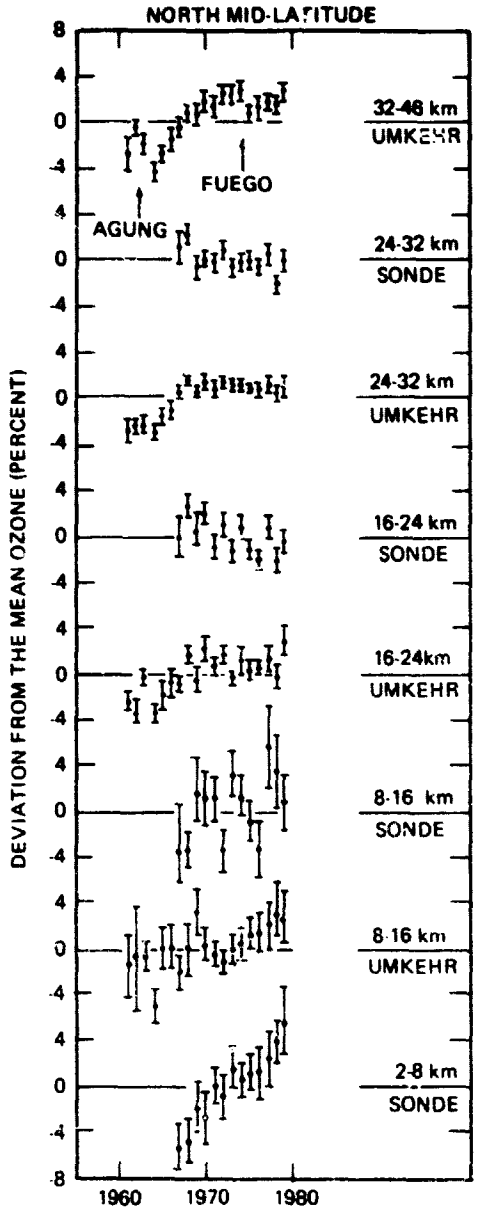

Figure 3-28. Observed ozone variations for different layers in the troposphere and stratosphere.

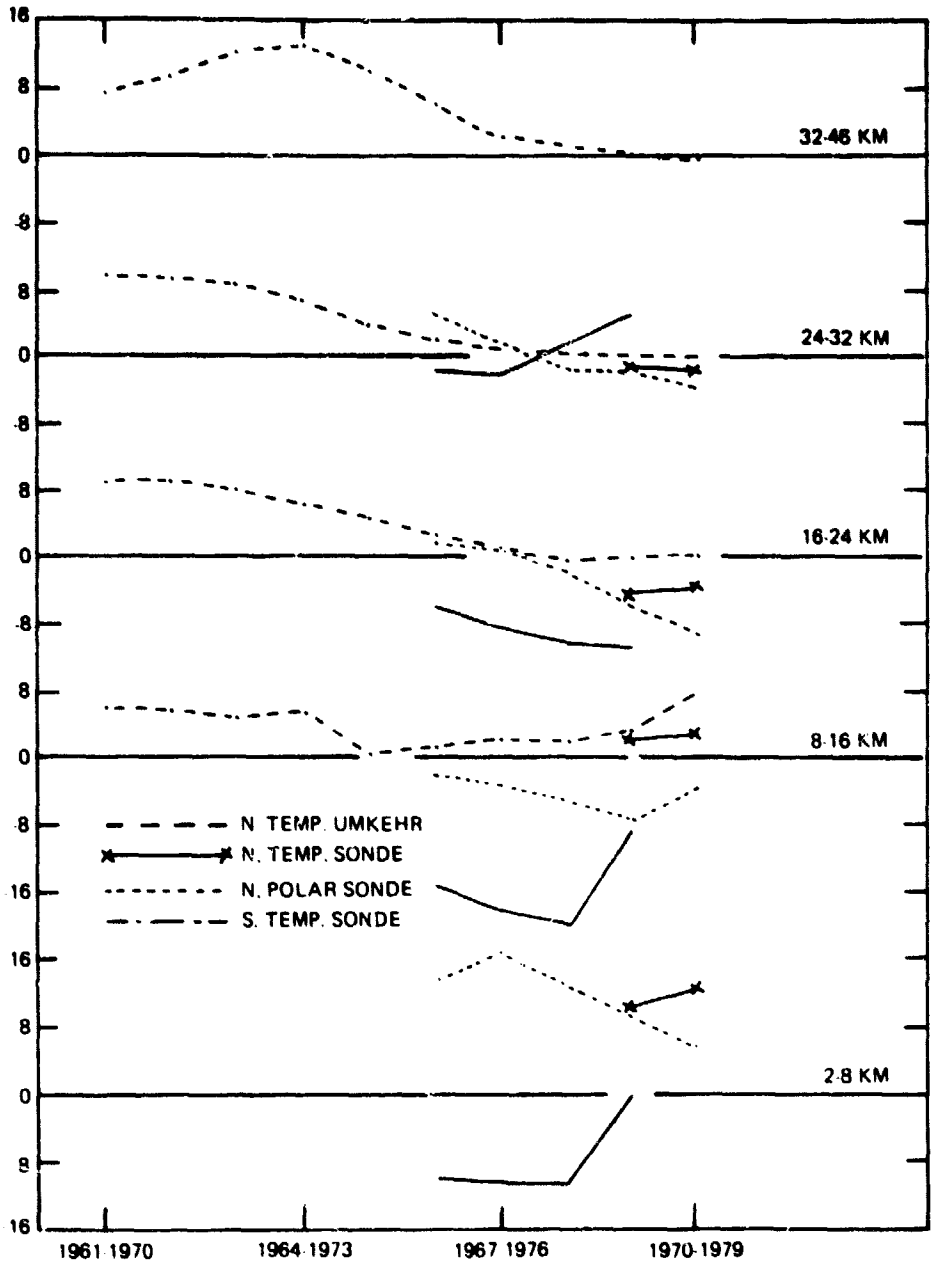

Figure 3-29. Decadal trends of ozone in the stratosphere from Umkehr and Ozonesonde observations.

In the 24 to 32 km layer the results are fairly compatible, but the differences are larger in the lower layers. Thus, in the 2 to 8 km tropospheric layer the Aspendale data suggest, until recently, a decadal ozone decrease rather than the large increase indicated by ozonesondes in north polar and north temperate latitudes. In the 16 to 24 km layer only, the observations in north temperate latitudes indicate a decadal ozone increase. Note that in the three middle layers the ozonesonde data for north temperate latitudes suggest more of a decadal ozone decrease than do the Umkehr data for this climatic zone, in accord with Figure 3-28.

In the critical 32 to 46 km layer dominated by photochemistry, the last few intervals (Figure 3-29) suggest essentially no change in ozone in north temperate latitudes.

Secular changes in ozone profiles in the 0.7 to 10 mbar region on a global scale have been derived by Heath (1981c) from an analysis of Nimbus 4 BUV and Nimbus 7 SBUV observations between 1970 and 1979. The Nimbus 4 instrument operated from April of 1970 to March of 1977 and the Nimbus 7 instrument began operations in November of 1978 and continues at present. See Chapter 2 for a description of the methods, coverage, and difficulties for these experiments.

The Nimbus 4 BUV data shows a continuous and large decrease in deduced ozone at all levels above 10 mbar (~31km). The major portion of this decrease is believed to be instrumental but its cause is not known with certainty. Because of such difficulties Heath (1981c) has used two methods for examining the BUV and SBUV data sets for trends in the ozone profile. The first method uses the 7-year BUV data set from Nimbus 4 and attempts to correct for the instrumental drift by normalization to the Umkehr profile results during satellite overpasses of the Umkehr stations. This correction is derived from a linear regression analysis of satellite overpass data by comparing BUV determined ozone concentrations with those obtained from the ground via the Umkehr technique. The number of overpasses ranged from about 500 in the first year to about 100 in the last year. The correction is then applied to the entire 7-year BUV data set resulting in the solid curve in Figure 3-30. The second method compares the data from the first 6 months of presumably well-calibrated Nimbus 7 data in 1978 and 1979 with the corresponding months in 1970 and 1971 of the Nimbus 4 data, also assumed to be well-calibrated at that point. This has been done on a month-by-month basis as a function of latitude and altitude.

The dashed curve in Figure 3-30 shows the globally integrated results for the SBUV in March of 1979 compared with the BUV for March of 1971. Heath (1981c) has also compared SBUV for March 1979 to BUV for March 1972 and finds a similar effect.

Both analyses seem to indicate a negative trend in the 3 to 6 mbar region (i.e., 35 to 40 km). They, however, show opposite effects (opposite sign in change per year) above 2 mbar which may be due to several possibilities: an incomplete correction of the BUV drift via the Umkehr comparison, some unidentified variation in either the atmosphere or in instrument calibration, or that the solar cycle has been responsible for the decrease up to 1976 and the subsequent increase from that time to 1979

The third possibility, that the upper portion of the change in the ozone profile is related to the solar cycle, is strongly dependent upon an assessment of the change in sensitivity of the BUV on Nimbus 4 over its 7-year lifetime. As discussed earlier, the determination of the rate of decreasing sensitivity of BUV over the 7-year period was derived from near overpass comparison with Umkehr observations where it was assumed that the sensitivity of the Umkehr network was invariant with time. This assessment of decreasing sensitivity of BUV indicated an approximately linear change of BUV sensitivity versus altitude, that is, about +0.35% per year at the mean pressure level 5 (22 mbar) and -1.5% per year at the mean pressure of level 9 (1.4 mbar).

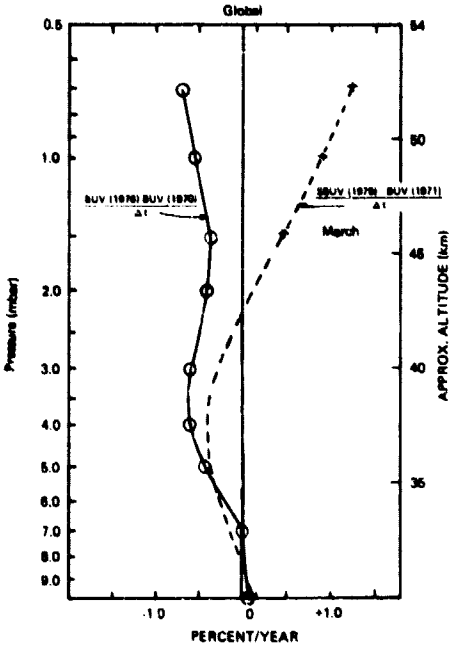

Figure 3-30. Inferred long-term ozone variations in the stratosphere from satellite observations.

The shape of the observed change near 40 km is similar to that predicted due to chemical releases of human origin, but to infer any cause-effect relationship rests upon many assumptions. In the comparison of SBUV (1978-1979) derived ozone with that from BUV (1970-1971) it has been assumed that the interannual variability in the mean does not represent a significant contributor to the effect. A further assumption is that the solar cycle effect on upper stratospheric ozone varies in phase with solar activity and increases monotonically with increasing altitude. This is in agreement with the analysis of Dütsch (1979) who also found a two year phase lag (ozone following solar activity) in the Umkehr data from Arosa. Solar cycle effects are certainly not yet fully understood theoretically. For instance, calculations of the response of ozone to changes in the solar UV flux, such as might be expected to occur over a solar cycle, indicate a maximum expected effect at about 40 km (Chandra, 1981; Brasseur and Simon, 1981). Thus, the problem becomes one of thus uniquely ascribing the 40 km change to its cause. A major argument for the reality of continuing ozone depletion in the altitude region of predicted sensitivity to chemicals of human origin rests upon the observation that the shape of the ozone profile near 40 km did not change in phase with the solar cycle between the beginning of BUV observation on Nimbus 4 and the first six months from Nimbus 7.

ESTIMATES OF UNCERTAINTY IN VERTICAL OZONE PROFILE TRENDS

The longest record of Umkehr observations comes from Arosa, (and those are available only since 1956), with a fairly continuous set of observations extending from 1961 to the present. These data have been analyzed using time series methods as described above (Penner et al., 1981). Other stations have records that span almost as long a period as Arosa, but contain significant gaps. Bloomfield et al. (1981), have developed a method for treating less complete data sets with maximum likelihood methods for first order Markov models. Both stochastic models are severely limited due to the limited data set available. Estimates for the uncertainty in the observed trend cannot therefore capture the entire range of uncertainty for determination of trends of human origin.

In developing uncertainty estimates we have, as far as possible, followed the breakdown used for the total column data analysis. Penner's (1981) study was restricted to a single station, and therefore yields an estimate of the "within-station" component of variance for Umkehr layers 7, 8, and 9 separately and summed. Bloomfield et al. (1981) studied 15 stations spanning six regions, and provided estimates of "within-stations", "among-stations-within-region", and "region-to-region" components, for layers 7, 8, and 9 combined. Even the latter study covers only two stations outside the north mid-latitude region. Also, it should be noted that, because of the strong decrease of ozone partial pressure with height in the mid-stratosphere, combining the data for layers 7, 8, and 9 effectively limits the analysis to layer 7 (~4 to 8 mbar). Statistical analysis of 8 years of balloonsonde data from Aspendale (Pittock, 1974b; 1977) has shown that in the lower and mid-stratosphere the variance of the observed partial pressure is too large to be able to detect a significant change over that short period. No new "hard" estimates are available for the other standard errors, but the "soft" estimates from NASA RP 1049 have in some cases been revised.

Table 3-15 summarizes estimates of the standard errors associated with estimates of the ozone changes over a data interval of 10 years at various indicated levels in the atmosphere, for balloonsondes, (using the Mast-Brewer or ECC-sondes), the Umkehr method, and the Nimbus 7 satellite system. The estimated standard errors are reasonably well established in cases where sufficient data exist and these estimates are underlined. Other estimates, notably for natural trend variations at various levels in the atmosphere, are soft and are quite uncertain. The latter are based on a consideration of possible sources of trends and their likely variations. This table represents a substantial revision of Table 6-15 in NASA RP 1049, where a more general qualitative discussion of the various sources of error will be found. Table 3-15 is more consistent with the corresponding table for error estimates on trends in total ozone data (see above). Estimates of errors in a rocketsonde network, which appeared in NASA RP 1049 have not been included because few new data are available.

Estimates of errors in trend estimates from satellite systems other than Nimbus 7 are not presented in Table 3-13 due to the shortness of record. However, data presented by Gille (1980) show that the LRIR, an infrared limb scanner, determined the monthly average zonal mean ozone amounts in the tropics at 40 km (2 to 3 mbar) with a standard deviation of 0.05 to 0.1 ppmv, or ~1%. This value includes both instrumental effects and geophysical variability.

The best trend estimates are expected to come from satellite vertical distribution measurements, where at 40 km for the Nimbus 7 system the estimated value of 2σ for a real trend is ±1.4% per decade. Umkehr measurements in layer 7, at 33 to 38 km altitude, are more reliable than Umkehr values in the upper layers, but the estimated 2σ value of ±10% per decade is much higher than for the satellite system. This uncertainty could be substantially reduced by a more representative global network, as is also true of the balloonsondes. If trend evaluation were restricted to the north temperate zone where most of the Umkehr and balloon ozonesonde data are obtained, σ_{spat} could be significantly reduced, although probably by no more than 50%.

The estimates of σ_{nat} are very soft, but it is clear that in the troposphere, which is subject to large meteorological effects, and in the high stratosphere, where solar variations become important, σ_{nat} might be quite large. This would also be true of the lower stratosphere, but less so in the middle stratosphere. The element, σ_{nat}, provides the dominant uncertainty in any effort to detect a human influence on the stratospheric ozone layer by satellite.

As discussed in Chapter 1, photochemical models of the effects of tropospheric NO_x either injected by aircraft or produced by combustion at the Earth's surface suggest that during the decade of the 1970s these sources taken separately might each have caused an increase in tropospheric ozone content of the order of 5 to 20% in the Northern Hemisphere, and perhaps 1 to 5% in the Southern Hemisphere. However, considerable disagreement exists about the relative

Table 13

Standard Error Estimates for Trends in Ozone Concentrations at Various Levels in the Atmosphere (in percent per decade).

Source	Balloonsondes (Refs. 1 and 2)		Umkehr (Refs. 3 and 4)				Nimbus 7 Satellite
	2-8 km	30 km	33-38 km	38-43 km	43-48 km	33-48 km	at 40 km
$\sigma_{stat.}$ within station (Synoptic + random noise)	5	3	2.4	7.0	15.5	2.3	0.1 at about 10 km vert. resol.
$\sigma_{instr.}$ between stations within regions	2	2	2	3	4	1.5	0.5
σ_{spat} region to region	7	4	4	4	4	5	0.5
σ_{nat} all stations	4	1	1.5	2	3	2	2
$2\sigma_{true}$*	18	11	10	17	33	11	1.4
$2\sigma_{human}$**	20	11	10	18	33	12	4

Note: Underlined figures are based on actual statistical analysis or otherwise reliable data while the remaining figures are qualitative estimates.

References: 1, WMO, 1981; 2, Pittock, 1974b; 3, Penner et al. 1981; 4, Bloomfield et al. 1981; and NASA RP 1049.

σ_{nat} will vary significantly with latitude.

* $2\sigma_{true} = 2(\sigma^2_{stat} + \sigma^2_{instr.} + \sigma^2_{spat})^{1/2}$

** $2\sigma_{human} = 2(\sigma^2_{true} + \sigma^2_{natural})^{1/2}$

importance of surface-emitted and aircraft-emitted NO_x due to problems in the treatment of removal by precipitation. The model results for these and other reasons must be considered very preliminary and uncertain.

A linear regression fit to the 2 to 8 km ozone data in Figure 3-28 which is for ozone in the north temperate zone, reveals a trend of about +7% per decade. The revealed uncertainties as indicated by the error bars in Figure 3-28 suggest that this might be a statistically significant trend. However, our estimate of $2\sigma_{true}$ in Table 3-15 is ±18% per decade. This includes estimates of uncertainties which are not revealed in such a limited data set, if it is to be taken as an estimate of the global trend. Among the terms included here is an estimate of ±7% per decade for $1\sigma_{spatial}$ which is higher than the revealed between regions in the north temperate zone. This was in part influenced by the one trend estimate obtained from a single station (Aspendale) in the Southern Hemisphere, which was about -20% per decade (Pittock, 1974b). If we wish to test for a significant trend in the north temperate zone only, the appropriate $\sigma_{spatial}$ will thus be smaller, which could reduce $2\sigma_{true}$ to about ±14% per decade. Thus we can conclude that the estimated trend in the data differs from zero by only about $1\sigma_{true}$. It thus has a probability of only about 2 in 3 of being a real trend.

Nevertheless, the order of magnitude agreement between the possible real observed increase in tropospheric ozone content in the north temperate zone and that tentatively predicted by the models is suggestive. More extensive analysis, measurements and modeling are clearly desirable in order to confirm or deny the reality of this possible effect of human activity on tropospheric ozone.

Because of the lack of continuous and constantly calibrated observations and the known degradation which occurred in the Nimbus 4 BUV data as discussed above, the dip apparently observed in the Nimbus 4 data and the comparison with Nimbus 7 in the ozone profile at around 40 km altitude is somewhat open to question. Nevertheless, if we accept the suggested explanation for the change in profile, namely that this is due to variation over the solar cycle, the data suggest that at 40 km the ozone concentration decreased between 1970 and 1979 by about 5%. This is greater than the estimated uncertainty of the trend 2σ of $\pm$1.4% per decade which is included in Table 3-15 for the Nimbus 7 system.

COMPARISON OF PHOTOCHEMICAL MODEL PREDICTIONS AND ESTIMATED OZONE TRENDS

The comparisons of predicted distributions of chemical species in the stratosphere and the corresponding observed distributions discussed in Chapter 1 provide a level of confidence in the adequacy of the existing theoretical models in describing many of the essential features of the stratosphere. However, in order to assess hypothesized potential changes in stratospheric chemical structure brought about by past and future human activities, the models must be able to predict some past events in a time dependent scenario. As preceding sections of this chapter have demonstrated, many such potential factors influencing ozone most likely have occurred during the past two decades and the models (1-D and some 2-D) have made predictions (estimates) of the expected changes. All "predictions" covering ozone changes over the past can in principle be evaluated with the appropriate observed ozone trends. Nevertheless due to limited data of varying quality and "unrevealed" influencing factors such comparisons are far from simple.

As was discussed before, the best available "global" total ozone records cover only the last two decades (1960-1980). Statistical analyses of the ground-based data yield the following estimates of the hypothesized linear trend for total ozone for the decade 1970-1980:

(1.7 ± 2.0)%	Bloomfield et al. (1981)
(0.8 ± 1.35)%	Reinsel et al. (1981a)
(1.1 ± 1.20)%	St. John et al. (1981)

(St. John et al. did not use a linear trend test function for this decade, but for the current purpose it is not necessary to discuss the details.)

Over this decade the major activities which could affect ozone are high altitude subsonic aircraft operations, CFC releases, and CO_2 increases. The corresponding model estimated trends (1970-1980) due to these perturbations are:

(-0.4 to -0.7)% for CFC-only scenario

(+0.5 to +1.5)% for subsonic-only scenario

(+0.2 to +0.4)% for CO_2-only scenario

These results reaffirm the point that the assumption of a CFC-only scenario for the past decade is clearly inconsistent with the observations. This is **not** to say that the statistical time series model of the observed ozone trend is inconsistent with the CFC release - ozone depletion hypothesis. In fact, using the best estimates of changes in the major source species for the past decade, the best combined scenario model predicts the 1970-1980 total ozone trend to be about (-.13 to +.13)%. (See section entitled "Combined Scenarios".) This range reflects the differences in HO_x and $ClONO_2$ chemistry as represented by chemistry B and chemistry D, respectively. (See section entitled "Model Prediction of Potential Anthropogenic Perturbations".) The full range of uncertainty in model predictions due to uncertainties in chemical reaction rate coefficients is expected to be much larger, but no new assessment has been made at this time.

In the statistical time series model the objective is not only to estimate the most likely trend but also to estimate the standard error range for the trend. For hypothesis testing, if the prediction is outside of the range then the common practice is to question the proposed mechanisms. If the prediction is within the range then the statistical model has not demonstrated any inconsistency between hypothesis and data.

During the past decade, the three principal perturbing influences on ozone appear to have been an increasing CFC content leading to a decrease in ozone in the middle stratosphere, an increasing CO_2 content leading to an increase in ozone in the upper stratosphere, and the emissions from subsonic aircraft affecting ozone in the lower stratosphere and upper troposphere. The combined effect of these on the vertical ozone distribution as predicted by models is shown in Figure 3-17.

The available data for comparisons are more limited and more uncertain than the total ozone data. Although the **preliminary** results of both upper stratospheric ozone and upper tropospheric ozone trends (section entitled Observed Changes in Vertical Ozone Profiles) all appear to be consistent with the model predictions, it is premature to make this assessment. The satellite and the Umkehr data must be further evaluated and analyzed. Many assumptions used in the analysis and interpretations of satellite data have not been confirmed or cross checked. Until then, one should consider the vertical ozone distribution changes to be one of the most challenging research problems of this time.

INTERPRETATION OF MODEL PREDICTIONS

Most of the predictions of ozone perturbations in this report are still derived from one-dimensional models (1-D). Although there are selected results from two-dimensional models (2-D), they generally confirm the findings of 1-D models and elaborate upon some details. Therefore it is useful to reiterate how one may interpret the predictions of 1-D models.

A one-dimensional model is phenomenological and is actually a composite of several submodels. Its vertical transport is fitted with the mean observed transport rate of long-lived trace species on time scales of a decade or more. Therefore, for these species (source species), the model represents a global average. Since there is no accurate procedure for obtaining all the globally averaged chemical and photochemical reaction rates, these must be evaluated locally. Furthermore, through theoretical experimentation it is found that 1-D models can best represent the ozone vertical distribution only at the mid-latitudes. With regard to ozone chemistry, 1-D models provide an analysis of the chemical interactions and balances under mid-latitude conditions. This has been demonstrated through comparisons with results from 2-D models. With a basic understanding of existing relations among mid-latitude, tropical and high-latitude ozone distributions, one can reasonably project small ozone perturbations at mid-latitudes to a global average. Of course this is quite subjective and requires validation by more elaborate models. Available 2-D models all seem to provide results consistent with 1-D models.

Current understanding indicates that photochemistry dominates over all other physical processes in determining ozone distributions in the upper stratosphere. Consequently, viewing 1-D models as pure local photochemical models is quite reasonable and there are no serious problems in accepting 1-D predictions of changes at these altitudes as globally representative. The principal concern about the quality of theoretical models in this region is with representation of physical processes such as solar heating due to ozone, H_2O, and CO_2 changes, possible solar UV variability, and others. Upper stratosphere ozone is more sensitive to these uncertainties, hence there is difficulty in modeling the "real" trend during the past decade in this region.

In addition to these technical considerations there is a subjective element in considering the model predictions. Uncertainties in measured solar flux intensity, chemical kinetics reaction rate coefficients, model boundary conditions, transport coefficients, source distributions, and others can, in principle, be evaluated. Although all these parameters are not known to similar degrees of accuracy, recent progress in analysis, techniques and measurement programs promise steady improvements in the years to come. Present analysis of the uncertainties inherent in the model predictions can be considered only as the best available information. The unquantified uncertainties, such as the possibility of missing chemistry, the adequacies of 1-D, 2-D or 3-D model transport formulations, diurnal, seasonal, or spatial averaging procedures for the nonlinear interactions, and the adequacy of model validation procedures, by necessity, must be evaluated on a mostly subjective basis.

Existing views of the model's ability to describe the present day atmosphere and predict potential perturbations span the range from a high level of confidence based on the positive results discussed in previous sections to strong reservations based on the still unquantified uncertainties. The subjective components in the interpretation of model predictions will probably persist.

The complementary relationship among 1-D, 2-D and 3-D models is widely accepted and current information strongly supports this view. Recent results from two-dimensional models on stratospheric ozone perturbation studies serve to elaborate on the seasonal and latitudinal variations of the ozone change but have not significantly altered global average predictions based on 1-D

models. Multi-dimensional models have pointed to new coupling processes, most notable in the troposphere, that could not be studied with 1-D models, (e.g., tropospheric-stratospheric exchange processes).

Theoretical models are only one component in the process of evaluating our understanding of ozone changes. The descriptive analysis and statistical analysis of time series models are the other components. Descriptive analysis provides a qualitative representation pointing out the variations in the ozone records. It does not necessarily establish a time trend with a statistically quantifiable degree of certainty. On the other hand the time series model of ozone trend can test any **given** hypothesis with **some** quantifiable degree of certainty. But it does not provide any information on why a certain trend is or is not observed.

A statistical time series model is perhaps the most systematic method for the analysis of past ozone records. It gives as good an estimate of the trend from the available data as pure analysis allows. However, analogous to the theoretical models, these models have their own set of sensitivities to uncertain input parameters, many of which have already been described. This type of model is more diagnostic than prognostic. In fact, the trend estimates and the test function (e.g., linear trend in the seventies) are guided by chemical model predictions. The question of the most appropriate test function is partially answered by the ability of the autoregressive model of the noise component (Equation (4)) to capture some of the unknown variations. For example, Figure 3-31 an autoregressive moving average model has been applied to the model of average total ozone of Figure 3-19.

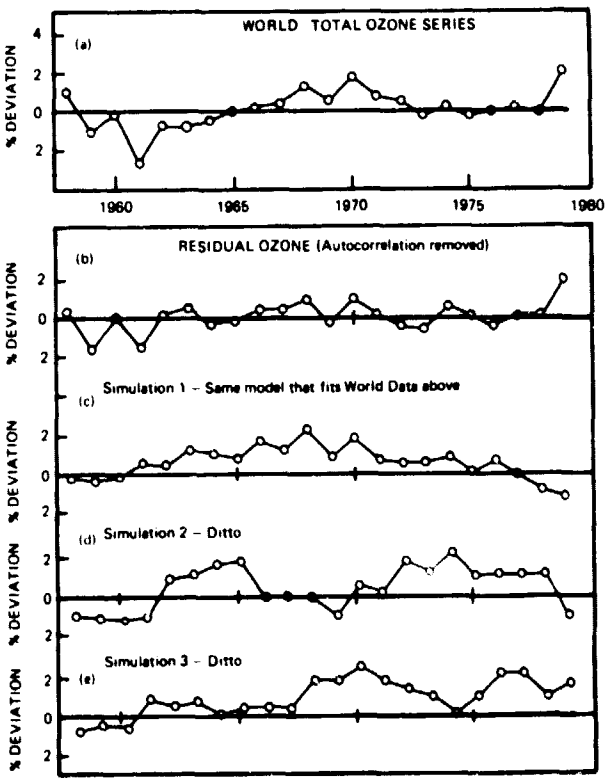

Figure 3-31. Autoregressive moving average analysis of worldwide total ozone.

Figure 3-31(a) shows the original record and Figure 3-31(b) shows the residual series after the autocorrelation is removed. The autocorrelation appears to capture the upswing in the 1960s and the downswing in the early 1970s. An estimate of the trend from 1970 to 1979 is (+1.3 ± 2.5)% decade which allows for the uncertainty associated with the presence of autocorrelation. This is calculated by fitting trend and autoregressive-moving average coefficients simultaneously in the same model and by assuming stationarity through 1969 followed by linear trend from 1970 to 1979. The two standard error limits indicate that the trend is not significant at the 95% level. The autocorrelation has inflated the uncertainty by a factor of approximately two and one-half over what would be expected from fitting the same model to random noise (e.g., residuals) alone, indicating that low and high frequency variations are captured in the uncertainty. For comparison, a simple linear decadal regression trend through the autocorrelated original data for period 1970-1979 is estimated to be (-0.2 ± 2.0)% decade. This could be a misleading result if taken as an estimate for the size, sign and uncertainty of a deterministic trend as described above.

Monte Carlo simulations (Figures 3-31(c)-(e)), using a randomly selected noise level, show what sort of patterns can be generated from the same autoregressive-moving average model that fits the world data series. These few simulations indicate apparent patterns of trends and cycles that are contained in the autocorrelation model. Therefore unhypothesized variation can be captured and represented as components of standard errors. Unfortunately the sensitivity relation between ozone data and the time series model is not clear. Reinsel et al. (1981b) has reanalyzed the data from 1960-1980 using a test function in the sixties similar to the suggested model predicted ozone change due to past atmospheric nuclear tests (Chang et al., 1979c) while retaining the linear trend in the seventies. The estimated trend and standard error have changed from the above result of (0.8 ± 1.35)% to (0.49 ± 1.35)% in the seventies. It was somewhat surprising that with a more elaborate test function (i.e., using more physical theory) these standard errors did not change. More studies on the relation of data length to model assumptions are required before the sensitivity of the trend estimate and standard errors on input assumptions can be understood.

Since the test functions are diagnostic, the only component of a time series model that may be predictive is the autoregressive model of the noise component. The autoregressive relations developed for most of the existing ozone records do not extend over a period of as much as a year. Therefore they are not able to "predict" over any length of time beyond a few months. Using the current data to estimate future trend will only increase the standard error proportionately (i.e., doubling the period will double the standard error). In general there can be no increase in diagnostic power without an increase in the length of the data record.

APPENDIX A

CHEMICAL KINETICS AND PHOTOCHEMISTRY

INTRODUCTION

The present compilation of rate constant data for use in stratospheric modeling was prepared jointly by the Task Group on Chemical Kinetics of CODATA and the NASA for Data Evaluation. A three day workshop was held in Boulder, Colorado, in March, 1981. The resulting set of recommendations was based mainly on prior evaluations by each group; i.e., JPL 81-3 for the NASA Panel and Baulch et al. (1981), for the CODATA group. For the most part, there were no large differences between the two previous evaluations, and where differences did exist, they were mainly due to the fact that the evaluations had been prepared at different times and, therefore, had different data available to them. Recommendations for cross sections were unchanged from those of JPL 81-3 and Baulch et al. (1980).

There were, however, areas of controversy within the joint panel. In a few cases, bearing on reactions of major importance, new data (or new interpretations of data) generated considerable debate as to the proper recommendation. In deciding the possible role of isomers in the ClO + NO_2 reaction, major disagreement existed, and the issue was decided by means of a majority vote.

PHILOSOPHY OF THE EVALUATION

Previous NASA and CODATA evaluations have been based primarily on published experimental data, with theory being invoked only where necessary to extrapolate or correlate laboratory measurements. In cases where the experimental data appeared to be inconsistent with theoretical expectations, this fact was pointed out as a warning that the data might be suspect. For the most part, these inconsistencies took the form of unreasonable A-factors in rate constants, which can easily arise when there are small, systematic errors in the measurement of rate constants as a function of temperature.

In the present joint evaluation a more expanded role of theory has been adopted. In taking this larger view the panel has not rejected out of hand the results of experimental studies, but has examined them more rigorously in the light of theoretical reasonableness. In addition to the previous practice of pointing out discrepancies between theory and experiment by means of textual discussion and the assignment of appropriate error limits, the panel has, in some cases, declined to recommend certain reported pressure and temperature dependences which seemed irreconcilable with theory. Theses changes applied mainly to HO_x chemistry, where, despite a thread of consistency between several experimental results by different researchers, the resulting kinetic behavior of some of the HO_x reactions appeared to be incompatible with theoretical interpretations. These issues are discussed specifically and in greater detail in later sections of this chapter dealing with individual reactions.

REACTION CATEGORIES

For purposes of tabulation it is convenient to divide reactions into two categories, bimolecular (Table A-1) and termolecular (Table A-2). However, some of the reactions in Table A-1 which are nominally bimolecular are actually more complex. To provide framework for explaining the anomalous pressure and temperature dependences occasionally seen in actions of this type, it is necessary to further divide the bimolecular class of reactions into the two subcategories of direct (concerted) and indirect (non-concerted) reactions.

Table A-1
Rate Constants for Second Order Reactions (continued)

Reaction	A-Factor	E/R‡ (E/R)	k(298 K)	Uncertainty Factor/298 K
$O + O_2 \underline{M} O_3$	(See Table A-2)			
$O + O_3 \rightarrow O_2 + O_2$	1.5×10^{-11}	2218±150	8.8×10^{-15}	1.15
$O_3 + NO \rightarrow NO_2 + O_2$	3.8×10^{-12}	1580±150	1.9×10^{-14}	1.15
$HO + NO_2 \underline{M} HNO_3$	(See Table A-2)			
$O + NO_2 \rightarrow NO + O_2$	9.3×10^{-12}	0^{+0}_{-150}	9.3×10^{-12}	1.1
$O + HNO_3 \rightarrow HO + NO_3$	–	–	$<3.0\times10^{-17}$	–
$O + HO_2NO_2 \rightarrow$ products	7.4×10^{-12}	2630±300	1.1×10^{-15}	2.0
$N + O_2 \rightarrow NO + O$	4.4×10^{-12}	3220±340	8.9×10^{-17}	1.25
$N + NO \rightarrow N_2 + O$	3.7×10^{-11}	0±100	3.7×10^{-11}	1.4
$HO + HNO_3 \rightarrow$ products	1.5×10^{-14}	$-(650^{+300}_{-650})$	1.3×10^{-13}	1.4
$HO + HO_2NO_2 \rightarrow$ products	4.0×10^{-12}	0±400	4.0×10^{-12}	+2;-4
$N + NO_2 \rightarrow N_2O + O$	–	–	1.4×10^{-12}	10
$N + O_3 \rightarrow NO + O_2$	–	–	$<1.0\times10^{-15}$	–
$NO_2 + O_3 \rightarrow NO_3 + O_2$	1.2×10^{-13}	2450±150	3.2×10^{-17}	1.15
$HO_2 + NO_2 \underline{M} HO_2NO_2$	(See Table A-2)			
$NO + NO_3 \rightarrow 2NO_2$	–	–	2.0×10^{-11}	3.0
$O(^1D) + N_2O \rightarrow N_2 + O_2$	4.4×10^{-11}	0±100	4.4×10^{-11}	1.4
$O(^1D) + N_2O \rightarrow NO + NO$	7.2×10^{-11}	0±100	7.2×10^{-11}	1.4
$O(^1D) + H_2O \rightarrow HO + HO$	2.3×10^{-10}	0±100	2.3×10^{-10}	1.2
$O(^1D) + CH_4 \rightarrow HO + CH_3$	1.4×10^{-10}	0±100	1.4×10^{-10}	1.2
$O(^1D) + CH_4 \rightarrow H_2 + CH_2O$	1.5×10^{-11}	0±100	1.5×10^{-11}	1.2
$O(^1D) + H_2 \rightarrow HO + H$	1.1×10^{-10}	0±100	1.1×10^{-10}	1.3
$O(^1D) + N_2 \rightarrow O + N_2$	1.8×10^{-11}	-(107±100)	2.6×10^{-11}	1.2
$O(^1D) + N_2 \underline{M} N_2O$	(See Table A-2)			
$O(^1D) + O_2 \rightarrow O + O_2$	3.2×10^{-11}	-(67±100)	4.0×10^{-11}	1.2
$O(^1D) + O_3 \rightarrow O_2 + O_2$	1.2×10^{-11}	0±100	1.2×10^{-10}	1.2

Table A-1
Rate Constants for Second Order Reactions (continued)

Reaction	A-Factor	E/R± (E/R)	k(298 K)	Uncertainty Factor/298 K
$O(^1D) + O_3 \rightarrow O_2 + O + O$	1.2×10^{-10}	0±100	1.2×10^{-10}	1.2
$O(^1D) + HCl \rightarrow HO + Cl$	1.4×10^{-10}	0±100	1.4×10^{-10}	1.3
$O(^1D) + CFCl_3 \rightarrow$ products	2.2×10^{-10}	0±100	2.2×10^{-10}	1.6
$O(^1D) + CF_2Cl_2 \rightarrow$ products	1.4×10^{-10}	0±100	1.4×10^{-10}	1.6
$O(^1D) + CCl_4 \rightarrow$ products	3.5×10^{-10}	0±100	3.5×10^{-10}	1.6
$O(^1D) + CCl_2O \rightarrow$ products	3.6×10^{-10}	0±100	3.6×10^{-10}	2.0
$O(^1D) + CFClO \rightarrow$ products	1.9×10^{-10}	0±100	1.9×10^{-10}	2.0
$O(^1D) + CF_2O \rightarrow$ products	2.3×10^{-10}	0±100	2.3×10^{-10}	2.0
$O(^1D) + NH_3 \rightarrow HO + NH_2$	2.5×10^{-10}	0±100	2.5×10^{-10}	1.3
$O(^1D) + CO_2 \rightarrow O + CO_2$	7.4×10^{-11}	-(117±100)	1.1×10^{-10}	1.2
$O + NO_3 \rightarrow O_2 + NO_2$	1.0×10^{-11}	0±150	1.0×10^{-11}	3.0
$O + N_2O_5 \rightarrow$ products	–	–	$<3.0\times10^{-16}$	–
$O_3 + HNO_2 \rightarrow O_2 + HNO_3$	–	–	$<5.0\times10^{-19}$	–
$HO + HO_2 \rightarrow H_2O + O_2$	8.0×10^{-11}	0±250	8.0×10^{-11}	2.0
$HO_2 + HO_2 \rightarrow H_2O_2 + O_2$	3×10^{-12}	0^{+500}_{-300}	3.0×10^{-12}	3.0
$NO + HO_2 \rightarrow NO_2 + HO$	3.7×10^{-12}	-(240±100)	8.3×10^{-12}	1.2
$HO_2 + O_3 \rightarrow HO + 2O_2$	1.4×10^{-14}	580^{+500}_{-100}	2.0×10^{-15}	1.5
$OH + O_3 \rightarrow HO_2 + O_2$	1.6×10^{-12}	940±300	6.8×10^{-14}	1.25
$O + HO \rightarrow O_2 + H$	2.3×10^{-11}	-(110±200)	3.3×10^{-11}	1.3
$O + HO_2 \rightarrow HO + O_2$	3.5×10^{-11}	0±350	3.5×10^{-11}	2.0
$O + H_2O_2 \rightarrow HO + HO_2$	1.0×10^{-11}	2500±1000	2.3×10^{-15}	2.0
$H + O_2 \; M \; HO_2$	(See Table A-2)			
$H + O_3 \rightarrow HO + O_2$	1.4×10^{-10}	470±200	2.9×10^{-11}	1.25
$HO + HO \rightarrow H_2O + O$	4.5×10^{-12}	275±275	1.8×10^{-12}	1.4
$HO + HO \; M \; H_2O_2$	(See Table A-2)			
$HO + H_2O_2 \rightarrow H_2O + HO_2$	2.9×10^{-12}	160±100	1.7×10^{-12}	1.25

Table A-1
Rate Constants for Second Order Reactions (continued)

Reaction	A-Factor	E/R† (E/R)	k(298 K)	Uncertainty Factor/298 K
$HO + CO \rightarrow CO_2 + H$	$1.35\times10^{-13}(1+P_{atm})$	0±200	$1.35\times10^{-13}(1+P_{atm})$	1.25
$HO + CH_4 \rightarrow CH_3 + H_2O$	2.4×10^{-12}	1710±200	7.7×10^{-15}	1.2
$HO + H_2 \rightarrow H_2O + H$	7.7×10^{-12}	2100±200	6.7×10^{-15}	1.2
$Cl + O_3 \rightarrow ClO + O_2$	2.8×10^{-11}	257±100	1.2×10^{-11}	1.15
$O + ClO \rightarrow Cl + O_2$	7.7×10^{-11}	130±130	5.0×10^{-11}	1.2
$NO + ClO \rightarrow NO_2 + Cl$	6.2×10^{-12}	-(294±100)	1.7×10^{-11}	1.15
$HO + HCl \rightarrow H_2O + Cl$	2.8×10^{-12}	425±100	6.6×10^{-13}	1.15
$HO + HOCl \rightarrow H_2O + ClO$	3.0×10^{-12}	150^{+850}_{-150}	1.8×10^{-12}	10.0
$Cl + CH_4 \rightarrow HCl + CH_3$	9.6×10^{-12}	1350±250	1.0×10^{-13}	1.1
$Cl + C_2H_6 \rightarrow HCl + C_2H_5$	7.7×10^{-11}	90±90	5.7×10^{-11}	1.1
$Cl + HO_2 \rightarrow HCl + O_2$	4.8×10^{-11}	0±250	4.8×10^{-11}	2.0
$ClO + NO_2 \underset{}{M} ClONO_2$	(See Table A-2)			
$O + ClONO_2 \rightarrow$ products	3.0×10^{-12}	808±200	2.0×10^{-13}	1.5
$HO + ClONO_2 \rightarrow$ products	1.2×10^{-12}	333±200	3.9×10^{-13}	1.5
$Cl + ClONO_2 \rightarrow$ products	1.7×10^{-12}	607±388	2.2×10^{-13}	2.0
$O + HCl \rightarrow HO + Cl$	1.1×10^{-11}	3370±350	1.4×10^{-16}	2.0
$O + HOCl \rightarrow HO + ClO$	1.0×10^{-11}	2200±1000	6.0×10^{-15}	10.0
$Cl + H_2 \rightarrow HCl + H$	3.5×10^{-11}	2290±200	1.6×10^{-14}	1.5
$Cl + H_2O_2 \rightarrow HCl + HO_2$	1.1×10^{-11}	980±500	4.1×10^{-13}	1.5
$Cl + HNO_3 \rightarrow$ products	$<1.0\times10^{-11}$	2170^{+2500}_{-500}	$<7.0\times10^{-15}$	
$Cl + H_2CO \rightarrow HCl + HCO$	8.2×10^{-11}	34±100	7.3×10^{-11}	1.15
$Cl + CH_3Cl \rightarrow CH_2Cl + HCl$	3.4×10^{-11}	1260±200	4.9×10^{-13}	1.2
$Cl + NO \underset{}{M} NOCl$	(See Table A-2)			
$Cl + ClNO \rightarrow NO + Cl_2$	3.0×10^{-11}	0^{+500}_{-250}	3.0×10^{-11}	2.0
$Cl + O_2 \underset{}{M} ClOO$	(See Table A-2)			

Table A-1
Rate Constants for Second Order Reactions (continued)

Reaction	A-Factor	E/R† (E/R)	k(298 K)	Uncertainty Factor/298 K
$Cl + ClOO \cdot Cl_2 + O_2$	1.4×10^{-10}	0±250	1.4×10^{-10}	3.0
$Cl + ClOO \cdot ClO + ClO$	8.0×10^{-12}	0±250	8.0×10^{-12}	3.0
$Cl + Cl_2O \cdot Cl_2 + ClO$	9.8×10^{-11}	0±250	9.8×10^{-11}	1.2
$O + Cl_2O \cdot ClO + ClO$	–	–	4.0×10^{-12}	1.5
$ClO + HO_2 \cdot HOCl + O_2$	4.6×10^{-13}	(710^{+250}_{-700})	5×10^{-12}	1.4
$ClO + H_2CO \cdot$ products	$<1.0\times10^{-12}$	>2060	$<1.0\times10^{-15}$	–
$ClO + HO \cdot$ products	–	–	9.1×10^{-12}	3.0
$ClO + CH_4 \cdot$ products	$<1.0\times10^{-12}$	>3700	$<4.0\times10^{-18}$	–
$ClO + H_2 \cdot$ products	$<1.0\times10^{-12}$	>4800	$<1.0\times10^{-19}$	–
$ClO + CO \cdot$ products	$<1.0\times10^{-12}$	>3700	$<4.0\times10^{-18}$	–
$ClO + N_2O \cdot$ products	$<1.0\times10^{-12}$	>4260	$<6.0\times10^{-19}$	–
$ClO + BrO \cdot Br + OClO$	6.7×10^{-12}	0±250	6.7×10^{-12}	2.0
$ClO + BrO \cdot Br + Cl + O_2$	6.7×10^{-12}	0±250	6.7×10^{-12}	2.0
$ClO + ClO \cdot$ products	–	–	–	–
$ClO + O_3 \cdot ClOO + O_2$	1.0×10^{-12}	>4000	$<1.0\times10^{-18}$	–
$ClO + O_3 \cdot OClO + O_2$	1.0×10^{-12}	>4000	$<1.0\times10^{-18}$	–
$Cl + OClO \cdot ClO + ClO$	5.9×10^{-11}	0±250	5.9×10^{-11}	1.25
$NO + OClO \cdot NO_2 + ClO$	2.5×10^{-12}	600±300	3.4×10^{-13}	1.5
$O + OClO \cdot ClO + O_2$	2.5×10^{-11}	1166±300	5.0×10^{-13}	1.5
$HO + CH_3Cl \cdot CH_2Cl + H_2O$	1.8×10^{-12}	1112±200	4.3×10^{-14}	1.2
$HO + CH_2Cl_2 \cdot CHCl_2 + H_2O$	4.5×10^{-12}	1032±200	1.4×10^{-13}	1.2
$HO + CHCl_3 \cdot CCl_3 + H_2O$	3.3×10^{-12}	1034±200	1.0×10^{-13}	1.2
$HO + CHFCl_2 \cdot CFCl_2 + H_2O$	8.9×10^{-13}	1013±200	3.0×10^{-14}	1.3
$HO + CHF_2Cl \cdot CF_2Cl + H_2O$	7.8×10^{-13}	1530±200	4.6×10^{-15}	1.2

Table A-1
Rate Constants for Second Order Reactions (continued)

Reaction	A-Factor	E/R± (E/R)	k(298 K)	Uncertainty Factor/298 K
$HO + CH_2ClF \cdot CFClF + H_2O$	2.0×10^{-12}	1134±150	4.4×10^{-14}	1.2
$HO + CH_3CCl_3 \cdot CH_2CCl_3 + H_2O$	5.4×10^{-12}	1820±200	1.2×10^{-14}	1.3
$HO + C_2Cl_4 \cdot$ products	9.4×10^{-12}	1200±200	1.7×10^{-13}	1.25
$HO + C_2HCl_3 \cdot$ products	5.0×10^{-13}	-(445±200)	2.2×10^{-12}	1.25
$HO + CFCl_3 \cdot$ products	1.0×10^{-12}	>3650	$<5.0\times10^{-18}$	–
$HO + CF_2Cl_2 \cdot$ products	1.0×10^{-12}	>3560	$<6.5\times10^{-18}$	–
$Br + O_3 \cdot BrO + O_2$	1.4×10^{-11}	755±200	1.1×10^{-12}	1.2
$O + BrO \cdot Br + O_2$	3.0×10^{-11}	0±250	3.0×10^{-11}	3.0
$BrO + NO \cdot NO_2 + Br$	8.7×10^{-12}	-(265±130)	2.1×10^{-11}	1.15
$BrO + NO_2 \text{ M } BrONO_2$	(See Table A-2)			
$BrO + BrO \cdot 2\,Br + O_2$	1.0×10^{-12}	-(244±250)	2.3×10^{-12}	1.5
$BrO + BrO \cdot Br_2 + O_2$	1.8×10^{-13}	-(244±250)	4.0×10^{-13}	1.5
$BrO + O_3 \cdot Br + 2\,O_2$	1.0×10^{-12}	>1600	$<5.0\times10^{-15}$	–
$Br + H_2O_2 \quad HBr + HO_2$	1.0×10^{-11}	>2500	$<2.0\times10^{-15}$	
$Br + HO_2 \cdot HBr + O_2$	–	–	–	–
$Br + H_2CO \quad HBr + HCO$	1.4×10^{-11}	750±250	1.1×10^{-12}	1.5
$HO + HBr \cdot H_2O + Br$	8.5×10^{-12}	0±250	8.5×10^{-12}	2.0
$O + HBr \cdot HO + Br$	7.6×10^{-12}	1570+300	3.9×10^{-14}	1.5
$BrO + HO_2 \cdot HOBr + O_2$		–	5.0×10^{-12}	5.0
$BrO + HO \cdot$ products		–	9.0×10^{-12}	5.0
$HO + CH_3Br \cdot CH_2Br + H_2O$	6.1×10^{-13}	825±200	3.8×10^{-14}	1.25
$F + O_3 \cdot FO + O_2$	2.8×10^{-11}	226±200	1.3×10^{-11}	2.0
$F + O_2 \text{ M } FO_2$	(See Table A-2)			
$F + H_2 \cdot HF + H$	2.0×10^{-10}	620±250	2.5×10^{-11}	1.5
$F + CH_2 \cdot HF + CH_3$	3.0×10^{-10}	400±300	8.0×10^{-11}	2.0

Table A-1.
Rate Constants for Second Order Reactions

Reaction	A-Factor	E/R± (E/R)	k(298 K)	Uncertainty Factor/298 K
$F + H_2O \cdot HF + OH$	2.2×10^{-11}	200±200	1.1×10^{-11}	5.0
$O + FO \cdot F + O_2$	5.0×10^{-11}	0±250	5.0×10^{-11}	3.0
$NO + FO \cdot NO_2 + F$	2.6×10^{-11}	0±250	2.6×10^{-11}	2.0
$FO + FO \cdot 2\,F + O_2$	1.5×10^{-11}	0±250	1.5×10^{-11}	3.0
$FO + O_3 \cdot F + 2\,O_2$	–	–	–	–
$FO + O_3 \cdot FO_2 + O_2$	–	–	–	–
$O + FO_2 \cdot FO + O_2$	5.0×10^{-11}	0±250	5.0×10^{-11}	5.0
$O(^1D) + HF \cdot OH + F$	1.0×10^{-10}	0±100	1.0×10^{-10}	5.0
$CH_3 + O_2 \overset{M}{\rightarrow} CH_3O_2$	(See Table A-2)			
$CH_3 + O_2 \cdot$ products	–	–	$<10^{-16}$	–
$CH_3 + O \cdot H_2CO + H$	1.3×10^{-10}	0±250	1.3×10^{-10}	1.5
$CH_3O_2 + NO \cdot CH_3O + NO_2$	7.4×10^{-12}	0±500	7.4×10^{-12}	1.25
$CH_3O_2 + NO_2 \overset{M}{\rightarrow} CH_3O_2NO_2$	(See Table A-2)			
$CH_3O_2 + O_3 \cdot CH_3O + 2O_2$	–	–	$<2\times10^{-17}$	–
$CH_3O_2 + HO_2 \cdot CH_3OOH + O_2$	6.0×10^{-12}	0^{+500}_{-1300}	6.0×10^{-12}	5.0
$CH_3O_2 + SO_2 \cdot$ products	–	–	$<5.0\times10^{-17}$	–
$CH_3O_2 + CH_3O_2 \cdot$ products	3.6×10^{-13}	0±300	3.6×10^{-13}	1.5
$CH_3O + O_2 \rightarrow H_2CO + HO_2$	1.0×10^{-12}	2050±750	1.0×10^{-15}	10.0
$HO + H_2CO \cdot HCO + H_2O$	1.0×10^{-11}	0±200	1.0×10^{-11}	1.25
$O + H_2CO \cdot$ products	3.0×10^{-11}	1550±250	1.6×10^{-13}	1.25
$HCO + O_2 \cdot CO + HO_2$	5.0×10^{-12}	0±250	5.0×10^{-12}	1.4
$HO + CH_3OOH \cdot$ products	2.2×10^{-12}	160±160	1.3×10^{-12}	5.0
$O + H_2S \cdot HO + SH$	1.4×10^{-11}	1920±750	2.2×10^{-14}	2.0
$O + OCS \cdot CO + SO$	2.1×10^{-11}	2200±150	1.3×10^{-14}	1.2
$O + CS_2 \cdot CS + SO$	2.4×10^{-11}	530±150	3.4×10^{-12}	1.2
$HO + H_2S \cdot SH + H_2O$	4.2×10^{-12}	0±220	4.2×10^{-12}	1.4
$HO + OCS \cdot$ products	–	–	$<1.0\times10^{-14}$	–
$HO + CS_2 \cdot$ products	–	–	$<1.5\times10^{-15}$	–

Table A-2
Rate Constants for Three-Body Reactions

	Low Pressure Limit $k_o(T) = k_o^{300}(T/300)^{-n}$		High Pressure Limit $k(T) = k^{300}(T/300)^{-m}$	
Reaction	k_o^{300}	n	k^{300}	m
$HO_2 + NO_2 \underset{\bullet}{M} HO_2NO_2$	(2.1±0.4)(-31)	5.0±2.0	(6.5±3.3)(-12)	2.0±2.0
$HO + NO_2 \underset{\bullet}{M} HNO_3$	(2.6±0.3)(-30)	2.9±0.7	(2.4±1.2)(-11)	1.3±1.3
$ClO + NO_2 \underset{\bullet}{M} ClONO_2$	$(4.5^{+12}_{-2})(-32)$	3.8±1.0	(1.5±0.7)(-11)	1.9±1.9
$\underset{\bullet}{M}$ isomer	$(1.2^{+0.7}_{-1.2})(-31)$	3.8±1.0	(1.5±0.7)(-11)	1.9±1.9
$CH_3 + O_2 \underset{\bullet}{M} CH_3O_2$	(2.2±1.1)(-31)	2.2±1.0	(2.0±1.0)(-12)	1.7±1.7
$O + O_2 \underset{\bullet}{M} O_3$	(6.2±0.9)(-34)	2.0±0.5	– –	–
$O(^1D) + N_2 \underset{\bullet}{M} N_2O$	(3.5±3.0)(-37)	$0.45^{+2.0}_{-.45}$	– –	–
$Cl + NO \underset{\bullet}{M} ClNO$	(9.0±2.0)(-32)	1.8±0.5	– –	–
$Cl + NO \underset{\bullet}{M} ClNO_2$ (ClONO)	(1.6±1.0)(-30)	1.9±1.0	(3.0±1.5)(-11)	1.0±1.0
$Cl + O_2 \underset{\bullet}{M} ClOO$	(2.0±1.0)(-33)	$1.3^{+2.0}_{-1.3}$	– –	–
$H + O_2 \underset{\bullet}{M} HO_2$	(5.5±0.5)(-32)	1.4±0.5	– –	–
$HO + NO \underset{\bullet}{M} HONO$	(6.7±1.2)(-31)	3.3±1.0	(3.0±1.5)(-11)	1.0±1.0
$F + O_2 \underset{\bullet}{M} FO_2$	(1.1±0.3)(-32)	1.7±1.0	– –	–
$HO + HO \underset{\bullet}{M} H_2O_2$	(2.5±1.3)(-31)	$0.8^{+2.0}_{-0.8}$	(3.0±1.5)(-11)	1.0±1.0
$CH_3O_2 + NO_2 \underset{\bullet}{M} CH_3O_2NO_2$	(1.5±0.8)(-30)	4.0±2.0	(6.5±3.2)(-12)	2.0±2.0
$F + NO \underset{\bullet}{M} FNO$	(6.6±3.3)(-32)	$1.0^{+2.0}_{-1.0}$	– –	–
$FO + NO_2 \underset{\bullet}{M} FNO_3$	(8.3±6.0)(-31)	$0.7^{+3.0}_{-0.7}$	(2.0±1.0)(-11)	1.5±1.5
$F + NO_2 \underset{\bullet}{M} FNO_2$ (FONO)	(1.3±0.7)(-30)	$1.7^{+2.0}_{-1.7}$	(3.0±1.5)(-11)	1.0±1.0
$BrO + NO_2 \underset{\bullet}{M} BrNO_3$	(5.0±1.0)(-31)	4.0±2.0	(2.0±1.0)(-11)	2.0±2.0
$NO_2 + NO_3 \underset{\bullet}{M} N_2O_5$	(1.4±0.7)(-30)	2.8±1.0	(8.0±4.0)(-13)	0±1.0
$O + NO \underset{\bullet}{M} N_2O_2$	(1.2±0.3)(-31)	1.8±0.5	(3.0±1.0)(-11)	0±1.0
$O + NO_2 \underset{\bullet}{M} NO_3$	(9.0±1.0)(-32)	2.0±1.0	(2.2±0.3)(-11)	0±1.0
$HO + SO_2 \underset{\bullet}{M} HOSO_2$	(3.0±1.5)(-31)	2.9±1.0	(2.0±1.5)(-12)	0±1.0

Note. $k(z) = k(M,T) = \left(\frac{k_o(T)[M]}{1 + k_o(T)[M]/k_\infty(T)}\right) 0.6^{\{1 + [\log_{10}(k_o(T)[M]/k_\infty(T))]^2\}^{-1}}$

(The values quoted are suitable for air as the third body, M)

A direct or concerted bimolecular reaction is one in which the reactants A and B proceed to products C and D without the intermediate formation of an A+B adduct which has appreciable bonding; i.e., no stable A-B molecule exists, and there is no reaction intermediate other than the transition state of the reaction, $(AB)^{\neq}$.

$$A + B \rightarrow (AB)^{\neq} \rightarrow C + D \qquad (1)$$

The reaction of HO with CH_4 forming $H_2O + CH_3$ is an example of a reaction in this class.

Very useful correlations between the expected structure of the transition state $[AB]^{\neq}$ and the A-factor of the reaction rate constant can be made, especially in reactions which are constrained to follow a well-defined approach of the two reactants in order to minimize energy requirements in the making and breaking of bonds.

The indirect or non-concerted class of bimolecular reactions is characterized by a more complex reaction path involving a potential well between reactants and products, leading to a bound adduct (or reaction complex) formed between the reactants A and B:

$$A + B \leftrightarrows [AB]^{*} \rightarrow C + D \qquad (2)$$

The intermediate $[AB]^{*}$ is different from the transition state $[AB]^{\neq}$, in that it is a bound molecule which has a finite lifetime and which can, in principle, be isolated. (Of course, transition states are involved in all of the above reactions, both forward and backward, but are not explicitly shown, for purposes of clarity). An example of this reaction type is ClO + NO, which normally produces Cl + NO_2 as a bimolecular product, but which undoubtedly involves ClONO (Chlorine nitrite) as an intermediate. This can be viewed as a chemical activation process forming $(ClONO)^{*}$ which decomposes unimolecularly to the ultimate products, Cl + NO_2. Reactions of the non-concerted type can have a more complex temperature dependence than those of the concerted type, and, in particular, can exhibit a pressure dependence if the lifetime of $[AB]^{*}$ is comparable to the rate of collisional deactivation of $[AB]^{*}$. This arises because the relative rate at which $[AB]^{*}$ goes to products C + D vs. reactants A + B is a sensitive function of its excitation energy. Thus, in actions of this type, the distinction between the bimolecular and termolecular classification becomes less meaningful, and it is particularly necessary to study such reactions under the temperature and pressure conditions in which they are to be used in model calculations.

TABLES OF RATE CONSTANT DATA

The rate constant tabulation for second-order reactions (Table 1-1) gives the following information:

- Reaction stoichiometry and products, if known.
- Arrhenius A-Factor.
- Temperature dependence and associated uncertainty (activation temperature, $E/R \pm \Delta E/R$).
- Rate constant at 298 K. (Based on all measurements, not just those at 298 K).
- Uncertainty factor at 298 K.

Third-order rate constants (Table A-2) are given in the form:

$$k_0(T) = k_0^{300}(T/300)^{-n} cm^6 s^{-1}, \qquad (3)$$

(where the value is suitable for air as the third body), together with the recommended value of n. Where pressure fall-off corrections are necessary, an additional entry gives the limiting high pressure rate constant in a similar form:

$$k_\infty(T) = k_\infty^{300}(T/300)^{-m} \text{ cm}^3\text{s}^{-1}. \tag{4}$$

To obtain the effective second-order rate constant for a given condition of temperature and pressure (altitude), the following formula is used:

$$k(z) = k(M,T) = \frac{k_0(T)[M]}{1 + k_0(T)[M]/k_\infty(T)} \, 0.6^{\left\{1 + [\log_{10}(k_0(T)[M]/k_\infty(T))]^2\right\}^{-1}}. \tag{5}$$

The number $F_c = 0.6$ is chosen as a unifying compromise for all of the three-body reactions of interest in the atmosphere. It should be noted that in reality the number decreases with increasing temperature and molecular size. It can be calculated from molecular parameters. The CODATA Panel prefers to assign F_c individual values for each reaction; however, the practical effect of the procedure is small for the present applications.

Thus, a compilation of rate constants of this type requires the stipulation of the four parameters, $k_0(300)$, n, $k_\infty(300)$, and m. These can be found in Table A-2. The discussion that follows outlines the general methods we have used in establishing this table.

LOW-PRESSURE LIMITING RATE CONSTANT $[k_0^x(T)]$

Troe (1977) has described a simple method for obtaining low-pressure limiting rate constants. In essence this method depends on the definition:

$$k_0^{\,x}(T) = \beta_x \, k_0^{\,sc}(T), \tag{6}$$

where sc signifies "strong" collisions, x denotes the bath gas, and β_x is an efficiency parameter ($0 < \beta > 1$) which provides a measure of energy transfer.

$$\frac{\beta_x}{1 - \beta_x^{1/2}} = \frac{\langle \Delta E \rangle_x}{F_E \, kT} \tag{7}$$

where $\langle \Delta E \rangle_x$ is the average energy transferred per collision and is quite sensitive to β. F_E is the correction factor of the energy dependence of the density of states (a quantity of the order of 1.1 for most species of stratospheric interest).

For many of the reactions of possible stratospheric interest reviewed here, there exist data in the low-pressure limit (or very close thereto), and we have chosen to evaluate and unify this data by calculating $k_0^{\,sc}(T)$ for the appropriate bath gas, x, and computing the value of β_x corresponding to the experimental value [Troe (1977)].

From the βx values (most of which are for N_2, i.e., β_{N_2}), we compute $\langle E \rangle_x$ according to Equation (7). Values of $\langle E \rangle_{N_2}$ of approximately 0.3 to 1 kcal mole-1 are generally expected. If multiple data exist, we average the values of $\langle E \rangle_{N_2}$ and recommend a rate constant corresponding to the N_2 computed as previously indicated.

Where no data exist, we have estimated the low-pressure rate constants by taking $\beta_{N_2} = 0.3$ at T=300K; a value based on those cases where data exist.

TEMPERATURE DEPENDENCE OF LOW-PRESSURE LIMITING RATE CONSTANTS: n

The value of n recommended here comes from a calculation of $< \Delta E >_{N_2}$ from the data at 300 K, and a computation of β_{N_2} (200 K) assuming that $< \Delta E >_{N_2}$ is independent of temperature. This β_{N_2} (200K) value is combined with the computed value of k_o^{SC} (200 K) to give the expected value of the actual rate constant at 200 K. This latter in combination with the value at 300 K yields the value of n.

This procedure can directly be compared with measured values of k_o(200 K) when those exist. Unfortunately, very few values at 200 K are available. There are often temperature-dependent studies, but some ambiguity exists when one attempts to extrapolate these down to 200 K. If data are to extrapolated out of the measured temperature range, a choice must be made as to the functional form of the temperature dependence. There are two general ways of expressing the temperature dependence of rate constants. Either the Arrhenius expression $k_o(T)=A_{exp}(E/RT)$ or the form $k(t) = A'T^{-n}$ is employed. Since neither of these extrapolation techniques is soundly based, and since they often yield values that differ substantially, we have used the method explained heretofore as the basis of our recommendations.

In JPL 79-27, we computed the extrapolated values at 200 K using both T^{-n} and Arrhenius forms when data are available over any reasonable temperature range. When these values are compared with the recommendation, it can be seen that the data are well accommodated by our methods.

HIGH-PRESSURE LIMITING RATE CONSTANTS [k_∞(T)]

High-pressure rate constants can often be obtained experimentally, but those for the relatively small species of atmospheric importance usually reach the high-pressure limit at inaccessibly high pressures. This leaves two sources of these parameters, the first being guesses based upon some model, and the second extrapolation of fall-off data up to higher pressures. Stratospheric conditions generally render reactions of interest much closer to the low-pressure limit, and thus are fairly insensitive to the high-pressure value. This means that while the extrapolation is long, and the value of k_∞(T) not very precise, a "reasonable guess" of k_∞(T) will then suffice. In some cases we have declined to guess since the low-pressure limit is always in effect over the entire range of stratospheric conditions.

TEMPERATURE DEPENDENCE OF HIGH-PRESSURE LIMITING RATE CONSTANTS: m

There are very little data upon which to base a recommendation for values of m. Values in Table A-2 are estimated, based on models for the transition state of bond association reactions and whatever data are available. In all cases the error limits encompass the possibility of no temperature dependence. The CODATA panel, based on some theoretical and experimental evidence (Quack and Troe 1977) prefers to put $m \geq 0$ for all three-body reactions. For pressures up to one atmosphere, this leads to only slightly differing representations of the T and P dependence of the rate constant under atmospheric conditions. Such differences then can be compensated for by different F_c values (see above). New experiments outside the range of atmospheric conditions (higher temperatures and higher pressures) are required to make the best choice between the alternatives for the representation of k(M,T) where M is the concentration of the third body. It should, however, be emphasized that the data for three-body reactions, with the current available accuracy, are represented equally well by the two procedures. Differences will become apparent only when the precision of the data is considerably improved.

ERROR ESTIMATES

Meaningful error assignment is a major problem in the evaluation of rate constant data, because measurement uncertainties tend to be somewhat random in nature. Although deviations from the central recommended value of the rate constants are usually assumed to be Gaussian in nature, this is not always the case and exceptions may occur in studies where systematic errors not recognized by the researcher or the evaluators are involved. One manifestation of this is that there are occasionally large "wings" to the error distribution, with significant probability for values of k many σ's from the central value.

In some cases, the measured values of a rate constant may center around two distinct ranges, such that the error curve is bimodal in nature. This situation arises not infrequently, largely due to measurements made by different groups using different techniques. This is a particularly difficult problem to reconcile, since often it is not clear which of the two extremes is most likely correct, and intermediate (average) values are almost certainly incorrect, and do not constitute a useful recommendation. Nevertheless, it is necessary to present uncertainty parameters in a tractable form which is suitable for uncertainty analysis in the composite photochemical model. The approach taken in this evaluation was to select a single recommendation for every reaction, and to make the corresponding uncertainties large enough to encompass the alternate value.

For second-order reactions, an estimate of the uncertainty in the rate constant at any given temperature (within the region 200-300 K) is given by the following expression:

$$f_T = f_{298} \exp\left(\frac{\Delta E}{R}\left|\frac{1}{T} - \frac{1}{298}\right|\right)$$

Thus, an upper or lower bound (corresponding roughly to one standard deviation of the rate constant) can be obtained at any temperature T by multiplying or dividing the value of the rate constant at that temperature by the factor f_T. The quantities f_{298} and $\Delta E/R$ are, respectively, the uncertainty in the rate constant at 298K and in the Arrhenius coefficient. These uncertainties were arrived at by a somewhat subjective procedure, involving factors such as the number of measurements, the agreement between them, the variety of techniques applied, the skill and reputation of the researcher, and the difficulty of the experiment.

For three-body reactions a somewhat analogous procedure was used. Uncertainties expressed as increments to k_0 and k_∞ (the limiting low pressure third order rate constant and high pressure second order rate constant, respectively) are given for these rate constants at room temperature. The additional uncertainty arising from the temperature extrapolation is expressed as an uncertainty in the temperature coefficients n and m.

DISCUSSION OF SOME SPECIFIC REACTIONS

This section reviews those reactions for which the recommendations have undergone significant changes, or for which there still exist serious unanswered questions about the constants or reaction mechanism. Fortunately, from the standpoint of the $CFC\text{-}O_3$ question, many of the important reaction rate constants, such as those for $Cl + O_3$, $NO + ClO$, $O + ClO$ and $OH + HCl$, have been measured reliably and recommendations can be made confidently. Several other crucial reactions, however, still pose major uncertainties.

The $ClO + NO_2 + M$ reaction is important in the lower stratosphere, where it couples the ClO_x and NO_x systems and impacts catalytic destruction of O_3 by tying up reactive radicals as relatively stable $ClONO_2$. The available kinetics data for this reaction fall into two sets, which are in substantial disagreement. Several independent low pressure determinations (Zahniser et al., 1977; Birks et al., 1977; Leu et al., 1977; Molina et al., 1980; Cox and Lewis, 1979) of the rate of ClO disappearance via the $ClO + NO_2 + M$ reaction are in excellent agreement and give a k_o (300) near 1.65×10^{-31} cm^6 s^{-1}. No product identification was carried out, and it was assumed that the reaction gave chlorine nitrate, $ClONO_2$. In contrast, direct measurements of the rate of thermal decomposition of $ClONO_2$ (Knauth, 1978; Schonle et al., 1979), combined with the equilibrium constant, give $k_o(300) = 4.5 \times 10^{-32}$ cm^6 s^{-1} for the three-body reaction forming $ClONO_2$. Since the measured rate of ClO disappearance seems well established, the Knauth results can only be reconciled with the higher number by three possible explanations: (1) the measured thermal decomposition rate is incorrect; (2) the equilibrium constant is in error by a factor of three (requiring that the ΔH_f's off by ~1 kcal/mole, which is outside the stated error limits); (3) all the data are correct, and the low pressure ClO disappearance studies measured not only a reaction forming $ClONO_2$, but another channel forming an isomer such as $OClNO_2$, ClOONO or OClONO (Chang et al., 1979a; Molina et al., 1980). Although the $ClONO_2$ form has a relatively low photolysis rate, it is often assumed that the other hypothetical isomers would have higher absorption cross sections and therefore be rapidly photolyzed. In past evaluations, the CODATA group recommended the higher rate constant, i.e., that corresponding to the measured rate of ClO disappearance via reaction with NO_2. The NASA Panel previously made two recommendations; one, the higher rate constant, assuming all $ClO + NO_2$ goes to $ClONO_2$, and the other, the lower rate constant assuming ~2/3 of the overall reaction forms an unknown, rapidly photolyzed isomer. For the present evaluation, the majority of the joint panel felt that a single recommendation should be made, in keeping with our practice on all other reactions. The majority opinion was that the isomer explanation best encompassed all experimental and theoretical information, and therefore the lower (Knauth) rate constant was adopted. Recognizing, however, that there is a significant possibility of error in the value derived from the thermal decomposition study, the error limit was made sufficiently large to encompass the higher value.

When the isomer-forming reaction is included in models, the fate of the isomer must also be stated - a difficult assignment for an unidentified, hypothetical species. While photolysis back to $ClO + NO_2$ seems most reasonable, an isomer of the form ClOONO could, in fact, dissociate to ClOO + NO and thus enhance catalytic destruction of ozone. In the absence of definitive information, the recommended approach is to consider that isomeric $ClONO_2$ rapidly photolyzes to $ClO + NO_2$, at a rate which dominates other possible paths such as isomerization to normal $ClONO_2$. This is equivalent to omitting the isomer-forming reaction altogether for sunlight conditions, because the assumed rapid photolysis to reform the original reactants has the effect of negating the isomer-forming portion of the reaction. It must be borne in mind, however, that at sunset the ClO will disappear at a rate corresponding to the total rate of the $ClO + NO_2$ reaction. Furthermore, the rate of appearance of ClO at sunrise will depend on two factors (presently unknown): (1) the residual distribution between isomeric and normal $ClONO_2$ at dawn, and (2) the relative cross sections of the two forms. The entire matter will remain speculative and unsettled until there is conclusive evidence for or against isomer formation, or until a substantial change in rate data occurs. The photolysis products of $ClONO_2$ itself are uncertain (Smith et al., 1977; Chang et al., 1979b) and additional studies are needed there as well.

A substantial change has been made in the recommendation for the $HO + HNO_3$ reaction since NASA RP 1049. The previous evaluations were based on two independent experimental studies by different techniques (Margitan et al., 1975; Smith and Zellner, 1975) giving a temperature invariant rate constant of 9×10^{-14} cm^3 s^{-1}. Recently, Wine et al. (1980) have remeasured k and found $k(298) = 1.3 \times 10^{-13}$ cm^3 s^{-1}, with a strong negative temperature dependence of E/R = -640K.

These results are being confirmed in two other studies by essentially the same technique (Kurylo, 1981; Margitan and Watson, 1981). Another investigation using several techniques including the same laser photolysis-resonance fluorescence technique (Nelson et al., 1981) resulted in $k(298) = 8 \times 10^{-14}$ cm^3 s^{-1}, but as yet does not include temperature dependence. The Wine et al. study, as confirmed by the other two, is recommended at the present time, although the source of error in the earlier studies is baffling; thus, the uncertainty limits are large enough to encompass the old value. With this new rate constant, the HO + HNO_3 reaction, presumably giving H_2O + NO_3 as products, (Nelson et al., 1981), is now the major sink for HO_x in the lower stratosphere. A verification of the new rate constant by a direct technique other than laser photolysis - resonance fluorescence is clearly needed, as is another determination of reaction products. The role of the reaction depends on the product distribution.

Another reaction whose rate constant has been recently revised and which further reduces HO_x in the lower stratosphere is the HO + HO_2NO_2 reaction. Two measurements of the rate constant are in good agreement (Littlejohn and Johnston, 1980; Trevor et al., 1981), considering the difficulties involved in measuring and handling HO_2NO_2 and yield rate constants significantly higher than previous estimates. Due to the enhanced importance of this reaction, additional studies are needed of k and its T dependence, as well as reaction products (three exothermic channels exist). Quantum yields and products for HO_2NO_2 photolysis are also needed, particularly in the 290 to 300 nm range.

The HO + HO_2 reaction has long been regarded as one of the major uncertainties in atmospheric chemistry. Although the recent revisions in rate data for HO + HNO_3 and HO + HNO_4 have diminished the role played by HO + HO_2 in controlling lower stratospheric HO_x densities, this reaction still remains the dominant sink for HO_x in the upper stratosphere, the region where projected O_3 depletion should first appear and, being the region where photochemistry controls species concentrations in a reasonably well understood manner, it offers the best possibility of partial model verification through measurements. Recent kinetic studies of the HO + HO_2 reaction have significantly reduced the discrepancies, and although the detailed reaction mechanism is far from being understood, the magnitude of the rate constant is coming into sharper focus. Studies of HO + HO_2 in systems near atmospheric pressure have consistently yielded rate constants near 1×10^{-10} cm^3 s^{-1} (Hochanadel et al., 1972, 1980; DeMore and Tschuikow-Roux, 1974; DeMore, 1979; Lii et al., 1980), in serious disagreement with a low pressure upper limit of 4×10^{-11} cm^3 s^{-1} (Chang and Kaufman, 1978). Since a pressure dependent rate constant seemed unlikely, the upper limit of the Chang and Kaufman study was recommended in previous evaluations. This was consistent with the value $k = 5 \times 10^{-11}$ cm^3 s^{-1} reported by Burrows et al. (1977), and 3×10^{-11} cm^3 s^{-1}, (Hack et al., 1978). However, these latter values are no longer under consideration due to changes in the reference reaction used in those studies, and inconsistencies subsequently induced in their other rate constants (see Sridharan et al., 1980). Recent direct low pressure results of Keyser (1981) now give $k = 6.5 \times 10^{-11}$ cm^3 s^{-1}, making it appear likely that the Chang and Kaufman work is in error. The panel is now recommending $k = 8 \times 10^{-11}$ cm^3 s^{-1}, with a factor of two uncertainty, which easily encompasses both low and high pressure values. The possibility of a pressure dependence still remains, but requires precise studies to be fully ascertained.

The rate constant now recommended for the HO_2 + HO_2 reaction is the same as in most earlier evaluations, but differs substantially from the JPL 81-3 value. Most experimental studies have been carried out near atmospheric pressure, and yield a room temperature value of 2.5×10^{-12} cm^3 s^{-1} (Hamilton and Lii, 1977; Cox and Burrows, 1979; Lii et al., 1979). This rate is known to be enhanced by the presence of water vapor (measured up to $\sim$26 mbar). Additionally, the temperature dependence, measured over a limited T range in direct studies, yielded $E/R = -1245$K. The Cox and Burrows study also indicated that the reaction was pressure dependent below 32 mbar at room temperature, with the P dependence extending to higher pressures at lower

temperatures. Limited data also indicated E/R=-680 K at 13 mbar. These combined P and T dependences were used in JPL 81-3 to calculate altitude dependent rate constants for stratospheric modeling. Since the origin and mechanism of these P and T dependences are not known with certainty, and since they are based on somewhat limited data, the panel chose to recommend a fixed value of $k = 3 \times 10^{-12}$ cm^3 s^{-1}, with a factor of three uncertainty to encompass the range of values one would obtain with the P, T dependent expressions. Further studies are clearly required, including product determinations, since the P dependence may indicate the possible formation of stabilized H_2O_4. Similar reasoning was used in formulating the P, T independent recommendation for the analogous $CH_3O_2 + HO_2$ reaction.

The recommended value for the $HO_2 + O_3$ reaction is based on the direct study of Zahniser and Howard (1980), which yields an unexpectedly low A factor. Three determinations of $k(HO_2 + O_3)$ relative to $k(HO_2 + HO_2)$ (DeMore and Tschuikow-Roux, 1974; Simonaitis and Heicklen, 1973; DeMore, 1979) are consistent with that recommendation if the high pressure T dependence (E/R = -1245 K) is used for the $HO_2 + HO_2$ reaction. Conversely, the directly measured $HO_2 + O_3$ rate constant can be coupled with the ratios to derive the strong negative T dependence of $HO_2 + HO_2$, over a wider T range than the direct studies. Because of the importance of the $HO_2 + O_3$ reaction, its inexplicable A-factor, and its potential bearing on the $HO_2 + HO_2$ rate constant, a remeasurement of $k(HO_2 + O_3)$ is needed. Our present recommendations for $k(HO_2 + O_3)$ and $k(HO_2 + HO_2)$ as a function of temperature are inconsistent with the experimental ratio measurements.

The present recommendation for the $HO + H_2O_2$ reaction rate constant is based on a least squares fit of the combined data of two recent, extensive studies (Keyser, 1980; Sridharan et al., 1980) which clearly show the earlier investigations to be in error. Although this reaction is of little importance in the stratosphere, it quite often plays a role in laboratory kinetic studies as a reference reaction, and the recent change has negated a large body of HO_2 rate constants obtained in certain relative studies (see Sridharan et al., for a more detailed discussion). The new Arrhenius parameters are in much better agreement with theoretical expectations than the earlier ones were. Based on this and the limited nature of data for the $O + H_2O_2$ reaction, we have chosen an A factor for that reaction slightly different from the reported value, and more consistent with other atom-molecule reaction A factors. The resultant change in recommended value of k is minor.

Recent kinetic studies of the $HO + ClO$ and $HO_2 + ClO$ reactions suggest that formation of HCl is minimal, thus diminishing their potential importance in the stratosphere as chain terminators. The strong negative T-dependence of the $HO_2 + ClO$ reaction does, however, indicate a potential role for HOCl in stratospheric chemistry. Its ultimate role, however, is probably minor since its effect as a sink (or reservoir) is counter-balanced by its possible action in a catalytic O_3 destruction cycle arising through its photolysis.

ATMOSPHERIC PHOTOCHEMISTRY - SOME CONCLUDING REMARKS

The ozone content of Earth's atmosphere can be considered to exist in three distinct regions: the troposphere, stratosphere, and mesosphere. The latter region is not discussed here. The unpolluted troposphere contains small amounts of ozone, which comes from both downward transport from the stratosphere and from in situ photochemical production. The chemistry of the global troposphere is complex, with both homogeneous and heterogeneous (e.g., rain-out) processes playing important roles. The homogeneous chemistry is governed by coupling between the carbon/nitrogen/hydrogen and oxygen systems and can be considered to be more complex than the chemistry of the stratosphere, due to the presence of higher hydrocarbons, long photochemical relaxation times, higher total pressures, and the high relative humidity which

may affect the reactivity of certain key species such as HO_2. Significant progress is being made in understanding the coupling between the different chemical systems, especially the mechanism of methane oxidation which partially controls the odd hydrogen budget. This is an important development, as reactions of the hydroxyl radical are the primary loss mechanism for compounds containing C-H (CH_4, CH_3Cl, CHF_2Cl, etc.) or C-C (C_2Cl_4, C_2HCl_3, C_2H_4, etc.), thus limiting the fraction transported into the stratosphere.

The stratosphere is the region of the atmosphere where the bulk of the ozone resides, with the concentration reaching a maximum value of about $5x10^{12}$ molecule cm^{-3} at an altitude of ~25 km. Ozone in the stratosphere is removed predominantly by catalytic (i.e., non-Chapman) processes, but the assignment of their relative importance and the prediction of their future impact is dependent on a detailed understanding of chemical reactions which form, remove and inter-convert the catalytic species. A model calculation of stratospheric composition may include some 150 chemical reactions and photochemical processes, which vary greatly in their importance in controlling the density of ozone. Laboratory measurements of the rates of these reactions have progressed rapidly in recent years, and have given us a basic understanding of the processes involved, particularly in the upper stratosphere. Despite the basically sound understanding of overall stratospheric chemistry which presently exists, much remains to be done to quantify errors, to identify reaction channels positively, and to measure reaction rates both under conditions corresponding to the lower stratosphere (~210 K, ~100 mbar) as well as the top of the stratosphere (~270K, ~1 mbar).

The chemistry of the upper stratosphere, i.e., 30 to 50 km, is reasonably well defined. In this region the chemical composition of the atmosphere is predominantly photochemically controlled and the photolytic lifetimes of temporary reservoir species such as HOCl, HO_2, NO_2, $ClONO_2$, N_2O_2 and H_2O_2 are short and hence they play a minor role. Thus the important processes above 30 km all involve atoms and small molecules. The majority of laboratory studies on these reactions have been carried out under the conditions of pressure and temperature which are encountered in the upper stratosphere, and their overall status appears to be good. No significant changes in rate coefficients for the key reactions such as Cl+O_3, O+ClO, NO+ClO, O+NO_2, NO+O_3, etc., have occured in the last few years. On the other hand, there have recently been rate and mechanistic studies on reactions such as HO+ClO and HO_2+ClO, which could play important roles throughout the stratosphere if they were to have product channels which generate significant amounts of HCl. Although the results to date suggest minor HCl pathways, their product distributions are at present inadequately estabalished for atmospheric modeling purposes.

A major area of concern in the chemistry of the upper stratosphere involves the reaction between HO and HO_2 radicals which, as previously discussed in this chapter, has had considerable uncertainty in the rate constant. This termination reaction plays an important role in determining the absolute concentrations of HO and HO_2, and since HO plays a central role in controlling the catalytic efficiencies of both NO_x and ClO_x it is a reaction of considerable importance. It should be noted that the new rate coefficients for the HO + H_2O_2, HO + HNO_3 and HO + HO_2NO_2 reactions have had little effect on the model predictions of odd HO_x concentrations above 30 km.

One area in which additional studies may be needed is that of excited state chemistry, i.e., to determine whether electronic or vibrational states of certain atmospheric constituents may be more important than hitherto recognized. Possible examples are O_2^*, O_3^*, or N_2^*. It has recently been suggested that the excited N_2 ($A^3\Sigma_u^+$) molecule may react with O_2 to form N_2O + O. This could possibly modify our understanding of the source of N_2O in the upper stratosphere.

There are numerous processes in the upper stratosphere which do not significantly affect the model predictions of ozone perturbations by fluorocarbons but for which accurate rate coefficients are required in order to interpret field measurement data. For example, reactions such as O + HO and O + HO_2 control the HO_x radical partitioning above 40 km. For reactions of this type the data base can only be considered to be fair, and some improvements need to be made before comparing theoretical predictions with certain field measurement data.

The chemistry of the lower stratosphere is quite complex, with significant coupling between the HO_x, NO_x and ClO_x families. It is within this region of the atmosphere (15 to 30 km) where both dynamics and photochemistry play key roles in controlling the trace gas distributions. Here the model calculations predict large changes in ozone concentration (absolute number density, not percentage) from chlorofluoromethanes. It is also within this region of the stratosphere that the question of the pressure and temperature dependences of the rate coefficients is most critical, due to the low temperatures (210-225 K) and the high total pressures (40 to 270 mbar). The previously discussed question of possible pressure and temperature dependences of HO and HO_2 reactions is highly pertinent here.

Our view of the chemistry of the lower stratosphere has changed radically in recent times, due to changes in rate constants which have in turn led to changes in the relative importance of reactions which control the HO_x budget in this region of the atmosphere. Prior to the appearance of new or revised kinetics data for the HO + H_2O_2, HO+HNO_3, and HO+HO_2NO_2 reactions, the major termination reaction for odd hydrogen species in models of the lower stratosphere was the HO+HO_2 → H_2O+O_2 reaction. Recent work on the HO+H_2O_2 and HO+HNO_3 rate constants has suggested that the previously accepted values were in error, especially at stratospheric temperatures, and that the previously undetermined rate coefficient for the HO+HO_2NO_2 reaction was significantly faster than has been estimated. The major effect occurred due to the change in rate constant for the OH+HNO_3 reaction (a factor of three faster at 220 K). The change in the rate constant for HO+H_2O_2 (a factor of five at 220 K) had relatively less effect.

There are several other processes which need to be re-studied in order to understand HO_x radical budgets in the lower stratosphere, especially HO_2+HO_2. The species HNO_3, HO_2NO_2, $ClNO_3$ and HOCl illustrate the strong coupling that exists between the HO_x, NO_x and ClO_x families. One disturbing problem is that while these species are currently thought to play an important role in stratospheric photochemistry, only HNO_3 has yet been positively observed by any field measurement study.

Table A-3
Reliability Estimates for Photochemical Rates

Species	Uncertainty Factor
O_2 (Schumann-Runge bands)	1.4
O_2 (Continua)	1.15
O_3	1.12
$O_3 \rightarrow O(^1D)$	1.4
NO_2	1.25
$NO_3 \rightarrow \begin{cases} NO + O_2 \\ NO_2 + O \end{cases}$	2.0
N_2O	1.2
N_2O_5	2.0
H_2O_2	1.4
HNO_3	1.15
NO_2NO_2	2.0
$CH_2O \rightarrow \begin{cases} H + HCO \\ H_2 + CO \end{cases}$	1.4
HCl	1.12
HOCl	1.4
$ClONO_2$	1.25
CCl_4	1.1
CCl_3F	1.05
CCl_2F_2	1.15
CH_3Cl	1.1
CF_2O	2.0
CH_3OOH	1.4
$BrONO_2$	1.4

Table A-4
Mathematical Expression for $O(^1D)$ Quantum Yields, φ, in the Photolysis of O_3

$$\varphi(\lambda,T) = A(\tau)\arctan[B(\tau)(\lambda-\lambda_0(\tau))] + C(\tau)$$

Where: $\tau = T - 230$ is a temperature function with T given in Kelvin, λ is expressed in nm, and arctan in radians.

The coefficients $A(\tau)$, $B(\tau)$, $\lambda_0(\tau)$ and $C(\tau)$ are expressed as interpolation polynomials of the third order:

$$A(\tau) = 0.332 + 2.565 \times 10^{-4}\tau + 1.152 \times 10^{-5}\tau^2 + 2.313 \times 10^{-8}\tau^3$$
$$B(\tau) = -0.575 + 5.59 \times 10^{-3}\tau - 1.439 \times 10^{-5}\tau^2 - 3.27 \times 10^{-8}\tau^3$$
$$\lambda_0(\tau) = 308.20 + 4.4871 \times 10^{-2}\tau + 6.9380 \times 10^{-5}\tau^2 - 2.5452 \times 10^{-6}\tau^3$$
$$C(\tau) = 0.466 + 8.883 \times 10^{-4}\tau - 3.546 \times 10^{-5}\tau^2 + 3.519 \times 10^{-7}\tau^3.$$

In the limits where $\varphi(\lambda,T) > 0.9$, the quantum yield is set $\varphi = 0.9$, and similarily for $\varphi(\lambda,T) < 0$, the quantum yield is set $\varphi = 0$.

Table A-5
NO_2 Absorption Cross Sections at 235 and 298 K

λ (nm)	$10^{20}\sigma$(cm2)		λ (nm)	$10^{20}\sigma$(cm2)	
	235 K	298 K		235K	298 K
185		26.0	300	10.9	11.7
190		29.3	305	16.7	16.6
195		24.2	310	18.3	17.6
200		25.0	315	21.9	22.5
205		37.5	320	23.5	25.4
210		38.5	325	25.4	27.9
215		40.2	330	29.1	29.9
220		39.6	335	31.4	34.5
225		32.4	340	32.3	38.8
230		24.3	345	34.3	40.7
235		14.8	350	31.1	41.0
240		6.70	355	43.7	51.3
245		4.35	360	39.0	45.1
250		2.83	365	53.7	57.8
255		1.45	370	48.7	54.2
260		1.90	375	50.0	53.5
265		2.05	380	59.3	59.9
270		3.13	385	57.9	59.4
275		4.02	390	54.9	60.0
280		5.54	395	56.2	58.9
285		6.99	400	66.6	67.6
290	6.77	8.18	405	59.6	63.2
295	8.52	9.67	410	53.2	57.7

Table A-6
Quantum Yields for NO_2 Photolysis

λ, nm	Φ	λ, nm	Φ	λ, nm	Φ
375	0.73	389	0.74	400	0.65
376	0.75	390	0.74	401	0.62
377	0.86	391	0.81	402	0.57
378	0.74	392	0.73	403	0.50
379	0.83	393	0.78	404	0.40
380	0.81	394	0.83	405	0.32
381	0.73	394.5	0.78	406	0.30
382	0.65	395	0.81	407	0.23
383	0.62	395.5	0.75	408	0.18
384	0.66	396	0.78	409	0.17
385	0.70	396.5	0.81	410	0.14
386	0.74	397	0.77	411	0.10
387	0.69	398	0.72	415	0.067
388	0.76	399	0.70	420	0.023

Table A-7
Mathematical Expression for Absorption Cross Sections of N_2O as a Function of Temperature

$$\ln \sigma(\lambda, T) = A_1 + A_2\lambda + A_3\lambda^2 + A_4\lambda^3 + A_5\lambda^4 + (T-300)\exp(B_1 + B_2\lambda + B_3\lambda^2 + B_4\lambda^3)$$

Where: T: temperature, Kelvin λ: nm

$A_1 = 68.21023$ $B_1 = 123.4014$

$A_2 = -4.071805$ $B_2 = -2.116255$

$A_3 = 4.301146 \times 10^{-2}$ $B_3 = 1.111572 \times 10^{-2}$

$A_4 = -1.777846 \times 10^{-4}$ $B_4 = -1.881058 \times 10^{-5}$

$A_5 = 2.520672 \times 10^{-7}$

Range: 173 to 240 nm; 194 to 320 K

Table A-8
Absorption Cross Sections of N_2O_5

λ (nm)	σ (cm^2)	λ (nm)	σ (cm^2)	λ (nm)	σ (cm^2)
206	6.6(-18)	246	4.3(-19)	286	7.8(-20)
208	5.9(-18)	248	3.8(-19)	288	7.1(-20)
210	5.2(-18)	250	3.5(-19)	290	6.3(-20)
212	4.4(-18)	252	3.0(-19)	292	5.7(-20)
214	3.7(-18)	254	2.72(-19)	294	4.9(-20)
216	3.0(-18)	256	2.55(-19)	296	4.4(-20)
218	2.48(-18)	258	2.33(-19)	298	3.8(-20)
220	2.06(-18)	260	2.12(-19)	300	3.2(-20)
222	1.71(-18)	262	1.97(-19)	302	2.7(-20)
224	1.41(-18)	264	1.86(-19)	304	2.4(-20)
226	1.23(-18)	266	1.7(-19)	306	2.1(-20)
228	1.06(-18)	268	1.64(-19)	308	1.8(-20)
230	9.3(-19)	270	1.52(-19)	310	1.5(-20)
232	8.4(-19)	272	1.42(-19)	320	7.5(-21)
234	7.5(-19)	274	1.31(-19)	330	4.0(-21)
236	6.9(-19)	276	1.2(-19)	340	2.7(-21)
238	6.3(-19)	278	1.15(-19)	350	1.8(-21)
240	5.7(-19)	280	1.07(-19)	360	1.0(-21)
242	5.3(-19)	282	9.9(-20)	370	4.7(-22)
244	4.7(-19)	284	8.9(-20)	380	1.3(-22)

Note: Numbers in parentheses signify powers of 10(e.g., 6.6(-18) = 6.6×10^{-18})

Table A-9
Absorption Cross Sections of H_2O_2 Vapor

λ (nm)	$10^{20}\sigma$ (cm^2)
210	37.3
220	27.0
230	19.2
240	13.2
250	9.0
260	5.6
270	3.5
280	2.1
290	1.2
300	0.71
310	0.42
320	0.24
330	0.15
340	0.09
350	0.05

Table A-10
Absorption Cross Sections of HNO_3 Vapor

λ (nm)	$10^{20}\sigma$ (cm^2)	λ (nm)	$10^{20}\sigma$ (cm^2)
190	1320	255	1.94
195	910	260	1.90
200	550	265	1.80
205	255	270	1.63
210	97.0	275	1.40
215	32.8	280	1.11
220	14.4	285	0.877
225	8.51	290	0.634
230	5.63	295	0.426
235	3.74	300	0.276
240	2.60	305	0.163
245	2.10	310	0.095
250	1.95	315	0.047
		320	0.018

Table A-11
Absorption Cross Sections of HO_2NO_2 Vapor
Molina and Molina (1980)

(nm)	$10^{20}\sigma(cm^2)$	(nm)	$10^{20}\sigma(cm^2)$
190	1010	265	22.4
195	816	270	17.8
200	563	275	13.4
205	367	280	9.3
210	241	285	6.3
215	164	290	4.0
220	120	295	2.6
225	95.2	300	1.6
230	80.8	305	1.1
235	69.8	310	0.7
240	59.1	315	0.4
245	49.7	320	0.3
250	41.8	325	0.2
255	35.1	330	0.1
260	27.8		

Table A-12
Absorption Cross Sections and Quantum Yields for the Photolysis of CH_2O

λ (nm)	$10^{20}\sigma$ (cm^2)	Φ_1 (H + HCO)	Φ_2 (H_2 + CO)
280	2.4	0.63	0.37
290	3.2	0.73	0.27
300	3.3	0.77	0.23
310	3.1	0.76	0.24
320	2.4	0.63	0.37
330	2.4	0.31	0.64
340	2.0	0	0.67
350	0.8	0	0.40
360	0.2	0	0.14

Table A-13
Absorption Cross Sections of HCl Vapor

λ (nm)	$10^{20}\sigma$ (cm^2)	λ (nm)	$10^{20}\sigma$ (cm^2)
140	211	185	31.3
145	281	190	14.5
150	345	195	6.18
155	382	200	2.56
160	332	205	0.983
165	248	210	0.395
170	163	215	0.137
175	109	220	0.048
180	58.8		

Table A-14
Absorption Cross Sections of HOCl

λ (nm)	$10^{20}\sigma$ (cm^2)	λ (nm)	$10^{20}\sigma$ (cm^2)
200	5.2	330	3.7
210	6.1	340	2.4
220	11.0	350	1.4
230	18.6	360	0.8
240	22.3	370	0.45
250	18.0	380	0.24
260	10.8	390	0.15
270	6.2	400	0.05
280	4.8	420	0.04
290	5.3		
300	6.1		
310	6.2		
320	5.0		

Table A-15
Absorption Cross Sections of $ClONO_2$

λ (nm)	$10^{20}\sigma(cm^2)$ 227K	243K	296K	λ (nm)	$10^{20}\sigma(cm^2)$ 227K	243K	296K
190	555	---	589	325	0.463	0.502	0.655
195	358	---	381	330	0.353	0.381	0.514
200	293	---	307	335	0.283	0.307	0.397
205	293	---	299	340	0.246	0.255	0.323
210	330	---	329	345	0.214	0.223	0.285
215	362	---	360	350	0.198	0.205	0.246
220	348	---	344	355	0.182	0.183	0.218
225	282	---	286	360	0.170	0.173	0.208
230	206	---	210	365	0.155	0.159	0.178
235	141	---	149	370	0.142	0.140	0.162
240	98.5	---	106	375	0.128	0.130	0.139
245	70.6	---	77.0	380	0.113	0.114	0.122
250	52.6	50.9	57.7	385	0.098	0.100	0.108
255	39.8	39.1	44.7	390	0.090	0.083	0.090
260	30.7	30.1	34.6	395	0.069	0.070	0.077
265	23.3	23.1	26.9	400	0.056	0.058	0.064
270	18.3	18.0	21.5	405	---	---	0.055
275	13.9	13.5	16.1	410	---	---	0.044
280	10.4	9.98	11.9	415	---	---	0.035
285	7.50	7.33	8.80	420	---	---	0.027
290	5.45	5.36	6.36	425	---	---	0.020
295	3.74	3.83	4.56	430	---	---	0.016
300	2.51	2.61	3.30	435	---	---	0.013
305	1.80	1.89	2.38	440	---	---	0.009
310	1.28	1.35	1.69	445	---	---	0.007
315	0.892	0.954	1.23	450	---	---	0.005
320	0.630	0.681	0.895				

Table A-16
Absorption Cross Sections of CCl_4

λ (nm)	$10^{20}\sigma$(cm^2)	λ (nm)	$10^{20}\sigma$ (cm^2)
174	995	206	56.5
176	1007	208	52.8
178	976	210	47.3
180	772	212	39.6
182	589	214	33.4
184	450	216	27.6
186	318	218	22.1
188	218	220	17.0
190	142	222	12.8
192	98.9	224	9.5
194	73.3	226	7.1
196	67.6	228	5.6
198	65.1	230	4.11
200	64.i	232	3.05
202	61.4	234	2.24
204	60.1	236	1.52
		238	1.25

Table A-17
Absorption Cross Sections of CCl_3F

λ (nm)	$10^{20}\sigma$ (cm^2)
186.0	243.0
187.8	217.0
189.6	186.0
191.4	159.0
193.2	133.0
195.1	111.0
197.0	90.3
199.0	73.0
201.0	57.3
203.0	45.2
205.1	33.3
207.3	23.9
209.4	16.8
211.6	11.5
213.9	7.6
216.2	5.0
218.6	3.1
221.0	2.0
223.5	1.2
226.0	0.8

Table A-18
Absorption Cross Sections of CCl_2F_2

λ (nm)	$10^{20}\sigma_{296}$ (cm^2)
186.0	106.0
187.8	85.4
189.6	64.6
191.4	48.7
193.2	35.3
195.1	24.5
197.0	16.6
199.0	10.8
201.0	6.87
203.0	4.36
205.1	2.59
207.3	1.50
209.4	0.89
211.6	0.51
213.9	0.29
216.2	0.17
218.6	0.095
221.0	0.05
223.5	<0.05
226.0	<0.05

Table A-19
Absorption Cross Sections of $CHClF_2$

λ (nm)	$10^{20}\sigma$ (cm^2)
174	5.94
176	4.06
178	2.85
180	1.99
182	1.30
184	0.825
186	0.476
188	0.339
190	0.235
192	0.157
194	0.100
196	0.070
198	0.039
200	0.026
202	0.022
204	0.013

Table A-20
Absorption Cross Sections of CH_3Cl

λ (nm)	$10^{20}\sigma(cm^2)$	λ (nm)	$10^{20}\sigma(cm^2)$
174	110	198	2.60
176	93.3	200	1.69
178	77.3	202	1.09
180	63.5	204	0.718
182	46.5	206	0.476
184	34.7	208	0.302
186	25.3	210	0.191
188	18.0	212	0.116
190	12.5	214	0.089
192	8.76	216	0.047
194	5.61	218	0.036
196	3.80	220	0.023

Table A-21
Absorption Cross Sections of CH_3CCl_3
Vanlaethem-Meuree et al. (1979)

λ (nm)	$10^{20}\sigma$ (cm^2)		
	295K	250K	210K
185	265	265	265
190	192	192	192
195	129	129	129
200	81.0	81.0	81.0
205	46.0	44.0	42.3
210	24.0	21.6	19.8
215	10.3	8.67	7.47
220	4.15	3.42	2.90
225	1.76	1.28	0.97
230	0.700	0.470	0.330
235	0.282	0.152	0.088
240	0.102	0.048	0.024

Table A-22
Absorption Cross Sections of CCl_2O, CClFO, and CF_2O

λ (nm)	$10^{20}\sigma(cm^2)$		
	CCl_2O	CClFO	CF_2O
184.9	204.0		4.7
186.0	189.0	15.6	5.5
187.8	137.0	14.0	5.2
189.6	117.0	13.4	4.5
191.4	93.7	12.9	4.0
193.2	69.7	12.7	3.3
195.1	52.5	12.5	2.8
197.0	41.0	12.4	2.3
199.0	31.8	12.3	1.9
201.0	25.0	12.0	1.4
203.0	20.4	11.7	1.1
205.1	16.9	11.2	0.86
207.3	15.1	10.5	0.65
209.4	13.4	9.7	0.48
211.6	12.2	9.0	0.36
213.9	11.7	7.9	0.26
216.2	11.6	6.9	0.21
218.6	11.9	5.8	0.15
221.0	12.3	4.8	0.12
223.5	12.8	4.0	0.10
226.0	13.2	3.1	0.08

Table A-23
Absorption Cross Sections of CH_3OOH

λ (nm)	$10^{20}\sigma$ (cm^2)	λ (nm)	$10^{20}\sigma$ (cm^2)	λ (nm)	$10^{20}\sigma$ (cm^2)
210	37.5	260	3.8	310	0.34
220	22.0	270	2.5	320	0.19
230	13.8	280	1.5	330	0.11
240	8.8	290	0.90	340	0.06
250	5.8	300	0.58	350	0.04

Table A-24
Absorption Cross Sections of $BrONO_2$

λ (nm)	σ (cm^2)	λ (nm)	σ (cm^2)
187	1.5(-17)	280	2.9(-19)
190	1.3(-17)	285	2.7(-19)
195	1.0(-17)	290	2.4(-19)
200	7.2(-18)	295	2.2(-19)
205	4.3(-18)	300	1.9(-19)
210	3.2(-18)	305	1.8(-19)
215	2.7(-18)	310	1.5(-19)
220	2.4(-18)	315	1.4(-19)
225	2.1(-18)	320	1.2(-19)
230	1.9(-18)	325	1.1(-19)
235	1.7(-18)	330	1.0(-19)
240	1.3(-18)	335	9.5(-20)
245	1.0(-18)	340	8.7(-20)
250	7.8(-19)	345	8.5(-20)
255	6.1(-19)	350	7.7(-20)
260	4.8(-19)	360	6.2(-20)
265	3.9(-19)	370	4.9(-20)
270	3.4(-19)	380	4.0(-20)
275	3.1(-19)	390	2.8(-20)

Note: Numbers in parentheses signify powers of 10 (e.g., 1.5(-17) = 1.5×10^{-17})

C-5

APPENDIX B

A REFERENCE SOLAR SPECTRAL IRRADIANCE FOR USE IN ATMOSPHERIC MODELING

INTRODUCTION

This appendix outlines the present state of knowledge concerning the absolute magnitude and temporal variability of the solar spectral irradiance with emphasis on wavelengths relevant to the mesosphere and stratosphere. Reference spectra for the wavelength region 175 to 850 nm appear in the tables including estimates for solar minimum and solar maximum conditions where appropriate. Values for the Lyman alpha emission are given separately.

The principal absorbing gases in the atmosphere are O_2 and O_3 which attenuate the incident irradiance via:

$$O_2 + h\nu \ (\lambda < 175 \text{ nm}) \rightarrow O(^3P) + O(^1D)$$
$$O_2 + h\nu \ (175 \text{ nm} < \lambda < 242.4 \text{ nm}) \rightarrow O(^3P) + O(^3P)$$
$$O_3 + h\nu \ (\lambda < 310 \text{ nm}) \rightarrow O_2 + O(^1D)$$
$$O_3 + h\nu \ (\lambda > 310 \text{ nm}) \rightarrow O_2 + O(^3P)$$

An accurate calculation of the solar irradiance which penetrates to a given level depends on the vertical distribution of absorbing gases and their cross sections as well as on the incident solar energy. In addition to the above processes, numerous trace gases dissociate in the spectral region 175 to 400 nm and play significant roles in the atmospheric photochemical system. Wavelengths less than 175 nm are absorbed principally in the Schumann-Runge continuum of O_2 at altitudes above the mesopause. Oxygen molecules absorb photons between 175 and 200 nm in the Schumann-Runge band system and thereby provide the largest source of odd oxygen in the mesosphere. Dissociation of O_2 in the stratosphere occurs in the Herzberg continuum at wavelengths between 200.0 and 242.4 nm. Ozone dissociates in the Hartley bands between 200 and 310 nm, in the Huggins bands between 310 and 340 nm, and in the Chappuis bands in the visible region of the spectrum.

MEASUREMENT TECHNIQUES

The accuracy of solar irradiance measurements is limited by the accuracy of the primary standards and their long term precision. Additional errors are accumulated in the transfer process from the primary to secondary standard and to the flight instrument. The variability of the flight instrument adds further uncertainties. Furthermore, all of these errors are wavelength dependent.

Ground-based measurements cover only the visible spectrum. The advantage is that the instruments can be kept in a benign environment and there is no degradation by solar ultraviolet or X-ray radiation. The primary standards can be compared directly with the Sun. The disadvantage of ground-based measurements is the required correction to zero air mass which can lead to rather large errors in the ultraviolet and the infrared.

Aircraft measurements are less influenced by the zero air mass correction. Aerosols are minimal, no interference from clouds is encountered, and the corrections due to water vapor are reduced. High altitude balloon measurements allow observations in the ultraviolet down to 200 nm. However, measurements between 240 and 270 nm are not reliable because of large optical depth effects. Balloon measurements have the advantage of no outgassing problems, and no damage

due to solar ultraviolet or X-ray radiation. The flight duration is several hours which allows measurements with high precision. Instruments are returned for post-flight calibration and the flight environment is less harsh than that of sounding rockets.

Sounding rocket observations cover all wavelengths into the X-ray region without significant absorption. Calibration can be carried out before and after flight. Their shortcomings are the harsh flight environment, limited rocket carrying capability, and the short flight duration which does not allow in-flight calibration and results in rather limited signal-to-noise ratios.

Solar irradiance measurements from satellites have a high precision over extended time periods and, therefore, allow observing the short term variation of the Sun. Their disadvantage is the long period between the last laboratory calibration and launch, and the fact that the instruments cannot be returned for post-flight calibration. In addition, the experiments suffer from severe degradation caused by solar ultraviolet and X-ray radiation and this requires that calibration checks be carried out by independent means.

In the future, the space shuttle will provide an additional platform. The primary advantage is longer flight duration (days to weeks) than sounding rockets, which allows in-flight calibration and better statistics. The shuttle can carry much larger instruments than sounding rockets and allows their return for post-flight calibration, but it has the same disadvantage of rockets, namely, a harsh flight environment (high vibration, outgassing).

ABSOLUTE IRRADIANCES AND TEMPORAL VARIABILITY

Variations in the solar irradiance occur on time scales ranging from seconds to hours for solar flares, days to weeks for the development of active regions and solar rotation, 11 years for the sunspot cycle, and perhaps longer periods such as the 90 year "Gleissberg cycle" which appears in the envelope of maximum sunspot numbers measured over many solar cycles (Heath, 1981a). A mechanism which provides for a significant variation in the full-disk solar irradiance is the change in the number of plage regions visible from Earth (Cook et al., 1980; Brueckner, 1981). This accounts for the 27-day period which is now firmly established as well as a solar cycle variation. In general, the percentage variation in full-disk irradiance assocated with active regions increases as wavelength decreases and at wavelengths longer than 210 nm becomes less than 1 to 2% (Cook et al., 1980; Brueckner, 1981). Early measurements from the Solar Backscatter Ultraviolet instrument on Nimbus 7 reveal both a 27-day and longer term variation. Although the variation with solar rotation is confirmed, it is still possible that the longer term change arises from an instrumental effect. Further analysis is required before definitive conclusions can be reached (Heath, 1981a). Between 200 and 300 nm, solar line blanketing reaches a maximum (Kurucz, 1981), and hence, it is conceivable that small changes in the opacity of the solar atmosphere might lead to measurable changes in emission. However, the reality of this mechanism as a cause of significant solar variability has not yet been established. Further discussion of the origin of solar variation is beyond the scope of this appendix.

Current knowledge of the solar irradiance in the spectral region 135 to 850 nm plus Lyman alpha is summarized below.

THE LYMAN-ALPHA LINE (121.6 nm)

Measurements of the integrated Lyman Alpha emission, q, for a low level of solar activity as reported by Vidal-Madjar (1975), Vidal-Madjar and Phissamay (1980), Hinteregger (1961), and Rottman (1981) are adequately summarized by:

$$q = (2.5 \pm 0.5) \times 10^{11} \text{ photons cm}^{-2}\text{s}^{-1}$$

The Lyman alpha irradiance varies with solar activity and is correlated with the 10.7 cm radio flux, F(10.7). A relationship between these quantities can be anticipated from the fact that both emissions originate in the solar chromosphere. For aeronomic application it is convenient to express q in terms of F(10.7) although any formula must be viewed as valid only in a statistical sense. Unfortunately the various dependencies of q on solar activity reported in the literature differ markedly among themselves. The results of Hinteregger (1981) imply larger changes in Lyman alpha than those of Vidal-Madjar (1975). Both of these data sets represent long-term observations from satellites. Comparison of results obtained from rockets by Mount et al. (1980) and Rottman (1981) support the smaller variations as does the plage model of Cook et al. (1980). However, as discussed by Hinteregger (1981), data from the five rocket flights of Rottman (1981) show a spread of more than a factor of two among themselves, making a reliable determination of the mean irradiance at solar minimum difficult. With the present state of knowledge the linear relationship:

$$q = 2.5 \times 10^{11} + 0.011 \times 10^{11} [F(10.7) - 65]$$

derived by Bossy and Nicolet (1981) is adequate for atmospheric modeling. Figure B-1 presents the Lyman alpha irradiances used to derive this equation plotted as a function of F(10.7) in watts $m^{-2}Hz^{-1}$. The data of Hinteregger (1981) which appear in the figure have been adjusted by Bossy and Nicolet (1981) to account for a hypothesized instrument drift. However, the proper magnitude of such a correction is uncertain and the recommended equation yields q values smaller than reported by Hinteregger (1981) for high levels of solar activity. It is possible that a linear relationship between q and F(10.7) is invalid for high levels of solar activity. Hence, any expression giving the Lyman-alpha irradiance in terms of F(10.7) is subject to modification as improved knowledge from satellite experiments becomes available.

THE SPECTRAL REGION 135 TO 175 nm

This wavelength region is relevant to the mesosphere in that it influences the atomic oxygen concentration near the upper boundary. The irradiance results reported by different observers show a wide spread as indicated in Table B-1 which compares the total number of photons $cm^{-2}s^{-1}$ between 135 and 175 nm as reported by various groups. The differences among the measurements in the 1972-1975 period surely represent systematic calibration differences. According to Hinteregger (1976), the minimum number of solar photons is 5.7×10^{11} $cm^{-2}s^{-1}$ integrated between 135 and 175 nm as compared to an average value from Rottman (1981) of $(9 \pm 1) \times 10^{11}$ $cm^{-2}s^{-1}$. The average of the extreme values for solar minimum is 7.5×10^{11} $cm^{-2}s^{-1}$ with a spread of ±30%. The results of Mount et al. (1980) and Mount and Rottman (1981) for high solar activity give an integrated irradiance of $1.3\text{-}1.5 \times 10^{12}$ $cm^{-2}s^{-1}$, or a ratio of maximum to minimum of 1.4 to 1.7 when data from similar instruments are compared. The plage model of Cook et al. (1980) and Brueckner (1981) suggests a ratio of 1.3 with a statistical uncertainty of ±30%, which is in good agreement with the measurements. It is clear that the irradiance between 135 and 175 nm shows a substantial variability over the solar cycle; however, in view of the discrepancies among irradiance data taken near solar minimum, the absolute values must be considered as certain to no more than ±25 to 30%.

THE SPECTRAL REGION 175 TO 200 nm

Several independent data sets exist for this wavelength region. These are compared in Figure B-2 which gives the ratio of several measured irradiances to those of Samain and Simon (1976) which refer to a quiet solar disk. Differences at the shorter wavelengths may represent true solar variations. In particular, the data of Mount et al. (1980) and Mount and Rottman (1981) refer to

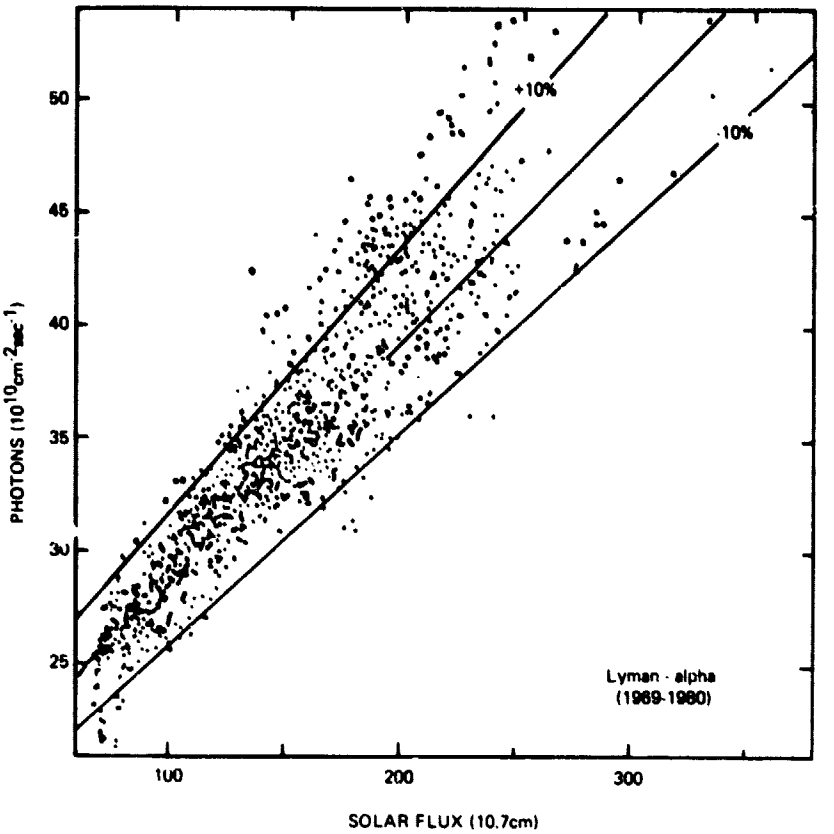

Figure B-1. Variation of the solar Lyman-alpha irradiance with the 10.7 cm radio flux. Measurements are from Vidal-Madjar (1975) and Hinteregger (1981) as compiled by Bossy and Nicolet (1981).

Table B-1
Observed Solar Irradiance Integrated Over the Spectral Range 135 to 175 nm

Date of Observation	10.7 cm flux	Irradiance (photons $cm^{-2}s^{-1}$)	Reference
2 November 1973	84	5.7×10^{11}	Heroux and Higgins (1977)
23 April 1974	74	5.2×10^{11}	Heroux and Higgins (1977)
13 December 1972	111	8.7×10^{11}	Rottman (1981)
30 August 1973	91	7.7×10^{11}	Rottman (1981)
28 July 1975	75	8.2×10^{11}	Rottman (1981)
18 February 1976	70	1.0×10^{12}	Rottman (1981)
9 March 1977	80	1.0×10^{12}	Rottman (1981)
5 June 1979	224	1.5×10^{12}	Mount et al. (1980)
15 July 1980	218	1.3×10^{12}	Mount and Rottman (1981)

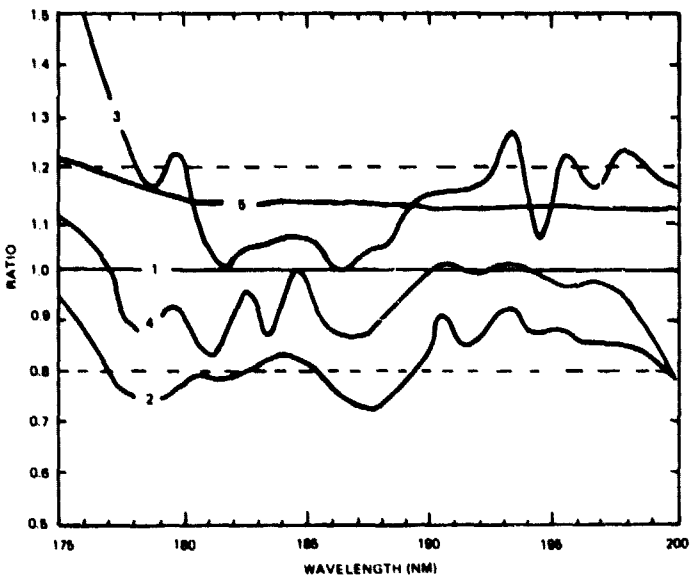

Figure B-2. Observed solar irradiance in the spectral range 175 to 200 nm expressed as ratios relative to Samain and Simon (1976). Dashed lines indicate a ± 20% range. The numbering is as follows:
1 = Samain and Simon (1976), 2 = Brueckner et al. (1976), 3 = Mount and Rottman (1981)
4 = Heath (1980), 5 = Prediction of plage model of Cook et al. (1980) for R_Z = 200 and the quiet Sun irradiance of Samain and Simon (1976).

solar maximum conditions. At wavelengths greater than 180 nm the results of Samain and Simon (1976), Brueckner et al. (1976), Mount et al. (1980), Mount and Rottman (1981) and the Nimbus 7 SBUV measurements of Heath (1980), generally agree to within 20%. The plage model of Cook et al. (1980) and Brueckner (1981) suggests irradiances near solar minimum which are smaller than those for a very large solar maximum, Zurich sunspot number R_Z = 320, by factors of 1.3, 1.2 and 1.2 at the wavelengths 176, 182, and 202 nm respectively. At 210 nm and longer wavelengths, only a low contrast exist between the background solar disk and plage regions and, hence, the plage model here predicts a variability of less than 1 to 2%.

The reference spectra appear in Table B-2 which contains the following information. The data of Samain and Simon (1976) are given as representative of solar minimum conditions while the values of Mount and Rottman (1981) are characteristic of the solar maximum in 1979. A reasonable error bar on both sets is ±20%. Reference to Figure B-2 shows that, when these uncertainties are included, the data by themselves cannot be taken to support a variation with solar activity since the error bars overlap. However, the plage model of solar variability provides a predictive tool based on a specific physical mechanism. For additional reference, Table B-2 contains a solar maximum spectrum generated from the Samain and Simon (1976) results using the plage model for R_Z = 200 which is characteristic of 1979. Comparison of the Mount and Rottman (1981) data with this computed spectrum shows an average difference of 2.4% with a one standard deviation spread of 11.5%. Because the full-disk irradiance varies with the number of active regions, the values for solar maximum presented in Table B-2 refer only to 1979. The emission at the maximum of one solar cycle generally will differ from that at other maxima. In the absence of longer term variability, not accounted for by the number of active regions, the irradiances at different solar minima will be similar.

Table B-2
Reference Solar Spectral Irradiance for Wavelengths 175-200 nm
Error Bars on Measured Spectra are ± 20 Percent.

Wavelength Interval (nm)	Solar Minimum[1] Irradiance (photons $cm^{-2}s^{-1}$)	Solar Maximum[2] Irradiance (photons $cm^{-2}s^{-1}$)	Computed[3] Solar Maximum Irradiance (photons $cm^{-2}s^{-1}$)
175.0-176.0	0.74×10^{11}	1.22×10^{11}	0.89×10^{11}
176.0-177.0	0.85	1.39	1.01
177.0-178.0	1.15	1.42	1.34
178.0-179.0	1.32	1.54	1.52
179.0-180.0	1.29	1.60	1.48
180.0-181.0	1.54	1.63	1.75
181.0-182.0	2.00	2.01	2.27
182.0-183.0	1.86	1.94	2.10
183.0-184.0	1.97	2.05	2.23
184.0-185.0	1.66	1.80	1.88
185.0-186.0	1.91	2.05	2.16
186.0-187.0	2.37	2.37	2.68
187.0-188.0	2.66	2.77	3.01
188.0-189.0	2.80	2.91	3.16
189.0-190.0	2.93	3.31	3.31
190.0-191.0	2.94	3.41	3.32
191.0-192.0	3.33	3.86	3.76
192.0-193.0	3.48	4.15	3.93
193.0-194.0	2.54	3.31	2.87
194.0-195.0	4.46	4.85	5.04
195.0-196.0	4.27	5.25	4.83
196.0-197.0	4.86	5.62	5.49
197.0-198.0	4.87	6.13	5.50
198.0-199.0	4.92	6.07	5.56
199.0-200.0	5.53	6.54	6.25

[1]Data of Samain and Simon (1976) for a quiet solar disk.

[2]Data of Mount and Rottman (1981).

[3]Computed from the plage model of Cook et al. (1980) for $R_Z = 200$ using the quiet sun results of Samain and Simon (1976).

THE SPECTRAL REGION 220 TO 330 nm

The only measurement of solar irradiance during solar cycle 20 which covered the wavelength range corresponding to the Hartley bands of ozone was performed by Broadfoot (1972) in June 1970. Irradiance values from 210 to 320 nm were published with a quoted accuracy of ±10% and a resolution of 0.3 nm. Observations at several discrete wavelengths were made in the same spectral range by the BUV spectrometer on board the Nimbus 4 satellite and published by Heath (1973). The bandpass of this latter instrument was 1 nm making difficult an accurate comparison with Broadfoot's data but the agreement seems reasonably good. On the other hand, Simon (1974) reported irradiance observations from 196 to 230 nm from a balloon-borne spectrometer with a bandpass of 0.6 nm which are from 30 to 15% lower than those published by Broadfoot (1972). The quoted accuracy is ±20%. The same balloon-borne spectrometer yielded irradiance data beyond 284 nm (Simon, 1975) with an accuracy of ±15% and the same resolution. The agreement with Broadfoot is good up to 305 nm. It should be mentioned that Broadfoot (1972) quoted larger uncertainties between 300 and 320 nm than at shorter wavelengths. Beyond 200 nm, other measurements performed from a Convair Jet aircraft were made by Arvesen et al. (1969) with a quoted accuracy of 25% at 300 nm. Disagreements reaching 40% appear between the data of Arvesen et al. (1969) and those of Broadfoot (1972) in the wavelength interval 300 to 320 nm, very important for the formation of $O(^1D)$ from the photodissociation of O_3. The values of Simon (1975) have been widely accepted as more reliable in this interval.

Since 1976, corresponding to the beginning of solar cycle 21, several measurements of the solar irradiance have been performed beyond 200 nm. They include observation by means of the Nimbus 7 satellite (Heath, 1980), rockets (Mount et al., 1980; Mount and Rottman, 1981; Mentall et al., 1981) and stratospheric balloons (Simon et al., 1981a,b). Dates, wavelength intervals and quoted accuracies for most of these appear in Table B-3. Figure B-3 presents the ratios of different measured irradiance values integrated over 5 nm intervals from 210 to 240 nm taking as a reference the data obtained by Heath (1980) from Nimbus 7. The 5 nm interval has been chosen to reduce the effect of the different spectrometer resolutions on irradiance values. The data of Simon (1974) are not presented in this figure for the sake of clarity, however, they agree with his more recent values to ±5% in this wavelength range (Simon et al., 1981a,b). Systematic divergences clearly appear between most of the measurements and are probably due to experimental errors. Differences between the balloon flights do not exceed 12%. The two last flights are in very close agreement, within 5%, with the data obtained by Heath (1980). They confirm that values of Broadfoot (1972) should be lowered by at least 25% in this wavelength range. The lowest values of Mount et al. (1980) do not seem reliable because they are not confirmed by the last rocket flight reported by Mount and Rottman (1981), using a similar spectrometer.

New measurements between 240 and 270 nm include those of Heath (1980), Mount and Rottman (1981) and Mentall et al. (1981). All are systematically lower in this wavelength interval than those of Broadfoot (1972). They diverge by 15% between 240 and 250 nm and agree quite well around 270 nm.

Figure B-4 presents the comparison of irradiance values integrated over 5 nm between 270 and 330 nm, taking as a reference the Nimbus 7 data of Heath (1980). The agreement between all the observations is rather good (±10%) up to 295 nm. Beyond this wavelength, the data of Mount and Rottman (1981) become significantly lower than the others such as those of Broadfoot (1972) longward of 305 nm. Some balloon observations exhibit discrepancies of up to 15% at longer wavelengths, but the results of Simon (1981a,b) agree with those of Heath (1980) to within 5%.

Table B-3
UV Solar Irradiance Observations Beyond 200 nm

Reference	Date of Observation	Wavelength Interval (nm)	Vehicle	Accuracy
Arvesen et al. (1969)	Aug. - Nov. 1967	300 - 2500	aircraft	± 25 - ± 3%
Broadfoot (1972)	June 15, 1970	210 - 320	rocket	± 10%
Simon (1975)	Sept. 23, 1972 May 16, 1973	285 - 355	balloon	± 15%
Heath (1980)	Nov. 7, 1978	160 - 400	satellite	± 10 - ± 3%
Mount et al. (1980)	June 7, 1979	120 - 256	rocket	± 15%
Neckel and Labs (1981)	1960s	330 - 1248	ground	± 1.5 - ± 1%
Simon et al. (1981a, b)	July 1, 1976 July 7, 1977 Sept. 14, 1979 June 24, 1980	270 - 330	balloon	± 10%
Mount and Rottman (1981)	July 15, 1980	120 - 318	rocket	± 15%
Mentall et al. (1981)	Sept. 15, 1980	200 - 330 nm	rocket	± 15%

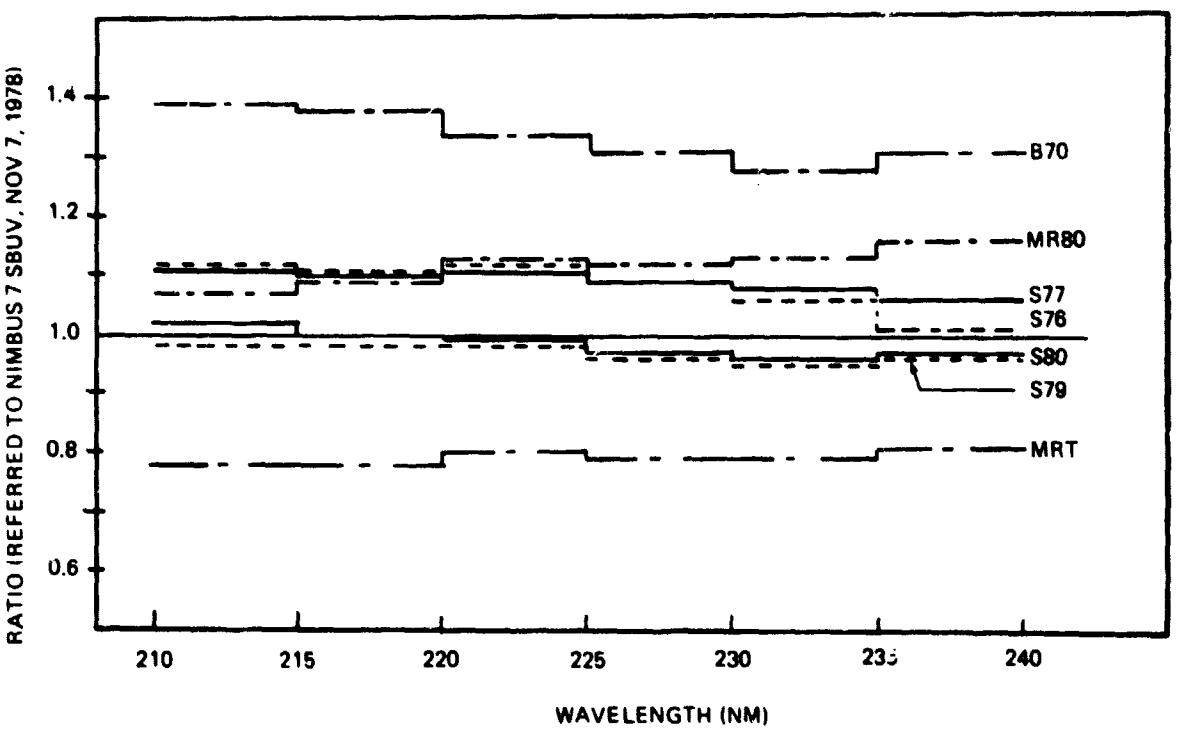

Figure B-3. Observed solar irradiance in the spectral range 210 to 240 nm expressed as ratios relative to the Nimbus 7 data of Heath (1980). Values are integrated over 5 nm intervals. The labeling is as follows: B70 = Broadfoot (1972), MR80 = Mount and Rottman (1981), S77, S76, S80, S79 = Simon et al. (1981a, b), MRT = Mount et al. (1980).

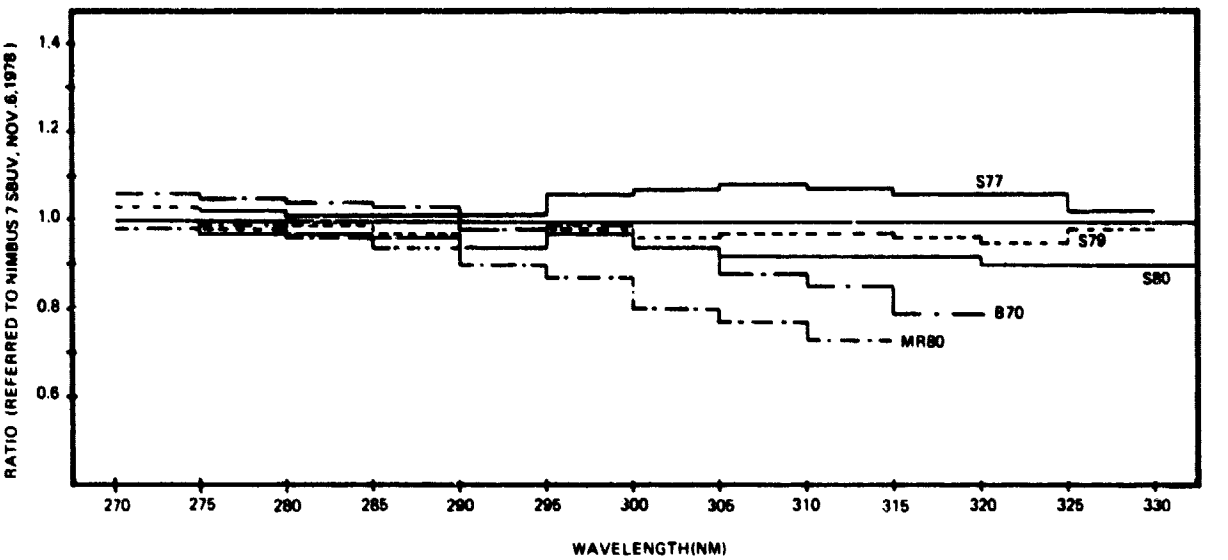

Figure B-4. Observed solar irradiance in the spectral range 270 to 330 nm expressed as ratios relative to the Nimbus 7 data of Heath (1980). Values are integrated over 5 nm intervals. The labeling is as follows: S77, S79, S80 = Simon et al. (1981a,b), B70 - Broadfoot (1972), MR80 = Mount and Rottman (1981).

Tables B-4 and B-5 contain the reference spectrum based on the data of Heath (1980). The error bar near 200 nm is ±15%, decreasing to ±10% near 300 nm. This spread encompasses both instrumental error as well as any true solar variability.

THE SPECTRAL REGION 330 TO 852.2 nm

Two sets of data cover this wavelength range, namely those of Arvesen et al. (1969) and those of Neckel and Labs (1981) which supersede the data published by Labs and Neckel (1970). The latest values are based on observations obtained during the 1960s from a high mountain observatory with a 2 nm resolution. They are probably the most reliable observations in the visible and their quoted accuracy is better than ±2%.

The aircraft data of Arvesen et al. (1969) cannot be directly adopted for several reasons: first, their wavelength scale has to be adjusted below 400 nm to align the Fraunhofer lines with their known positions. Second, the data suffer from uncertainties due to changes in the spectral irradiance scale of the National Bureau of Standards in 1973. Third, the solar constant value of 139 mW cm^{-2} deduced from their observations is larger than the value generally adopted of 137 mW cm^{-2} based on the recent observations of Willson et al. (1981). Consequently, the irradiance values of Arvesen et al. (1969) have to be adjusted either by comparison with the data of Neckel and Labs (1981) or the accepted solar constant. Both methods produce results which lie within ~3% of each other to wavelengths beyond 400 nm.

The reference spectrum of Table B-5 is based on the data of Heath (1980) to 330 nm and the data of Arvesen et al. (1969) adjusted to a solar constant of 137 mW cm^{-2} at longer wavelengths. The accuracy in the visible region is better than ±3% but degrades toward the ultraviolet to ±10%. Any long term variability in this spectral region cannot be detected in the available irradiance data buy may manifest itself via measurements of the solar constant.

Table B-4
Reference Solar Spectral Irradiance for Wavelengths 200.0-307.7 nm
See Text for Discussion of Error Bars.

Wavenumber Interval (cm^{-1})	Wavelength Interval (nm)	Solar Irradiance (photons $cm^{-2}s^{-1}$)
50,000-49,500	200.0-202.0	1.40×10^{12}
49,500-49,000	202.0-204.1	1.69
49,000-48,500	204.1-206.2	2.07
48,500-48,000	206.2-208.3	2.52
48,000-47,500	208.3-210.5	4.21
47,500-47,000	210.5-212.8	7.23
47,000-46,500	212.8-215.0	7.79
46,500-46,000	215.0-217.4	8.45
46,000-45,500	217.4-219.8	1.05×10^{13}
45,500-45,000	219.8-222.2	1.19
45,000-44,500	222.2-224.7	1.51
44,500-44,000	224.7-227.3	1.33
44,000-43,500	227.3-229.9	1.31
43,500-43,000	229.9-232.6	1.51
43,000-42,500	232.6-235.3	1.32
42,500-42,000	235.3-238.1	1.50
42,000-41,500	238.1-241.0	1.34
41,500-41,000	241.0-243.9	2.02
41,000-40,500	243.9-246.9	1.82
40,500-40,000	246.9-250.0	1.88
40,000-39,500	250.0-253.2	1.83
39,500-39,000	253.2-256.4	2.25
39,000-38,500	256.4-259.7	4.65
38,500-38,000	259.7-263.2	4.44
38,000-37,500	263.2-266.7	1.07×10^{14}
37,500-37,000	266.7-270.3	1.18
37,000-36,500	270.3-274.0	1.08
36,500-36,000	274.0-277.8	1.04
36,000-35,500	277.8-281.7	7.54×10^{13}
35,500-35,000	281.7-285.7	1.48×10^{14}
35,000-34,500	285.7-289.9	2.17
34,500-34,000	289.9-294.1	3.46
34,000-33,500	294.1-298.5	3.39
33,500-33,000	298.5-303.0	3.24
33,000-32,500	303.0-307.7	4.40

Table B-5
Reference Solar Spectral Irradiance for Wavelengths 307.5-852.5 nm (Values are Irradiance Integrated Over 5 nm Centered on Wavelength Given) See Text for Discussion of Error Bars.

Wavelength (nm)	Solar Irradiance (photons $cm^{-2}s^{-1}$)	Wavelength (nm)	Solar Irradiance (photons $cm^{-2}s^{-1}$)
310	4.95×10^{14}	530	2.55×10^{15}
315	5.83	535	2.51
320	6.22	540	2.49
325	6.96	545	2.55
330	8.61	550	2.53
335	8.15	555	2.54
340	8.94	560	2.50
345	8.44	565	2.57
350	8.69	570	2.58
355	9.14	575	2.67
360	8.23	580	2.67
365	1.07×10^{15}	585	2.70
370	1.08	590	2.62
375	9.72×10^{14}	595	2.69
380	1.11×10^{15}	600	2.63
385	8.98×10^{14}	605	2.68
390	1.18×10^{15}	610	2.66
395	9.34×10^{14}	615	2.59
400	1.69×10^{15}	620	2.69
405	1.70	625	2.61
410	1.84	630	2.62
415	1.97	635	2.62
420	1.95	640	2.63
425	1.81	645	2.60
430	1.67	650	2.55
435	1.98	655	2.48
440	2.02	660	2.57
445	2.18	665	2.61
450	2.36	670	2.61
455	2.31	675	2.62
460	2.39	680	2.62
465	2.38	685	2.57
470	2.39	690	2.52
475	2.44	695	2.60
480	2.51	700	2.58
485	2.30	705	2.52
490	2.39	710	2.51
495	2.48	715	2.48
500	2.40	720	2.45
505	2.46	725	2.48
510	2.49	730	2.45
515	2.32	735	2.44
520	2.39	740	2.39
525	2.42	745	2.40

Table B-5. Reference Solar Spectral Irradiance for Wavelengths 307.5-852.5 nm (continued)

Wavelength (nm)	Solar Irradiance (photons $cm^{-2}s^{-1}$)	Wavelength (nm)	Solar Irradiance (photons $cm^{-2}s^{-1}$)
750	2.41×10^{15}	800	2.27
755	2.40	805	2.27
760	2.38	810	2.20
765	2.34	815	2.22
770	2.32	820	2.18
775	2.30	825	2.20
780	2.33	830	2.14
785	2.34	835	2.14
790	2.29	840	2.13
795	2.29	845	2.09
		850	2.05

THE SOLAR CONSTANT

The mean value of the solar constant is 136.831 mW cm^{-2} (Willson et al. 1981). Short term variations show average amplitudes of ±0.05%. Up to 0.2% decreases in the solar constant over a 7-day period have been observed and are correlated with the development of sunspot groups. Any long term changes in the solar constant are still highly speculative.

CONCLUSIONS AND FUTURE DIRECTION FOR SOLAR IRRADIANCE MEASUREMENTS

Two basic problems remain concerning our knowledge of the solar irradiance values presently used for studies of atmospheric chemistry.

(1) The absolute value for solar irradiance is known with an accuracy of ±30% at the shortest wavelength, 120 nm, and improves to ±10% at 300 nm. A factor of two improvement in accuracy is desirable if the irradiance values are to be useful in validating photochemical models by comparing their predictions with trace gas measurements.

(2) Our knowledge of solar variability is still masked by insufficient relative accuracy and precision in available observations. Satellite observations between 120 and 400 nm give evidence of a solar rotation effect over time periods of months, however, a solar cycle variability above 200 nm is not obvious when irradiance data are examined in light of overall error budgets. Only at wavelengths less than 200 nm is the existence of a solar cycle variability well-established. However, its magnitude is uncertain.

To overcome these observational difficulties, the following improvements are required:

(1) Available standards must be improved. Present ultraviolet transfer standards, both radiance and irradiance, have inherent uncertainties as large as ±10% and discrepancies between standards often exceed the stated accuracies. Widespread use of synchrotron radiation (e.g., the NBS SURF II facility) is likely to improve the absolute accuracy of the primary standard to a range of ±1 to 2% for future measurements.

(2) It is essential that a stable reference source be maintained over extended periods, at least over a solar cycle, to ensure continuity of instrument calibration programs.

(3) Observers must be encouraged to coordinate and intercompare their observations. A standard format for error budget analysis would validate the agreements or disagreements.

(4) The close symbiotic relationship between rocket, balloon and satellite experiments must be continued and improved. Long-term drifts in the satellite sensitivity must be determined by frequent rocket, balloon, and shuttle observations. On the other hand, quick "snap-shots" of the Sun must be interpreted with the aid of satellite monitoring to filter short and intermediate term solar variations. The future use of the space shuttle will improve solar irradiance measurements considerably over those obtained by sounding rockets.

(5) To obtain reliable information from which to estimate the ultraviolet irradiance at various time in the solar cycle, continuous monitoring is essential.

APPENDIX C

STRATOSPHERIC INSTRUMENTS AND ANALYSES

GROUND BASED INSTRUMENTS

DOBSON OZONE SPECTROPHOTOMETER

The instrument contains (a) a double monochromator for isolating two suitable wavelengths, (b) a photomultiplier and amplifier, and (c) two optical wedges whose position (and therefore absorption) is controlled by a graduated dial for measuring the relative intensities of these wavelengths. The two wavelengths fall on to the same photomultiplier, but a rotating shutter admits first one wavelength and then the other. By means of the optical wedges, the stronger wavelength is reduced in intensity until the photomultiplier gives the same current for each wavelength. After suitable calibration the position of the optical wedges will give the relative intensities of the two wavelengths.

The purpose of the instrument is to measure the total amount of ozone. This is deduced from the measured reduction in the intensity of sunlight in its passage through the atmosphere. Since it is much easier to measure the relative absorption of two wavelengths than the absolute absorption of one wavelength, two wavelengths are used having very different absorption coefficients. The pairs in common use are: A (305.5 and 325.4 nm), B (308.8 and 329.1 nm), C (311.45 and 332.4 nm), D (317.6 and 339.8 nm) and C' (332.4 and 453.6 nm). Measurements may be made from the direct Sun, the clear blue zenith sky, or from the cloudy zenith sky. Observations are archived by the Atmospheric Environment Service, Downsview, Ontario, Canada.

Vertical profiles of ozone may be deduced from "Umkehr" observations on the zenith blue sky for solar zenith distances between 36° and 90°. The inversion of the observations in terms of ozone profiles is done by the Atmospheric Environment Service. For a recent discussion of the status of methods for estimating total ozone and ozone profiles from Dobson data, see Mateer, 1980.

In Table C-1 are listed stations for which total ozone observations are being made as of 1980, with an indication of the length and completeness of the data set. In Table C-2 are listed the stations currently making Umkehr observations.

FILTER OZONOMETER (M-83)

This instrument currently is a two-channel filter photometer with nominal center wavelengths at 299.0 nm (22.5 nm full width at half power) and at 324.7 nm (15.0 nm full width at half power). A photocell is used for direct sun observations; a photomultiplier for observation of the zenith sky. Information on stations in operation as of 1980 is included in Table C-1.

OZONESONDES (SMALL BALLOONS)

Three Brewer-type electrochemical instruments are presently available for routine operation: the MAST sonde, instruments produced in the German Democratic Republic, and those produced in India. Two Komhyr types are available: the ECC and the KC-Japan. Stations in operation as of 1980 are listed in Table C-3.

Table C-1
Total Ozone Stations in Operation as of 1980

Station	Initial Year (since 1958)	Months of Missing Data
North Temperate		
Europe		
Aarhus	1958	12
Arosa	1958	2
Belsk	1963	2
Biscarrosse	1976	1
Bracknell (Camborne)	1958	11
Bucharest	1980	0
Budapest	1967	40
Cagliari	1958	4
Cairo	1978	0
Hohenpeissenberg	1968	0
Hradec Kralove	1961	1
Lerwick	1958	15
Lisbon	1968	10
Magny-Les-Hameaux	1980	0
Oslo	1978	0
Potsdam	1964	11
Sestola	1977	0
Uccle	1973	3
Vigne de Valle	1958	0
Casablanca	1971	24
North America		
Bismark	1963	3
Boulder	1964	2
Caribou	1963	4
Churchill	1965	3
Edmonton	1958	2
Goose Bay	1962	1
Nashville	1963	3
Toronto	1960	5
Wallops Island	1972	1
White Sands	1972	0
Japan		
Kagoshima	1958	3
Naha	1974	0
Sapporo	1958	0
Tateno	1958	0
India-Pakistan		
Mount Abu	1958	3
New Delhi	1958	0
Poona	1973	5
Quetta	1968	9
Srinagar	1964	6
Varanasi	1964	1

Table C-1
Total Ozone Stations in Operation as of 1980 (Continued)

Station	Initial Year (since 1958)	Months of Missing Data
China		
Kunming	1980	0
Shiangher	1979	2
Soviet Union (M-83)		
Alma Ata	1958	11
Ashkhabad	1962	9
Bolshaya Elan	1963	14
Dikson Island	1958	100
Dushanbe	1963	7
Irkutsk	1960	9
Kiev	1960	19
Kuybyshev	1962	5
Leningrad	1958	30
Moscow	1962	12
Murmansk	1962	25
Nagaevo	1962	40
Odessa	1962	4
Omsk	1962	4
Riga	1961	26
Sverdlovsk	1962	4
Vladivostok	1962	13
Yakutsk	1962	33
North Polar		
Barrow	1974	25
Resolute	1958	26
Reykjavik	1958	70
Tropics		
Bangkok	1978	10
Cairns (Darwin)	1966	7
Huancayo	1964	1
Kodaikanal	1958	4
Mahe	1976	0
Manila	1979	0
Mauna Loa	1961	0
Mexico City	1974	6
St. Helena	1977	0
Samoa	1976	0
Singapore	1979	0
South Temperate		
Aspendale	1958	0
Brisbane	1958	0
Buenos Aires	1966	1

Table C-1
Total Ozone Stations in Operation as of 1980 (Continued)

Station	Initial Year (since 1958)	Months of Missing Data
South Temperate (Continued)		
Hobart	1967	16
Invercargill	1970	13
Macquarie Island	1963	3
Perth	1969	1
South Polar		
Amundsen Scott	1962	104
Syowa	1966	78

Table C-2
Umkehr Stations in Operation as of 1980

Station	Initial Year (since 1958)	Months of Missing Data
Europe		
Arosa	1961	6
Belsk	1963	46
Cairo	1978	13
Lisbon	1967	39
North America		
Boulder	1978	1
Edmonton	1974	18
Japan		
Kagoshima	1958	88
Naha	1976	31
Sapporo	1958	96
Tateno	1958	23
India		
Mount Abu	1964	30
New Delhi	1965	57
Poona	1975	27
Srinagar	1976	14
Varanasi	1964	72
Australia		
Aspendale	1958	24
Brisbane	1959	22
Macquarie Island	1961	20

Goose Bay and Churchill have reported old data. But no data for 1979 or 1980.

Table C-3
Ozonesonde Stations in Operation as of 1980

Station	Initial Year (since 1958)	Months of Missing Data
North America		
Churchill	1973	0
Edmonton	1973	0
Cold Lake	1977	26
Goose Bay	1969	0
Palestine	1977	18
Toronto	1976	26
Wallops Island	1970	26
Europe		
Biscarrosse	1976	0
Hohenpeissenberg	1966	0
Legionowo	1980	0
Lindenberg (Tempelhof)	1967	11
Thalwil/Payerne	1968	0
Uccle	1965	20
North Polar		
Resolute	1966	5
Tropics		
Natal	1979	2
Australia		
Aspendale	1965	6
Japan		
Kagoshima	1968	19
Sapporo	1968	35
Tateno	1968	23

SATELLITE INSTRUMENTS

BUV (BACKSCATTER ULTRAVIOLET SPECTROMETER)

The Nimbus 4 Backscatter Ultraviolet (BUV) Spectrometer experiment was designed to monitor the vertical distribution and total amount of atmospheric ozone on a global scale by measuring the intensity of UV radiation backscattered by the Earth/atmosphere system in the 250 to 380 nm spectral region. The primary instrumentation consisted of a double monochromator containing all reflective optics and a photomultiplier detector. The double monochromator was composed of two Fastie-Ebert instruments in tandem. Each had a 64 by 64 mm grating with 2400 lines per mm; the triangular slits were 1.0 mm full width at half-maximum. Light from a 0.05 steradian solid angle (subtending a square of about 200 km on the Earth's surface from a satellite altitude of about 1100 km) entered the nadir pointing instrument through a depolarizing filter. A motor-driven cam stepped the gratings to monitor the intensity at 12 different wavelength bands. For ground reflectivity, a filter photometer measured the UV radiation in an ozone-free absorption area near 380 nm. Signals from both units were read by separate range-switching electrometers. During each data frame (of 32 s duration) the monochromator measured the intensity of the UV radiation in each of the 12 wavelength bands while the photometer simultaneously measured the UV intensity in a single wavelength band. The dwell time at each wavelength was 1.8 s; during this interval, four analog UV intensity measurements were taken at 400 ms intervals in addition to an integrated pulse count measurement of the UV intensity and energetic particle flux. Once each orbit, a diffuser plate deployed to monitor the Sun directly. Total ozone was obtained from data at 312.5 and 339.8 nm; the vertical distribution was obtained by mathematical inversion of data for wavelengths between 273.5 and 305.8 nm. For a complete description of the BUV experiment, see Section 7 in The Nimbus IV User's Guide, available from the NSSDC.

HIRS (HIGH RESOLUTION INFRARED RADIATION SOUNDER)

The Nimbus 6 High Resolution Infrared Radiation Sounder (HIRS) supported the GARP data test set by providing vertical temperature profiles twice daily on a global basis, extending up to approximately 40 km, and information on the water vapor distribution in the troposphere. The HIRS measured radiances primarily in five spectral regions -- (1) seven channels near the 15-micrometer CO_2 absorption band, (2) two channels in the IR window, 11.1 and 3.7 micrometers, (3) two channels in the water vapor absorption band, 8.2 and 6.7 micrometers, (4) five channels in the 4.3-micrometer band, and (5) one channel in the visible 0.69-micrometer region. The sounder consisted of a Cassegrain telescope, scanning mirror, dichroic beam splitter, filter wheel, chopper, and associated electronics. The HIRS scanned the Earth's surface in a plane normal to the spacecraft's orbital path with a maximum scan angle of 30° to either side of nadir.

IRIS (INFRARED INTERFEROMETER SPECTROMETER)

This is a Twyman-Green modification of Michelson interferometer spectrometer operating in the 6.5 to 40 micrometer wavelength region. Radiation from a cone of atmosphere, whose base on the surface of the Earth is a circle 98 km in diameter, is reflected into the instrument from a plane mirror which rotates to provide image motion compensation. The radiation is split into two beams, one of which is reflected from a moving mirror, recombined and focused onto a bolometer detector. Interference effects result from the path length differences in the two beams as the mirror moves. It travels about 2 mm in 13 seconds to give an interferogram which is recorded on tape. Observations are begun 16 seconds apart in which time the spacecraft travels about 120 km; thus, there is no overlap in successive observations. After recording 14 interferograms, two calibration observations are made, one for a reference blackbody at 300 K and

one for outer space. A Fourier transformation, performed by digital computer, must be made on each telemetered interferogram to produce a spectrum. Then, to relate this to atmospheric conditions, appropriate spectra absorption regions must be chosen and employed in an inversion of the radiative transfer equations.

ITPR (INFRARED TEMPERATURE PROFILE RADIOMETER)

ITPR measures IR radiation in four spectral intervals of the 15-micrometer carbon dioxide band, a spectral interval of the rotational water vapor band, and in the 2.8 and 11-micrometer spectral windows. Coverage is cluster-sampled in three clusters of 10 by 14 instantaneous fields-of-view per cluster distributed symmetrically about either side of nadir but staggered by cluster in the orbital direction. Each cluster matrix contains 140 resolution elements. Measurements in the carbon dioxide and water vapor absorption bands will be used to calculate the temperature profiles and the total water vapor in the lower stratosphere and troposphere by inverting the radiative transfer equation using numerical and mathematical techniques. The statistical fluctuations of the radiation data from the independent resolution elements will be used in the solution to account for the attenuation of the clouds in addition to the two window measurements, which should enable cloud contamination of the radiances to be detected and eliminated, thus permitting actual determination of temperature profiles down to the Earth's surface.

LIMS (LIMB INFRARED MONITOR OF THE STRATOSPHERE)

The objective of the Limb Infrared Monitor of the Stratosphere (LIMS) experiment is to map the vertical profiles of temperature and the concentration of ozone, water vapor, nitrogen dioxide, and nitric acid in the lower to middle stratosphere range, with extension to the stratopause for water vapor and into the lower mesosphere for temperature and ozone. The instrument has a six-channel infrared radiometer that incorporates Hg-Cd-Te detectors cooled by a two-stage solid cryogen cooler. The radiometer maps vertical profiles of thermal IR emission coming from the horizon in six bands. Two of the channels are used to determine radiance profiles of emission by CO_2. These profiles are mathematically inverted to obtain temperature versus pressure. The inferred temperature profile, together with radiance profiles in the other spectral bands, are then used to infer the vertical distribution of trace constituents.

The temperature is determined to an accuracy of about 1.5 K. Constituent concentrations are determined with an accuracy of about 20%, with the exception of NO_2 which is determined to within about 50%. Instantaneous vertical field-of-view at the horizon is 2 km for the temperature, ozone, and nitric acid channels and 4 km for the NO_2 and water vapor channels.

LRIR (LIMB RADIANCE INVERSION RADIOMETER)

The Nimbus 6 Limb Radiance Inversion Radiometer (LRIR) provided calibrated radiance versus altitude profiles by intercepting radiation emanating from an atmospheric path which is tangential to a particular geocentric height. The LRIR sensed radiation in four spectral intervals -- (1) the 14.6- to 15.9-micrometer CO_2 band, (2) the 14.2- to 17.3-micrometer CO_2 band, (3) the 8.8- to 10.1-micrometer ozone band, and (4) the 20- to 25-micrometer water vapor rotational band. Measurements taken in the two CO_2 channels and the water vapor channel were used to calculate global temperature and water vapor profiles in the stratosphere and lower mesosphere. In addition, values of the geostrophic wind up to 1 mbar (approximately 48 km) were derived analytically from the deduced temperature profiles. The radiometer included an optical system, a scanning mirror, choppers, associated electronics and employed an ammonia-methane cooler system for three of the four detector channels. While the deduced

temperature profiles had an root mean square accuracy of ±3 K at heights above 15 km, the values for ozone were accurate to within ±20% at 1 mbar. Water vapor values at the same height were within 50%.

MFR (MULTICHANNEL FILTER RADIOMETER)

The Multichannel Filter Radiometer (MFR), also called Special Sensor H (SSH) is a Vertical Temperature Profile Radiometer (VTPR). The objective of this experiment is to obtain vertical temperature, water vapor, and ozone profiles of the atmosphere to support Department of Defense requirements in operational weather analysis and forecasting. The SSH is a 16-channel sensor with one channel (1022 cm^{-1}) in the 12-micrometer atmospheric window, six channels (747, 725, 708, 695, 676, 668.5 cm^{-1}) in the 15-micrometer CO_2 absorption band, and eight channels (535, 408.5, 441.5, 420, 374, 397.5, 355, 353.5 cm^{-1}) in the 22- to 30-micrometer rotational water vapor absorption band. The experiment consists of an optical system, detector and associated electronics, and a scanning mirror. The scanning mirror is stepped across the satellite subtrack, allowing the SSH to view 25 separate columns of the atmosphere every 32 s over cross track ground swath of 2000 km. While the scanning mirror is stopped at a scene station, the channel filters are sequenced through the field-of-view. The surface resolution is approximately 39 km at nadir. The radiance data are transformed into temperature water vapor and ozone profiles by a mathematical inversion technique. A more complete description of the experiment can be found in the report by Nichols (1975).

PMR (PRESSURE MODULATED RADIOMETER)

The Nimbus 6 Pressure Modulated Radiometer (PMR) experiment took radiometric measurements in the 15-micrometer CO_2 band at altitudes between 45 and 70 km on a global scale. By appropriate mathematical retrieval methods, the temperature structures of the upper stratosphere and lower mesosphere were then deduced. The pressure modulation technique permitted the extension of selective chopping techniques to higher altitudes where the pressure-broadened emission lines in the 15-micrometer CO_2 band became so narrow that conventional spectrometers and interferometers had insufficient spectral resolution. In addition to pressure scanning (in discrete steps), the radiometer also employed Doppler scanning along the direction of flight. The PMR comprised two similar radiometer channels, each consisting of a plane scanning mirror, reference blackbody, pressure modulator cell, and detector assembly. The plane mirror was gold-coated and mounted at 45° on a 90° stepping motor so that the field-of-view of the channel could be directed to space or the internal reference blackbody for inflight range and zero calibration. The motor was mounted on a pair of flexible pivots so that the mirror could be rotated through ±7-1/2° from its rest position to give the required doppler scan. Major components in the pressure modulator cell were a movable piston, a diaphragm, and a magnetic drive coil. The detector assembly consisted of a field lens, a condensing light pipe, and pyroelectric flake bolometer. Each radiometer had a field-of-view that was 20° whole angle across the spacecraft's line-of-flight and 4° whole angle parallel to the line-of-flight.

SAGE (STRATOSPHERIC AEROSOL AND GAS EXPERIMENT)

The objectives of the Stratospheric Aerosol and Gas Experiment (SAGE) are to determine the spatial distribution of stratospheric aerosols and ozone on a global scale. Specific objectives are (1) to develop a satellite-based remote sensing technique for stratospheric aerosols and ozone, (2) to map aerosol and ozone concentrations on a time scale shorter than major stratospheric changes, (3) to locate stratospheric aerosol and ozone sources and sinks, (4) to monitor circulation and transfer phenomena, (5) to observe hemispheric differences, and (6) to investigate the optical properties of aerosols and assess their effects on global climate. The SAGE instrument consists of a Cassegrainian telescope and a detector subassembly which measures the

attenuation of solar radiation at four wavelenths (0.38, 0.45, 0.6, and 1.0 micrometers) during solar occultation. As the spacecraft emerges from the Earth's shadow, during sunrise the sensor will acquire the Sun and measure the attenuation of solar radiation by different atmospheric layers. This procedure is repeated during spacecraft sunset. Two vertical scannings are obtained during each orbit, with each scan requiring approximately 0.5 minute of time to cover the atmosphere above the troposphere. The instrument has a field-of-view of approximately 1 minute of arc which will result in a vertical resolution of less than 1 km.

SAMS (STRATOSPHERIC AND MESOSPHERIC SOUNDER)

The objective of SAMS was to observe emission from the limb of the atmsophere through various pressure modulator radiometers and to determine temperature and vertical concentrations of H_2O, N_2O, CH_4, CO, and NO in the stratosphere and mesosphere to approximately 90 km. Measurements of zonal wind in this region were attempted by observing the Doppler shift of atmospheric emission lines. Radiation from the limb of the atmosphere was incident on a telescope of 15-cm aperture. In front of the telescope a plane mirror scanned the limb, viewed space for calibration, and viewed the atmosphere obliquely to obtain vertical profiles. Three adjacent fields-of-view, each 28 by 2.8 mrad (corresponding to 100 km by 10 km at the limb), focused onto a field-splitting mirror which directed radiation to six detectors. The remaining division into channels was accomplished through dichroic beam splitters. There were seven pressure modulator cells (PMC), two containing CO_2, the remainder N_2O, NO, CH_4, CO, and H_2O. Pressure in the cells could be varied on command by changing the temperature of a small container of molecular sieve material attached to each PMC. The spectral parameters for the H_2O channel were 2.7 micrometers and 25 to 100 micrometers. All other channels lay within the range of 4.1 to 15 micrometers. Within the telescope, a chopper operating at 250 Hz allowed measurement of two separate signals from all detectors, one at 250 Hz and one at the PMC frequency. Comparison of these signals permitted eliminating emission from interfering gases within a particular spectral interval. In front of the chopper a small black body at known temperature could be introduced for calibration.

SAM II (STRATOSPHERIC AEROSOL MEASUREMENT - II)

The objective of SAM II is to map the concentration and optical properties of stratospheric aerosols as a function of altitude, latitude, and longitude. When no clouds are present in the instrument field-of-view (IFOV), the tropospheric aerosols can also be mapped. The instrument, basically a Sun photometer, measures the extinction of solar radiation at 1.0-micrometer wavelength during spacecraft sunrise and sunset. The photometer views a portion of the solar disk with a 5 arc min IFOV and a sampling rate of 50 samples per second. As the spacecraft first views the sunrise, the photometer-pointing axis is depressed approximately 0.52 rad with respect to the spacecraft horizontal. The photometer continues looking at the Sun until its depression angle is on the order of 0.44 rad (approximately 1.4 minutes observing time). Before sunset, the photometer head rotates 3.14 rad in azimuth and views the Sun from a depression of approximately 0.44 to 0.52 rad as the spacecraft orbits to the dark side of the Earth. For the expected high noon orbit, latitudes of between 1.12 and 1.40 rad (64° to 80° latitude) in both hemispheres are scanned for 3 months. The extinction measurements are inverted for the number-density times the aerosol scattering cross section by using the Lambert-Beer Law and assuming the atmosphere to be composed of layers. To determine the stratospheric aerosol optical properties, ground-truth in situ balloon borne aerosol measurements are also made.

SBUV/TOMS (SOLAR AND BACKSCATTER ULTRAVIOLET/TOTAL OZONE MAPPING SYSTEM)

The objectives of the SBUV/TOMS are to determine the vertical distribution of ozone, map the total ozone and monitor the incident solar ultraviolet irradiance and ultraviolet radiation backscattered from the Earth. The SBUV spectrometer measures solar UV that is backscattered by the Earth's atmosphere at 12 wavelengths between 250 and 330 nm with a spectral band pass of 1.0 nm. The instrument field-of-view of 0.20 rad is directed at the nadir. A parallel photometer channel at 340 nm measures the reflectivity of the atmosphere's lower boundary in the same 0.20 rad field-of-view . Both channels also view the Sun for calibration through the use of a diffuser plate deployed near the terminator. The contribution functions for the eight shortest wavelengths are centered at levels ranging from 55 to 28 km and are used to infer the vertical ozone profile. The four longest wavelengths have contribution functions in the troposphere which are used to compute the total ozone amount. The SBUV spectrometer has a second mode of operation that allows a continuous spectral scan from 160 to 400 nm for detailed examination of the solar spectrum and its temporal variations. The TOMS systems, operating in parallel with the SBUV, step scans across a 105° field-of-view normal to the orbital track with an FOV of approximately 0.052 rad. At each scan position the Earth Radiance is monitored at six wavelengths between 310 and 380 nm to infer the total ozone amount. The instrument consists principally of three Ebert-Fastie monochromators, two of which are operated in tandem for stray light rejection. TOMS uses the third monochromator, which is equipped with a spatial scan mechanism at the entrance slit. The signal-to-noise ratio of the SBUV is greater than $5x10^3$. The TOMS signal-to-noise ratio is greater than $1x10^5$.

SCR (SELECTIVE CHOPPER RADIOMETER) (6 CHANNEL)

The Nimbus 4 Selective Chopper Radiometer (SCR) observed the emitted infrared radiation in the 15-micrometer absorption band of carbon dioxide. From these measurements, the temperature of six successive 10-km layers of the atmosphere were determined from Earth or cloudtop level to 60-km height. Height resolution was obtained by a combination of optical multilayer filters and selective absorption of radiation using carbon dioxide-filled cells within the experiment. The SCR had six channels, which were arranged in three units of two. The four lower channels were called single cell channels. The optics of each channel included a cantilever-mounted blade shutter that oscillated at 10 Hz and successively chopped the field-of-view between Earth and space. The chopped radiation was then passed through a 10-cm path length of carbon dioxide, the pressure being set for each channel to define the viewing depth of the atmosphere. Behind the carbon dioxide path was a narrow-band filter, the centers of which were different for each channel, and a light pipe which converged the radiation on a thermistor bolometer detector. To obtain adequate height resolution in the upper layers of the atmosphere, the upper two channels operated on a slightly different principle and were known as double cell channels. The technique consisted of switching the radiation between two half-cells, semicircular in shape and of 1-cm path length, containing different pressures of carbon dioxide. A movable 45° mirror was used in place of the oscillating shutter used in the lower four channels. During one half-period, Earth radiation passed through one half-cell and space radiation through the other. The situation was reversed during the other half-period. The radiation then passed through a light pipe onto a thermistor bolometer detector. Inflight calibration was carried out by viewing of an internal reference blackbody of known temperature prior to the view of space.

SCR (SELECTIVE CHOPPER RADIOMETER) (16 CHANNEL)

The Nimbus 5 Selective Chopper Radiometer (SCR) was designed to: (1) observe the global temperature structure of the atmosphere up to 50 km in altitude, (2) make supporting observations of water vapor distribution, and (3) determine the density of ice particles in cirrus

clouds. To accomplish these objectives, the SCR measured emitted radiation in 16 spectral intervals separated into the following four groups -- (1) eight CO_2 channels between 13.8 and 15.0 micrometers, (2) an IR window channel at 11.1 micrometers and a water vapor channel at 18.6 micrometers, (3) two channels at 49.5 and 133.3 micrometers, and (4) 2.08, 2.59, 2.65, and 3.5 micrometers. From an average satellite altitude of 1100 km, the radiometer viewed a 48-km circle on the Earth's surface. The CO_2 channels measured over a height range similar to the Nimbus 4 SCR but to a greater accuracy.

SIRS B (SATELLITE INFRARED SPECTROMETER)

The instrument, a modification of the SIRS A, is a Fastie-Ebert fixed-grating infrared spectrometer with the following features: (1) a plane, light-collecting mirror to provide one fixed and two variable Earth-viewing angles; (2) a balanced rotating chopping mirror which serves alternatively to collect space radiation, and Earth radiation; (3) a spherical mirror of 0.318 m focal length; (4) a 6.35 cm with 49.2 lines per mm diffraction grating; (5) a set of 14 exit slits with associated interference filters for order limitation, and 14 wedge-immersed or similar thermistor bolometers; and (6) a blackbody radiation source for calibration purposes. The 15-micrometer radiation data is transformed into a single temperature-pressure profile by mathematical inversion. A similar technique yields the altitude profile of water vapor from the 18 to 35-micrometer data. The 11.1-micrometer data compared with a blackbody temperature calibration curve yields surface or cloudtop temperatures. The bands monitored are centered at 11.12, 13.33, 14.01, 14.16, 14.31, 14.45, 14.76, 14.95, 18.82, 22.91, 23.50, 34.31, 33.11, 35.71 micrometers. Data is accumulated in 6-second intervals to give profiles each 80 km along the strip.

TOVS (TIROS OPERATIONAL VERTICAL SOUNDER)

TOVS is an operational vertical sounder system first flown on TIROS-N in 1978 and expected to continue in use on successive NOAA satellites until the late 1980s. It consists of three separate and independent instruments, the data from which may be combined for the computation of atmospheric temperature profiles, humidity and ozone. The three instruments are:

1. The High Resolution Infrared Radiation Sounder (HIRS 2). A filter radiometer using both the 4.3 and 15 μm CO_2 bands for temperature sounding and the 9.6 μm band for total ozone measurement.

2. The Stratospheric Sounding Unit (SSU). A pressure modulated radiometer using selective absorption of incoming radiation in the 15 μm band by three CO_2 filled cells at different pressures. The design is based on techniques used in the earlier Nimbus 6 PMR.

3. The Microwave Sounding Unit (MSU). A passive radiometer with four channels operating in the 50-60 GHz oxygen band.

Although the SSU (provided by the U.K. Meteorological Office) is the prime sounding instrument in the stratosphere, HIRS 2 and MSU also have channels sensitive to radiation originating in the stratosphere.

In addition to the operational processing of all global data at NOAA/NESS, a subset of the data (comprising Earth-located SSU instrumental outputs and radiances calculated from SSU, MSU and HIRS 2 channels with peak responses in the stratosphere) is passed via a data link to the U.K. Meteorological Office where global stratospheric analyses are performed daily about 24 hours in arrears. An archive is maintained including SSU instrument data, processed radiances and derived analyses.

Since all TOVS instruments are side scanning and two satellites are usually in orbit at the same time, this archive provides virtually complete global coverage and observations at four different solar times, thus allowing study of diurnal variations. If archiving is continued throughout the life of the satellite system it will also result in the longest period of stratospheric data obtained with similar instruments.

The channels used for stratospheric temperature retrievals from the TOVS have weighting functions peaking from around 10 to 45 km. (125 to 1.5 mbar). The details are (in order of ascending height) MSU 23: 10 km, HIRS 3: 15 km, MSU 24: 17 km, HIRS 2: 19 km, HIRS 1: 22 km (but extending much higher), HIRS 17: 28 km, SSU 25: 30 km, SSU 26: 38 km, SSU 27: 45 km. This allows effective retrieval of thickness from 100 to 1 mbar.

VTPR (VERTICAL TEMPERATURE PROFILE RADIOMETER)

The ITOS-G Vertical Temperature Profile Radiometer (VTPR) sensed the radiant energy from atmospheric CO_2 in six narrow spectral regions centered at 15.0, 14.8, 14.4, 14.1, 13.8, and 13.4 micrometers. The gross atmospheric water vapor content was determined from measurements centered at 18.7 micrometers. Measurements were taken in the 12.0-micrometer spectral region to determine surface/cloudtop temperatures. The VTPR consisted of an optical system, detector and associated electronics, and a scanning mirror. The mirror scanned the Earth's surface perpendicular to the satellite's orbital path. As each area is scanned, the optical system collected, filtered, and detected the radiation from the Earth and separated it into the eight spectral intervals. The ground area covered by one sample of data was approximately 50 to 50 km. The radiometer operated continuously, taking measurements over every part of the Earth's surface twice a day. The data were recorded throughout the orbit and were played back upon command when the satellite was within communication range of a command and data acquisition station. Ground personnel used the data to compute temperature-pressure profiles to altitudes as high as 30 km. All operational data from this experiment were handled by NOAA and eventually archived at the National Climatic Center, Asheville, North Carolina. Identical experiments were flown on ITOS-D, -E, and -F.

INVESTIGATIONS USING STRATOSPHERIC SATELLITE DATA

ANALYSIS OF SATELLITE TOTAL OZONE DATA

The analysis of total ozone measurements has led to a number of scientific investigations of the variability of total ozone both considered by itself and as related to the changes in other atmospheric phenomena or parameters such as temperature, dynamics, and composition. Studies relating total ozone variability directly to solar flux changes also are being undertaken. Table C-4 summarizes some of the published analyses of total ozone using the IRIS, MFR, TOVS, BUV, SBUV, and TOMS instruments mentioned earlier.

Table C-4
Published Studies of Total Ozone Using Satellite Data

Instrument	Authors (Year)	Title
IRIS	Blackshear and Tolson, 1978	High correlations between variations in monthly averages of solar activity and total atmospheric ozone.
	Hanel et al., 1972	The Nimbus 4 infrared spectroscopy experiment 1. Calibrated thermal emission spectra.
	Keating, 1978	Relation between monthly variations of global ozone and solar activity.
	London and Reber, 1979	Solar activity and total atmospheric ozone
	Prabhakara et al., 1970	Remote sensing of atmospheric ozone using the 9.6 micron band.
	Prabhakara et al., 1976	The Nimbus 4 infrared spectroscopy experiment 3. Observations of the lower stratospheric thermal structure and total ozone.
MFR	Lovill et al., 1978	Total ozone retrieval from satellite Multichannel Filter Radiometer measurements.
	Luther, et al. 1980	Global distribution of total ozone during January and February 1979 as determined from DMSP Multichannel Filter Radiometer measurements.
TOVS	Crosby et al., 1980	Evaluation and comparison of total ozone fields derived from TOVS and SBUV.
BUV, SBUV, TOMS	Crosby et al., 1980	Evaluation and comparison of total ozone fields derived from TOVS and SBUV.
	Fleig et al., 1978	Global total ozone determinations from Nimbus 4 BUV spacecraft data.
	Ghazi, 1974	Nimbus 4 observations of changes in total ozone and stratospheric temperatures during a sudden warming.
	Ghazi, 1980a	Anamolous variations of radiative heating/cooling in the tropical stratosphere.

Table C-4
Published Studies of Total Ozone Using Satellite Data (continued)

Instrument	Authors (Year)	Title
BUV, SBUV, TOMS (continued)	Ghazi, 1980b	Atlas der Globalverteilung des Gesamtozonbetrages nach Satellitenvermungen.
	Ghazi 1980c	Ozone effects on radiative damping in the stratosphere.
	Ghazi and Barnett, 1980	Ozone behaviour and stratospheric thermal structure during southern hemisphere spring.
	Ghazi et al., 1976	A study of satellite observations of ozone and stratospheric temperatures during 1970-1971.
	Ghazi et al., 1979	Acceleration of upper stratospheric radiative damping: Observational evidence.
	Hilsenrath et al., 1979	Seasonal and interannual variations in total ozone revealed by the Nimbus-4 backscattered ultraviolet experiment.
	Hilsenrath and Schlesinger, 1981	Total ozone seasonal and internannual variations derived from the 7 year Nimbus-4 data set.
	A. Miller et al., 1977a	Stratospheric ozone transport during the mid-winter warming of December 1970 - January 1971.
	A. Miller et al., 1977b	Comparison of Backscatter Ultraviolet (BUV) and ground-based total ozone fields for December 1970.
	A. Miller et al., 1978a	Variations in the 100 mb height fields as an indicator of long-term trends of total ozone at individual sampling sites.
	A. Miller et al., 1978b	Verification of Nimbus 4 BUV total ozone data and the requirements for operational satellite monitoring.

Table C-4
Published Studies of Total Ozone Using Satellite Data (continued)

Instrument	Authors (Year)	Title
BUV, SBUV, TOMS (continued)	A. Miller et al., 1979a	Comparison of Backscatter Ultraviolet (BUV) total ozone and vertical profile information with ground-based data and meteorological analyses.
	A. Miller et al., 1979b	Preliminary comparisons of daily total ozone fields derived from SBUV, TOMS and HIRS-2 satellite instruments.
	A. Miller et al., 1979c	Comparison of Backscatter Ultraviolet (BUV) and ground-based total ozone fields for December 1970.
	A. Miller et al., 1979d	Utilization of 100 mb midlatitude height fields as an indicator of sampling effects on total ozone variations.
	A. Miller et al., 1980	Results and analyses of ground-based and satellite ozone observations - A review.
	Tolson, 1981	Spatial and temporal variations of monthly mean total columnar ozone derived from 7 years of BUV data.

ANALYSIS OF OZONE VERTICAL PROFILE DATA

The ozone concentration profile data analysis, like the total ozone data analysis, is a relatively mature activity with many investigations completed, in progress or planned. This should be expected when one considers: (a) the emphasis which has been placed on the importance of stratospheric ozone, beginning with the CIAP program in the early 1970s; (b) the Congressional mandate to government agencies to study the possibility of ozone depletion due to the release of fluorocarbons; and, (c) two of the longest stratospheric satellite data sets, BUV and SBUV, contain information which is applicable to the study of both total ozone and ozone vertical profiles at altitudes above the peak mixing ratio ievel (i.e., about 35 km). Table C-5 lists papers that have been published using ozone profile satellite data.

ANALYSIS OF VERTICAL TEMPERATURE PROFILE DATA

The analysis of the temperature data sets is normally a part of a meteorological analysis or to analysis of the relationships between temperature and some other constituents such as ozone. This is reflected in the data analysis descriptions presented in the following. Table C-6 lists studies that have been published using satellite-derived stratospheric temperature data.

Table C-5
Published Studies of Ozone Profile Satellite Data

Instrument	Authors (Year)	Title
BUV, SBUV	Anderson et al., 1980	LRIR observations of diurnal ozone variation in the mesosphere.
	Gille, 1980	Ozone distributions by infrared limb scanning: Preliminary results from the LRIR.
	Gille et al., 1980c	Observations of the interaction of ozone and dyanmics.
	Gille et al., 1980d	Comparison of near coincident LRIR and OAO-3 measurements of equatorial night ozone profiles.
	Heath et al., 1977	Solar proton event: Influence on stratospheric ozone.
	A. Miller et al., 1979a	Comparison of Backscatter Ultraviolet (BUV) total ozone and vertical profile information with ground-based data and meteorological analyses.
	A. Miller et al., 1980	Results and analyses of ground-based and satellite ozone observations - A review.
LIMS	Gille et al., 1980b	Temperature and composition measurements from the LRIR and LIMS experiments on Nimbus 6 and 7.
	Gille et al., 1980e	The Limb Infrared Monitor of the Stratosphere (LIMS) experiment: Temperature and O_3 results.
	Remsberg et al., 1980	The validation of LIMS ozone profiles using correlative ECC and Dobson data sets.
	Russell et al., 1981	Satellite observation of upper atmosphere O_3 and HNO_3 from the Limb Infrared Monitor of the Stratosphere (LIMS) experiment on Nimbus 7.
SAGE	McCormick et al., 1980	Satellite profile measurements of stratosphereic ozone.
	McCormick et al., 1981b	Stratospheric aerosol and ozone measurements by the SAM II and SAGE satellite sensors.

Table C-6
Some Published Studies Using Satellite-Derived Stratospheric Temperature Data

Instrument	Authors (Year)	Title
IRIS	Hanel et al., 1972	The Nimbus infrared spectroscopy experiment 1. Calibrated thermal emission spectra.
	Prabhakara et al., 1976	The Nimbus 4 infrared spectroscopy experiment 3. Observations of the lower stratospheric thermal structure and total ozone.
SCR, PMR	Aanensen, 1973	The use of Nimbus 4 radiance and radio-sonde data in the construction of stratospheric contour charts.
	Asgeirsson and Stanford, 1977	Systematic deviations of Nimbus-5 atmospheric temperature fields from radio-sonde data over the winter Antarctic.
	Austen et al., 1976	Satellite observations of planetary waves in the mesosphere.
	Austen et al., 1977	Satellite temperature measurements in the 40-90 km region by the Pressure Modulator Radiometer.
	Barnett, 1973a	Remote sounding of the atmosphere.
	Barnett, 1973b	Analysis of stratospheric measurements by the Nimbus IV and V selective Chopper Radiometers.
	Barnett, 1974	The mean meridional temperature behaviour of the stratosphere from November 1970 to November 1971 derived from measurements by the Selective Chopper Radiometer on Nimbus IV.
	Barnett, 1975a	Hemispheric coupling - evidence of a cross-equatorial planetary wave-guide in the stratosphere.
	Barnett, 1975b	Large sudden warming in the southern hemisphere.
	Barnett, 1977	The Antarctic atmosphere as seen by satellites.

Table C-6
Some Published Studies Using Satellite-Derived Stratospheric Temperature Data (continued)

Instrument	Authors (Year)	Title
SCR, PMR (continued)	Barnett, 1980	Satellite measurements of middle atmosphere temperature structure.
	Barnett, 1981	Middle atmosphere climatology.
	Barnett and Walshaw, 1972	Temperature measurements from a satellite: Applications and achievements.
	Barnett et al., 1971	Stratospheric warming observed by Nimbus 4.
	Barnett et al., 1972	The first year of the Selective Chopper Radiometer on Nimbus 4.
	Barnett et al., 1973	Stratospheric observations from Nimbus 5.
	Barnett et al., 1975a	The temperature dependence of the ozone concentration near the stratopause.
	Barnett et al., 1975b	Comparison between radiosonde, rocketsonde and satellite observations of atmospheric temperatures.
	Barnett et al., 1977	Comparison between satellite radiance observations and those derived from a stratospheric numerical model.
	Barnett et al., 1978	Observations of the stratosphere and mesosphere from Nimbus satellites.
	Brown and John, 1979	Vertical penetration of planetary waves into the lower ionosphere.

Table C-6
Some Published Studies Using Satellite-Derived Stratospheric Temperature Data (continued)

Instrument	Authors (Year)	Title
SCR, PMR (continued)	Chapman and McGregor, 1978	The application of complex demodulation to meteorological satellite data.
	Chapman and Miles, 1981	Planetary-scale wave guides in the troposphere and stratosphere.
	Chapman et al., 1974	A spectral analysis of global atmospheric temperature fields observed by the Selective Chopper Radiometer on the Nimbus 4 satellite during the year 1970-1.
	Chiu, 1975	A self contained iterative algorithm for a numerical solution to the radiative transfer equation.
	Coy and Leovy, 1977	A comparison of midwinter stratospheric warmings in the southern and northern hemispheres.
	Crane, 1979a	Aspects of the energetics of the upper stratosphere during the January-February 1973 major sudden warming.
	Crane, 1979b	Annual and semiannual waves in the temperature of the mesosphere as deduced from Nimbus 6 PMR measurements.
	Crane and Barnett, 1977	Energetics of the upper stratosphere during a sudden warming.
	Crane et al., 1980	Mean meridional circulations of the stratosphere and mesosphere.
	Deland, 1977	Evidence of downward propagating planetary-scale waves in the southern hemisphere winter stratosphere.
	Ellis et al., 1970	First results from the Selective Chopper Radiometer on Nimbus 4.

Table C-6
Some Published Studies Using Satellite-Derived Stratospheric Temperature Data (continued)

Instrument	Authors (Year)	Title
SCR, PMR (continued)	Fraser, 1976	The covariance of temperature and ozone due to planetary-wave forcing.
	Fraser and Wratt, 1976	Experimental investigations of ionospheric/stratospheric coupling in southern mid-latitudes - 2. Comparison of mesospheric electron densities and drifts with stratospheric temperatures and winds.
	Ghazi, 1980c	Ozone effects on radiative damping in the stratosphere.
	Ghazi and Barnett, 1980	Ozone behaviour and stratospheric thermal structure during southern hemisphere spring.
	Hartmann, 1976a	The dynamical climatology of the stratosphere in the southern hemisphere during late winter 1973.
	Hartmann, 1976b	The structure of the stratosphere in the southern hemisphere during late winter 1973 as observed by satellite.
	Hartmann, 1976c	Dynamic studies of the southern hemisphere stratosphere.
	Hartmann, 1977a	Comments on "Stratospheric long waves: Comparison of thermal structure in the northern and southern hemispheres".
	Hartmann, 1977b	On potential vorticity and transport in the stratosphere.
	Harwood, 1975	The temperature structure of the southern hemisphere stratosphere: August-October 1971.
	Harwood, 1976	Some recent investigations of the upper atmosphere by remote sounding satellites.

Table C-6
Some Published Studies Using Satellite-Derived Stratospheric Temperature Data (continued)

Instrument	Authors (Year)	Title
SCR, PMR (continued)	Harwood, 1980	Dynamical models of the middle atmosphere for tracer studies.
	Harwood and Pyle, 1975	A two-dimensional mean circulation model for the atmosphere below 80 km.
	Harwood and Pyle, 1977	Studies of the ozone budget using a zonal mean circulation model and linearized photochemistry.
	Harwood and Pyle, 1978	The fluxes of ozone from a zonal mean circulation model of the atmosphere.
	Harwood and Pyle, 1980	The dynamical behaviour of a two-dimensional model of the stratosphere.
	Heasman and Crane, 1978	Determination of mesospheric height fields up to 80 km from Nimbus 6 PMR measurements.
	Hirota, 1975	Spectral analysis of planetary waves in the summer stratosphere and mesosphere.
	Hirota, 1976	Seasonal variation of planetary waves in the stratosphere observed by the Nimbus 5 SCR.
	Hirota, 1978	Equatorial waves in the upper stratosphere and mesosphere in relation to the semiannual oscillation of the zonal wind.
	Hirota, 1979	Kelvin waves in the equatorial middle atmosphere observed by the Nimbus 5 SCR.

Table C-6
Some Published Studies Using Satellite-Derived Stratospheric Temperature Data (continued)

Instrument	Authors (Year)	Title
SCR, PMR	Hirota, 1980	Observational evidence of the semiannual oscillation in the tropical middle atmosphere - a review.
	Hirota and Barnett, 1977	Planetary waves in the winter mesosphere - preliminary analysis of Nimbus 6 PMR results.
	Hirota et al., 1973	Structure and behavior of the Aleutian anticyclone as revealed by meteorological rocket and satellite observations.
	Houghton, 1972	The Selective Chopper Radiometer on Nimbus 4.
	Houghton 1978	The stratosphere and mesosphere.
	Johnson, 1977	Variations in static stability in the stratosphere and lower mesosphere during a winter disturbance.
	Johnson and Rodenhuis, 1977	Potential vorticity transport during a stratospheric warming.
	Kanzawa, 1978	On the behaviour of mean zonal flow and planetary waves during the 1973 sudden warming observed by the Nimbus 5 SCR.
	Kanzawa, 1980	The behavior of mean zonal wind and planetary-scale disturbances in the troposphere and stratosphere during the 1973 sudden warming.
	Kanzawa and Hirota, 1981	The behaviour of mean zonal winds and planetary waves during the 1973 sudden warming.
	Koshelkov, 1980	Mean values of meteorological parameters in the upper stratosphere and mesosphere of the southern hemisphere.
	Labitzke, 1971	Synoptic-scale motions above the stratopause.

Table C-6
Some Published Studies Using Satellite-Derived Stratospheric Temperature Data (continued)

Instrument	Authors (Year)	Title
SCR, PMR (continued)	Labitzke, 1972a	Temperature changes in the mesosphere and stratosphere connected with circulation changes in winter.
	Labitzke, 1972b	The interaction between stratosphere and mesosphere in winter.
	Labitzke, 1974	The temperature in the upper stratosphere: Differences between hemispheres.
	Labitzke, 1976a	Comparison of the stratospheric temperature distribution over northern and southern hemispheres.
	Labitzke, 1976b	On the use of single channel radiances for estimating temperatures at discrete pressure levels in the upper stratosphere.
	Labitzke and Barnett, 1973	Global time and space changes of satellite radiances received from the stratosphere and lower mesosphere.
	Labitzke and Barnett, 1979	Review of climatological information obtained from remote sensing of the stratosphere and mesosphere.
	Labitzke and Barnett, 1981	Review of the radiance distribution in the upper mesosphere as observed from the Nimbus 6 Pressure Modulator Radiometer (PMR).
	Leovy and Webster, 1976	Stratospheric long waves: Comparison of thermal structure in the northern and southern hemispheres.
	McGregor and Chapman, 1978	Observations of the annual and semi-annual wave in the stratosphere using Nimbus 5 SCR data.
	McGregor and Chapman, 1979	Stratospheric temperatures and geostrophic winds during 1973-1974.

Table C-6
Some Published Studies Using Satellite-Derived Stratospheric Temperature Data (continued)

Instrument	Authors (Year)	Title
SCR, PMR (continued)	Noxon, 1978	Stratospheric NO_2 in the Antarctic winter.
	Offermann et al., 1979	Atmospheric temperature structure during the Western European winter anomaly campaign 1975/76.
	Prata and Rodgers, 1981	A comparison of 5-day and 2-day travelling wave observations with Hough modes modified by meridional shear.
	Quiroz, 1978	The contribution of satellite remote sounding data in stratospheric analysis and research.
	Quiroz et al., 1975	A comparison of observed and simulated properties of sudden stratospheric warmings.
	Rodgers, 1976	Evidence for the five-day wave in the upper stratosphere.
	Rodgers, 1977b	Morphology of upper atmosphere temperatures.
	Rodgers and Prata, 1981	Evidence for a travelling 2-day wave in the middle atmosphere.
	Schlapp, 1980	Lunar tides in the middle atmosphere from Nimbus 5 data.
	Schlapp, 1981	Lunar tides in the stratosphere and mesosphere from Nimbus 6 data.
	Stanford and Dunkerton 1978	The character of ultra-long stratospheric temperature waves during the 1973 Austral winter.
	Van Loon et al., 1972	Half-yearly wave in the stratosphere.
	Venne, 1981	A 4-day winter polar stratosphere temperature wave: Observation and theory.
	Webster et al., 1977	Equatorial waves in the upper stratosphere.

Table C-6
Some Published Studies Using Satellite-Derived Stratospheric Temperature Data (continued)

Instrument	Authors (Year)	Title
SAMS	Drummond et al., 1980	The Stratospheric and Mesospheric Sounder on Nimbus 7.
	Taylor et al., 1981	Performance and early results from the Stratospheric and Mesospheric Sounder (SAMS) on Nimbus 7.
NOAA Data Sets	Gelman et al., 1980	An evaluation of stratospheric meteorological analyses using satellite sounder and rocketsonde data.
	Groves and Tuck, 1980	An investigation of the ability of a radiative-photochemical model to reproduce the temporal variation of ozone and temperature in the stratosphere.
	Labitzke, 1981	The amplification of height wave 1 in January 1979: A characteristic precondition for the major warming in February.
	Palmer, 1981a	Diagnostic study of a wavenumber-2 stratospheric sudden warming in a transformed Eulerian-mean formalism.
	Palmer, 1981b	Aspects of stratospheric sudden warmings studied from a transformed Eulerian-mean viewpoint.
	Pick and Brownscombe, 1981	Early results based on the stratospheric channels of TOVS on the TIROS-N series of operational satellites.
LRIR	Gille et al., 1979	Middle atmosphere processes revealed by satellite observations.
	Gille et al., 1980c	Observations of the interaction of ozone and dynamics.
	Kohri, 1981	LRIR observations of the structure and propagation of the stationary planetary waves in the Northern Hemisphere during December 1975.
LIMS	Gille et al., 1980a	Temperature and composition measurements from the LRIR and LIMS experiments on Nimbus 6 and 7.
	Gille et al., 1980e	The Limb Infrared Monitor of the Stratosphere (LIMS) experiment: Temperature and O_3 results.

D1

APPENDIX D

STRATOSPHERIC AEROSOLS AND PRECURSOR GASES

MEASUREMENTS

The data base for studying stratospheric aerosols is exceptionally diverse. Measurements have been made of the aerosol size, height and geographical distributions, their composition and optical properties, and their temporal variation with season and following large volcanic eruptions. Sulfur-bearing gases have been measured in situ in the stratosphere, and studies of the chemical and physical processes which control gas-to-particle conversion have been carried out in the laboratory. Finally, the existing body of scientific knowledge which pertains to stratospheric chemistry and dynamics can be brought to bear on the problem of stratospheric aerosols.

PRECURSOR GASES

The first measurements of stratospheric SO_2 concentrations were made by Jaeschke et al. (1976), who extended their technique (collection by means of a wet chemical filter with subsequent chemiluminescent analysis) to heights just above the tropopause. More recent efforts using dry filters and chemiluminescent analysis have obtained data to about 15 km, yielding SO_2 mixing fractions in the range 0.01 to 0.1 ppbv with a mean value of about 0.05 ppbv above 6 km (Georgii and Meixner, 1980). The uncertainty in these measurements is probably a factor of two.

Inn et al. (1981a) trapped sulfur gases cryogenically during U-2 aircraft flights and analyzed the samples by means of gas chromatography using a flame photometric detector. They were thus able to extend the SO_2 observations up to 21 km. The results obtained are similar to those reported by Georgii and Meixner (1980), namely 0.036 to 0.051 ppbv SO_2 throughout the lower stratosphere. The principal uncertainties in the Inn et al. data arise in the collection process rather than the laboratory analysis. The uncertainties include errors in the total sample volume, the cryogenic collection efficiency for the gases in question, and the accuracy of the transfer of the sample to the chromatograph. The estimated errors are ±50% for SO_2 and ±20% for COS.

Earlier, Sagawa and Itoh (1977) used a mass spectrometer to detect stratospheric SO_2, but obtained unrealistically high concentrations of 30 ppmv. SO_2 can also be detected through its near-ultraviolet absorption band, but experiments to do so in the stratosphere have not yet been perfected. Inn et al. (1981b), measured SO_2 mixing ratios on the order of 100 ppb at 14 km in the eruption plume of Mount St. Helens about one day after the May 18, 1980, eruption.

Inn et al. (1979, 1981a) measured COS in the stratosphere, finding about 0.3 to 0.5 ppbv at altitudes ~15 km (just above the tropopause) and rapidly decreasing concentrations with height above 15 km. The stratospheric values are consistent with tropospheric measurements made during the GAMETAG program (Maroulis et al., 1977; Torres et al., 1980). The in situ measurements are shown in Figure 1-6. Mankin et al. (1979) measured the stratospheric column abundance of COS, and found it to agree with the in situ observation and to show little variation with season or latitude.

Inn et al. (1981a) attempted to detect CS_2 in the stratosphere, but were not able to identify it definitely. A small feature in their gas chromatograms may have indicated the presence of CS_2 at abundances of about 0.001 ppbv just above the tropopause. Maroulis and Bandy (1980) measured only ~30 pptv of CS_2 in air near the surface far from sources of pollution. This concentration is too small to make CS_2 of any direct significance to the stratosphere.

Stratospheric H_2SO_4 concentrations have recently been deduced using measurements of stratospheric negative ion mass spectra coupled with laboratory rate coefficients for H_2SO_4 ion-molecule reactions (Arnold and Fabian, 1980; Arnold et al., 1981; Viggiano and Arnold, 1981; Arijs et al., 1981). The results generally indicate H_2SO_4 concentrations of about $10^5 cm^3$ below 27 km, increasing rapidly to $\sim 10^7 cm^3$ near 34 km, then perhaps declining again above 34 km. The rapid increase between 27 and 34 km appears to follow a characteristic H_2SO_4 vapor pressure curve (Arnold et al., 1981).

The uncertainties in the ion technique lie in two general areas; first, the uncertainties in the measured ion cluster concentrations because the ions are subject to breakup in the mass spectrometer inlet, and second, the uncertainties in the ion chemistry rate coefficient and equilibrium constants. In view of these factors, an uncertainty in the H_2SO_4 concentration of a factor of two to three is possible.

Arnold and Henschen (1981) detected massive ion clusters comprised of H_2SO_4, H_2O, HNO_3 and other stratospheric gases, and suggested that these may play a role as aerosol "precondensation" nuclei. Research into the possible connections between stratospheric ions and aerosols is continuing.

AEROSOL MEASUREMENTS

Junge et al. (1961), in their earliest work, used cascase impacters and gummed glass slides to collect stratospheric aerosols, with balloons as the instrumental platform. A U-2 aircraft was later employed (Junge and Manson, 1961). Particle size distributions were determined for altitudes from 12 to 21 km by visual analysis of electron micrographs of collection surfaces. Chemical analysis of the samples revealed that the particles contained sulfur as a major constituent.

Farlow and coworkers (1979), and Ferry and Lem (1974) collected particles on carbon-coated palladium wires mounted below the wing of a U-2 aircraft. The wires were examined with a scanning electron microscope to obtain size distributions and absolute particle concentrations. Initial analyses of aerosol composition revealed nitrosyl and ammonium sulfates (Farlow et al., 1977, 1978). However, after modifying the instrument to protect the samples from exposure to the atmosphere after collection, no ammonium sulfate was detected. Apparently, ammonia was absorbed by the aerosols in the lower atmosphere after collection (Hayes et al., 1980). Impactors have also been employed to study stratospheric aerosols by Mossop (1965), Bigg (1975, 1976), Gras and Laby (1978), and Gras and Michael (1979).

A large number of aerosol filter samples have been collected and analyzed for composition. This work is described in papers by Shedlovsky and Paisley (1966), Lazrus et al. (1971), Lazrus and Gandrud (1974a, 1977), Castleman et al. (1974), Delaney et al. (1974) and Lezberg et al. (1979). Castleman et al. (1974) studied isotopic sulfur ratios (S^{32}/S^{34}), and provided direct evidence of the in situ chemical origin of the sulfate aserosols.

Rosen (1964) developed an in situ optical detector for particles based on the light-scattering characteristics of aerosols in the size ranges $\geq$0.15 μm and $\geq$0.25 μm radius. Optical systems have also been used by Miranda and Fenn (1974), Kaselau et al. (1974) and Podzimek et al. (1975). The optical counters are often used in tandem with a condensation chamber to determine the background condensation nuclei abundance. Rosen (1971) also evaporated stratospheric aerosols in situ and noted that their boiling point is consistent with a 75% H_2SO_4 aqueous solution (Toon and Pollack, 1973).

In addition to in situ sampling of the aerosol layer, much data on stratospheric characteristics have been obtained with remote sensing by ground- and aircraft-based optical radar (lidar) systems. The lidar data (aerosol backscatter) are used to detect the spatial temporal variations in the layer and to deduce aerosol properties such as reported by McCormick et al. (1978), Fox et al. (1973), and Fiocco and Grams (1964). Recently, another remote technique has been developed which promises a global measurement capability. In this, satellite instruments are used to observe the attenuation due to atmospheric aerosols during spacecraft sunrise and sunset. The first such experiment was carried out during the Apollo-Soyuz program in 1975 (Pepin et al., 1977) using a simple photometer which the astronauts pointed at the Sun. The more recent SAM II and SAGE unmanned satellite experiments were developed specifically to monitor stratospheric aerosols by this technique with an automated acquisition system to provide continuous global-scale monitoring of the aerosols (McCormick et al., 1979).

Figure D-1 illustrates the global distribution of aerosol extinction as determined from the SAGE satellite for the month of April 1979 (McCormick, 1981a). The stratospheric layer is seen to follow the tropopause (dash-dot line) with latitude with the layer peak at higher altitudes in the tropics. The mixing ratio is likewise the highest over equatorial latitudes suggesting a source region for the layer. The high values of extinction below the tropopause are due to tropospheric clouds. Such extinction maps are useful for climate and radiation studies and to determine the source and sink regions for stratospheric aerosols. Figure D-2 presents the extinction map for the May 18, 1980 Mount St. Helens eruption cloud (McCormick, 1981a). The data are zonally averaged for the month of July and half of August. Interestingly, the satellite data indicate significant aerosol opacities at high northern latitudes, with little apparent effect of the volcano at low latitudes. The new satellite data, as with earlier analyses of global aerosol distribution (e.g., Lazrus and Gandrud, 1974a; Hofmann et al., 1975a; Rosen et al., 1975; Farlow et al., 1979; Oberbeck et al., 1981), will prove useful in studies of stratospheric transport process, stratosphere/troposphere exchange and stratospheric variability.

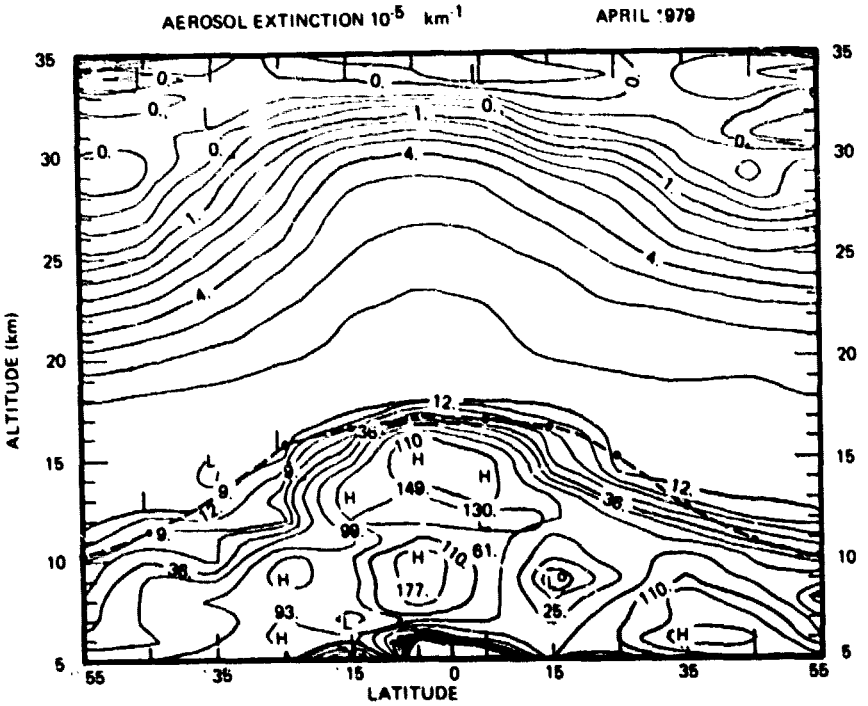

Figure D-1. Global distribution of aerosol extinction obtained with the SAGE satellite. The units are 10^{-5}/km. Data are zonally averaged values for April, 1979 (McCormick, 1981a)

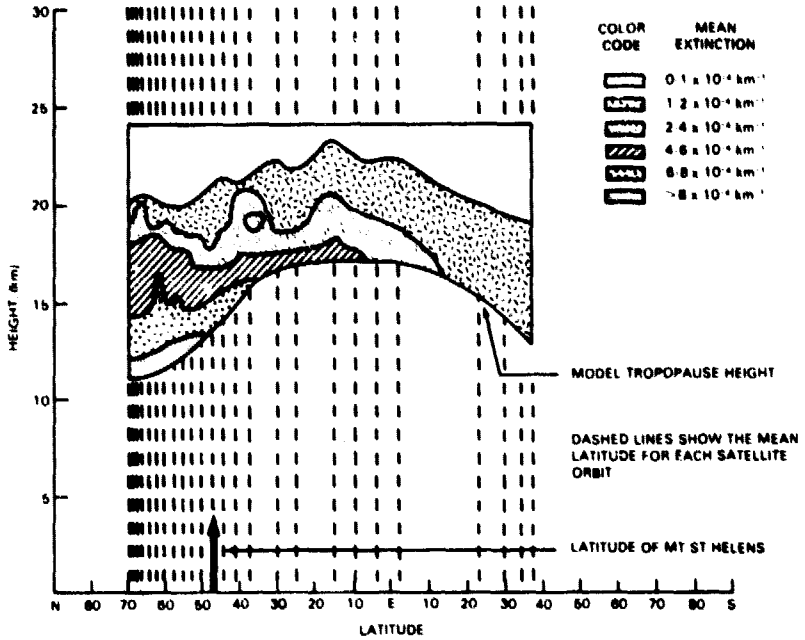

Figure D-2. SAGE extinction measurements (zonal mean) for July 1-August 12, 1980, 2 to 3 months following the Mount St. Helens eruption on May 18, 1980 (McCormick, 1981a)

McCormick et al. (1978) and Swissler et al. (1981) made a series of lidar observations of the aerosol layer following the Fuego volcanic eruption in October 1974. The observed 'e-folding' decay times of the vertically integrated particulate opacity, and the peak ratio of particulate-to-gaseous backscattering, were 9 and 7.5 months, respectively. The short lifetimes are evidently the result of the low altitude of injection of the volcanic particles, and their larger mean size compared to the ambient aerosols. In addition to particles, measurements indicate that volcanos can also inject substantial amounts of sulfur gases, particularly SO_2 and chlorine and water vapor directly into the stratosphere (Inn et al., 1981b).

NACREOUS CLOUDS

Nacreous clouds are observed only during the winter months and are quite rare, being reported on the average only a few times per year during the previous century (Stanford and Davis, 1974). Stanford (1973) pointed out that temperatures in the Antarctic stratosphere are commonly as low as 183 K so that much more persistent clouds might be expected there. During the winters of 1950 and 1951 persistent widespread stratospheric clouds were observed in Antarctica. These clouds, which were optically thin and did not noticeably extinguish starlight, were observable only under the proper twilight conditions.

Recently the SAM II satellite has detected dense, persistent, high altitude particle layers over Antarctica that are probably nacreous clouds. Figure D-3 shows a year of Antarctic SAM II data averaged weekly and the corresponding temperature fields which are also weekly averaged over the same geographical location as the SAM II measurements (McCormick et al., 1981). The clouds are persistent in the wintertime (McCormick, 1982) and are thought to be composed of ice crystals from freezing of the sulfuric acid aerosol and subsequent growth (Hamill et al., 1980). The locations of the clouds correspond closely with regions of very low temperature. The clouds

persist throughout the winter period. If the preliminary satellite data are correct, these stratospheric clouds may be far more common than was previously thought. Accordingly, a careful evaluation of the role of the clouds in the high-latitude radiation balance and in the stratospheric water vapor budget is warranted (Hamill et al., 1980). The connection of the clouds with stratospheric aerosols also requires investigation (Toon and Farlow, 1981).

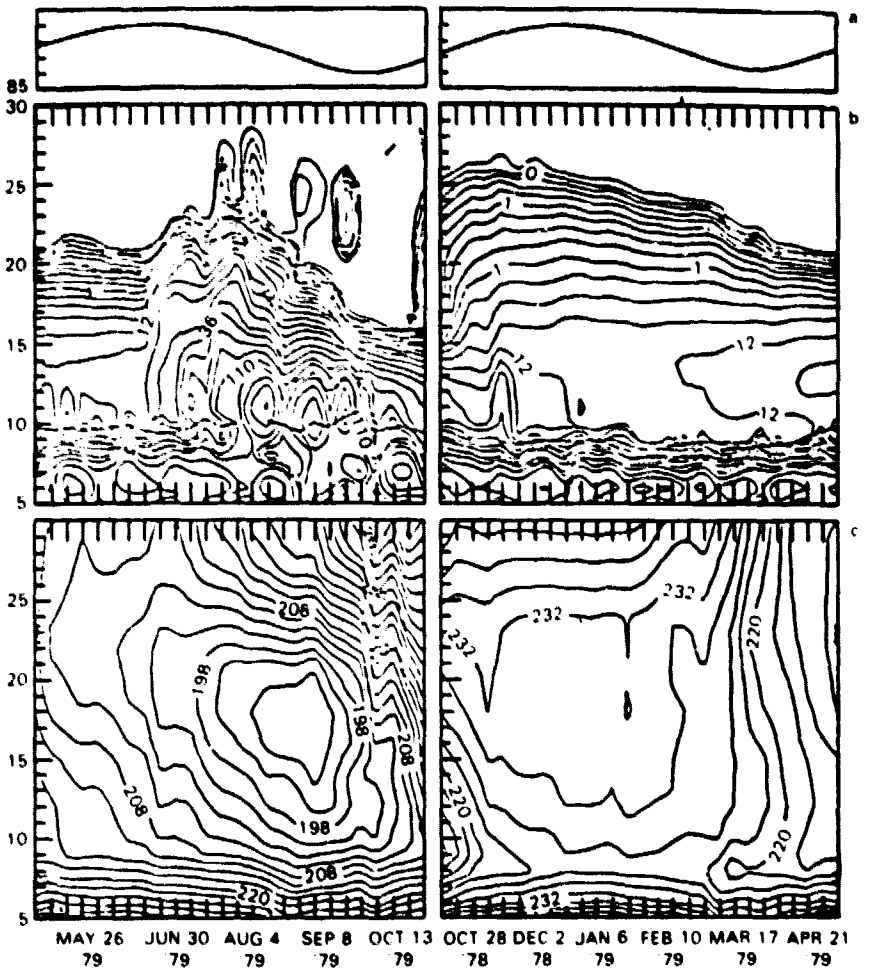

Figure D-3. SAM-II satellite observations over the Antarctic (McCormick et al., 1981) panel (1), shows the latitude of observation versus time. The middle panel meteorological network temperatures.

COMPARISON OF THEORY AND MEASUREMENTS

Theoretical models of the stratospheric aerosol layer must treat a wide spectrum of physical and chemical processes in order to describe accurately the formation and evolution of the particles. Only then can meaningful comparisons with data be made. Below, the current state-of-the-art model predictions of high-altitude particles are compared with observations.

AEROSOL PRECURSOR GASES

Detailed studies have been made of the tropospheric COS cycle and the stratospheric sulfur balance during volcanically quiescent times (e.g., Turco et al., 1980a,b). Figure D-4 illustrates the estimated flow of sulfur into and out of the stratosphere. The CS_2 flux may be greatly overestimated in Figure D-4 because recent CS_2 measurements indicate very low background concentrations above the boundary layer (Maroulis and Bandy, 1980). Thus, COS appears to be the dominant sulfur source for the stratospheric aerosol layer during periods of low volcanic activity, as originally proposed by Crutzen (1976). Sulfuric acid aerosols which diffuse above ~30 km are thermodynamically unstable, and evaporate. This explains the downward flux of H_2SO_4 seen at these altitudes in Figure D-4. Predicted concentration profiles of sulfur gases in the troposphere and stratosphere are compared with observations in Figure D-5. Notice that COS is the predominant sulfur-bearing constituent in the atmosphere of the Earth. The concentration curves marked '312.5 nm' in Figure D-5 roughly correspond to the flux curves given in Figure D-4. Using a combination of SO_2, COS and sulfate aerosol data, Turco et al. (1981d) deduced that stratospheric HO concentrations are lower than photochemical ozone models predicted (in 1980). Such results demonstrate that aerosols are closely coupled with the major photochemical cycles of the stratosphere.

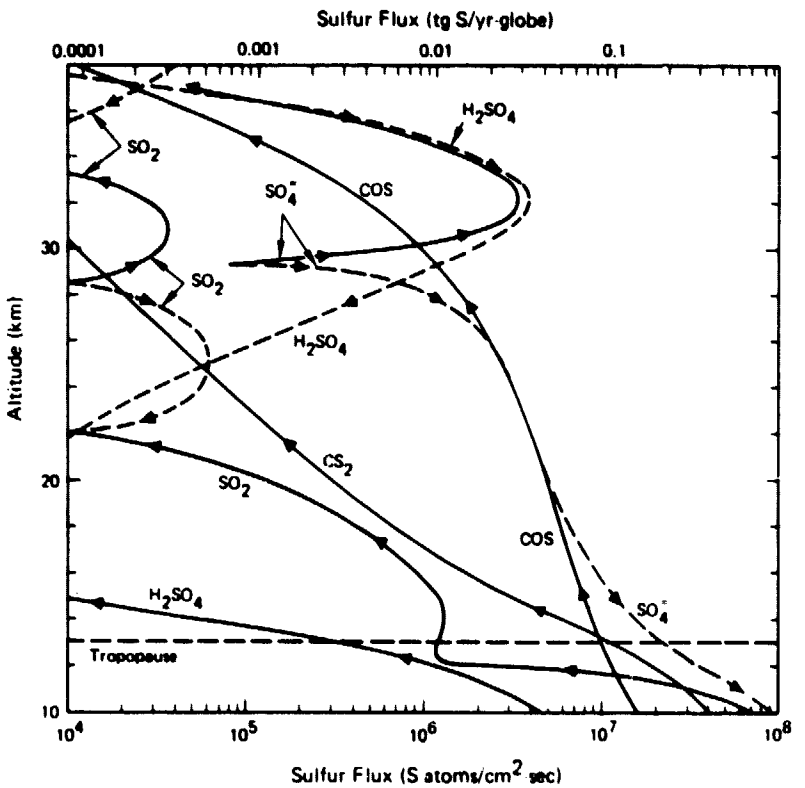

Figure D-4. The balance of stratospheric sulfur gases and sulfate aerosols in a one-dimensional model. Equivalent sulfur-atom fluxes are given. The arrows indicate direction of sulfur flow (Turco et al., 1980a).

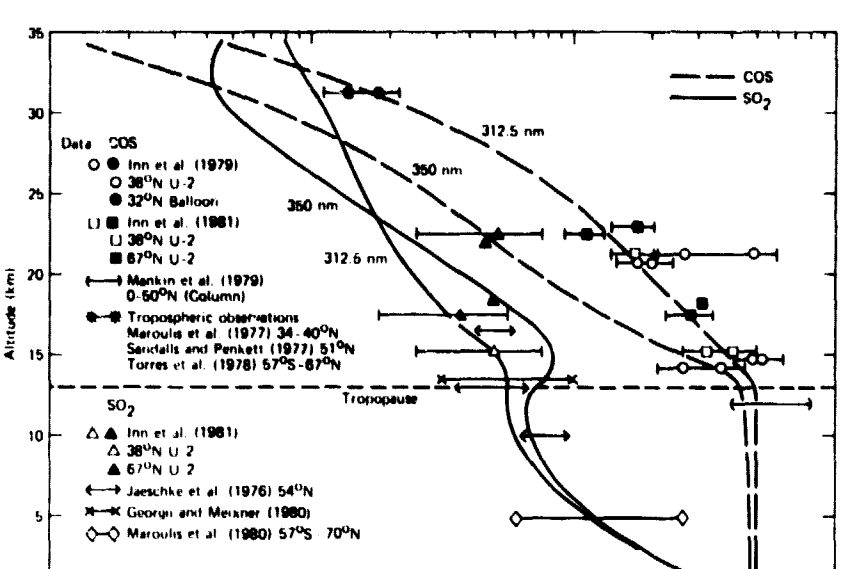

Figure D-5. Calculated and observed SO_2 and COS concentrations in the stratosphere. The curves marked 312.5 nm and 350 nm refer to the assumed long-wavelength cutoff for COS photodissociation (Turco et al., 1981c).

Sulfuric acid vapor concentrations are difficult to calculate because they are controlled by heterogeneous processes. Figure D-6 shows several profiles calculated with an interactive H_2SO_4 solution/H_2SO_4-vapor model (Turco et al., 1981a). The first reliable H_2SO_4 measurements are also shown in Figure D-6. The calculated profiles are in excellent accord with the observations between 23 and 33 km (Arnold et al., 1981; Viggiano et al., 1981). The data appear to support the idea that the aerosols are volatile H_2SO_4/H_2O droplets below ~34 km.

Meteoric metal profiles are also shown in Figure D-6 (Turco et al., 1981a). These results indicate that heterogeneous processes remove the meteoric metal vapors at the uppermost extent of the aerosol layer. Thus, the metals cannot interact significantly with the other reaction cycles of the stratosphere; in the condensed state, metal sulfates are extremely stable compounds.

AEROSOL PROPERTIES

The measured properties of the stratospheric aerosols obtained with a variety of field instruments provide strict constraints on model predictions. Toon et al. (1979) made extensive comparisons between model calculations and in situ observations for a variety of parameters, including the total particle mixing ratio, the sulfate mass mixing ratio, the large particle ($r > 0.15$ μm) mixing ratio, the particle size ratio (number >0.15 μm/number >0.25 μm), and the particle composition and size distribution. They found generally good agreement in each case. Measurements of the total particle concentration obtained with present-day condensation nuclei counters are probably limited to particle sizes >0.01 μm radius. In Figure D-7 typical observational values are compared with model calculations (Hamill et al. 1981). The comparison suggests that many of the aerosols detected in the lower stratosphere may be generated in the upper troposphere, possibly by homogeneous nucleation.

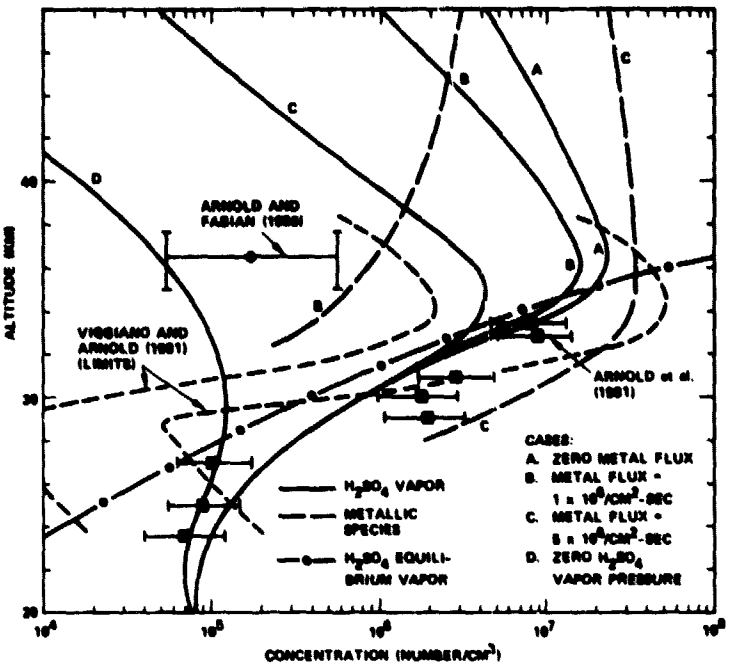

Figure D-6 Predicted stratospheric distributions of H_2SO_4 vapor and metallic meteoric vapors (Turco et al., 1981a).

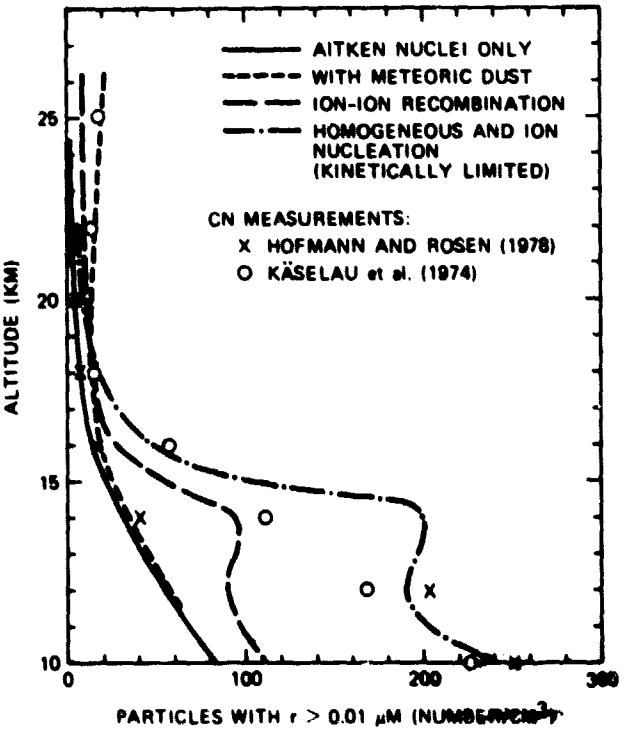

Figure D-7. Total aerosol particle concentrations in the lower stratosphere (i.e., particles with radii >0.01 μm). Model predictions (lines) are compared with data: the predictions were made with different aerosol nucleation sources (Hamill et al., 1981).

Figure D-8 contrasts calculated and observed sulfate mass mixing ratios in the stratosphere. Considering the variability of the measurements, the model calculations provide a reasonable fit to the data. The continual influx of extraterrestrial (meteoric) debris has a small, but perceptible, effect on the aerosol mass (Figure D-8). Note that, at high altitudes (above ~35 km), sulfuric acid vapor contributes substantially to the total sulfate mass; above 35 km, H_2SO_4 vapor is dominant sulfate compound (notwithstanding possible absorption and neutralization of H_2SO_4 on meteoritic particles (Turco et al., 1981a).

Calculated and observed aerosol particle size ratios are illustrated in Figure D-9. The ratio typically has values ~4 to 6 below 25 km. Above 25 km, the behavior of the size ratio is uncertain. The measurements of Hofmann and Rosen (1981a) suggest a rapidly increasing ratio with height, but the scatter and uncertainty in the data at these altitudes preclude a firm conclusion. The theoretical simulations of Turco et al. (1981a) show a sharp increase in the size ratio above 35 km in a model assuming pure sulfuric acid droplets, because the droplets evaporate rapidly above 35 km. This point of view (i.e., volatile aerosols up to 35 km) is supported by recent measurements of the H_2SO_4 vapor profile (Arnold et al., 1981). On the other hand, Turco et al. (1981a) noted that, if the aerosols are nonvolatile, a steady increase in the size ratio begins near 25 km (where sedimentation overwhelms diffusion), which is in close agreement with the data of Hofmann and Rosen (1981) (See Figure D-9).

Measurements suggest that the composition of the stratospheric aerosols is basically 75% sulfuric acid aqueous solution (Rosen, 1971) with an admixture of solid granules and dissolved nitrosyl sulfates (Farlow et al., 1977, 1978). The model of Turco et al. (1979) predicts a slightly variable acid composition with height of between 75 to 78% H_2SO_4 by weight, and a small (<10%) concentration of extraterrestrial material in the aerosols (Turco et al., 1981a).

The meteoric dust size distribution below ~0.1 m radius is dominated by coagulated smoke particles (Hunten et al., 1980). Above ~ 0.1 μm, micrometeorites (which do not ablate completely upon entering the atmosphere) determine the size distribution. Predicted meteoric particle sizes fit the current meager data base on meteoric dust (Brownlee, 1978).

Detailed microphysical models of volcanic cloud formation and dispersion are presently under development (e.g., Turco et al., 1981b). These models will complement observational studies of volcanic aerosols and climate.

CONCLUSIONS

The major conclusions regarding observations and modeling of stratospheric aerosols may be summarized as follows:

- A broad base of data exists which describes the properties of stratospheric aerosols including their concentrations, spatial distributions, temporal variations, size dispersion, and composition. The global climatology is just now emerging, especially from the satellite experiments. Less information is available for the sulfur precursor gases (e.g., their abundances and photochemical reactions), but here also the data base has been rapidly expanding in the past few years.

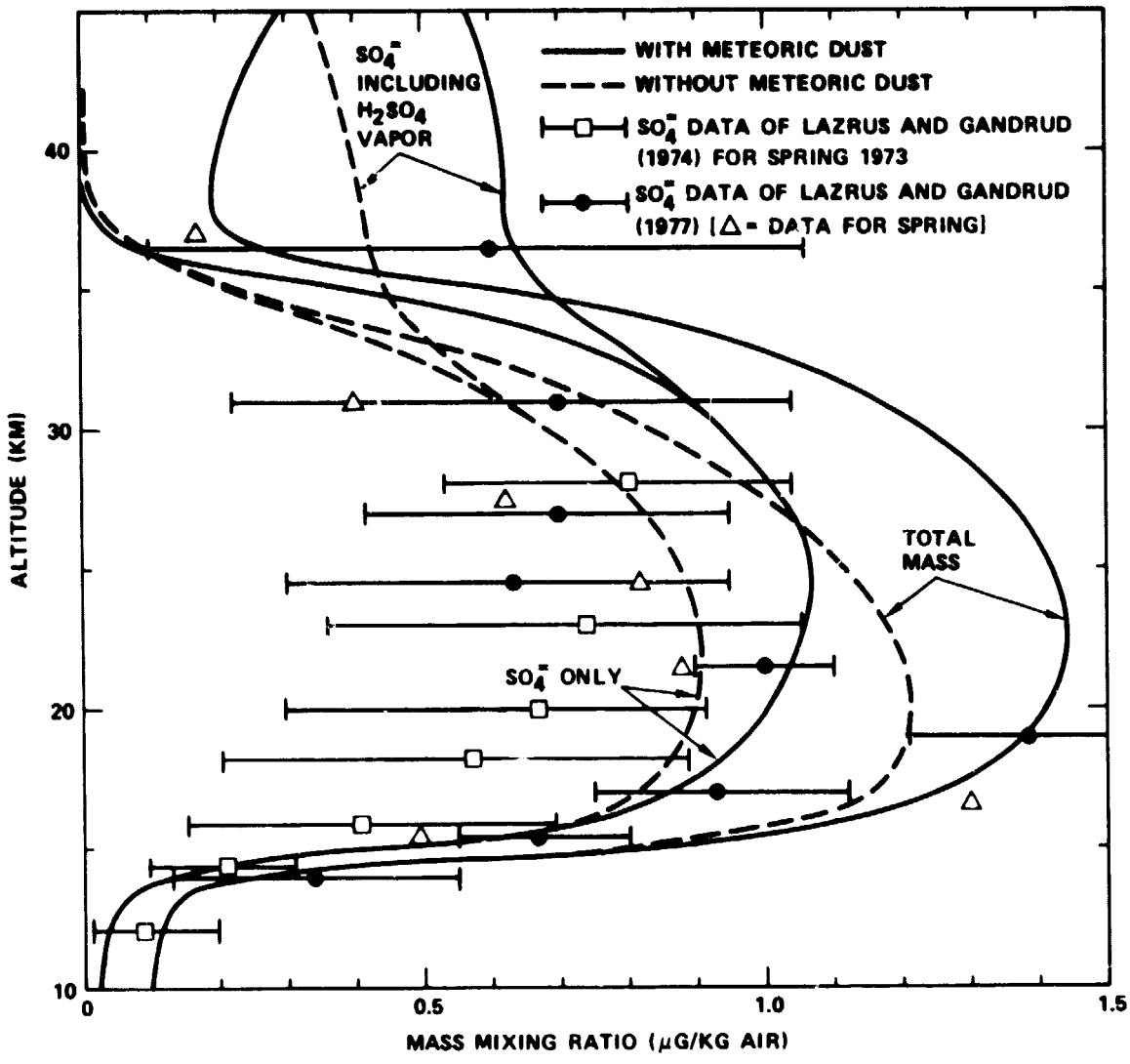

Figure D-8. Particulate mass mixing ratios calculated with and without meteoric dust. The corresponding SO_4 mass mixing ratios are shown, and are compared to the data of Lazrus and Gandrud (1974a, 1977). The Lazrus and Gandrud (1974a) measurements were made in Spring 1973 in the Northern Hemisphere. Data points correspond roughly to average values at a fixed elevation with respect to the mean tropopause level. The range of individual measurements is indicated by a cross bar. The Lazrus and Gandrud (1977) SO_4 data points represent average values of measurements made during 1976, with one standard deviation indicated by a cross bar. Average Spring 1976 data, more appropriate for comparison with the model, are plotted as well (standard deviations for these points were not published). The 1976 measurements may have been influenced to some extent by the eruption of Volcano Fuego (14.5 degrees N) in October 1974 (Turco et al., 1981a).

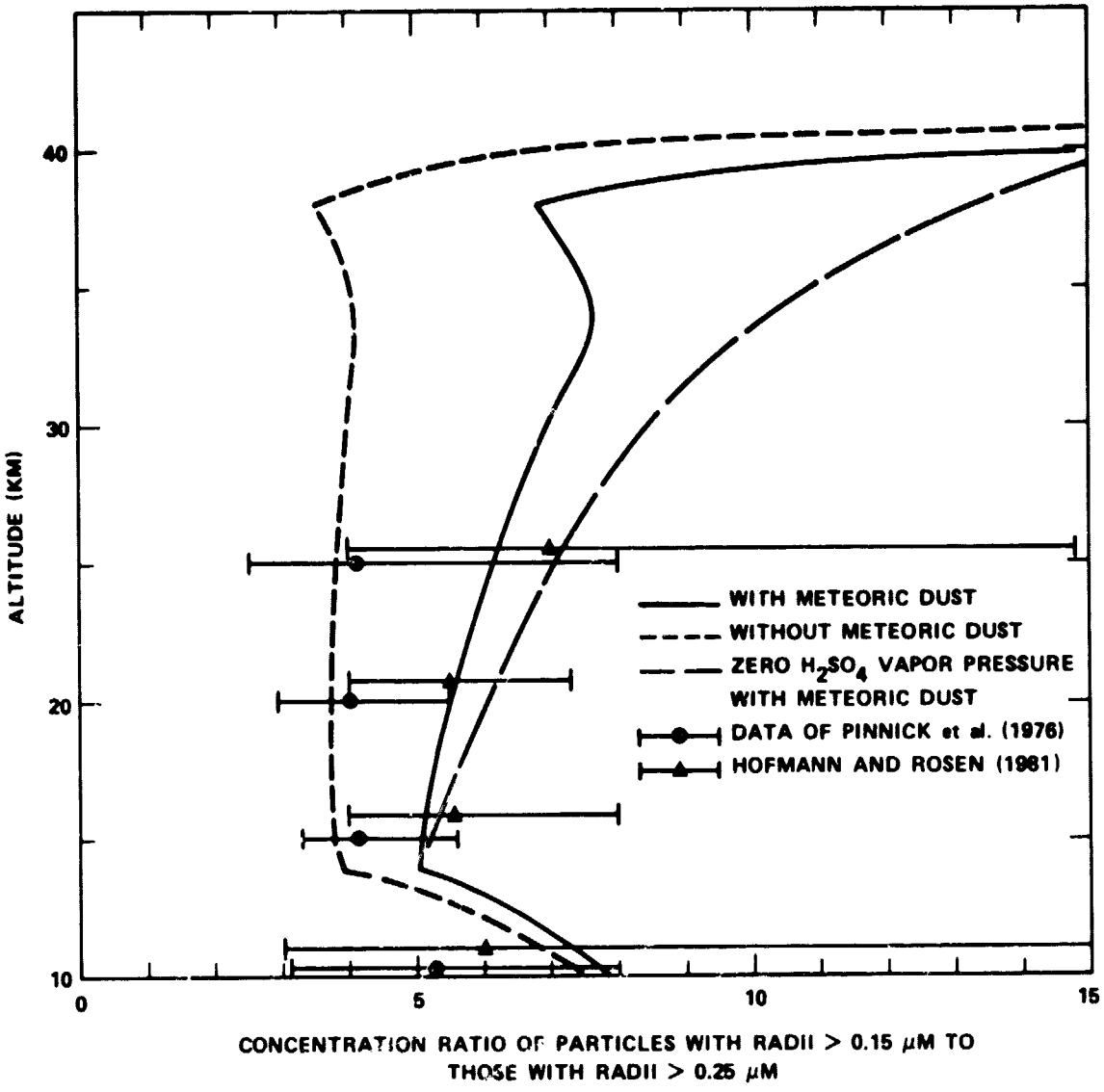

Figure D-9. Particle size ratios calculated with and without meteoric dust. For comparison, the measurements of Pinnick et al. (1976) made worldwide between 1971 and 1974, and Hofmann and Rosen (1981) taken at Laramie, Wyoming, during 1978 and 1979, are shown. In each case, an average value and the range of individual measurements are given. The observations of Hofmann and Rosen are most appropriate for the background aerosol layer in the absence of volcanic activity (Turco et al., 1981a).

- Comprehensive physicochemical models of the aerosols are available. These models incorporate appropriate particle microphysical processes such as nucleation, condensation, coagulation, and sedimentation. To be most useful, chemical processes must also be treated "interactively" in these simulations.

- Model predictions for the aerosols and precursor gases compare favorably with observational data in most important respects. Areas requiring further investigation include the aerosol size distribution below 0.05 m radius, the height extent of the aerosol layer, and the rates of SO_2 oxidation under stratospheric conditions.

- Intensive experimental and theoretical studies will be required in the future to determine:

  --The nucleation source of the aerosols.
  --The processes influencing the global distribution of the aerosols.
  --The precise concentrations and chemical interaction rates of aerosol precursor gases.
  --The physicochemical development and disposition of volcanic eruption clouds.
  --The mechanisms coupling aerosols and climate.
  --The importance of heterogeneous reactions to stratospheric composition.
  --The physical connections between dust, aerosols and ions throughout the middle atmosphere.

omit to end

APPENDIX E

REFERENCES

Aanensen, C. J. M., The use of Nimbus 4 radiance and radio-sonde data in the construction of stratospheric contour charts, Quart. J. Roy. Meteorol. Soc., **99**, 657-668, 1973.

Acharya, Y. B., R. N. Misra, S. Lal, and B. H. Subbaraya, A rocket borne solar MUV photometer for measurement of ozone concentrations in the stratosphere, J. Instn. Electr. & Telecom. Engrs., **25**, 254-257, 1979.

Ackerman, M., and C. Müller, Stratospheric methane and nitrogen dioxide from infrared spectra, Pure Appl. Geophys., **106-108**, 1325-1335, 1973.

Ackerman, M., D. Frimout, and R. Pastels, New ultraviolet solar flux measurements at 2000A using a balloon borne instrument, New Techniques in Space Astronomy; Proceedings of the Symposium, Munich, West Germany, 1970, F. Labuhn and R. Lüst, editors, Reidel Publishing Co., 251-253, 1971.

Ackerman, M., J. C. Fontanella, D. Frimout, A. Girard, N. Louisnard, and C. Muller, Simultaneous measurements of NO and NO_2 in the stratosphere, Planet. Space Sci., **23**, 651-660, 1975.

Ackerman, M., D. Frimout, A. Girard, M. Gottignier, and C. Müller, Stratospheric HCl from infrared spectra, Geophys. Res. Lett., **3**, 81-83, 1976.

Ackerman, M., D. Frimout, C. Müller, and D. J. Wuebbles, Stratospheric methane measurements and predictions, Pure Appl. Geophys., **117**, 367-380, 1978/79.

Aikin, A. C., and E. J. R. Maier, Balloon-borne photoionization mass spectrometer for measurement of stratospheric gases, Rev. Sci. Instrum., **49**, 1034-1040, 1978.

Aimedieu, P., J. Barat, and P. Rigaud, Mesures de la concentration en ozone de la stratosphère au lever et au coucher du Soleil, C. R. Acad. Sci. Paris, B, **288** 89-92, 1979.

Aimedieu, P., J. Barat, C. Bernard, and J. Ohayon, Ozonomètres stratosphériques à chimiluminescence en phase gazeuse utilisant des éthyléniques comme réactifs, Proceedings of the Quadrennial International Ozone Symposium, IAMAP, J. London, editor, pp. 212-215, 1980.

Aimedieu, P., P. Rigaud, and J. Barat, The sunrise ozone depletion problem of the upper stratosphere, Geophys. Res. Lett., **8**, 787-789, 1981.

Ainsworth, J. E., and J. R. Hagemeyer, Measurement of ozone by a Dasibi ozone monitor, in The Stratcom VIII Effort, E. I. Reed, editor, NASA Technical Paper 1640, pp. 95-100, April 1980.

Ainsworth, J. E., J. R. Hagemeyer, and E. I. Reed, Error in Dasibi flight measurements of atmospheric ozone due to instrument wall-loss, Geophys. Res. Lett., **8**, 1071-1074, 1981.

Allam. R. I., K. S. Groves, and A. F. Tuck, Global OH distribution derived from general circulation model fields of ozone and vapor, J. Geophys. Res., **86**, 5303-5320, 1981.

Altshuller, A. P., Average tropospheric concentration of carbon tetrachloride based on industrial production, usage and emissions, Environ. Sci. and Tech., **10**, 596-598, 1976.

Anderson, J. G., Rocket-borne ultraviolet spectrometer measurement of OH resonance fluorescence with a diffusive transport model for mesospheric photochemistry, J. Geophys. Res., 76, 4634-4652, 1971a.

Anderson, J. G., Rocket measurement of OH in the mesosphere, J. Geophys. Res., 76, 7820-7824, 1971b.

Anderson, J. G., The absolute concentration of $O(^3P)$ in the Earth's stratosphere, Geophys. Res. Lett., 2, 231-238, 1975.

Anderson, J. G., The absolute concentration of OH ($X^2\pi$) in the Earth's stratosphere, Geophys. Res. Lett., 3, 165-168, 1976.

Anderson, J. G., Free radicals in the Earth's stratosphere: A review of recent results. Proceedings of the NATO Advanced Study Institute on Atmospheric Ozone, A. C. Aikin, editor, FAA-EE-80-20, pp 233-251, 1980.

Anderson, J. G., J. J. Margitan, and D. H. Stedman, Atomic chlorine and the chlorine monoxide radical in the stratosphere: Three in situ observations, Science, 198, 501-503, 1977.

Anderson, G. P., J. C. Gille, P. L. Bailey, and S. Solomon, LRIR observations of diurnal ozone variation in the mesosphere, Proceedings of the Quadrennial International Ozone Symposium, IAMAP, pp 580-585, J. London, editor, 1980.

Anderson, J. G., H. J. Grassl, R. E. Shetter, and J. J. Margitan, Stratospheric free chlorine measured by balloon-borne in situ resonance fluorescence, J. Geophys. Res. 85, 2869-2887, 1980.

Anderson, J. G., H. J. Grassl, R. E. Shetter, and J. J. Margitan, HO_2 in the stratosphere: Three in situ observations, Geophys. Res. Lett., 8, 289-292, 1981.

Andrews, D. G., and M. E. McIntyre, Planetary waves in horizontal and vertical shear: The generalized Eliassen-Palm relation and the mean zonal acceleration, J. Atmos. Sci., 33, 2031-2048, 1976.

Andrews, D. G., and M. E. McIntyre, Generalized Eliassen-Palm and Charney-Drazin theorems for waves in axisymmetric mean flows in compressible atmospheres, J. Atmos. Sci., 35, 175-185, 1978a.

Andrews, D. G., and M. E. McIntyre, An exact theory of nonlinear waves in a Langrangian-mean flow, J. Fluid Mech., 89, 609-646, 1978b.

Andrews, D. G., J. D. Mahlman, and R. W. Sinclair, The use of the Eliassen-Palm flux as a diagnostic of wave, mean-flow interaction in a general circulation model, Handbook for MAP, Volume 2, S. K. Avery, editor, pp 99-100, 1981.

Angell, J. K., and J. Korshover, Quasi-biennial and long-term fluctuations in total ozone, Mon. Weather Rev., 101, 426-443, 1973.

Angell, J. K., and J. Korshover, Global analysis of recent total ozone fluctuations, Mon. Weather Rev., 104, 63-75, 1976.

Angell, J. K., and J. Korshover, Estimate of the global change in temperature, surface to 100 mb, between 1958 and 1975, Mon. Weather Rev., 105, 375-385, 1977.

Angell, J. K., and J. Korshover, Global ozone variations: An update into 1976, Mon. Weather Rev., 106, 725-737, 1978a.

Angell, J. K., and J. Korshover, Global temperature variations, surface-100mb: An update into 1977, Mon. Weather Rev., 106, 755-770, 1978b.

Apruzese, J. P., An efficient two-stream numerical model of infrared cooling in the earth's atmosphere, Science Applications, Inc. Report No. SAI-80-147-WA, 1980.

Apruzese, J. P., M. R. Schoeberl, and D. F. Strobel, The zonally averaged circulation of the middle atmosphere calculated with IR radiant transfer, submitted to J. Atmos. Sci., 1981.

Arakawa, A., and V. R. Lamb, Computational design of the basic dynamical processes of the UCLA general circulation model, Methods in Computational Physics, 17, edited by J. Chang, Academic Press, New York, 1977.

Arijs, E., D. Nevejans, P. Frederick, and J. Ingels, Negative ion composition measurements in the stratosphere, Geophys. Res. Lett., 8, 121-124, 1981.

Arnold, F., and R. Fabian, First Measurements of gas phase sulphuric acid in the stratosphere, Nature, 283, 55-57, 1980.

Arnold, F., and G. Henschen, Mass spectrometric detection of pre-condensation nuclei in the stratosphere - evidence for a stratospheric gas to particle conversion mechanism, Geophys. Res. Lett., 8, 83-86, 1981.

Arnold, F., and D. Krankowsky, Water vapour concentrations at the mesopause, Nature, 268, 218-219, 1977.

Arnold, F., R. Fabian, G. Henschen, and W. Joos, Stratospheric trace gas analysis from ions: H_2O and HNO_3, Planet. Space Sci., 28, 681-685, 1980.

Arnold, F., R. Fabian, and W. Joos, Measurements of the height variation of sulfuric acid vapor concentrations in the stratosphere, Geophys. Res. Lett., 8, 293-296, 1981.

Arvesen, J. C., R. N. Griffin, Jr., and B. D. Pearson, Jr., Determination of extraterrestrial solar spectral irradiance from a research aircraft, Appl. Optics, 8, 2215-2232, 1969.

Asgeirsson, V., and J. L. Stanford, Systematic deviations of Nimbus-5 atmospheric temperature fields from radiosonde data over the winter Antarctic, Geophys. Res. Lett., 4, 445-447, 1977.

Atkinson, R., R. A. Perry, and J. N. Pitts, Jr., Rate constants for the reaction of OH radicals with COS, CS_2 and CH_3SCH_3 over the temperature range 299-430 K, Chem. Phys. Lett., 54, 14-18, 1978.

Atkinson, R., K. R. Darnall, A. C. Lloyd, A. M. Winer, and J. N. Pitts, Jr., Kinetics and mechanisms of the reactions of the hydroxyl radical with organic compounds in the gas phase, Advances in Env. Sci. and Tech., 11, 375-488, 1979.

Attmannspacher, W., and H. U. Dütsch, International Ozonesonde Intercomparison at the Observatory Hohenpeissenberg, 15 January - 5 February 1970, Ber. Deutschen Wetterd., 16, 11 pp, 1970.

Austen, M. D., J. J. Barnett, P. D. Curtis, C. G. Morgan, J. T. Houghton, C. D. Rodgers, and E. J. Williamson, Satellite observations of planetary waves in the mesosphere, Nature, 260, 594-596, 1976.

Austen, M. D., J. J. Barnett, P. D. Curtis, J. T. Houghton, C. G. Morgan, C. D. Rodgers, and E. J. Williamson, Satellite temperature measurements in the 40-90 km region by the Pressure Modulator Radiometer, COSPAR Space Research XVII, 111-115, 1977.

Bangham, M. J., A. Bonetti, R. H. Bradsell, B. Carli, J. G. Harries, F. Mencaraglia, D. G. Moss, J. Pollitt, E. Rossi, and N. R. Swann, New measurements of stratospheric composition using submillimeter and infrared emission spectroscopy, unpublished manuscript, 1980.

Barnett, J. J., Remote sounding of the atmosphere. D. Phil. Thesis, Clarendon Laboratory, Oxford University, 1973a.

Barnett, J. J., Analysis of stratospheric measurements by the Nimbus IV and V Selective Chopper Radiometer, Proceedings of International Symposium on Meteorological Satellites, 173-188, 1973b.

Barnett, J. J., The mean meridional temperature behaviour of the stratosphere from November 1970 to November 1971 derived from measurements by the Selective Chopper Radiometer on Nimbus-IV, Quart. J. Roy. Meteorol. Soc., 100, 505-530, 1974.

Barnett, J. J., Hemispheric coupling - evidence of a cross-equatorial planetary wave-guide in the stratosphere, Quart. J. Roy. Meteorol. Soc., 101, 835-845, 1975a.

Barnett, J. J., Large sudden warming in the Southern Hemisphere, Nature, 255, 387-389, 1975b.

Barnett, J. J., The Antarctic atmosphere as seen by satellites, Phil. Trans. Roy. Soc., Lon. Ser. B, 279, 247-259, 1977.

Barnett, J. J., Satellite measurements of middle atmosphere temperature structure, Roy. Soc. Lon. Phil. Trans., A296, 41-57, 1980.

Barnett, J. J., Middle Atmosphere Climatology, Extended Abstracts from International Symposium on Middle Atmosphere Dynamics and Transport, Handbook for MAP, Volume 2, S. K. Avery, editor, pp 45-50, 1981.

Barnett, J. J., and C. D. Walshaw, Temperature measurements from a satellite: Applications and achievements, Environ. Remote Sensing, 187-213, 1972.

Barnett, J. J., M. J. Cross, R. S. Harwood, J. T. Houghton, C. G. Morgan, G. E. Peckham, C. D. Rodgers, S. D. Smith, and E. J. Williamson, The first year of the Selective Chopper Radiometer on Nimbus 4, Quart. J. Roy. Meteorol. Soc., 98, 17-37, 1971.

Barnett, J. J., R. S. Harwood, J. T. Houghton, S. G. Morgan, C. D. Rodgers, E. J. Williamson, G. E. Peckman, and S. D. Smith, Stratospheric warming observed by Nimbus 4, Nature, 230, 47-48, 1971.

Barnett, J. J., J. T. Houghton, C. G. Morgan, D. R. Pick, C. D. Rodgers, E. J. Williamson, M. J. Cross, D. Flower, G. Peckham, and S. D. Smith, Stratospheric observations from Nimbus 5, Nature, 245, 141-145, 1973.

Barnett, J. J., J. T. Houghton, and J. A. Pyle, The temperature dependence of the ozone concentration near the stratopause, Quart. J. Roy. Meteorol. Soc., 101, 245-257, 1975a.

Barnett, J. J., R. S. Harwood, J. T. Houghton, C. G. Morgan, C. D. Rodgers, and E. J. Williamson, Comparison between radiosonde, rocketsonde and satellite observations of atmospheric temperatures, Quart. J. Roy. Meteorol. Soc., 101, 423-436, 1975b.

Barnett, J. J., F. N. Alyea, and D. M. Cunnold, Comparison between satellite radiance observations and those derived from a stratospheric numerical model, Extended Summaries IAGA/IAMAP Joint Assembly, Seattle, pp 17(1-9), 1977.

Barnett, J. J., J. T. Houghton, and G. D. Peskett, Observations of the stratosphere and mesosphere from Nimbus satellites, Presented at COSPAR Plenary Meeting, Innsbruck, Austria, 7p (Available from AIAA-TIS no. A78-48613), 1978.

Bass, A. M., L. C. Glasgow, C. Miller, J. P. Jesson, and D. L. Filkin, Temperature dependent absorption cross sections for formaldehyde (CH_2O): The effect of formaldehyde on stratospheric chlorine chemistry, Proceedings of the NATO Advanced Institute on Atmospheric Ozone, A. C. Aikin, editor, FAA-EE-80-20, 467-477, 1980.

Bates, J. R., Dynamics of stationary ultra-long waves in middle latitudes, Quart. J. Roy. Meteorol. Soc., 103, 397-430, 1977.

Bates, D. R., and M. Nicolet, The photochemistry of atmospheric water vapor, J. Geophys. Res., 55, 301-327, 1950.

Bauer, E., A catalog of perturbing influences on stratospheric ozone, 1955-1975, J. Geophys. Res. 84, 6929-6940, 1979.

Bauer, E., A catalogue of perturbing influences on stratospheric ozone, 1955-1975, Federal Aviation Administration Report No. FAA-EQ-78-20, U.S. Department of Transportation, Washington, D.C., September, 1978.

Baulch, D. L., R. A. Cox, R. F. Hampson, Jr., J. A. Kerr, J. Troe, and R. T. Watson, Evaluated kinetic and photochemical data for atmospheric chemistry, J. Phys. Chem. Ref. Data, 9, 295-471, 1980.

Berg, W. W., and J. W. Winchester, Organic and inorganic gaseous chlorine concentrations in relation to the particle size distribution of chloride in the marine aerosol, J. Geophys. Res., 82, 5948-5943, 1977.

Berg, W. W., P. J. Crutzen, F. E. Grahek, S. N. Gitlin, and W. A. Sedlacek, First measurements of total chlorine and bromine in the lower stratosphere, Geophys. Res. Lett., 7, 937-940, 1980.

Berggren, R., and K. Labitzke, A detailed study of the horizontal and vertical distribution of ozone, Tellus, 18, 761-772, 1966.

Berggren, R., and K. Labitzke, The distribution of ozone on pressure surfaces, Tellus, 20, 88-97, 1968.

Bigg, E. K. Stratospheric particles, J. Atmos. Sci., 32, 910-917, 1975.

Bigg, E. K., Size distributions of stratospheric aerosols and their variations with altitude and time, J. Atmos. Sci., 33, 1080-1086, 1976.

Birks, J. W., B. Shoemaker, T. J. Leck, R. A. Borders, and L. J. Hart, Studies of reactions of importance in the stratosphere II. Reactions involving chlorine nitrate and chlorine dioxide, J. Chem. Phys., 66, 4591-4599, 1977.

Birrer, W. H., Some critical remarks on trend analysis of total ozone data, Pure Appl. Geophys., 112, 523-532, 1974.

Birrer, W., Homogenisierung und discussion der totalozon-messreihe von Arosa 1926-1971, Laboratory for Atmospheric Physics ETH, Zürich, Switzerland, 196 pp, 1975.

Bischof, W., P. Fabian, and R. Borchers, Decrease in CO_2 mixing ratio observed in the stratosphere, Nature, 288, 347-348, 1980.

Bishop, L., and W. J. Hill, Analyzing stratospheric ozone for the natural and man-made trend variability, Proceedings of the Environmetrics's 81 Conference, Washington, D.C., 1981.

Blackmon, M. L., A climatological spectral study of the 500 mb geopotential height of the Northern Hemisphere, J. Atmos. Sci., 33, 1607-1623, 1976.

Blackshear, W. T., and R. H. Tolson, High correlations between variations in monthly averages of solar activity and total atmospheric ozone, Geophys. Res. Lett., 5, 921-924, 1978.

Blake, D., and R. S. Lindzen, Effect of photochemical models on calculated equilibria and cooling rates in the stratosphere, Mon. Weather Rev., 101, 783-802, 1973.

Blatherwick, R. D., A. Goldman, D. G. Murcray, F. J. Murcray, G. R. Cook, and J. W. VanAllen, Simultaneous mixing ratio profiles of stratospheric NO and NO_2 as derived from balloon-borne infrared solar spectra, Geophys. Res. Lett., 7, 471-473, 1980.

Bleck, R., Short-range prediction in isentropic coordinates with filtered and unfiltered numerical models, Mon. Weather Rev., 102, 813-829, 1974.

Bleck, R., Simulation of coastal upwelling frontogenesis with an isopycnic coordinate model, J. Geophys. Res., 83 6163-6172, 1978.

Bloomfield, P., Fourier Analysis of Time Series: An Introduction, New York: Wiley, 1976.

Bloomfield, P., M. L. Thompson, G. S. Watson, and S. Zeger, Frequency domain estimation of trends in stratospheric ozone, Tech. Rpt. 182, Dept. of Statistics, Princeton University submitted to J. Geophys. Res., 1981.

Borucki, W. J., R. C. Whitten, H. T. Woodward, L. A. Capone, C. A. Riegel, and S. Gaines, Stratospheric ozone decrease due to chlorofluoromethane photolysis: Predictions of latitude dependence, J. Atmos. Sci., 37, 686-697, 1980.

Bossy, L., and M. Nicolet, On the variability of Lyman alpha with solar activity, Planet. Space Sci., 29, 907-914, 1981.

Bourke, W., A multi-level spectral model. I. Formulations and hemispheric integrations, Mon. Weather Rev., 102, 687-701, 1974.

Boyd, J. P., The noninteraction of waves with the zonally averaged flow on a spherical earth and the interrelationships of eddy fluxes of energy, heat and momentum, J. Atmos. Sci., 33, 2285-2291, 1976.

Box, G. E. P., and G. M. Jenkins, Time Series Analysis Forecasting and Control, 2nd ed., Holden-Day, San Francisco, 1976.

Brasseur, G., A two-dimensional model of minor constituents in the stratosphere, Presented at the WMO Workshop on Two-Dimensional Models in Toronto, Canada, February, 1980.

Brasseur, G., and M. Bertin, The action of chlorine on the ozone layer as given by a zonally averaged two-dimensional model, Pure Appl. Geophys., 117, 436-447, 1978.

Breiland, J. G., Comparison of the vertical distribution of thermal stability in the lower stratosphere with the vertical distribution of atmospheric ozone, J. Atmos. Sci., 24, 569-576, 1967.

Breiland, J. G., Some large-scale features of the vertical distribution of atmospheric ozone associated with the thermal structure of the atmosphere, J. Geophys. Res., 73, 5021-5028, 1968.

Brewer, A. W., Evidence for a world circulation provided by the measurements of helium and water vapour distribution in the stratosphere, Quart. J. Roy. Meteorol. Soc., 75, 351-363, 1949.

Brezgin, N. I., A. Ph. Chizhov, and O. V. Shtyrkov, Ozone and turbidity rocket measurements in the middle atmosphere of the tropics of the Indian Ocean during MONEX-79, (Abstract), IAMAP Third Scientific Assembly, Hamburg, Federal Republic of Germany, August, 1981.

Briggs, J., and W. T. Roach, Aircraft observations near jet streams, Quart. J. Roy. Meteorol. Soc., 89, 225-247, 1963.

Brinza, D. E., H. M. Pickett, and E. A. Cohen, Pressure induced broadening of ^{35}ClO and $^{16}O_2$ millimeter wavelength transitions by N_2, Paper presented at the Topical Meeting on Spectroscopy in Support of Atmospheric Measurements, November 10-12, 1980.

Broadfoot, A. L., The solar spectrum 2100 - 3200 A, Astrophys. J., 173, 681-689, 1972.

Brown, G. M., and J. I. John, Vertical penetration of planetary waves into the lower ionosphere, J. Atmos. Terr. Phys., 41, 379-385, 1979.

Brownlee, D. E., Microparticle studies by sampling techniques, in Cosmic Dust, J. McDonnell, editor, Wiley, New York, pp 295-336, 1978.

Brownlee, D. E., G. V. Ferry, and D. Tomandl, Stratospheric aluminum oxide, Science, 191, 1270-1271, 1976.

Brueckner, G. E., The variability of the Sun's ultraviolet radiation, Planetary Aeronomy and Astronomy, Advances in Space Research, 7, No 9 Pergamon, 101-116, 1981.

Brueckner, G. E., J.-D. F. Bartoe, O. K. Moe, and M. E. VanHoosier, Absolute solar ultraviolet intensities and their variations with solar activity I: The wavelength region 1750 - 2100 A, Astrophys. J., 209, 935-944, 1976.

Bruner, F., CMA-Universita deli Studi di Urbine research project-CMA ref 78-265R-final report, 1980.

Buijs, H. L., G. L. Vail, G. Tremblay, and D. J. W. Kendall, Simultaneous measurements of the volume mixing ratio of HCl and HF in the stratosphere, Geophys. Res.Lett., 7, 205-208, 1980.

Burkhardt, E. G., C. A. Lambert, and C. K. N. Patel, Stratospheric nitric oxide: Measurements during daytime and sunset, Science, 188, 1111-1113, 1975.

Burnett, C. R., Terrestrial OH abundance measurement by spectroscopic observation of resonance absorption of sunlight, Geophys. Res. Lett., 3, 319-322, 1976.

Burnett, C. R., Spectroscopic measurement of atmospheric OH abundance, Bull. Am. Phys. Soc., 22, 539, 1977.

Burnett, C. R., and E. B. Burnett, Spectroscopic measurements of the vertical column abundance of hydroxyl (OH) in the earth's atmosphere, J. Geophys. Res., 86, 5185-5202, 1981.

Burrows, J. P., G. W. Harris, and B. A. Thrush, Rates of reaction of HO_2 with HO and O studied by laser magnetic resonance, Nature, 267, 233-234, 1977.

Bush, Y. A., A. L. Schmeltekopf, F. C. Fehsenfeld, D. L. Albritton, J. R. McAfee, P. D. Goldan, and E. E. Ferguson, Stratospheric measurements of methane at several latitudes, Geophys. Res. Lett., 5, 1027-1029, 1978.

Bytchart, N., S. A. Clough, T. N. Palmer, and P. J. Trevelyan, Simulations of an observed stratospheric warning with quasigeostrophic refraction index as a model diagnostic, Quart. J. Roy. Meteorol. Soc., submitted 1981.

Callis, L. B., and J. E. Nealy, Solar UV variability and its effect on stratospheric thermal structure and trace constituents, Geophys. Res. Lett., 5, 249-252, 1978.

Campbell, M. J., J. C. Sheppard, and B. F. Au, Measurement of hydroxyl concentration in boundary layer air by monitoring CO oxidation, Geophys. Res. Lett., 6, 175-178, 1979.

Carlson, E. R., M. V. Schneider, and T. F. McMaster, Subharmonically pumped millimeter wave mixers, IEEE Trans. Microwave Theory Tech., 26, 706-715, 1978.

Castleman, A. W., Jr., H. R. Munkelwitz, and B. Manowitz, Isotopic studies of the sulfur component of the stratospheric aerosol layer, Tellus, 26, 222-234, 1974.

C.E.Q., Global Energy Futures and the Carbon Dioxide Problem, Council on Environmental Quality, U.S. Government Printing Office, Washington, D.C., 1981.

Chaloner, C. P., J. R. Drummond, J. T. Houghton, R. F. Jarnot, and H. K. Roscoe, Infrared measurements of stratospheric composition I. The balloon instrument and water vapour measurements, Proc. Roy. Soc. London A, 364, 145-159, 1978.

Chameides, W. L., The photochemical role of tropospheric nitrogen oxides, Geophys. Res. Lett., 5, 17-20, 1978.

Chameides, W. L., and D. D. Davis, Iodine: Its possible role in tropospheric photochemistry, J. Geophys. Res., 85, 7383-7398, 1980.

Chameides, W. L., and A. Tan, The two-dimensional diagnostic model for tropospheric OH: An uncertainty analysis, J. Geophys. Res., 86, 5209-5223, 1981.

Chameides W., and J. C. G. Walker, A photochemical theory of tropospheric ozone, J. Geophys. Res., 78, 8751-8760, 1973.

Chandra, S., An assessment of possible ozone-solar cycle relationships inferred from Nimbus-4 BUV data, J. Geophys. Res., submitted, 1981.

Chang, J. S. and H. S. Johnston, The effect of NO_x effluents on ozone, in Proceedings of the 3rd Conference on CIAP, A. J. Broderick and T. M. Hard, editors, DOT-TSC-OST-74-15, pp 323-329, 1974.

Chang, J. S., and F. Kaufman, Upper bound and probable value of the rate constant of the reaction $OH + HO_2 \rightarrow H_2O + O_2$, J. Phys. Chem., 82, 1683-1687, 1978.

Chang S. W., and R. -J. Madala, Numerical simulation of the influence of sea surface temperatures on translating tropical cyclones, J. Atmos. Sci., 37, 2617-2630, 1980.

Chang, J. S., and J. E. Penner, Analysis of global budgets of halocarbons, Atmos. Environ., 12, 1867-1873, 1978.

Chang, J. S., A. C. Baldwin, and D. M. Golden, An explanation of the preferential formation of less stable isomers in three body reactions: $Cl + NO_2 + M$; $ClO + NO_2 + M$, J. Chem. Phys., 71, 2021-2024, 1979a.

Chang, J. S., J. R. Barker, J. E. Davenport, and D. M. Golden, Chlorine nitrate photolysis by a new technique: Very low pressure photolysis, Chem. Phys. Lett., 60, 385-390, 1979b.

Chang, J. S., D. J. Wuebbles, and W. H. Duewer, The atmospheric nuclear tests of the 1950s and 1960s: A possible test of ozone depletion theories, J. Geophys. Res., 84, 1755-1765, 1979c.

Chapman, W. A., and J. McGregor, The application of complex demodulation to meteorological satellite data, Quart. J. Roy. Meteorol. Soc., 104, 213-223, 1978.

Chapman, W. A., and T. Miles, Planetary-scale wave guides in the troposphere and stratosphere, Nature, 293, 108-112, 1981.

Chapman, W. A., M. J. Cross, D. A. Flower, G. E. Peckham, and S. D. Smith, A spectral analysis of global atmospheric temperature fields observed by the Selective Chopper Radiometer on the Nimbus 4 satellite during the year 1970-1, Proc. Roy. Soc. London A, 338, 57-76, 1974.

Charney, J. G., and P. G. Drazin, Propagation of planetary-scale disturbances from the lower into the upper atmosphere, J. Geophys. Res., 66, 83-109, 1961.

Chatfield, R., and H. Harrison, Tropospheric ozone, 2, Variations along a meridional band, J. Geophys. Res., 82, 5969-5976, 1977.

Chemical Manufacturers Association, World production and release of chlorofluorocarbons 11 and 12 through 1980, CMA Fluorocarbons Project Panel, 1981.

Chiu J. S. U., A self contained iterative algorithm for a numerical solution to the radiative transfer equation, Beitrage Phy. Atm., 48, 185-198, 1975.

Chleck, D., Measurements of upper atmosphere water vapor made in situ with a new moisture sensor, Geophys. Res. Lett., 6, 379-381, 1979.

CIAP, The Stratosphere Perturbed by Propulsion Effluents, CIAP Monograph III, DOT-TST-75-53, 1975a.

CIAP, The Natural Stratosphere of 1974, CIAP Monograph 1, DOT-TST-75-51, 1975b.

Cicerone, R. J., Atmospheric carbon tetrafluoride: a nearly inert gas, Science, 206, 59-61, 1979.

Cicerone, R. J., Halogens in the atmosphere, Rev. Geophys. Space Phys., 19, 123-139, 1981.

Cicerone, R., and S. Walters, NO_2-catalyzed removal of stratospheric HO_x, Presented at the 14th Informal Conference on Photochemistry, Newport Beach, Calif., 1980.

Clark, J. H. E., A quasi-geostrophic model of the winter stratospheric circulation, Mon. Weather Rev., 98, 443-461, 1970.

Clark, J. H. E., and T. G. Rogers, The transport of conservative trace gases by planetary waves, J. Atmos. Sci., 35, 2232-2235, 1978.

Clough, S. A., Two-dimensional chemical modelling in the U. K. Meteorological Office, Presented at the WMO Workshop on Two-Dimensional Models Toronto, Canada held during February, 1980

Coffey, M. T., W. G. Mankin, and A. Goldman, Simultaneous spectroscopic determination of the latitudinal, seasonal, and diurnal variability of stratospheric N_2O, NO, NO_2, and HNO_3, J. Geophys. Res., 86, 7331-7341, 1981.

COMESA, The Report of the Committee on Meteorological Effects of Stratospheric Aircraft (1972-1975), U.K. Meteorological Office, Bracknell, 1975.

Connell, P. S., R. A. Perry, and C. J. Howard, Tunable diode laser measurement of nitrous oxide in air, Geophys. Res. Lett., 7, 1093-1096, 1980.

Cook, J. W., G. E. Brueckner, and M. E. VanHoosier, Variability of the solar flux in the far ultraviolet 1175 - 2100 A, J. Geophys. Res., 85, 2257-2268, 1980.

Cox, R. A., and J. P. Burrows, Kinetics and mechanism at the disproportionation of HO_2 in the gas phase, J. Phys. Chem., 83, 2560-2568, 1979.

Cox, R. A., and R. G. Derwent, Gas phase chemistry of the minor constituents of the troposphere, Gas Kinetics and Energy Transfer, 4, 189-230, Royal Society of Chemistry, London, 1981.

Cox, R. A., and R. Lewis, Kinetics of ClO radical reactions using modulated photolysis, Part 3, Pressure and temperature dependence of the reaction: $ClO + NO_2 (+ M) \rightarrow ClONO_2 (+ M)$, J. Chem. Soc. Lon. Farad. Trans. 1, 75, 2649-2661, 1979.

Coy, L., and C. Leovy, A comparison of mid-winter stratospheric warmings in the southern and northern hemispheres, Extended Summaries, IAMAP/IAGA Joint Assembly, Seattle, pp 46(1-5), 1977.

Craig, R. A., The observations and photochemistry of atmospheric ozone and their meteorological significance, Meteorological Monographs, 1(2), 50 pp, 1950.

Craig, R. A., The Upper Atmosphere, Meteorology and Physics. Academic Press: New York and London, 209 pp, 1965.

Crane, A. J., Aspects of the energetics of the upper stratosphere during the January-February 1973 major sudden warming, Quart. J. Roy. Meteorol. Soc., 105, 185-206, 1979a.

Crane, A. J., Annual and semiannual waves in the temperature of the mesosphere as deduced from Nimbus 6 PMR measurements, Quart. J. Roy. Meteorol. Soc., 105, 509-520, 1979b.

Crane, A. J., and J. J. Barnett, Energetics of the upper stratosphere during a sudden warming, Extended Summaries, IAGA/IAMAP Joint Assembly, Seattle, pp 53(1-8), 1977.

Crane, A. J., J. D. Haigh, J. A. Pyle, and C. F. Rogers, Mean meridional circulations of the stratosphere and mesophere, Pure Appl. Geophys, 118, 307-328, 1980.

Cronn, D., and E. Robinson, Tropospheric and lower stratospheric vertical profiles of ethane and acetylene, Geophys. Res. Lett., 6, 641-644, 1979.

Cronn, D. R., R. A. Rasmussen, E. Robinson, and D. E. Harsch, Halogenated compound identification and measurement in the troposphere and lower stratosphere, J. Geophys. Res., 82, 5935-5944, 1977.

Crosby, D. S., W. G. Planet, A. J. Miller, and R. M. Nagatani, Evaulation and comparison of total ozone fields derived from TOVS and SBUV, Proceedings of the Quadrennial International Ozone Symposium, IAMAP, J. London, editor, pp 161-167, 1980.

Crutzen, P. J., Ozone production rates in an oxygen, hydrogen-nitrogen oxide atmosphere, J. Geophys. Res., 76, 7311-7327, 1971.

Crutzen, P. J., Photochemical reactions initiated by and influencing ozone in unpolluted tropospheric air, Tellus, 26, 47-57, 1974.

Crutzen, P. J., The possible importance of CSO for the sulfate layer of the stratosphere, Geophys. Res. Lett., 3, 73-76, 1976.

Crutzen, P. J., Solar variability--the stratosphere and mesosphere, in The Solar Output and Its Variations, Oran R. White, editor, Colorado Associated University Press, Boulder, pp 13-16, 1977.

Crutzen, P. J., and L. T. Gidel, A two-dimensional, photochemical model of the atmosphere below 55 km, Presented at the WMO Workshop on Two-Dimensional Models, Toronto, Canada, February, 1980.

Crutzen, P. J., L. E. Heidt, J. P. Krasnec, W. H. Pollock, and W. Seiler, Biomass burning as a source of atmospheric gases CO, H_2, N_2O, NO, CH_3Cl and COS, Nature, 282, 253-256, 1979.

Cunnold, D., F. Alyea, N. Phillip, and R. Prinn, A three-dimensional dynamical-chemical model of atmospheric ozone, J. Atmos. Sci., 32, 170-194, 1975.

Cunnold, D. M., F. N. Alyea, and R. G. Prinn, Preliminary calculations concerning the maintenance of the zonal mean ozone distribution in the northern hemisphere, Pure Appl. Geophys., 118, 329-354, 1980.

Danielsen, E. F., A determination of the mass transported from the stratosphere to the troposphere over North America during a thirty-six hour interval, Mitt. Deut. Wetterdienstes, 20, 10-11, 1959.

Danielsen, E. F., Stratospheric-tropospheric exchange based on radioactivity, ozone and potential vorticity, J. Atmos. Sci., 25, 502-518, 1968.

Danielsen, E. F., An objective method for determining the generalized transport tensor for two dimensional Eulerian models, J. Atmos. Sci., 38, 1319-1339, 1981.

Danielsen, E. F., and R. S. Hipskind, Stratospheric-tropospheric exchange at polar latitudes in summer, J. Geophys. Res., 85, 393-400, 1980.

Danielsen, E. F., and V. A. Mohnen, Project Dustorm report: Ozone transport, in situ measurements, and meteorological analyses of tropopause folding, J. Geophys. Res., 82, 5867-5877, 1977.

Danielsen, E. F., K. H. Bergman, and C. A. Paulsen, Radioisotopes, potential temperature and potential vorticity, A study of stratospheric-tropospheric exchange processes, Dept. of Meteorology and Climatology, University of Washington, 54 pp, 1962.

Danielson, E. F., R. Bleck, J. Shedlovsky, A. Wartburg, P. Haagenson, and W. Pollock, Observed distribution of radioactivity, ozone, and potential vorticity associated with tropopause folding, J. Geophys. Res., 75, 2353-2361, 1970.

Dave, J. V., C. L. Mateer, and J. J. DeLuisi, An examination of the effect of haze on the short Umkehr method for deducing the vertical distribution of ozone, Proceedings of the Quadrennial International Ozone Symposium, IAMAP, J. London, editor, 222-229, 1980.

Davis, D. D., Project Gametag: An overview, J. Geophys. Res., 85, 7285-7292, 1980.

Davis, D. D., W. Heaps, and T. McGee, Direct measurements of natural tropospheric levels of OH via an aircraft-borne tunable dye laser, Geophys. Res. Lett., 3, 331-333, 1976.

Davis, D. D., W. Heaps, D. Philen, and T. McGee, Boundary layer measurements of the OH radical in the vicinity of an isolated power plant plume: SO_2 and NO_2 chemical conversion times, Atmos. Env., 13, 1197-1203, 1979.

Davis, D. D., W. L. Chameides, D. Philen, W. Heaps, A. Ravishankara, and M. Rodgers, Hydroxyl radical measurements in the marine boundary layer at tropical and sub-tropical latitudes, J. Geophys. Res., submitted, 1981a.

Davis, D. D., M. O. Rodgers, S. D. Fischer, and K. Asai, An experimental assessment of the O_3/H_2O interference problem in the detection of natural levels of OH via laser induced fluorescence, Geophys. Res. Lett., 8, 69-72, 1981b.

Davis, D. D., M. O. Rodgers, S. D. Fischer, and W. S. Heaps, A theoretical assessment of the O_3/H_2O interference problem in the detection of natural levels of OH via laser induced fluorescence, Geophys. Res. Lett., 8, 73-76, 1981c.

Dawson, G. A., Nitrogen fixation by lightning, J. Atmos. Sci., 37, 174-178, 1980.

Deland, R. J., Spectral analysis of traveling planetary scale waves: Vertical structure in middle latitudes of Northern Hemisphere, Tellus, 25, 355-373, 1973.

Deland, R. J., Evidence of downward propagating planetary-scale waves in the Southern Hemisphere winter stratosphere, Extended Summaries, IAMAP/IAGA Assembly, Seattle, pp 4(1-6), 1977.

Delany, A. C., J. P. Shedlovsky, and W. H. Pollock, Stratospheric aerosol: The contribution from the troposphere, J. Geophys. Res., 79, 5646-5650, 1974.

DeLuisi, J. J., Umkehr vertical ozone profile errors caused by the presence of stratospheric aerosols, J. Geophys. Res., 84, 1766-1770, 1979.

DeMore, W. B., Reaction of HO_2 with O_3 and the effect of water vapor on HO_2 kinetics, J. Phys. Chem., 83, 1113-1118, 1979.

DeMore, W. B., and E. Tschuikow-Roux, Temperature dependence of the reactions of OH and HO_2 with O_3, J. Phys. Chem., 78, 1447-1451, 1974.

DeMore, W. B., L. J. Stief, F. Kaufman, D. M. Golden, R. F. Hampson, M. J. Kurylo, J. J. Margitan, M. J. Molina, and R. T. Watson, Chemical Kinetic and Photochemical Data for Use in Stratospheric Modeling, JPL Publication 79-27, Jet Propulsion Laboratory, Pasadena, California, USA, 1979.

Derwent, R. G., Two-dimensional model studies of the impact of aircraft exhaust emissions on tropospheric ozone, Atmos. Environ., (to be published), 1981.

Derwent, R. G., and A. R. Curtis, Stratospheric Ozone Depletion Estimates for Global Halocarbon Usage Estimated by the Linear Superposition of Contributions from Individual Halocarbons, AERE Report-R10168, Her Majesty's Stationery Office, London, 1981.

Derwent, R. G., and E. J. Eggleton, Halocarbon lifetimes and concentration distributions calculated using a two-dimensional tropospheric model, Atmos. Environ. 12, 1261-1269, 1978.

Derwent, R. G., and E. J. Eggleton, Two-dimensional model studies of methyl chloroform in the troposphere, Quart. J. Roy. Meteorol. Soc., 107, 231-242, 1981.

Dickinson, R. E., On the exact and approximate linear theory of vertically propagating planetary Rossby waves forced at a spherical lower boundary, Mon. Weather Rev., 96, 405-415, 1968a.

Dickinson, R. E., Planetary Rossby waves propagating vertically through weak westerly wind wave guides, J. Atmos. Sci., 25, 984-1002, 1968b.

Dickinson, R. E., Vertical propagation of planetary Rossby waves through an atmosphere with Newtonian cooling, J. Geophys. Res., 94, 929-938, 1969.

Dickinson, R. E., Development of a Rossby wave critical level, J. Atmos. Sci., 27, 627-633, 1970.

Dickinson, R. E., Planetary waves: Theory and observation in Orographic Effects in Planetary Flows, WMO GARP Publ. No 23, 51-84, 1980.

Dobson, G. M. B., Observations of the amount of ozone in the earth's atmosphere and its relation to other geophysical conditions - Part IV, Proc. Roy. Soc. London, A, 129, 411-433, 1930.

Dobson, G. M. B., Origin and distribution of polyatomic molecules in the atmosphere, Proc. Roy. Soc. London, A, 236 , 187-193, 1956.

Dobson, G. M. B. and D. N. Harrison, Measurements of the amount of ozone in the earth's atmosphere and its relation to other geophysical conditions, Proc. Roy. Soc. London, A, 110, 660-693, 1926.

Dobson, G. M. B., D. N. Harrison, and J. Lawrence, Measurements of the amount of ozone in the earth's atmosphere and its relation to other geophysical conditions, Part II, Proc. Roy. Soc. London, A, **114**, 521-541, 1927.

Dobson, G. M. B., D. N. Harrison, and J. Lawrence, Measurement of the amount of ozone in the earth's atmosphere and its relation to other geophysical conditions, Proc. Roy. Soc. London, A, **122**, 456-486, 1929.

Dobson, G. M. B., A. W. Brewer, and B. Cwilong, Meteorology of the lower stratosphere, Proc. Roy. Soc. London, A, **185**, 144-175, 1946.

Drummond, J. W., Atmospheric measurements of nitric oxide using a chemiluminescent detector, PhD. Thesis, University of Wyoming, 1977.

Drummond J. R., and R. F. Jarnot, Infrared measurements of stratospheric composition II. Simultaneous NO and NO_2 measurements, Proc. Roy. Soc. London, A, **364**, 237-254, 1978.

Drummond, J. W., J. M. Rosen, and D. J. Hofmann, Balloon-borne chemiluminescent measurement of NO to 45 km, Nature, **265**, 319-320, 1977.

Drummond, J. W., D. Kley, M. McFarland, A. L. Schmeltekopf, J. M. Rosen, and D. H. Hofmann, Stratospheric measurements of ozone using a nitric oxide-ozone chemiluminescence detector, (abstract) EOS Trans. AGU, **60**, 269, 1979.

Drummond, J. R., J. T. Houghton, G. D. Peskett, C. D. Rodgers, M. J. Wale, J. Whitney, and E. J. Williamson, The Stratospheric and Mesospheric Sounder on Nimbus 7, Phil. Trans. Roy. Soc. Lon. A, **296**, 219-241, 1980.

Duewer, W. H., D. J. Wuebbles, and J. S. Chang, Effects of NO photolysis on NO_y mixing ratios, Nature, **265**, 523-525, 1977.

Dunkerton, T., On the mean meridional mass motions of the stratosphere and mesosphere, J. Atmos. Sci., **35**, 2325-2333, 1978.

Dunkerton, T., On the role of the Kelvin wave in the westerly phase of the semiannual zonal wind oscillation, J. Atmos. Sci., **36**, 32-41, 1979.

Dunkerton, T., A Lagrangian mean theory of wave, mean-flow interaction with applications to nonacceleration and its break down--large-scale atmospheric dynamics, Rev. Geophys. Space Sci., **18**, 387-400, 1980.

Dunkerton, T., C. P. Hsu, and M. E. McIntyre, Some Eulerian and Lagrangian diagnostics for a model stratospheric warming, J. Atmos. Sci., **38**, 819-843, 1981.

Du Pont, Some concerns with recent EPA communications on the fluorocarbon/ozone issue, E. I. du Pont de Nemours & Company, Wilmington, Delaware, June, 1980.

Dütsch, H. U., Photochemische theorie des atmosphärischen ozons unter Berucksichtigung von Nichtgleichgewichtszustanden und Luftbewegungen, Zürich, Doctoral Dissertation, 1946.

Dütsch, H. U., Ozone distribution and stratospheric temperature field over Europe during the sudden stratospheric warming in January/February 1958, Beitr. Physik Atmos., **35**, 87-107, 1962.

Dütsch, H. U., Atmospheric ozone and ultraviolet radiation, World Survey of Climatology, Vol 4, Climate of the Free Atmosphere, D. F. Rex., Editor, Elsevier, pp 383-432, 1969.

Dütsch, H. U., Photochemistry of atmospheric ozone, Advances in Geophysics, **15**, Academic Press, pp 219-232, 1971.

Dütsch, H. U., Regular ozone soundings at the aerological station of the Swiss Meteorological Office at Payerne, Switzerland, 1968-1972, Lapeth-10, Laboratorium für Atmosphärenphysik ETH, Zürich, 337 pp. (NTIS N75-2185415GA), 1974.

Dütsch, H. U., Vertical ozone distribution on a global scale, Pure Appl. Geophys., **116**, 511-529, 1978.

Dütsch, H. U., The search for solar-cycle ozone relationships, J. Atmos. Terr. Phys., **41**, 771-785, 1979.

Dütsch, H. U., and C. Ling, Six years of regular ozone soundings over Switzerland, Pure Appl. Geophys., **106-108**, 1151-1168, 1973.

Dutton, J. A., The Ceaseless Wind, McGraw-Hill, 579, 1976.

Edmon, H. J., Jr., B. J. Hoskins, and M. E. McIntyre, Eliassen-Palm cross sections for the troposphere, J. Atmos. Sci., **37**, 2600-2616, 1980.

Ehhalt, D. H., The atmospheric cycle of methane, Tellus, **26**, 58-70, 1974.

Ehhalt, D. H., In situ measurements of stratospheric trace constitutents, Rev. Geophys. Space Phys., **16**, 217-224, 1978.

Ehhalt, D. H., Des Atmosphärische Kreislauf von methan, Naturwissenschaften, **66**, 307-311, 1979.

Ehhalt, D. H., In situ observations, Phil. Trans. Roy. Soc. London, **A196**, 175-189, 1980.

Ehhalt, D. H., and L. E. Heidt, The concentration of molecular H_2 and CH_4 in the stratosphere, Pure Appl. Geophys., **106-108**, 1352-1360, 1973a.

Ehhalt, D. H., and L. E. Heidt, Vertical profiles of CH_4 in the troposphere and stratosphere, J. Geophys. Res., **78**, 5265-5271, 1973b.

Ehhalt, D. H., and L. E. Heidt, Vertical profiles of molecular H_2 and CH_4 in the stratosphere, AIAA Journal **12**, 822-825, 1974.

Ehhalt, D. H., and A. Tönnissen, Hydrogen and carbon compounds in the stratosphere, Proceedings of the NATO Advanced Study Institute on Atmospheric Ozone, A. C. Aikin, editor, pp 129-151, FAA-EE-80-20, 1980.

Ehhalt, D. H., L. E. Heidt, R. H. Lueb, and N. Roper, Vertical profiles of CH_4, H_2, CO, N_2O, and CO_2 in the stratosphere, Proc. III CIAP Conf., Boston, MA, A. J. Broderick and T. M. Hard, editors, DOT-TSC-OST-74-15, U. S. Department of Transportation, pp 153-159, 1974.

Ehhalt, D. H., L. E. Heidt, R. H. Lueb, and E. A. Martell, Concentrations of CH_4, CO, CO_2, H_2, H_2O, and N_2O in the upper stratosphere, J. Atmos. Sci., 32, 163-169, 1975a.

Ehhalt, D. H., L. E. Heidt, R. H. Lueb, and W. Pollock, The vertical distribution of trace gases in the stratosphere, Pure Appl. Geophys., 113, 389-402, 1975b.

Ehhalt, D. H., U. Schmidt, and L. E. Heidt, Vertical profiles of molecular hydrogen in the troposphere and the stratosphere, J. Geophys. Res., 82, 5907-5911, 1977.

Eliassen, A., and E. Palm, On the transfer of energy in stationary mountain waves, Geofys. Publ., 22, No. 3, 1-23, 1961.

Ellis, P. J., G. Peckham, S. D. Smith, J. T. Houghton, C. G. Morgan, C. D. Rodgers, and E. J. Williamson, First results from the Selective Chopper Radiometer on Nimbus 4, Nature, 228, 139-143, 1970.

Ellsaesser, H. W., J. E. Harries, D. Kley, and R. Penndorf, Stratospheric H_2O, Planet. Space Sci., 28, 827-835, 1980.

EPA, Regulating Chlorofluorocarbon Emission: Effects on Chemical Production, EPA-860/12-80-0016, 1980.

Evans, W. F. J., H. Fast, J. B. Kerr, C. T. McElroy, R. S. O'Brien, D. I. Wardle, J. C. McConnell, and B. A. Ridley, Stratospheric constituent measurements from project stratoprobe, Proc. WMO Symposium on the Geophysical Aspects and Consequences of Change in the Composition of the Stratosphere, WMO Publ. 511, World Meteorological Organization, Geneva, 55-60, 1978.

Evans, W. F. J., I. A. Asbridge, J. B. Kerr, C. L. Mateer, and R. A. Olafson, The effects of SO_2 on Dobson and Brewer total ozone measurements, Proceedings of the International Ozone Symposium, J. London, editor, 48-56, 1980.

Eyre, J. R., and H. K. Roscoe, Radiometric measurements of Stratospheric HCl, Nature, 226, 243-244, 1977.

Fabian, P., and P. G. Pruchniewicz, Meridional distribution of ozone in the troposphere and its seasonal variation, J. Geophys. Res., 82, 2063-2073, 1977.

Fabian, P., R. Borchers, K. H. Weiler, U. Schmidt, A. Volz, D. H. Ehhalt, W. Seiler, F. Muller, Simultaneously measured vertical profiles of H_2, CH_4, CO, N_2O, $CFCl_3$ and CF_2Cl_2 in the mid-latitude stratosphere and troposphere, J. Geophys. Res., 84, 3149-3154, 1979.

Fabian, P., R. Borchers, G. Flentje, W. A. Matthews, W. Seiler, H. Giehl, K. Bunse, F. Muller, U. Schmidt, A. Volz, A. Khedim, and F. J. Johnen, The vertical distribution of stable trace gases at mid-latitudes, J. Geophys. Res., 86, 5179-5184, 1981.

Farlow, N. H., D. M. Hayes, and H. Y. Lem, Stratospheric aerosols: Undissolved granules and physical state, J. Geophys. Res., 82, 4921-4929, 1977.

Farlow, N. H., K. G. Snetsinger, D. M. Hayes, H. Y. Lem, and B. M. Tooper, Nitrogen-sulfur compounds in stratospheric aerosols, J. Geophys. Res., 83, 6207-6211, 1978.

Farlow, N. H., G. V. Ferry, H. Y. Lem, and D. M. Hayes, Latitudinal variations of stratospheric aerosols, J. Geophys. Res., 84, 733-743, 1979.

Farmer, C. B., and O. F. Raper, The HF:HCl ratio in the 14-38 km region of the stratosphere, Geophys. Res. Lett., 4, 527-529, 1977.

Farmer, C. B., O. F. Raper, and R. H. Norton, Spectroscopic detection and vertical distribution of HCl in the troposphere and stratosphere, Geophys. Res. Lett., 3, 13-16, 1976.

Farmer, C. B., O. F. Raper, B. D. Robbins, R. A. Toth, and C. Müller, Simultaneous spectroscopic measurements of stratospheric species: O_3, CH_4, CO, CO_2, N_2O, H_2O, HCl and HF at northern and southern mid-latitudes, J. Geophys. Res., 85, 1621-1632, 1980.

Feely, H. W., and J. Spar, Tungsten-185 from nuclear bomb tests as a tracer for stratospheric meteorology, Nature, 188, 1062-1064, 1960.

Feely, H. W., H. Seitz, R. J. Lagomarsino, and P. E. Biscaye, Transport and fallout of stratospheric radioactive debris, Tellus, 18, 316-328, 1966.

Fels, S. B., A parameterization of scale dependent radiation rates in the middle atmosphere, J. Atmos. Sci., submitted, 1981.

Fels, S. B., and M. D. Schwarzkopf, The simplified exchange approximation - A new method for radiative transfer calculations, J. Atmos. Sci., 32, 1475-1488, 1975.

Fels, S. B., and M. D. Schwarzkopf, An efficient, accurate algorithm for calculating CO_2 15 μm band cooling rates, J. Geophys. Res., 86, 1205-1232, 1981.

Fels, S. B., J. D. Mahlman, M. D. Schwarzkopf, and R. W. Sinclair, Stratospheric sensitivity to perturbations in ozone and carbon dioxide: Radiative and dynamical response, J. Atmos. Sci., 37, 2265-2297, 1980.

Ferry, G. V., and H. Y. Lem, Aerosols in the stratosphere, Proceedings of the Third Conference on the Climatic Impact Assessment Program, Report DOT-TSC-OST-74-15, Department of Transportation, Washington, D. C., A. J. Broderick and T. M. Hard, editors, pp 310-317, 1974.

Fiocco, G., and G. Grams, Observation of aerosol layer of 20 km by optical radar, J. Atmos. Sci., 21, 323-324, 1964.

Fiocco, G., G. Grams, and A. Mugnai, Energy exchange and temperature of aerosols in the earth's atmosphere (0-60 km), J. Atmos. Sci., 33, 2415-2424, 1976.

Flocco, G., G. Grams, and A. Mugnai, Energy exchange and equilibrium temperature of aerosols in the earth's atmosphere, Proceedings of the Symposium on Radiation in the Atmosphere, H. J. Bolle, editor, Science Press, Princeton, New Jersey, pp 74-78, 1977.

Fischer, H., F. Fergg, and D. Rabus, Radiometric measurements of stratospheric H_2O, HNO_3, and NO_2 profiles, Proc. Intl. Radiation Symposium, Fort Collins, August 1980.

Fishman, J., The distribution of NO_x and the production of ozone: Comments on 'On the origin of tropospheric ozone' by S. C. Liu et al., J. Fishman, J. Geophys. Res., 86, 12,161-12,164, 1981.

Fishman, J., and P. J. Crutzen, A numerical study of tropopsheric photochemistry using a one-dimensional model, J. Geophys. Res., 82, 5897-5906, 1977.

Fishman, J., V. Ramanathan, P. J. Crutzen, and S. C. Liu, Tropospheric ozone and climate, Nature, 282, 818-820, 1979a.

Fishman, J., S. Solomon, and P. J. Crutzen, Observational and theoretical evidence in support of a significant in-situ photochemical source of tropospheric ozone, Tellus, 31, 432-446, 1979b.

Fleig, A. J., R. S. Fraser, B. W. Guenther, D. F. Heath, E. Hilsenrath, L. V. Novak, V. G. Kaveeshwar, R. D. McPeters, C. L. Mateer, and A. J. Miller, Global total ozone determinations from Nimbus-4 BUV spacecraft data, in Remote Sensing of the Atmosphere: Inversion Methods and Applications, A. Fymat and V. E. Zuev, editors, Elsevier, Scientific Publishing Company, Amsterdam, Netherlands, Dev. Atmos. Sci., 9, 97-105, 1978.

Fleig, A. J., V. G. Kaveeshwar, K. F. Klenk, M. R. Hinman, P. I. Bhartia, and P. M. Smith, Characteristics of space and ground based total ozone observing systems investigated by intercomparison of Nimbus 4 backscattered ultraviolet (BUV) data with Dobson and M-83 results, Proceedings of the Quadrennial International Ozone Symposium, IAMAP, J. London, editor, pp 9-16, 1980.

Fontanella, J. C., A. Girard, L. Gramont, and N. Louisnard, Vertical distribution of NO, NO_2, and HNO_3 as derived from stratospheric absorption infrared spectra, Appl. Opt., 14, 825-839, 1975.

Fox, R. J., G. W. Grams, B. G. Schuster, and J. A. Weinman, Measurements of stratospheric aerosols by airborne laser radar, J. Geophys. Res., 78, 7789-7801, 1973.

Fraser, G. J., The covariance of temperature and ozone due to planetary-wave forcing, NASA preprint X-911-76-192, Goddard Space Flight Center, 1976.

Fraser, G. J., and M. R. Thorpe, Experimental investigations of ionospheric/stratospheric coupling in southern mid-latitudes - 1. Spectra and cross-spectra of stratospheric temperatures and the ionospheric f-min parameters, J. Atmos. Terr. Phys., 38, 1003-1011, 1976.

Fraser, G. J. and D. S. Wratt, Experimental investigations of ionospheric/stratospheric coupling in southern mid-latitudes - 2. Comparison of mesospheric electron densities and drifts with stratospheric temperatures and winds, J. Atmos. Terr. Phys., 38, 1013-1016, 1976.

Fraser, P. J. B., and G. I. Pearman, Atmospheric halocarbons in the southern hemisphere, Atmos. Environ., **12**, 839-844, 1978.

Frederick, J. E., and R. D. Hudson, Atmospheric opacity in the Schumann-Runge bands and the aeronomic dissociation of water vapor, J. Atmos. Sci., **37**, 1088-1098, 1980.

Frederick, J. E., and J. E. Mentall, Solar irradiance in the stratosphere: Implications for the Herzberg continuum absorption of O_2, Geophys. Res. Lett., submitted, 1981.

Frederick, J. E., B. W. Guenther, P. B. Hays, and D. F. Heath, Ozone profiles and chemical loss rates in the tropical stratosphere deduced from Backscatter Ultraviolet measurements, J. Geophys. Res., **83**, 953-958, 1978.

Fritz, S., Earth's radiation to space at 15 microns: Stratospheric temperature variations, J. Appl. Meteorol., **9**, 815-824, 1970.

Fritz, S., and S. D. Soules, Large-scale temperature changes in the stratosphere observed from Nimbus-3, J. Atmos. Sci., **27**, 1091-1097, 1970.

Gadd, A. J., A split explicit integration scheme for numerical weather prediction, Quart. J. Roy. Meteorol. Soc., **104**, 569-582, 1978.

Galbally, I. E., Man-made carbon tetrachloride in the atmosphere, Science, **193**, 573-576, 1976.

Garcia, R. R., and D. L. Hartmann, The role of planetary waves in the maintenance of the zonally averaged ozone distribution of the upper stratosphere, J. Atmos. Sci., **37**, 2248-2264, 1980.

Geisler, J. E., and R. E. Dickinson, The five-day wave on a sphere with realistic zonal winds, J. Atmos. Sci., **33**, 632-641, 1976.

Geller, M. A., and J. C. Alpert, Planetary wave coupling between the troposphere and the middle atmosphere as a possible sun-weather mechanism, J. Atmos. Sci., **37**, 1197-1215, 1980.

Gelman, M. E., R. M. Nagatani, A. J. Miller, J. D. Laver, and F. C. Finger, An evaluation of stratospheric meteorological analyses using satellite sounder and rocketsonde data, Proceedings of International Symposium on Middle Atmosphere Dynamics and Transport, Urbana, Illinois, Handbook for MAP, Vol. 2, S. K. Avery, editor, pp 1-9, 1980.

Georgii, H. -W., and F. X. Meixner, Measurement of the tropospheric and stratospheric SO_2 distribution, J. Geophys. Res., **85**, 7433-7438, 1980.

German, K. R., Radiative and predissociative lifetimes of the $V' = 0$, 1 and 2 levels of the $A^2\Sigma^+$ state of OH and OD, J. Chem. Phys., **63**, 5252-5255, 1975.

German, K. R., Collision and quenching cross sections in the $A^2\ \Sigma^+$ state of OH and OD, J. Chem. Phys., **64**, 4065-4068, 1976.

Ghazi, A., Nimbus 4 observations of changes in total ozone and stratospheric temperatures during a sudden warming, J. Atmos. Sci., **31**, 2197-2206, 1974.

Ghazi, A., Infrared cooling during a stratospheric warming, J. Atmos. Terr. Phys., 39, 895-898, 1977.

Ghazi, A. Anamolous variations of radiative heating/cooling in the tropical stratosphere, Space Res. 20, 33-39, 1980a.

Ghazi, A., Atlas der Globalverteilung des Gesamtozonbetrages nach Satellitenmessungen (April 1970-Mai 1972), Mittl. Inst. Geophys. Meteor., Univ. Colonge (FRG), 28, 1980b.

Ghazi, A., Ozone effects on radiative damping in the stratosphere, Proceedings of the Quadrennial International Ozone Symposium, IAMAP, J. London, editor, pp 1048-1052, 1980c.

Ghazi, A., and J. J. Barnett, Ozone behavior and stratospheric thermal structure during southern hemisphere spring, Beitr. Phys. Atm., 53, 1-13, 1980.

Ghazi, A., A. Ebei, and D. F. Heath, A study of satellite observations of ozone and stratospheric temperatures during 1970-1971, J. Geophys. Res., 81, 5365-5373. 1976.

Ghazi, A., V. Ramanathan, and R. E. Dickinson, Acceleration of upper stratospheric radiative damping: Observational evidence, Geophys. Res. Lett, 6, 437-440, 1979.

Gille, J. C., Middle atmosphere processes revealed by satellite observations, J. Atmos. Terr. Phys., 41, 707-722, 1979.

Gille, J. C., Ozone distributions by infrared limb scanning: Preliminary results from the LRIR, in Proceedings of the NATO Advanced Study Institute on Atmospheric Ozone, A. C. Aikin, editor, DOT Report FAA-EE-80-20, pp 103-121, 1980.

Gille, J. C., P. L. Bailey, R. A. Craig, F. B. House, and G. P. Anderson, Sounding the stratosphere and mesosphere by infrared limb scanning from space, Science, 208, 397-399, 1980a.

Gille, J. C., P. L. Bailey, and J. M. Russell, III, Temperature and composition measurements from the LRIR and LIMS experiments on Nimbus 6 and 7, Phil. Trans. Roy. Soc. London, A, 296, 205-218, 1980b.

Gille, J. C., G. P. Anderson, W. J. Kohri, and P. L Bailey, Observations of the interaction of ozone and dynamics, Proceedings of the Quadrennial International Ozone Symposium, IAMAP, J. London, editor, pp 1007-1011, 1980c.

Gille, J. C., G. P. Anderson, and P. L. Bailey, Comparison of near coincident LRIR and OAO-3 measurements of equatorial night ozone profiles, Geophys. Res.Lett., 7, 525-528, 1980d.

Gille, J. C., J. M. Russell, III, and P. L. Bailey, The Limb Infrared Monitor of the Stratosphere (LIMS) Experiment: Temperature and O_3 results, IAMAP, Collection of Extended Abstracts Presented at the ICHUA Sessions, IUGG Symposium Dec. 18, 1979, Canberra, Australia, pp 269-276, 1980e.

Gille, J. C., R. R. Garcia, and W. J. Kohri, Early winter meridional motions in the stratosphere and mesosphere determined from LRIR data, AMS 3rd Conference on the Meteorology of the Upper Atmosphere, San Diego, 20-22 January, Abstracts, p 63, 1981.

Girard, A., J. Besson, R. Giraudet, and L. Gramont, Correlated seasonal and climate variations of trace constituents in the stratosphere, Pure Appl. Geophys., **117**, 381-394, 1978/79.

Goldan, P. D., W. C. Kuster, D. L. Albritton, and A. L. Schmeltokopf, Stratospheric $CFCl_3$, CF_2Cl_2, and N_2O height profile measurements at several latitudes, J. Geophys. Res., **85**, 413-423, 1980.

Goldan, P. D., W. C. Kuster, A. L. Schmeltekopf, F. C. Fehsenfeld, and D. L. Albritton, Correction of atmospheric N_2O mixing-ratio data, J. Geophys. Res., 5385-5386, 1981.

Goldman, A., F. G. Fernald, W. J. Williams, and D. G. Murcray, Vertical distribution of NO_2 in the stratosphere as determined from balloon measurements of solar spectra in the 4500 A region, Geophys. Res.Lett., **5**, 257-260, 1978.

Gordon, H. B., A flux formulation of the spectral atmospheric equations suitable for use in long-term climate modeling, Mon. Weather Rev., **109**, 56-64, 1981.

Grant, A., 1979 world production and sales of fluorocarbons FC-11 and FC-12, Alexander Grant Co., Washington, D. C., 1980.

Gras, J. L., and J. E. Laby, Southern hemisphere stratospheric aerosol measurements, 1. Simultaneous impactor and in-situ single-particle (light scatter) detection, J. Geophys. Res., **83**, 1869-1874, 1978.

Gras, J. L., and C. G. Michael, Measurement of the stratospheric aerosol particle size distribution, J. Appl. Meteorol, **18**, 855-860, 1979.

Grimsrud, E. P., and R. A. Rasmussen, The analysis of chlorofluorocarbons in the troposphere by gas chromatography-mass spectrometry, Atmos. Environ., **9**, 1010-1013, 1975.

Grobecker, A. J., S. C. Coroniti, and R. H. Cannon, Jr., The Effects of Stratospheric Pollution by Aircraft, DOT-TST-75-50, Dept. of Transportation, Washington D.C., 1974.

Groves, K. S., and A. F. Tuck, An investigation of the ability of a radiative-photochemical model to reproduce the temporal variation of ozone and temperature in the stratosphere, Proceedings of the Quadrennial International Ozone Symposium, IAMAP, J. London, editor, pp 837-844, 1980.

Groves, K. S., S. R. Mattingly, and A. F. Tuck, Increased atmospheric carbon dioxide and stratospheric ozone, Nature, **273**, 771-715, 1978.

Gudiksen, P. H., A. W. Fairhall, and R. S. Reed, Roles of mean meridional circulation and eddy diffusion in the transport of trace substances in the lower stratosphere, J. Geophys. Res., **73**, 4461-4473, 1968.

Hack, W., A. W. Preuss, and H. Gg. Wagner, Messung der Geschwindigkeit der Reaction von OH- und HO_2-radikalen mit hilfe der laser-magnetischen resonanz, Ber. Bunsenges. Phys. Chem., 82, 1167-1171, 1978.

Haggard, K. V., and W. L. Grose, Energetics of a sudden stratospheric warming simulated with a three-dimensional spectral, quasi-geostrophic model, NASA Technical Publication-1847, 1981.

Haigh, J. D., and J. A. Pyle, A two-dimensional calculation including atmospheric carbon dioxide and stratospheric ozone, Nature, 279, 222-224, 1979.

Haigh, J. D. and J. A. Pyle, Ozone perturbation experiments in a two-dimensional circulation model, Quart. J. Roy. Meteorol. Soc., (to be published), 1981.

Hall, W. D., and H. R. Pruppacher, The survival of ice particles falling from cirrus clouds in subsaturated air, J. Atmos. Sci., 33, 1995-2006, 1976.

Hameed, S., R. D. Cess, and J. S. Hogan, Response of the global climate to changes in atmospheric chemical composition due to fossil fuel burning, J. Geophys. Res., 85, 7537-7545, 1980.

Hamill, P., M. P. McCormick, W. P. Chu, T. J. Swissler, H. M. Steele, and R. P. Turco, Stratospheric cloud sightings by the SAM II satellite system, Abstracts of the 1980 IAMAP International Radiation Symposium, Colorado State University, Fort Collins, Colorado, August 11-16, pp 32-34, 1980.

Hamill, P., R. P. Turco, O. B. Toon, C. S. Kiang, and R. C. Whitten, On the formation of sulfate aerosol particles in the stratosphere, J. Atmos. Sci., submitted, 1981.

Hamilton, E. J., Jr., and R. R. Lii, The dependence on H_2O and on HN_3 of the kinetics of the self reaction of HO_2 in the gas phase formation of $HO_2 \cdot H_2O$ and $HO_2 \cdot NH_3$ complexes, Int. J. Chem. Kinet., 9, 875-885, 1977.

Hanel, R. A., B. J. Conrath, V. G. Kunde, C. Prabhakara, I. Revah, V. V. Salomonson, and G. Wolford, The Nimbus 4 infrared spectroscopy experiment 1. Calibrated thermal emission spectra, J. Geophys. Res., 77, 2629-2641, 1972.

Hansen, J. E., W. Wang, and A. A. Lacis, Mt. Agung eruption provides test of a global climatic perturbation, Science, 199, 1065-1068, 1978.

Hanser, F. A., and B. Sellers, Variations of $O(^1D)$ photoproduction rate for the 1977 Gametag flights, J. Geophys. Res., 85, 7377-7382, 1980.

Hanser, F. A., B. Sellers, and D. C. Briehl, Ultraviolet spectrophotometer for measuring columnar atmospheric ozone from aircraft, Appl. Opt., 17, 1649-1656, 1978.

Hanst, P. L., J. W. Spence, and E. O. Edney, Carbon monoxide production in photooxidation of organic molecules in the air, Atmos. Environ., 14, 1077-1088, 1980.

Harries, J. E., The distribution of water vapor in the stratosphere, Rev. Geophys. Space Phys., 14, 565-575, 1976.

Harries, J. E., D. G. Moss, N. R. W. Swann, G. F., Neill, and P. Gildwarg, Simultaneous measurements of H_2O, NO_2, and HNO_3 in the daytime stratosphere from 15 to 35 km, Nature, **259**, 300-302, 1976.

Harrison, H., J. E. Johnson, and J. D. Cline, Light hydrocarbon in the atmospheric boundary layer over the north Pacific, Unpublished Manuscript, Dept. of Atmos. Sci., Univ. of Washington, Seattle, Washington, 1979.

Hartmann, D. L., The dynamical climatology of the stratosphere in the southern hemisphere during late winter 1973, J. Atmos. Sci., **33**, 1789-1802, 1976a.

Hartmann, D. L., The structure of the stratosphere in the southern hemisphere during late winter 1973 as observed by satellite, J. Atmos. Sci., **33**, 1141-1154, 1976b.

Hartmann, D. L., Dynamic studies of the southern hemisphere stratosphere, COSPAR Space Research XVII, 167-174, 1976c.

Hartmann, D. L. Comments on "Stratospheric long waves: Comparison of thermal structure in the northern and southern hemispheres", J. Atmos. Sci., **34**, 434-435, 1977a.

Hartmann, D. L., On potential vorticity and transport in the stratosphere, J. Atmos. Sci., **34**, pp 968-977, 1977b.

Hartmann, D. L., A note concerning the effect of varying extinction on radiative-photochemical relaxation, J. Atmos. Sci., **35**, 1125-1130, 1978.

Hartmann, D. L., Baroclinic instability of realistic zonal-mean states to planetary waves, J. Atmos. Sci., **36**, 2336-2349, 1979.

Hartmann, D. L., and R. R. Garcia, A mechanistic model of ozone transport by planetary waves in the stratosphere, J. Atmos. Sci., **36**, 350-364, 1979.

Hartmann, G. K., K. F. Kunzi, and A. K. Randegger, Composition and temperature profile of the terrestrial atmosphere derived from thermal emission at microwave frequencies, (Abstract) IAMAP Third Scientific Assembly, Hamburg, Federal Republic of Germany, August, 1981.

Harwood, R. S., The temperature structure of the Southern Hemisphere stratosphere: August-October 1971, Quart. J. Roy. Meteorol. Soc., **101**, 75-91, 1975.

Harwood, R. S., Some recent investigations of the upper atmosphere by remote sounding satellites, Colston Papers, **28**, Ed. Curtis and Barrett, Briston, 1976.

Harwood, R. S., Dynamical models of the middle atmosphere for tracer studies, Phil. Trans. Roy. Soc. Lond., **A296**, 103-127, 1980.

Harwood, R. S., and J. A. Pyle, A time-dependent two-dimensional model of the atmosphere below 80 km. Proceedings of the International Conference on Structure, Composition and General Circulation of the Upper and Lower Atmosphere and Possible Anthropogenic Perturbations, Melbourne, pp 809-834, 1974.

Harwood, R. S., and J. A. Pyle, A two-dimensional mean circulation model for the atmosphere below 80 km, Quart. J. Roy. Meteorol. Soc., 101, 723-747, 1975.

Harwood, R. S., and J. A. Pyle, Studies of the ozone budget using a zonal mean circulation model and linearized photochemistry, Quart. J. Roy. Meteorol. Soc., 103, 319-343, 1977.

Harwood, R. S., and J. A. Pyle, The fluxes of ozone from a zonal mean circulation model of the atmosphere, Atmospheric and Oceanic Physics, 14, 50-56, 1978.

Harwood, R. S., and J. A. Pyle, The dynamical behaviour of a two-dimensional model of the stratosphere, Quart. J. Roy. Meteorol. Soc., 106, 395-420, 1980.

Hasebe, F., A global analysis of the fluctuation of total ozone I. Application of the optimum interpolation to the network data with random and systematic errors, J. Meteorol. Soc. Japan, 58, 95-103, 1980.

Haurwitz, B., Atmospheric ozone as a constituent of the atmosphere, Bull Amer. Meteorol. Soc., 19, 417-424, 1938.

Hayes, D., K. Snetsinger, G. Ferry, V. Oberbeck, and N. Farlow, Reactivity of stratospheric aerosols to small amounts of ammonia in the laboratory environment, Geophys. Res. Lett, 11, 974-976, 1980.

Hays, P. B., and R. G. Roble, Observation of mesospheric ozone at low latitudes, Planet. Space Sci., 21, 273-279, 1973.

Heaps, W. S., Measurement of hydroxyl radical in the upper atmosphere using lidar from the space shuttle, Appl. Opt., 19, 243-249, 1980.

Heaps, Wm. S., and T. J. McGee, Balloon borne lidar measurements of stratospheric hydroxyl radical, J. Geophys. Res., submitted, 1981.

Heaps, W. S., R. D. Hudson, T. J. McGee, and L. O. Caudill, Balloon borne lidar measurements of stratospheric hydroxyl and ozone, (abstract) IAMAP Third Scientific Assembly, Hamburg, Federal Republic of Germany, 17-28 August 1981. Also see EOS Trans. AGU, 62, 344, 1981.

Heasman, C. C., and A. J. Crane, Determination of mesospheric height fields up to 80 km from Nimbus-6 PMR measurements, Presented at COSPAR, 21st Plenary meeting, Innsbruck, Austria. Available from AIAA, citation no. 78A 48592#, 1978.

Heath, D. F., Space observations of the variability of solar irradiance in the near and far ultraviolet, J. Geophys. Res., 78, 2779-2792, 1973.

Heath, D. F., Spatial and temporal variability of ozone as seen from space, Proc. NATO Advanced Study Inst. on Atmospheric Ozone, A. Aikin, editor, Report No. FAA-EE-80-20, pp 45-101, 1980.

Heath, D. F., A review of observational evidence for short and long term ultraviolet flux variability of the sun, Proceedings of the International Conference on Sun and Climate, 30 September - 3 October, 1980, Toulouse, to be published, 1981a.

Heath, D. F., On the adequacy of the fixed locations of the surface based international network for inferring ozone trends, J. Geophys. Res., In Press, 1981b.

Heath, D. F., Secular changes in atmospheric ozone from satellite observations (1970-1979), submitted to Science, 1981c.

Heath, D. F., and M. P. Thekaekara, The solar spectrum between 1200 and 3000A, in The Solar Output and its Variation, Oran R. White, editor, Colorado Associated University Press, Boulder, Colorado, pp 193-212, 1977.

Heath, D. F., A. J. Krueger, and C. L. Mateer, The Nimbus-4 BUV atmospheric ozone experiment; two years operation, Pure Appl. Geophys., **106-108**, 1238-1253, 1973.

Heath, D. F., E. Hilsenrath, A. J. Krueger, W. Nordberg, C. Prabhakara, and J. S. Theon, Observations of the global structure of the stratosphere and mesosphere with sounding rockets and with remote sensing techniques from satellites, Structure and Dynamics of the Upper Atmosphere, F. Veriani, editor, Developments in Atmospheric Science, 1, Elsevier Scientific Publishing Company, Amsterdam, pp 131-198, 1974.

Heath, D. F., A. J. Krueger, and P. J. Crutzen, Solar proton event: Influence on stratospheric ozone, Science, **197**, 886-889, 1977.

Heidt, L. E., and D. H. Ehhalt, Corrections of CH_4 concentrations measured prior to 1974, Geophys. Res. Lett., 7, 1023, 1980

Heidt, L. E., R. Lueb, W. Pollock, and D. H. Ehhalt, Stratospheric profiles of CCl_3F, and CCl_2F_2, Geophys. Res. Lett., 2, 445-447, 1975.

Heidt, L. E., J. P. Krasnec, R. A. Lueb, W. H. Pollock, B. E. Henry, and P. J. Crutzen, Latitudinal distri- tions of CO and CH_4 over the Pacific, J. Geophys. Res., **85**, 7329-7336, 1980.

Hering, W. S., Ozone and atmospheric transport processes, Tellus, **18**, 329-336, 1966.

Hering, W., and T. R. Borden, Jr., Ozonesonde Observations over North America, Vol. II, Environmental Research Paper, **38**, AFCRL Report 64-30, 1964.

Herman, J. R., The response of stratospheric constituents to a solar eclipse, sunrise, and sunset, J. Geophys. Res., **84**, 3701-3710, 1979.

Heroux, L., and J. E. Higgins, Summary of full-disk solar fluxes between 250 and 1940 A, J. Geophys. Res., **82**, 3307-3310, 1977.

Hester, N. E., E. R. Stephens, and O. C. Taylor, Fluorocarbon air pollutants, Measurements in the lower stratosphere, Environ. Sci. and Tech., **9**, 875-876, 1975.

Hidalgo, H., and P. J. Crutzen, The tropospheric and stratospheric composition perturbed by NO_x emissions of high altitude aircraft, J. Geophys. Res., **82**, 5833-5866, 1977.

Hill, R. D., R. G. Rinker, and H. D. Wilson, Atmospheric nitrogen fixation by lightning, J. Atmos. Sci., **37**, 179-192, 1980.

Hill, W. J., P. N. Sheldon, and J. J. Tiede, Analyzing worldwide total ozone for trends, Geophys. Res. Lett., **4**, 21-24, 1977.

Hilsenrath, E., Ozone measurements in the mesosphere and stratosphere during two significant geophysical events, J. Atmos. Sci., 28, 295-297, 1971.

Hilsenrath, E., Standard ozone profiles from balloon and rocket data, unpublished manuscript, 1979.

Hilsenrath, E., Rocket observations of the vertical distribution of ozone in the polar night and during a mid-winter stratospheric warming, Geophys. Res. Lett., 7, 581-584, 1980.

Hilsenrath, E., and T. E. Ashenfelter, A balloon ozone measurement utilizing an optical absorption cell and an ejector air sampler, NASA Technical Note D-8281, 9 pp, 1976.

Hilsenrath, E., and P. T. Kirschner, Recent assessment of the performance and accuracy of a chemiluminescent rocket sonde for upper atmospheric ozone measurements, Rev. Sci. Instr., 51, 1381-1389, 1980.

Hilsenrath, E., and B. Schlesinger, The seasonal and interannual variability of total ozone as revealed by the BUV Nimbus-4 experiment, Fourth NASA Weather and Climate Program Science Review, NASA Conference Publication 2076, E. R. Kreins, editor, pp 277-286, 1979.

Hilsenrath, E., and B. M. Schlesinger, Total ozone seasonal and interannual variations derived from the 7 year Nimbus-4 data set, J. Geophys. Res., 86, 12087-12096, 1981.

Hilsenrath, E., R. L. Coley, P. T. Kirschner, and B. Gammill, A rocket ozonesonde for geophysical research and satellite intercomparsions, NASA Technical Memorandum 79712, 52 p, 1979a.

Hilsenrath, E., D. F. Heath, and B. M. Schlesinger, Seasonal and interannual variations in total ozone revealed by the Nimbus 4 Backscattered Ultraviolet experiment, J. Geophys. Res., 84, 6969-6979, 1979b.

Hines, C. O., A possible mechanism for the production of sun-weather correlations, J. Atmos. Sci., 31, 589-591, 1974.

Hinteregger, H. E., EUV fluxes in the solar spectrum below 2000 A., J. Atmos. Terr. Phys., 38, 791-806, 1976.

Hinteregger, H. E., Representations of solar EUV fluxes for aeronomical applications, The Mesophere and Thermosphere, Adv. Space Res. 1, No. 1, Pergamon, 39-52, 1981.

Hirota, I., Spectral analysis of planetary waves in the summer stratosphere and mesosphere, J. Meteorol. Soc. Japan, 53, 33-44, 1975.

Hirota, I., Seasonal variation of planetary waves in the stratosphere observed by the Nimbus 5 SCR, Quart. J. Roy. Meteorol. Soc., 102, 757-770, 1976.

Hirota, I., Equatorial waves in the upper stratosphere and mesosphere in relation to the semiannual oscillation of the zonal wind, J. Atmos. Sci., 35, 714-722, 1978.

Hirota, I., Kelvin waves in the equatorial middle atmosphere observed by the Nimbus 5 SCR, J. Atmos. Sci., 36, 217-222, 1979.

Hirota, I., Observational evidence of the semiannual oscillation in the tropical middle atmosphere - A review, Pure Appl. Geophys., 118, 217-238, 1980.

Hirota, I., and J. J. Barnett, Planetary waves in the winter mesophere - preliminary analysis of Nimbus 6 PMP results, Quart. J. Roy. Meteorol. Soc., 103, 487-498, 1977.

Hirota, I., K. Saotome, T. Suzuki, and S. Ikeda, Structure and behavior of the Aleutian anticyclone as revealed by meteorological rocket and satellite observations, J. Meteorol. Soc. Japan, 51, 353-363, 1973.

Hochanadel, C. J., J. A. Ghormley, and P. J. Ogren, Absorption spectrum and reaction kinetics of HO_2 radical in the gas phase, J. Phys. Chem., 56, 4416-4432, 1972.

Hochanadel, C. J., T. J. Sworski, and P. J. Ogren, Rate constants for the Reactions of HO_2 with OH and HO_2, J. Phys. Chem., 84, 3274-3277, 1980.

Hoell, J. M., C. N. Harward, and B. S. Williams, Remote infrared heterodyne radiometer measurements of atmospheric ammonia profiles, Geophys. Res. Lett., 7, 313-316, 1980.

Hofmann, D. J., and J. M. Rosen, Balloon observations of a particle layer injected by a stratospheric aircraft at 23 km, Geophys. Res.Lett., 5, 511-514, 1978.

Hofmann, D. J., and J. M. Rosen, On the background stratospheric aerosol layer, J. Atmos. Sci., 38, 168-181, 1981.

Hofmann, D. J., J. M. Rosen, T. J. Pepin, and R. G. Pinnick, Stratospheric aerosol measurements I: Time variations at northern mid latitudes, J. Atmos. Sci., 32, 1446-1456, 1975a.

Hofmann, D. J., D. E. Carroll, and J. M. Rosen, Estimate of the contribution of the Space Shuttle effluent to the natural stratospheric aerosol, Geophys. Res.Lett., 2, 113-116, 1975b.

Holdeman, J. D., and G. D. Nastrom, Ozone contamination in aircraft cabins; Results from GASP data and analyses, NASA Technical Memorandum 81671, 15 p, 1981.

Holton, J. R., Forcing of mean flows by stationary waves, J. Atmos. Sci., 31, 942-945, 1974.

Holton, J. R., Wave propagation and transport in the middle atmosphere, Phil. Trans. Roy. Soc. London, A296, 73-85, 1980.

Holton, J. R., An advective model for two-dimensional transport of stratospheric trace species, J. Geophys. Res., 86, 11,989-11,994, 1981.

Holton, J. R., and H. C. Tan, The influence of the equatorial quasi-biennial oscillation on the global circulation at 50 mb, J. Atmos. Sci., 37, 2200-2208, 1980.

Holton, J. R., and W. M. Wehrbein, The role of forced planetary waves in the annual cycle of the zonal mean circulation of the middle atmosphere, J. Atmos. Sci., 37, 1968-1983, 1980a.

Holton, J. R., and W. M. Wehrbein, A numerical model of the zonal mean circulation of the middle atmosphere, Pure Appl. Geophys. 118, 284-306, 1980b.

Holton, J. R., and W. M. Wehrbein, A further study of the annual cycle of the zonal mean circulation in the middle atmosphere, J. Atmos. Sci., 38, 1504-1509, 1981.

Horntveth, K., and I. Isaksen, Preliminary results from a 2-D Lagrangian global transport model for the troposphere and the stratosphere, preprint, 1981.

Horvath, J. J., and C. J. Mason, Nitric oxide mixing ratios near the stratosprause measured by a rocket-borne chemiluminescent detector, Geophys. Res. Lett., 5, 1023-1026, 1978.

Houghton, J. T., The Selective Chopper Radiometer on Nimbus 4, Bull Amer. Met. Soc. 53, 27-28, 1972.

Houghton, J. T., The Selective Chopper Radiometer on Nimbus 4, Bull Amer. Meteorol. Soc., 53, 27-28, 1972.

Hsu, C. P. F, Air parcel motions during a numerically simulated sudden stratospheric warming, J. Atmos. Sci., 37, 2768-2792, 1980.

Hsu, C. P. F., A numerical study of the role of wave-wave interactions during sudden stratospheric warmings, J. Atmos. Sci., 38, 189-214, 1981.

Huebert, B. J., and A. L. Lazrus, Tropospheric gas-phase and particulate nitrate measurements, J. Geophys. Res., 85, 7322-7328, 1980.

Hunt, B. G., Experiments with a stratospheric general circulation model, III. Large-scale diffusion of ozone including photochemistry, Mon. Weather Rev., 97, 287-306, 1969.

Hunt, B. G., The maintenance of the zonal mean state of the upper atmosphere as represented in a three-dimensional general circulation model extending up to 100 km, J. Atmos. Sci., 38, 2172-2186, 1981.

Hunt, B. G., and S. Manabe, Experiments with a stratospheric general circulation model I: Radiative and dynamic aspects, Mon. Weather Rev. ,96, 477-502, 1968.

Hunten, D. M., R. P. Turco, and O. B. Toon, Smoke and dust particles of meteoric origin in the mesosphere and stratosphere, J. Atmos. Sci., 37, 1342-1357, 1980.

Husain, L., P. E. Coffey, R. E. Meyers and R. T. Cederwall, Ozone transport from stratosphere to troposphere, Geophys. Res. Lett., 4, 363-365, 1977.

Husain, L., V. A. Dutkiewicz, and A. Rusheed, Origin of tropospheric ozone, IUGG XVII General Assembly, Int. Union of Geod. and Geophys. Canberra, Australia, Dec. 1979.

Hyson, P., Stratospheric water vapor measurements over Australia, 1973-1976, Quart. J. Roy. Meteorol. Soc., 104, 225-227, 1978.

Hyson, P., P. J. Fraser, and G. I. Pearman, A two-dimensional transport simulation model for trace atmospheric constituents, J. Geophys. Res., 85, 4443-4455, 1980.

Ilyas, M., Temporal variability and latitudinal asymmetry in the Woomera (31°S) ozone data, Proceedings of the Quadrennial International Ozone Symposium, IAMAP, J. London, editor, pp 526-533, 1980.

Inn, E. C. Y., J. F. Vedder, B. J. Tyson, and D. O'Hara, COS in the stratosphere, Geophys. Res.Lett., 6, 191-193, 1979.

Inn, E. C. Y., J. F. Vedder, and D. O'Hara, Measurement of stratospheric sulfur constituents, Geophys. Res.Lett., 8, 5-8, 1981a.

Inn, E. C. Y., J. F. Vedder, E. P. Condon, and D. O'Hara, Gaseous constituents in the plume from eruptions of Mount St. Helens, Science, 211, 821-823, 1981b.

Isaksen, I. S. A., A two-dimensional transport/chemistry model of the troposphere and stratosphere, preprint NASA Stratospheric Modeling Workshop, December, 1980.

Isaksen, I. S. A., and H. Rodhe, A two-dimensional model for the global distribution of gases and aerosol particles in the troposphere, Univ. of Stockholm Report HC-47, 1978.

Iyer, R. S., and F. S. Rowland, A significant upper limit for the rate of formation of OCS from the reaction of OH with CS_2, Geophys. Res. Lett., 10, 797-800, 1980.

JPL 79-27, Chemical Kinetic and Photochemical Data for Use in Stratospheric Modelling, Evaluation No. 2, NASA Panel for Data Evaluation, Jet Propulsion Laboratory, Pasadena, California, USA, 124 pp, 1979.

JPL 81-3, Chemical Kinetic and Photochemical Data for Use in Stratospheric Modelling, Evaluation Number 4, NASA Panel for Data Evaluation, Jet Propulsion Laboratory, Pasadena, California, USA, 124 pp, 1981.

Jaeschke, W., R. Schmitt, and H. -W. Georgii, Preliminary results of stratospheric SO_2 measurements, Geophys. Res.Lett., 3, 517-519, 1976.

Jeong, K. -M., and F. Kaufman, Rates of the reactions of 1,1,1-trichloroethane and 1,1,2-trichloroethane with OH, Geophys. Res. Lett., 6, 757-759, 1979.

Jesson, J. P., Release of industrial halocarbons and tropospheric budget, Proc. of NATO Adv. Study Inst. on Atmospheric Ozone: Its Variation and Human Influences, A. C. Aikin, editor, U.S. Department of Transportation Report. No. FAA-EE-80-20, 373-396, 1980.

Johnson, K. W., Variations in static stability in the stratosphere and lower mesosphere during a winter disturbance, Extended Summaries, IAMAP/IAGA Assembly, Seattle, pp 18(1-5), 1977.

Johnson, K. W., and D. R. Rodenhuis, Potential vorticity transport during a stratospheric warming, Extended Summaries, IAMAP/IAGA Assembly, Seattle, pp 49(1-5), 1977.

Johnston, H., Reduction of stratospheric ozone by nitrogen oxide catalysts from supersonic transport exhaust, Science, 173, 517-522, 1971.

Johnston, H. S., and S. Solomon, Thunderstorms as possible micrometeorological sink for stratospheric water, J. Geophys. Res., **84**, 3155-3158, 1979.

Johnston, H., G. Whitten, and J. Birks, Effect of nuclear explosions on stratospheric nitric oxide and ozone, J. Geophys. Res., **78**, 6107-6135, 1973.

Johnston, H. S., D. Kattenhorn, and G. Whitten, Use of excess carbon-14 data to calibrate models of stratospheric ozone depletion by supersonic transports, J. Geophys. Res., **81**, 368-380, 1976.

Junge, C. E., Global ozone budget and exchange between stratosphere and troposphere, Tellus, **14**, 363-377, 1962.

Junge, C. E., Air Chemistry and Radioactivity, Academic Press Inc., 380 pp, 1963.

Junge, C. E., and G. Czeplak, Some aspects of the seasonal variation of carbon dioxide and ozone, Tellus, **20**, 422-434, 1968.

Junge, C. E., and J. E. Manson, Stratospheric aerosol studies, J. Geophys. Res., **66**, 2163-2182, 1961.

Junge, C. E., C. W. Chagnon, and J. E. Manson, Stratospheric aerosols, J. Meteorol., **18**, 81-108, 1961.

Kanzawa, H., On the behaviour of mean zonal flow and planetary waves during the 1973 sudden warming observed by the Nimbus 5 SCR, Symp. on Use of Satellite Data in Met. Res., Tokyo, pp 102-107, 1978.

Kanzawa, H., The behavior of mean zonal wind and planetary-scale disturbances in the troposphere and stratosphere during the 1973 sudden warming, J. Meteorol. Soc. Japan, **58**, 329-356, 1980.

Kanzawa, H., and I. Hirota, The behavior of mean zonal winds and planetary waves during the 1973 sudden warming, Ext. Abstracts of Int. Symp. on Middle Atmos. Dynamics and Transport, Urbana, 1980, Handbook for MAP, Volume 2, S. K. Avery, editor, pp 165-174, 1981.

Karol, I. L., Radioisotopes and global transport in the atmosphere, Jerusalem, Israel, Program for Scientific Translation, 336 pp, 1974.

Karol, I. L., I. I. Polyak, and K. Ya. Vinnikov, Statistically correct determination of long-lived trends in geophysical data series, Pure Appl. Geophys., **114**, 965-974, 1976.

Käselau, K. H., P. Fabian, and H. Röhrs, Measurements of aerosol concentration up to a height of 27 km, Pure Appl. Geophys., **112**, 877-885, 1974.

Keating, G. M., Relation between monthly variations of global ozone and solar activity, Nature, **274**, 873-874, 1978.

Keating, G. M., L. R. Lake, and J. Y. Nicholson, III, Global ozone - Solar activity relationship from satellite measurements, Proceedings of the Quadrennial International Ozone Symposium, IAMAP, J. London, editor, 1075-1082, 1980.

Keating, G. M., L. R. Lake, J. Y. Nicholson, III, and M. Natarajan, Global ozone long-term trends from satellite measurements and the response to solar activity variations, J. Geophys. Res., **86** 9873-9880, 1981.

Keeling, C. D., R. B. Bacastow, A. E. Bainbridge, C. A. Ekdahl, Jr., P. R. Guenther, L. S. Waterman, and J. F. -S. Chin, Atmospheric carbon dioxide variations at Mauna Loa Observatory, Hawaii, Tellus, **28**, 538-551, 1976.

Kennett, J. P., and R. C. Thunell, On explosive Cenozoic volcanism and climatic implications, Science, **196**, 1231-1234, 1977.

Kerr, J. B., and C. T. McElroy, Measurement of stratospheric nitrogen dioxide from the AES stratospheric balloon program, Atmosphere, **14**, 166-171, 1976.

Kerr, J. B., C. T. McElroy, and R. A. Olafsen, Measurements of ozone with the Brewer ozone spectrophotometer, Proceedings of the Quadrennial International Ozone Symposium, IAMAP, J. London, editor, pp 74-79, 1980.

Keyser, L. F., Absolute rate constant of the reaction OH + H_2O_2 → HO_2 + H_2O from 245-423 K, J. Phys. Chem., **84**, 1659-1663, 1980.

Keyser, L. F., Absolute rate constant of the reaction OH + HO_2 → H_2O + O_2, J. Phys. Chem., **85**, 3667-3673, 1981.

Khalil, M. A. K., and R. A. Rasmussen, Atmospheric methylchloride (CH_3Cl), Chemosphere, in press, 1981.

Khrgian, A. Kh., The Physics of Atmospheric Ozone, trans. by D. Lederman, Israel Program for Scientific Translations, Jerusalem, Available from NTIS, 1975.

Kida, H., A numerical investigation of the atmospheric general circulation and stratospheric tropospheric mass exchange, I. Long term integration of a simplified general circulation model, J. Meteorol. Soc. Japan, **55**, 52-70, 1977.

Kley, D., and M. McFarland, Chemiluminescence detector for NO and NO_2, Atmos. Technol., **12**, 63-68, 1980.

Kley, D., E. J. Stone, W. R. Henderson, J. W. Drummond, W. J. Harrop, A. L. Schmeltekopf, T. L. Thompson, and R. H. Wrinkler, In situ measurements of the mixing ratio of water vapor in the stratosphere, J. Atmos. Sci., **36**, 2513-2524, 1979.

Kley, D., J. W. Drummond, and A. L. Schmeltekopf, On the structure and microstructure of statrospheric water vapor, in Atmospheric Water Vapor, A. Deepak, T. D. Wilkerson and L. H. Ruhnke, editors, Academic Press, 315-327, 1980.

Kley, D., J. W. Drummond, M. McFarland, and S. C. Liu, Tropospheric profiles of NO_x, J. Geophys. Res., 86, 3153-3161, 1981.

Knauth, H-D, Uber den thermischen zerfall von $ClONO_2$ in gegenwert von NO, ClNO and N_2, Ber Bunsenges. Phys. Chem., 82, 212-216, 1978.

Ko, M. K. W., M. Livshits, and N. D. Sze, Atmospheric ozone: Comparison of observations with two-dimensional model calculation, Proceedings of the Quadrennial International Ozone Symposium, IAMAP, J. London, editor, pp 884-891, 1980.

Ko, M. K. W., M. Livshits, P. B. Ryan, and N. D. Sze, Status Report to the Chemical Manufacturers Association for AER 2-D Model Project, April, 1981.

Kohri, W. J., LRIR observations of the structure and propagation of the stationary planetary waves in the Northern Hemisphere during December 1975, Ph.D. Dissertation, Drexel University, Philadelphia, 1981.

Komhyr, W. D., A carbon-iodine sensor for atmospheric soundings, Proc. Ozone Symposium, WMO, Albuquerque, New Mexico, 1964.

Komhyr, W. D., Dobson spectrophotometer systematic total ozone measurement error, Geophys. Res. Lett., 7, 161-163, 1980.

Komhyr, W. D., and R. D. Evans, Dobson spectrophotometer total ozone measurement errors caused by interfering absorbing species such as SO_2, NO_2 and photochemically produced O_3 in polluted air, Geophys. Res. Lett., 7, 157-160, 1980.

Komhyr, W. D., and T. B. Harris, Development of an ECC ozonesonde, NOAA Technical Report ERL-APCL 18, Boulder, Colorado, 1971.

Komhyr, W. D., E. W. Barrett, G. Slocum, and H. K. Weickmann, Atmospheric total ozone increase during the 1960s, Nature, 232, 390-391, 1971.

Komhyr, W. D., R. D. Grass, E. D. Dutton, R. K. Leonard, and R. D. Evans, Trend determinations from provisional and corrected 1963-1979 Bismark total ozone data, Proceedings of the Quadrennial International Symposium, IAMAP, J. London, editor, pp 371-377, 1980.

Konkov, V. I., V. A. Kononkov, and S. P. Perov, A chemiluminescent method of rocket measurement of ozone vertical distribution, (Abstract) International Association of Meteorology and Atmospheric Physics, Third Scientific Assembly, Hamburg, Federal Republic of Germany, 17-28 August 1981.

Koshelkov, Yu. P., Mean values of meteorological parameters in the upper stratosphere and mesosphere of the southern hemisphere, Leningrad, Gidrometeoisdat, 1980.

Krey, P. W., R. J. Lagomarsino, and L. E. Toonkel, Gaseous halogens in the atmosphere in 1975, J. Geophys. Res., 82, 1753-1766, 1977.

Krueger, A. J., The mean ozone distribution from several series of rocket soundings to 52 km at latitudes from 58°S to 64°N, Pure Appl. Geophys., **106-108**, 1272-1280, 1973.

Krueger, A. J., and R. A. Minzner, A mid-latitude ozone model for the 1976 U.S. Standard Atmosphere, J. Geophys. Res., **81**, 4477-4481, 1976.

Krueger, A., D. Heath, and C. Mateer, Variations in the stratospheric ozone field inferred from NIMBUS satellite observations, Pure Appl. Geophys., **106-108**, 1254-1263, 1973.

Kuhn, P. M., In-situ and overburden measurement of water vapour - infrared and direct, in Atmospheric Water Vapor, A. Deepak, T. D. Wilkerson, and L. H. Ruhnke, editors, Academic Press, pp 291-301, 1980.

Kurucz, R. L., Model atmospheres for G, F, A, B, and O stars, Astrophys. J. Suppl. Series, in press, 1981.

Kurylo, M. J., Flash photolysis resonance fluorescence investigation of the reactions of OH radicals with OCS and CS_2, Chem. Phys. Lett., **58**, 238-242, 1978.

Kurylo, M. J., P. C. Anderson, and O. Klais, A flash photolysis resonance fluorescence investigation of the reaction $OH+CH_3CCl_3 \rightarrow H_2O+CH_2CCl_3$, Geophys. Res. Lett., **6**, 760-762, 1979.

Kutzbach, J. E., and R. A. Bryson, Variance spectrum of Holocene climatic fluctuations in the North Atlantic sector, J. Atmos. Sci, **31**, 1958-1963, 1974.

Labitzke, K., Synoptic-scale motions above the stratopause, NCAR ms. 71-139, Presented at IUGG Assembly, Moscow, 1971.

Labitzke, K., Temperature changes in the mesosphere and stratosphere connected with circulation changes in winter, J. Atmos. Sci., **29**, 756-766, 1972a.

Labitzke, K. The interaction between stratosphere and mesophere in winter, J. Atmos. Sci., **29**, 1395-1399, 1972b.

Labitzke, K., The temperature in the upper stratosphere: Differences between hemispheres, J. Geophys. Res., **79**, 2171-2175, 1974.

Labitzke, K., Comparison of the stratospheric temperature distribution over northern and southern hemispheres, COSPAR Space Research 17, pp 159-165, 1976a.

Labitzke, K., On the use of single channel radiances for estimating temperature at discrete pressure levels in the upper stratosphere, COSPAR Space Research 17, 151-157, 1976b.

Labitzke, K., The amplification of height wave 1 in January, 1979: A characteristic precondition for the major warming in February, Mon. Weather Rev., **109**, 983-989, 1981.

Labitzke, K., and J. J. Barnett, Global time and space changes of satellite radiances received from the stratosphere and lower mesosphere, J. Geophys. Res., **78**, 483-496, 1973.

Labitzke, K., and J. J. Barnett, Review of climatological information obtained from remote sensing of the stratosphere and mesosphere, COSPAR Space Research, **21**, 97-106, 1979.

Labitzke, K., and J. J. Barnett, Review of the radiance distribution in the upper mesosphere as observed from the Nimbus 6 Pressure Modulator Radiometer (PMR), Planet. and Space Sci., **29**, 673-685, 1981.

Labs, D., and H. Neckel, Transformation of the absolute solar radiation data into the 'International Practical Temperature Scale of 1968', Solar Phys., **15**, 79-87, 1970.

Lacis, A. A., and J. E. Hansen, A parameterization for the absorption of solar radiation in the earth's atmosphere, J. Atmos. Sci., **31**, 118-133, 1974.

Lamb, H. H., The Changing Climate, Methuen (London), 236 pp, 1966.

Lamb, H. H., Volcanic dust in the atmosphere: With a chronology and assessment of its meteorological significance, Phil. Trans. Roy. Soc. Lond., **A266**, 425-533, 1970.

Lamb, H. H., Climate: Present, Past and Future, Vol. 2 Climatic History and the Future, Methuen, London, 1977.

Landsberg, H. E., and J. M. Albert, The summer of 1816 and volcanism, Weatherwise, **27**, 63-66, 1974.

Lau, N. -C., and J. M. Wallace, On the distribution of horizontal transports by transient eddies in the Northern Hemisphere winter time circulation, J. Atmos. Sci., **36**, 1844-1863, 1979.

Lazrus, A. L., and B. W. Gandrud, Stratospheric sulfate aerosol, J. Geophys. Res., **79**, 3424-3431, 1974a.

Lazrus, A. L., and B. W. Gandrud, Distribution of stratospheric nitric acid vapor, J. Atmos. Sci., **31**, 1102-1108, 1974b.

Lazrus, A. L., B. W. Gandrud, and R. D. Cadle, Chemical composition of air filtration samples of the stratospheric sulfate layer, J. Geophys. Res., **76**, 8083-8088, 1971.

Lazrus, A. L., B. W. Gandrud, J. Greenberg, J. Bonelli, E. Mroz, and W. A. Sedlacek, Midlatitude seasonal measurements of stratospheric acidic chlorine vapor, Geophys. Res. Lett., **4**, 587-589, 1977.

Lean, J. L., Observation of the diurnal variation of atmospheric ozone, J. Geophys. Res., submitted, 1981.

Lee, Robert B., III, B. W. Gandrud, D. E. Robbins, L. C. Rossi, and N. R. W. Swann, LIMS instrument package (LIP) balloon experiment - Nimbus 7 satellite correlative temperature, ozone, water vapor, and nitric acid measurements, NASA Technical Memorandum, estimated publication date, 1982.

Lengel, R. K., and D. R. Crosley, Rotational dependence of vibrational relaxation in $A^2\Sigma^+$ OH, Chem. Phys. Lett., **32**, 261-264, 1975.

Leovy, C. B., Simple models of thermally driven mesopheric circulations, J. Atmos. Sci., 21, 327-341, 1964.

Leovy, C. B., and P. J. Webster, Stratospheric long waves: Comparison of thermal structure in the northern and southern hemispheres, J. Atmos. Sci., 33, 1624-1638, 1976.

Leu, M. T., C. L. Lin, and W. B. DeMore, Rate constant for formation of chlorine nitrate by the reaction ClO + NO_2 + M, J. Phys. Chem., 81, 190-195, 1977.

Levy, H., Normal atmosphere: Large radical and formaldehyde concentrations predicted, Science, 173, 141-143, 1971.

Levy, H., II, J. D. Mahlman, and W. J. Moxim, A preliminary report on the numerical simulation of the three-dimensional structure and variability of atmospheric N_2O, Geophys. Res. Lett., 6, 155-158, 1979.

Levy, H., II, J. D. Mahlman, and W. J. Moxim, A stratospheric source of reactive nitrogen in the unpolluted troposphere, Geophys. Res. Lett., 7, 441-444, 1980.

Lezberg, E. A., F. M. Humenik, and D. A. Otterson, Sulfate and nitrate mixing ratios in the vicinity of the tropopause, Atmos. Environ., 13, 1299-1304, 1979.

Libby, W. F., Radioactive strontium fallout, Proc. Natl. Acad. Sci., 42, 365-390, 1956.

Liebl, K. H., and W. Seiler, CO and H_2 destruction at the soil surface, Microbial Production and Utilization of Gases, H. E. Schlegel, G. Gottschalk, N. Pfennig, editors, Akademie der Eissenschaften, Gottingen, FRG, 215-230 1976.

Lii, R. -R., R. A. Gorse, Jr., M. C. Sauer, Jr., and S. Gordon, Negative activation energy for the self reaction of HO_2 in the gas phase, J. Phys. Chem., 83, 1803-1804, 1979.

Lii, R. -R., R. A. Gorse, Jr., M. C. Sauer, Jr., and S. Gordon, Rate constant for the reaction of OH with HO_2, J. Phys. Chem., 84, 819-821, 1980.

Lindzen, R. S., Tides and gravity waves in the upper atmosphere, Mesospheric models and related experiments, G. Fiocco, editor, D. Reidel, pp 122-130, 1971.

Lindzen, R. S., Tides in the middle atmosphere, International Symposium on Middle Atmosphere Dynamics and Transport, July 28-August 1, Urbana, Illinois, 1980.

Lindzen, R. S., Turbulence and stress owing to gravity wave and tidal breakdown, J. Geophys. Res., 86, 9707-9714, 1981.

Lippens, C., and C. Muller, Atmospheric nitric acid and chlorofluoromethane from interferometric spectra obtained at the "Observatories du Pic du Midi", Aeronomica Acta, A227, Inst. d'Aeronomie Spatiale Belgique, Brussels, 1980.

Littlejohn, D., and H. S. Johnston, Rate constant for the reaction of hydroxyl radicals and peroxynitric acid, (abstract), EOS Trans. AGU, 61, 966, 1980.

Liu, S. C., Possible effects on tropospheric O_3 and OH due to NO emissions, Geophys. Res. Lett., **4**, 325-328, 1977.

Liu, S. C., Modeling of stratospheric and tropospheric ozone - A review, Proceedings of Quadrennial International Ozone Symposium, IAMAP, J. London, editor, 829-836, 1980.

Liu, S. C., T. M. Donahue, R. J. Cicerone, and W. L. Chameides, Effect of water vapor on the destruction of ozone in the stratosphere perturbed by Cl_x or NO_x pollutants, J. Geophys. Res., **81**, 3111-3118, 1976.

Liu, S. C., D. Kley, M. McFarland, J. D. Mahlman, and H. Levy II, On the origin of tropospheric ozone, J. Geophys. Res., **85**, 7546-7552, 1980.

Llewellyn, E. J., and G. Witt, The measurement of ozone concentrations at high latitude during the twilight, Planet. Space Sci., **25**, 165-172, 1977.

Loewenstein, M., and H. Savage, Latitudinal measurements of NO and O_3 in the lower stratosphere from 5° to 82° north, Geophys. Res. Lett., **2**, 448-450, 1975.

Loewenstein, M., H. F. Savage, and R. C. Whitten, Seasonal variation of NO and O_3 at altitudes of 18.3 and 21.3 km, J. Atmos. Sci., **32**, 2185-2190, 1975.

Loewenstein, M., H. F. Savage, and J. G. Borucki, Geographical variations of NO and O_3 in the lower stratosphere, International Conference on Problems Related to the Stratosphere, Utah State University, Logan, Utah, JPL Publication 77-12, 230-233, 1977.

Loewenstein, M., W. J. Starr, and D. G. Murcray, Stratospheric NO and HNO_3 observations in the northern hemisphere for three seasons, Geophys. Res. Lett., **5**, 531-534, 1978a.

Loewenstein, M., W. J. Borucki, H. F. Savage, J. G. Borucki, and R. C. Whitten, Geographical variations of NO and O_3 in the lower stratosphere, J. Geophys. Res., **83**, 1874-1882, 1978b.

Logan, J. A., M. Prather, S. Wofsy, and M. B. McElroy, Atmospheric chemistry: Response to human influence, Phil. Trans. Roy. Soc. London, Ser. A, **290**, 187-234, 1978.

Logan, J. A., M. B. McElroy, S. C. Wofsy, and M. J. Prather, Oxidation of CS_2 and COS: Sources for atmospheric SO_2, Nature, **281**, 185-188, 1979.

Logan, J. A., M. J. Prather, S. C. Wofsy, and M. B. McElroy, Tropospheric chemistry: A global perspective, J. Geophys. Res., **96**, 7210-7254, 1981.

London, J., Ozone variations and their relation to stratospheric warmings, Proc. Symp. Stratospheric and Mesospheric Circulation, Berlin, pp 99-310, 1962.

London, J., and J. Angell, The observed distribution of ozone and its variations, Stratospheric Ozone and Man, Vol. I, Stratospheric Ozone, F. A. Bower and R. B. Ward, editors, CRC press, 1982.

London, J., and S. J. Oltmans, The global distribution of long-term total ozone variations during the period 1957-1975, Pure Appl. Geophys., **117**, 345-354, 1978/79.

London, J., and C. A. Reber, Solar activity and total atmospheric ozone, Geophys. Res. Lett., 6, 869-872, 1979.

London, J., J. E. Frederick, and G. P. Anderson, Satellite observations of the global distribution of stratospheric ozone., J. Geophys. Res., 82, 2543-2556, 1977.

Lordi, N. J., A. Kasahara, and S. K. Kao, Numerical simulation of sudden warmings with a primitive equation spectral model, J. Atmos. Sci., 37, 2746-2767, 1980.

Louis, J. F., A two-dimensional transport model of the atmosphere, Ph.D. dissertation, Univ. of Colorado, Boulder, Colorado, 1974.

Louisnard, N., G. Fergant, and A. Girard, Simultaneous measurements of methane and water vapor vertical profiles in the stratosphere, Proceedings of the Quadrennial International Ozone Symposium, IAMAP, J. London, editor, pp 797-802, 1980a.

Louisnard, N., A. Girard, and G. Eichen, Mesures du profil vertical de concentration de la vapeur d'eau stratosphérique, C. R. Acad. Sci., Paris, Ser. B, 290, 385-388, 1980b.

Lovelock, J. E., Atmospheric fluorine compounds as indicators of air movement, Nature, 230, 379, 1971.

Lovelock, J. E. Atmospheric turbidity and CCl_3F concentrations in rural southern England and southern Ireland, Atmos. Environ., 6, 917-925, 1972.

Lovelock, J. E., Atmospheric halocarbons and stratospheric ozone, Nature, 252, 292-294, 1974.

Lovelock, J. E., Natural halocarbons in the air and in the sea, Nature, 256, 193-194, 1975.

Lovelock, J. E., Methyl chloroform in the troposphere as an indicator of OH radical abundance, Nature, 267, 32, 1977.

Lovelock, J. E., R. J. Maggs, and R. J. Wade, Halogenated hydrocarbons in and over the Atlantic, Nature, 241, 194-196, 1973.

Lovill, J. E., Characteristics of the general circulation of the atmosphere and the global distribution of total ozone as determined by the Nimbus III satellite infrared interferometer spectrometer, Atmospheric Science Paper No. 180, Colorado State University, Fort Collins, Colorado, 72 pp, 1972.

Lovill, J. E., T. J. Sullivan, R. L. Weichel, J. S. Ellis, J. G. Huebel, J. A. Korver, P. P. Weidhaas, and F. A. Phelps, Total ozone retrieval from satellite Multichannel Filter Radiometer measurements, UCRL-52473, Lawrence Livermore Laboratory, University of California/Livermore, 1978.

Luther, F. M., Monthly mean values of eddy diffusion coefficients in the lower stratosphere, AIAA Paper 73-498, AIAA/AMS Conference, Denver, Colorado, 1973.

Luther, F. M., Annual report of Lawrence Livermore Laboratory to the High Altitude Pollution Program, 1978, UCRL-50042-78, Lawrence Livermore Laboratory, University of California/Livermore, 1978.

Luther, F. M., and R. J. Gelinas, Effect of molecular multiple scattering and surface albedo on atmospheric photodissociation rates, J. Geophys. Res., 81, 1125-1132, 1976.

Luther, F. M., D. J. Wuebbles, W. H. Duewer, and J. S. Chang, Effect of multiple scattering on species concentrations and model sensitivity, J. Geophys. Res., 83, 3563-3570, 1978.

Luther, J. M., J. S. Ellis, J. E. Lovill, T. J. Sullivan, and R. L. Weichel, Global distribution of total ozone during January and February 1979 as determined from DMSP Multichannel Filter Radiometer measurements, Proceedings of the Quadrennial International Ozone Symposium, IAMAP, J. London, editor, pp 406-413, 1980.

Luther, F. M., J. S. Chang, W. H. Duewer, J. E. Penner, R. L. Tarp, and D. J. Wuebbles, Potential environmental effects of aircraft emissions, UCRL-52811, Lawrence Livermore Laboratory, University of California/Livermore, 1979.

Machta, L., Discussion of meteorological factors and fallout distribution, U.S. Dept. Commerce, Weather Bureau, 11 pp, 1957.

Machta, L., and R. J. List, Analysis of stratospheric strontium^{90} measurements, J. Geophys. Res., 64, 1267-1276, 1959.

Machta, J., and K. Telegades, Examples of stratospheric transport, Proc. Second Conf. Climatic Impact Assessment Program, A. J. Broderick, editor, DOT-TSC-OST-73-4, 47-56, 1973.

Machta, L., K. Telegadas, and R. J. List, The slope of the surface of maximum tracer concentration in the lower stratospheres, J. Geophys. Res., 75, 2279-2288, 1970.

Mahlman, J. D., Atmospheric general circulation and transport of radioactive debris, Atmospheric Science Paper No. 103, Department of Atmospheric Science, Colorado State University, 184 pp, 1966.

Mahlman, J. D., Eddy transfer processes in the stratosphere during major and 'minor' breakdowns of the polar night vortex, J. Geophys. Res., 75, 1701-1705, 1970.

Mahlman, J. D., On the maintenance of the polar front jet stream, J. Atmos. Sci., 30, 554-557, 1973.

Mahlman, J. D., Some fundamental limitations of simplified transport models as implied by results from a three-dimensional general circulation/tracer model, Proc. Fourth Conference Climatic Impact Assesment Program, T. M. Hard and A. J. Broderick, editors, DOT-TSC-OST-75-38, U. S. Department of Transportation, Washington, D.C., 132-146, 1975.

Mahlman, J. D., Coupling of atmospheric observation with comprehensive numerical models, Proc. of iCMUA Sessions and IUGG Symposium 18, XVII IUGG General Assembly, Canberra, Australia, 253-259, 1980.

Mahlman, J. D., and W. J. Moxim, Tracer simulation using global general circulation model: Results from a midlatitude instantaneous source experiment, J. Atmos. Sci., 35, 1340-1374, 1978.

Mahlman, J. D., and R. W. Sinclair, Tests of various numerical algorithms applied to a simple trace constituent air transport problem, Fate of Pollutants in the Air and Water Environments, Part 1, 8, I. H. Suffet, editor, John Wiley & Sons, Inc., 1977.

Mahlman, J. D., and R. W. Sinclair, Recent results from the GFDL troposphere-stratosphere-mesophere general circulation model, Proc. of ICMUA Sessions and IUGG Symposium 18, XVII IUGG General Assembly, Canberra, Australia, 11-18, 1980.

Mahlman, J. D., H. Levy II, and W. J. Moxim, Three-dimensional tracer structure and behavior as simulated in two ozone precursor experiments, J. Atmos. Sci., 37, 655-685, 1980.

Mahlman, J. D., D. G. Andrews, H. U. Dütsch, D. L. Hartmann, T. Matsuno, R. J. Murgatroyd, and J. F. Noxon, Transport of trace constituents in the stratosphere, Report of Study Group 2 of the Middle Atmosphere Program, Map Handbook III, pp 2(14-43), 1981.

Maier, E. J., A. C. Aikin, and J. E. Ainsworth, Stratospheric nitric oxide and ozone measurements using photoionization mass spectrometer and UV absorption, Geophys. Res. Lett., 5, 37-40, 1978.

Manabe, S., and B. G. Hunt, Experiments with a stratospheric general circulation model: I. Radiative and dynamic effects, Mon. Weather Rev., 96, 477-539, 1968.

Manabe, S., and J. D. Mahlman, Simulation of seasonal and interhemispheric variations in the stratospheric circulation, J. Atmos. Sci., 33, 2185-2217, 1976.

Manabe, S., D. G. Hahn, and J. L. Holloway, Jr., The seasonal variation of the hydrologic cycle as simulated by a global model of the atmosphere, J. Atmos. Sci., 31, 43-83, 1974.

Mankin, W. G., M. T. Coffey, D. W. T. Griffith, and S. R. Drayson, Spectroscopic measurement of carbonyl sulfide (OCS) in the stratosphere, Geophys. Res. Lett., 6, 853-856, 1979.

Marché, P., A. Barbe, C. Secroun, J. Corr, and P. Jouve, Ground based spectroscopic measurements of HCl, Geophys. Res. Lett., 7, 869-872, 1980a.

Marché, P., A. Barbe, C. Secroun, J. Corr, and P. Jouve, Mesures des acides fluorhydrique et chlorhydrique dans l'atmosphère par spectroscopie infrarogue à partir du sol, C. R. Acad. Sci. Paris, 290, 369-371, 1980b.

Margitan, J. J., F. Kaufman, and J. G. Anderson, Kinetics of the reaction OH + HNO_3 → H_2O + NO_3, Int. J. Chem. Kinet., Symp. No. 1, 281-287, 1975.

Maroulis, P. J., and A. R. Bandy, Measurements of atmospheric concentrations of CS_2 in the Eastern United States, Geophys. Res. Lett., 7, 681-684, 1980.

Maroulis, P. J., A. L. Torres, and A. R. Bandy, Atmospheric concentrations of carbonyl sulfide in the Southwestern and Eastern United States, Geophys. Res. Lett., 4, 510-512, 1977.

Maroulis, P. J., A. L. Torres, A. B. Goldberg, and A. R. Bandy, Atmospheric SO_2 measurements on Project Gametag, J. Geophys. Res., 85, 7345-7349, 1980.

Mason, C. J., and J. J. Horvath, The direct measurement of nitric oxide concentration in the upper atmosphere by a rocket-borne chemiluminescent detector, Geophys. Res. Lett., 3, 391-394, 1976.

Mass, C., and S. H. Schneider, Statistical evidence on the influence of sunspots and volcanic dust on long-term temperature records, J. Atmos. Sci., 34, 1995-2004, 1977.

Mastenbrook, H. J., Water vapor distribution in the stratosphere and high troposphere, J. Atmos. Sci., 25, 299-311, 1968.

Mastenbrook, H. J., and R. E. Daniels, Measurements of stratospheric water vapor using a frost point hygrometer, in Atmospheric Water Vapor, A. Deepak, T. W. Wilkerson, and L. H. Ruhnke, editors, Academic Press, pp 329-342, 1980.

Mateer, C. L., A review of some unresolved problems in measurement/estimation of total ozone and the vertical ozone profile, Proceedings of the Quadrennial International Ozone Symposium, IAMAP, J. London, editor, pp 1-8, 1980.

Mateer, C. L., J. J. DeLuisi, and C. C. Porco, The short Umkehr method, part I: Standard ozone profiles for use in the estimation of ozone profiles by the inversion of short Umkehr observations, NOAA Technical Memorandum ERL ARL-86, 20 pp, 1980.

Matsuno, T., Vertical propagation of stationary planetary waves in the winter Northern Hemisphere, J. Atmos. Sci., 27, 871-883, 1970.

Matsuno, T., A dynamical model of the stratospheric warming, J. Atmos. Sci., 28, 1479-1494, 1971.

Matsuno, T., Presented at CIAP workshop on computational modeling of the atmosphere, Pacific Grove, California, 1972.

Matsuno, T., Lagrangian motion of air parcels in the stratosphere in the presence of planetary waves, Pure Appl. Geophys., 118, 189-216, 1980.

Matsuno, T., and K. Nakamura, The Eulerian and Lagrangian mean meridional circulations in the stratosphere at the time of a sudden warming, J. Atmos. Sci., 36, 640-654, 1979.

Mauersberger, K., Measurement of heavy ozone in the stratosphere, Geophys. Res. Lett., 8, 935-937, 1981.

Mauersberger, L., and R. Finstad, Carbon dioxide measurements in the stratosphere, Geophys. Res. Lett., 7, 873-876, 1980.

Mauersberger, K., R. Finstad, S. Anderson, and D. Robbins, A comparison of ozone measurements, Geophys. Res. Lett., 8, 361-364, 1981.

McCarthy, R. L., F. A. Bower, and J. P. Je on, The fluorocarbon-ozone theory I: World production and release of CCl_3F and CCl_2F_2 (fluorocarbon 11 and 12) through 1975, Atmos. Environ., 11, 491-497, 1977.

McConnell, J. C., and H. I. Schiff, Methyl chloroform: Impact on stratospheric ozone, Science, 199, 174-177, 1978.

McCormick, M. P., Stratospheric aerosols, NASA Technical Memorandum 83217, 19 pp, 1981a.

McCormick, M. P., Stratospheric aerosol and ozone measurements by the SAM II and SAGE satellite sensors, (abstract), Third Scientific Assembly of IAMAP, Hamburg, FDR, 17-28 August, 1981b.

McCormick, M. P., T. J. Swissler, W. P. Chu, and W. H. Fuller, Jr., Post-volcanic stratospheric aerosol decay as measured by lidar, J. Atmos. Sci., 35, 1296-1303, 1978.

McCormick, M. P., P. Hamill, T. J. Pepin, W. P. Chu, T. J. Swissler, and L. R. McMaster, Satellite studies of the stratosphere aerosol, Bull. Amer. Meteorol. Soc., 60, 1038-1046, 1979.

McCormick, M. P., T. J. Swissler, W. P. Chu, M. Osborn, and H. Steele, Satellite profile measurements of stratospheric ozone, Proceedings of the Quadrennial International Ozone Symposium, IAMAP, J. London, editor, pp 184-189, 1980.

McCormick, M. P., W. P. Chu, G. W. Grams, P. Hamill, B. M. Herman, L. R. McMaster, T. J. Pepin, P. B. Russell, H. M. Steele, and T. J. Swissler, High-latitude stratospheric aerosols measured by the SAM II satellite system in 1978-1979, Science, 214, 328-331, 1981.

McCormick, M. P., H. M. Steele, P. Hamill, W. P. Chu, and T. J. Swissler, Polar stratospheric cloud sightings by SAM II, J. Atmos. Sci., in press, 1982.

McElroy, M. B., S. C. Wofsy, and Y. L. Yung, The nitrogen cycle: Perturbations due to man and their impact on atmospheric N_2O and O_3, Phil. Trans. Roy. Soc. Lon. Ser. B., 277, 159-181, 1977.

McFarland, M., D. Kley, J. W. Drummond, A. L. Schmeltekopf, and R. H. Winkler, Nitric oxide measurements in the equatorial Pacific region, Geophys. Res. Lett, 6, 605-608, 1979.

McGee, T. J., and T. J. McIlrath, Absolute OH absorption cross-sections for lidar measurements, NASA Technical Report, 1982.

McGregor, J., and W. A. Chapman, Observations of the annual and semi-annual wave in the stratosphere using Nimbus 5 SCR data, J. Atmos. Terr. Phys., 40, 677-684, 1978.

McGregor, J. and W. A. Chapman, Stratospheric temperatures and geostrophic winds during 1973-1974, Quart. J. Roy. Meteorol. Soc., 105, 241-261, 1979.

McInturff, R. M., A. J. Miller, J. K. Angell, and J. Korshover, Possible effects on the stratosphere of the 1963 Mt. Agung volcanic eruption, J. Atmos. Sci., 28, 1304-1307, 1971.

McIntyre, M. E., An introduction to the generalized Lagrangian-mean description of wave, mean-flow interaction, Pure Appl. Geophys., 118, 152-176, 1980a.

McIntyre, M. E., Towards a Lagrangian-mean description of stratospheric circulations and chemical transports, Phil. Trans. Roy. Soc. London, A, 296, 129-148, 1980b.

Mentall, J. E., J. R. Herman, and B. Zak, Ozone profile and solar fluxes from a grating spectrometer, The Stratcom VIII Effort, NASA Technical Paper 1640, E. Reed, editor, pp 117-123, April 1980.

Mentall, J. E., J. E. Frederick, and J. R. Herman, The solar irradiance from 200-330 nm, J. Geophys. Res., 86, 9881-9884, 1981.

Menzies, R. T., Remote measurement of ClO in the stratosphere, Geophys. Res. Lett., 6, 151-154, 1979.

Menzies, R. T., C. W. Rutledge, R. A. Zanteson, and D. L. Spears, Balloon-borne laser heterodyne radiometer for measurements of stratospheric trace species, Appl. Opt., 20, 536-553, 1981.

Metra Gruppe, Social and economic implications of controlling the use of chlorofluorocarbons in the EEC, U/77/336/(234), 1978.

Mihelcic, D., D. H. Ehhalt, G. F. Kulessa, J. Klomfass, M. Trainer, U. Schmidt, and H. Röhrs, Measurements of free radicals in the atmosphere by matrix isolation and electron paramagnetic resonance, Pure Appl. Geophys., 116, 530-536, 1978.

Miller, A. J., R. M. Nagatani, K. B. Labitzke, E. Klinker, K. Rose, and D. F. Heath, Stratospheric ozone transport during the mid-winter warming of December 1970-January 1971, Proc. Joint Symp. Atmos. Ozone., Dresden, German Democratic Republic, pp 135-148, 1977a.

Miller, A. J., H. Korty, and D. F. Heath, Comparison of Backscatter Ultraviolet (BUV) and ground-based total ozone fields for December 1970, Paper presented IUGC/IAMAP, Seattle, Washington, 1977b.

Miller, A. J., R. M. Nagatani, and J. D. Laver, Variations in the 100 mb height fields as an indicator of long-term trends of total ozone at individual sampling sites, Paper presented at AMS Conference on the Meteorology of the Upper Atmosphere, October 1978, Boston, Massachusetts, 1978a.

Miller, A. J., B. Korty, E. Hilsenrath, A. J. Fleig, and D. F. Heath, Verification of Nimbus 4 BUV total ozone data and the requirements for operational satellite monitoring, Proc. WMO Symposium on the Geophysical Aspects and Consequences of Change in the Composition of the Stratosphere, Toronto, Canada, WMO Publ. 511, World Meteorological Organization, pp 153-160, 1978b.

Miller, A. J., T. G. Rogers, R. M. Nagatani, D. F. Heath, A. J. Fleig, and V. G. Kaveeshwar, Comparison of Backscatter Ultraviolet (BUV) total ozone and vertical profile information with ground-based data and meteorological analyses, Proceedings XVII General Assembly of the International Union of Geodesy and Geophysics, 1979a.

C-6

Miller, A. J., T. G. Rogers, R. M. Nagatani, D. F. Heath, A. J. Krueger, W. Planet, and D. Crosby, Preliminary comparisons of daily total ozone fields derived from SBUV, TOMS and HIRS-2 satellite instruments, Proceedings XVII General Assembly of the International Union of Geodesy and Geophysics, 1979b.

Miller, A. J., B. Korty, and D. F. Heath, Comparison of Backscatter Ultraviolet (BUV) and ground-based total ozone fields for December 1970, Pure Appl. Geophys., 117, 355-360, 1978/1979c.

Miller, A. J., R. M. Nagatani, J. D. Laver, and B. Korty, Utilization of 100 mb midlatitude height fields as an indicator of sampling effects on total ozone variations, Mon. Weather Rev., 107, 782-787, 1979d.

Miller, A. J., T. G. Rogers, R. M. Nagatani, D. F. Heath, A. J. Fleig, and V. G. Kaveeshwar, Results and analyses of ground-based and satellite ozone observations - a review, Proceedings of the Quadrennial International Ozone Symposium, IAMAP, J. London, editor, pp 285-305, 1980.

Miller, A. J., R. M. Nagatani, T. G. Rogers, A. J. Fleig, D. F. Heath, and V. G. Kaveeshwar, Total ozone variations 1970-1974 using Backscattered Ultraviolet (BUV) and ground-based observations, J. of App. Met., submitted, 1981.

Miller, C., Two-dimensional model predictions: Long-lived tracers, chlorine species, and chlorine perturbations, preprint, December 1980.

Miller, C., D. L. Filkin, and J. P. Jesson, The fluorocarbon ozone theory - VI Atmospheric modeling: Calculation of the diurnal steady state, Atmos. Environ., 13, 381-394, 1979.

Miller, C., D. L. Filkin, and J. P. Jesson, Summary of the Du Pont 2-D model, Presented at the WMO Workshop on Two-Dimensional Models, Toronto, Canada, February, 1980a.

Miller, C., J. M. Steed, D. L. Filkin, and J. P. Jesson, Two-dimensional model calculations of stratospheric HCl and ClO, Nature, 288, 461-464, 1980b.

Miller, C., D. L. Filkin, A. J. Owens, J. M. Steed, and J. P. Jesson, A two-dimensional model of stratospheric chemistry and transport, J. Geophys. Res., 86, 12,039-12,065, 1981.

Miranda, H. ., Jr., and R. Fenn, Stratospheric aerosol sizes, Geophys. Res. Lett., 1, 201-203, 1974.

Molina, L. T., and M. J. Molina, Ultraviolet absorption cross sections for HO_2NO_2 vapor, presented at the 14th Informal Conference on Photochemistry, Newport Beach, California, also U. S. DOT Report FAA-EE-80-7, 1980.

Molina, M. J., L. T. Molina, and T. Ishiwata, Kinetics of the ClO + NO_2 reaction, J. Phys. Chem., 84, 3100-3104, 1980.

Mossop, S. C., Stratospheric particles at 20 km altitude, Geochim. Cosmochim. Acta, 29, 201-207, 1965.

Mount, G. H., and G. J. Rottman, The solar spectral irradiance 1200-3184A near solar maximum: 15 July 1980, J. Geophys. Res., 86, 9193-9198, 1981.

Mount, G. H., G. J. Rottman, and J. G. Timothy, The solar spectral irradiance 1200-2550 A at solar maximum, J. Geophys. Res., 85, 4271-4274, 1980.

Moxim, W. J., and J. D. Mahlman, Evaluation of various total ozone sampling networks using the GFDL 3-D tracer model, J. Geophys. Res., 85, 4527-4539, 1980.

Mroz, E. J., A. L. Lazrus and J. C. Bonnelli, Direct measurements of stratospheric fluoride, Geophys. Res. Lett., 4, 149-150, 1977.

Murcray, D. G., A. Goldman, W. J. Williams, F. H. Murcray, J. N. Brooks, J. Van Allen, R. N. Stocker, J. J. Kosters, D. B. Barker, and D. E. Snider, Recent results of stratospheric trace-gas measurements from balloon-borne spectrometers, Proc. Third CIAP Conf., A. J. Broderick and T. M. Hard, editors, DOT-TSC-OST-74-15, U. S. Dept. of Transportation, Washington, D. C., pp 184-192, 1974.

Murcray, D. G., D. B. Barker, J. N. Brooks, A. Goldman, and W. J. Williams, Seasonal and latitudinal variation of the stratospheric concentration of HNO_3, Geophys. Res. Lett., 2, 223-225, 1975.

Murcray, D. G., W. J. Williams, D. B. Barker, A. Goldman, C. Bradford, and G. Cook, Measurements of constituents of interest in the chemistry of the ozone layer using IR techniques, Proc. WMO Symposium on the Geophysical Aspects and Consequences of Change in the Composition of the Stratosphere, WMO No. 511, pp 61-68, Toronto, Canada, June, 1978.

Murcray, D. G., A. Goldman, F. H. Murcray, F. J. Murcray, and W. J. Williams, Stratospheric distribution of $ClONO_2$, Geophys. Res. Lett., 6, 857-859, 1979.

Murgatroyd, R. J., Ozone and water vapor in the upper troposphere and lower stratosphere, WMO Technical Note, No. 68, 68-94, 1965.

Murgatroyd, R. J., and R. M. Goody, Sources and sinks of energy from 30 to 90 km, Quart. J. Roy Meteorol. Soc., 84, 225-234, 1958.

Murgatroyd, R. J., and A. O'Neill, Interaction between the troposphere and stratosphere, Phil. Trans. Roy Soc. London, A, 296, 87-102, 1980

Murgatroyd, R. J., and F. Singleton, Possible meridional circulation in the stratosphere and mesosphere, Quart. J. Roy Meteorol. Soc., 87, 125-135, 1961.

NASA RP-1010, Chlorofluoromethanes and the Stratosphere, NASA Reference Publication 1010, R. D. Hudson, editor, 266 pp, 1977.

NASA RP 1049, The Stratosphere: Present and Future, NASA Reference Publication 1049, R. D. Hudson and E. I. Reed, editors, 432 pp, 1979.

Namias, J., Large-scale and long-term fluctuations in some atmospheric and oceanic variables, Proceedings of the 20th Nobel Symposium, Almquist and Wiksell, 27-48, 1972.

Namias, J., and P. F. Clapp, Confluence theory of the high tropospheric jet stream, J. Meteorol., 6, 330-336, 1949.

Nastrom, G. D., Vertical and horizontal fluxes of ozone at the tropopause from the first year of GASP data, J. Appl. Meteorol., 16, 740-744, 1977.

Nastrom, G. D., and A. D. Belmont, Periodic variations in stratospheric-mesopheric temperature from 20-65 km at 80°N to 30°S, J. Atmos. Sci., 32, 1715-1722, 1975.

Nastrom, G. D., J. D. Holdeman, and P. J. Perkins, Measurements of cabin and ambient ozone in B747 airplanes, J. Aircraft, 17, 246-249, 1980.

National Academy of Sciences, Environmental Impact of Stratospheric Flight, National Academy of Sciences, Washington, D.C., 348 pp, 1975.

National Academy of Sciences, Stratospheric Ozone Depletion By Halocarbons: Chemistry and Transport, Washington, D.C., 352 pp., 1979.

National Academy of Sciences, Halocarbons: Effects on Stratospheric Ozone, Washington, D.C., 1976.

National Research Council, Carbon Dioxide and Climate, a Scientific Assessment, National Academy of Sciences, Washington, D.C., 1979.

Naudet, J. P., P. Rigaud, and D. Huguenin, Stratospheric NO_2 at night from stellar spectra in the 440 nm region, Geophys. Res. Lett., 7, 701-703, 1980.

Naudet, J. P., D. Huguenin, P. Rigaud, and D. Cariolle, Stratospheric observations of NO_3 and its experimental and theoretical distribution between 20 and 40 km, Planet. Space Sci., 29, 707-712, 1981.

Neckel, H., and D. Labs, Improved data of solar spectral irradiance from 0.33 to 1.25 μm, Solar Phys., 74, 231-249, 1981.

Neely, and Agin, Environmental fate of methyl chloroform, Proceedings of the Conference on Methyl Chloroform and Other Halocarbon Pollutants, EPA-600/3-80-003, Environmental Sciences Research Lab., Research Triangle Park, North Carolina, 1980.

Neely, W. B., and J. H. Plonka, Estimation of the time-averaged hydroxyl radical concentration in the troposphere, Env. Sci. and Tech., 12, 317-321, 1978.

Nelson, H. H., W. J. Marinelli, and H. S. Johnston, The kinetics and product yield of the reaction of HO with HNO_3, Chem. Phys. Lett., 78, 495-499, 1981.

Newell, R. E., The transort of trace substances in the atmosphere and their implications for the general circulation of the stratosphere, Geofisica Pura e Appl., 49, 137-158, 1961.

Newell, R. E., The general circulation of the atmosphere and its effects on the movement of trace substances, J. Geophys. Res., 68, 3949-3962, 1963a.

Newell, R. E., Transfer through the tropopause and within the stratosphere, Quart. J. Roy. Meteorol. Soc., 89, 167-204, 1963b.

Newell, R. E., Further ozone transport calculations and the spring maximum in ozone amount, Pure Appl. Geophys., 59, 191-206, 1964.

Newell, R. E., The general circulation of the atmosphere and its effects on the movement of trace substance, Part 2, Tellus, 18, 363-380, 1965.

Newell, R. E., The general circulation of the atmosphere above 60 km, Meteorological Monographs, 9, 98-113, 1968.

Newell, R. E., The global circulation of atmospheric pollutants, Sci. Am., 224, 32-42, 1971.

Newell, R. E., and S. Gould-Stewart, The stratospheric fountain, J. Atmos. Sci., 28, in press, 1981.

Newell, R. E., and M. -F. Wu, A pilot study of concomitant changes in total ozone and atmospheric general circulation, Quart. J. Roy. Meteorol. Soc., 104, 999-1003, 1978.

Newell, R. E., J. W. Kidson, D. G. Vincent, and G. J. Boer, The General Circulation of the Tropical Atmosphere and Interactions with Extra-tropical Latitudes, MIT Press, Cambridge, 258 pp, 1972.

Newson, R. L., An experiment with a tropospheric and stratospheric three-dimensional general-circulation model, Proc. Third Conference on CIAP, A. J. Broderick and T. M. Hard, editors, Dept. of Transportation DOT-TSC-OST-74-15, pp 461-474, 1974.

Nichols, D. A., DMSP Block 5D meteorological sensor H, optical subsystem, Opt. Engr., 14, 284-288, 1975.

Nicolet M., L'ozone et ses relations avec la situation atmospherique, Inst. Roy. Meteorol. de Belgique, Misc., Fasc., 19, 36 pp, 1946.

Nicolet, M., Stratospheric zone: An introduction to its study, Rev. Geophys. Space Phys., 13, 593-636, 1975.

Nicolet, M., The solar spectral irradiance and its action in the atmospheric photodissociation processes, Planet. Space Sci., 29, 951-974, 1981.

Nimbus Project, Nimbus IV Users Guide, National Space Science Data Center, NASA, Goddard Space Flight Center, Greenbelt, MD, 1970.

Niple, E., W. G. Mankin, A. Goldman, D. G. Murcray, and F. J. Murcray, Stratospheric NO_2 and H_2O mixing ratio profiles from high resolution infrared solar spectra using nonlinear least squares, Geophys. Res. Lett., 7, 489-492, 1980.

Nolt, I. G., and L. P. Stearns, Infrared water vapor measurements from the Kuiper airborne observatory, Atmospheric Water Vapor, A. Deepak, T. D. Wilkerson, and K. H. Ruhnke, editors, Academic Press, pp 343-353, 1980.

Normand, C. Atmospheric ozone and the upper air conditions, Quart. J. Roy. Meteorol. Soc., 79, 39-50, 1953.

Noxon, J. F., Stratospheric NO_2 in the Antarctic winter, Geophys. Res. Lett., 5, 1021-1022, 1978.

Noxon, J. F., Stratospheric NO_2, Global behavior, J. Geophys. Res., 84, 5067-5076, 1979.

Noxon, J. F., Correction, J. Geophys. Res., 85, 4560-4561, 1980.

Noxon, J. F., E. C. Whipple, Jr., and R. S. Hyde, Stratospheric, NO_2, I. Observational method and behavior at mid-latitude, J. Geophys. Res., 84, 5047-5065, 1979.

Oberbeck, V. R., N. H. Farlow, G. V. Ferry, H. Y. Lem, and D. M. Hayes, A study of stratospheric aerosol maturity, Geophys. Res. Lett., 8, 18-20, 1981.

Offerman, D., P. Curtis, J. M. Cisneros, J. Satrustegui, H. Lauche, G. Rose, and K. Petzoldt, Atmospheric temperature structure during the Western European winter anomaly campaign 1975/76, J. Atmos. Terr. Phys., 41, 1051-1062, 1979.

O'Brien, R. S., and W. F. J. Evans, Rocket measurements of the distribution of water vapor in the stratosphere at high latitudes, J. Geophys. Res., 86, 12,101-12,107, 1981.

OECD, Report of chlorofluorocarbons, ENV (80) 32, Paris, France, 1981.

Ogawa, T., K. Shibasaki, and K. Suzuki, Balloon observation of the stratospheric NO_2 profile by visible absorption spectroscopy, J. Meteorol. Soc. Japan, 59, 410-416, 1981.

Ogawa, T., and T. Watanabe, Summary of the mesospheric ozone measurements during 1970-1979 in Japan, Proceedings of the Quadrennial International Ozone Symposium, IAMAP, J. London, editor, pp 520-525, 1980.

Oliver, R. C., E. Bauer, H. Hidalgo, K. A. Gardner, and W. Wasylkiwskyj, Aircraft emissions: Potential effects on ozone and climate, a review and progress report, Report FAA-EQ-77-3, U.S. Department of Transportation, Washington, D.C. March 1977.

Oltmans, S. J., Surface ozone measurements in clear air, J. Geophys. Res., 86, 1174-1180, 1981.

O'Neill, A., The dynamics of stratospheric warmings generated by a general circulation model of the troposphere and stratosphere, Quart. J. Roy. Meteorol. Soc., 106, 659-690, 1980.

O'Neill, A., R. L. Newson, and R. J. Murgatroyd, An analysis of the large scale features of the upper troposphere and stratosphere in a global, three dimensional, general circulation model, Quart. J. Roy. Meteorol. Soc., in press, 1981.

Oort, A. H., Adequacy of the rawinsonde network for global circulation studies tested through numerical model output, Mon. Weather Rev., 106, 174-195, 1978.

Oort, A. H., and E. M. Rasmusson, Atmospheric circulation statistics NOAA Professional Paper 5, U.S. Govt. Print. Off., 1971.

Ortgies, G., D. -H. Gericke, and F. J. Comes, Is UV laser induced fluorescence a method to monitor tropospheric OH?, Geophys. Res. Lett., 7, 905-908, 1980.

Pack, D. H., J. E. Lovelock, G. Cotton, and C. Curthoys, Halocarbon behavior from a long time series, Atmos. Environ., 11, 329-344, 1977.

Palmer, T. N., Diagnostic study of a wavenumber-2 stratospheric sudden warming in a transformed Eulerian-mean formalism, J. Atmos. Sci., 38, 844-855, 1981a.

Palmer, T. N., Aspects of stratospheric sudden warmings studied from a transformed Eulerian-mean viewpoint, J. Geophys. Res., 86, 9679-9687, 1981b.

Papathakos, L. C., and D. Briehl, NASA global atmospheric sampling program (GASP) data report for tape VL0015, VL0016, VL0017, VL0018, VL0019, and VL0020, NASA Technical Memorandum 81661, 94 pp, June 1981.

Parrish, A., R. L. deZafra, P. M. Solomon, J. W. Barrett and E. R. Carlson, Chlorine oxide in the stratospheric ozone layers: Ground-based detection and measurement, Science, 211, 1158-1161, 1981.

Patel, C. K., N. E. G. Burkhardt, and C. A. Lambert, Spectroscopic measurements of stratospheric nitric oxide and water vapor, Science, 184, 1173-1176, 1974.

Penfield, H., M. M. Litvak, C. A. Gotlieb, and A. E. Lilley, Mesospheric ozone measured from ground-based millimeter wave observations, J. Geophys. Res., 81, 6115-6120, 1976.

Penkett, S. A., K. A. Brice, R. G. Derwent, and A. E. J. Eggleton, Measurement of CCl_3 and CCl_4 at Harwell over the period January 1975-November 1977, Atmos. Environ., 13, 1011-1019, 1979.

Penkett, S. A., N. J. D., Prosser, R. A. Rasmussen, and M. A. K. Khalil, Measurement of $CHFCl_2$ (F-21) in background tropospheric air, Nature, 286, 793-795, 1980.

Penkett, S. A., N. J. D. Prosser, R. A. Rasmussen, and M. A. K. Khalil, Atmospheric measurements of CF_4 and other fluorocarbons containing the CF_3 grouping, J. Geophys. Res., 86, 5172-5178, 1981.

Penner, J. E., Trend prediction for O_3: An analysis of model uncertainty with comparison to detection thresholds, Atmos. Environ., submitted, 1981.

Penner, J. E. and J. S. Chang, Possible variations in atmospheric ozone related to the eleven-year solar cycle, Geophys. Res. Lett., 5, 817-820, 1978.

Penner, J. E., L. P. Golen, and R. W. Mensing, A time series analysis of Umkehr data from Arosa, J. Geophys. Res., in press, 1981.

Pepin, T. J., M. P. McCormick, W. P. Chu, F. Simon, T. J. Swissler, R. R. Adams, K. H. Crumbly, and W. H. Fuller, Stratospheric Aerosol Measurements, NASA Special Publication-421, 1977.

Perner, D., D. H. Ehhalt, H. W. Pätz, U. Platt, E. P. Röth, and A. Volz, OH radicals in the lower troposphere, Geophys. Res. Lett., 3, 466-468, 1976.

Perner, D., D. H. Ehhalt, H. W. Pätz, U. Platt, E. P. Röth, and A. Volz, Comment on Improved airborne measurements of OH in the atmosphere using the technique of laser-induced fluorescence; by C. C. Wang, L. I. Davis, Jr., P. M. Selzer, and R. Munoz, J. Geophys. Res., 86, 12,155, 1981.

Pick, D. R., and J. L. Brownscombe, Early results based on the stratospheric channels of TOVS on the TIROS-N series of operational satellites, First FGGE Results from Satellites, Adv. Space Res. Vol. 1. No. 4, 247-260, 1981.

Pierotti, D., and R. A. Rasmussen, Combustion as a source of nitrous oxide in the atmosphere, Geophys. Res. Lett., 3, 265-267, 1976.

Pierotti, D., L. E. Rasmussen, and R. A. Rasmussen, The Sahara as a possible sink for trace gases, Geophys. Res. Lett., 5, 1001-1004, 1978.

Pinnick, R. G., J. M. Rosen and D. J. Hofmann, Stratospheric aerosol measurements III: Optical model calculations, J. Atmos. Sci., 33, 304-314, 1976.

Pinto, et al., J. Geophys. Res., submitted, 1981.

Pittock, A. B., On the representativeness of mean ozone distributions, Quart. J. Roy. Meteorol. Soc., 96, 32-39, 1970.

Pittock, A. B., Global meridional interactions in stratosphere and troposphere, Quart. J. Roy. Meteorol. Soc., 99, 424-437, 1973.

Pittock, A. B., Global interactions in stratosphere and troposphere, Proceedings of the International Conference on Structure, Composition and General Circulation of the Upper and Lower Atmospheres and Possible Anthropogenic Perturbations, pp 716-726, 1974a.

Pittock, A. B., Ozone climatology trends and the monitoring problem, Proceedings of the International Conference on Structure, Composition and General Circulation of the Upper and Lower Atmospheres and Possible Anthropogenic Perturbations, Melbourne, Australia, pp 455-466, 1974b.

Pittock, A. B., Climatology of the vertical distribution of ozone over Aspendale (38°S 145°E), Quart. J. Roy. Meteorol. Soc., 103, 575-584, 1977.

Plumb, R. A., Eddy fluxes of conserved quantities by small-amplitude waves, J. Atmos. Sci., 36, 1699-1704, 1979.

Plumb, R. A., Instability of the distorted polar night vortex: A theory of stratospheric warmings, J. Atmos. Sci., in press, 1981.

Podzimek, J., J. B. Haberl, and W. A. Sedlacek, Recent measurements of Aitken nuclei in the lower stratosphere, Proceedings of the Fourth Conference on the Climatic Impact Assessment Program, T. J. Hard and A. J. Broderick, editors, U. S. Dept. Transportation, DOT-TSC-OST-75-38, pp 519-526, 1975.

Pollack, J. B., O. B. Toon, A. Summers, W. Van Camp and B. Baldwin, Estimates of the climatic impact of aerosols produced by space shuttles, SSTs and other high flying aircraft, J. Appl. Meteorol., 15, 247-258, 1976b.

Pollack, J. B., O. B. Toon, C. Sagan, A. Summers, B. Baldwin and W. VanCamp, Volcanic explosions and climatic change: A theoretical assessment, J. Geophys. Res., 81, 1071-1083, 1976c.

Pollock, W., L. E. Heidt, R. Lueb, and D. H. Ehhalt, Measurement of stratospheric water vapor by cryogenic collection, J. Geophys. Res., 85, 5555-5568, 1980.

Pommereau, J.P., and A. Hauchecorne, Observations spectroscopiques depuis le sol du dioxyde d'azote atmosphèrique, C. R. Acad. Sc. Paris, Ser. B., 288, 135-138, 1979.

Popoff, I. G., W. A. Page, and A. P. Margozzi, editors, 1977 Intertropical Convergence Zone Experiment, NASA Technical Memorandum 78577, 506 pp, 1979.

Poynter, R. L., and H. M. Pickett, Submillimeter, Millimeter and Microwave Spectral Line Catalogue, JPL Publication 80-23, Pasadena, California, 141 pp, 1981.

Prabhakara, C., B. J. Conrath, R. A. Hanel, and E. J. Williamson, Remote sensing of atmospheric ozone using the 9.6 micron band, J. Atmos. Sci., 27, 689-697, 1970.

Prabhakara, C., E. B. Rodgers, B. J. Conrath, R. A. Hanel, and V. G. Kunde, The Nimbus 4 infrared spectroscopy experiment 3. Observations of the lower stratospheric thermal structure and total ozone, J. Geophys. Res., 81, 6391-6399, 1976.

Prata, H. J., Some observations of traveling waves in the stratosphere and mesosphere, Ph. D. Thesis, University of Oxford, England, 1980.

Prata, A. J., and C.D. Rodgers, A comparison of 5-day and 2-day travelling wave observations with Hough modes modified by meridional shear, Extended Abstracts, International Symposium on Middle Atmosphere Dynamics and Transport, Urbana, Illinois, Volume II of the Handbook for MAP, S.K. Avery, editor, pp 147-156, 1981.

Prather, M. J., Ozone in the upper stratosphere and mesosphere, J. Geophys. Res., 86, 5325-5338, 1981.

Pruchniewicz, P. G., The average tropospheric ozone content and its variation with season and latitude as a result of global ozone circulation, Pure Appl. Geophys., 106-108, 1058-1073, 1973.

Pyle, J. A., A calculation of the possible depletion of ozone by chlorofluorocarbons using a two-dimensional model, Pure Appl. Geophys., 118, 355-377, 1980.

Pyle, J. A., and C. F. Rogers, A modified diabatic circulation model for stratospheric tracer transport, Nature, 287, 711-714, 1980.

Quack, M., and J. Troe, Unimolecular processes V: Maximum free energy criterion for the high pressure limit of dissociation reactions, Ber. Bunsenges. Phys. Chem., 81, 329-377, 1977.

Quiroz, R. S., The contribution of satellite remote sounding data in stratospheric analysis and research, COSPAR Plenary Meeting, Innsbruck, Austria, May 29-June 10, 1978. (Also see Remote Sounding of the Atmosphere from Space, H. J. Bolle, editor, Oxford, Pergamon Press, pp 69-82, 1979.

Quiroz, R. S., Stratospheric temperatures during solar cycle 20, J. Geophys. Res., 84, 2415-2420, 1979.

Quiroz, R. S., A. J. Miller, and R. M. Nagatani, A comparison of observed and simulated properties of sudden stratospheric warmings, J. Atmos. Sci., 32, 1723-1736, 1975.

Radford, H. E., M. M. Litvak, C. A. Gottlieb, E. W. Gottlieb, S. K. Rosenthal, and A. E. Lilley, Mesospheric water vapor measured from ground-based microwave observations, J. Geophys. Res., 82, 472-478, 1977.

Ramanathan, V., Radiative transfer within the earth's troposphere and stratosphere: A simplified radiative convective model, J. Atmos. Sci., 33, 1330-1346, 1976.

Ramanathan, V., Troposphere-stratosphere feedback mechanism: Stratospheric warming and its effects on the polar energy budgets and the tropospheric circulation, J. Amos. Sci., 34, 439-447, 1977.

Ramanathan, V., Climate effects of anthropogenic trace gases, Interaction of Energy and Climate, edited by Bach, et al., D. Reidel, 269-280, 1980a.

Ramanathan, V., Climate effects of ozone changes - A review, Low Latitude Aeronomical Processes, COSPAR Symposium Series, 8, Pergaman Press, 223-236, 1980b.

Ramanathan, V., and R. E. Dickinson, The role of stratospheric ozone in the zonal and seasonal radiative energy balance of the earth-troposphere system, J. Atmos. Sci., 36, 1084-1104, 1979.

Randhawa, J., Ozone measurements near sunrise, Nature, (Physical Science), 233, 101-102, 1971.

Randhawa, J., and M. Izquierdo, Ozone measurements at 48 km, J. Photochem., 6, 147-148, 1976-1977.

Rao-Vupputuri, R. K., Numerical experiments on the steady state meridional structure and ozone distribution in the stratosphere, Mon. Weather Rev., 101, 510-527, 1973.

Rao-Vupputuri, R. K., The structure of the natural stratosphere and the impact of chlorofluoromethane on the ozone layer investigated in a 2-D time dependent model, Pure Appl. Geophys., 117, 448-485, 1979.

Rao-Vupputuri, R. K., A comprehensive summary of the AES two-dimensional model, WMO Workshop on Two-dimensional Models, Toronto, Canada, February, 1980a.

Rao-Vupputuri, R. K., The natural stratospheric distributions of odd oxygen and odd nitrogen as simulated in the AES two-dimensional models, NASA/Stratospheric Modeling Workshop, 1980b.

Raper, O. F., C. B. Farmer, R. A. Toth, and B. D. Robbins, The vertical distribution of HCl in the stratosphere, Geophys. Res.Lett., 4, 531-534, 1977.

Rasmussen, R. A. and M. A. K. Khalil, Atmospheric halocarbons: Measurements and analyses of selected trace gases, Proc. of NATO Adv. Study Inst. on Atmospheric Ozone: Its Variation and Human Influences, A. C. Aikin, editor, FAA-EE-80-20, Dept. of Transportation, pp 209-231, 1980.

Rasmussen, R. A. and M. A. K. Khalil, Increase in the concentration of atmospheric methane, Atmos. Environ., 15, 883-886, 1981.

Rasmussen, R. A., S. A. Penkett, and N. Prosser, Measurement of carbon tetrafluoride in the atmosphere, Nature, 277, 549-551, 1979.

Rasmussen, R. A., M. A. K. Khalil, S. A. Penkett, and N. J. Prosser, $CHClF_2$ (F-22) in the earth's atmosphere, Geophys. Res. Lett., 7, 809-812, 1980a.

Rasmussen, R. A., L. E. Rasmussen, M. A. K. Khalil, and R. W. Dalluge, Concentration distribution of methyl chloride in the atmosphere, J. Geophys. Res., 85, 7350-7356, 1980b.

Rasmussen, R. A., M. A. K. Khalil, and R. W. Dalluge, Atmospheric trace gases in Antarctica, Science, 211, 285-287, 1981a.

Rasmussen, R. A., M. A. K. Khalil, and J. S. Chang, Atmospheric trace gases over China, J. Geophys. Res., in press, 1981b.

Ravishankara, A. R., N. M. Kreutter, R. C. Shah, and P. H. Wine, Rate of reaction of OH with COS, Geophys. Res. Lett., 7, 861-864, 1980.

Reber, C. A. and F. T. Huang, Total ozone - Solar activity relationships, J. Geophys. Res., 86, in press, 1981.

Reed, E. I., The Stratcom VIII Effort, NASA Technical Paper 1640, 219 pp, 1980.

Reed, E., Participants in the SABE effort include J. Ainsworth, J. Drummond, R. Evans, W. Komhyr, A. Krueger, D. Wright, J. Mentall, L. Rossi, and D. Robbins; a report is being coordinated by E. Reed, Goddard Space Flight Center, Greenbelt, Maryland, USA, 1981.

Reed, R. J., The role of vertical motions in ozone-weather relationships, J. Meteorol., 7, 263-267, 1950.

Reed, R. J. A study of a characteristic type of upper level frontogenesis, J.Meteorol., 12, 226-237, 1955.

Reed, R. J., and K. E. German, A contribution to the problem of stratospheric diffusion by large-scale mixing, Mon. Weather Rev., 93, 313-321, 1965.

Reed, R. J., and A. L. Julius, A quantitative analysis of two proposed mechanisms for vertical ozone transport in the lower stratosphere. J. Meteorol., 8, 321-325, 1951.

Reinsel, G., G. C. Tiao, M. N. Wang, R. Lewis, and D. Nychka, Statistical analysis of stratospheric ozone data for detection of trends, Atmos. Environ. 15, 1569-1577 1981a.

Reinsel, G., G. C. Tiao, and R. Lewis, A statistical analysis of total ozone data from the BUV satellite experiment, Preliminary Report, Dept. of Statistics, University of Wisconsin, Madison, 1981b.

Reinsel, G., G. C. Tiao, and R. Lewis, Statistical analysis of stratospheric ozone data for trend detection, Proceedings of the Environmetrics '81 Conference, Washington, DC, April, 1981c.

Remsberg, E. E., J. M. Russell, III, L. L. Gordley, J. C. Gille, and P. L. Bailey, The validation of LIMS ozone profiles using correlative rocket, ECC, and Dobson data sets, Proceedings of the Quadrennial International Ozone Symposium, IAMAP, J. London, editor, pp 190-196, 1980.

Ridley, B. A., and D. R. Hastie, Stratospheric odd-nitrogen: NO measurements at 51°N in summer, J. Geophys. Res., 86, 3162-3166, 1981.

Ridley, B. A., and L. C. Howlett, An instrument for nitric oxide measurements in the stratosphere, Rev. Sci. Instr., 45, 742-746, 1974.

Ridley, B. A., and H. I. Schiff, Stratospheric odd-nitrogen: Nitric oxide measurements at 32N in autumn, J. Geophys. Res., 86, 3167-3172, 1981.

Ridley, B. A., M. McFarland, J. T. Bruin, H. I. Schiff, and J. C. McConnell, Sunrise measurements of stratospheric nitric oxide, Can. J. Phys., 55, 212-221, 1977.

Riehl, H., and J. S. Malkus, On the heat balance in the equatorial trough zone, Geophysica, 6, 503-538, 1958.

Rigaud, P., Photodissociation de l'ozone au moment du lever du Soleil entre 40 et 65 km d'altitude, Ann. Geophys., 30, 319-328, 1974.

Rigaud, P., O. Steiger, D. Huguenin, Destruction de l'ozone de la haute atmosphére par les oxydes d'azote au moment du level du Soleil, C. R. Seances Soc. Phys. Hist. Natur. Geneve, 9, 84-90, 1974.

Rigaud, P., J. P. Naudet, and D. Huguenin, Étude de la répartition verticale de NO_2 stratosphérique durant la nuit, C. R. Acad. Sci. Paris, Ser. B, 284, 331-334, 1977.

Roach, W. T., Some aircraft observations of fluxes of solar radiation in the atmosphere, Annals of the International Geophysical Year, 32, 63-70, 1964.

Roach, W. T., On the effect of radiative exchange on the growth by condensation of a cloud or fog droplet, Quart. J. Roy. Meteorol. Soc., 102, 361-372,1976.

Robbins, D. E., NASA-JSC Ozone Observations for Validation of Nimbus 7 - LIMS Data, NASA Technical Memorandum 58227, 44 pp, April, 1980.

Robbins, D. E., and J. G. Carnes, Variations in the upper stratosphere's ozone profile, WMO Symposium on the Geophysical Aspects and Consequences of Changes in the Composition of the Stratosphere, Toronto, Canada, Pub. 511, World Meteorological Organization, Geneva, pp 131-137, 1978.

Robert, A. J., The integration of a spectral mode of the atmosphere by the implicit method, Proc. WMO/IUGG Symposium on Numerical Weather Prediction, Tokyo Meteor. Soc., Japan, VII-19-VII-24, 1969.

Robinson, G. D., The transport of minor atmospheric constituents between troposphere and stratosphere, Quart. J. Roy. Meteorol. Soc., 106, 227-253, 1980.

Robinson, E., R. Rasmussen, J. Krasnec, D. Pierotti, and M. Jakubovic, Detailed halocarbon measurements across the Alaskan tropopause, Geophys. Res. Lett., 3, 323-326, 1976.

Robock, A., The 'Little Ice Age': Northern hemisphere average observations and model calculations, Science, 206, 1402-1404, 1979.

Rodgers, C. D., Evidence for the five-day wave in the upper stratosphere, J. Atmos. Sci., 33, 710-711, 1976.

Rodgers, C. D., Statistical principles of inversion theory, Inversion Methods in Atmospheric Remote Sounding, A. Deepak, editor, Academic Press, 117-138, 1977. (Also NASA Conference Publication 004, 1977)

Rodgers, C. D., Morphology of upper atmosphere temperatures, Dynamical and Chemical Coupling Between the Neutral and Ionized Atmosphere, NATO Advanced Study, B. Grandal and J. A. Holtet, editors, D. Reidel, pp 3-16, 1977b.

Rodgers, C. D., and A. J. Prata, Evidence for a travelling two-day wave in the middle atmosphere, Extended Abstracts, International Symposium on Middle Atmosphere Dynamics and Transport, Volume II of the Handbook for MAP, S. K. Avery, editor, pp 138-146, 1981. Also J. Geophys. Res., 86, 9661-9664, 1981.

Rodhe, H., and I. Isaksen, Global distribution of sulfur compounds in the troposphere estimated in a height/latitude transport model, J. Geophys. Res., 85, 7401-7409, 1980.

Rogers, J. W., A. T. Stair, Jr., T. C. Degges, C. L. Wyatt, and D. J. Baker, Rocketborne measurement of mesospheric H_2O in the auroral zone, Geophys. Res. Lett., 4, 366-368, 1977.

Roscoe, H. K., J. R. Drummond, and R. F. Jarnot, Infrared measurements of stratospheric composition III. The daytime changes of NO and NO_2, Proc. Roy. Soc. London, A, 375, 507-528, 1981.

Rosen, J. M., The vertical distribution of dust to 30 kilometers, J. Geophys. Res., 69, 4673-4676, 1964.

Rosen, J. M., The boiling point of stratospheric aerosols, J. Appl. Meteorol., 10, 1044-1046, 1971.

Rosen, J. M., D. J. Hofmann, and J. Laby, Stratospheric aerosol measurements II: The worldwide distribution, J. Atmos. Sci., 32, 1457-1462, 1975.

Rottman, G. J., Rocket measurements of solar spectral irradiance during solar minimum, 1972 to 1977, J. Geophys. Res., 86, 6697-6705, 1981.

Routhier, F., and D. D. Davis, Free tropospheric/boundary-layer airborne measurements of H_2O over the latitude range of 58°S to 70°N: Comparison with simultaneous ozone and carbon monoxide measurements, J. Geophys. Res., 85, 7293-7306, 1980.

Routhier, F., R. Dennett, D. D. Davis, A. Wartburg, P. Haagenson, and A. C. Delany, Free tropospheric and boundary-layer airborne measurements of ozone over the latitude range of 58°S to 70°N, J. Geophys. Res., 85, 7307-7321, 1980.

Rowland, F. S., S. C. Tyler, and D. C. Montague, Global tropospheric distributions of CH_3CCl_3, CCl_3F and CCl_2F_2 July 1979, Proceedings of the Quadrennial International Ozone Symposium, IAMAP, J. London, editor, p 808, 1980.

Roy, C. R., I. E. Galbally, and B. A. Ridley, Measurements of nitric oxide in the stratosphere of the southern hemisphere, Quart. J. Roy. Meteorol. Soc., 106, 887-894, 1980.

Rudolph, J., and D. H. Ehhalt, Measurements of C_2 - C_5 hydrocarbons over the North Atlantic, J. Geophys. Res., 86, 11,959-11,964, 1981.

Rudolph, J., D. H. Ehhalt, and G. Gravenhorst, Recent measurements of light hyrdocarbons in remote areas, Proceedings of the First European Symposium on Physico-chemical Behavior of Atmospheric Pollutants, Ispra, Oct. 16-18, Commission of the European Communities, 41-51, 1979.

Rudolph, J., D. H. Ehhalt, and A. Tönnissen, Vertical profiles of ethane and propane in the stratosphere, J. Geophys. Res., 86, 7267-7272, 1981.

Russell, J. M., and J. C. Gille, The Limb Infrared Monitor of the Stratosphere (LIMS) Experiment, The Nimbus 7 User's Guide, C. R. Madrid, editor, NASA Goddard Space Flight Center, Greenbelt, Maryland, pp 71-103, 1978.

Russell, J. M., J. C. Gille, E. E. Remsberg, and L. L. Gordley, Satellite observations of upper atmosphere O_3 and HNO_3 from the Limb Infrared Monitor of the Stratosphere (LIMS) Experiment on Nimbus 7, First FGGE Results from Satellites, Adv. Space Res., 1, No. 4, 271-277, 1981.

Sagawa, E., and T. Itoh, Mass spectrometric observation of SO_2 in the stratosphere, Geophys. Res.Lett., 4, 29-32, 1977.

Salby, M. L., The 2-day wave in the middle atmosphere: Observations and theory, J. Geophys. Res., 86, 9654-9660, 1981.

Samain, D., and P. C. Simon, Solar flux determination in the spectral range 150-210 nm, Solar Physics, 49, 33-41, 1976.

Sandalls, F. J., and S. A. Penkett, Measurements of carbonyl sulphide and carbon disulphide in the atmosphere, Atmos. Environ., 11, 197-199, 1977.

Sangster, W. E., A method of representing the horizontal pressure force without reduction of station pressures to sea level, J. Meteorol., 17, 166-176, 1960.

Schereschewky, M. P., La pénétration de la stratosphère par les protubérances des enclumes des cumulonimbus, C. R. Acad. Sci. Paris, Ser B, 284, 33-35, 1977.

Schlapp, D. M., Lunar tides in the middle atmosphere from Nimbus 5 data, J. Atmos. Terr. Phys., 42, 529-532, 1980.

Schlapp, D. M., Lunar tides in the stratosphere and mesosphere from Nimbus 6 data, J. Atmos. Terr. Phys., 43, 205-207, 1981.

Schlesinger, M. E., and Y. Mintz, Numerical simulation of ozone production, transport and distribution with a global atmospheric general circulation model, J. Atmos. Sci., 36, 1325-1361, 1979.

Schmeltekopf, A. L., P. D. Goldan, W. R. Henderson, W. J. Harrop, T. L. Thompson, F. C. Fehsenfeld, H. I. Schiff, P. J. Crutzen, I. S. A. Isaksen, and E. E. Ferguson, Measurements of stratospheric $CFCl_3$, CF_2Cl_2, and N_2O, Geophys. Res. Lett., 2, 393-396, 1975.

Schmidt, U., The latitudinal and vertical distribution of molecular hydrogen in the troposphere, J. Geophys. Res., 83, 941-946, 1978.

Schmidt, U., G. Kulessa, and E. P. Röth, The atmospheric H_2 cycle, Proceedings of the NATO Advanced Study Institute on Atmospheric Ozone, A. C. Aikin, editor, Dept. of Transportation, FAA-EE-80-20, pp 307-322, 1980a.

Schmidt, U., J. Rudolph, F. J. Johnen, D. H. Ehhalt, A. Volz, E. P. Röth, R. Borchers, and P. Fabian, The vertical distribution of CH_3Cl, $CFCl_3$, and CF_2Cl_2 in the midlatitude stratosphere, Proceedings of the Quadrennial International Ozone Symposium, IAMAP, J. London, editor, pp 816-823, 1980b.

Schoeberl, M. R., and M. A. Geller, The structure of stationary planetary waves in winter in relation to the polar night jet intensity, Geophys. Res. Lett., 3, 177-180, 1976.

Schoeberl, M. R., and D. F. Strobel, The zonally averaged circulation of the middle atmosphere, J. Atmos. Sci., 35, 577-591, 1978a.

Schoeberl, M. R., and D. F. Strobel, The response of the zonally averaged circulation to stratospheric ozone reductions, J. Atmos. Sci., 35, 1751-1757, 1978b.

Schoeberl, M. R., and D. F. Strobel, Numerical simulation of sudden stratospheric warmings, J. Atmos. Sci., 37, 214-236, 1980.

Schoeberl, M. R., D. F. Strobel, and J. P. Apruzese, The NRL stratosphere-mesosphere model, WMO Workshop on Two-Dimensional Models, Toronto, Canada, February, 1980.

Schönle, G., H. D. Knauth, and R. N. Schindler, Pressure dependence of the exchange reaction between $ClONO_2$ and $^{15}NO_2$, J. Phys. Chem., 83, 3297-3302, 1979.

Schumacher, N. I., Upper air temperatures over an Antarctic station, Tellus, 7, 87-95, 1955.

Seiler, W. and J. Fishman, The distribution of carbon monoxide and ozone in the free troposphere, J. Geophys. Res., 86, 7255-7265, 1981.

Sekiguchi, Y., The relation between total ozone amount and temperature in the lower stratosphere over the Northern Hemisphere, Geophys. Mag., 31, 653-666, 1963.

Shedlovsky, J. P., and S. Paisley, On the meteoritic component of stratospheric aerosols, Tellus, 18, 499-503, 1966.

Simmons, A. J., Planetary-scale disturbances in the polar winter stratosphere, Quart. J. Roy. Meteorol. Soc., 100, 76-108, 1974.

Simon, P. C., Balloon measurements of solar fluxes between 1960A and 2300A, Proceedings of the Third Conference on the Climatic Impact Assessment Program, A. J. Broderick and T. M. Hard, editors, Dept. of Transportation DOT-TSC-057-74-15, pp 137-141, 1974.

Simon, P. C., Nouvelles mesures de l'ultraviolet solaire dans la stratosphère, Bull. Acad. Sci. Roy. Belgique, Cl. Sci., 6, 399-409, 1975.

Simon, P. C., Observation of the solar ultraviolet radiation, Proceedings of the NATO Advanced Study Institute on Atmospheric Ozone, A. C. Aikin, editor, DOT Report FAA-EE-80-20, pp 529-553, 1980.

Simon, P. C., and W. Peetermans, Ozone trend in the upper stratosphere: Results from Solar UV absorption measurements from 1976-1980, (Abstract) International Association of Meteorology and Atmospheric Physics, Third Scientific Assembly, Hamburg, Federal Republic of Germany, 17-28 August 1981.

Simon, P. C., R. Pastiels, and D. Nevejans, Balloon observations of solar ultraviolet irradiance at solar minimum, Planet. Space Sci., in press, 1981a.

Simonaitis, R., and J. Heicklen, The reaction of HO_2 with O_3, J. Phys. Chem., 77, 1932-1935, 1973.

Singh, H. B., Atmospheric Halocarbons: Evidence in favor of reduced average hydroxyl radical concentrations in the troposphere, Geophys. Res. Lett., 4, 101-104, 1977a.

Singh, H. B., Preliminary estimation of average tropospheric HO concentrations in the northern and southern hemispheres, Geophys. Res. Lett., 4, 453-456, 1977b.

Singh, H. B., and P. L. Hanst, Peroxyacetyl nitrate (PAN) in the unpolluted atmosphere: An important reservoir for nitrogen oxides, Geophys. Res. Lett., 8, 941-944, 1981.

Singh, H. B., D. P. Fowler, T. O. Peyton, Atmospheric carbon tetrachloride: Another man-made pollutant, Science, 192, 1231-1234, 1976.

Singh, H. B., L. J. Salas, and L. A. Cavanagh, Distribution, sources and sinks of atmospheric halogenated compounds, J. Air Pollut. Contr. Assn, 27, 332-336, 1977a.

Singh, H. B., L. Salas, H. Shigeishi, and A. Crawford, Urban-nonurban relationships of halocarbons, SF_6, N_2O and other atmospheric trace constituents, Atmos. Environ., 11, 819-828, 1977b.

Singh, H. B., F. L. Ludwig, and W. B. Johnson, Tropospheric ozone: Concentrations and variabilities in clean remote atmospheres, Atmos. Environ., 12, 2185-2196, 1978.

Singh, H. B., L. J. Salas, H. Shigeishi, and E. Scribner, Atmospheric halocarbons, hydrocarbons and sulfur hexafluoride: Global distributions, sources, and sinks, Science, 203, 899-903, 1979.

Singh, H. B., L. J. Salas, and R. Stiles, Trace Chemicals in the Clean Troposphere, SRI Project 8893, interim report prepared for U.S. EPA, SRI International, Menlo Park, California, 1981.

Smith, I. W. M., and R. Zellner, Rate measurements of reactions of OH by resonance absorption IV. Reactions of OH with NH_3 and HNO_3, Int. J. Chem. Kinet., Symp. No. 1, 341-351, 1975.

Smith, W. S., C. C. Chou, and F. S. Rowland, The mechanism for ultraviolet photolysis of gaseous chlorine nitrate at 302.5 nm, Geophys. Res. Lett., 4, 517-519, 1977.

Solomon, S., One- and two-dimensional photochemical modeling of the chemical interactions in the middle atmosphere, Ph.D. Thesis, University of California and National Center for Atmospheric Research, 1981.

Somayajulu, Y. V., S. Sampath, and K. S. Zalpuri, Rocket measurement of ozone density distribution in the equatorial stratosphere and mesosphere, Proceedings of the Quadrennial International Ozone Symposium, IAMAP, J. London, editor, pp 534-540, 1980.

Sridharan, U. C., B. Reimann, and F. Kaufman, Kinetics of the reaction OH + H_2O_2 HO_2 + H_2O, J. Chem. Phys., 73, 1286-1293, 1980.

St. John, D. S., S. P. Bailey, W. H. Fellner, J. M. Minor, and R. D. Snee, Time series search for trend in total ozone measurements, J. Geophys. Res., 86, 7299-7311, 1981.

Stanford, J. L., Possible sink for stratospheric water vapor at the winter Antarctic pole, J. Atmos. Sci., 30, 1431-1436, 1973.

Stanford, J. L., and J. S. Davis, A century of stratospheric cloud reports: 1870-1972, Bull. Amer. Meteorol. Soc., 55, 213-219, 1974.

Stanford, J. L., and T. J. Dunkerton, The character of ultra-long stratospheric temperature waves during the 1973 Austral, winter, Beitr. Phys. Atmos., 51, 174-188, 1978.

Starr, W. L., M. Loewenstein, and R. A. Craig, Measurements of NO and O_3 from U-2 aircraft: 1977 Tropical Convergence Zone Experiment, in 1977 Intertropical Convergence Zone Experiment, I. G. Poppoff, W. A. Page, and A. P. Margozzi, editors, NASA Technical Memorandum 78577, pp 35-50, 1979.

Starr, W. L., R. A. Craig, M. Loewenstein, and M. E. McGhan, Measurements of NO, O_3, and temperature at 19.8 km during the total solar eclipse of 26 February 1979, Geophys. Res. Lett., 7, 553-555, 1980.

Stewart, R. W., S. Hameed, and J. P. Pinto, Photochemistry of tropospheric ozone, J. Geophys. Res., 82, 3134-3140, 1977.

Stolarski, R. S., and R. J. Cicerone, Stratospheric chlorine: A possible sink for ozone, Can. J. Chem., 52, 1610-1615, 1974.

Straus, D. M., Long-wave baroclinic instability in the troposphere and stratosphere with spherical geometry, J. Atmos. Sci., 38, 409-426, 1981.

Strobel, D. F., Parameterization of the atmospheric heating rate from 15 to 120 km due to O_2 and O_3 absorption of solar radiation, J. Geophys. Res., 83, 6225-6230, 1978.

Strobel, D. F., Parameterization of the thermal relaxation rate in the stratosphere, J. Geophys. Res., 84, 2469-2470, 1979.

Strobel, D. F., Parameterization of linear wave chemical transport in planetary atmospheres by eddy diffusion, J. Geophys. Res., 86, 9806-9810, 1981.

Subbaraya, B. H., S. Lal, and A. Jayaraman, In-situ measurement of ozone concentration profiles at stratospheric and mesospheric altitudes over Thumba, (Abstract), IAMAP Third Scientific Assembly, Hamburg, Federal Republic of Germany, August, 1981.

Sundararaman, N., International ozone rocketsonde intercomparison, IAMAP Third Scientific Assembly, Hamburg, Federal Republic of Germany, August, 1981.

Sundararaman, N., T. Perry, Jr., W. Gurkin, E. Jackson, B. Horton, J. Lean, E. Llewellyn, B. Solheim, W. F. J. Evans, B. H. Subbaraya, S. Lal, T. Ogawa, T. Watanabe, E. Hilsenrath, and A. Krueger, International ozone rocketsonde intercomparison, Proceedings of the Quadrennial International Ozone Symposium, IAMAP, J. London, editor, pp 421-422, 1980.

Swissler, T. J., P. Hamill, M. Osborn, P. B. Russell, and M. P. McCormick, A comparison of lidar and balloon-borne particle counter measurements of the stratospheric aerosol 1974-1980, J. Atmos. Sci., submitted, 1981.

Sze, N. D., Stratospheric fluorine: A comparison between theory and measurement, Geophys. Res. Lett., 5, 781-783, 1978.

Sze, N. D., and M. K. W. Ko, Is CS_2 a precursor for atmospheric COS, Nature, 278, 731-732, 1979a.

Sze, N. D., and M. K. W. Ko, CS_2 and COS in the stratospheric sulphur budget, Nature, 280, 308-310, 1979b.

Sze, N. D., and M. K. W. Ko, Photochemistry of COS, CS_2, CH_3SCH_3 and H_2S: Implications for the atmospheric sulfur cycle, Atmos. Environ., 14, 1223-1239, 1980.

Sze, N. D., and M. K. W. Ko, The photochemistry of carbon monosulfide: A possible source for atmospheric OCS, Geophys. Res. Lett., 8, 765-768, 1981.

Taylor, F. W., J. J. Barnett, I. Colbeck, R. L. Jones, C. D. Rodgers, M. I. Wale, and E. J. Williamson, Performance and early results from the Stratospheric and Mesospheric Sounder (SAMS) on Nimbus 7, First FGGE Results from Satellites, Advances in Space Research, 1, No. 4, 261-265, 1981.

Telegadas, K., and R. J. List, Are particulate radioactive tracers indicative of stratospheric motions, J. Geophys. Res., 74, 1339-1350, 1969.

Thekaekara, M. P., Radiation scales on which standard values of the solar constant and solar spectral irradiance are based, Proc. of the Sixth Space Simulation Conference, New York 1-3 May 1972, 947-953, 1972.

Thompson, B. A., P. Harteck and R. R. Reeves, Jr., Ultraviolet absorption coefficents of CO_2, CO, O_2, H_2O, N_2O, NH_3, NO, SO_2, and CH_4 between 1850 A and 4000 A, J. Geophys. Res., 68, 6431-6436, 1963.

Tohmatsu, T., Altitude distributions of minor atmospheric species in the mesosphere and lower thermosphere as measured in optical absorption and emission, Space Research, 17, M. J. Rycroft, editor, Pergamon Press, pp 247-251, 1977.

Tolson, R. H. Spatial and temporal variations of monthly mean total columnar ozone derived from 7 years of BUV data, J. Geophys. Res., 86, 7312-7330, 1981.

Toon, O. B., and N. H. Farlow, Particles above the tropopause: Measurements and models of stratospheric aerosols, meteoric debris, nacreous clouds, and noctilucent clouds, Ann. Rev. Earth Planet. Sci., 9, 19-58, 1981.

Toon, O. B., and J. B. Pollack, Physical properties of the stratospheric aerosols, J. Geophys. Res., 78, 7051-7056, 1973.

Toon, O. B., R. P. Turco, P. Hamill, C. S. Kiang, and R. C. Whitten, A one-dimensional model describing aerosol formation and evolution in the stratosphere. II. Sensitivity studies and comparison with observations, J. Atmos. Sci., 36, 718-736, 1979.

Torres, A. L., P. J. Maroulis, A. B. Goldberg, and A. R. Bandy, Atmospheric OCS measurements on Project GAMETAG, J. Geophys. Res., 85, 7357-7360, 1980.

Troe, J., Theory of thermal unimolecular reactions at low pressures. I. Solutions of the master equation, J. Chem. Phys., 66, 4745-4757, 1977.

Tuck, A. F., A comparison of one-, two- and three-dimensional model representations of stratospheric gases, Phil. Trans. Roy. Soc., Lon., A290, 477-494, 1979.

Turco, R. P., and R. C. Whitten, A note on the diurnal averaging of aeronomical models, J. Atmos. Terr. Phys., 40, 13-20, 1978.

Turco, R. P., P. Hamill, O. B. Toon, R. C. Whitten, and C. S. Kiang, A one-dimensional model describing aerosol formation and evolution in the stratosphere. I. Physical processes and mathematical analogs, J. Atmos. Sci., 36, 699-717, 1979.

Turco, R. P., R. C. Whitten, O. B. Toon, J. B. Pollack, and P. Hamill, OCS, stratospheric aerosols and climate, Nature, 283, 283-286, 1980a.

Turco, R. P., R. C. Whitten, O. B. Toon, J. B. Pollack, and P. Hamill, Carbonyl sulfide, stratospheric aerosols and terrestrial climate, Environmental and Climatic Impact of Coal Utilization, J. J. Singh and A. Deepak, editors, Academic Press, New York, pp 331-356, 1980b.

Turco, R. P., O. B. Toon, J. B. Pollack, R. C. Whitten, I. G. Poppoff, and P. Hamill, Stratospheric aerosol modification by supersonic transport and space shuttle operations - climate implications, J. Appl. Meteorol., 19, 78-89, 1980c.

Turco, R. P., O. B. Toon, P. Hamill, and R. C. Whitten, Effects of meteoric debris on stratospheric aerosols and gases, J. Geophys. Res., 86, 1113-1128, 1981a; Correction, 86, 7471, 1981a

Turco, R. P., O. B. Toon, R. C. Whitten, and R. G. Keesee, The Mt. St. Helens eruptions of May and June 1980: Model studies of the physical and chemical processes occurring in the volcanic clouds, Proc. Sym. Mt. St. Helens, Washington, DC, 18-19 November 1980, Spectrum Press, in press, 1981b.

Turco, R. P., R. J. Cicerone, E. C. Y. Inn, and L. A. Capone, Long wavelength carbonyl sulfide photodissociation, J. Geophys. Res., 86, 5373-5377, 1981c.

Turco, R. P., R. C. Whitten, O. B. Toon, E. C. Y. Inn, and P. Hamill, Stratospheric hydroxyl radical concentrations: New limitations suggested by observations of gaseous and particulate sulfur, J. Geophys. Res., 86, 1129-1139, 1981d.

Twomey, S., Cloud nucleation in the atmosphere and the influence of nucleus concentration levels in atmospheric physics, J. Phys. Chem., 84, 1459-63, 1980.

Tyson, B. J., J. F. Vedder, J. C. Arvesen, and R. B. Brewer, Stratospheric measurements of CF_2Cl_2 and N_2O, Geophys. Res. Lett., 5, 369-372, 1978.

U. K. DOE, Chlorofluorocarbons and Their Effect on Stratospheric Ozone, Pollution Paper No. 15, Her Majesty's Stationery Office, London, 1979.

U. S. Standard Atmosphere, 1962, Supt. of Documents, U.S. Government Printing Office, Washington, D.C., 1962.

U. S. Standard Atmosphere, 1976, NOAA-S/T76-1562, Supt. of Documents, U.S. Government Printing Office, Washington, D.C., 1976.

Uryu, M., Mean zonal flows induced by a vertically propagating Rossby wave packet, J. Meteorol. Soc. Japan, 52, 481-490, 1974.

Vanlaethem-Meurée, H., J. Wisemberg, and P. C. Simon, Ultraviolet absorption spectrum of methylchloroform in the vapor phase, Geophys. Res. Lett., 6, 451-454, 1979.

Van Loon, H., Temperature in the southern hemisphere, Meteorology of the Southern Hemisphere, Meteorological Monographs, 13, C. W. Newton, editor, Amer. Meteorol. Soc. pp 25-58, 1972.

Van Loon, H., K. Labitzke, and R. L. Jenne, Half-yearly wave in the stratosphere, J. Geophys. Res., 77, 3846-3855, 1972.

Van Loon, H., R. L. Jenne, and K. Labitzke, Zonal harmonic standing waves, J. Geophys. Res., 78, 4463-4471, 1973.

Vedder, J. F., B. J. Tyson, R. B. Brewer, C. A. Boitnott, and E. C. Y. Inn, Lower stratosphere measurements of variation with latitude of CF_2Cl_2, $CFCl_3$, CCl_4, and N_2O profiles in the northern hemisphere, Geophys. Res. Lett., 5, 33-36, 1978.

Vedder, J. F., E. C. Y. Inn, B. J. Tyson, C. A. Boitnott, and D. O'Hara, Measurements of CF_2Cl_2, $CFCl_3$, and N_2O in the lower stratosphere between 2°S and 73°N latitude, J. Geophys. Res., 86, 7363-7368, 1981.

Venne, D. E., A 4-day winter polar stratosphere temperature wave: Observation and theory, Extended Abstracts Int. Symp. on Middle Atmos. Dynamics, Handbook for MAP, Volume 2, S. K. Avery, editor, pp 157-164, 1981.

Vidal-Madjar, A., Evolution of the solar Lyman-alpha flux during four consecutive years, Solar Phys., 40, 69-86, 1975.

Vidal-Madjar, A., and B. Phissamay, The solar Lyman-alpha flux near solar minimum, Solar Phys., 66, 259-271, 1980.

Viggiano, A. A., and F. Arnold, Extended sulfuric acid vapor concentration measurements in the stratosphere, Geophys. Res. Lett., 8, 583-586, 1981.

Vincent, D. G., Mean meridional circulation in the northern hemisphere and lower stratosphere during 1964 and 1965, Quart. J. Roy. Meteorol. Soc., 94, 333-349, 1968.

Volz, A., D. H. Ehhalt, L. E. Heidt, and W. Pollock, Vertical profiles of CH_4, CO and CO_2 in the stratosphere, Proceedings of the Joint Symposium on Atmospheric Ozone, Aug. 1976, Dresden, GDR, Vol. II, 219, 1977.

Volz, A., D. H. Ehhalt, and R. G. Derwent, Seasonal and latitudinal variation of ^{14}CO and the tropospheric concentrations of OH radicals, J. Geophy. Res., 86, 5163-5171, 1981.

Volz, A., U. Schmidt, J. Rudolph, D. H. Ehhalt, F. J. Johnson, and A. Khedim, Vertical profiles of trace gases at mid-latitudes, Jul-Report No. 1742, Kernforschungsanlage, Jülich, Federal Republic of Germany, 1981b.

Vonder Haar, T. H., and J. S. Ellis, Atlas of radiation budget measurements from satellites (1962-1970), Atmospheric Science Paper No. 231, Dept. of Atmospheric Science, Colorado State Univ., Fort Collins, Colorado, 1974.

Vupputuri, R. K. R., A comprehensive summary of the AES two-dimensional model, WMO Workshop on Two-Dimensional Models, Toronto, Canada, February, 1980a.

Vupputuri, R. K. R., The natural stratospheric distributions of odd oxygen and odd nitrogen as simulated in the AES two-dimensional model, preprint at NASA Stratospheric Modeling Workshop, December 1980b.

Wallace, J. M., Trajectory slopes, contergradient heat fluxes and mixing by lower stratospheric waves, J. Atmos. Sci., 35, 554-558, 1978.

Wang, W-C., J. P. Pinto, and Y. L. Yung, Climatic effects due to halogenated compounds in the Earth's atmosphere, J. Atmos. Sci., 37, 333-338, 1980.

Wang, C. C., L. I. Davis, Jr., P. M. Selzer, and R. Munoz, Improved airborne measurements of OH in the atmosphere using the technique of laser-induced fluorescence, J. Geophys. Res., 86, 1181-1186, 1981a.

Wang, C. C., L. I. Davis, Jr., P. M. Selzer, and R. Munoz, Reply, J. Geophys. Res., 86, 12,156, 1981b.

Waters, J. W., J. J. Gustincic, P. N. Swanson, and A. R. Kerr, Measurements of upper atmospheric H_2O emission at 183 GHz, Atmospheric Water Vapor, A. Deepak, T. D. Wilkerson, and L. H. Ruhnke, editors, Academic Press, pp 229-440, 1980.

Waters, J. W., J. C. Hardy, R. F. Jarnot, H. M. Pickett, Chlorine monoxide radical, ozone and hydrogen peroxide: Stratospheric measurements by microwave limb sounding, Science, 214, 61-64, 1981.

Watson, A. J., J. E. Lovelock, and D. H. Stedman, The problem of atmospheric methyl chloride, Proc. of NATO Adv. Study Inst. on Atmospheric Ozone: Its Variation and Human Influence, A. C. Aikin, editor, U. S. Department Transportation Report No. FAA-EE-80-20, pp 365-372, 1980.

Webster, P. J., L. Coy, and C. Leovy, Equatorial waves in the upper stratosphere, Extended Summaries IAMAP/IAGA Joint Assembly, Seattle, August 22-September 3, pp 2(1-4), 1977.

Wehrbein, W. M., and C. B. Leovy, Middle-atmosphere project: A radiative heating and cooling algorithm for a numerical model of the large scale stratospheric circulation, NASA Contractor Report 164646 Rept-2, Dept. of Atmos. Sciences, Washington University, Seattle, 1981.

Weiler, K. H., P. Fabian, G. Flentje, and W. A. Matthews, Stratospheric NO measurements: A new balloon-borne chemiluminescent instrument, J. Geophys. Res., 85, 7445-7452, 1980.

Weinstock, E. M., M. J. Phillips, and J. G. Anderson, In-situ observations of ClO in the stratosphere: A review of recent results, J. Geophys. Res., 86, 7273-7278, 1981.

Weiss, R. F., The temporal and spatial distribution of tropospheric nitrous oxide, J. Geophys. Res., 86, 7185-7195, 1981.

Weiss, R. F., and H. Craig, Production of atmospheric nitrous oxide by combustion, Geophys. Res. Lett., 3, 751-753, 1976.

Weiss, R. F., C. D. Keeling, and H. Craig, The determination of tropospheric nitrous oxide, J. Geophys. Res., 86, 7197-7202, 1981.

Wexler, H., W. B. Moreland, and W. S. Weyant, A preliminary report on ozone observations at Little America, Antarctica, Mon. Weather Rev., 88, 43-54, 1960.

Whitten, R. C., W. J. Borucki, V. R. Watson, T. Shimazaki, H. T. Woodward, C. A. Riegel, L. A. Capone, and T. Becker, The NASA Ames Research Center one- and two-dimensional stratospheric models, Part II: The two-dimensional model, NASA Technical Paper 1003, 1977.

Whitten, R. C., W. J. Borucki, H. T. Woodward, L. A. Capone, C. A. Riegel, R. P. Turco, I. G. Poppoff, and K. Santhanam, Implications of smaller concentrations of stratospheric OH: A two-dimensional model study of ozone perturbations, Atmos. Environ., 15, 1583-1589, 1981.

Widhopf, G. F., and L. Glatt, The aerospace time dependent 2-dimensional, photochemical model of the atmosphere, WMO Workshop on Two-Dimensional Models, Toronto, Canada, 1980, report in preparation, 1981.

Wilkniss, P. E., R. A. Lamontagne, R. E. Larson, J. W. Swinnerton, C. R. Dickson, and T. Thompson, Atmospheric trace gases in the southern hemisphere, Nature, 245, 45-47, 1973.

Wilkniss, P. E., J. W. Swinnerton, D. J. Bressan, R. A. Lamontagne, and R. E. Larson, CO, CCl_4, Freon-11, CH_4 and Rn-222 concentrations at low altitude over the Arctic Ocean in January 1974, J. Atmos. Sci., 32, 158-162, 1975a.

Wilkniss, P. E., J. W. Swinnerton, R. A. Lamontagne, and D. J. Bressan, Trichlorofluoromethane in the troposphere, distribution and increase, 1971 to 1974, Science, 187, 832-834, 1975b.

Wilkniss, P. E., R. A. Lamontagne, R. E. Larson, and J. W. Swinnerton, Atmospheric trace gases and land and sea breezes at the Sepik River Coast of Papua New Guinea, J. Geophys. Res., 83, 3672-3674, 1978.

Williams, W. J., J. J. Kostus, A. Goldman, and D. G. Murcray, Measurements of the stratospheric mixing ratio of HCl using an infrared absorption technique, Geophys. Res. Lett., 3, 383-385, 1976.

Willson, R. C., S. Gulkis, M. Janssen, H. S. Hudson, and G. A. Chapman, Observations of solar irradiance variability, Science, 211, 700-702, 1981.

Wilson, W. J., and P. R. Schwartz, Diurnal variations of mesospheric ozone using millimeter-wave measurements, J. Geophys. Res., 86, 7385-7388, 1981.

Wine, P. H., R. C. Shah, and A. R. Ravishankara, Rate of reaction of OH with CS_2, J. Phys. Chem., 84, 2499-2503, 1980.

Wine, P. H., W. L. Chameides, and A. R. Ravishankara, Potential role of CS_2 photooxidation in tropospheric sulphur chemistry, Geophys. Res. Lett., 8, 543-546, 1981a.

Wine, P. H., A. R. Ravishankara, N. M. Kreutter, R. C. Shah, J. M. Nicovich, R. L. Thompson and D. J. Wuebbles, Rate of reaction of OH with HNO_3, J. Geophys. Res., 86, 1105-1112, 1981b.

WMO, Assessment of Performance Characteristics of Various Ozone Observing Systems, Report of the meeting of experts, Boulder, July 1980, WMO Global Ozone Research and Monitoring Project Report No. 9, 67 pp, published 1981.

Wofsy, S. C., and M. B. McElroy, HO_x NO_x and ClO_x: Their role in atmospheric photochemistry, Can. J. Chem., 52, 1582-1591, 1974.

Wright, D. U., A. J. Krueger, and G. M. Foster, Rocket ozone sounding network data, quarterly report, NASA Technical Memorandum 73283, 29 pp, Nov. 1979.

Wu, M.-F., Observation and analysis of trace constituents in the stratosphere, annual report, Contract DOT-05-20217, Env. Res. Tech., Lexington, Mass., 1973.

Wuebbles, D. J., A summary of current two-dimensional models of the troposphere and stratosphere, Lawrence Livermore National Laboratory Report, 1980.

Wuebbles, D. J., Treatment of dynamical processes in two-dimensional models of the troposphere and stratosphere, UCID-188771, 1980.

Wuebbles, D. J., The relative efficiency of a number of halocarbons for destroying stratospheric ozone, Lawrence Livermore National Laboratory, UCID 18924, 1981.

Wuebbles, D. J., and W. H. Duewer, Effect on recent kinetics measurements on our understanding of chemical processes in the troposphere and stratosphere, UCRL-83960, 1980.

Wuebbles, D. J., and F. M. Luther, Effect of coupled anthropogenic perturbations on stratospheric ozone, Preprint, 1981.

Yule, G. U., On a method of investigating periodicities in disturbed series, with special reference to Wolfer's sunspot numbers, Phil. Trans. Roy. Soc. London, A226, 267-298, 1927.

Zafonte, L., N. E. Hester, E. R. Stephens, and O. C. Taylor, Background and vertical atmospheric measurements of Fluorocarbon-11 and Fluorocarbon-12 over Southern California, Atmos. Environ., 9, 1007-1009, 1975.

Zahniser, M. S., and C. J. Howard, Kinetics of the reaction of HO_2 with ozone, J. Chem. Phys., 73, 1620-1626, 1980.

Zahniser, M. S., J. Chang, and F. Kaufman, Chlorine nitrate: kinetics of formation by ClO + NO_2 + M and of reaction with OH, J. Chem. Phys., 67, 997-1003, 1977.

Zander, R., Présence de HF dans la stratosphère supérieure, C. R. Acad. Sci. Paris, B, 281, 213-214, 1975.

Zander, R., Recent observations of HF and HCl in the upper stratosphere, Geophys. Res. Lett., 8, 413-416, 1981, corrections to the paper, 8, 850, 1981.

Zander, R., H. Leclercq, and L. D. Kaplan, Concentration of carbon monoxide in the upper stratosphere, Geophys. Res. Lett., 8, 365-368, 1981a.

Zerefos, C. S., and H. T. Mantis, Climatic fluctuations in the northern hemisphere stratosphere, Arch. Meteor. Geoph. Biokl., Ser. B, 25, 33-39, 1977.

Zimmerman, P. R., R. B. Chatfield, J. Fishman, P. J. Crutzen, and P. L. Hanst, Estimates on the production of CO and H_2 from the oxidation of hydrocarbon emissions from vegetation, Geophys. Res. Lett., 5, 679-682, 1978.

APPENDIX F

CHEMICAL FORMULAE AND NOMENCLATURE

SYMBOL	NAME
CFC	chlorofluorcarbon
HC	hydrocarbon
NMHC	non-methane hydrocarbons
PAN	peroxyacetyl nitrate
O	atomic oxygen
O_2	molecular oxygen
O_3	ozone
N_2O	nitrous oxide
NO	nitric oxide
NO_2	nitrogen dioxide
NO_3	nitrogen trioxide
N_2O_5	nitrogen pentoxide
HNO_3, $HONO_2$	nitric acid
HNO_4, HO_2NO_2	peroxynitric acid
NH_3	ammonia
H_2O	water vapor
H_2O_2	hydrogen peroxide
HO	hydroxyl radical
HO_2	hydroperoxyl radical
CO	carbon monoxide
CO_2	carbon dioxide
CS_2	carbon disulfide
COS	carbonyl sulfide
SO_2	sulfur dioxide
SF_6	sulfur hexafluoride

H_2SO_4	sulfuric acid
HF	hydrogen fluoride
HCl	hydrogen chloride
HOCl	hypochlorous acid
ClO	chlorine oxide
$ClONO_2$	chlorine nitrate
CH_4	methane
C_2H_6	ethane
C_3H_8	propane
C_2H_4	ethylene
C_2H_2	acetylene
CH_2O	formaldehyde
CH_3CHO	acetaldehyde
$(CH_3)_2CO$	acetone
CH_3O_2H	methyl peroxide
CH_2CHCHO	acrolein
CCl_4	carbon tetrachloride
C_2Cl_4	tetrachloroethylene
CH_3Cl	methyl chloride
CH_2Cl_2	ethylene dichloride
$CHCl_3$	chloroform
CH_3CCl_3	methyl chloroform
CF_4	tetrafluoromethane
C_2F_6	hexafluoroethane
CCl_3F	trichlorofluoromethane (FC-11)
CCl_2F_2	dichlorodifluoromethane (FC-12)

$CHCl_2F$	dichlorofluoromethane (FC-21)
$CHClF_2$	chlorodifluoromethane (FC-22)
CCl_2FCClF_2	trichlorotrifluoroethane (FC-113)
$CClF_2CClF_2$	dichlorotetrafluoroethane (FC-114)
$CClF_2CF_3$	chloropentafluoroethane (FC-115)
CH_3I	methyl iodide
$CBrF_3$	trifluorobromomethane

APPENDIX G

PRESSURE-ALTITUDE CONVERSION CHART

PRESSURE-ALTITUDE

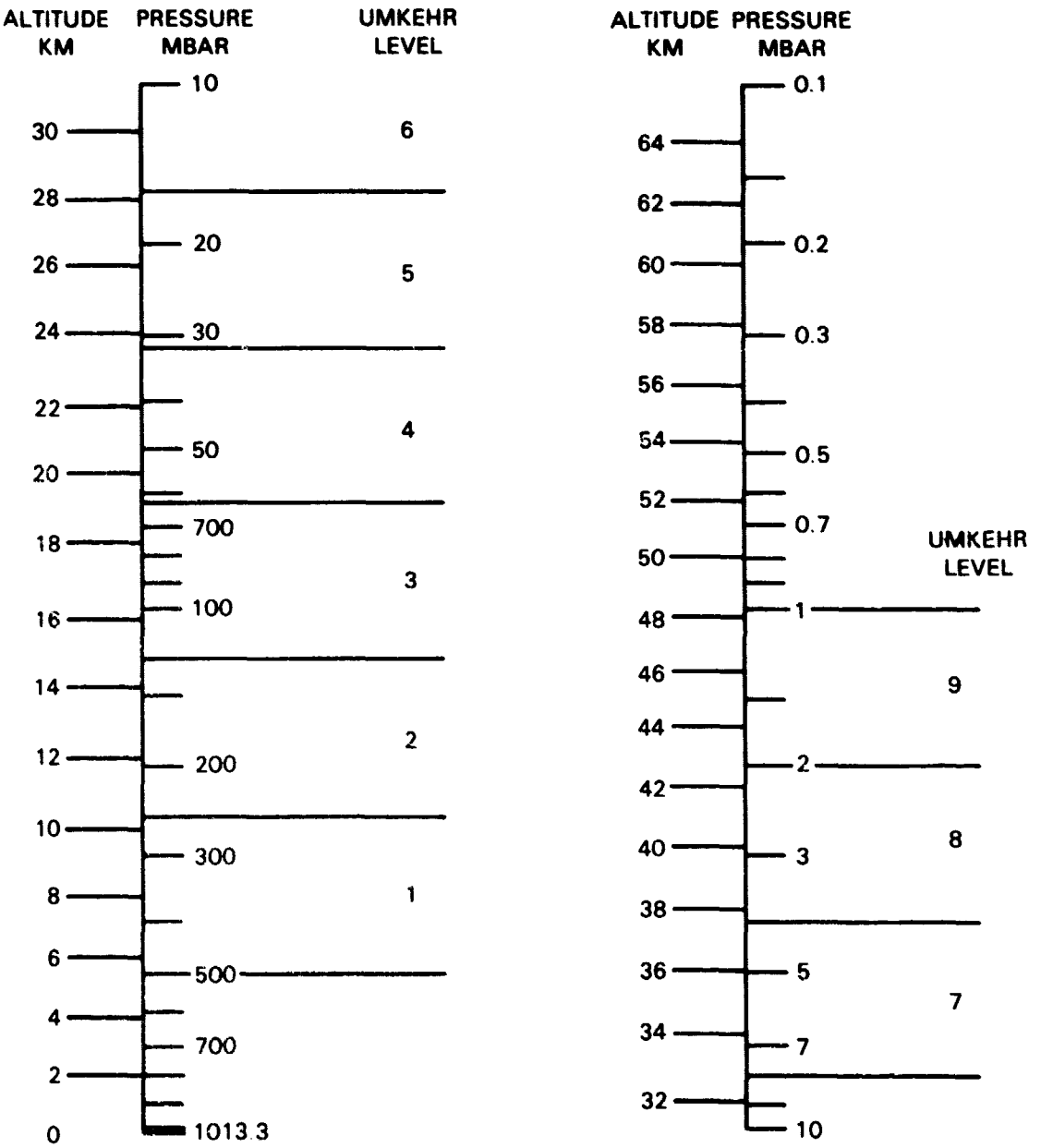

ALTITUDES ARE BASED ON U.S. STANDARD ATMOSPHERE, 1976. THE ACTUAL ALTITUDE FOR A GIVEN PRESSURE MAY DIFFER BY AS MUCH AS 2 KM, DEPENDING ON SEASON, LATITUDE, AND SHORT TERM VARIATIONS.

APPENDIX H

ACRONYMS

Units, Instruments, Satellites, and Programs

AE	Atmosphere Explorer
AEM	Applications Explorer Mission
BMLS	Balloon-borne Microwave Limb Sounder
BSU	Basic Sounding Unit
BUV	Backscattered Ultraviolet Spectrometer
CIAP	Climatic Impact Assessment Program
DMSP	Defense Meteorological Satellite Program
DU	Dobson Unit=milliatm-cm=2.687×10^{16} molecules cm^{-2}
ECC	Electrochemical cell (ozone sonde)
ERBS	Earth Radiation Budget Satellite
GARP	Global Atmospheric Research Program
GATE	GARP Atlantic Tropical Experiment
GCM	General Circulation Model
GMCC	Geophysical Monitoring for Climatic Change
GOES	Geosynchronous Operational Environmental Satellite
HALOE	Halogen Occultation Experiment
HAPP	High Altitude Pollution Program
HIRS	High Resolution Infrared Radiation Sounder
IORI	International Ozone Rocket Intercomparison
IRIS	Infrared Interferometer Spectrometer
ITCZ	Intertropical Convergence Zone
ITOS	Improved TIROS Operational Satellite
ITPR	Infrared Temperature Profile Radiometer
LHR	Laser Heterodyne Radiometer
LIMS	Limb Infrared Monitor of the Stratosphere
LRIR	Limb Radiance Inversion Radiometer
MFR	Multichannel Filter Radiometer
MM	Mechanistic Model
MST	Mesosphere, Stratosphere, Troposphere (radar)
MSU	Microwave Sounding Unit
MUSE	Monitor of Ultraviolet Solar Energy
NOPS	Nimbus Operational Processing System
OAO	Orbiting Astronomical Observatory
OGO	Orbiting Geophysical Observatory
OSO	Orbiting Solar Observatory
PEPSIOS	Poly-Etalon Pressure Scanned Interferometer
PMR	Pressure Modulated Radiometer

SAGE	Stratospheric Aerosol and Gas Experiment
SAM II	Stratospheric Aerosol Measurement II
SAMS	Stratospheric and Mesospheric Sounder
SBUV	Solar and Backscattered Ultraviolet Spectrometer
SCR	Selective Chopper Radiometer
SIRS	Satellite Infrared Spectrometer
SME	Solar Mesosphere Explorer
SSH	Special Sensor H (also called MFR)
SST	Supersonic Transport
SSU	Stratospheric Sounding Unit
TIROS	Television and Infrared Observation Satellite
TOMS	Total Ozone Mapping System
TOVS	TIROS Operational Vertical Sounder
UARS	Upper Atmosphere Research Satellite
VTPR	Vertical Temperature Profile Radiometer

Institutions

AER, Inc.	Atmospheric and Environmental Research, Incorporated 872 Massachusetts Avenue Cambridge, Massachusetts 02139 USA
AERE Harwell	Atomic Energy Research Establishment Harwell Oxfordshire OX11 ORA, United Kingdom
AES	Atmospheric Environment Service 4905 Dufferin Street Downsview, Ontario M3H 5T4, Canada
AIAA	American Institute of Aeronautics and Astronautics, Inc. Technical Information Service 555 West 57th Street New York, New York 10019 USA
ARC	Ames Research Center Moffett Field, California 94035 USA
ASL	Atmospheric Sciences Laboratory White Sands Missile Range New Mexico, 88002 USA
BMO	Meteorological Office London Road Bracknell, Berkshire RG12 2SZ, United Kingdom
CMA	Chemical Manufacturers Association 2501 M Street, N.W. Washington, D.C. 20037 USA
CNRS	Center National de la Recherche Scientifique 91370 Verrieres le Buisson, France
CODATA	Committee on Data for Science and Technology 51 Boulevard de Montmorency Paris, France
COMESA	Committee on Meteorological Effects of Stratospheric Aircraft Meteorological Office Bracknell, United Kingdom
CSIRO	Commonwealth Scientific and Industrial Research Organization Australia
DoD	Department of Defense (USA)
DOT	Department of Transportation (USA)

Du Pont	E.I. du Pont de Nemours & Co. Experimental Station Wilmington, Delaware 19898 USA
EERM	Météorologie Nationale EERM Boulogne-Billancourt France
EPA	Environmental Protection Agency, Washington, D.C. 20460 USA
FAA	Federal Aviation Administration U.S. Dept. of Transportation Washington, D.C. 20591 USA
GFDL	Geophysical Fluid Dynamics Laboratory P.O. Box 308, Princeton University, Princeton, New Jersey 08540 USA
GISS	Goddard Institute for Space Studies New York, New York 10025 USA
GIT	Georgia Institute of Technology Atlanta, GA 30332 USA
GSFC	Goddard Space Flight Center Greenbelt, Maryland 20771 USA
IAS	Institut d'Aéronomie Spatiale Brussels, Belgium
JPL	Jet Propulsion Laboratory 4800 Oak Grove Drive Pasadena, California 91103 USA
KFA	Institut fur Chemie der Kernforschungsanlage Julich Postfach 1913, D-5170 Jülich Federal Republic of Germany
LaRC	Langley Research Center Hampton, Virginia 23665 USA
LLNL	Lawrence Livermore National Laboratory P.O. Box 808 Livermore, California 94550 USA
MIT	Massachusetts Institute of Technology Cambridge, Massachusetts 02139 USA
MPI-Lindau	Max Planck Institute für Aeronomie Postfach 20, D-3411 Katlenburg, Lindau 3 Federal Republic of Germany

MPIC, MPI-Mainz	Max Planck Institut für Chemie Saarstrasse 23, D-65 Mainz Federal Republic of Germany
NAS	National Academy of Sciences 2101 Constitution Avenue, N.W. Washington, D.C. 20418 USA
NASA	National Aeronautics and Space Administration Headquarters Washington, D.C. 20546 USA
NCAR	National Center for Atmospheric Research P.O. Box 3000 Boulder, Colorado 80307 USA
NCC	National Climatic Center, Asheville, North Carolina 28801 USA
NESS	National Earth Satellite Service Suitland, Maryland 20233 USA
NOAA	National Oceanic and Atmospheric Administration Headquarters Rockville, Maryland 20852 USA
NSF	National Science Foundation Washington, D.C. USA
NSSDC	National Space Science Data Center Goddard Space Flight Center Greenbelt Maryland 20771 USA
NTIS	National Technical Information Service Springfield, Virginia 22151 USA
OECD	Organization for Economic Cooperation and Development Paris, France
OHP	Observatoire de Haute Provence France
ONR	Office of Naval Research, USA
NWS	National Weather Service Silver Spring, Maryland 20910 USA
R&D	R and D Associates P. O. Box 9695 Marina del Rey, California 90291 USA

UK DOE	United Kingdom Department of the Environment
UNEP	United Nations Environment Program Nairobi, Kenya
Univ. of Oxford	University of Oxford Oxford, United Kingdom
WMO	World Meteorological Organization Case Postal No. 5 Geneva 20, Switzerland

APPENDIX I

WORKSHOP COMMITTEE AND CONTRIBUTORS

WORKSHOP COMMITTEE

Executive Council	Robert D. Hudson, Co-Chairman Rumen D. Bojkov, Co-Chairman Marvin Geller Edith I. Reed Richard S. Stolarski Narasimhan Sundararaman Robert T. Watson
Chapter 1:	Dieter Ehhalt Thomas J. McGee
Chapter 2:	James R. Holton Jordan Alpert
Chapter 3:	Julius Chang Julius London Paul Guthrie
Appendix A:	William B. DeMore
Appendix B:	John E. Frederick
Appendix C:	Marvin Geller
Appendix D:	Robert D. Hudson

CONTRIBUTORS

Marcel E. H. Ackerman
Institut d' Aéronomie Spatiale de Belgium
Brussels, Belgium

Daniel L. Albritton
NOAA/Environmental Research Laboratory
Boulder, Colorado, USA

Jordan Alpert
NASA/Goddard Space Flight Center
Greenbelt, Maryland, USA

James G. Anderson
Harvard University
Cambridge, Massachusetts, USA

James K. Angel
NOAA/Air Resources Laboratory
Silver Spring, Maryland, USA

Peter Bloomfield
Princeton University
Princeton, New Jersey, USA

Rumen D. Bojkov
World Meteorological Organization
Geneva, Switzerland

B. W. Boville
Willowdale, Ontario, Canada

G. Brasseur
Institut d' Aéronomie Spatiale
Brussels, Belgium

Guenter E. Brueckner
Naval Research Laboratory
Washington, D. C., USA

D. Cariolle
Meteorologie Nationale EERM
Boulogne-Billancourt, France

Sushil Chandra
NASA/Goddard Space Flight Center
Greenbelt, Maryland, USA

Julius Chang
Lawrence Livermore National Laboratory
Livermore, California, USA

Ralph J. Cicerone
National Center for Atmospheric Research
Boulder, Colorado, USA

David S. Crosby
American University
Washington, D.C., USA

Paul Crutzen
Max Planck Institut fur Atmos. Chemie
Mainz, Federal Republic of Germany

Derek M. Cunnold
Georgia Institute of Technology
Atlanta, Georgia, USA

Edwin F. Danielsen
NASA/Ames Research Center
Moffett Field, California, USA

William B. DeMore
Jet Propulsion Laboratory
Pasadena, California, USA

R. G. Derwent
AERE Harwell
Oxfordshire, United Kingdom

Richard F. Donnelly
NOAA/Environmental Research Laboratory
Boulder, Colorado USA

Hans U. Dütsch
Laboratory for Atmospheric Physics, ETH
Zürich, Switzerland

Dieter Ehhalt
Institut für Chemie der KFA (3)
Jülich, Federal Republic of Germany

Wayne Evans
Atmospheric Environment Service
Downsview, Ontario, Canada

C. B. Farmer
Jet Propulsion Laboratory
Pasadena, California, USA

Giorgio Fiocco
Citta Universitaria
Roma, Italy

John E. Frederick
NASA/Goddard Space Flight Center
Greenbelt, Maryland, USA

Marvin Geller
NASA/Goddard Space Flight Center
Greenbelt, Maryland, USA

Anver Ghazi
Comm. of European Communities
Brussels, Belgium

John C. Gille
National Center for Atmospheric Research
Boulder, Colorado, USA

A. Girard
Office Nat. d'Etudes et de Recherche
Aerospatiale
Chatillon sous Bagneux, France

William L. Grose
NASA/Langley Research Center
Hampton, Virginia, USA

Paul Guthrie
NASA/Goddard Space Flight Center
Greenbelt, Maryland, USA

John E. Harries
Rutherford and Appleton Laboratories
Slough, United Kingdom

Dennis L. Hartmann
University of Washington
Seattle, Washington, USA

Donald F. Heath
NASA/Goddard Space Flight Center
Greenbelt, Maryland, USA

William J. Hill
Allied Chemical Corporation
Buffalo, New York, USA

Hans E. Hinteregger
Air Force Geophysics Laboratory
Bedford, Massachusetts, USA

James R. Holton
University of Washington
Seattle, Washington, USA

Robert D. Hudson
NASA/Goddard Space Flight Center
Greenbelt, Maryland, USA

Donald Hunten
University of Arizona
Tucson, Arizona, USA

I.S.A. Isaksen
University of Oslo
Oslo, Norway

J. Peter Jesson
E. I. du Pont de Nemours & Company
Wilmington, Delaware, USA

Harold S. Johnston
University of California
Berkeley, California, USA

Frederick Kaufman
University of Pittsburgh
Pittsburgh, Pennsylvania, USA

Gerald M. Keating
NASA/Langely Research Center
Hampton, Virginia, USA

Dieter Kley
NOAA/Environmental Research Laboratory
Boulder, Colorado, USA

Walter D. Komhyr
NOAA/Air Resources Laboratory - GMCC
Boulder, Colorado, USA

Cecil E. Leith
National Center for Atmospheric Research
Boulder, Colorado, USA

Conway B. Leovy
University of Washington
Seattle, Washington, USA

Hiram Levy II
NOAA/Geophysical Fluid Dynamics Laboratory
Princeton, New Jersey, USA

Shaw Chen Liu
NOAA/Environmental Research Laboratory
Boulder, Colorado, USA

Jennifer Logan
Harvard University
Cambridge, Massachusetts, USA

Julius London
University of Colorado
Boulder, Colorado, USA

Frederick M. Luther
Lawrence Livermore National Laboratory
Livermore, California, USA

Rowland Madden
National Center for Atmospheric Research
Boulder, Colorado, USA

Jerry D. Mahlman
NOAA/Geophysical Fluid Dynamics Laboratory
Princeton, New Jersey, USA

William Mankin
National Center for Atmospheric Research
Boulder, Colorado, USA

Carl Mateer
Atmospheric Environment Service
Downsview, Ontario, Canada

M. Patrick McCormick
NASA/Langley Research Center
Hampton, Virginia, USA

Michael McElroy
Harvard University
Cambridge, Massachusetts, USA

Thomas J. McGee
NASA/Goddard Space Flight Center
Greenbelt, Maryland, USA

A. James Miller
NOAA/National Meteorological Center
Washington, D. C., USA

Chester Miller
E. I. du Pont de Nemours & Company
Wilmington, Delaware, USA

Mario Molina
University of California
Irvine, California, USA

Marcel Nicolet
Ionosphere Research Laboratory
Pennsylvania State University
University Park, Pennsylvania, USA

T. Ogawa
University of Tokyo
Tokyo, Japan

Aaron J. Owens
E. I. du Pont de Nemours & Company
Wilmington, Delaware, USA

Hans Panofsky
Pennsylvania State University
University Park, Pennsylvania, USA

Joyce E. Penner
Lawrence Livermore National Laboratory
Livermore, California, USA

Barrie Pittock
CSIRO Div. of Atmospheric Physics
Mordialloc, Victoria, Australia

John Pyle
Clarendon Laboratory, Oxford University
Oxford, United Kingdom

V. Ramanathan
National Center for Atmospheric Research
Boulder, Colorado, USA

Carl A. Reber
NASA/Goddard Space Flight Center
Greenbelt, Maryland, USA

Edith I. Reed
NASA/Goddard Space Flight Center
Greenbelt, Maryland, USA

Gregory Reinsel
University of Wisconsin
Madison, Wisconsin, USA

George D. Robinson
Center for Environment and Man, Inc.
Hartford, Connecticut, USA

James W. Rogers
Federal Aviation Administration
Washington, D. C., USA

Gary J. Rottman
University of Colorado
Boulder, Colorado, USA

F. Sherwood Rowland
University of California
Irvine, California, USA

James M. Russell III
NASA/Langley Research Center
Hampton, Virginia, USA

Harold I. Schiff
York University
Downsview, Ontario, Canada

Arthur L. Schmeltekopf
NOAA/Enviromental Research Laboratory
Boulder, Colorado, USA

Mark R. Schoeberl
Naval Research Laboratory
Washington, D. C., USA

Paul C. Simon
Institut d'Aéronomie de Belgique
Brussels, Belgium

Hanwant B. Singh
SRI International
Menlo Park, California, USA

Daniel S. St. John
E. I. du Pont de Nemours & Company
Wilmington, Delaware, USA

Richard S. Stolarski
NASA/Goddard Space Flight Center
Greenbelt, Maryland, USA

Narasimhan Sundararaman
Federal Aviation Administration
Washington, D.C., USA

N. Dak Sze
Atmospheric and Environmental Research, Inc.
Cambridge, Massachusetts, USA

F. Taylor
Clarendon Laboratory, Oxford University
Oxford, United Kingdom

George C. Tiao
University of Wisconsin
Madison, Wisconsin, USA

Robert H. Tolson
NASA/Langley Research Center
Hampton, Virginia, USA

Adrian F. Tuck
Meteorological Office
Berkshire, United Kingdom

Richard P. Turco
R&D Associates
Marina del Rey, California, USA

Andreas Volz
Institut für Chemie der KFA (3)
Jülich, Federal Republic of Germany

R.K.R. Vupputuri
Atmospheric Environment Service
Downsview, Ontario, Canada

Robert T. Watson
NASA Headquarters
Washington, D.C., USA

Robert C. Whitten, Jr.
NASA/Ames Research Center
Moffett Field, California, USA

Robert W. Wilcox
Control Data Corporation
Minneapolis, Minnesota, USA

Donald J. Wuebbles
Lawrence Livermore National Laboratory
Livermore, California, USA

Zhou Xiuji
Institute of Atmospheric Physics, Academia Sinica
Beijing, Peoples Republic of China